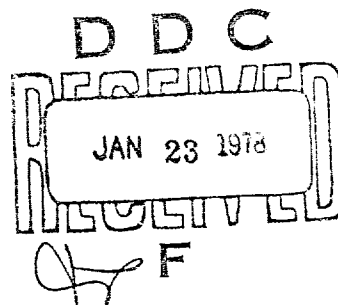


AD A049017

SUPPRESSIVE SHIELDS

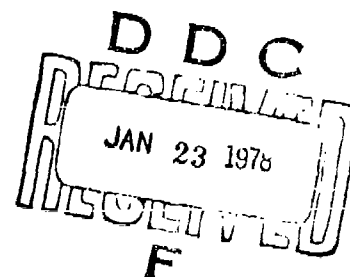
STRUCTURAL DESIGN AND
ANALYSIS HANDBOOK



DISTRIBUTION STATEMENT A
Approved for public release
Distribution Unlimited

U.S. ARMY
CORPS OF ENGINEERS
HUNTSVILLE DIVISION

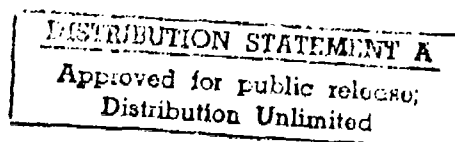
SUPPRESSIVE SHIELDS
STRUCTURAL DESIGN
AND
ANALYSIS HANDBOOK



This project was accomplished as part of the U.S. Army manufacturing technology program. The primary objective of this program is to develop, on a timely basis, manufacturing processes, techniques, and equipment for use in production of Army material.

U.S. ARMY CORPS OF ENGINEERS
HUNTSVILLE DIVISION

18 Nov 1977



LIST OF EFFECTIVE PAGES

INSERT LATEST CHANGED PAGES.

DESTROY SUPERSEDED PAGES.

Total number of pages in this manual is 552 consisting of the following:

Page No.	Change No. & Date
Title	0 - 18 Nov 77
A	0 - 18 Nov 77
Foreword	0 - 18 Nov 77
Blank	0 - 18 Nov 77
Acknowledgements	0 - 18 Nov 77
Safety Approval Disclaimer	0 - 18 Nov 77
Blank	0 - 18 Nov 77
i thru xv	0 - 18 Nov 77
xvi Blank	0 - 18 Nov 77
1-1 thru 1-11	0 - 18 Nov 77
1-12 Blank	0 - 18 Nov 77
2-1 thru 2-12	0 - 18 Nov 77
3-1 thru 3-75	0 - 18 Nov 77
3-76 Blank	0 - 18 Nov 77
4-1 thru 4-17	0 - 18 Nov 77
4-18 Blank	0 - 18 Nov 77
5-1 thru 5-117	0 - 18 Nov 77
5-118 Blank	0 - 18 Nov 77
6-1 thru 6-78	0 - 18 Nov 77
7-1 thru 7-7	0 - 18 Nov 77
7-8 Blank	0 - 18 Nov 77
8-1 thru 8-19	0 - 18 Nov 77
8-20 Blank	0 - 18 Nov 77
A-1 thru A-119	0 - 18 Nov 77
A-120 Blank	0 - 18 Nov 77
B-1 thru B-47	0 - 18 Nov 77
B-48 Blank	0 - 18 Nov 77
C-1 thru C-8	0 - 18 Nov 77

Zero in the Change No. Column indicates an original page.

Change 0,
18 Nov 1977

FOREWORD

The information in this handbook is the result of recent investigation of explosive environment inside containment structures and of structural response to the contained blast. Prediction techniques have been corroborated by some testing and represent the state-of-the-art in containing explosives. The data furnished is not always the most accurate or complete; however, it does meet our immediate requirements. Accordingly, later editions will be improved and updated. A supplement containing complete design examples is being prepared and will be published next year.

Comments for corrections and improvements are invited from individuals or organizations in industry and the U.S. Government.

CONTACT: Mr. Washington T. Char
US Army Engineer Division, Huntsville
PO Box 1600
Huntsville, AL 35807

Phone: 205-895-5410

ACCESSION for	
NTIS	WFO Section <input checked="" type="checkbox"/>
DDC	DDC Section <input type="checkbox"/>
UNCLASSIFIED	<input type="checkbox"/>
J S I D E N	
BY	
DISTRIBUTION/AVAILABILITY CODES	
SPECIAL	
A	

ACKNOWLEDGEMENTS

In any effort of the magnitude of the Suppressive Shielding Study conducted by Edgewood Arsenal during the past four years, the final product is a result of the combined efforts of many people and it is impossible to name every individual. However, the following individuals have had a major role in the preparation of this handbook:

Dr. David J. Katsanis, Chemical Systems
Laboratory (formerly Edgewood Arsenal)
Bruce W. Jezek, Chemical Systems Laboratory
(formerly Edgewood Arsenal)
Washington T. Char, US Army Engineer Division,
Huntsville
Murray F. Burnette, US Army Engineer Division,
Huntsville
Dr. Robert E. Crawford, Civil/Nuclear Systems
Corporation
Dr. Edward H. Bultmann, Civil/Nuclear Systems
Corporation
Laverne E. Romesberg, Civil/Nuclear Systems
Corporation
Dr. Wilford E. Baker, Southwest Research
Institute
F. James Schroeder, AAI Corporation

In addition to the direction of the effort by Edgewood Arsenal and preparation of this handbook by the US Army Corps of Engineers, Huntsville Division, the following organizations have had a major part in developing the technology data on which this handbook is based, and the quality of this handbook is, in large part, a representation of the technical competence of these organizations.

Ballistic Research Laboratory
NASA National Space Technology Laboratory
Dugway Proving Grounds

HNDM-1110-1-2

Naval Surface Weapons Center, White Oak
Picatinny Arsenal
Southwest Research Institute
AAI Corporation

Details of the role played by each organization are in the
Introduction.

SAFETY APPROVAL DISCLAIMER

In order to assure the accuracy and acceptability of the engineering design methods recommended in this handbook, it has been reviewed by the Suppressive Shielding Technical Steering Committee which includes the following individuals:

- Dr. David J. Katsanis, Chairman, Chemical Systems Laboratory
- Dr. Thomas A. Zaker, DOD Explosives Safety Board
- Mr. Walter G. Queen, US Army Materiel Development and Readiness Command
- Mr. Richard Vitali, US Army Ballistics Research Laboratories
- CPT Harvey L. Burnsteel, US Army Armament Command
- Mr. John J. Canavan, Large Caliber Weapon Systems Laboratory
- Mr. Albert T. Dybacki, Office of Project Manager for Munition Production Base Modernization and Expansion

Correct use of this handbook should assure that the resulting Suppressive Shielding Designs will meet the requirements of Command Safety Offices; however, it must be recognized that the Command Safety Offices will always maintain their prerogative of review and approval of plant layouts and barricade designs. Approval will be based upon the application of sound engineering principles where the technologies have been developed or by successful performance of proof tests where technology is undeveloped.

CONTENTS

<u>Chapter</u>		<u>Page</u>
I	INTRODUCTION	1- 1
	1.1 OBJECTIVE	1- 1
	1.2 SCOPE	1- 1
	1.3 BACKGROUND	1- 2
	1.4 ORIGIN AND DEVELOPMENT OF THE SUPPRESSIVE SHIELD CONCEPT	1- 3
	1.5 USE OF THE HANDBOOK	1- 6
	1.6 REFERENCES	1-11
II	SAFETY APPROVED SUPPRESSIVE SHIELDS	2- 1
	2.1 INTRODUCTION	2- 1
	2.2 SELECTION OF A SUPPRESSIVE SHIELD DESIGN	2- 4
	2.2.1 Identify Hazardous Operations	2- 4
	2.2.2 Determine Space Requirements	2- 4
	2.2.3 Determine Charge Parameters	2- 4
	2.2.4 Determine Fragment Parameters	2- 6
	2.2.5 Determine Specific Requirements of the Installation	2- 6
	2.3 APPROVAL OF NEW SUPPRESSIVE SHIELD DESIGNS	2- 7
	2.4 SUPPRESSIVE SHIELD GROUP DESIGNS	2- 8
	2.4.1 Shield Groups 1, 2 and 3	2- 8
	2.4.2 Shield Groups 4 and 5	2- 9
	2.4.3 Shield Group 6	2-10
	2.4.4 Shield Group 81-mm	2-10
	2.5 REFERENCES	2-12
III	EXPLOSIVE ENVIRONMENTS	3- 1
	3.1 INTRODUCTION	3- 1
	3.2 BLAST WAVES IN AIR	3- 1
	3.2.1 General	3- 1
	3.2.2 TNT Equivalence	3- 3
	3.2.3 Scaling	3- 4
	3.2.4 Prediction of Free-Field Airblast Parameters	3- 7

CONTENTS (continued)

<u>Chapter</u>		<u>Page</u>
3.3	INTERNAL AIRBLAST	3-12
	3.3.1 General	3-12
	3.3.2 Prediction of Internal Blast Loads	3-14
3.4	VENTING	3-17
	3.4.1 Introduction	3-17
	3.4.2 Vent Area Ratio	3-17
3.5	QUASI-STATIC PRESSURES	3-18
	3.5.1 General	3-18
	3.5.2 Prediction of Quasi-Static Pressure Parameters	3-18
3.6	AIRBLAST OUTSIDE SUPPRESSIVE SHIELDS	3-22
	3.6.1 General	3-22
	3.6.2 Prediction Methods	3-25
3.7	FRAGMENTATION	3-28
	3.7.1 Introduction	3-28
	3.7.2 Prediction of Primary Fragmentation	3-30
	3.7.3 Prediction of Secondary Fragmentation	3-32
3.8	IMPACT AND PENETRATION	3-35
	3.8.1 Introduction	3-35
	3.8.2 Prediction of Penetration of Steel Plate	3-37
	3.8.3 Prediction of Penetration of Concrete Panels	3-44
3.9	FIREBALL AND THERMAL ENVIRONMENT	3-50
3.10	ILLUSTRATIVE EXAMPLES	3-52
	3.10.1 Shield Group 4 Airblast Loading Parameters	3-52
	3.10.2 Shield Group 4 Effective Vent Area Ratio	3-53
	3.10.3 Shield Group 4 Design Blowdown Time and External Pressure	3-56
	3.10.4 Primary Fragment Mass and Velocity	3-58
	3.10.5 Secondary Fragment Velocity	3-59

CONTENTS (continued)

<u>Chapter</u>		<u>Page</u>
	3.10.6 Fragment Impact on Shield Group 3 Wall Panel	3-60
	3.10.7 Fragment Impact on Shield Group 4 Panel	3-63
	3.11 LIST OF SYMBOLS	3-68
	3.12 REFERENCES	3-71
IV	SUPPRESSIVE SHIELD STRUCTURAL BEHAVIOR	4- 1
	4.1 INTRODUCTION	4- 1
	4.2 PROPERTIES OF STRUCTURAL MATERIALS	4- 1
	4.2.1 Steel	4- 1
	4.2.2 Concrete	4- 5
	4.3 STRUCTURAL DUCTILITY	4- 9
	4.3.1 General	4- 9
	4.3.2 Structural Steel	4-11
	4.3.3 Reinforced Concrete	4-11
	4.3.4 Summary	4-12
	4.4 LIST OF SYMBOLS	4-16
	4.5 REFERENCES	4-17
V	STRUCTURAL DESIGN AND ANALYSIS	5- 1
	5.1 INTRODUCTION	5- 1
	5.2 STRUCTURAL RESISTANCE	5- 3
	5.3 PROPERTIES OF STRUCTURAL ELEMENTS	5- 6
	5.3.1 General	5- 6
	5.3.2 Structural Steel Elements	5- 6
	5.3.3 Reinforced Concrete Elements	5-12
	5.3.4 Cylinders	5-19
	5.3.5 Spheres	5-24
	5.3.6 Natural Frequencies of Common Systems	5-24
	5.4 EQUIVALENT SINGLE DEGREE OF FREEDOM SYSTEMS	5-29
	5.4.1 General	5-29
	5.4.2 Transformation Factors for Beams and Slabs	5-31
	5.4.3 Dynamic Reactions	5-48

CONTENTS (continued)

<u>Chapter</u>		<u>Page</u>
5.5	DYNAMIC RESPONSE OF STRUCTURAL SYSTEMS	5- 50
5.5.1	Introduction	5- 50
5.5.2	Energy Methods	5- 52
5.5.3	Numerical Integration	5- 61
5.5.4	Spherical Chambers	5- 64
5.6	ILLUSTRATIVE EXAMPLES	5- 65
5.6.1	Response of the Group 3 Suppres- sive Shield Wall	5- 65
5.6.2	Numerical Integration Technique for Determining Response of a Steel Beam Subjected to Blast Loading	5- 71
5.6.3	Design of Roof Slab for Group 3 Type Suppressive Shield (Type I Construction Ref. 5-5)	5- 77
5.6.4	Analysis of Shield Group 6A Design	5- 85
5.6.5	Response of Removable Column in 81-mm Suppressive Shield	5- 89
5.6.6	Analysis of Base Plate Ring and Reinforcing Steel in Foundation Slab for Group 3 Suppressive Shield	5- 98
5.6.7	Design of Upper Connection for Removable Column in 81-mm Sup- pressive Shield	5-102
5.6.8	Structural Response of Group 3 Suppressive Shield Ring Beam	5-107
5.7	LIST OF SYMBOLS	5-111
5.8	REFERENCES	5-116
VI	STRUCTURAL DETAILS	6- 1
6.1	INTRODUCTION	6- 1
6.2	UTILITY PENETRATIONS	6- 1
6.2.1	General	6- 1
6.2.2	Design Concept and Rationale	6- 2
6.2.3	Method of Structural Analysis	6- 4
6.2.4	Location of Utility Penetrations	6- 8

CONTENTS (continued)

<u>Chapter</u>		<u>Page</u>
6.3	VACUUM LINE PENETRATION	6- 8
6.3.1	Design Requirements	6- 8
6.3.2	Design Concept and Rationale	6-13
6.3.3	Method of Structural Analysis	6-15
6.3.4	Location of Vacuum Line	6-32
6.4	ENVIRONMENT CONDITIONING PENETRATION	6-33
6.4.1	Design Concept and Rationale	6-33
6.4.2	Design Procedure	6-34
6.5	ACCESS PENETRATIONS	6-37
6.5.1	Requirements	6-37
6.5.2	Safety Considerations	6-39
6.5.3	Personnel Door	6-40
6.5.4	Product Door	6-42
6.6	SHIELD LINERS	6-45
6.6.1	Functional Requirements	6-45
6.6.2	Design Considerations	6-45
6.6.3	Recommended Configurations	6-46
6.7	ILLUSTRATIVE EXAMPLES	6-51
6.7.1	Bending in Box Structure Cover Plate	6-51
6.7.2	Buckling of Utility Box Side Members	6-52
6.7.3	Shear in Shield Group 81-mm Split Collar at the Vacuum Line/Suppressive Shield Interface	6-56
6.7.4	Stress in Group 3 Shield External Disposal Line Shield Caused by Munition Explosion	6-59

CONTENTS (continued)

<u>Chapter</u>		<u>Page</u>
	6.7.5 Stress in Group 3 Shield Disposal Line Shield Caused by an Airborne Dust Explosion	6-62
	6.7.6 Stress in Disposal Line Shield Caused by Dust Sediment Explosion	6-63
	6.7.7 Fragment Hazard From Detonation of Explosive Dust Sediment in Disposal Line	6-65
	6.7.8 Determine the Area of the Environmental Conditioning Exhaust Stack for the Milan 81-mm Suppressive Shield	6-68
	6.7.9 Determination of Exhaust Stack Height	6-68
	6.7.10 Stress in Environmental Conditioning Exhaust Stack	6-70
	6.7.11 Stress in the Shaft of the Rotary Product Door Caused by the Accidental Detonation of Munitions During Production	6-72
	6.8 LIST OF SYMBOLS	6-75
	6.9 REFERENCES	6-78
VII	ECONOMIC ANALYSIS	7- 1
	7.1 THE PROBLEM	7- 1
	7.2 CONSIDERATIONS	7- 1
	7.3 METHOD	7- 4
	7.4 EXAMPLE ECONOMIC ANALYSES	7- 5
	7.5 REFERENCES	7- 7
VIII	ASSURING STRUCTURAL QUALITY	8- 1
	8.1 INTRODUCTION	8- 1
	8.2 STEEL	8- 1
	8.2.1 Structural Steel	8- 1
	8.2.2 Reinforcing Steel	8- 2
	8.3 WELDING	8- 2
	8.3.1 General	8- 2
	8.3.2 Welding Processes	8- 3
	8.3.3 Welding Defects	8- 3

CONTENTS (continued)

<u>Chapter</u>		<u>Page</u>
	8.3.4 Weld Inspection Methods	8-10
	8.3.5 Weld Repairs	8-12
8.4	CONCRETE	8-13
	8.4.1 General	8-13
	8.4.2 Mixing	8-13
	8.4.3 Placing	8-14
	8.4.4 Curing	8-15
	8.4.5 Quality Control	8-16
8.5	FIBER REINFORCED CONCRETE	8-17
8.6	REFERENCES	8-19
 <u>Appendix</u>		
A	SAFETY APPROVED SUPPRESSIVE SHIELDS	A- 1
A.1	INTRODUCTION	A- 1
A.2	SHIELD GROUP 3	A-12
	A.2.1 Description	A-12
	A.2.2 Application	A-26
	A.2.3 Modification	A-27
A.3	SHIELD GROUP 4	A-28
	A.3.1 Description	A-28
	A.3.2 Application	A-44
	A.3.3 Modification	A-45
A.4	SHIELD GROUP 5	A-45
	A.4.1 Description	A-45
	A.4.2 Application	A-68
	A.4.3 Modification	A-70
A.5	SHIELD GROUP 6	A-70
	A.5.1 Description	A-70
	A.5.2 Application	A-84
	A.5.3 Modification	A-85
A.6	SHIELD GROUP 81-mm	A-86
	A.6.1 Description	A-86

CONTENTS (continued)

<u>Appendix</u>		<u>Page</u>
	A.6.2 Application	A-112
	A.6.3 Modification	A-117
	A.7 REFERENCES	A-119
B	RESPONSE CHARTS	B- 1
	B.1 INTRODUCTION	B- 1
	B.2 USE OF CHARTS	B- 2
	B.3 ILLUSTRATIVE EXAMPLES	B- 3
	B.3.1 Response of Group 3 Wall Beam Element to Airblast Loading	B- 3
C	METRIC CONVERSION FACTORS	C- 1

ILLUSTRATIONS

<u>Figure</u>		<u>Page</u>
1- 1	Early Model Suppressive Shield	1- 4
2- 1	General Configuration of Suppressive Shield Groups	2- 3
3- 1	Ideal Blast Wave	3- 3
3- 2	Hopkinson-Cranz Scaling of Airblast Parameters	3- 7
3- 3	Incident Airblast Parameters for Spherical TNT Free Air burst	3- 9
3- 4	Shock Front Velocity as a Function of Peak Overpressure at Sea Level	3-11
3- 5	Schematic Representation of Shock Reflections from Interior Walls of a Suppressive Shield	3-13
3- 6	Reflected Airblast Parameters for Spherical TNT Free Air Burst	3-15
3- 7	Definition of Vent Area Ratios for Various Structural Configurations	3-19
3- 8	Internal Pressure Loading at Inner Surface of a Suppressive Shield	3-20
3- 9	Peak Quasi-Static Pressure	3-21
3-10	Scaled Blowdown Time Versus Scaled Maximum Pressure	3-23
3-11	Stages During the Transmission of a Shock Wave Through a Single Slit in a Plate	3-24
3-12	Calculated Pressures Outside Group 3 Cylindrical Blast Shield with 48-lb Charge	3-26
3-13	Possible Mechanisms for Steel Plate Damage	3-36
3-14	Possible Mechanisms for Concrete Panel Impact Damage	3-37
3-15	Prediction of Fragment Penetration of Steel Plate	3-38
3-16	Perforation Factor Versus Vent Area Ratio for Drilled Hole Patterns	3-42
3-17	Fragment Penetration of 5,000 psi Concrete	3-46
3-18	Limits of Concrete Spalling and Perforation	3-47
3-19	Residual Velocity of Primary Fragment After Perforation	3-49

ILLUSTRATIONS (continued)

<u>Figure</u>		<u>Page</u>
4- 1	Typical Stress-Strain Curves for Various Grades of Steel	4- 3
4- 2	Typical Stress-Strain Curves for Concrete	4- 7
4- 3	Effect of Age on Concrete Compressive Strength f'_c	4- 7
4- 4	Elastic-Plastic Resistance Function	4- 9
5- 1	Idealized Resistance Functions	5- 3
5- 2	Idealized Resistance Function for Uniform Loaded Fixed End Beam	5- 5
5- 3	Plastic Section Moduli for Structural Shapes	5- 8
5- 4	Cylindrical Structural Configuration	5-21
5- 5	Hoop Stress in Thick Wall Cylinder Subjected to Internal Pressure Only	5-23
5- 6	Natural Frequencies of Beam Elements with Concentrated Masses	5-25
5- 7	Fundamental Frequencies of Thin Flat Plates of Uniform Thickness	5-27
5- 8	Natural Frequencies of Beams of Uniform Section and Uniformly Distributed Mass	5-28
5- 9	Equivalent Single Degree of Freedom System	5-30
5-10	Assumed Yield Lines for Two-Way Slabs	5-46
5-11	External Work and Internal Energy for Long Duration Load	5-52
5-12	Impulsive Loading	5-53
5-13	Multiple Triangle Approximation of Loading Function	5-56
5-14	Impulsive Load Plus Long Duration Component	5-57
5-15	Acceleration Versus Time Plots	5-60
6- 1	Typical Utility Penetration	6- 3
6- 2	Transverse and Longitudinal Cross Section Through Group 4 Shield Panel	6-8
6- 3	Typical Location of Utility Penetration in Shield Groups 4, 5 and 81-mm	6-9
6- 4	Typical Location of Utility Penetrations in Shield Group 3	6-10

ILLUSTRATIONS (continued)

<u>Figure</u>		<u>Page</u>
6- 5	Typical Vacuum Line Penetration	6-14
6- 6	Waste Disposal Vacuum Line Entry Into Suppressive Shield	6-16
6- 7	Joint Design for the Shielded Disposal Vacuum Line	6-17
6- 8	Typical Vacuum Line - Suppressive Shield Interface	6-19
6- 9	Maximum Response of Elasto-Plastic One-Degree Systems (Undamped) Due to Constant Force With Finite Rise Time	6-25
6-10	Estimate of Dust Sediment on Bottom of Inner Liner - Shielded Disposal Line Concept	6-27
6-11	Cross Section of Disposal Line with Explosive Dust Sediment	6-29
6-12	Typical Environmental Conditioning Penetration	6-35
6-13	Cubicle with Partial Roof	6-36
6-14	Design Chart for Vent Area Required to Limit Pressures at Any Range Outside a 4-Wall Cubicle	6-38
6-15	Sliding Personnel Door	6-41
6-16	Rotating Product Door	6-43
6-17	Typical Installation of Thin Metal Liners	6-47
6-18	Typical Installation of Thin Plastic Liners	6-49
6-19	Waste Disposal Line Entry Into Suppressive Shield	6-58
8- 1	Cracking of Weld	8- 4
8- 2	Porosity in Weld	8- 7
8- 3	Incomplete Fusion at Sidewall and Incomplete Joint Penetration at Root	8- 8
8- 4	Undercut Weld and Incomplete Penetration at Root	8- 9
A- 1	Group 3 Suppressive Shield	A-13
A- 2	Group 3 Shield Construction Details	A-15
A- 3	Door - Group 3 Shield	A-25
A- 4	Group 4 Suppressive Shield	A-29
A- 5	Group 4 Shield Construction Details	A-31
A- 6	Schematic of Group 4 Shield Frame	A-42

ILLUSTRATIONS (continued)

<u>Figure</u>		<u>Page</u>
A- 7	Group 5 Suppressive Shield	A- 46
A- 8	Center Framework Connection - Group 5 Shield	A- 47
A- 9	Edge Framework - Group 5 Shield	A- 48
A-10	Corner Anchor Plate - Group 5 Shield	A- 49
A-11	Group 5 Shield Construction Details	A- 51
A-12	Group 6A Suppressive Shield	A- 71
A-13	Group 6B Suppressive Shield	A- 72
A-14	Group 6A Shield Schematic	A- 73
A-15	Group 6A Shield Construction Details	A- 75
A-16	Group 6B Shield Schematic	A- 77
A-17	Group 6B Shield Construction Details	A- 79
A-18	Prototype 81-mm Suppressive Shield	A- 87
A-19	Prototype 81-mm Shield Construction Details	A- 89
A-20	Milan 81-mm Suppressive Shield Construction Details	A-101
A-21	Revised Structural Frame Corner Design	A-113
A-22	Milan 81-mm Suppressive Shield Foundation Attachment	A-114
A-23	Milan 81-mm Suppressive Shield Removable Column	A-115
B- 1	Response Chart for $C_1 = 0.60$ and $C_2 = 0.40$	B- 7
B- 2	Response Chart for $C_1 = 0.61$ and $C_2 = 0.39$	B- 8
B- 3	Response Chart for $C_1 = 0.62$ and $C_2 = 0.38$	B- 9
B- 4	Response Chart for $C_1 = 0.63$ and $C_2 = 0.37$	B- 10
B- 5	Response Chart for $C_1 = 0.64$ and $C_2 = 0.36$	B- 11
B- 6	Response Chart for $C_1 = 0.65$ and $C_2 = 0.35$	B- 12
B- 7	Response Chart for $C_1 = 0.66$ and $C_2 = 0.34$	B- 13
B- 8	Response Chart for $C_1 = 0.67$ and $C_2 = 0.33$	B- 14
B- 9	Response Chart for $C_1 = 0.68$ and $C_2 = 0.32$	B- 15
B-10	Response Chart for $C_1 = 0.69$ and $C_2 = 0.31$	B- 16
B-11	Response Chart for $C_1 = 0.70$ and $C_2 = 0.30$	B- 17
B-12	Response Chart for $C_1 = 0.71$ and $C_2 = 0.29$	B- 18
B-13	Response Chart for $C_1 = 0.72$ and $C_2 = 0.28$	B- 19

ILLUSTRATIONS (continued)

<u>Figure</u>		<u>Page</u>
B-14	Response Chart for $C_1 = 0.73$ and $C_2 = 0.27$	B-20
B-15	Response Chart for $C_1 = 0.74$ and $C_2 = 0.26$	B-21
B-16	Response Chart for $C_1 = 0.75$ and $C_2 = 0.25$	B-22
B-17	Response Chart for $C_1 = 0.76$ and $C_2 = 0.24$	B-23
B-18	Response Chart for $C_1 = 0.77$ and $C_2 = 0.23$	B-24
B-19	Response Chart for $C_1 = 0.78$ and $C_2 = 0.22$	B-25
B-20	Response Chart for $C_1 = 0.79$ and $C_2 = 0.21$	B-26
B-21	Response Chart for $C_1 = 0.80$ and $C_2 = 0.20$	B-27
B-22	Response Chart for $C_1 = 0.81$ and $C_2 = 0.19$	B-28
B-23	Response Chart for $C_1 = 0.82$ and $C_2 = 0.18$	B-29
B-24	Response Chart for $C_1 = 0.83$ and $C_2 = 0.17$	B-30
B-25	Response Chart for $C_1 = 0.84$ and $C_2 = 0.16$	B-31
B-26	Response Chart for $C_1 = 0.85$ and $C_2 = 0.15$	B-32
B-27	Response Chart for $C_1 = 0.86$ and $C_2 = 0.14$	B-33
B-28	Response Chart for $C_1 = 0.87$ and $C_2 = 0.13$	B-34
B-29	Response Chart for $C_1 = 0.88$ and $C_2 = 0.12$	B-35
B-30	Response Chart for $C_1 = 0.89$ and $C_2 = 0.11$	B-36
B-31	Response Chart for $C_1 = 0.90$ and $C_2 = 0.10$	B-37
B-32	Response Chart for $C_1 = 0.91$ and $C_2 = 0.09$	B-38
B-33	Response Chart for $C_1 = 0.92$ and $C_2 = 0.08$	B-39
B-34	Response Chart for $C_1 = 0.93$ and $C_2 = 0.07$	B-40
B-35	Response Chart for $C_1 = 0.94$ and $C_2 = 0.06$	B-41
B-36	Response Chart for $C_1 = 0.95$ and $C_2 = 0.05$	B-42
B-37	Response Chart for $C_1 = 0.96$ and $C_2 = 0.04$	B-43
B-38	Response Chart for $C_1 = 0.97$ and $C_2 = 0.03$	B-44
B-39	Response Chart for $C_1 = 0.98$ and $C_2 = 0.02$	B-45
B-40	Response Chart for $C_1 = 0.99$ and $C_2 = 0.01$	B-46
B-41	Response Chart for $C_1 = 1.00$ and $C_2 = 0.00$	B-47

TABLES

<u>Table</u>		<u>Page</u>
1- 1	Hazard Level	1- 7
2- 1	Summary of Suppressive Shield Groups	2- 2
2- 2	Charge Parameters for Safety Approved Shields	2- 5
3- 1	TNT Equivalence Factors for Chemical Explosives	3- 5
3- 2	Mott Scaling Constants for Mild Steel Casings and Various Explosives	3-31
3- 3	Gurney Energy Constants for Various Explosives	3-33
3- 4	Initial Primary Fragment Velocity for Various Cross-Sectional Shapes	3-34
3- 5	Empirical Constants for Predicting Compact Fragment Limit Velocity for Mild Steel Targets	3-40
3- 6	Empirical Constants for Predicting Compact Fragment Residual Velocity for Mild Steel Targets	3-40
4- 1	Dynamic Yield Stresses for Steel	4- 5
4- 2	Dynamic Increase Factors for Concrete	4- 8
4- 3	Recommended Ductility Ratios	4-15
5- 1	Maximum Thickness Ratios for Steel Members	5-10
5- 2	Transformation Factors for Beams and One-Way Slabs	5-33
5- 3	Transformation Factors for Beams and One-Way Slabs	5-34
5- 4	Transformation Factors for Two-Way Slabs Simple Supports, Uniform Load	5-36
5- 5	Transformation Factors for Two-Way Slabs: Fixed Supports - Uniform Load	5-37
5- 6	Transformation Factors for Two-Way Slabs: Short Edges Fixed - Long Edges Simply Supported	5-39
5- 7	Transformation Factors for Two-Way Slabs: Short Sides Simply Supported - Long Sides Fixed	5-41
5- 8	Transformation Factors for Circular Slabs	5-43
6- 1	Pressure and Pressure Increase Rates for Air- borne Dust Explosions	6- 24
6- 2	Summary of Proposed Liners for Suppressive Shields	6- 50

TABLES (continued)

<u>Table</u>		<u>Page</u>
7- 1	Representative Items to Consider in an Economic Analysis	7- 3
A- 1	Suppressive Shield Group 1	A- 2
A- 2	Suppressive Shield Group 2	A- 3
A- 3	Suppressive Shield Group 3	A- 4
A- 4	Suppressive Shield Group 4	A- 5
A- 5	Suppressive Shield Group 5	A- 6
A- 6a	Suppressive Shield Group 6A	A- 7
A- 6b	Suppressive Shield Group 6B	A- 8
A- 7	Suppressive Shield Group 7	A- 9
A- 8a	Prototype 81-mm Shield	A-10
A-8b	Milan 81-mm Suppressive Shield	A-11

CHAPTER 1

INTRODUCTION

1.1 OBJECTIVE

The objective of this handbook is to provide the designer of facilities for handling explosive material with procedures for design of suppressive shields and a basis for deciding whether suppressive shields are cost effective alternatives to other protective systems.

1.2 SCOPE

This handbook presents procedures for design, analysis, quality control and economic analysis of suppressive shields. A suppressive shield is a vented steel enclosure which controls or confines the hazardous blast, fragment, and flame effects of detonations. Such shields must meet the requirements of Ref. 1-1 for protective barricades or operational shields to provide safety in loading munitions as well as munitions modification, renovation, and demilitarization.

Suppressive shields are but one option for providing protective systems. Reference 1-2 presents methods for design and construction of conventional reinforced concrete protective facilities. The information contained herein supplements Ref. 1-2 and provides procedures for evaluation of economic factors concomitant to the use of suppressive shields. Suppressive shields should be used where they provide cost effective alternatives to conventional facilities or provide additional benefits. References 1-3 through 1-7 provide the user of this handbook additional technical and regulatory guidance on explosive safety procedures.

The Department of Defense Explosives Safety Board has approved five basic suppressive shield designs for use in

hazardous operations. This handbook presents the design details of these approved shields with engineering guidance on their selection and modification to meet operational requirements. In addition, techniques are presented for the design of new shields for cases where existing safety approved shields will not meet requirements. Proof test and safety approval procedures are also included.

1.3 BACKGROUND

Suppressive shields are a relatively new concept for providing protection to the area surrounding hazardous operations in munitions plants. At present, the protection methods most commonly used are

- Wide dispersal distances between hazardous operations.
- Reinforced concrete barricades.

The hardwall concrete concept is designed to withstand the anticipated blast effects. Concrete cubicles typically used to protect hazardous operations have one side and/or the top open and the blast is not confined on the open sides. Neither method will contain all the fragments generated by a detonation.

Since a suppressive shield is a complete enclosure, it will

- Contain all fragments from a detonation.
- Attenuate blast overpressure in all directions to a safe level at a prescribed distance.
- Reduce the diameter of the fireball.

Suppressive shields are designed for quick erection and modification and to provide the maximum degree of protection

at minimal cost. Under normal service conditions, the shields are long lived and maintenance free. Other attractive advantages are that suppressive shields can provide improved personnel safety, lend themselves to rapid plant conversion, and can reduce real estate needs and equipment costs by reducing quantity-distance requirements. Through reduction of the structural loads on the building housing the hazardous operation, the use of suppressive shielding will result in a reduced building cost. In addition, suppressive shields will minimize downtime and equipment/facility restoration costs by confining the destructive effects resulting from accidental detonations.

1.4 ORIGIN AND DEVELOPMENT OF THE SUPPRESSIVE SHIELD CONCEPT

Concepts similar to suppressive shields have been used in the past to provide various forms of protection. For example, closed cubicles have often been used to completely confine detonation effects in testing with explosives, and homogeneously vented blast mats have been used in quarries and construction blasting. However, a technology base for systematic, scientific design of homogeneously vented structures was not available prior to the development of suppressive shield technology.

Early investigation of protective measures for the 4.2-inch white phosphorus mortar projectile by Edgewood Arsenal during 1968 resulted in the initial concept for suppressive shields. From these early tests, data were obtained to design several prototype structures.

A small cubical test fixture uniformly vented on five sides was designed to contain fragments and provide controlled venting of product gases from the detonation of a 4.2-inch white phosphorus mortar projectile. Successful testing with this 4-foot cubical led to the decision to apply the concept

to a portable shield for use in explosive ordnance disposal. Edgewood Arsenal, working with the NASA National Space Technology Laboratories, designed, fabricated, and tested the cylindrical shield shown in Fig. 1-1 at Dugway Proving Ground, Utah. The shield is nominally 5 feet in diameter and 5 feet long. It is uniformly vented on the cylindrical surface and at both ends. The shield is constructed with an interior layer of nested angles covered with a double layer of perforated sheet steel. All members are separated sufficiently to allow gas flow through the walls but not far enough to permit fragments to pass between structural members. Structural grade steel is used throughout. Successful tests with a maximum charge weight of 5 pounds of C-4 were considered to verify the concept in general. Additional tests were conducted using up to 20 pounds of C-4. Test data are reported in Refs. 1-8 and 1-9.



Figure 1-1. Early Model Suppressive Shield

These early tests indicated the feasibility of suppressive shielding for hazardous munitions handling operations, and under the direction of the Project Manager for Munitions Production Base Modernization and Expansion, an extensive manufacturing technology project was undertaken by Edgewood Arsenal to design and proof test several prototype structures and to develop a technology base for suppressive shield design. This handbook is one of the results of that effort.

The design procedures and analytical techniques presented herein are the result of extensive testing of both scale model and prototype structures. This work was the cooperative effort of

- Ballistic Research Laboratories, which was tasked with major efforts in the areas of blast and fragment definition, blast and fragment suppression, fireball definition, structural analysis, and shield testing.
- NASA National Space Technology Laboratories and Dugway Proving Ground, which performed testing of suppressive shields fabricated as part of the hardware development program. Extensive instrumentation was used to record blast pressure data and structural response data for verification of predictive analytical techniques.
- Naval Surface Weapons Center (formerly Naval Ordnance Laboratory), which provided blast codes for defining gas pressures inside suppressive shields.

- Southwest Research Institute, which provided contractual support in all analytical development areas and developed scale model laws for defining the blast pressure attenuation outside of suppressive shields.
- Huntsville Division, Corps of Engineers, which identified current design techniques and conducted numerous design investigations in support of the Group 3 and 81-mm suppressive shields, including the preparation of construction specifications and engineering drawings.
- AAI Corporation which provided contractual support to develop shield penetrations for utility lines, vacuum lines, and environmental conditioning ducts.

1.5 USE OF THE HANDBOOK

The designer of a facility for munitions loading, maintenance, modification, renovation, or demilitarization must perform a hazards analysis of each operation and determine which operations involve potentially catastrophic Category III or IV hazards; see Table 1-1. The facility design must provide adequate safety for these hazardous operations. It may be that conventional protective barricades with appropriate separation distances or suppressive shields can be used, or that the operation can be isolated by separating it from other parts of the facility using quantity-distance specifications in Ref. 1-1. All safety considerations being equal, the decision as to which method will be used is based on economic factors. An economic analysis of alternative methods of protection must be performed considering facility, real estate, and equipment costs as well

Table 1-1
HAZARD LEVEL (Ref. 1-3)

Category	Hazard Level	Comment
I	Negligible	Will not result in personnel injury or system damage
II	Marginal	Can be counteracted or controlled without injury to personnel or major system damage
III	Critical	Will cause personnel injury or major system damage, or will require immediate corrective action for personnel or system survival
IV	Catastrophic	Will cause death or severe injury to personnel or system loss

as maintenance, operation, useful life, replacement, and renovation or modification costs insofar as they can be estimated.

In order to evaluate these economic factors, the designer must develop facility concepts using alternative methods of protection. He will use Ref. 1-1 for quantity-distance considerations, Ref. 1-2 for conventional reinforced concrete cubicles, and this handbook for suppressive shields. Costs will be estimated and compared over the facility life to determine the most economical mode of protection.

A major factor which must be considered in deciding which form of protection to use is the requirement for approval of the facility design by Department of Defense safety offices. If the designer can adapt one of the safety approved suppressive shields, either directly or by modification, and support the adaptation with proven, accepted analytical techniques, he can reasonably expect that the safety offices will approve his design. The designer should, therefore, begin development of a facility concept which employs suppressive shields using the safety approved shields which are described in more detail in Chapter 2 and Appendix A of this handbook.

Safety approved suppressive shields should meet most requirements by using the shield as designed or with slight modification of the shield dimensions. Facility safety approval will not be jeopardized by a modified shield if charge weight to volume ratio is maintained, the scaled distance to the shield wall is not reduced, and the shield maximum rated charge weight is not exceeded. When a modified safety approved shield design is proposed, it would be prudent to submit the modified design for approval prior to committing the entire facility concept to the modified shield application.

In submissions of proposed new shield designs or significant modifications to previously approved designs, documentation should summarize test results and analytical procedures which demonstrate the claimed level of protection to operators

or to the general public. The documentation should also show, if appropriate, that this level at least equals the protection provided by existing explosives safety standards applicable in the absence of such engineered safeguards as suppressive shields or any other type of explosion-resistant construction.

In exceptional situations where no safety approved shield can be made to fit a desired application, a new shield must be designed. The procedures for obtaining safety approval of a new shield design are described in Chapter 2. Chapters 3, 4, 5, and 6 provide the guidance needed to design a new shield. Hazardous environments resulting from internal and external airblast, fragmentation and fireball phenomena are presented in Chapter 3. Information contained in that chapter is used to determine venting requirements, airblast loads on the structure, and protection required to defeat fragments.

Structural behavior is addressed in Chapter 4. Typical construction material physical properties, ranges of structural response, structural failure modes, and acceptable damage levels are discussed. Information presented in Chapter 4 is a guide to the physical properties of the materials to be used in the structural analysis of suppressive shield designs. This chapter also includes guidance for determination of acceptable deformation limits.

A suppressive shield is usually designed with the maximum allowable venting which will meet blast overpressure suppression requirements. Then, using the structural design and analysis methods of Chapter 5, the structure is designed to have sufficient strength to withstand the pressure and fragmentation loads. Each suppressive shield installation will have specific requirements for utility penetrations, doors for personnel, equipment and products, and so on. Guidance on the provision of acceptable structural details such as these is presented in Chapter 6. Information on structural details which have been successfully proof tested is also contained in Chapter 6.

Once a shield design which meets blast, fragment, and flame suppression requirements has been achieved, its cost can be estimated and the data used in an economic analysis to determine the cost effectiveness of the design. The economic analysis of alternative facility concepts is a complex process which is unique to each facility. A completely general procedure suitable to analysis of all facilities would be so complicated that it would be useless. However, this handbook would be incomplete if the vital element of economics were ignored. Economic analysis of protective systems is discussed in Chapter 7, and two examples of economic analyses of facilities where suppressive shields were considered are presented as Refs. 7-5 and 7-6. One example is a melt-pour operation for 105-mm projectiles. The other is for a load, assembly, pack (LAP) operation with improved conventional munitions (ICM). These two examples illustrate the many factors that must be considered, show the magnitude of detail required, and can be used as a guide for other analyses.

It was demonstrated during the testing of suppressive shields that the strength of welds and concrete components is often the determining factor in the overall strength of a shield. Therefore, suppressive shield design packages must include specifications for assurance of the quality of concrete and the strength of welds, as well as basic design and material specifications. Guidance on quality assurance is contained in Chapter 8.

1.6 REFERENCES

- 1-1 Safety Manual, AMCR 385-100, Hq. U.S. Army Materiel Command, Alexandria, Va., Latest Edition. (U)
- 1-2 Structures to Resist the Effects of Accidental Explosions, TM5-1300, Department of the Army Technical Manual, NAVFAC P-397, Department of the Navy Publication, AFM 88-22, Department of the Air Force Manual, Washington, D.C., June 1969. (U)
- 1-3 System Safety Program for Systems and Associated Subsystems and Equipment Requirements for, Mil Std 882, U.S. Government Printing Office, Washington, D.C., 15 July 1969. (U)
- 1-4 Ammunition and Explosives Ashore, Department of the Navy Publication, OP-5, including Volume I, NAVSEA OP-5/1 "Safety Regulations for Handling, Storing, Renovation and Shipping", Volume II, NAVORD OP-5/2, "Storage Data", Volume III, NAVSEA OP-5/3, "Advance Bases", and all revisions thereto. (U)
- 1-5 Explosive Safety Manual, AFM 127-100, Department of the Air Force, Washington, D.C., 2 December 1971. (U)
- 1-6 Ammunition and Explosives Safety Standards, DOD 5154.4S, Department of Defense, Office of the Assistant Secretary of Defense (Installations and Logistics), March 1976. (U)
- 1-7 Shields, Operational for Ammunition Operations, Criteria for Design of, and Tests for Acceptance, Mil Std 398, U.S. Government Printing Office, Washington, D.C., 5 November 1976. (U)
- 1-8 Tanner, W.S. and Warnicke, C.H., Support Test for the Fabrication and Test of a Suppressive Shield for a Naval Ordnance Disposal Facility, DPG-DR-74-304, US Army Dugway Proving Ground, Dugway, Utah, December 1973. (U)
- 1-9 Warnicke, C.H., Added Support Tests of the Suppressive Shield for Naval Ordnance Disposal Facility, DPG-DRI-74-313, US Army Dugway Proving Ground, Dugway, Utah, September 1974. (U)

CHAPTER II

SAFETY APPROVED SUPPRESSIVE SHIELDS

2.1 INTRODUCTION

There are eight suppressive shield design groups that have been developed to various stages of definition. These shield groups are summarized in Table 2-1 and illustrated schematically in Fig. 2-1. Some of the shield group designs have been safety approved by the Department of Defense Explosives Safety Board; others are still in the criteria development and preliminary design stage. Two of the groups, Shield Group 6 and Shield Group 81-mm, have two versions (or adaptations), both of which have been safety approved. More detailed information on each of the eight shield group designs is presented in Tables A-1 through A-8 in Appendix A.

The five suppressive shield group designs approved by the Department of Defense Explosives Safety Board (Groups 3, 4, 5, 6 and 81-mm) have been designed to meet requirements for most applications to ammunition load, assembly, pack (LAP) in the Munitions Production Base Modernization and Expansion Program. However, specific shield requirements will vary with other applications and, even with LAP applications, design details will vary from plant to plant and between munitions or different operations on the line. It will, therefore, frequently be necessary to modify the approved shields to adapt them to the operation under consideration.

This chapter describes the safety approved shield group designs and provides guidance concerning acceptable modifications and recommended procedures for securing safety approval of new shield designs. Summary information on overall dimensions of the shield structure, charge capacity, rated overpressure, fragment stopping wall thickness, and type of construction of the five approved basic shield groups is included in Appendix A, Tables A-3 through A-6 and Table A-8.

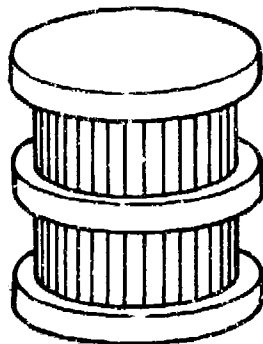
Table 2-1
SUMMARY OF SUPPRESSIVE SHIELD GROUPS

Shield Group	Hazard Parameter		Representative Applications	Level of Protection*
	Blast	Fragmentation		
1	High	Severe	Porcupine Melter (2000 lbs) plus 2 pour units 250 lbs each	Reduce blast pressure at intraline distance** by 50%
2	High	Severe	HE bulk (750 lbs) Minute Melter	Reduce blast pressure at intraline distance** by 50%
3	High	Moderate	HE bulk (37 lbs) Detonators, fuses	Category I hazard*** at 6.2 feet from shield
4	Medium	Severe	HE bulk (9 lbs) Processing rounds	Category I hazard*** at 19 feet from shield
5	Low	Light	30 lbs Illuminant Igniter slurry mixing HE processing (1.84 lbs)	Category I hazard*** at 3.7 feet from shield
6	Very High	Light	Laboratory, handling, and transportation	Category I hazard*** at 1 foot from shield
7	Medium	Moderate	Flame/fireball attenuation	Category I hazard*** at 5 feet from shield
81 mm	High	Moderate	81 mm mortar drill-and-face and/or cast-finishing operation	Category I hazard*** at 3 feet from shield

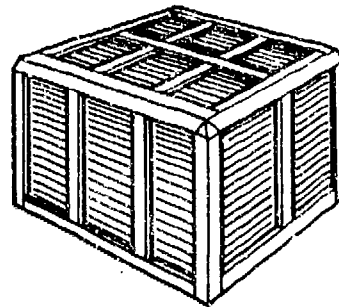
* All shield groups contain all fragments.

** Unbarricaded intraline distance as defined by Table 17-12, Ref. 2-1

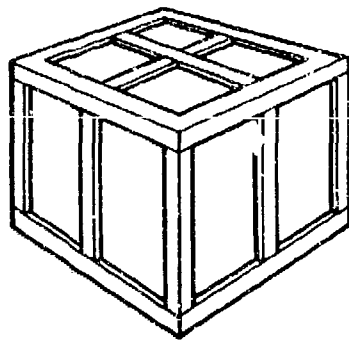
*** Category I hazard (2.3 psi level) as defined by Ref. 2-3



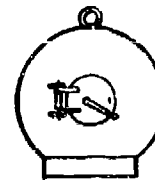
a. Suppressive Shield
Groups 1, 2 and 3



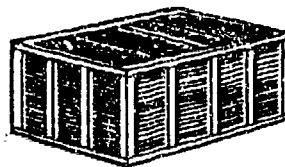
b. Suppressive Shield
Group 4



c. Suppressive Shield
Group 5



d. Suppressive Shield
Group 6



e. Suppressive Shield
Group 81-mm

Figure 2-1. General Configuration of Suppressive Shield Groups

Copies of the fabrication drawings for each approved shield design are included in Appendix A. Authorized agencies may attain full-size copies of the drawings from the Division Engineer, US Army Engineer Division, Huntsville, HNDED-CS, P. O. Box 1600, West Station, Huntsville, Alabama 35807.

2.2 SELECTION OF A SUPPRESSIVE SHIELD DESIGN

The procedure to follow in selecting an approved shield design for a particular application is outlined below. The same procedure would be followed for modification of an approved design or establishing the requirement for a new design.

2.2.1 Identify Hazardous Operations

The designer initially develops a facility concept, decides on the operations to be performed, and selects the equipment to be used. A hazard analysis is then performed to determine where protection from hazardous operations is required.

2.2.2 Determine Space Requirements

This step requires consideration of the size and shape of equipment and work space required inside the shield to estimate the approximate size and shape of the shield required. Space available for the operation on the line or in the building will also place limitations on overall shield base dimensions and height.

2.2.3 Determine Charge Parameters

Charge parameters which govern shield requirements are: charge weight (W), shape, confinement and composition; ratio of charge weight to shield internal volume (W/V); and scaled distance (Z) from the charge to nearest wall or roof of the shield ($Z = R/W^{1/3}$, where R is the distance from the center of the charge to the nearest wall or roof in feet and W is in pounds). Parameters for approved shield groups are summarized in Table 2-2. These charge parameters are used to determine

the overpressure, impulse, and quasi-static overpressure loads on the suppressive structure. Calculations are typically made in terms of TNT equivalency. Determination of TNT equivalency is discussed in Chapter 3. A tabulation of conversion factors (Table 3-1) is presented there with guidance on how pressure and impulse for other types explosive are obtained.

Table 2-2

CHARGE PARAMETERS FOR SAFETY APPROVED SHIELDS

Shield Group	Min Z (ft/lb ^{1/3})		Max W/V (lb/ft ³)
	Wall	Roof	
3	1.63	1.45	0.04157
4	2.23	2.19	0.00762
5	4.14	6.79	0.00215
6A	1.01*	N/A	0.2297*
6B	1.22*	N/A	0.132*
Prototype 81 mm	3.62	3.21	0.0034
Milan 81 mm	4.23	3.75	0.0028

* Based on single equivalent charge

The shield selected for a given application must be approved for a design charge weight which equals or exceeds that of the application of interest. The internal dimensions of the shield must be such that the design charge-to-volume ratio (W/V) of the approved shield is not exceeded in the application. In addition, location of the charge must be such that the scaled distance Z in the application of interest is greater than or equal to the Z for the approved shield.

It may be possible in some cases to modify specific dimensions of a safety approved shield to accommodate a particular application. For example, it would be possible to increase the volume of a given shield design by increasing its length, which would reduce the W/V ratio (for the same charge weight) without altering the scaled distance Z to the nearest shield wall. A modification that would not be permitted without supporting engineering analyses to verify adequacy of shield strength would be to move the charge closer to a shield wall. This would decrease the scaled distance Z, even though the W/V ratio (for the same charge weight) might be greatly reduced by an increased length or height of the shield. Guidance concerning acceptable modifications to all safety approved shield groups is given in Appendix A.

2.2.4 Determine Fragment Parameters

Both primary and secondary fragment hazards and suppression must be considered. Classified Ref. 2-2 should be consulted to determine primary fragment hazards for standard ammunition. If this reference is not available, methods presented in Chapter 3 are used to determine primary fragment threats. Chapter 3 also describes methods for analysis of surrounding equipment to estimate secondary fragment hazards. Fragment hazards, interpreted in terms of a fragment perforation thickness from Chapter 3, are compared with the nominal wall thickness for the shield design being considered. Where a fragment perforation thickness exceeds the nominal wall thickness of the approved shield, the approved suppressive shield under consideration is inadequate and must be discarded for another shield with a larger nominal wall thickness.

2.2.5 Determine Specific Requirements of the Installation

After an approved suppressive shield has been selected and/or modified to meet space, explosive charge, and fragment conditions, the specific details of the installation

such as environmental conditioning; product, access and conveyor doors; utility penetrations; and liners must be incorporated into the design. Recommended practices for the preparation of these design details in a manner that will not compromise safety of the installed shield are presented in Chapter 6.

2.3 APPROVAL OF NEW SUPPRESSIVE SHIELD DESIGNS

In some instances, none of the safety approved shield designs will be satisfactory for a particular application, even with permissible modifications to the design such as discussed above. In such cases, a suitable shield must be designed for the prescribed conditions utilizing the procedures and guidance contained in Chapters 3, 4, 5 and 6 of this handbook.

Any new design, or radical modification of an approved design, will require formal safety approval before the concept can be utilized in an operational installation. Obtaining safety approval for a suppressive shield design concept requires demonstrating conclusively that the design will accomplish its intended function. It may be possible in some cases to demonstrate the adequacy of a design analytically with the use of proven, accepted structural dynamic analysis procedures. If the adequacy cannot be proven analytically, proof-testing will be required. In such cases, the design concept is tested at 125 percent its rated design charge, i.e., a concept designed for 100 pounds of explosive would be tested with an actual charge of 125 pounds. Detailed requirements for planning, conducting and reporting the proof tests are presented in Ref. 2-3.

Safety approval is obtained by forwarding a Safety Approval Package through the safety chain of command. See Ref. 2-4 for samples of Safety Approval Documentation. Within the Department of the Army, this will require an approval by the Development and Readiness Command Safety Office and the Department of Defense Explosive Safety Board in addition to the internal reviews required by each subordinate command. The Safety Approval

Package describes the design concept; the analysis procedures and/or test operations employed to validate the concept; presents the analysis and/or test results; and evaluates and interprets the analysis/test results with respect to adequacy of the design concept. The documentation should also show, if appropriate, that this level at least equals the protection provided by existing explosives safety standards applicable in the absence of such engineered safeguards as suppressive shields or any other type of explosion-resistant construction.

2.4 SUPPRESSIVE SHIELD GROUP DESIGNS

Currently available safety approved shield designs range from units having about 4.2 cubic feet of interior volume weighing 165 pounds to assemblies with approximately 944 cubic feet of usable interior space weighing 45 tons. Preliminary design concepts are also complete for additional suppressive shield designs weighing up to 2880 tons with volumes to about 63,100 cubic feet and the capability for suppressing the hazardous effects from an accidental detonation of 2870 pounds of TNT. In general, as the size and weight of a suppressive shield increase, the charge weight that the shield is designed to suppress also increases. Appendix A contains design data for each shield group.

2.4.1 Shield Groups 1, 2 and 3

Shield Groups 1, 2 and 3 are scaled geometrically relative to each other. The Group 3 design has been safety approved. The Group 1 and 2 designs have not been safety approved and testing may be required for approval. The Group 1 shield is a very large structure measuring 45 ft in diameter and 52 ft in height externally. The blast environment is rated as high and the fragment hazard severe; see Table 2-1. The performance goals are to reduce blast pressure by 50 percent at the intra-line distance as defined in Table 17-12 in Ref. 2-1 and to contain 100 percent of the fragments generated. The unbarricaded

intraline distance can be approximated by $R = 18W^{1/3}$. The Group 1 shield can be applied at installations similar to a porcupine melt pour facility for which the concept has been developed.

The Group 2 shield design concept measures 34.3 ft in diameter and stands 33 ft tall externally. The blast environment is rated as high and the fragmentation hazard severe. Performance goals set for this group are to reduce the blast pressure by 50 percent at the intraline distance and to contain all fragments. The Group 2 shield would be appropriate for applications such as a minute melter (861 lb TNT equivalent).

The Group 3 shield, which was originally designed as a 1/4-scale Group 1 shield, stands 12.8 ft tall and measures 13.3 ft in diameter. Both dimensions are measured externally. The blast environment is again high, since all three groups (1, 2 and 3) are rated for the same internal blast pressure. However, the fragment hazard for the Group 3 shield is rated as moderate. The shield design has been tested and found to reduce the external pressure to 2.3 psi at a distance of 6.2 ft from the exterior of the shield. All fragments were contained by the shield. Also, the fireball was restricted to within four feet of the exterior wall. A typical application for the Group 3 shield would be for the high explosive incendiary (HEI) press operation in loading 20/30 mm HEI projectiles.

2.4.2 Shield Groups 4 and 5

Shield Groups 4 and 5 are depicted in Fig. 2-1 as rectangular parallelepipeds. The sizes of the two shields are similar, but the application and construction are different; both designs have been safety approved. The Group 4 shield measures 16.4 ft long by 11.5 ft wide by 10.4 ft high externally. The internal blast environment is rated as medium with a severe fragment hazard. Proof tests have shown that the external blast pressure is reduced to 2.3 psi at 19 feet from the external surface, all fragments are contained, and the fireball is restricted

to within 10 ft of the exterior of the shield. A 105-mm high explosive projectile fuze-insert-and-torque operation would be a typical application for this shield group.

The Group 5 shield overall external dimensions are 12.6 ft square in plan and 9.2 ft high. The shield design blast environment is rated as low, and the fragment hazards associated with typical applications are light. Tests to verify the design adequacy indicate that external blast pressures are reduced to 2.3 psi at 3.7 ft from the exterior of the shield; the fireball extends two feet outside the shield; and all fragments are contained. The primary application for the Group 5 shield is operations involving propellants and pyrotechnics, i.e., an igniter slurry mixing operation.

2.4.3 Shield Group 6

The two similar designs of Shield Group 6 are both rated for very high blast loads and light fragment hazards. Both shield groups are spherical and measure nominally 24.5 inches in diameter externally. Both shields have been tested and safety approved. External pressures were reduced to less than 2.3 psi at a distance of 2 ft. All fragments were contained. Typical applications of these shield designs would be to safely transport or store small quantities of explosive, such as in a detonator loading facility or laboratory.

2.4.4 Shield Group 81-mm

The 81-mm shield group also has two approved designs. Both designs are rated for a high blast environment and a fragment hazard that is moderate. The original design, now referred to as the Prototype, measures 20 ft long x 15.4 ft wide x 13.1 ft high externally. Tests have demonstrated that blast pressures are reduced to 2.3 psi peak external pressure at three feet from any exterior shield wall; all fragments are contained within the shield; and the fireball is contained within the shield.

The adaptation of the Prototype 81-mm Shield design has been named Milan 81-mm and can be used in applications which do not require as much floor area as the Prototype 81-mm Shield and which involve smaller charge weights. The Milan 81-mm design measures 15.4 ft on a side and is 13.1 ft tall externally and was designed specifically for the 81-mm mortar projectile application to the fuze cavity facing operation on line "C" at Milan AAP. Predicted blast pressures are reduced to 2.3 psi at 7.3 ft from the external surfaces and no fragments perforate the shield walls.

Additional details on the safety approved suppressive shield designs are presented in Appendix A.

2.5 REFERENCES

- 2-1 Safety Manual, AMCR 385-100, U.S. Army Materiel Command, Alexandria, Va., Latest Edition. (U)
- 2-2 Joint Munitions Effectiveness Manual, FM101-62-3, Manual of Fragmentation Data, 15 September 1973.
(C-XGDS-3)
- 2-3 Shields, Operational for Ammunition Operations, Criteria for Design of, and Tests for Acceptance, Mil Std 398, US Government Printing Office, Washington, D.C., 5 November 1976. (U)
- 2-4 Katsanis, D.J., Safety Approval of Suppressive Shields, EM-TR-76088, Edgewood Arsenal, Aberdeen Proving Ground, Md., August 1976. (U)

CHAPTER III

EXPLOSIVE ENVIRONMENTS

3.1 INTRODUCTION

General airblast phenomenology is presented in this chapter along with a discussion of TNT equivalency, blast scaling, the process of venting through the perforated walls of suppressive structures, and external airblast properties. Prediction methods are presented which allow a designer to estimate internal blast loads on suppressive shields or other types of containment structures. Methods are given for predicting both the initial reflected shock loading and the later relatively long term gas venting overpressure which can significantly load structures with small or no venting.

Prediction of fragment effects is divided into definition of fragment threat and to penetration of fragments. Both primary and secondary fragments are considered. A general discussion of fireball and thermal effects including attenuation by suppressive structures is given next. No prediction methods for thermal effects have been included because of insufficient data.

3.2 BLAST WAVES IN AIR

3.2.1 General

Blast wave formation and transmission through air have been studied extensively over the last 60 years, so the general characteristics of these waves are relatively well known and documented (see, e.g., Ref. 3-1). Airblast waves of interest in suppressive shielding are typically the result of an explosion. The word explosion as used in this handbook implies a process by which a pressure wave of finite amplitude is generated in air by a rapid release of energy. The energy source

will be, almost without exception, a compact quantity of chemical materials insofar as this handbook is concerned. Regardless of the source of the initial finite pressure disturbance, the properties of air as a compressible gas will cause the front of this disturbance to steepen as it passes through the air until it exhibits nearly discontinuous increases in pressure, density, and temperature. The resulting shock front moves supersonically. The air particles are also accelerated by the passage of the shock front, producing a net particle velocity in the direction of travel of the front.

If it is assumed that an explosion occurs in a still, homogeneous atmosphere and that the source is spherically symmetric, the characteristics of the blast wave are functions only of the properties of the explosive, the distance R from the center of the source and the time t . Let it be assumed that an ideal pressure transducer, which offers no resistance to flow behind the shock front and follows perfectly all variations in pressure, is used to record the time history of incident overpressure at some given fixed distance R from the explosion. The record that such a gage would produce is shown in Fig. 3-1. When the shock front arrives at arrival time t_a , the pressure rises quite abruptly to a peak value P_{so} . The pressure then decays to ambient in a time t_o , drops to a partial vacuum of amplitude P_{so}^- , and eventually returns to ambient in total time $t_a + t_o + t_o^-$. The quantity P_{so} is termed the peak side-on overpressure, as opposed to reflected overpressure.

The portion of the time-history curve above ambient pressure is called the positive phase. That portion of the time-history below ambient pressure is called the negative phase. The areas under these curves define the airblast wave incident positive and negative impulse, respectively. The negative phase of the blast wave is not important in the design and analysis of suppressive shields and will not be treated in this handbook.

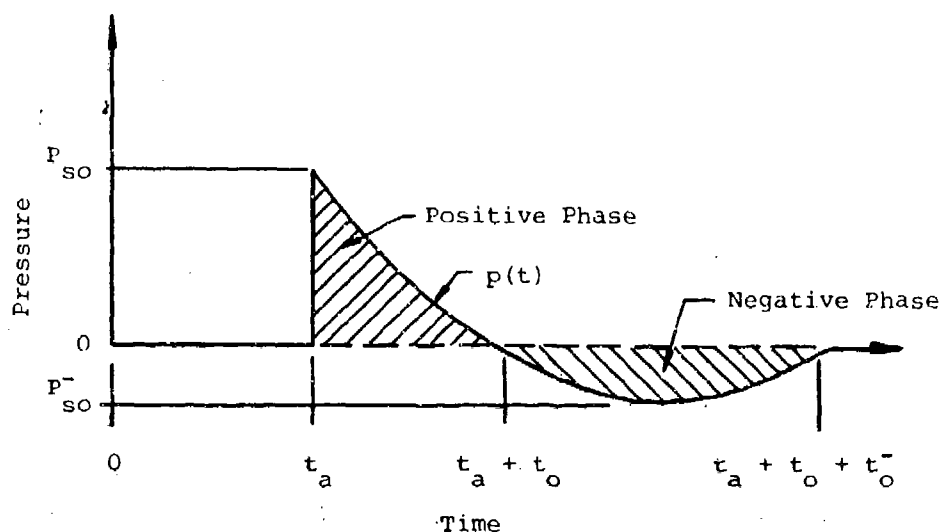


Figure 3-1. Ideal Blast Wave

The airblast wave depicted in Fig. 3-1 is a free-field phenomenon, i.e., the blast wave as it would appear over an ideal surface and under ideal conditions. Upon encountering any solid or dense object, the free-field blast waves are seriously modified as they reflect from and diffract around the object. These processes are of more interest in the external airblast loading of structures than in suppressive shielding and are covered in some detail in Refs. 3-2 and 3-3. Reflected airblast, which is of primary interest in suppressive shielding, will be covered in a later paragraph on internal airblast.

3.2.2 TNT Equivalence

The standard explosive for determination of blast effects in this handbook will be TNT. Other chemical explosives generate airblast waves which differ somewhat in their characteristics from TNT. The general wave characteristics are quite similar, but detailed properties such as peak pressure and impulse are measurably different for identical charge weights. Conversion of other types of explosive to their TNT equivalent, e_t , can be accomplished on the basis of charge weight, i.e.,

$$W_{\text{TNT}} = e_t \times W \quad (3-1)$$

where

W_{TNT} = equivalent charge weight of TNT, lb

e_t = factor from Table 3-1

W = explosive of interest charge weight, lb

The TNT equivalence factors listed in Table 3-1 have been developed by ratio of relative heats of explosion (Refs. 3-1 and 3-4). These factors are best average values and are recommended for suppressive shields only. They take into consideration the need for data on quasi-static pressure as well as blast impulse and related overpressures. For close-in explosions ($Z < 3.0 \text{ ft/lb}^{1/3}$) and for shapes of explosives other than spheres, the TNT equivalence factors can be much greater than those obtained from relative heats of explosion. Much work has been done on determination of TNT equivalency for specific compositions, distances, and shapes. References 3-5 through 3-14 are typical examples of these types of data.

Determination of airblast effects for use with the methods presented in this handbook, then, will be on the basis of an equivalent charge weight of TNT established in accordance with Eq. 3-1.

3.2.3 Scaling

A number of blast scaling laws have been proposed, (see, e.g., Ref. 3-1), but by far the most widely accepted are the Hopkinson-Cranz and Sachs laws. These two laws have been very well verified by experiment. The Hopkinson-Cranz law was formulated independently by B. Hopkinson in England and by C. Cranx in Germany during World War I. It allows prediction of blast wave properties from small scale experiments for any other scale, over all corresponding scaled distances, provided the type of explosive source, the geometry of the source and the

Table 3-1

TNT EQUIVALENCE FACTORS FOR
CHEMICAL EXPLOSIVES

Explosive	e_t (TNT Equivalent)
Amatol 60/40 (60% ammonium nitrate, 40% TNT)	0.586
Baronal (50% barium nitrate, 35% TNT, 15% aluminum)	1.051
Comp B (60% RDX, 40% TNT)	1.148
C-4 (91% RDX, 9% plasticizer)	1.078
Explosive D (ammonium picrate)	0.740
H-6 (45% RDX, 30% TNT, 20% Al, 5% D-2 wax)	0.854
HBX-1 (40% RDX, 38% TNT, 17% Al, 5% D-2 wax)	0.851
HMX	1.256
Lead Azide	0.340
Lead Styphnate	0.423
Mercury Fulminate	0.395
Nitroglycerine (liquid)	1.481
Nitroguanidine	0.668
Octol, 70/30 (70% HMX, 30% TNT)	0.994
PETN	1.282
Pentolite, 50/50 (50% PETN, 50% TNT)	1.129
Picric Acid	0.926
RDX (Cyclonite)	1.185
Silver Azide	0.419
Tetryl	1.00
TNT	1.00
Torpex (42% RDX, 40% TNT, 18% Al)	1.667
Tritonal (80% TNT, 20% Al)	1.639

(Pefs. 3-1 and 3-4)

experiment are identical. Sachs scaling, formulated by R. G. Sachs during World War II, allows prediction of the effects of detonations in different atmospheric conditions. It is unlikely that suppressive shields will be located at high enough altitudes for ambient atmospheric conditions to be significantly different from conditions at sea level; therefore, Sachs scaling is not included in this handbook.

The Hopkinson-Cranz law states that self-similar blast (shock) waves are produced at identical scaled distances when two explosive charges of similar geometry and the same explosive composition, but of different size, are detonated in the same atmosphere. The customary scaled distance Z is defined as

$$Z = R/W^{1/3} \quad (3-2)$$

where

R = distance from the center of the explosive source
to the point of interest, ft

W = explosive charge weight, lb

Scaling of airblast parameters is illustrated in Fig. 3-2. An observer located a distance R from the center of an explosive source of characteristic dimension d will be subjected to a blast wave with an amplitude (peak overpressure) P_{so} , a duration t_o , and a characteristic pressure-time history $p(t)$. The positive impulse i in the blast wave is defined as the area under the positive phase of the airblast pressure-time history curve. The Hopkinson-Cranz scaling law states that an observer stationed a distance λR from the center of a similar explosive source of characteristic dimension λd detonated in the same atmosphere will feel a blast wave of a similar form, the same amplitude P_{so} , but a duration λt_o and impulse λi . All characteristic times, such as arrival time t_a , are scaled by the same factor as the length scale factor λ . In Hopkinson-Cranz scaling, pressures and velocities are the same at scaled distances at scaled times.

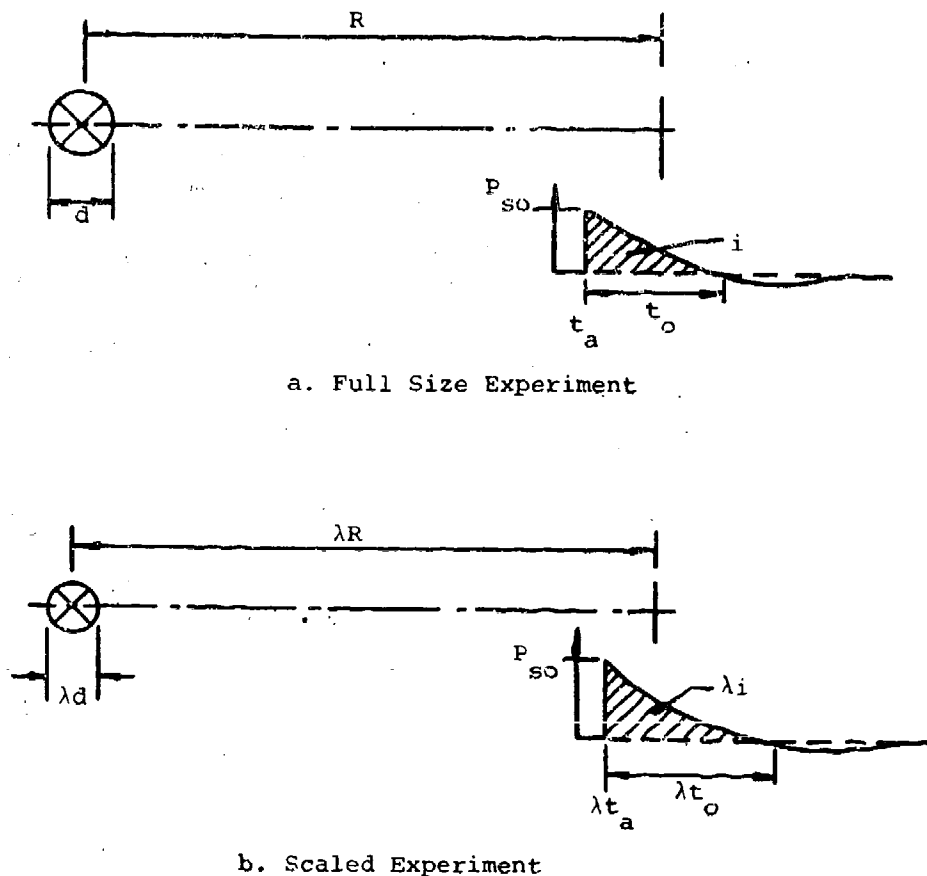


Figure 3-2. Hopkinson-Cranz Scaling of Airblast Parameters

The Hopkinson-Cranz scaling law has become so universally used that chemical explosive blast data are almost always presented in terms of Hopkinson-Cranz scaled parameters. That is, pressures, times and impulses, both incident and reflected, can be conveniently presented as unique functions of the scaled distance Z .

3.2.4 Prediction of Free-Field Airblast Parameters

There are a number of data sources for scaled blast parameters. References 3-1 and 3-4 give shock front properties for incident and normally reflected waves, as well as scaled times and impulses, for spherical Pentolite charges detonated

in free air (far from any reflecting surface). Data are given in Ref. 3-15 for incident waves from surface bursts of TNT which are generally accepted as the standard curves for this reflection situation. References 3-2, 3-16 and 3-17 contain compilations for both free-air and surface bursts of TNT.

If properly used, all of these references will give predictions of blast wave properties which are reasonably close to each other (with the possible exception of durations, t_0), although not all cover identical ranges of scaled distance. Free-field, or incident, blast wave properties which are important in the loading of suppressive shields are presented in Fig. 3-3. These parameters include P_{so} , i_s , t_a and t_0 . Reflected airblast parameters are presented in a later paragraph on internal blast in this handbook. All parameters are scaled according to the Hopkinson-Cranz law, using in-lb-sec units, and data are presented for spherical TNT charges in free air. Standard sea level atmospheric conditions are assumed (ambient pressure $P_0 = 14.696$ psi and sound speed $a_0 = 1117$ ft/sec).

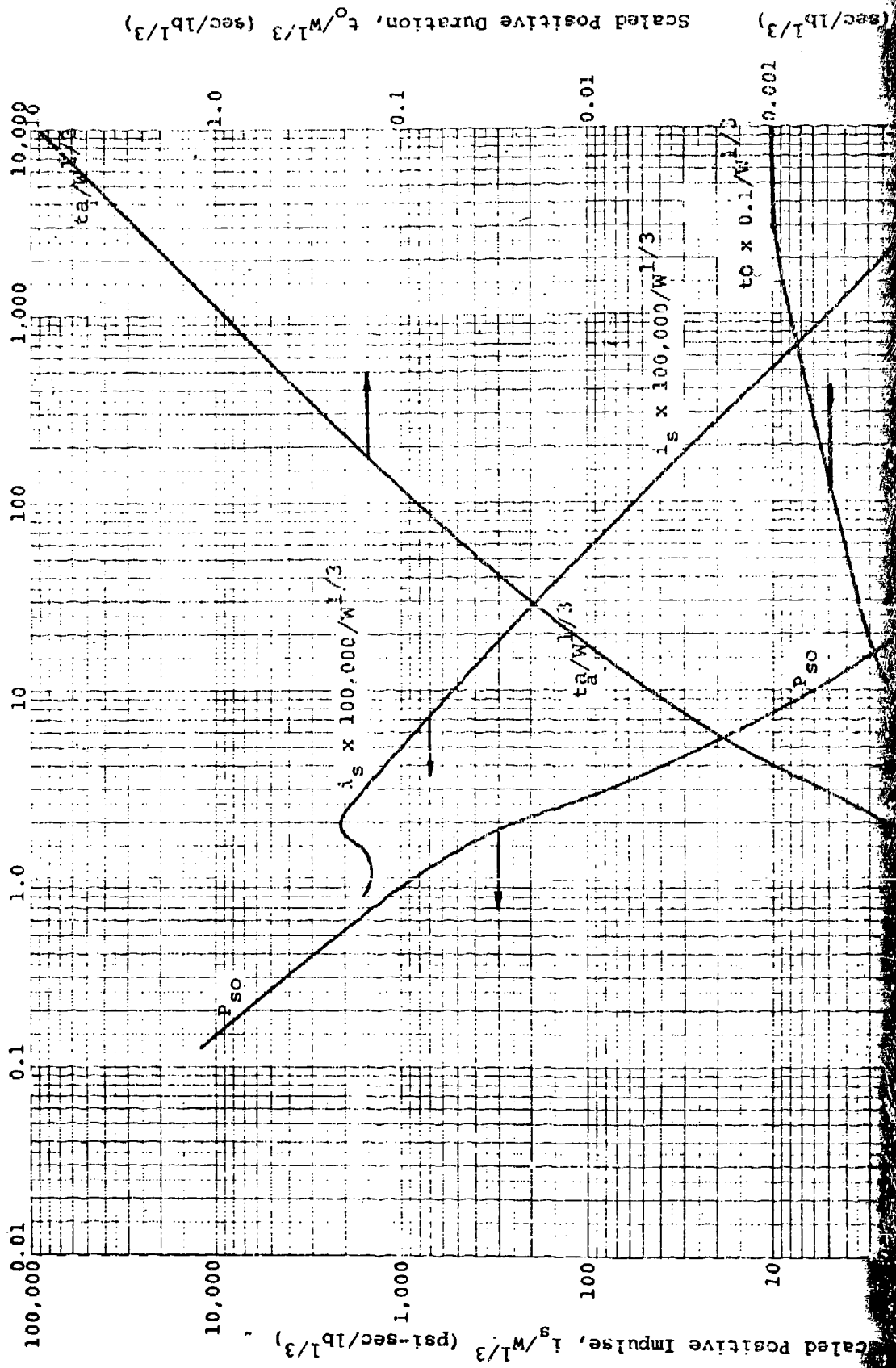
These curves can be used to estimate data for surface bursts by using an effective charge weight which accounts for ground reflection. The suggested conversion is

$$W_e = 1.8 W \quad (3-3)$$

where W_e is the effective charge weight in pounds of TNT to be used for estimating surface burst effects with the free air charts presented herein. This conversion has been shown to give good agreement with the data reported in Ref. 3-15.

It is sometimes necessary to estimate the velocity U at which the shock front of an airblast wave is traveling. The shock front velocity is a function of the peak overpressure and can be found from Fig. 3-4.

Scaled Distance, $Z = R/W^{1/3}$ (ft/lb^{1/3})



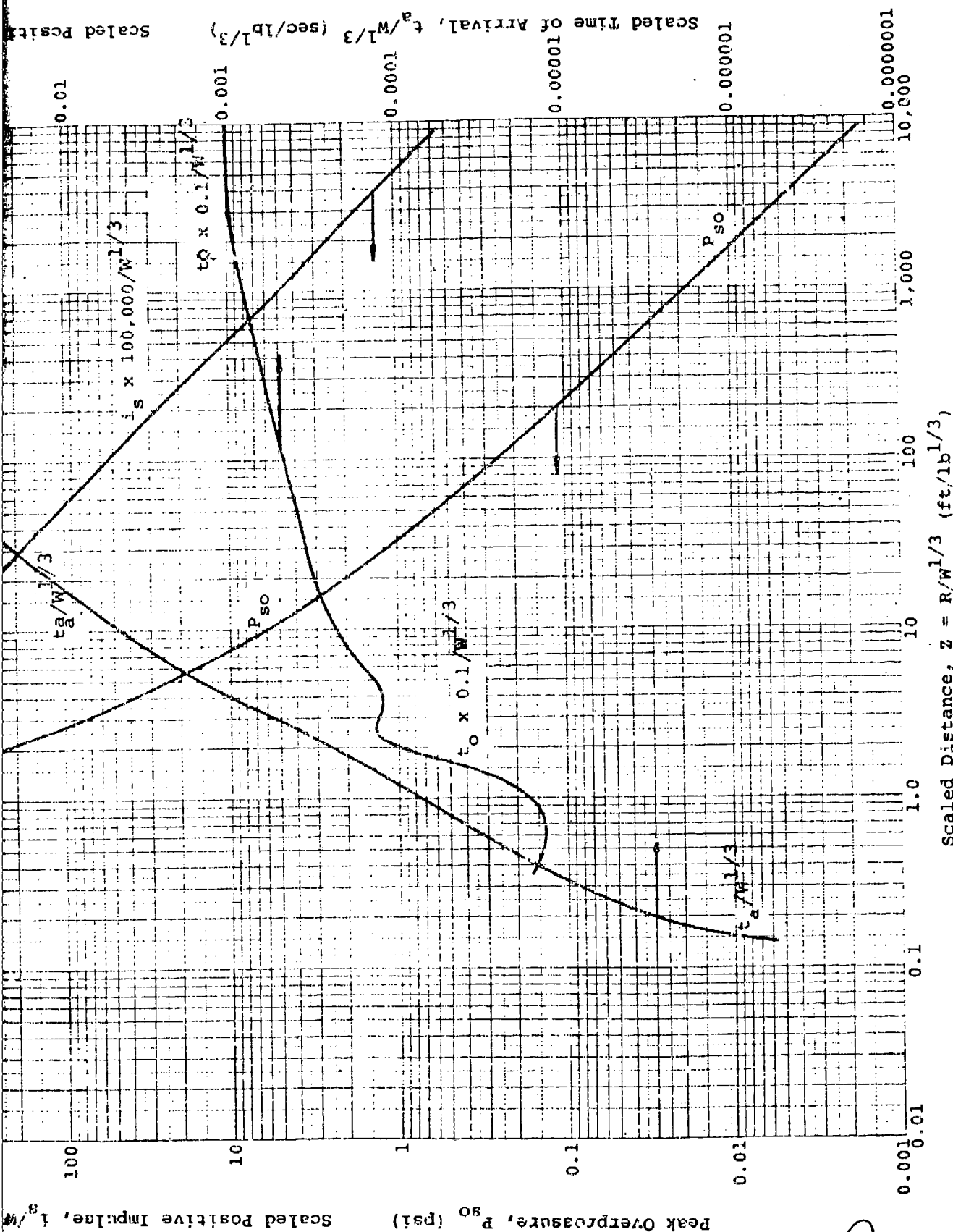


Figure 3-3. Incident Airblast Parameters for Spherical TNT Free Air Burst
(Southwest Research Institute)

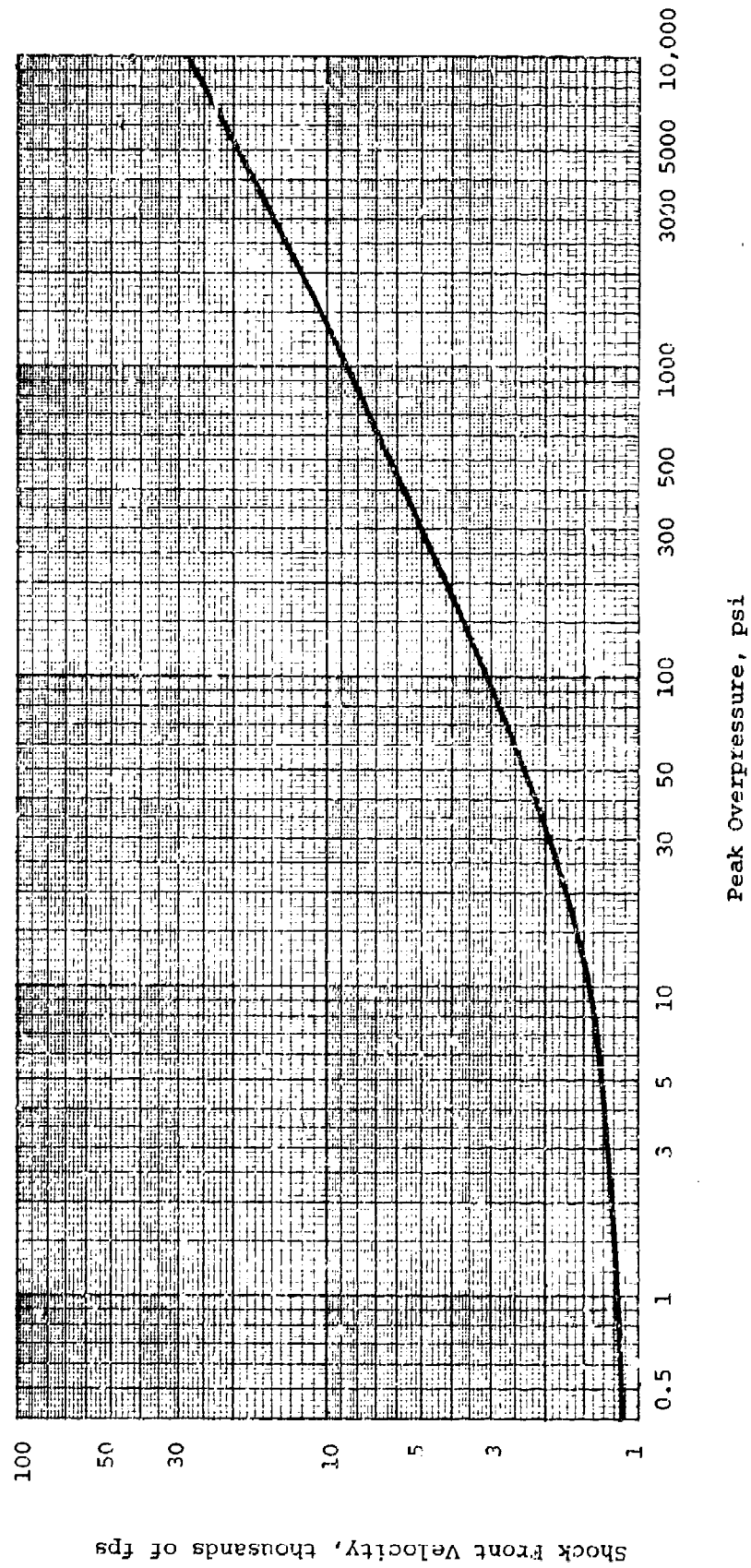


Figure 3-4. Shock Front Velocity as a Function of Peak Overpressure at Sea Level
(Ref. 3-3)

3.3 INTERNAL AIRBLAST

3.3.1 General

The loading from an explosive charge detonated within a vented or unvented structure consists of two almost distinct phases. The first phase is the reflected blast loading, which consists of an initial high pressure, short duration reflected wave, plus perhaps several later reflected pulses arriving at times closely approximated by twice the average first pulse arrival time at the chamber walls. These later pulses are usually attenuated in amplitude because of irreversible thermodynamic processes and are very complex in waveform because of the nature of the reflection process within the structure, whether vented or unvented. The second loading phase is a quasi-static pressure pulse and is discussed in a following paragraph.

The simplest case of blast wave reflection is that of normal reflection of a plane shock wave from a plane, rigid surface. In this case, the incident wave moves at velocity U through still air at ambient conditions. The conditions immediately behind the shock front are those for the free air shock wave discussed above. When the incident shock wave strikes the plane rigid surface, it is reflected therefrom. The reflected wave now moves away from the surface with a velocity U_r into the flow field and compressed region associated with the incident wave. In the reflection process, the incident particle velocity u_s is arrested ($u_s = 0$ at the reflecting surface), and the pressure, density, and temperature of the reflected wave are all increased above the values in the incident wave. The overpressure at the wall surface is termed the reflected overpressure and is designated P_r . For very weak shocks, $P_{s0} \ll P_0$, acoustic approximations are valid, and the reflected overpressure is twice the incident overpressure, $P_r = 2P_{s0}$. For stronger incident shocks, the enhancement of reflected pressure is increased by a factor of up to eight or more.

The durations of normally reflected waves are assumed to be not greatly different from those of incident waves. Reflected overpressures, however, are much higher than incident overpressures with the result that the reflected impulses are much greater than the incident impulses.

Following the initial shock wave reflection from the internal walls of a suppressive shield, the internal blast pressure loading becomes quite complex in nature. Figure 3-5 shows a stage in the loading for the cylindrical Group 3 suppressive shield. At the instant shown, portions of the cap, base and cylindrical surface are loaded by the reflected shock and the incident shock is reflecting obliquely from all three internal surfaces. The oblique reflection process can generate Mach waves (see Ref. 3-1 for a description of Mach waves), if the angle of incidence is great enough and pressures can be greatly enhanced on entering corners or reflecting near the axis of a cylindrical structure. In box-shaped suppressive shields, the reflection process can be even more complex.

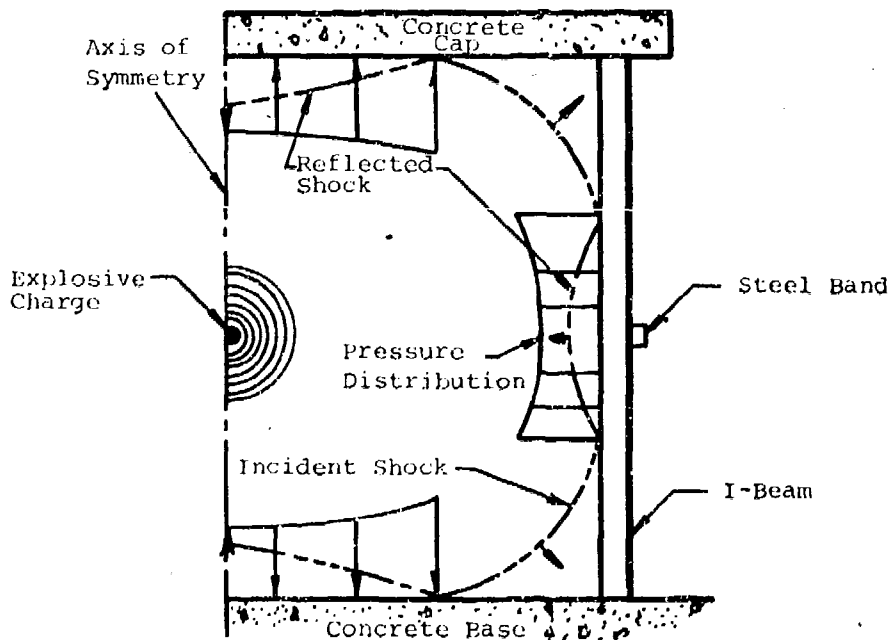


Figure 3-5. Schematic Representation of Shock Reflections from Interior Walls of a Suppressive Shield (Ref. 3-18)

Following the initial internal blast loading, the shock waves reflected inward will tend to strengthen as they impinge toward the center of the structure and then re-reflect to load the structure again. As noted earlier, each of these later shocks will usually be less severe than the preceding shock. After several such reflections, which occur in a very short time, the initial internal blast phase of the loading is over.

3.3.2 Prediction of Internal Blast Loads

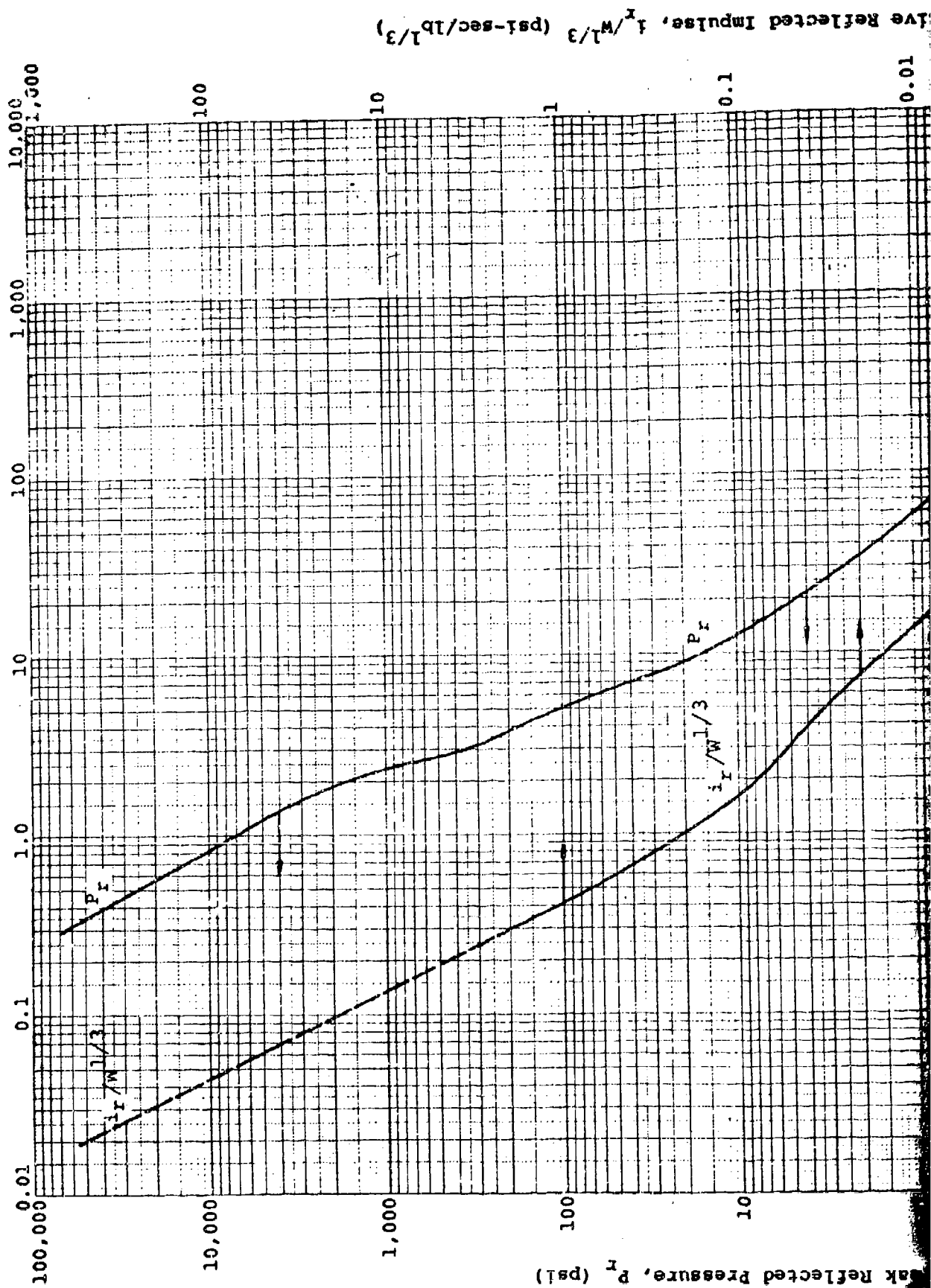
The air shock loading on the interior surfaces of suppressive shields is quite complex for all real structural geometries. Fortunately, however, approximate loading predictions suitable for the purposes of this handbook can be made with the aid of various simplifying assumptions. First, it is assumed that the initial reflected airblast parameters can be taken as the ideal normally reflected parameters, even for oblique reflections from the structure walls. This assumption is almost exactly true for strong shock waves up to an angle of incidence of about 40 degrees and for weak shock waves up to about 70 degrees, provided the slant range from the center of the charge to the point of interest is used for R in Eq. 3-2, pg. 3-6. Since most suppressive shield designs are reasonably symmetrical with length-to-height and width-to-height ratios of near one, and because well-designed suppressive shields will have the charge essentially centrally located, shock reflections from the walls will be fairly regular almost everywhere.

Ideal normally reflected blast parameters for a free air burst of spherical TNT are presented in Fig. 3-6. The time of duration of the initial reflected pulse is taken as

$$t_r = 2i_r/P_r \quad (3-4)$$

The re-reflected aftershocks are neglected in the simplified structural response methods presented in this handbook; therefore, the reflected impulse (i_r) and peak reflected pressure (P_r)

Scaled Distance, $z = R/W^{1/3}$ (ft/lb^{1/3})



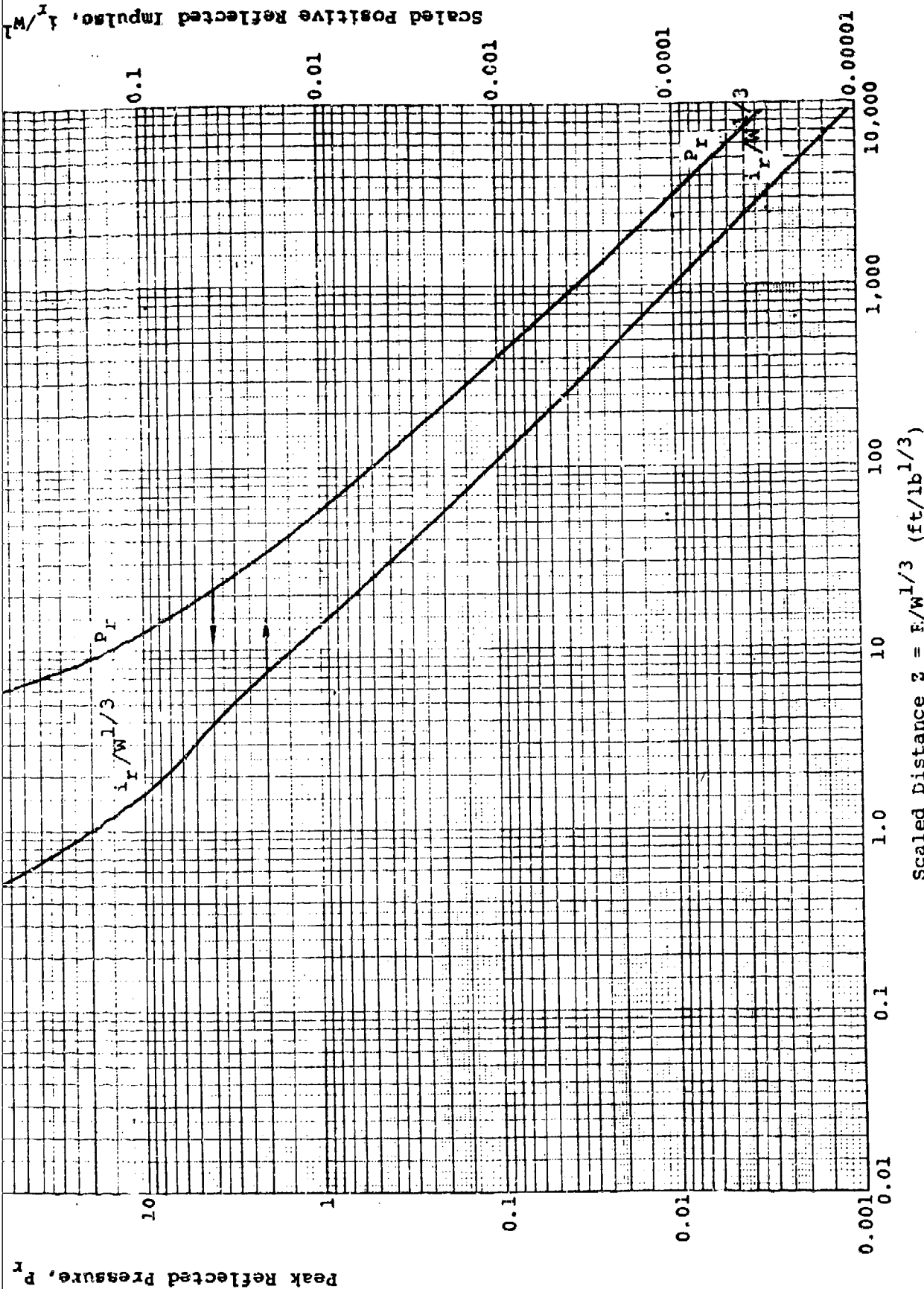


Figure 3-6. Reflected Airblast Parameters for Spherical TNT Free Air Burst
(Southwest Research Institute)

are the only initial internal blast parameters needed. For more exact calculations of loading, arrival times of the shock front and re-reflected aftershocks as a function of position in the structure can be important and should be considered.

3.4 VENTING

3.4.1 Introduction

The discussion of airblast loading up to this point has been largely in terms of solid containment vessels, i.e., structures with no venting. The desired function of a suppressive shield is to reduce the effects of an accidental explosion to an acceptable level as economically as possible. An optimum amount of venting can contribute materially to meeting this objective. Venting is essential for suppressive shields designed for containment of deflagrating materials (e.g., Shield Group 5); otherwise, the deflagration can escalate to a detonation if the gaseous products are not dissipated at an adequate rate.

3.4.2 Vent Area Ratio

The vent area ratio for a single layer structure is the vent area divided by the total area of the wall. The vent area ratio for a multi-layer structure proposed in Ref. 3-19 is

$$\frac{1}{\alpha_e} = \sum_{i=1}^n \frac{1}{\alpha_i} \quad (3-5)$$

where α_e is the multi-layer and α_i is the single layer vent area ratio for an n-layer structure.

The vent area ratio for a perforated plate is simply

$$\alpha_i = A_{vi}/A_{wi} \quad (3-6)$$

where A_{vi} and A_{wi} are the vent area and wall area of the ith layer, respectively. For cubicles with a portion or all of a wall or roof missing, the vent area is the area of the opening

and the appropriate value for α_e is the ratio of the open area to the total interior area of the cubicle.

Procedures for calculating vent area ratios for various structural configurations which have been used for suppressive shields are presented in Fig. 3-7. The procedures shown in Fig. 3-7, which are developed in Ref. 3-19, are believed to be self-explanatory, except possibly for the interlocked I-beams. The vent areas number 2 and 3 for this case are to take account of the two equal spaces b associated with each I-beam.

3.5 QUASI-STATIC PRESSURES

3.5.1 General

When an explosion occurs within a suppressive structure, the overpressure eventually settles to a slowly decaying level, which is a function of the volume and vent area of the structure and the nature and energy release of the explosion. A typical time history of overpressure at the wall of a suppressive structure is shown in Fig. 3-8a. The typical actual time history shown in Fig. 3-8a is idealized to the two triangle pulse depicted in Fig. 3-8b for use with the simplified structural response methods of this handbook.

Determination of the short duration initial impulsive portion of the idealized loading function has been addressed in paragraph 3.3 above. Prediction of the idealized long duration quasi-static portion of the loading is presented below.

3.5.2 Prediction of Quasi-Static Pressure Parameters

The two parameters of interest for construction of the quasi-static portion of the idealized loading function are the peak quasi-static pressure, P_{qs} , and the time, t_b , at which the quasi-static pressure returns to ambient. This time to return to ambient pressure is often referred to as the blowdown time.

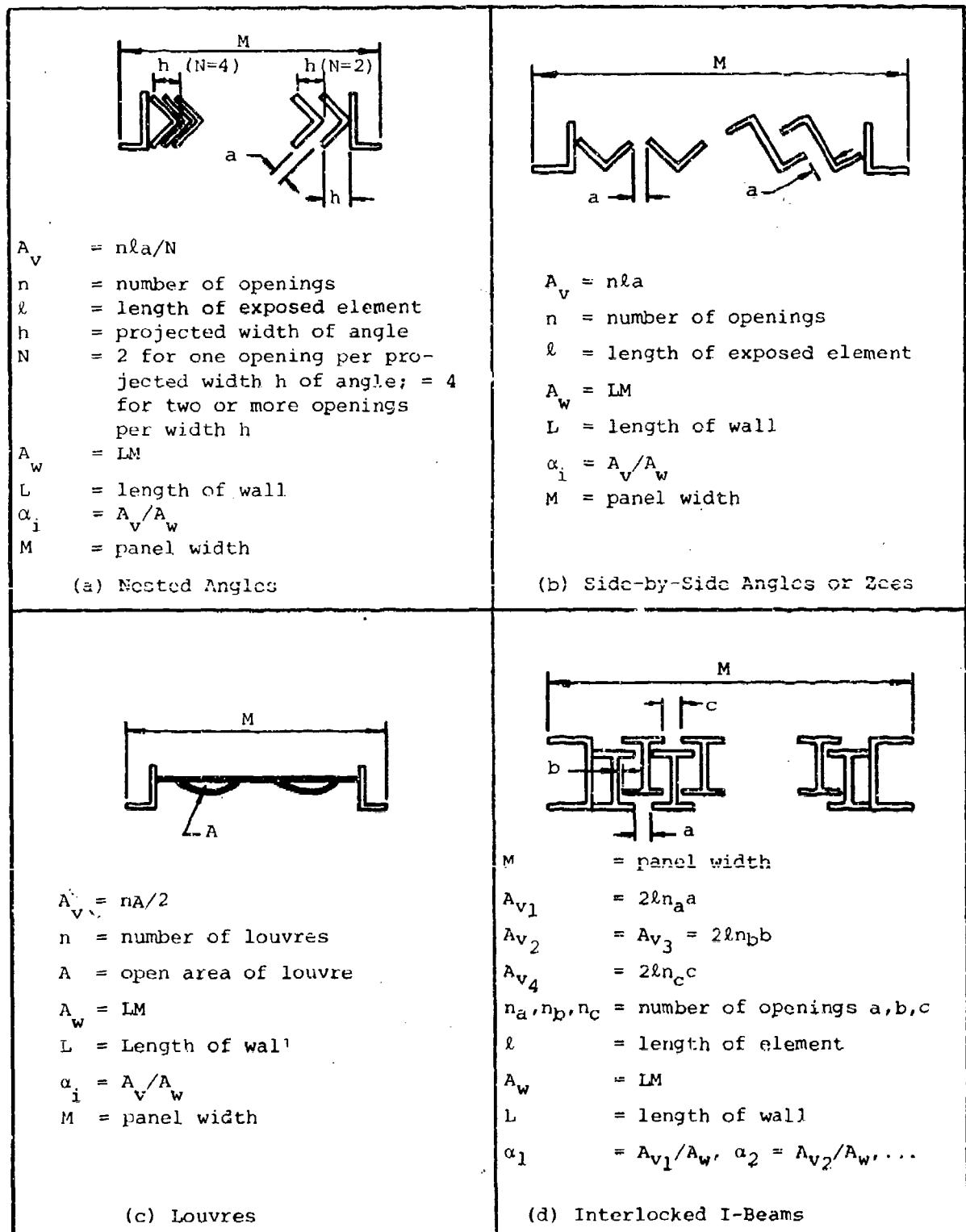
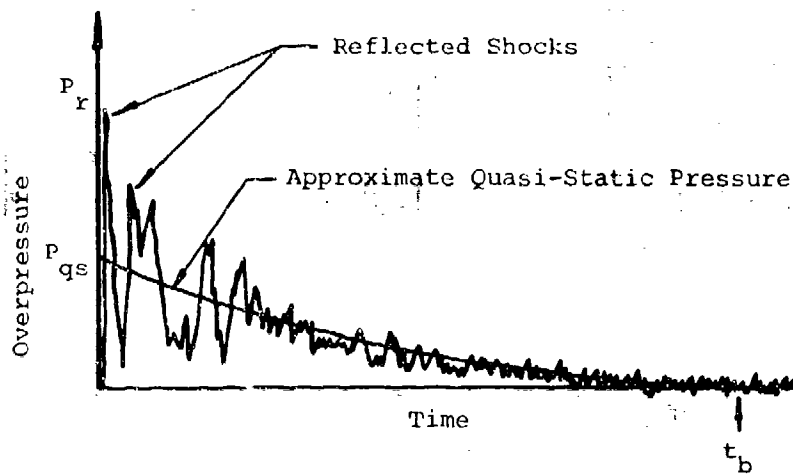
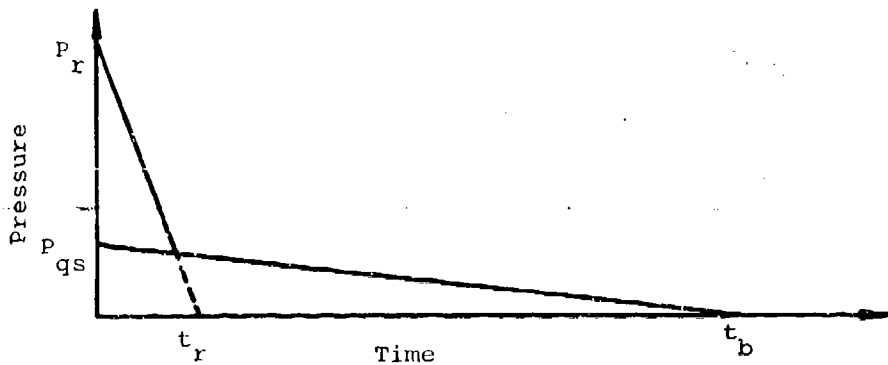


Figure 3-7. Definition of Vent Area Ratios for Various Structural Configurations (Ref. 3-19)



a. Typical Actual Pressure-Time History (Electronically Filtered)



b. Idealized Pressure-Time History

Figure 3-8. Internal Pressure Loading at Inner Surface of a Suppressive Shield

The maximum value for the quasi-static pressure in the long duration phase of the loading is the pressure rise which would occur in an unvented enclosure before heat transfer effects attenuate it. From data and analyses reported in Refs. 3-19 through 3-25, the curve of Fig. 3-9 has been shown to yield good predictions of P_{qs} as a function of the charge to volume ratio W/V . The charge weight W in Fig. 3-9 is in pounds of TNT and the internal volume, V , of the structure is in cubic feet.

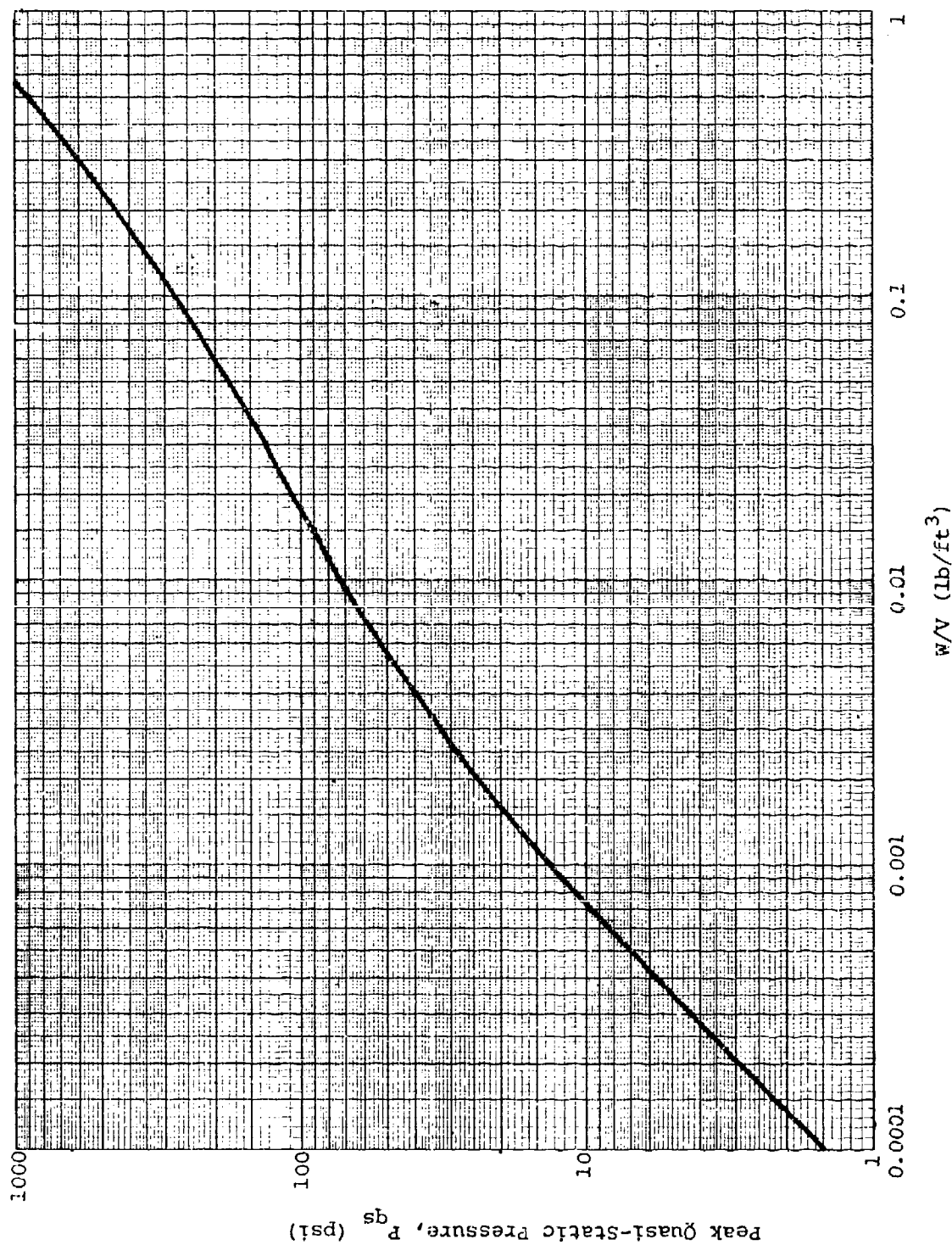


Figure 3-9. Peak Quasi-Static Pressure
(Southwest Research Institute)

The blowdown time, t_b , can be determined with Fig. 3-10 once P_{qs} has been established. In using Fig. 3-10,

P_o = ambient pressure, psi

a_o = speed of sound, 1117 ft/sec

V = internal volume of suppressive shield, ft^3

A_i = internal vented surface area of suppressive shield, ft^2

α_e = vent area ratio, Eq. 3-5, pg. 3-17

The internal vented surface area is the total surface area of those surfaces which are vented. For example, if the side walls are vented, but the roof and floor are not, A_i is equal to the total interior surface area of the walls, i.e., the roof and floor areas are not included.

3.6 AIRBLAST OUTSIDE SUPPRESSIVE SHIELDS

3.6.1 General

Most of the suppressive shield group designs have walls, or walls and roof, which have been designed to provide uniform venting. The vented wall/roof panel designs, which are discussed in more detail in Appendix A, consist of various combinations of perforated plates, nested angles or zees, louvres, and interlocked I-beams.

As each incident shock wave strikes the inner surface of a vented panel in a suppressive structure as shown in Fig. 3-11(a), it is partially reflected and partially transmitted undiminished in strength into the holes or slits in the first layer of the panel. The influence of viscosity is seen as a build-up of vortices at the entrance; see Fig. 3-11(a). At a later time, this vortex becomes detached and is swept into the restriction, forming a contraction (vena contracta) as shown in Figs. 3-11(b) through (d). The transmitted wave emerges from the restriction,

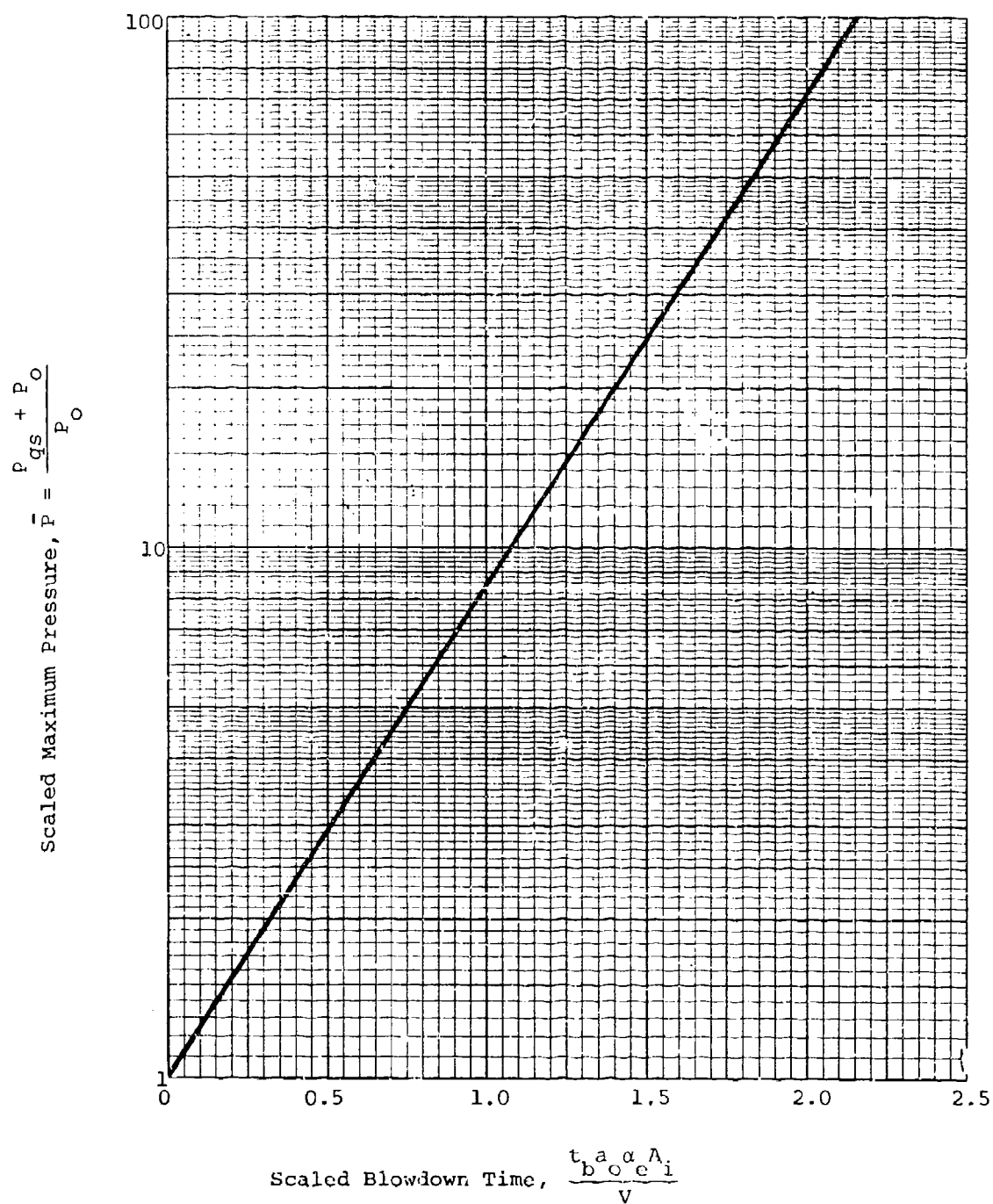


Figure 3-10. Scaled Blowdown Time Versus Scaled Maximum Pressure (Ref. 3-26)

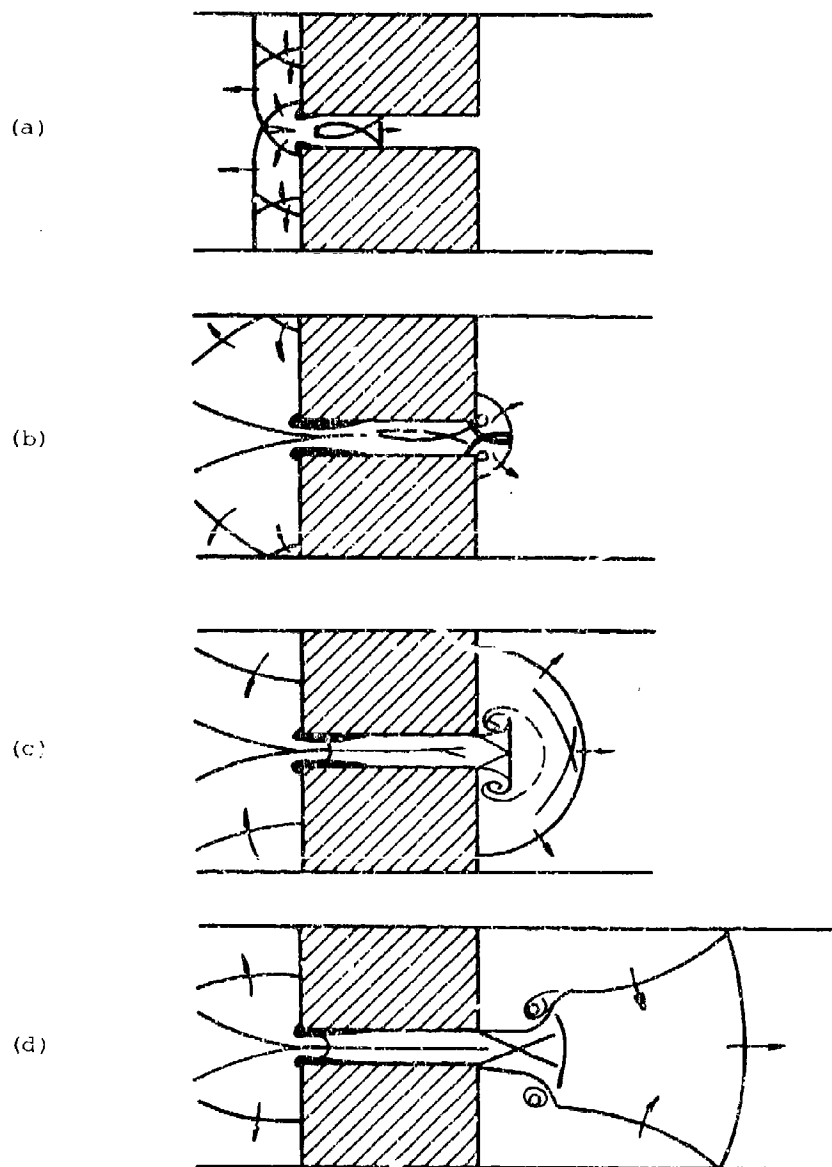


Figure 3-11. Stages During the Transmission of a Shock Wave Through a Single Slit in a Plate (Ref. 3-27)

becomes detached, and expands to fill the area behind the plate; see Fig. 3-11(d). The transmitted wave then reflects from the second layer and is again partially transmitted. This process continues for each layer until an attenuated shock emerges from the panel and reforms outside the structure. The detailed processes of reflection and transmission are very complex and result in multiple shocks. Even for transmission of a single shock through a single slit in a plate, the process is not simple, as can be seen in Fig. 3-11.

Various computer programs have been developed and used to attempt to predict intrapanel pressures and pressures transmitted through multi-layer panels. References 3-26 through 3-29 report intrapanel pressure predictions, and Ref. 3-30 reports predicted pressure transmission through an interlocked I-beam panel. Figure 3-12 illustrates typical results of the interlocked I-beam calculations of Ref. 3-30.

From the outset of suppressive structures testing and evaluation, measurements have been made of the characteristics of these external blast waves over a range of distances from the structures. References 3-21 and 3-31 through 3-36 contain the majority of such data. The following prediction methods presented are based upon these experimental data.

3.6.2 Prediction Methods

The prediction methods which follow have been developed by fitting curves to measured experimental data. They are strictly valid, therefore, only within the ranges of the variables for which measurements were obtained. Use of these expressions outside their range of applicability should be done only with extreme caution.

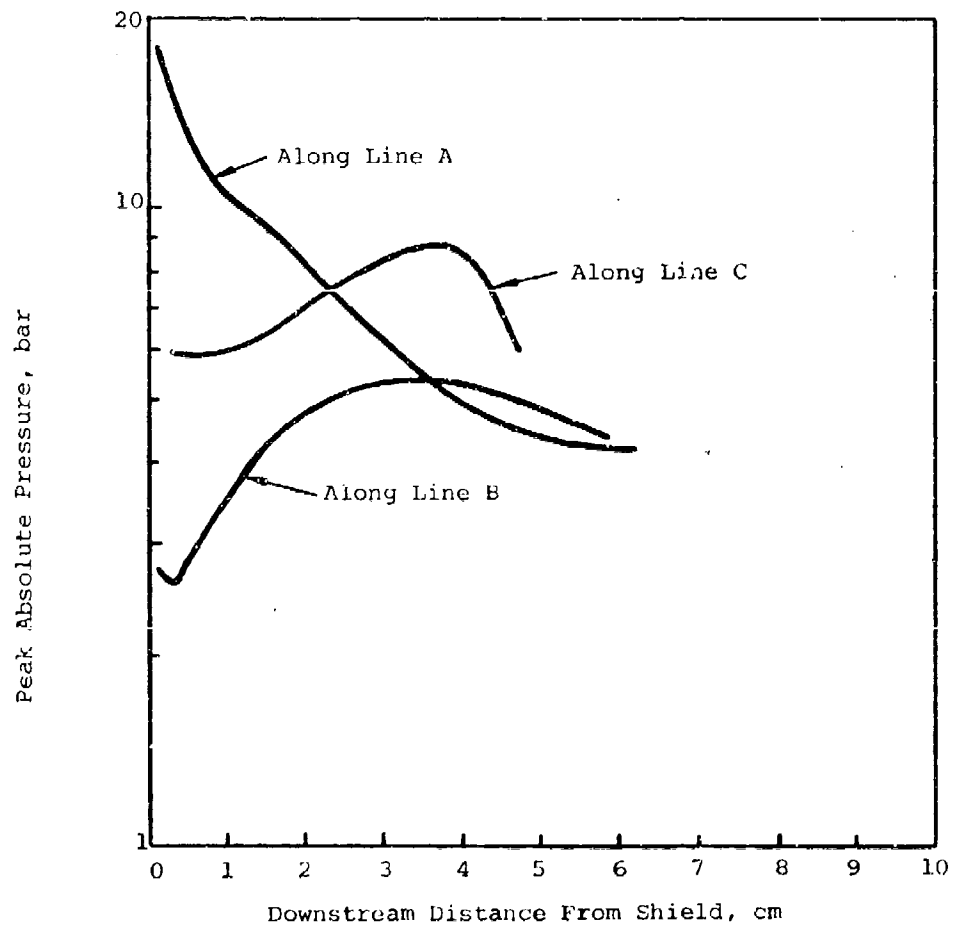
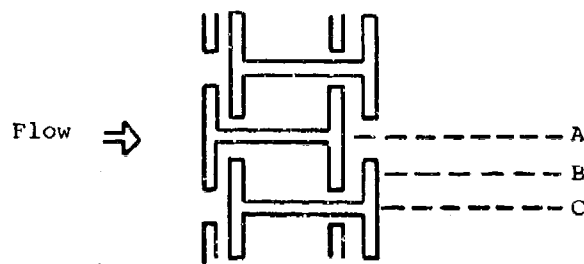


Figure 3-12. Calculated Pressures Outside Group 3 Cylindrical Blast Shield with 48-lb Charge (Ref. 3-30)

The expression for peak overpressure in psi outside a suppressive shield is (Ref. 3-19)

$$P_{so} = 957 \left(\frac{1}{Z} \right)^{1.66} \left(\frac{R}{X} \right)^{0.27} \left(\alpha_e \right)^{0.64} \quad (3-7)$$

where

Z = scaled distance, Eq. 3-2, pg. 3-6

R = distance from center of explosive charge to point of interest, ft

X = characteristic length of structure, ft;
side dimension for square structure; square root of plan area for rectangular structure; cube root of the volume for cylindrical structure

α_e = effective vent area ratio, Eq. 3-5, pg. 3-17

The limits for applicability of this equation are

$$2.93 \leq Z \leq 21.3$$

$$0.69 \leq R/X \leq 4.55$$

$$0.01 \leq \alpha_e \leq 0.13$$

and the expected error (standard deviation) is ± 19.9 percent.

The incident positive phase impulse in psi-ms outside a suppressive shield is given by (Ref. 3-19)

$$i_s = \left[218 \left(\frac{1}{Z} \right)^{0.98} \left(\frac{R}{X} \right)^{0.008} \left(\alpha_e \right)^{0.45} \right] W^{1/3} \quad (3-8)$$

where W is in pounds of TNT and the other terms are as previously defined. The limits of applicability of this equation are

$$2.93 \leq Z \leq 15.0$$

$$1.16 \leq R/X \leq 4.55$$

$$0.008 \leq \alpha_e \leq 0.13$$

and the expected error (standard deviation) is ± 19.2 percent. Additional equations are available for specific panel designs with smaller standard deviations (Ref. 3-19).

Equations 3-7 and 3-8 apply to any vented panel configuration which has been tested (e.g., all safety approved shields) and to uniformly vented structures, i.e., structures vented in the same manner through all sides and the roof.

3.7 FRAGMENTATION

3.7.1 Introduction

Fragments of interest in suppressive shielding may be classified as either primary or secondary. The term primary fragment denotes a fragment from an explosive-filled container which ruptures into many small pieces under detonation of the explosive material. Secondary fragments consist of objects which are located near an explosive source and are accelerated by the blast wave from the explosion. Secondary fragments may be initially restrained or fastened in some manner, or they may be unrestrained. Both types of fragments are discussed below.

a. Primary Fragments

Consider a cased high explosive charge such as a shell or missile warhead. The process of casing expansion and fracture on detonation of the explosive filler is well described in Ref. 3-37. The very high pressures generated by the detonating explosive cause the casing to expand to up to twice its original diameter. Radial cracks start on the outer surface of the casing but propagate only a short distance through the thickness. Failure is predominately in shear in the inner

part of the casing. Recovered fragments typically exhibit reductions in wall thickness of 40-60 percent according to Ref. 3-37.

The number and mass distribution of fragments formed during casing failure is a function of casing thickness, type of explosive, and metallurgy of the casing material. Natural fragments from cylindrical casings will often be portions of longitudinal strips and, consequently, will be rather long and slender. Numbers of fragments generated are usually quite large, typically in the thousands. Velocities of primary fragments are a function of the composition and geometry of the explosive charge and casing and the ratio of total explosive mass (or energy) to casing mass. Typically, primary fragment velocities from cased charges will be at least several thousand feet per second and can exceed seven thousand feet per second.

b. Secondary Fragments

Consider next the generation of secondary fragments. Loose or restrained objects located close to explosive sources can be accelerated by the strong blast waves from these sources and become potentially damaging fragments. In suppressive structures, these objects could be rollers on a conveyor line, motors and pieces of equipment used in munition plant operations, or a host of other items. Potential sources for secondary fragments can be determined from detailed study of specific plant operations and designs.

The initial reflected and diffracted blast waves accelerate the secondary fragments located close to the explosive source. Further from the source, both diffraction and drag forces can contribute to the acceleration. The mass and shape of potential secondary fragments can be estimated with a reasonable degree of certainty by inspection of the equipment and appurtenances at the hazardous location. Prediction of the velocity of secondary fragments is based upon impulse-momentum principles.

3.7.2 Prediction of Primary Fragmentation

Prediction of striking velocities of primary fragments for bursting munitions can be made with reasonable accuracy, but accurate prediction of mass and shape of these fragments for naturally fragmenting casings which do not employ pre-formed fragments is difficult. An unclassified expression for predicting primary fragment weight based upon Refs. 3-38 and 3-39 which has been partially verified by fragmentation tests using mild steel cylindrical casings filled with various explosives (Ref. 3-40) is

$$W_f = C \left[\ln \left(\frac{W_c}{2C} \right) \right]^2 \quad (3-9)$$

where

W_f = weight of the next to largest fragment, lb

$$C = \left[B t^{5/6} d_i^{1/3} (1 + t/d_i) \right]^2, \text{ lb}$$

B = constant depending upon type of explosive,
Table 3-2

t = thickness of casing, inches

d_i = inside diameter of casing, inches

W_c = weight of casing, lb

Prediction of primary fragment initial velocity can be accomplished with a semi-empirical procedure based upon the Gurney energy constant. The initial velocity of a primary fragment from a cylindrical metal case of uniform thickness filled with an evenly distributed explosive can be estimated with (Ref. 3-2)

$$v_o = \sqrt{2E'} \left[\frac{W/W_c}{1 + W/2W_c} \right]^{1/2} \quad (3-10)$$

Table 3-2
 MOTT SCALING CONSTANTS FOR MILD STEEL CASINGS
 AND VARIOUS EXPLOSIVES (Ref. 3-40)

Explosive	B (lb ^{1/2} inches ^{-7/6})
Paratol	0.128
Comp B	0.0554
Cyclotol (75/25)	0.0493
H-6	0.0690
HBX-1	0.0639
HBX-3	0.0808
Pentolite (50/50)	0.0620
PTX-1	0.0554
PTX-2	0.0568
TNT	0.0779
Comp A-3	0.0549
RDX/WAX (95/5)	0.0531
Tetryl	0.0681

where

v_o = initial primary fragment velocity, ft/sec

$\sqrt{2E^*}$ = Gurney energy constant; Table 3-3

W = charge weight, lb

W_c = weight of the cylindrical portion of the metal casing, lb

Initial primary fragment velocities for other than cylindrical cross sectional shapes are shown in Table 3-4.

The primary fragment striking velocity, v_s , can be taken equal to the initial velocity for distances up to 20 feet from the detonation (Ref. 3-2). Since suppressive shield walls will typically be at or within this range, it is recommended that the fragment striking velocity be taken equal to the initial velocity for suppressive shielding applications.

3.7.3 Prediction of Secondary Fragmentation

The only expression presently available for estimating the initial velocity of secondary fragments is the semi-empirical relationship

$$v_{os} = \frac{A_p R_e g_s}{M} \left[0.556 \left(\frac{R_e}{R} \right) + 2.75 \left(\frac{R_e}{R} \right)^2 \right] \quad (3-11)$$

where

v_{os} = initial velocity of secondary fragment, in/sec

A_p = area of secondary fragment presented to explosive, in²

R_e = radius of spherical explosive charge, inches

M = mass of secondary fragment, lb-sec²/in

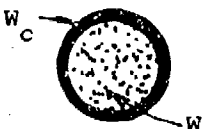
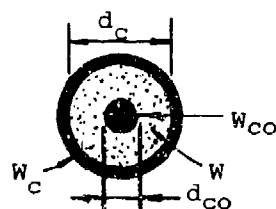
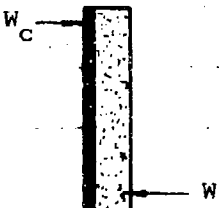
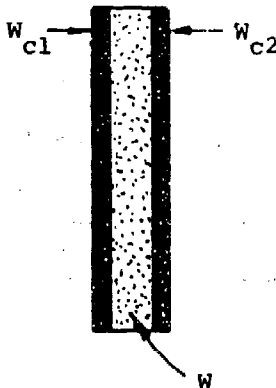
R = range from center of explosive charge to nearest face of secondary fragment, inches

Table 3-3
 GURNEY ENERGY CONSTANTS
 FOR VARIOUS EXPLOSIVES (Ref. 3-41)

Explosive	$\sqrt{2E'}$ (ft/sec)
RDX	9,610
Comp C-3	8,790
TNT	7,780
Tritonal	7,610
Comp B	8,890
HMX	9,740
PBX-9404	9,510
Tetryl	8,200
TACOT	6,960
Nitromethane	7,910
PETN	9,610
Detasheet EL506D	7,480
Detasheet EL506L	7,220
Pentolite (50/50)	8,400

Table 3-4

INITIAL PRIMARY FRAGMENT VELOCITY
FOR VARIOUS CROSS-SECTIONAL SHAPES (Ref. 3-42 & 3-2)

Type	Cross Section	Initial Fragment Velocity
Sphere		$v_o = \sqrt{2E'} \left[\frac{W/W_c}{1 + 3W/5W_c} \right]^{1/2}$
Steel Cored Cylinder		$v_o = \sqrt{2E'} \left[\frac{W/W_c}{1 + \frac{(3+a)W}{6(1+a)W_c}} \right]^{1/2}$ <p>where $a = \frac{d_{co}}{d_c}$</p>
Plate		$v_o = \sqrt{2E'} \left[\frac{\frac{3W}{5W_c}}{1 + \frac{W}{5W_c} + \frac{4W_c}{5W}} \right]^{1/2}$ <p>if $W_{c1} \neq W_{c2}$</p>
Sandwich Plates		$v_o = \sqrt{2E'} \left[\frac{W}{W_{c1} + W_{c2}g^2 + \frac{W}{3}(1-g+g^2)} \right]^{1/2}$ <p>where $g = \frac{W_{c1} + \frac{W}{2}}{W_{c2} + \frac{W}{2}}$</p> <p>if $W_{c1} = W_{c2} = W_c$</p> $v_o = \sqrt{2E'} \left[\frac{\frac{W}{2W_c}}{1 + \frac{W}{6W_c}} \right]^{1/2}$

$W, W_c, W_{cc}, W_{c1}, W_{c2}$ (lbs) d_c, d_{co} (inches) $v_o, \sqrt{2E'}$ (ft/sec)

g_s = secondary fragment shape factor

= 2/3 for sphere

= $\pi/4$ for side-on cylinder

= 1 for end-on cylinder or plane surface

The limits of applicability of Eq. 3-11 are

$$1.5 \leq \frac{R}{R_e} \leq 6.0$$

$$0.18 \frac{\text{lb-sec}}{\text{in}^3} \leq \frac{Mv_o}{A_p R_e g_s} \leq 2.0 \frac{\text{lb-sec}}{\text{in}^3}$$

In addition to its rather narrow limits of validity, Eq. 3-11 is strictly applicable only to spherical charges of Comp B explosive and unrestrained secondary fragments of spherical or cylindrical shape. The speed calculated for an unconstrained secondary fragment represents an upper limit and, hence, conservative estimate of the speed of a constrained secondary fragment. Until further analytical and experimental work is completed, however, Eq. 3-11 is the best method available for predicting secondary fragment velocities.

3.8 IMPACT AND PENETRATION

3.8 Introduction

The accidental detonation in an explosive processing plant can result in the generation of many primary and/or secondary fragments. On contact with a suppressive shield, the fragment will either penetrate some distance into the structure and be stopped, or perforate completely through and emerge from the back face with some residual velocity and mass. Whether partial penetration or perforation occurs depends on a variety of parameters including the thickness, construction details and material properties of the barrier; the geometry and material

characteristics of the fragment, fragment mass, presented area, striking velocity and angle at which the fragment strikes the wall. Several characteristic mechanisms for penetration that have been observed in steel plates are illustrated in Fig. 3-13. Plugs are most likely to be found in very hard plates of moderate thickness, while petalling is most frequently observed in thin plates struck at or below ordnance velocities (2500 fps). A combination of ductile failure and spalling is characteristic for perforation of thick plates of medium or low hardness.

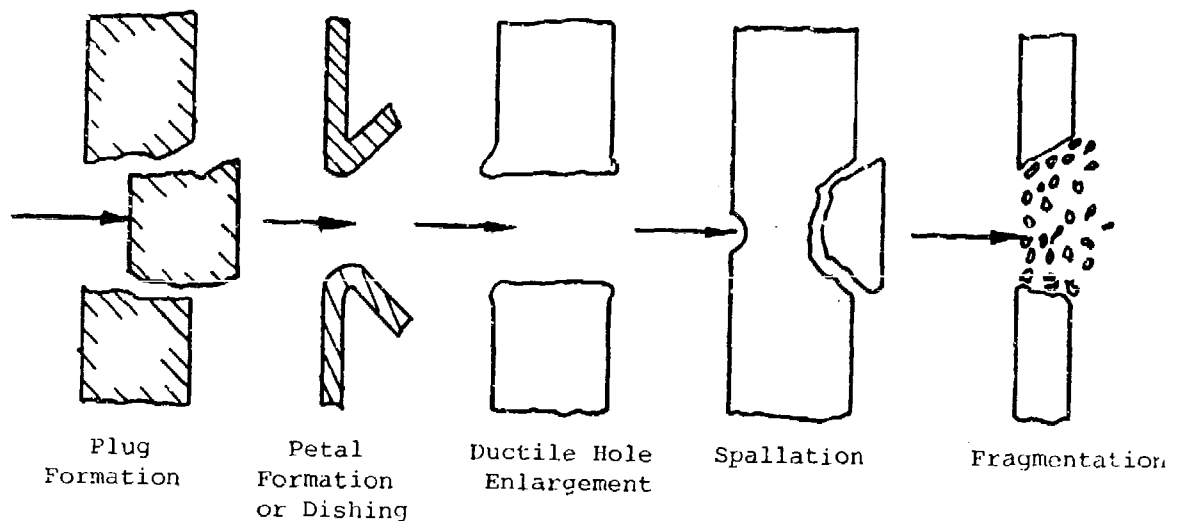


Figure 3-13. Possible Mechanisms for Steel Plate Damage

Three possible mechanisms of fragment impact damage of concrete panels are shown in Fig. 3-14. At low velocities, the fragment strikes the panel and rebounds without causing any local damage. As the velocity increases, pieces of concrete are spalled off of the front face of the target. This spalling forms a spall crater that extends over a substantially greater area than the cross sectional area of the striking fragment. As the velocity continues to increase, the fragment will penetrate the target to depths beyond the depth of the spall crater,

forming a cylindrical penetration hole with a diameter only slightly greater than the fragment diameter. Further increases in velocity produce cracking of the concrete on the back surface followed by scabbing of concrete from this rear surface. The zone of scabbing will generally be much wider, but not as deep as the front face spall crater. Once scabbing begins, the depth of penetration will increase rapidly. As the fragment velocity increases further, perforation of the target will occur as the penetration hole extends through to the scabbing crater. Still higher velocities will cause the missile to exit from the rear face of the target.

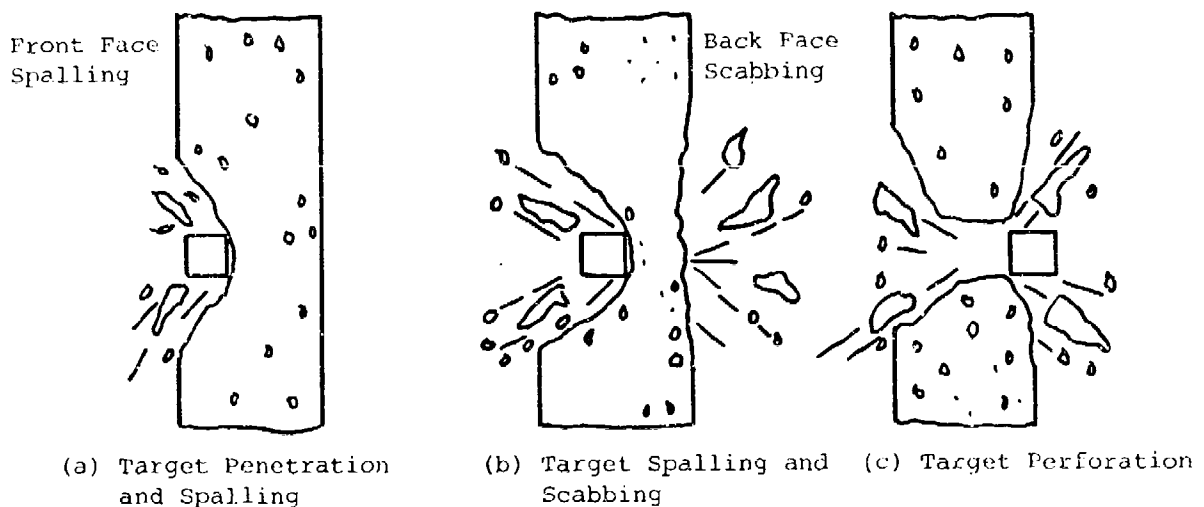


Figure 3-14. Possible Mechanisms for Concrete Panel Impact Damage (Ref. 3-43)

3.8.2 Prediction of Penetration of Steel Plate

The recommended method for predicting fragment penetration of steel plate(s) is based on the procedures of Ref. 3-44 and is shown in outline form in Fig. 3-15. The prediction method and quantities required for its utilization are discussed further below.

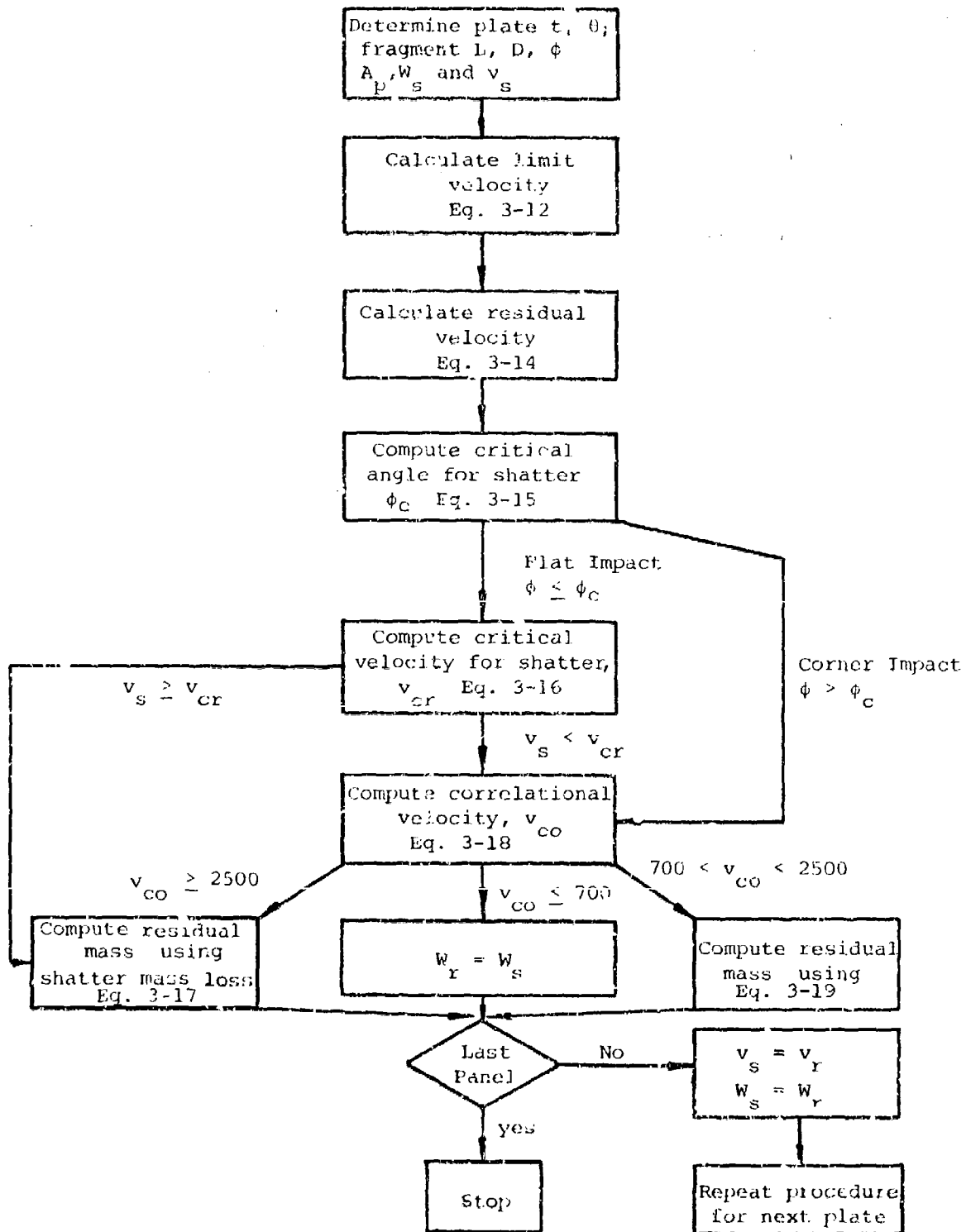


Figure 3-15. Prediction of Fragment Penetration of Steel Plate

a. Input Parameters

Quantities needed to begin the procedure are

- Plate thickness, t inches
- Angle of obliquity = angle between line of flight of fragment and the normal to the plate surface, θ degrees
- Orientation angle = least angle between any flat fragment surface and the plate surface, ϕ degrees
- Fragment length to diameter ratio, L/D
- Fragment area presented to plate, A_p in²
- Fragment striking weight, W_s lb
- Fragment striking velocity, v_s fps

These quantities will either be known or can be estimated for the problem of interest. Otherwise, they must be assumed.

b. Ballistic Limit Velocity

The ballistic limit velocity is defined as the lowest striking velocity that results in perforation of the target with zero residual velocity. The ballistic limit velocity for compact fragments striking mild steel targets can be estimated as

$$v_l = \frac{A_o}{\sqrt{W_s}} A_p^m (t \sec \theta)^n \quad (3-12)$$

where v_l is the ballistic limit velocity in fps; A_o , m and n are constants defined in Table 3-5; and the other terms are as previously defined.

Equation 3-12 is also applicable to perforated plates with the substitution of $R^2 A_p$ for A_p , where R is the perforation factor. The perforation factor is defined as

Table 3-5

EMPIRICAL CONSTANTS FOR PREDICTING COMPACT FRAGMENT
LIMIT VELOCITY FOR MILD STEEL TARGETS
(Southwest Research Institute)

L/D	$\frac{t}{R\sqrt{A_p}} *$	A_o	m	n
≤ 5	$0 \leq 0.46$	1414	0.295	0.910
≤ 5	$0.46 \leq 1.06$	1936	0.096	1.310
≤ 5	≥ 1.06	2039	0.064	0.430
> 5	-	1261	0.427	0.647

* R is the perforation factor for perforated plates;
see Eq. 3-13 or Fig. 3-16.

Table 3-6

EMPIRICAL CONSTANTS FOR PREDICTING COMPACT FRAGMENT
RESIDUAL VELOCITY FOR MILD STEEL TARGETS

Constant	L/D < 5	L/D \geq 5
a	1.12	1.10
b	0.52	0.80
c	1.29	1.45

(Southwest Research Institute)

$$R = 1 - d_p/h_p \quad (3-13)$$

where d_p is the diameter of the perforations and h_p is the average center-to-center distance between perforations. Values of the perforation factor as a function of vent area ratio, α , for hexagonal and square hole patterns are shown in Fig. 3-16.

c. Residual Velocity

In order to predict the residual velocity of a fragment that has perforated a mild steel plate, a quantity

$$x = \frac{v_s}{v_\ell} - 1$$

is computed first where v_s is the striking velocity and v_ℓ the ballistic limit velocity. Then,

$$v_r = v_\ell \beta \left[\frac{ax^2 + bx + c\sqrt{x}}{x + 1} \right] \quad (3-14)$$

$$\text{but } v_r \leq v_s$$

where

$$\beta = \frac{1}{\left[1 + \gamma A_p t / W_s \right]^{1/2}} \quad \text{for } L/D \leq 2$$

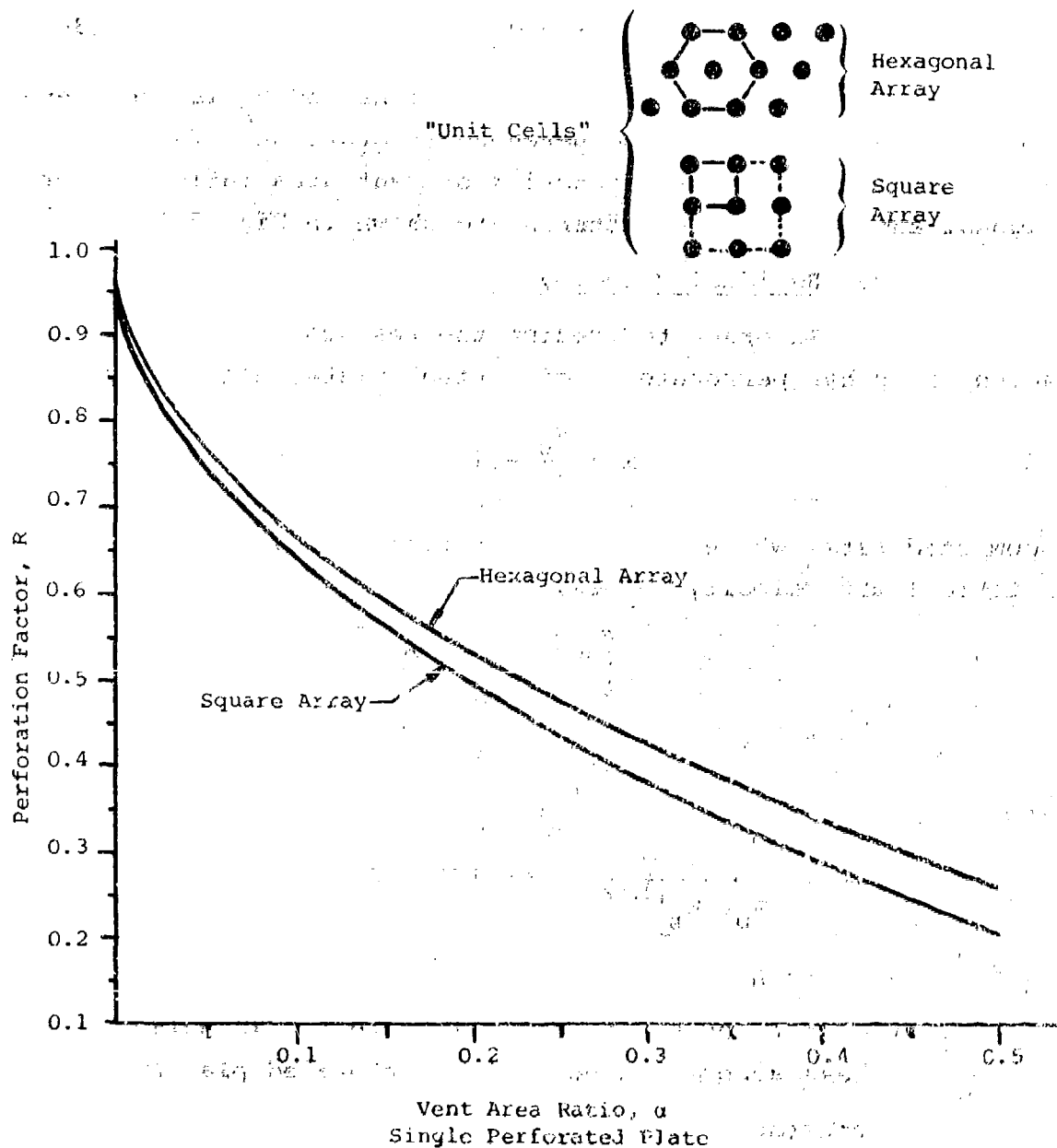
$$\beta = 1 \quad \text{for } L/D > 2$$

$$\gamma = \text{density of the target plate, lb/in}^3 \text{ (should take account of holes for perforated plates)}$$

$$a, b, c = \text{constants from Table 3-6}$$

d. Critical Angle for Shatter

A fragment which has perforated a mild steel plate may or may not lose mass depending upon the orientation angle ϕ between any flat fragment face and the target. If ϕ is small enough, the impact is essentially flat, or $\phi \leq \phi_c$, where ϕ_c is the critical orientation angle in degrees for shatter.



$$\phi_c = \arcsin(v_s \cos \theta / c_p) \quad (3-15)$$

where c_p = sonic velocity of the plate = 18,010 fps for steel.
If $\phi > \phi_c$, the impact is considered to be a corner or edge impact.

Define a critical velocity as

$$v_{cr} = 2000 \text{ fps} / \cos \theta \quad (3-16)$$

Then, for a flat impact with a striking velocity equal to or greater than the critical velocity, i.e.,

$$\phi \leq \phi_c$$

$$v_s \geq v_{cr}$$

the fragment will be in the shatter mass loss mode. The residual weight of the fragment for this case is determined by

$$W_r = W_s \left[1 - 0.002063 t^{0.138} W_s^{0.074} (\sec \theta)^{0.143} v_s^{0.761} \right] \quad (3-17)$$

where all terms are as previously defined.

For flat impacts with a striking velocity less than the critical velocity, i.e.,

$$\phi \leq \phi_c$$

$$v_s < v_{cr}$$

and for all corner or edge impacts, i.e.,

$$\phi > \phi_c$$

the fragment is in the deformation mass loss mode. To determine the fragment residual mass for this mode, a correlation velocity is computed first. The correlation velocity in fps is defined as

$$v_{co} = \frac{v_s}{1 + \frac{\cos\theta}{\frac{0.6t\gamma A}{W_s} P + 0.15}} \quad (3-18)$$

where all terms are as previously defined. Then,

For $v_{co} \leq 700$ fps: $W_r = W_s$

$v_{co} \geq 2500$ fps: $W_r = \text{Eq. 3-17}$

$700 \text{ fps} < v_{co} < 2500 \text{ fps}$:

$$W_r = W_s \left[1 - 0.0000151(v_{co} - 700)^{1.42} \right] \quad (3-19)$$

The penetration prediction method outlined above can be expected to give conservative results, particularly for fragment residual mass estimates. Two further assumptions can be made when investigating multi-layer panels that will increase the conservatism of the method and reduce the number of calculations required. These are (1) to set $\beta = 1$ in Eq. 3-14, and (2) to neglect any fragment loss of mass. If the panel defeats the fragment with the resulting known higher residual velocity and larger mass, it is clearly safe. If the fragment defeats the panel with these two assumptions, the calculations can be repeated with the more realistic fragment residual velocity and mass.

3.8.3 Prediction of Penetration of Concrete Panels

For a very quick and crude rule-of-thumb estimate of the effectiveness of reinforced concrete panels in resisting penetration by steel fragments, it can be assumed that one inch of mild steel is equivalent to nine inches of concrete, i.e., if it is known that a one-inch thickness of mild steel will defeat a particular fragment threat, it can be estimated that nine inches of reasonable quality reinforced concrete will also defeat the fragment. When more realistic estimates of concrete

penetration are desired, the methods from Ref. 3-2 summarized below can be utilized.

a. Armor-Piercing Fragments

A certain amount of experimental data analogous to primary fragment penetration has been accumulated in connection with projects to determine the effects of bomb and projectile impact on concrete structures. These data were analyzed and relationships developed where the amount of fragment penetration into concrete elements could be expressed in terms of the physical properties of both the metal fragment and the concrete. The general expression for the maximum penetration X_f in inches of a compact armor-piercing fragment was derived in terms of the fragment weight W_{fo} in ounces and striking velocity v_s in fps, i.e.,

$$X_f = 1.62 \times 10^{-5} W_{fo}^{0.4} v_s^{1.8} \quad (3-20)$$

Equation 3-20 is based on a concrete compression strength f'_c equal to 5,000 psi. Maximum penetrations of fragments in concrete of other strengths may be obtained by multiplying the value of X_f of Eq. 3-20 by the square root of the ratio of 5,000 psi to the compressive strength of the concrete in question. Figure 3-17 is a plot of the maximum penetration through 5,000 psi concrete for various fragment sizes and striking velocities.

The limiting thickness of concrete at which perforation will occur can be obtained from Fig. 3-18 and is a function of the coefficient C_1 , the fragment weight, striking velocity, and maximum penetration and the dilatational velocity c_s of the elastic wave through concrete where

$$c_s = 5.16 E_c^{1/2} \text{ (ft/sec)} \quad (3-21)$$

and the modulus of elasticity E_c is defined to be

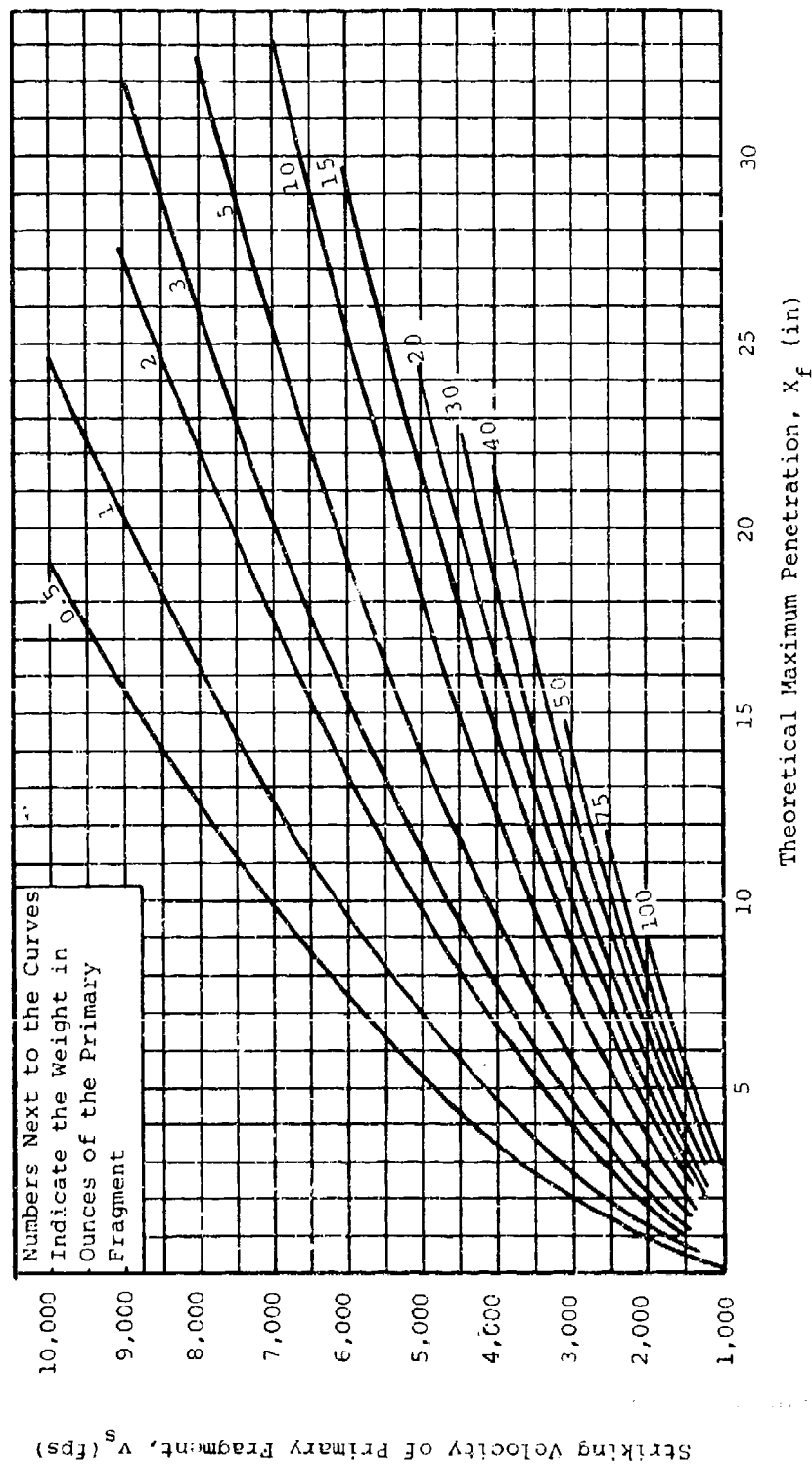


Figure 3-17. Fragment Penetration of 5,000 psi Concrete (Ref. 3-2)

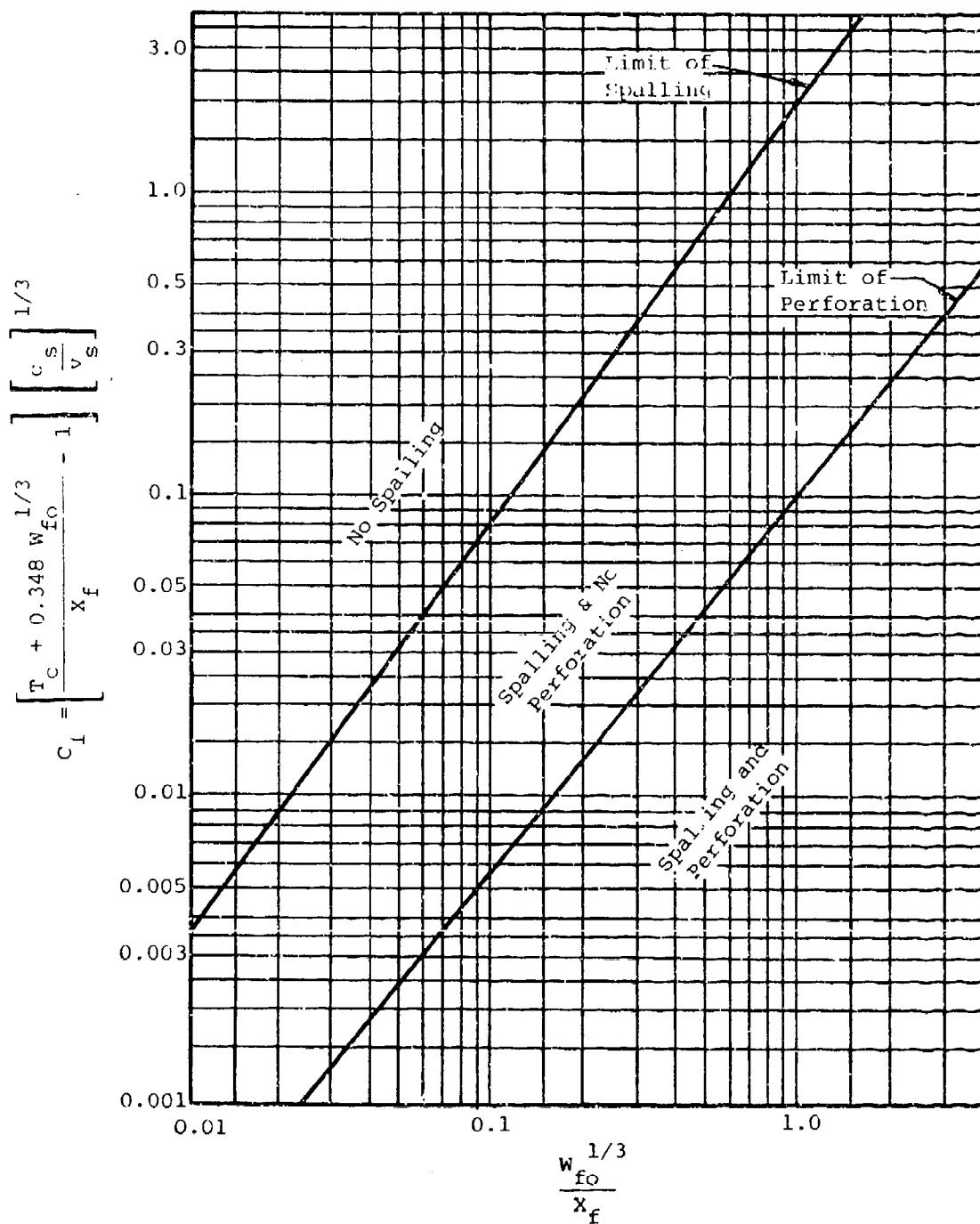


Figure 3-18. Limits of Concrete Spalling and Perforation (Ref. 3-2)

$$E_c = 33w^{1.5} \sqrt{f'_c} \quad (\text{psi}) \quad (3-22)$$

where

w = weight density of concrete, lb/ft³

f'_c = static unconfined compressive strength of concrete, psi

Fragments which perforate a concrete element will have a residual velocity v_r which may endanger the receiver system. The magnitude of this velocity may be approximated from the expression which defines the velocity of the fragment at any time as it penetrates the concrete, i.e.,

$$\left(\frac{v_r}{v_s} \right)^{1.8} = 1 - \frac{T_c}{X_f} \quad (3-23)$$

where

T_c = thickness of concrete element, inches

v_r = residual velocity of the fragment as it leaves the concrete element, fps

Equation 3-23 applies when the depth of penetration is greater than 2 fragment diameters. If the depth of penetration is less than 2 fragment diameters, Ref. 3-45 recommends

$$\left(\frac{v_r}{v_s} \right)^{1.8} = 1 - \left(\frac{T_c}{X_f} \right)^2 \quad (3-24)$$

This handbook does not include procedures for estimating fragment diameters. If other information on fragment size is not available, it is recommended that Eq. 3-24 be used to estimate the fragment residual velocity. Plots of the ratio v_r/v_s against T_c/X_f are given in Fig. 3-19.

b. Other Fragments

To estimate the concrete penetration of metal

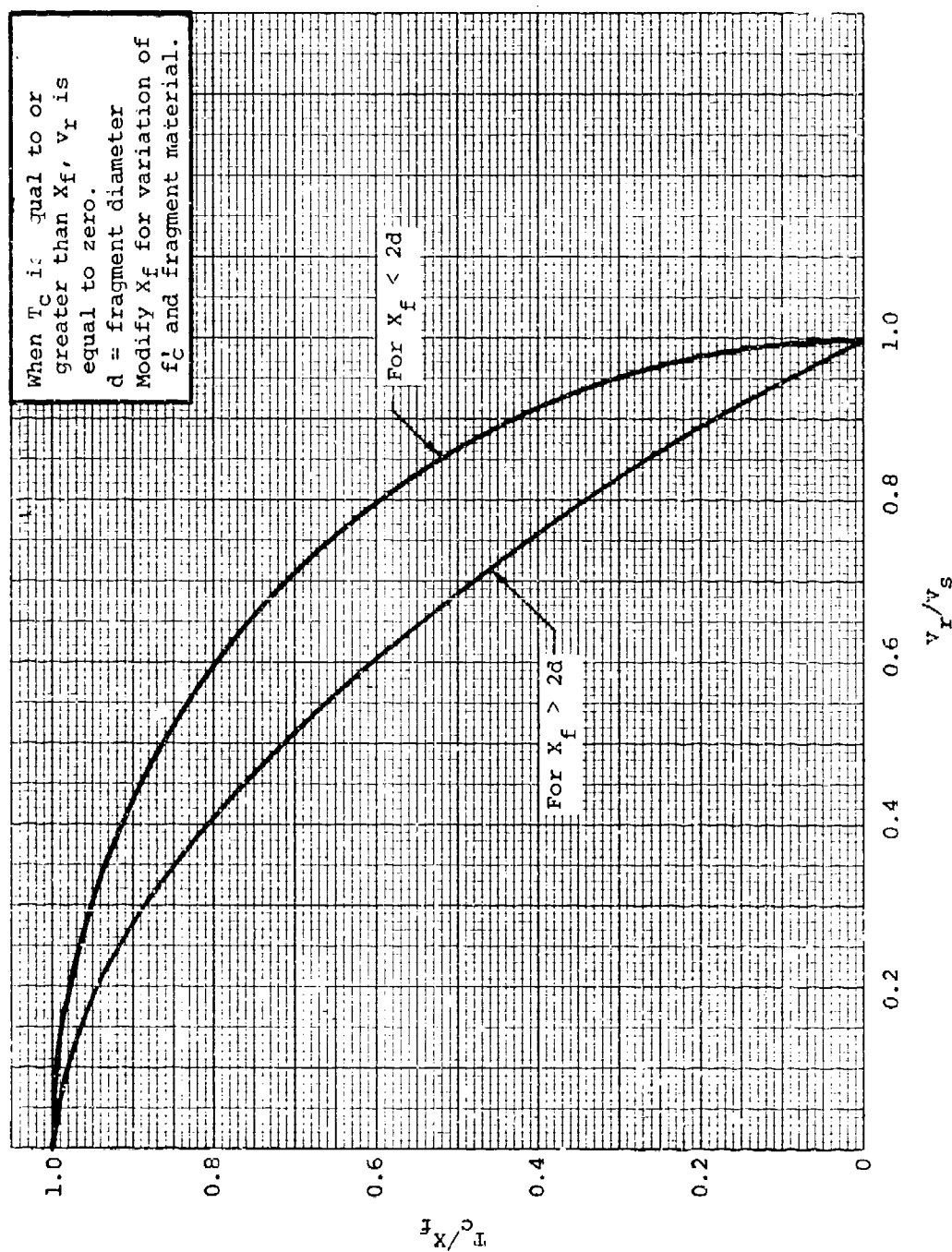


Figure 3-19. Residual Velocity of Primary Fragment After Perforation
 (Refs. 3-2 and 3-45)

fragments other than armor piercing, a procedure has been developed to relate the concrete penetrating capabilities of such fragments to those of armor-piercing fragments. This relationship is expressed in terms of relative metal hardness (the ability of the metal to resist deformation) and density, and is represented by constant C_2 in Eq. 3-25 (Ref. 3-2)

$$X_f' = C_2 X_f \quad (3-25)$$

where

X_f' = maximum penetration in concrete of metal fragments other than armor-piercing

The numerical values of C_2 for several of the more common casing metals are listed below:

<u>Type of Metal</u>	<u>C_2</u>
Armor-piercing steel.	1.00
Mild steel.	0.70
Lead.	0.50
Aluminum.	0.25

3.9 FIREBALL AND THERMAL ENVIRONMENT

The fireball and thermal environment resulting from an accidental explosion or deflagration can conceivably create as much damage as blast and fragmentation. An equally important function of a suppressive shield, therefore, is to suppress or attenuate the fireball and thermal environment to acceptable levels as well as blast and fragments.

The following expressions from Ref. 3-46 can be used to estimate the diameter and time of duration of a fireball in free air.

$$D_f = 9.56W^{0.325} \quad (3-26)$$

$$t_f = 0.196W^{0.349} \quad (3-27)$$

where

D_f = fireball diameter, ft

t_f = fireball time of duration, sec

W = charge weight, lb

Suppressive shields shall be designed to limit exposure of personnel to a critical heat flux value based on total time of exposure (Ref. 3-47). This value of heat flux shall be determined by

$$f = 0.62/t^{0.7423} \quad (3-28)$$

where

f = heat flux, cal/cm²-sec

t = total time of exposure, sec

Unfortunately, there are no methods currently available with which attenuation of the fireball/thermal environment by a suppressive shield can be predicted. Until such time as proven analytical prediction methods do become available, demonstration of the ability of a suppressive shield design to satisfy the criteria of Eq. 3-28 will require an experimental program. Guidelines for planning and conducting the necessary experimental program are presented in Ref. 3-47.

All safety approved suppressive shields suppress the fireball to acceptable levels and can be used where fireball suppression is required.

3.10 ILLUSTRATIVE EXAMPLES

3.10.1 Shield Group 4 Airblast Loading Parameters

a. Given

The Shield Group 4 design features and charge weights shown in Table A-4. Summarizing, the interior dimensions for airblast calculations are 9.48 feet high x 9.66 feet wide x 14.56 feet long; the design charge weight is 9 pounds of 50/50 Pentolite; the proof charge weight is 11.25 pounds of 50/50 Pentolite.

The roof and wall are almost the same distance from the charge. Although the roof is a little closer than the wall, it is significantly stronger because of additional cross bracing and smaller panels. Therefore, this analysis will be concerned with the wall, since that is the most vulnerable member.

b. Find

The reflected pressure and the reflected impulse on the shield sidewall and the peak quasi-static pressure for both the design and proof charge weights.

c. Solution

First, convert the Pentolite charge weights to equivalent weights of TNT with Table 3-1.

$$\text{Design : } 9 \text{ lb} \times 1.129 = 10.16 \text{ lb TNT}$$

$$\text{Proof : } 11.25 \times 1.129 = 12.70 \text{ lb TNT}$$

Next, determine the scaled distance from the charge, which is centrally located within the shield, to the nearest sidewall with Eq. 3-2, pg. 3-6. The distance R to the nearest wall for both charge weights is $9.66/2 = 4.83 \text{ ft.}$

$$\text{Design : } Z = 4.83/(10.16)^{1/3} = 2.23 \text{ ft/lb}^{1/3}$$

$$\text{Proof : } Z = 4.83/(12.70)^{1/3} = 2.07 \text{ ft/lb}^{1/3}$$

Enter Fig. 3-6 with these values for Z and read

$$\text{Design : } \underline{P_r} = 1150 \text{ psi}$$

$$i_r/W^{1/3} = 6.8 \times 10^{-2} \text{ psi-sec/lb}^{1/3}$$

$$\underline{i_r} = 147 \text{ psi-ms}$$

$$\text{Proof : } \underline{P_r} = 1480 \text{ psi}$$

$$i_r/W^{1/3} = 7.3 \times 10^{-2} \text{ psi-sec/lb}^{1/3}$$

$$\underline{i_r} = 170 \text{ psi-ms}$$

The charge to volume ratio is needed to compute the peak quasi-static pressure. The volume is

$$V = 9.48 \times 9.66 \times 14.56 = 1333.4 \text{ ft}^3$$

The charge to volume ratios are

$$\text{Design : } 10.16/1333.4 = 0.0076 \text{ lb/ft}^3$$

$$\text{Proof : } 12.70/1333.4 = 0.0095 \text{ lb/ft}^3$$

Enter Fig. 3-9 with these values of W/V and read

$$\text{Design : } \underline{P_{gs}} = 62 \text{ psi}$$

$$\text{Proof : } \underline{P_{gs}} = 70 \text{ psi}$$

3.10.2 Shield Group 4 Effective Vent Area Ratio

a. Given

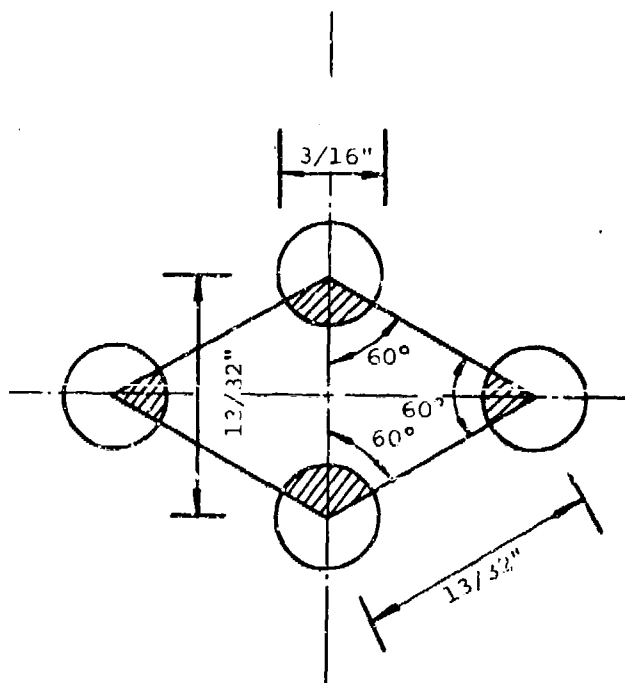
The Shield Group 4 design as shown in Fig. A-5.

b. Find

The effective vent area ratio, α_e , for the shield.

c. Solution

The Group 4 panel cross section contains six layers of baffle elements as shown schematically in Fig. A-4. It can be determined from Fig. A-5 that the perforations of the 3/16-inch plates consist of 3/16-inch diameter holes on a 60 degree staggered pattern at 13/32-inch centers; see following sketch.



Group 4 Shield Panel Plate Perforation Pattern

Referring to the sketch, the ratio of the perforations to the solid plate can be found to be

$$\alpha = \frac{0.25\pi(0.1875)^2}{(4)(0.5)(0.406\sin 60^\circ)(0.203)} = 0.193$$

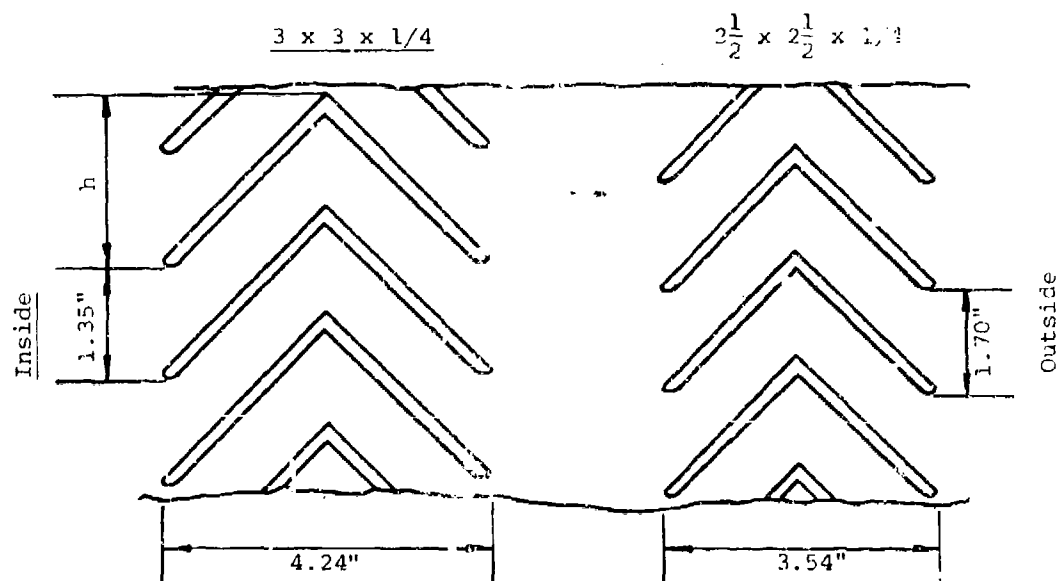
The exposed perforated plate area between columns and mounting bracket angles can be estimated to be 45 x 111 inches and the gross panel area can be taken as 55 x 111 inches; see Fig. A-5. The vent area ratio for the perforated plate panel is, therefore,

$$\alpha_1 = \frac{A_{v1}}{A_w} = \frac{(0.193)(4995)}{6105} = 0.158$$

The vent area for the nested angles can be determined by

$$A_v = nla/N$$

as shown in Fig. 3-7. The nested angle geometry is illustrated below.



Group 4 Shield Panel Nested Angle Geometry

From Fig. A-5d, it can be seen that one half-panel has 42 stacked $3 \times 3 \times 1/4$ angles; this makes the number of openings $n = 41$ for a half-panel and $n = 82$ for the full panel. The exposed length of the angles is 45 inches as shown on Fig. A-5d. The projected width of the $3 \times 3 \times 1/4$ angles is

$$h = 3\sin 45^\circ = 2.12 \text{ inches}$$

and the opening is 1.35 inches as shown on the above sketch. The number of openings per projected width is $2.12/1.35 = 1.57$, which is near 2, so take $N = 4$ as per Fig. 3-7. The distance between the angles is

$$a = 1.35\sin 45^\circ = 0.95 \text{ inches}$$

The vent area for the 3 x 3 x 1/4 angles is, therefore,

$$A_{v2} = (82)(45)(0.95)/4 = 876.4 \text{ in.}^2$$

It can be determined from Fig. A-5 that L = 111 inches and M = 55 inches, resulting in $A_w = (111)(55) = 6105 \text{ in.}^2$ and

$$\alpha_2 = A_{v2}/A_w = 876.4/6105 = 0.144$$

Going through the above steps for the 2-1/2 x 2-1/2 x 1/4 angle geometry leads to

$$\alpha_3 = \frac{A_{v3}}{A_w} = \frac{(66)(45)(1.20)/2}{6105} = 0.292$$

As may be seen in Fig. A-4, there are four perforated plates (α_1) and one layer each of the 3 x 3 and 2-1/2 x 2-1/2 angles (α_2, α_3). The effective vent area ratio by Eq. 3-5, pg. 3-17 is

$$\frac{1}{\alpha_e} = \frac{4}{0.158} + \frac{1}{0.144} + \frac{1}{0.292} = 35.7$$

$$\underline{\underline{\alpha_e = 0.03}}$$

The effective vent area ratio calculated above is actually for one full panel of the Shield Group 4 design. Due to the way α_e was calculated, however, with the wall area A_w taken as center to center of the columns, $\alpha_e = 0.03$ for the entire shield. The venting area blocked by the longitudinal roof beam (see Fig. A-6a) could be subtracted from the overall vented area (the walls and roof), but the effect on α_e is negligible in this case.

3.10.3 Shield Group 4 Design Blowdown Time and External Pressure

a. Given

The Shield Group 4 design as shown in Fig. A-5.

b. Find

The blowdown time and the incident overpressure at a point 19 feet from the exterior shield wall for the design charge weight.

c. Solution

The design quasi-static pressure found in paragraph 3.10.1 above is 62 psi. Find \bar{P} with which to enter Fig. 3-10.

$$\bar{P} = \frac{P_{qs} + P_o}{P_o} = \frac{62 + 15}{15} = 5.13$$

Enter Fig. 3-10 with $\bar{P} = 5.13$ and find

$$\frac{t_b a_o \alpha_e A_i}{V} = 0.77$$

Take

$$a_o = 1117 \text{ fps (par. 3.5.2)}$$

$$\alpha_e = 0.03 \text{ (par. 3.10.2)}$$

$$V = 1333.4 \text{ ft}^3 \text{ (par. 3.10.1)}$$

$$\begin{aligned} A_i &= 2(9.48)(14.56) + 2(9.48)(9.66) + (9.66)(14.56) \\ &= 599.9 \text{ ft}^2 \end{aligned}$$

Then,

$$t_b = \frac{(0.77)(1333.4)}{(1117)(0.03)(599.9)} = 0.051 \text{ sec}$$

$$\underline{\underline{t_b = 51 \text{ ms}}}$$

The peak incident pressure 19 feet outside the shield can be found with Eq. 3-7, pg. 3-27. Take $R = 4.83 + 19 = 23.83$, say 24 ft. Then

$$z = 24/(10.16)^{1/3} = 11.08 \text{ ft/lb}^{1/3}$$

for the design charge weight. Take

$$X = (9.66 \times 14.56)^{1/2} = 11.86 \text{ ft}$$

and $\alpha_e = 0.03$ as before. From Eq. 3-7,

$$P_{so} = 957 \left(\frac{1}{11.08} \right)^{1.66} \left(\frac{24}{11.86} \right)^{0.27} (0.03)^{0.64}$$

$$\underline{P_{so} = 2.3 \text{ psi}}$$

3.10.4 Primary Fragment Mass and Velocity

a. Given

A cylindrical cased explosive charge loaded with TNT. The charge weight W is 0.191 lb; the case weight W_c is 4.2 lb; the case thickness t is 0.5 inches; and the internal case diameter d_i is 2.0 inches.

b. Find

The weight and initial velocity of the largest expected primary fragment.

c. Solution

The weight of the largest expected primary fragment can be estimated with Eq. 3-9, pg. 3-30. Go to Table 3-2 and find that the constant $B = 0.0779$ for TNT. Then, calculate

$$C = \left[(0.0779) (0.5)^{5/6} (2.0)^{1/3} (1 + 0.5/2.0) \right]^2$$

$$C = 0.00474 \text{ lb}$$

With Eq. 3-9, estimate the largest primary fragment weight to be

$$W_f = 0.00474 \left[\ln \left(\frac{4.2}{2 \times 0.00474} \right) \right]^2$$

$$\underline{W_f = 0.176 \text{ lb}}$$

The primary fragment initial velocity can be estimated with Eq. 3-10, pg. 3-30. First, find the Gurney energy

constant for TNT in Table 3-3 to be 7780 fps. Then, from Eq. 3-10,

$$v_o = 7780 \left[\frac{0.191/4.2}{1 + 0.191/(2)(4.2)} \right]^{1/2}$$

$$\underline{v_o = 1640 \text{ fps}}$$

3.10.5 Secondary Fragment Velocity

a. Given

A front roller support axle for the 105-mm projectile fuze insert and torquing machinery would be a typical secondary fragment. The axle is located side-on to the projectile; is cylindrical in shape with a circular area of 0.194 in²; has a length of 2.74 inches and weighs 0.15 lb. The equivalent spherical charge of Comp B has a radius R_e of 2.57 inches and the range R from the center of the equivalent charge to the edge of the axle is 3.89 inches.

b. Find

The initial velocity of the axle as a secondary fragment.

c. Solution

The initial velocity will be estimated with Eq. 3-11, pg. 3-32. Establish that

$$g_s = \pi/4 = 0.785$$

$$M = 0.15/386 = 0.000389 \text{ lb-sec}^2/\text{in}$$

$$R_e/R = 2.57/3.89 = 0.66$$

The estimated initial velocity of the secondary fragment by Eq. 3-11 is

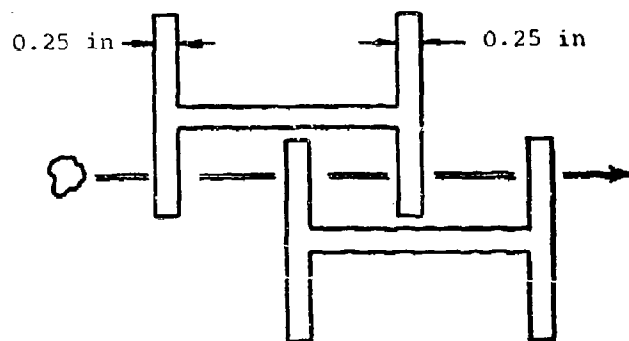
$$v_{os} = \frac{(0.194)(2.57)(0.785)}{0.000389} [(0.556)(0.66) + (2.75)(0.66)^2]$$

$$\underline{v_{os} = 1575 \text{ fps}}$$

3.10.6 Fragment Impact on Shield Group 3 Wall Panel

a. Given

The compact mild steel primary fragment predicted in paragraph 3.10.4 striking the Shield Group 3 wall panel as shown in the following sketch.



Shield Group 3 Wall Panel Geometry

The fragment is blunt and of roughly cylindric shape so that the length to diameter ratio is $L/D = 1.0$. The fragment threat parameters for the first element are

$$W_s = 0.176 \text{ lb}$$

$$v_s = 1640 \text{ fps}$$

$$\theta = 0^\circ$$

$$\phi = 0^\circ$$

$$t = 0.25 \text{ inches}$$

$$A_p = 0.674 \text{ in}^2$$

$$L = 0.926 \text{ inches}$$

b. Find

The penetration depth of the impacting fragment.

c. Solution

To determine the constants used for estimating the limit velocity for the first panel, the ratio $t/(R\sqrt{A_p})$ is calculated. The perforation factor R is one for solid plate.

$$\frac{t}{R\sqrt{A_p}} = \frac{0.25}{1.0\sqrt{0.674}} = 0.305$$

Using Table 3-5 and Eq. 3-12, pg. 3-39, the limit velocity is

$$v_l = \frac{1414}{\sqrt{0.176}} (0.674)^{0.295} (0.25 \sec 0^\circ)^{0.910}$$

$$v_l = 849 \text{ fps}$$

To calculate the residual velocity, first find

$$x = \frac{v_s}{v_l} - 1 = \frac{1640}{849} - 1 = 0.932$$

Then, using Eq. 3-14, pg. 3-41 and the constants in Table 3-6, the residual velocity is

$$v_r = 849 \left[\frac{1.12(0.932)^2 + 0.52(0.932) + 1.29(0.932)^{1/2}}{1.932} \right]$$

$$v_r = 1188 \text{ fps}$$

The term β could be set to unity to obtain a quick overestimate of residual velocity. However, to get a more accurate result, β is calculated as defined under Eq. 3-14. (Take the density of solid steel plate as 0.284 lb/in^3).

$$\beta = \frac{1}{[1 + (0.284)(0.674)(0.25)/0.176]^{1/2}} = 0.887$$

and the residual velocity becomes 1050 fps.

To estimate the residual weight, first determine the critical angle for shatter ϕ_c from Eq. 3-15, pg. 3-43.

$$\phi_c = \arcsin\left[\frac{1640\cos 0^\circ}{18010}\right] = 5.22^\circ$$

Since $\phi < \phi_c$, the impact is considered flat, and the critical velocity for shatter must be found with Eq. 3-16, pg. 3-43.

$$v_{cr} = 2000/\cos 0^\circ = 2000 \text{ fps}$$

Since $v_s < v_{cr}$, the velocity is insufficient for shatter, and the deformation mass loss equations must be used. The first step is to calculate the correlational velocity v_{co} from Eq. 3-18, pg. 3-44.

$$v_{co} = \frac{1640}{1 + \frac{\cos 0^\circ}{\frac{(0.6)(0.25)(0.284)(0.674)}{0.176} + 0.15}}$$

$$v_{co} = 391 \text{ fps}$$

This velocity is less than the threshold velocity for any deformation to occur (700 fps), so the residual mass is unchanged, i.e.,

$$W_r = W_s$$

The fragment threat parameters for the second element thus become

$$W_s = 0.176 \text{ lb}$$

$$v_s = 1050 \text{ fps}$$

$$\theta = 0^\circ$$

$$\phi = 0^\circ$$

$$t = 0.25 \text{ inches}$$

$$A_p = 0.674 \text{ in}^2$$

$$L = 0.926 \text{ inches}$$

All parameters remain unchanged from the initial conditions, except for the striking velocity, v_s . The striking velocity does not enter the limit velocity expression, Eq. 3-12, pg. 3-39, so v_l is the same as for the first element. Determine the residual velocity quantity

$$x = \frac{1050}{849} - 1 = 0.237$$

Then, since $\beta = 0.887$ as before, the residual velocity after perforating the second element is

$$v_r = (849)(0.887) \left[\frac{1.12(0.237)^2 + 0.52(0.237) + 1.29(0.237)^{1/2}}{1.237} \right]$$

$$v_r = 496 \text{ fps}$$

Since the velocity of the fragment leaving the second element is less than the limit velocity of the next element, $v_r = 496 \text{ fps} < v_l = 849 \text{ fps}$, the fragment will be defeated by the third element of the shield wall panel shown in the sketch on pg. 3-60.

3.10.7 Fragment Impact on Shield Group 4 Panel

a. Given

The secondary fragment predicted in paragraph 3.10.5 striking the Shield Group 4 panel shown in Fig. A-4. The fragment is assumed to strike end-on with zero obliquity. The pertinent features of the panel section shown in Fig. A-4 are summarized in the following table (pg. 3-64).

The fragment threat parameters for the first element are

$$W_s = 0.15 \text{ lb}$$

$$v_s = 1575 \text{ fps}$$

$$\theta = 0^\circ$$

$$\phi = 0^\circ$$

Shield Group 4 Panel Features

Element No.	t (in)	θ (deg)	Type Element
1	0.188	0	Perforated
2	0.25	45	Solid
3	0.25	45	Solid
4	0.188	0	Perforated
5	0.168	0	Perforated
6	0.188	0	Perforated
7	0.25	45	Solid
8	0.25	45	Solid

$$t = 0.188 \text{ inch}$$

$$A_p = 0.194 \text{ in}^2$$

$$L = 2.74 \text{ inches}$$

$$D = 0.50 \text{ inch}$$

b. Find

The depth to which the fragment penetrates the panel.

c. Solution

First, determine R for the first element, which is a perforated plate. It was found in paragraph 3.10.2 that the vent area ratio α for the Group 4 perforated plate was 0.193. From Fig. 3-16, $R = 0.54$ for $\alpha = 0.193$ and a hexagonal array (Eq. 3-13, pg. 3-41, could also be used to determine R). Since $L/D = 2.74/0.50 = 5.5$, use the long rod ($L/D > 5$) constants from Table 3-5 to find the limit velocity. Recall that $R^2 A_p$ is substituted for A_p in Eq. 3-12, pg. 3-39, for perforated plates.

$$v_l = \frac{1261}{\sqrt{0.15}} [(0.54)^2 (0.194)]^{0.427} (0.189 \sec 0^\circ)^{0.647}$$

$$v_l = 324 \text{ fps}$$

The quantity x needed to compute the residual velocity is

$$x = \frac{1575}{324} - 1 = 3.86$$

and the residual velocity from Eq. 3-14, pg. 3-41, with the long rod ($L/D > 5$) constants from Table 3-6 is

$$v_r = (324)(1) \left[\frac{1.1(3.86)^2 + 0.80(3.86) + 1.45(3.86)^{1/2}}{4.86} \right]$$

$$= 1483 \text{ fps}$$

Since $\phi = 0^\circ$, the impact is flat. The critical velocity for shatter, Eq. 3-16, pg. 3-43, is

$$v_{cr} = 2000 / \cos 0^\circ = 2000 \text{ fps}$$

and $v_s < v_{cr}$. Compute the correlational velocity with Eq. 3-18, pg. 3-44. The density γ in Eq. 3-18 is reduced to take account of the perforations in the plate, i.e., $\gamma = (0.284)(0.807) = 0.229 \text{ lb/in}^3$.

$$v_{co} = \frac{1575}{1 + \frac{\cos 0^\circ}{\frac{(0.6)(0.188)(0.229)(0.194)}{0.15} + 0.15}}$$

$$v_{co} = 244 \text{ fps}$$

Since $v_{co} < 700 \text{ fps}$, no mass loss occurs.

The fragment threat parameters for the second element are

$$W_s = 0.15 \text{ lb}$$

$$v_s = 1488 \text{ fps}$$

$$\theta = 45^\circ$$

$$\phi = 45^\circ$$

$$t = 0.25 \text{ inch}$$

$$A_p = 0.194 \text{ in}^2$$

$$L/D = 5.5$$

$$R = 1.0$$

The limit velocity for the second element with Eq. 3-12, pg. 3-39, and the long rod constants from Table 3-5 thus becomes

$$v_\ell = \frac{1261}{\sqrt{0.15}} (0.194)^{0.427} (0.25 \sec 45^\circ)^{0.647}$$

$$v_\ell = 825 \text{ fps}$$

Calculate the residual velocity as before.

$$x = \frac{1488}{825} - 1 = 0.80$$

$$v_r = (825)(1) \left[\frac{1.1(0.80)^2 + 0.80(0.80) + 1.45(0.80)^{1/2}}{1.80} \right]$$

$$v_r = 1210 \text{ fps}$$

The critical angle for shatter is

$$\phi_c = \arcsin \left[\frac{1488 \cos 45^\circ}{18010} \right] = 3.35^\circ$$

Since $\phi > \phi_c$, the impact is a corner or edge impact, and the fragment is in the deformation mass loss mode. The correlational velocity is

$$v_{co} = \frac{1488}{1 + \frac{\cos 45^\circ}{\frac{0.6(0.25)(0.284)(0.194)}{0.15} + 0.15}}$$

$$v_{co} = 335 \text{ fps}$$

The correlational velocity is too small for any mass loss, i.e., $v_{co} < 700 \text{ fps}$. Since the remaining elements are identical to

either the first or second element, and since the striking velocities must be less than those for the first two, the correlational velocities for all remaining elements will also be too small for any mass loss. Therefore, the mass of this fragment remains unchanged after every impact.

Consequently, only residual velocity calculations need be repeated until it is found that the residual velocity after perforating an element is less than the limit velocity of the next element. The results of these calculations are summarized below.

Element No. 3

$$v_s = 1210 \text{ fps}$$

$$v_l = 825 \text{ fps}$$

$$x = 0.47$$

$$v_r = 906 \text{ fps}$$

Element No. 4

$$v_s = 906 \text{ fps}$$

$$v_l = 324 \text{ fps}$$

$$x = 1.80$$

$$v_r = 804 \text{ fps}$$

Element No. 5

$$v_s = 804 \text{ fps}$$

$$v_l = 324 \text{ fps}$$

$$x = 1.48$$

$$v_r = 700 \text{ fps}$$

Element No. 6

$$v_s = 700 \text{ fps}$$

$$v_l = 324 \text{ fps}$$

$$x = 1.16$$

$$v_r = 595 \text{ fps}$$

Recall that Element No. 7 has the same features as Element Nos. 2 and 3, i.e., a limit velocity of 825 fps. Since the striking velocity on Element No. 7 is only 595 fps, it is predicted that the fragment is stopped at Element No. 7.

3.11 LIST OF SYMBOLS

a	Equation constant
a	Speed of sound in air at sea level (ft/sec)
A	Open area of louvre (in ²)
A _i	Internal surface area of suppressive shield (ft ²)
A _O	Equation constant
A _P	Area of fragment (in ²)
A _V	Vent area (in ²)
A _{vi}	Vent area for i-th layer of wall (in ²)
A _w	Area of wall (in ²)
A _{wi}	Area of i-th layer of wall (in ²)
b	Equation constant
B	Explosive constant (lb ^{1/2} inches ^{-7/6})
c	Equation constant
c _p	Velocity of sound in metal plate (ft/sec)
c _s	Dilatational velocity of elastic wave through concrete (ft/sec)
C, C ₁ , C ₂ , C ₃ , ...,	Equation constants
d _c	Charge diameter (inches)
d _{co}	Diameter of core element (inches)
d _i	Inside diameter (inches)
d _p	Diameter of perforations (inches)
D	Diameter (inches)
D _f	Fireball diameter (ft)
e _t	TNT equivalent factor
E _c	Modulus of elasticity of concrete (psi)
f	Heat flux (cal/cm ² -sec)
f' _c	Static unconfined compressive strength of concrete (psi)
g	Equation constant (Table 3-4)
g _s	Shape factor
h	Projected width (inches)
h _p	Center-to-center distance between perforations (inches)

i_r	Reflected pressure impulse (psi-sec)
i_s	Positive incident impulse (psi-sec)
l, L	Length (inches)
m	Equation constant
M	(1) Mass of secondary fragment (lb-sec ² /in) (2) Panel width (inches)
n	(1) Number of items or openings (2) Number of different types or sizes of panel members (3) Equation constant
N	Equation constant
$p(t)$	Pressure as a function of time (psi)
P_o	Ambient pressure at sea level (psi)
P_{qs}	Peak quasi-static pressure (psi)
P_r	Peak reflected overpressure (psi)
P_{so}	Peak positive incident pressure (psi)
P_{so}^-	Peak negative incident pressure (psi)
R	(1) Distance from the center of the explosive source to the point of interest (ft, inches) (2) Perforation factor
R_e	Radius of spherical explosive source (inches)
t	(1) Time (sec) (2) Thickness (inches)
t_a	Shock front arrival time (sec)
t_b	Duration of quasi-static pressure (sec)
t_f	Duration of fireball (sec)
t_o	Duration of positive pressure pulse (sec)
t_o^-	Duration of negative pressure pulse (sec)
t_r	Duration of positive reflected pressure (sec)
T_c	Thickness of concrete element (inches)
u_s	Incident particle velocity (ft/sec)
U	Airblast shock front velocity (ft/sec)
v_{co}	Correlational velocity (ft/sec)
v_{cr}	Critical velocity (ft/sec)
v_l	Ballistic limit velocity (ft/sec)

v_o	Initial primary fragment velocity (ft/sec)
v_{os}	Initial velocity of secondary fragment (in/sec)
v_r	Residual velocity of fragment (ft/sec)
v_s	Striking velocity of fragment (ft/sec)
V	Volume (ft ³)
w	Unit weight of concrete (lb/ft ³)
W	Charge weight of explosive (lbs)
W_c	Weight of casing (lbs)
W_{cl}, W_{c2}	Weight of sandwich plates (lbs)
W_{co}	Weight of core element (lbs)
W_e	Effective charge weight in pounds of TNT
W_f	Weight of fragment (lbs)
W_{fo}	Weight of fragment (oz)
W_r	Residual weight of fragment (lbs)
W_s	Striking weight of fragment (lbs)
W_{TNT}	Equivalent charge weight of TNT (lbs)
x	Equation parameter
X	Characteristic length of structure (ft)
x_i	Maximum penetration depth in concrete of armor piercing fragment (inches)
x'_f	Maximum penetration depth in concrete of other than armor piercing fragment (inches)
Z	Scaled distance (ft/lb ^{1/3})
α_e	Vent area ratio of shield
α_i	Vent area ratio for single layer of multiple layer wall
β	Equation coefficient
γ	Density of target plate (lb/in ³)
θ	Angle of obliquity (degrees)
λ	Scalar multiplier
ϕ	Orientation angle (degrees)
ϕ_c	Critical orientation angle (degrees)
$\sqrt{2E'}$	Gurney energy constant (ft/sec)

3.12 REFERENCES

- 3-1 Engineering Design Handbook: Explosions in Air, Part I, AMC Pamphlet 706-181, Headquarters U.S. Army Materiel Command, Latest Edition. (U)
- 3-2 Structures to Resist the Effects of Accidental Explosions, TM5-1300, Department of the Army, Washington, D.C., June 1969. (U)
- 3-3 Crawford, R.E., Higgins, C.J. and Bultmann, E.H., The Air Force Manual for Design and Analysis of Hardened Structures, AFWL TR 74-102, Air Force Weapons Laboratory, Kirtland AFB, N.M., October 1974. (U)
- 3-4 Tomlinson, W.R., Jr. and Sheffield, O.E., Engineering Design Handbook, Properties of Explosives of Military Interest, AMC Pamphlet No. 706-177, Headquarters, U.S. Army Materiel Command, January 1971. (U)
- 3-5 Safety Criteria for Modernization and Expansion Projects, DRCPM-PBM Memorandum No. 385-3, Latest Edition. (U)
- 3-6 Napadensky, H. and Swatosh, J., TNT Equivalency of Black Powder, (Vol I & II) IITRI TR J6265-3, IIT Research Institute, Chicago, Ill., September 1972. (U)
- 3-7 Swatosh, J. and Napadensky, H., TNT Equivalency N-5 Slurry and Paste, IITRI TR J6278, IIT Research Institute, Chicago, Ill., September 1972. (U)
- 3-8 Swatosh, J. and Napadensky, H., TNT Equivalency of Nitroglycerine, IITRI TR J6312, IIT Research Institute, Chicago, Ill., September 1973. (U)
- 3-9 Napadensky, H. and Swatosh, J., TNT Equivalency of Large Charges of Black Powder, IITRI TR J6289-4, IIT Research Institute, Chicago, Ill., February 1974. (U)
- 3-10 Napadensky, H., Swatosh, J., Humphreys, A., and Rindner, R., TNT Equivalency Three Pyrotechnic Composition, PA TR 4628, Picatinny Arsenal, Dover, N.J., June 1974. (U)
- 3-11 Levmore, S., Air Blast Parameters and Other Characteristics of Nitroguanidine and Guanidine Nitrate, PA TR 4865, Picatinny Arsenal, Dover, N.J., November 1975. (U)

- 3-12 Swatosh, J., et al, and Levmore, S., Blast Parameters of Lead Styphnate, Lead Azide, and Tetracene, PA TR 4900, Picatinny Arsenal, Dover, N.J., December 1974. (U)
- 3-13 Swatosh, J., et al, and Price, P., TNT Equivalency of M1 Propellant (Bulk), PA TR 4885, Picatinny Arsenal, Dover, N.J., December 1975. (U)
- 3-14 Swatosh, J., Cook, J., and Price, P., Blast Parameters of M26E1 Propellant, PA TR 4901, Picatinny Arsenal, Dover, N.J., December 1976. (U)
- 3-15 Kingery, C.N., Air Blast Parameters Versus Distance for Hemispherical TNT Surface Bursts, BRL Report No. 1344, Aberdeen Proving Ground, Maryland, September 1966. (U)
- 3-16 Petes, J., "Blast and Fragmentation Characteristics," Annals of the New York Academy of Sciences, Vol. 152, Article 1, October 1968, pp. 283-317. (U)
- 3-17 Swisdak, M.M., Jr., Explosion Effects and Properties: Part I - Explosion Effects in Air, NSWC/WOL/TR 75-116, Naval Surface Weapons Center, White Oak, Silver Spring, Maryland, October 1975. (U)
- 3-18 Gregory, F.H., Analysis of the Loading and Response of a Suppressive Shield When Subjected to an Internal Explosion, Minutes of the 17th Explosive Safety Seminar, Denver, Colorado, September 1976. (U)
- 3-19 Esparza, E.D., Baker, W.E., and Oldham, G.A., Blast Pressures Inside and Outside Suppressive Structures, EM-CR-76042, Report No. 8, Edgewood Arsenal, Aberdeen Proving Ground, Maryland, December 1975. (U)
- 3-20 Kingery, C.N., Schumacher, R.N., and Ewing, W.O., Jr., Internal Pressures from Explosions in Suppressive Structures, BRL Interim Memorandum Report No. 403, Aberdeen Proving Ground, Maryland, June 1975. (U)
- 3-21 Schumacher, R.N., Kingery, C.N., and Ewing, W.O., Jr., Airblast and Structural Response Testing of a 1/4 Scale Category 1 Suppressive Shield, BRL Memorandum Report No. 2623, Aberdeen Proving Ground, Maryland, May 1976. (U)
- 3-22 Weibull, H.R.W., Pressures Recorded in Partially Closed Chambers at Explosion of TNT Charges, Annals of the New York Academy of Sciences, 152, Art. 1, pp. 356-361, October 1968. (U)

- 3-23 Keenan, W.A. and Tancreto, J.E., Blast Environment from Fully and Partially Vented Explosions in Cubicles, Technical Report R828, Civil Engineering Laboratory, Naval Construction Battalion Center, Port Hueneme, California, November 1975. (U)
- 3-24 Zilliagus, S., Phyllaier, W.E., and Shorrow, P.K., The Response of Clamped Circular Plates to Confined Explosive Loadings, Naval Ship R&D Center Report 3987, NSRDC, Bethesda, Maryland, February 1974. (U)
- 3-25 Kinney, G.F. and Sewell, R.G.S., Venting of Explosions, Naval Weapons Center, NWC Technical Memorandum 2448, China Lake, California, July 1974. (U)
- 3-26 Baker, W.E. and Oldham, G.A., Estimates of Blowdown of Quasi-Static Pressures in Vented Chambers, EM-CR-76029, Report No. 2, Edgewood Arsenal, Aberdeen Proving Ground, Maryland, November 1975. (U)
- 3-27 Oertel, F.H., Jr., Evaluation of Simple Models for the Attenuation of Shock Waves by Vented Plates, BRL Report No. 1906, Aberdeen Proving Ground, Maryland, August 1976. (U)
- 3-28 Proctor, J.F. and Filler, W.S., A Computerized Technique for Blast Loads from Confined Explosions, 14th Annual Explosives Safety Seminar, New Orleans, Louisiana, 8-10 November 1972, pp. 99-124. (U)
- 3-29 Proctor, J.F., Internal Blast Damage Mechanisms Computer Program, 61 JTCG/ME-73-3, Joint Technical Coordinating Group for Munitions Effectiveness, April 1973. (U)
- 3-30 Proctor, J.F., Blast Suppression/Predictive Model, WBS 4333, Monthly Technical Report, November 1975, Naval Surface Weapons Center, White Oak, Silver Spring, Maryland. (U)
- 3-31 Lasseigne, A.H., Static and Blast Pressure Investigation for the Chemical Agent Munition Demilitarization System: Sub-Scale, Rpt. EA-FR-4C04, November 30, 1973. (U)
- 3-32 Koger, D.M. and McKown, G.L., Category 5 Suppressive Shield Test Report, EM-TR-76001, Edgewood Arsenal, Aberdeen Proving Ground, Maryland, October 1975. (U)

- 3-33 Study of Suppressive Structures Applications to an 81 mm Automated Assembly Facility, Report EA 1002, Edgewood Arsenal, Aberdeen Proving Ground, Maryland, 16 April 1973. (U)
- 3-34 81 mm Suppressive Shielding Technical Data Package, Report EA-4E33, Edgewood Arsenal, Aberdeen Proving Ground, Maryland, January 1974. (U)
- 3-35 Final Report Application of Suppressive Structure Concepts to Chemical Agent Munition Demilitarization System (CAMDS), Report EA-FR-2B02, Edgewood Arsenal, Aberdeen Proving Ground, Maryland, July 27, 1973. (U)
- 3-36 Schumacher, R.N. and Ewing, W.O., Jr., Blast Attenuation Outside Cubical Enclosures Made Up of Selected Suppressive Structures Panel Configurations, BRL Memorandum Report No. 2537, Aberdeen Proving Ground, Maryland, September 1975. (U)
- 3-37 Hoggatt, C.R. and Recht, R.F., Fracture Behavior of Tubular Bombs, J. Appl. Physics, Vol. 39, No. 3, February 1968, pp. 1856-1862. (U)
- 3-38 Mott, N.F., The Theory of Fragmentation, AC 3348 (British), January 1943. (U)
- 3-39 Mott, N.F., A Theoretical Formula for the Distribution of Weights of Fragments, AC 3742 (British) March 1943. (U)
- 3-40 Johnson, C. and Moseley, J.W., Preliminary Warhead Terminal Ballistic Handbook Part I, Terminal Ballistic Effects, NWL Report No. 1821, NAVWEPS Report No. 7673, U.S. Naval Weapons Laboratory, Dahlgren, Virginia, March 1964. (U)
- 3-41 Kennedy, J.E., Explosive Output for Driving Metal, in Behavior and Utilization of Explosives in Engineering Design, ASME and Univ. of New Mexico, March 1972, Albuquerque, New Mexico. (U)
- 3-42 Henry, I.G., The Gurney Formula and Related Approximations for the High Explosive Deployment of Fragments, PUR-189, Hughes Aircraft Co., AD813398, April 1967. (U)
- 3-43 Kennedy, R.P., A Review of Procedures for the Analysis of Design of Concrete Structures to Resist Missile Impact Effects, Nuclear Engineering and Design, Vol. 37, 1976, pp. 183-203. (U)

- 3-44 Ricchiazzi, A.J. and Barb, J.C., A Tentative Model for Predicting the Terminal Ballistic Effects of Blunt Fragments Against Single and Spaced Targets, A Comparison of Predicted and Experimental Results, BRL Memorandum Report 2578, Aberdeen Proving Ground, Maryland, January 1976. (U)
- 3-45 Headey, John, et al, Primary Fragment Characteristics and Impact Effects on Protective Barriers, PA TR 4903, Picatinny Arsenal, Dover, N.J., December 1975. (U)
- 3-46 Rakaczky, J.A., The Suppression of Thermal Hazards from Explosions of Munitions: A Literature Survey, BRL Interim Memorandum Report No. 377, Aberdeen Proving Ground, Maryland, May 1975. (U)
- 3-47 Shields, Operational for Ammunition Operations, Criteria for Design of, and Tests for Acceptance, Mil Std 398, U.S. Government Printing Office, Washington, D.C., 5 November 1976. (U)

CHAPTER IV

SUPPRESSIVE SHIELD STRUCTURAL BEHAVIOR

4.1 INTRODUCTION

Suppressive shields are subjected to large, high pressure loads very rapidly applied. The allowance of inelastic behavior of the shield structural elements enables much more efficient use of the structural material and does not impair the function of the shield, always provided, of course, that the inelastic behavior is maintained within acceptable limits.

In following paragraphs, the behavior and properties of structural steel and concrete under static and dynamic loading are discussed. The behavior of structural materials is followed by a discussion of ductility ratios pertaining to suppressive shield applications.

4.2 PROPERTIES OF STRUCTURAL MATERIALS

The structural materials of primary interest in suppressive shielding are steel and reinforced concrete. Although steel will normally be preferred in suppressive shield applications because of its isotropic material properties and workability/machinability, reinforced concrete will typically be utilized for shield foundations and could be used for shield primary load-carrying members. Reference 4-1 should be consulted for a comprehensive coverage of blast resistant reinforced concrete design.

4.2.1 Steel

a. Stress-Strain Properties

Structural metals can be separated into two general groups according to the shape of their stress-strain curves. In one group are those metals which do not exhibit a

sharp yield point. Many of the high strength steels and structural aluminum alloys are included in this group. The second group includes those metals which exhibit definite yield points and pronounced yielding zones. This group includes the standard structural carbon and low alloy steels. Typical static stress-strain curves for various grades of steel are shown in Fig. 4-1.

The major point to be gained from examination of Fig. 4-1 is that the higher the strength of a steel, the less ductility it exhibits. Ductility in this case is measured by the length of the stress-strain curve between the yield point and the onset of strain hardening. As may be noted on Fig. 4-1, the higher strength steels have no well defined yield point nor appreciable ductile (plastic) range where increasing strain may occur with no increase in stress. The yield point of high strength steels is usually specified in terms of the stress at some arbitrary strain (normally 0.002 to 0.005).

The low carbon structural grade steels are preferred for most structural applications because of their greater ductility. Because of this ductility, structural steels are able to undergo large deformations beyond the elastic limit without fracture. This is a desirable feature for all structures, but it is especially advantageous for suppressive shields which must resist very large dynamic loads. In general, only structural grade steels should be used in suppressive shield design.

b. Rapidly Applied Loads

The mechanical properties of some structural materials are affected by the rate at which straining takes place. Those metals having definite yield points and pronounced yielding zones show a marked variation in mechanical properties with changes in loading rate. In general, yield strengths will be higher under rapid strain rates than under slowly applied loads and a higher stress is required to produce a yielding strain.

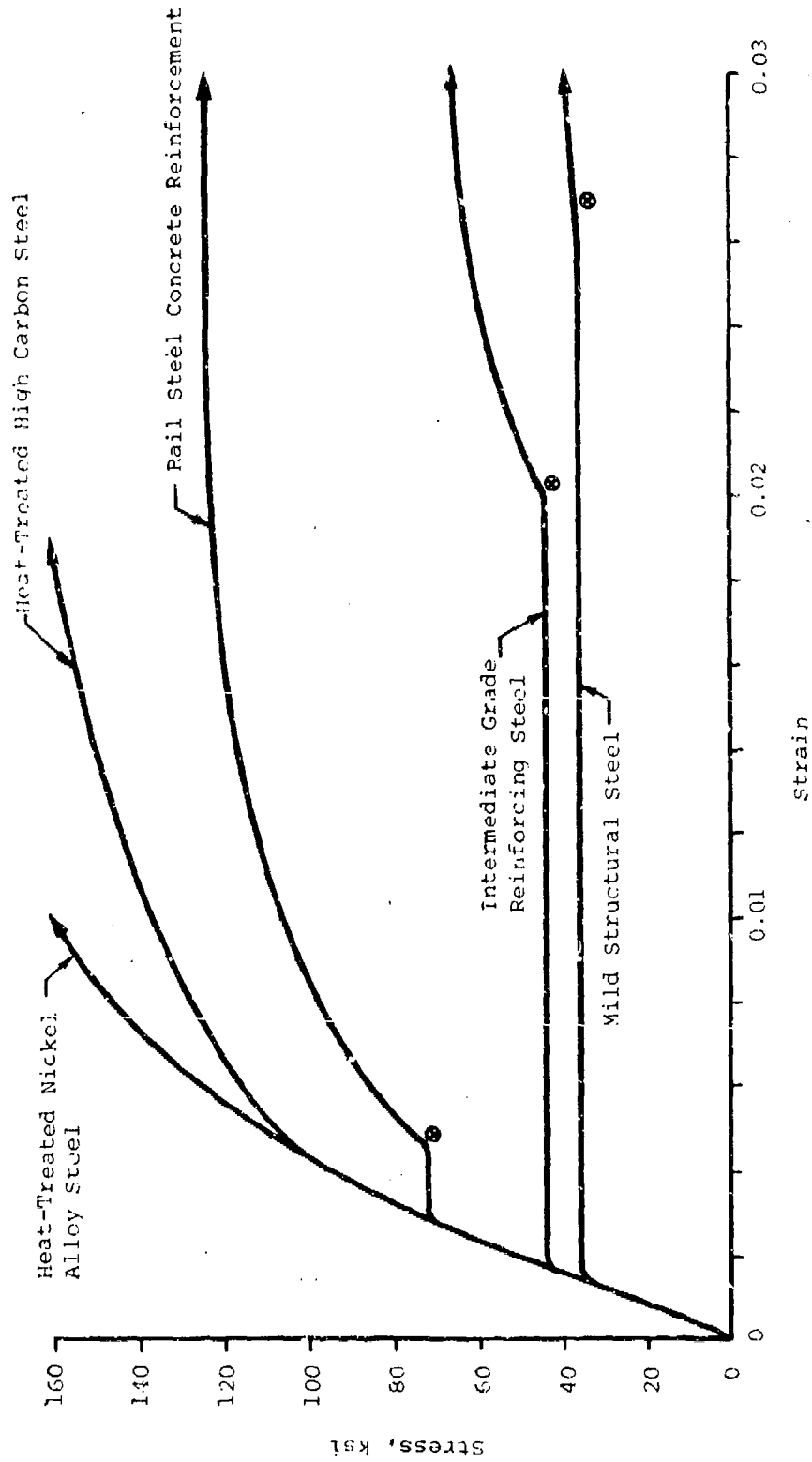


Figure 4-1. Typical Stress-Strain Curves for Various Grades of Steel

Strain rates in a specific member are dependent on the characteristics of the loading function and the manner in which loads are transmitted to the member. The modulus of elasticity of the material is assumed to be unaffected by strain rate, which makes it possible to utilize a static load deformation relationship with a dynamic yield stress for design and analysis of structures subjected to blast loads. The limited amount of experimental data that are available support this approach. As the strain rate increases, the yield stress increases to some dynamic value while the modulus of elasticity remains essentially constant. Because of the higher yield strength and constant modulus of elasticity, there is also an increase in the yield-point strain. In addition, there is an increase in the strain at which strain hardening begins and some slight increase in ultimate strength.

In view of the uncertainties involved in determining the blast response of structures, great precision in evaluation of strain rate effects is not normally justified. It is generally accepted (Refs. 4-1 and 4-2) that strain rate effects resulting from airblast loadings can be estimated to increase the static tensile yield strength of structural steels by about 10 percent. Reference 4-1 suggests that under some conditions the increase in yield strength may be greater. The higher strength steels ($f_y > 60,000$ psi), without definite yield points and pronounced plastic ranges, have not been found to exhibit as high an increase as other structural steels. It is recommended that the high strength steel dynamic yield strengths be taken equal to the static values. The strain rate effect on ultimate strength is usually neglected for all steels. The dynamic shear yield strength is normally taken equal to 0.55 times the dynamic tensile yield strength.

Table 4-1 summarizes recommended dynamic flexural yield stresses for various structural steels used in suppressive shields. The yield stresses in Table 4-1 represent a 10 percent increase in the normal static yield stresses specified for these

steels. If the actual strain rates in a structure can be accurately determined, and these strain rates justify larger increases in yield strength, the higher dynamic yield strengths can be used. See Refs. 4-1, 4-6, 4-7, 4-8 and 4-9 for further guidance. Other allowable dynamic stresses are obtained from the tensile yield stresses using guidance provided in Ref. 4-3. Also included in Table 4-1 are recommended dynamic tensile yield stresses for A615 Grade 40 and 60 reinforcing steels.

Table 4-1

DYNAMIC YIELD STRESSES FOR STEEL

Steel	Flexural Dynamic Yield Stress (ksi) f_{dy}	Shearing Stress (ksi)
<u>Structural Steels*</u>		
A-36	39.6	} $0.55 f_{dy}$
A441 Grade 40	44.0	
Grade 42	46.2	
Grade 46	50.6	
Grade 50	55.0	
A572 Grade 42	46.2	
Grade 45	49.5	
Grade 50	55.0	
Grade 55	60.5	
Grade 60	66.0	
<u>Reinforcing Steels</u>		
A615 GR 40	48.0	} Not Applicable
A615 GR 60	72.0	

* See paragraph 8.3 for welding requirements.

4.2.2 Concrete

The primary application of reinforced concrete in suppressive shielding technology is for foundations, although the Group 3 shield design does employ a reinforced concrete roof. Reference 4-1 should be consulted in situations where it

is found desirable to utilize reinforced concrete facilities for the primary protective structures.

a. Stress-Strain Properties

Since concrete is used mostly in compression, its compressive stress-strain characteristics are of primary importance. Figure 4-2 shows a typical set of stress-strain curves for uniaxial compression cylinder tests at normal, moderate, loading rates on concrete 28 days old. Several important characteristics of concrete can be noted in these curves. First, the stress-strain relationship is obviously nonlinear over most of its range. Second, concrete is a brittle material in comparison with structural steel and reaches its maximum strength at strains near the yield point of some reinforcing steels. Third, the slope of the initial portion of the stress-strain curve increases with increasing compressive strength. A modulus of elasticity for concrete can be estimated with the empirical relationship (Ref. 4-1)

$$E_c = 33w^{1.5} \sqrt{f'_c} \text{ psi} \quad (4-1)$$

where

w = unit weight of concrete, lb/ft³

f'_c = specified compressive strength of concrete, psi

As shown in Fig. 4-3, the strength of a concrete mix will normally continue to increase beyond its 28-day strength. While it is conservative to neglect this increase for design purposes, the analyst should be aware that the actual strength of a concrete may be 50 percent or more greater than that specified at 28 days.

Although concrete is normally used in compression, its tensile strength may be of significance in some applications. The flexural tension strength (modulus of rupture) of concrete is usually related to its tensile splitting strength.

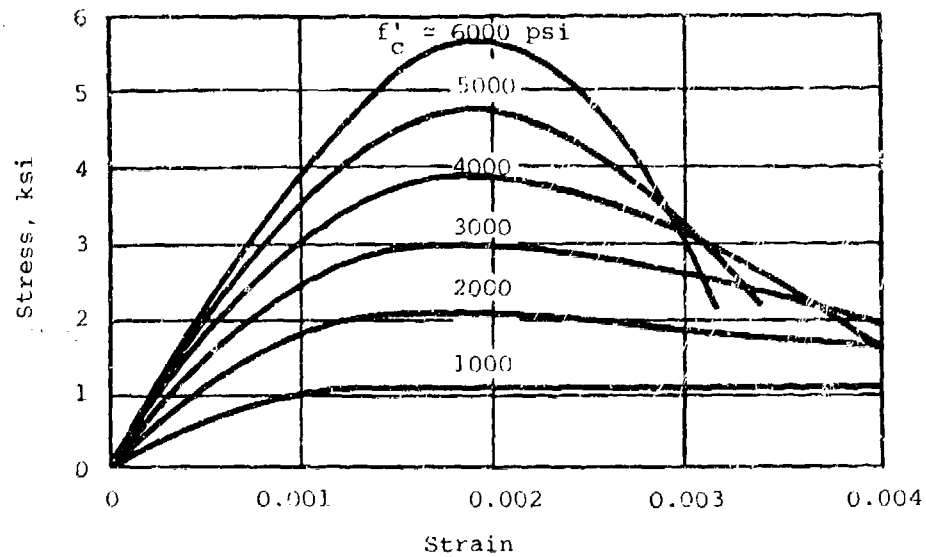


Figure 4-2. Typical Stress-Strain Curves for Concrete (Ref. 4-4)

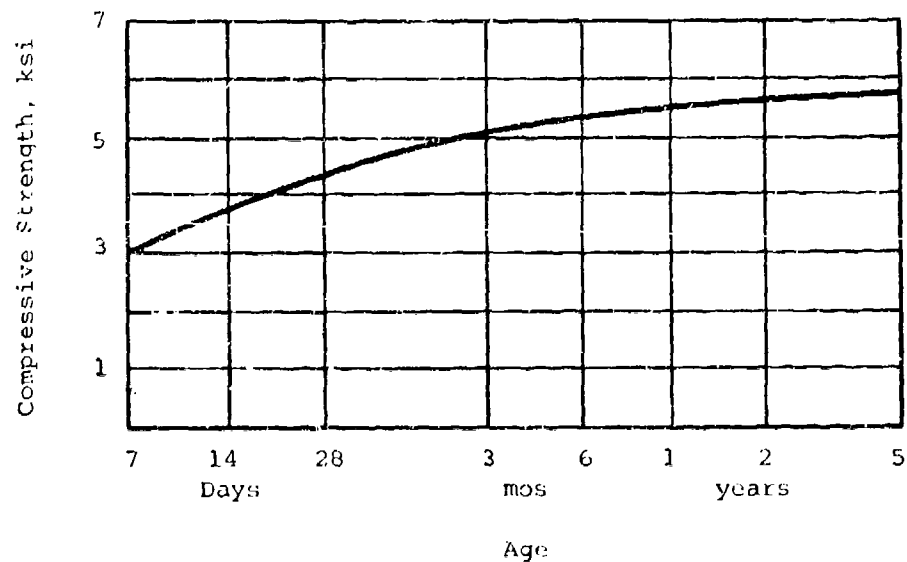


Figure 4-3. Effect of Age on Concrete Compressive Strength f'_c (Ref. 4-4)

For sand-gravel concretes, Ref. 4-4 states that the tensile splitting strength can be reasonably estimated as 6 to 7 times $\sqrt{f'_c}$, and the modulus of rupture as 1.25 to 1.75 times the tensile splitting strength. The smaller of the above factors applies to higher strength ($f'_c > 3500$ psi) concretes and the larger to lower strength concretes.

b. Rapidly Applied Loads

Experimental data indicate that the unconfined (uniaxial) compressive strength of concrete increases with rate of loading. Based on the experimental data that are available, the generally accepted practice (Ref. 4-1) is to assume a 25 percent increase in the unconfined compressive strength of concrete due to rapid loading, unless sufficient data and/or information are available for a particular application to use a greater or lesser value. Reference 4-1 also recommends a 10 percent increase in the direct shear strength of members due to rapid loading.

It is recommended that no increase in diagonal tension or bond strength be allowed for rapid loading. Table 4-2 summarizes dynamic increase factors (DIF) for stresses in concrete members for rapid loading.

Table 4-2

DYNAMIC INCREASE FACTORS FOR CONCRETE (Ref. 4-1)

Stress	Dynamic Increase Factor
Compression	1.25
Tension	1.0
Diagonal Tension	1.0
Direct Shear	1.1
Bond	1.0

4.3 STRUCTURAL DUCTILITY

4.3.1 General

Allowance of inelastic behavior of suppressive shield structural elements enables much more efficient use of the structural material and does not impair the function of the shield, provided that the inelastic behavior is maintained within acceptable limits. In most cases, the resistance-displacement function is assumed to be represented by a simple elastic-plastic function such as shown in Fig. 4-4. This and other types of resistance functions are discussed in Chapter 5.

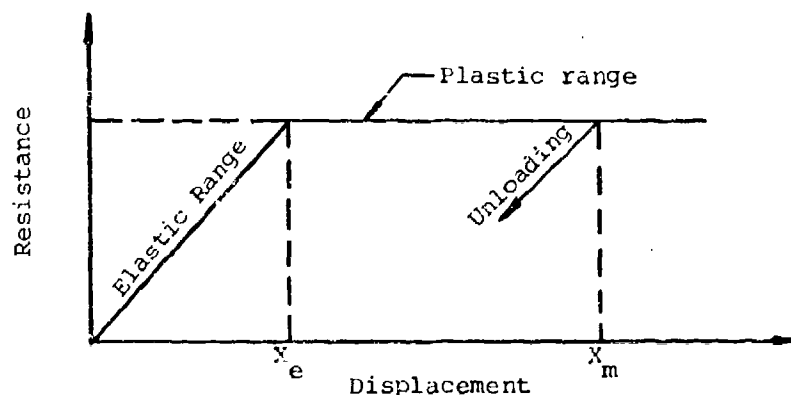


Figure 4-4. Elastic-Plastic Resistance Function

Inelastic structural deformations are often described in terms of a ductility ratio. The ductility ratio in blast resistant design is typically defined as the ratio of a maximum displacement or strain to the elastic displacement or strain, i.e.,

$$\mu = X_m / X_e \quad (4-2)$$

Elastic behavior is indicated by $\mu \leq 1$ and inelastic behavior

by $\mu > 1$. The allowable ductility ratio depends on the properties of the material from which the element is fabricated and the function of the element in the structural system. In some cases, large inelastic deformations are permissible. In other cases, elastic behavior is required. The mode of failure is also important in that brittle catastrophic failures must be avoided, while some inelastic response of a ductile nature is tolerable in most instances. When inelastic behavior is desirable, it is frequently necessary to construct load deformation relationships considering the geometry and proportions of the member as well as its material properties in order to derive a reasonably realistic ductility ratio. While the concept of ductility ratio is strictly applicable only to those systems where the effective response can be described by one coordinate, it is sometimes applied to more complex structures by the use of simplifying assumptions regarding their mode of response.

Ultimate strength, or plastic design, concepts are normally used in the design of suppressive shields. These concepts include the assumption of plastic hinge formation at critical points on the structure or structural element.

In order for these hinges to form and redistribution of moment to occur in a structure, the structural elements must possess the ability to withstand rotations associated with the plastic moment. Other factors such as local buckling, insufficient shear capacity, brittle failure modes, etc., can cause members to fail before developing their full flexural capacity. Premature failure due to these factors must be prevented to ensure that rotation capacity is sufficient to develop the full plastic strength of the element.

Just as it is desirable to maintain inelastic deformations within acceptable limits, it is also necessary that the rotation capability of a member not be exceeded. It is stated

in Ref. 4-5 that hinge rotation under uniform moment up to about 12 times the rotation that had occurred at the elastic limit is not unreasonable for properly proportioned steel members. Reference 4-1 states that properly designed reinforced concrete members can withstand rotations at the supports of from 2 to 12 degrees, depending upon the details of the reinforcing provided. For design of suppressive shield reinforced concrete structural elements, it is recommended that rotations of members at the supports be limited to 2 degrees which Ref. 4-1 defines to be Type I construction.

4.3.2 Structural Steel

Most structural steels of interest begin to yield at strains of about 0.002 or less. As shown in Fig. 4-1, the more ductile steels can undergo fairly large strains beyond this point before the onset of strain hardening. Ultimate strain at rupture of mild steel is typically on the order of 0.20 to 0.25, more than 100 times the yield point strain. The higher strength steels exhibit much lower ultimate strains at rupture, and the ratio of strain at rupture to yield point strain may be on the order of 10 or less. On the basis of strain alone, ductility ratios of 15 to 20 or higher would be permissible for the low carbon structural steels. Ductility ratios of these magnitudes are probably satisfactory for some redundant or secondary elements in shields required to suppress only one explosive. When a shield may be required to withstand more than one event, or when more margin for error is desired, ductility ratios of 6 are normally used for flexural modes of response. A ductility ratio of 1 is recommended for elements fabricated from high strength steels.

4.3.3 Reinforced Concrete

As shown in Fig. 4-2, the maximum load (stress) capacity of concrete occurs at a strain of about 0.002 and drops off rapidly at higher strains. It is obvious that when strength

of the structural element is controlled by crushing of the concrete, only low ductility ratios are allowable. Similarly, reinforced concrete elements without stirrups whose strength depends on direct shear and diagonal tension have brittle modes of failure and show limited to low ductility ratios.

Due to the limited ductility and low tensile strength of concrete, concrete structural elements are always reinforced with steel in blast resistant design. If the member is under-reinforced, yielding of the steel in flexure will occur before the concrete crushes. Since large strains can occur in ductile reinforcing steels before the onset of strain hardening, the ductility of a properly reinforced concrete member can approach that of a steel member. However, at very large strains, cracking of the concrete reduces the compression area, and a brittle concrete compression failure is likely to occur.

As in the case of steel structures, functional requirements must be considered in determining an allowable ductility ratio. A ductility ratio of 1.3 is recommended for reinforced concrete columns. For underreinforced concrete beams and slabs, a ductility ratio, between 6 and 15, is recommended; however, sufficient stirrups must be provided to prevent brittle diagonal tension failure (i.e., minimum $p_v = .0025$). In any case, the flexure member must be checked for direct shear using a ductility ratio of 1.3.

4.3.4 Summary

The following guidelines and Table 4-3 summarize the recommendations made in previous paragraphs with regard to allowable ductility ratios. Obviously, it is impossible to give detailed guidelines on all possible structural concepts and the designer must always evaluate the effect of displacements on the integrity of the suppressive shield. Ductility ratios for different types of members are recommended.

- REINFORCED CONCRETE COLUMNS AND BEAMS AND SLABS WITHOUT STIRRUPS. Their strength depends on compression, direct shear, or diagonal tension. A ductility ratio of 1.3 is recommended for these elements.
- REINFORCED CONCRETE BEAMS AND SLABS WITH STIRRUPS. These would include under-reinforced concrete beams and slabs designed for multiple events. A ductility ratio of 6 is recommended for these elements.
- REINFORCED CONCRETE BEAMS AND SLABS WITH STIRRUPS. These would include under-reinforced concrete beams and slabs designed for a single event. A ductility ratio of 15 is recommended for these elements.
- HIGH STRENGTH STEEL PLATES. These resist tensile stresses, e.g., the Group 6B shields. These are designed for multiple events. A ductility ratio of 1 is recommended for these elements.
- STRUCTURAL STEEL BEAMS AND PLATES FABRICATED FROM LOW CARBON DUCTILE STEELS. These resist flexural and/or tensile stresses. Beams and plates are designed for multiple events or for limited deformation, e.g., wall panels, door elements, and steel hoops. A ductility ratio of 6 is recommended for these elements.

- STRUCTURAL STEEL BEAMS AND PLATES FABRICATED FROM LOW CARBON DUCTILE STEELS. These resist flexural and/or tensile stresses. Beams and plates are designed for a single event and large plastic deformations, e.g., the wall beam columns in the Group 1, 2, and 3 suppressive shields. A ductility ratio of 15 is recommended for these elements.

Table 4-3
RECOMMENDED DUCTILITY RATIOS

Member	Failure Mode	Ductility Ratio, μ	Number of Events
Reinf. Conc. Cols.	Compression (Brittle)	1.3	—
Underreinforced Conc., Bms & Slabs Without Stirrups	Direct Shear (Brittle)	1.3	—
	Diagonal Tension (Brittle)	1.3	—
	Flexure (Ductile)	6.0	Multiple
		15.0	Single
Underreinforced Conc., Bms & Slabs With Stirrups	Direct Shear (Brittle)	1.3	—
	Flexure, Diagonal Tension (Ductile)	6.0	Multiple
		15.0	Single
High Strength Steel Plates	Tension	1.0	Multiple
Low Carbon Structural Steel Plates and Beams	Flexure Tension	6.0	Multiple
Low Carbon Structural Steel Plates and Beams	Flexure Tension	15.0	Single

4.4 LIST OF SYMBOLS

E_c	Modulus of elasticity of concrete (psi)
f'_c	Static unconfined compressive strength of concrete (psi)
f_{dy}	Dynamic tensile yield stress (psi)
f_y	Static tensile yield stress (psi)
w	Unit weight of concrete (psi)
x_e	Elastic limit displacement (inches)
x_m	Maximum displacement (inches)
μ	Ductility ratio
ρ_v	Stirrup Reinforcing Steel Ratio

4.5 REFERENCES

- 4-1 Structures to Resist the Effects of Accidental Explosions, TM5-1300, Department of the Army, Washington, D.C., June 1969. (U)
- 4-2 Crawford, R.E., Higgins, C.J. and Bultmann, E.H., The Air Force Manual for Design and Analysis of Hardened Structures, AFWL TR 74-102, Air Force Weapons Laboratory, Kirtland AFB, N.M., October 1974. (U)
- 4-3 Manual of Steel Construction, Seventh Edition, American Institute of Steel Construction, Inc., New York, N.Y., 1970. (U)
- 4-4 Winter, G., et al, Design of Concrete Structures, McGraw-Hill Book Co., New York, N.Y., 1964. (U)
- 4-5 Beedle, L.S., Plastic Design of Steel Frames, John Wiley and Sons, Inc., New York, N.Y., 1958. (U)
- 4-6 Healey, John, et al, Design of Steel Structures to Resist the Effects of HE Explosions, Technical Report 4837, Picatinny Arsenal, Dover, New Jersey, August 1975. (U)
- 4-7 Symonds, P.S., ASME Colloquium on Behavior of Materials Under Dynamic Loading, Ed., N.J. Huffington, November 1965. (U)
- 4-8 Malvern, L.E., Propagation of Longitudinal Waves of Plastic Deformation in a Bar of Material Exhibiting a Strain-rate Effect, J. App. Mech., Vol. 18, pp. 203-8. (U)
- 4-9 Shelter Design and Analysis, TR-20 (Vol. 4), Defense Civil Preparedness Agency, Washington, DC, July 1972. (U)

CHAPTER V

STRUCTURAL DESIGN AND ANALYSIS

5.1 INTRODUCTION

The design and analysis of structural components subjected to dynamic loads differs from conventional static design procedures in that the time varying characteristics of the loading and the inertial characteristics of the structure must be considered. Following paragraphs of this chapter describe techniques which are sufficiently accurate for preliminary designs in all cases, and in most cases, adequate for final designs. These methods deal primarily with the dynamic loadings imposed by internal explosions.

The type of operation and the explosive size and characteristic to be contained within the suppressive shield dictate configuration and dimensions for the structure. With the explosive data and structural dimensions established, the internal airblast environment and fragment hazard can be defined using the procedures presented in Chapter 3. Safety criteria determine the allowable venting ratio. The internal airblast pressures determine the strength of structural elements and the fragment weights and velocities often determine the minimum thickness of these elements.

Structural design to resist dynamic loads is an iterative procedure. After an explosive environment is defined for a suppressive shield element, a trial structural section is selected to perform the first design calculation. If required by the first design calculation, the trial section is modified and used as the trial section for the second design calculation. The process is repeated until the resistance of the selected section is equal to or slightly greater than

the required resistance. Very seldom are more than three iterations needed.

On the other hand structural analysis of existing structures does not always require iterations. A closed form solution is used to obtain structural deformation or ductility ratios for a specified loading. If the objective of the analysis is to determine the maximum explosive charge an existing structure can withstand, an iterative process is still required.

Before proceeding with either design or analysis discussed above, a decision must have been made as to what damage to the structure is acceptable. Damages are measured by ductility ratios. Chapter 4 defines, discusses and recommends acceptable ductility ratios. If the recommended ductility ratios are used, the safety criteria for containment of airblast, fragments, and fireball will be met.

5.2 STRUCTURAL RESISTANCE

As noted in Chapter 4, most suppressive shield structural elements are designed under the assumption that some inelastic response is acceptable and desirable. For these elements, the displacement-resistance function is nonlinear and is assumed to be represented by one of the idealized functions shown in Fig. 5-1. Resistance is proportional to displacement up to the point of yielding. Beyond the point of yielding, the resistance of the element may increase, remain constant or even decrease. An increase in resistance may result from strain hardening of the material or the development of membrane action in the element. A decaying resistance might be the result of local buckling or axial compressive loads on the element. This type of resistance-displacement function is undesirable and can normally be avoided by proper design of the structural system. Neglect of strain hardening or membrane action results in a more conservative design; however, it is often difficult to ascertain exactly how much benefit might accrue from these effects. The elastic-plastic resistance functions used in this handbook neglect any enhancement or degradation of structure resistance from the above effects.

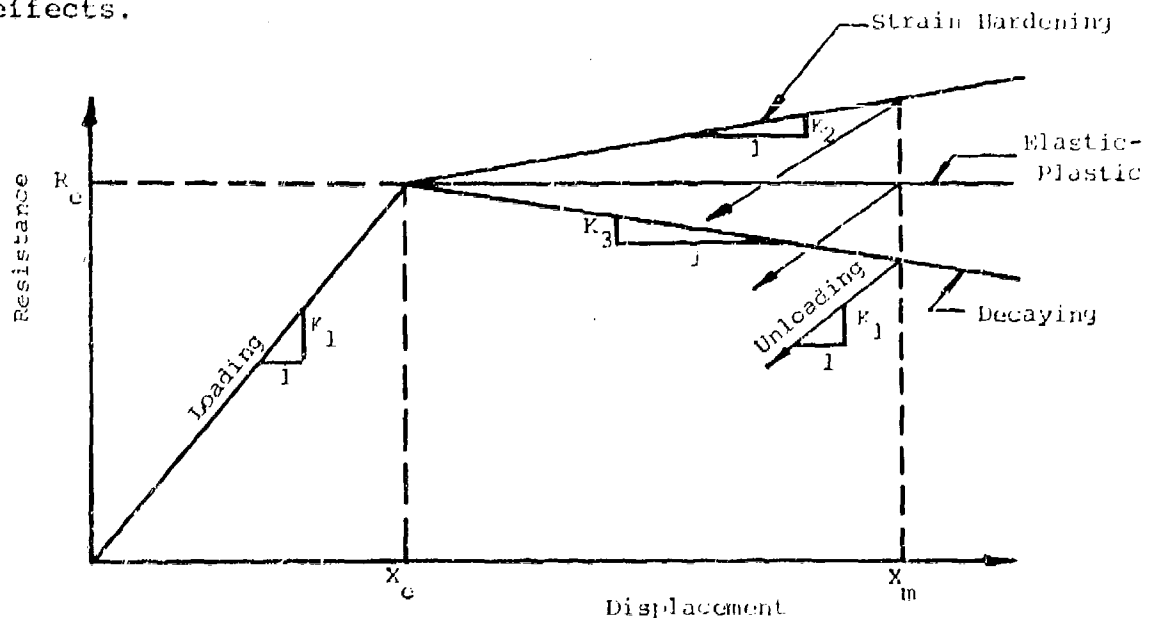


Figure 5-1. Idealized Resistance Functions

For elastic-plastic systems, the response is elastic up to the elastic limit X_e . The resistance then remains constant over the displacement range, $X_e \leq X \leq X_m$, where X_m is the maximum displacement. As the displacement starts to decrease, the response or rebound is again assumed to be elastic.

The resistance functions shown in Fig. 5-1 are representative of the idealized elastic-plastic behavior of statically determinate structures such as a simple beam. That is, as the load (assumed uniform) is increased on the beam, the displacement at midspan increases to some value X_e at which point the moment capacity of the beam has been reached and a plastic hinge forms at midspan. Assuming perfectly plastic behavior, the displacement can now increase indefinitely with no further increase in load.

Statically indeterminate structures possess additional load carrying capacity beyond formation of the first plastic hinge(s). A uniformly loaded beam with both ends fixed would have a resistance function similar to that shown in Fig. 5-2. As the load increases, the moments at the fixed supports increase until the plastic moment capacity of the beam is reached and plastic hinges form. This portion of the resistance function is that shown in Fig. 5-2 as zero to 1.

Although the beam section has yielded and plastic hinges have formed at the fixed supports, the member is still capable of supporting increased load as a simple beam. This portion of the resistance function is that from 1 to 2 in Fig. 5-2. Point 2 represents the formation of a plastic hinge at midspan which converts the beam into a mechanism theoretically capable of increasing deflection without limit with no increase in load.

It is frequently found convenient in the accomplishment of simplified dynamic analyses to replace the bilinear curve 0-1-2 in Fig. 5-2 with the single line 0-3. This equivalent resistance function can be constructed by equating the areas under the

actual and equivalent curves. The equivalent deflection X_E can be found by

$$X_E = X_e + X_p(1 - R_e/R_m) \quad (5-1)$$

and the equivalent stiffness K_E of the system by

$$K_E = R_m/X_E \quad (5-2)$$

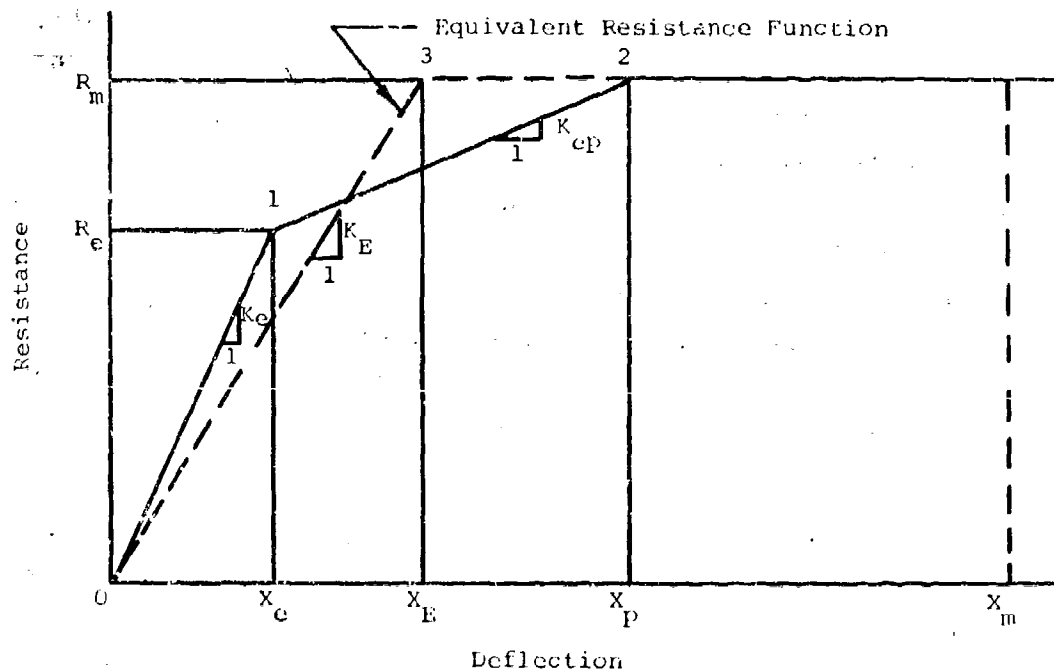


Figure 5-2. Idealized Resistance Function for Uniform Loaded Fixed End Beam

The curves shown in Fig. 5-2 are elastic-perfectly plastic, i.e., they contain elastic portions with a linear relationship between load and deflection and perfectly plastic portions where indefinite deflection is possible at constant load. When very large deflections (strains) are considered, the elastic portion of the resistance can be neglected and the behavior considered to be rigid-plastic (i.e., the resistance function could be taken as a horizontal line with ordinate R_m) with little error.

5.3 PROPERTIES OF STRUCTURAL ELEMENTS

5.3.1 General

The design or analysis of structures and structural elements to resist dynamic loads requires a determination of the static load carrying capacity of the element. A dynamic analysis is performed to obtain a required static resistance or to translate a given static resistance into one under dynamically applied loads. This section presents conventional expressions for the flexural, shear and axial load capacity of steel and reinforced concrete elements. These expressions are utilized in paragraph 5.4 to obtain the resistances of beams and slabs with various end conditions and span ratios. Also presented are expressions for the load capacity of cylindrical and spherical pressure vessels. As noted in Chapter 4, dynamic tensile or compressive strengths should be used to obtain the strength of elements subjected to dynamic loadings.

The design or analysis of structural members for suppressive shields will almost always be based upon inelastic behavior of the member. For steel, the design procedure is referred to as plastic design; for concrete, it is ultimate strength design. These methods assume both ultimate strength behavior (plastic moments) and the redistribution of load due to formation of plastic hinges.

5.3.2 Structural Steel Elements

In designing or analyzing the ability of steel members to resist blast effects, many of the concepts and equations developed for the plastic analysis of steel structures under static loads are used. A number of references (such as Refs. 5-1 and 5-2) contain discussions of plastic analysis and design of steel structures for static loads and can be consulted for more detailed guidance.

a. Flexure

If a steel member is subjected to pure bending, its ultimate moment capacity is given by

$$M_p = f_{dy} Z \quad (5-3)$$

where Z is the plastic section modulus of the member and f_{dy} is the dynamic yield strength of the steel. Reference 5-2 includes plastic section modulus tables for common structural steel sections, and Fig. 5-3 gives general expressions for the plastic section modulus of several structural shapes for bending about a horizontal centroidal axis.

Equation 5-3 assumes that the member is properly supported and proportioned so as to allow development of a plastic hinge at critical sections. If the member is not properly supported or proportioned, buckling may occur before the fully plastic moment can be developed. To ensure the ability of a steel member to sustain fully plastic hinge formation, it is necessary that the member be properly braced to prevent lateral-torsional buckling and that the elements of the member meet minimum thickness requirements for initial loading and rebound (see Ref. 5-3). Table 5-1 gives maximum width-thickness ratios for flanges of rolled, wide-flange shapes and similar built-up single-web shapes that are subjected to compression involving hinge rotation under ultimate loading.

b. Shear

Shear is of interest in steel members primarily because of its possible influence on the plastic moment capacity of the member. It has been found experimentally that the member will achieve its full plastic moment capacity if the average shear stress over the full web area is less than the yield stress in shear (Ref. 5-1).

From Ref. 5-2, the shear capacity of WF or I-shaped steel sections with unstiffened webs is given by

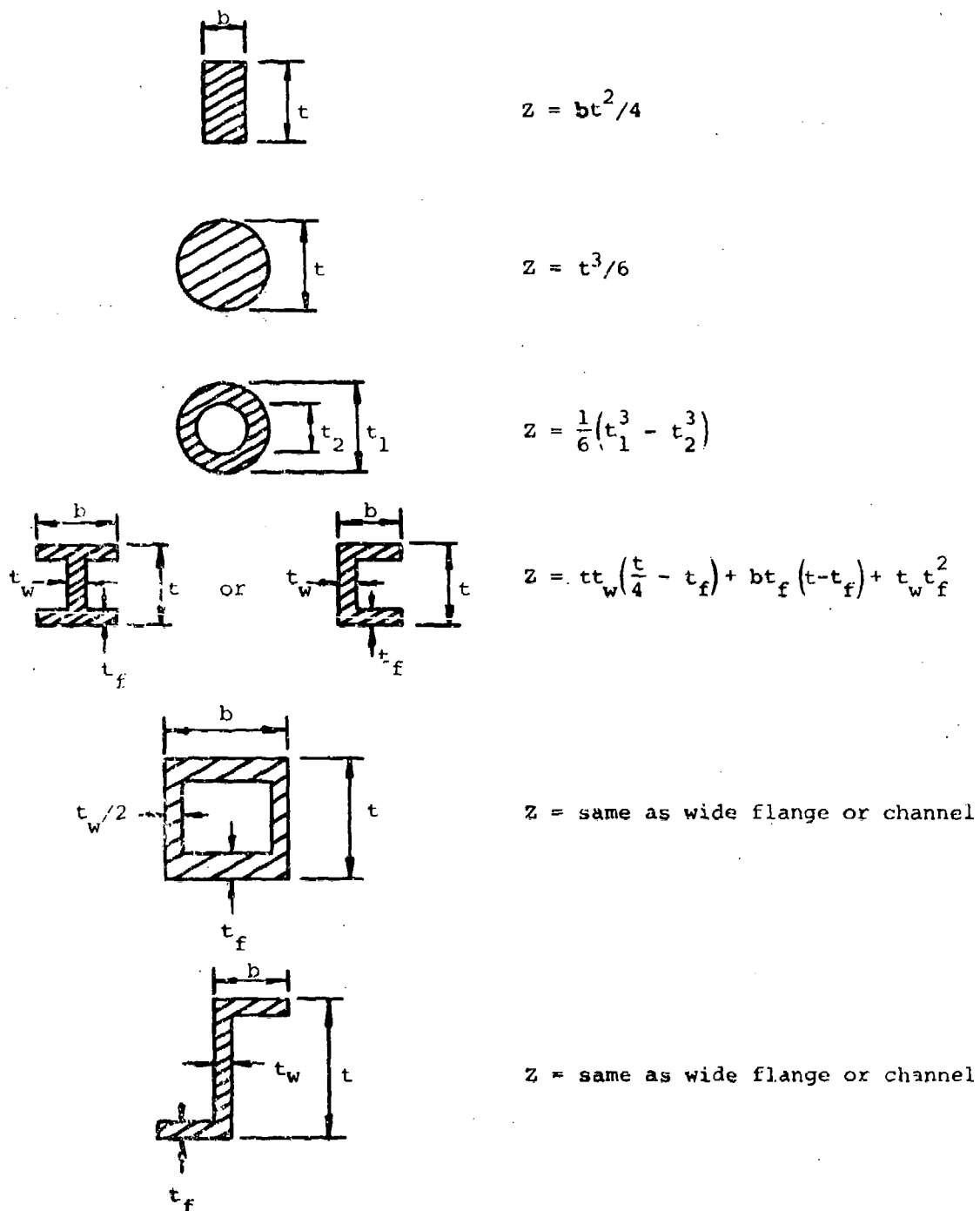
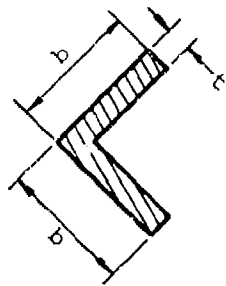
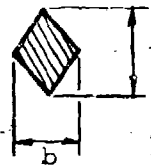


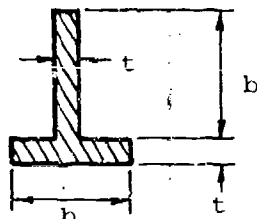
Figure 5-3a. Plastic Section Moduli for Structural Shapes



$$z = \frac{b^2 t}{\sqrt{2}}$$

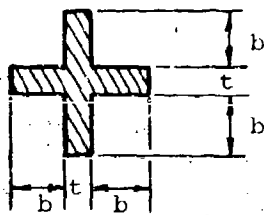


$$z = \frac{bt^2}{12}$$



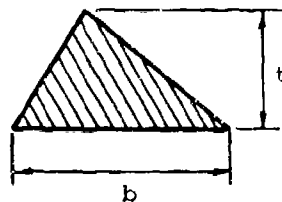
$$z = \frac{b^2 t}{2}$$

$$t \ll b$$



$$z = \frac{bt}{2} (2b + 3t)$$

$$t \ll b$$



$$z = 0.0976 bt^2$$

Figure 5-3b. Plastic Section Moduli for Structural Shapes (concluded)

Table 5-1

MAXIMUM THICKNESS RATIOS FOR STEEL MEMBERS (Ref. 5-2)

f_y , ksi	$b/2t_f$	d_w/t_w
36	8.5	43
42	8.0	40
45	7.4	38
50	7.0	36
55	6.6	35
60	6.3	33
65	6.0	32

b = width of flange; t_f = thickness of flange (if thickness of flange varies, use average thickness); d_w = depth of web; t_w = thickness of web.

$$V_u = 0.55f_{dy}t_w t \quad (5-4)$$

where

V_u = ultimate shear capacity

t_w = web thickness

t = total depth of member

When the web of a built-up section is designed to carry a significant part of the total moment requirement of the section, the shear influence cannot be neglected and the member should be investigated for possible moment capacity loss through shear yield. Reference 5-3 recommends that the moment capacity of such a section be defined by

$$M_P = bf_{dy}t_f d_w \left\{ 1 + 0.25 \left(\frac{t_w d_w}{t_f b} \right) \left[1 - \left(\frac{V}{V_y} \right)^2 \right] \right\} \quad (5-5)$$

where

b = flange width

t_f = flange thickness

d_w = depth of web = $t - 2t_f$

V = total shear acting on section

$V_y = 0.55f_{dy}t_w d_w$ = shear capacity of web

c. Axial Loads

Due to the nature of suppressive shield structural configurations (i.e., loaded from the interior such as pressure vessels), compressive axial loads will rarely, if ever, be a consideration. Even with those configurations that utilize columns, such columns properly proportioned for the rated blast loads will almost certainly be adequate for the normal static service loads and rebound loads. Such adequacy can be readily verified by the procedures presented in Refs. 5-1 and 5-2.

Tensile axial loads can also reduce the moment capacity of steel members. However, columns and roof beams proportioned for moment due to blast loads by the methods of this handbook are not expected to experience any significant reduction in load-carrying capability due to combined tensile and flexural forces. Reference 5-1 or 5-3 is recommended should the occasion arise to investigate the effects of combined axial and flexural forces on steel members.

5.3.3 Reinforced Concrete Elements

The only reinforced concrete structural elements of potential interest for suppressive shields are beams and slabs (plates). These elements may be utilized for suppressive shield foundations or roof slabs. The use of reinforced concrete in cylindrical and spherical structural configurations is not recommended for suppressive shielding applications.

Ultimate strength design methods are used for reinforced concrete elements, and a properly designed and proportioned reinforced concrete member is theoretically as ductile in flexure as a structural steel member. If reinforced concrete members are used, they should be Type I construction as defined in Chapter 4.

a. Flexure

The flexural mode of response is heavily dependent upon the percentage of tensile steel employed. If insufficient steel is used, the steel may be incapable of resisting the tensile force carried by the concrete before cracking. If, on the other hand, an excessively large percentage of steel is used, the concrete crushes on the compression side before the tensile steel yields. To avoid either of these undesirable characteristics and to ensure ductile response, reinforced concrete flexural members with tensile reinforcing only should be proportioned so that (Ref. 5-4)

$$p \leq \frac{55,463 B_1}{87,000 + f_y} \left[\frac{f'_c}{f_y} \right] \quad (5-6)$$

where

p = tensile reinforcing steel ratio = A_s/bd

A_s = cross sectional area of tensile steel

b = width of concrete member

d = effective depth of concrete member (Distance from the compression outer fiber to the centroid of the tensile reinforcing steel)

f'_c = static unconfined compressive strength of concrete

f_y = static yield strength of steel

B_1 = .85 for $f'_c \leq 4,000$ psi and is reduced at a rate of 0.05 for each 1,000 psi increase in f'_c over 4,000 psi.

The ultimate moment capacity of a rectangular member with tensile reinforcing only and subjected to bending only is given by

$$M_p = pf_{dy}bd^2(1 - 0.59pf_{dy}/f'_{dc}) \quad (5-7)$$

where f'_{dc} is the dynamic compressive strength of the concrete and all other terms are as previously defined.

The addition of compression steel has little effect on the ultimate moment capacity of underreinforced members (those meeting the criteria of Eq. 5-6). It is recommended that the member be proportioned according to Eq. 5-7 and that for small shields, 25% of the rebars be conservatively provided on the opposite face for rebound resistance but that no increase in moment capacity be claimed due to the presence of reinforcing steel in the compression area. If there is found to be some overriding reason to take account of the effects of compression reinforcement, Ref. 5-4 or 5-5 should be consulted. If the required rebound resistance is determined by dynamic analysis, the reinforcing steel in the opposite face should provide this resistance. See Section 5.5.5 (to be added) for rebound calculations.

It is often necessary to calculate the moment of inertia of a reinforced concrete element. Reference 5-6 recommends that the moment of inertia be taken equal to the average of that for the cracked and uncracked transformed cross sections. For rectangular cross sections, Ref. 5-6 recommends the approximation

$$I_a = \frac{bd^3}{2} (5.5p + 0.083) \quad (5-8)$$

b. Shear

Shear failures are generally brittle in nature with little advance warning of distress in the member. In order to assure ductile behavior of reinforced concrete members, it is necessary that members be designed against shear failure by following recommended ductility ratios in Table 4-3. The static compressive allowable stress should be used in expressions for the shear strength of reinforced concrete members.

There are two modes of shear failure, direct shear and diagonal tension. The direct shear mode of failure is characterized by the rapid propagation of a nearly vertical crack through the depth of the member in the region of the support. Horizontal reinforcement inhibits the formation and propagation of such cracks. Direct shear failures can occur in members properly proportioned for suppressive shielding applications. Direct shear should always be investigated. The direct shear stress that can be taken by the concrete is given by (Ref. 5-5)

$$v_d = \frac{V_d}{b_1} = 0.18f'_c \text{ psi} \quad (5-9)$$

where V_d is the total shear at the support in pounds and the other terms are as previously defined. Equation 5-9 may be used for either conventional (span/depth > 5) or deep (span/depth < 5) members.

The diagonal tension failure mode is characterized by diagonal cracks which propagate through the member from

a point near the tensile steel toward the compression face. When the crack has penetrated to a point where the remaining compression zone of the concrete is insufficient to sustain the bending stresses, the concrete crushes and the member fails.

The critical section for diagonal tension in conventional members is taken at a distance d (the effective depth of the member) from the support. The allowable shear stress on the concrete is given by (Ref. 5-7)

$$v_c = (1.9\sqrt{f'_c} + 2500pdv_c / M_c) \quad (5-10)$$

where

V_c = total shear on critical section (typically at distance d from the support)

M_c = moment at the critical section

The value of the term dV_c/M_c in Eq. 5-10 shall not be taken greater than 1.0. Reference 5-7 states that the shearing stress obtained from Eq. 5-10 should not exceed $3.5\sqrt{f'_c}$. Reference 5-5 recommends a more conservative value of $2.28\sqrt{f'_c}$. A review of test data reported in Ref 5-8 indicates that the value of $2.28\sqrt{f'_c}$ is perhaps overly conservative.

The added shear capacity contributed by shear reinforcing is given by (Ref. 5-9)

$$V_s = d \frac{A_v f_y}{s} \quad (5-11)$$

where

s = spacing of vertical web reinforcing

A_v = total cross section area of web reinforcing over distance s

The vertical web reinforcing ratio is defined as the ratio of the area of the vertical web reinforcing to the gross horizontal area, bs . Equation 5-11 assumes the web reinforcing is placed perpendicular to the longitudinal axis of the member. Reference 5-7 states that V_s/bd should not exceed

$8\sqrt{f'_c}$ psi. The total shear capacity is then given by

$$V_u = V_c + V_s \quad (5-12)$$

where V_c equals the allowable concrete shear stress from Eq. 5-10, v_c times bd . The shear stress calculated from Eq. 5-12, i.e., V_u/bd , should not exceed $11.5\sqrt{f'_c}$ psi. Reference 5-5 recommends a more conservative value of $10\sqrt{f'_c}$.

The critical section for diagonal tension (shear) in deep members is assumed to occur at a distance $0.15L$ from the support for uniformly loaded members, one-half the distance between a concentrated load and the support for concentrated loads, but not over a distance d from the support for either case. The allowable shear stress on the concrete for deep members is given by (Ref. 5-8)

$$v_c = (3.5 - 2.5M_c / V_c d) (1.9\sqrt{f'_c} + 2500pdv_c / M_c) \quad (5-13)$$

with the provisions that

$$1.0 \leq (3.5 - 2.5M_c / V_c d) \leq 2.5$$

and

$$v_c \leq 6\sqrt{f'_c}$$

with all terms as previously defined.

When web reinforcing is needed to supply additional shear capacity for deep members, it is recommended that such reinforcement be provided by an orthogonal vertical and horizontal system of bars. The shear capacity contributed by such a system is given by (Ref. 5-7)

$$V_s = f_{dy} d \left[\frac{A_v}{12s} \left(1 + \frac{L}{d} \right) + \frac{A_{vh}}{12s_H} \left(11 - \frac{L}{d} \right) \right] \quad (5-14)$$

where

A_v = total cross section area of vertical web reinforcing over distance s

s = horizontal spacing of vertical web reinforcing

L = span of member

A_{vH} = total cross section area of horizontal web reinforcing over distance s_H

s_H = vertical spacing of horizontal web reinforcing

The total shear stress, i.e., V_u/bd with V_u from Eq. 5-12, to be allowed on a deep member shall be limited to $10\sqrt{f'_c}$ psi.

The web reinforcing systems described above are the conventional methods of providing shear reinforcement for reinforced concrete members. Where shear reinforcement is required for conventional members, the amount of such reinforcement provided shall be

$$A_v \geq \frac{50bs}{f_{dy}}$$

and s shall not exceed $d/2$ or 24 inches. Where required in deep members, the area of shear reinforcement A_v perpendicular to the main reinforcement shall be not less than $0.0015bs$ and s shall not exceed $d/5$ or 18 inches. The area of shear reinforcement A_{vH} parallel to the main reinforcement shall not be less than, $0.0025bs_H$ and s_H shall not exceed $d/3$ or 18 inches.

The situation may arise where it is desirable to utilize a reinforced concrete element where the loading conditions are such that the allowable total shear values stated above ($V_u/bd \leq 11.5\sqrt{f'_c}$ or $\leq 10\sqrt{f'_c}$) are exceeded. In such a case, increase the depth of the member.

c. Bond and Anchorage

All modes of failure of reinforced concrete elements are closely coupled to and are, in fact, inseparable from a bond mode of failure. If a bond failure is not prevented, the bars will not serve their function in the other modes of behavior considered.

The tension or compression forces in the reinforcement at each section must be developed on each side of that section by an adequate embedment length or end anchorage or a combination of the two. If no mechanical end anchorage is provided, the tension or compression forces in the reinforcing must be resisted by shear-type bond stresses distributed over the contact area between the bars and the concrete. Bars without deformations shall not be used. The projecting ribs of deformed bars bear against the surrounding concrete and provide greatly increased bond strength over that of plain bars.

Reference 5-4 states that the ultimate resisting bond force, in force per unit length of bar, is largely independent of bar size or perimeter. Since the force in the bar causing bond failure increases with its area, bond is a more serious problem with the larger bars. The critical sections for development of reinforcement in flexural members are generally at points of maximum moment gradient. The required development length of deformed bars in tension is given by (Ref. 5-7)

$$L_D = 0.04A f_{dy} / \sqrt{f'_c}$$

but not less than

(5-15)

$$0.0004D f_{dy}$$

where L_D is in inches, A is the cross section area of an individual bar in square inches and D is the diameter of the bar in inches. If the reinforcement is placed horizontally in the top of a member with more than 12 inches of concrete below it, the values obtained from Eq. 5-15 are multiplied by 1.4. For reinforcement whose f_{dy} is greater than 60,000 psi, the values

obtained from Eq. 5-15 are multiplied by the factor $[2 - (60,000/f_{dy})]$. Equation 5-15 is limited to #11 reinforcing bars and smaller. Bars larger in diameter than #11 are not recommended for suppressive shielding applications.

The development length for bars in compression is given by

$$L_D = 0.02f_{dy}D/\sqrt{f'_c} \quad (5-16)$$

but not less than

$$0.0003f_{dy}D \text{ or } 8 \text{ inches}$$

Additional guidance on development of bond strength is presented in Ref. 5-7.

d. Axial Compression Loads

There are no currently approved suppressive shielding applications which employ reinforced concrete columns. As discussed previously for steel, such columns properly proportioned for the outward blast loads would almost assuredly be satisfactory for the normal vertical static service loads and rebound loads. The adequacy is readily verified by procedures presented in Ref. 5-7.

5.3.4 Cylinders

The cylindrical pressure vessel is not normally used for suppressive shielding applications. Although Shield Groups 1, 2 and 3 are cylindrical in shape, they are an assemblage of beam, ring and plate elements. However, the equations for design or analysis of cylindrical pressure vessels can be applied to pipelines, ductwork, spheres and steel hoops and are, therefore, of interest for suppressive shield applications. It is also possible that the cylinder might be adapted to some future suppressive shielding application. In suppressive shield applications, the cylinder would be subjected to large internal dynamic pressure loads and zero or near zero external loads. The structural material will be responding primarily in tension, and

buckling and moment loads, which are so important for cylinders subjected to external load, will be insignificant except in the vicinity of the end caps. Stresses in the vicinity of the juncture between the end caps and the cylinder walls are a function of the relative stiffnesses of these elements. Their prediction is complex and cannot be treated here.

The cylinder shown in Fig. 5-4 can be considered thin walled, if its wall thickness is equal to or less than one-tenth the internal radius. The average stress calculated for the wall thickness is a good approximation of the maximum stress in the wall. The force P acting on the end cap and base plate is the product of the internal pressure and the internal cross sectional area

$$P = p \times \pi R^2$$

where p is the internal pressure and R is the internal radius. The longitudinal stress in the cylinder wall depicted in Fig. 5-4 can be found from

$$\text{(Thin Wall)} \quad \sigma_{\ell} = P/A_{\text{wall}} = \frac{pR}{2t} \quad (5-17)$$

The radius to the mid section of the wall of thickness t can be taken equal to the internal radius with little error for thin wall cylinders.

The total force P on the base plate is the same as on the hemispherical cap. This force could be divided equally among the bolts that are shown or distributed around the circumference for welding when determining the end cap connection requirements.

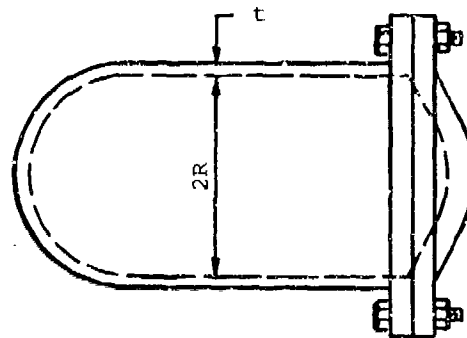
The cylinder hoop forces are also depicted in Fig. 5-4. For the unit width strip shown,

$$F = 2Rp = 2H = 2\sigma_h t$$

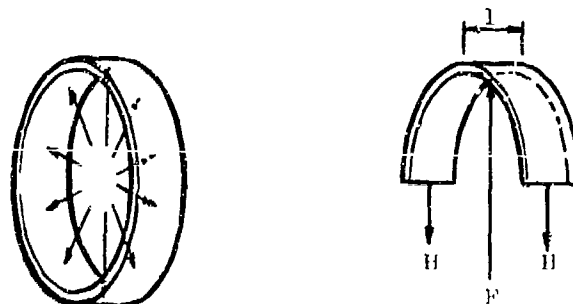
and the hoop stress

$$\text{(Thin Wall)} \quad \sigma_h = \frac{pR}{t} \quad (5-18)$$

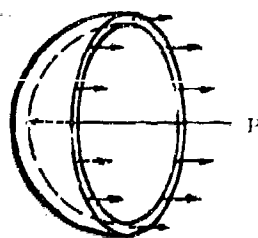
with all terms as previously defined.



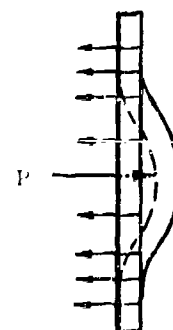
a. Side View of Structure



b. Hoop Section



c. Hemispherical Cap



d. Base Plate

Figure 5-4. Cylindrical Structural Configuration

In cases where the cylinder wall thickness exceeds one-tenth of the internal radius, expressions for stress in thick wall cylinders should be used. The maximum hoop stress in a thick wall cylinder subjected to internal pressure only expressed as a ratio of the thin wall stress and a function of the outside and inside radii is shown in Fig. 5-5. Expressions from Ref. 5-10 for the maximum hoop, radial and longitudinal stresses in thick walled cylinders subjected to internal pressure only are summarized below.

$$\text{(Thick Wall)} \quad \sigma_h = \frac{p(R_o^2 + R_i^2)}{R_o^2 - R_i^2} \quad (5-19)$$

$$\text{(Thick Wall)} \quad \sigma_r = p \quad (5-20)$$

$$\text{(Thick Wall)} \quad \sigma_l = \frac{pR_i^2}{R_o^2 - R_i^2} \quad (5-21)$$

where R_i is the inside radius, R_o is the outside radius of the thick wall cylinder and the other terms are as previously defined.

The stresses given by Eqs. 5-19 and 5-20 are maximum values and occur at the inside wall of the cylinder. The maximum value that a radial stress may attain is equal to the internal pressure. The hoop stress is normally larger than the radial stress for the conditions of interest in suppressive shielding.

The longitudinal stress, Eq. 5-21, can be assumed to be uniformly distributed on any transverse wall section which is not close to a capped end. Near a capped end, the influence of the cap will cause nonuniformity in the stress distribution. It will usually be found that values of σ_l are small relative to those of σ_h and σ_r .

Equations 5-17 through 5-21 can be used for design or analysis of suppressive shields by taking the allowable stress equal to f_{dy} .

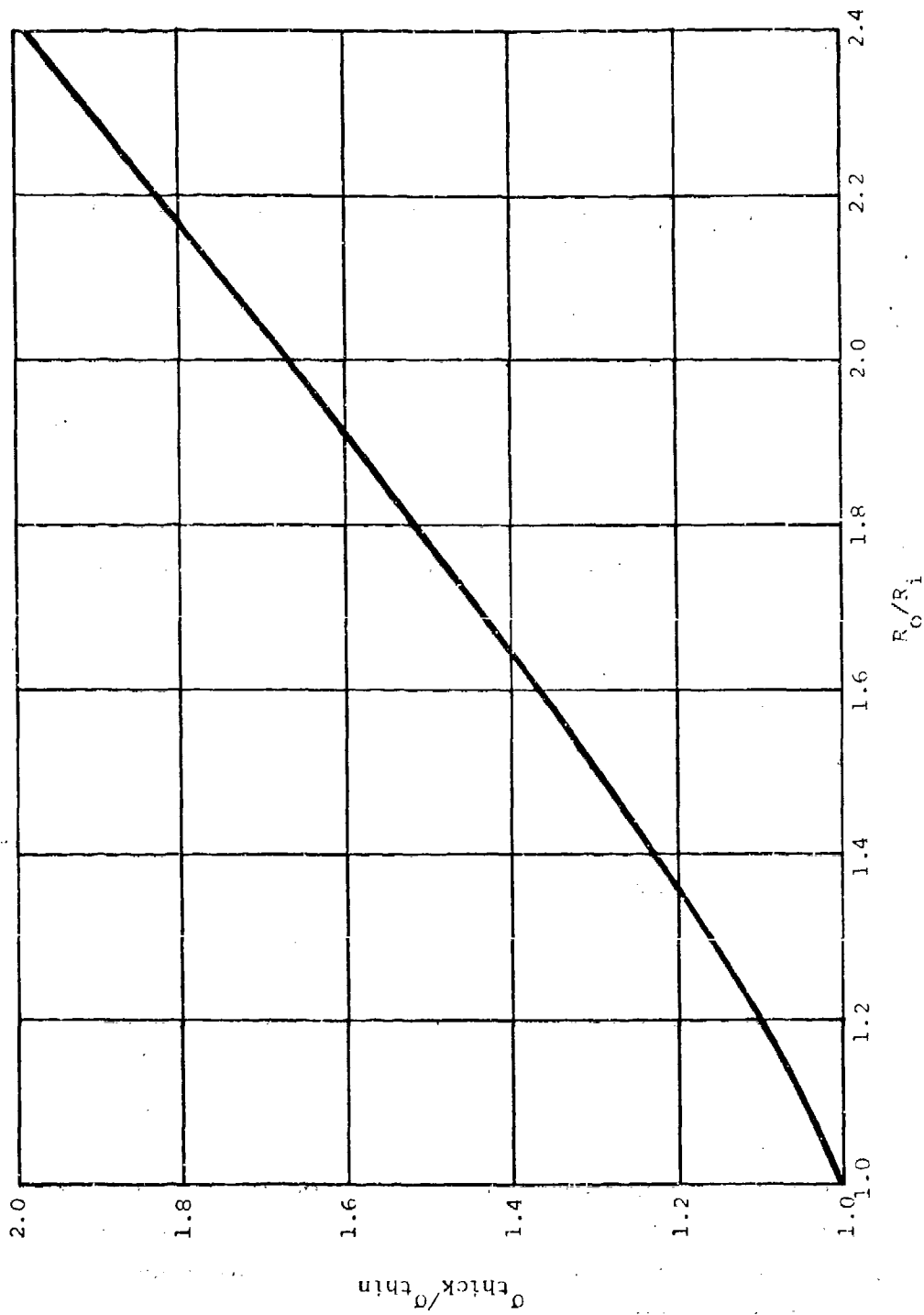


Figure 5-5. Hoop Stress in Thick Wall Cylinder Subjected to Internal Pressure Only

5.3.5 Spheres

Spherical chambers are used for some suppressive shield applications where the fragment hazards are minimal. Equations 5-17 and 5-21 can be used for calculating the maximum stresses in thin and thick wall spheres, respectively, subjected to an internal pressure only. The maximum static resistance of a spherical chamber would be obtained by taking the calculated stress equal to f_{dy} .

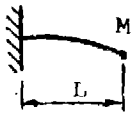

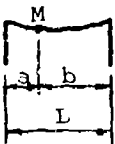
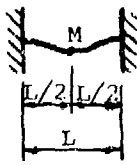
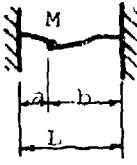
5.3.6 Natural Frequencies of Common Systems

Calculating natural frequencies is one of the important steps in the analysis of most systems. The expressions given in this section can be used to calculate the circular natural frequencies or period of vibration of various types of structural elements which remain elastic. The circular natural frequency and period of vibration of an element are related by

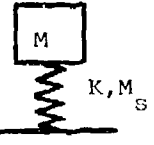
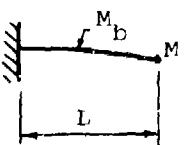
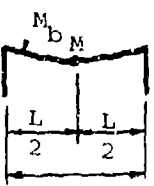
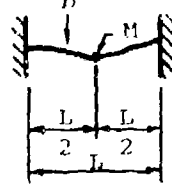
$$T_N = \frac{2\pi}{\omega_N} \quad (5-22)$$

where T_N is the period of vibration of the element in seconds and ω_N is the circular natural frequency in radians per second. If the period of vibration and load duration are known, the equations and charts of paragraph 5.5 and Appendix B can be used to obtain the maximum response of the system.

Figure 5-6 presents solutions for the circular natural frequency of various types of beams or one-way slabs. In Fig. 5-6(a), the mass of the beam is assumed to be very small compared to that of the supported load. The solutions given in Fig. 5-6(b) include consideration of both the mass of the beam and the supported mass. They do not include consideration of the stiffness added by attached plates or boxes. The importance of added stiffness depends on how much is added and over what portion of the span it extends. No general solution can be given here.

Fixed-Free End Load	Hinged-Hinged Center Load	Hinged-Hinged Off-Center Load	Fixed-Fixed Center Load	Fixed-Fixed Off-Center Load
				
$\omega_N = \sqrt{\frac{3EI}{ML^3}}$	$\omega_N = 4\sqrt{\frac{3EI}{ML^3}}$	$\omega_N = \frac{1}{ab}\sqrt{\frac{3EIL}{M}}$	$\omega_N = 8\sqrt{\frac{3EI}{ML^3}}$	$\omega_N = \frac{1}{ab}\sqrt{\frac{3EIL^3}{Mab}}$

(a) Massless Beams with Concentrated Mass Loads

Mass-Helical Spring	Fixed-Free End-Load	Hinged-Hinged Center Load	Fixed-Fixed Center Load
			
$\omega_N = \sqrt{\frac{K}{M + \frac{M_s}{3}}}$	$\omega_N = \sqrt{\frac{3EI}{L^3 (M + 0.23M_b)}}$	$\omega_N = \sqrt{\frac{48EI}{L^3 (M + 0.5M_b)}}$	$\omega_N = 14\sqrt{\frac{EI}{L^3 (M + 0.375M_b)}}$

(b) Massive Springs (Beams) with Concentrated Mass Loads

- M = Mass of Load, lb-sec²/in
 M_s (M_b) = Total Mass of Spring (Beam), lb-sec²/in
 K = Stiffness of Spring lb/in
 L = Length of Beam, inches
 I = Area Moment of inertia of Beam Cross Section, in⁴
 E = Young's Modulus, lb/in²
 ω_N = Natural Frequency, rad/sec

Figure 5-6. Natural Frequencies of Beam Elements with Concentrated Masses (Ref. 5-11)

Figure 5-7 presents solutions for the natural frequencies of circular and square slabs with various edge conditions. Figure 5-8 presents solutions for the natural frequencies of beams or one-way slabs with uniformly distributed mass and various support conditions.

The solutions presented in Figs. 5-6 through 5-8 are for the lowest (fundamental) mode of vibration. They do not include consideration of the effects of rotary motion and shearing forces on natural frequencies. These effects are small except for beams with small span to depth ratios, i.e., short, deep beams, or beams vibrating in higher mode shapes. Reference 5-11 presents guidance regarding adjustment of natural frequencies in those cases where these effects might be considered important.

Some cylindrical suppressive shields are strengthened with circumferential steel hoops. Under the radial loads imposed by the longitudinal beam columns they support, these steel hoops will respond in the extensional mode (all segments move radially together - in or out). The frequency of vibration of a steel hoop in this mode is given by

$$\omega_N = \sqrt{\frac{EA}{mR^2}} \quad (5-23)$$

where

A = cross section area of beam, in²

m = mass per unit length of beam, lb-sec²/in²

R = radius to center of beam, inches

The fundamental mode of vibration of a sphere would consist of simultaneous radial motion of all points on its surface. From Ref. 5-12, the natural period of vibration in the fundamental mode is given by

$$T_N = 2\pi \sqrt{\frac{\rho a^2 (1-\nu)}{2E}} \quad (5-24)$$

$$\omega_N = B \sqrt{\frac{Et^2}{\rho a^4 (1-\nu^2)}} \text{ rad/sec}$$

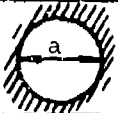


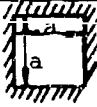
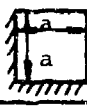
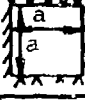


E = Young's Modulus, lb/in²

t = Thickness of Plate, inches

ρ = Mass Density, lb-sec²/in⁴

a = Diameter of Circular Plate or Side of Square Plate, inches

ν = Poisson's Ratio

Shape of Plate	Diagram	Edge Conditions	Value of B
CIRCULAR		Clamped at Edge	11.84
CIRCULAR		Simply Supported at Edge	5.90
SQUARE		One Edge Clamped-Three Edges Free	1.01
SQUARE		All Edges Clamped	10.40
SQUARE		Two Edges Clamped-Two Edges Free	2.01
SQUARE		One Edge Clamped-Three Edges Simply Supported	6.83
SQUARE		Two Edges Clamped-Two Edges Simply Supported	8.37
SQUARE		All Edges Simply Supported	5.70

Massless Circular Plate with Concentrated Center Mass

Clamped Edges



$$\omega_N = 4.09 \sqrt{\frac{Et^3}{Ma^2 (1-\nu^2)}}$$

Simply Supported Edges



$$\omega_N = 4.09 \sqrt{\frac{Et^3}{Ma^2 (1-\nu) (3+\nu)}}$$

Figure 5-7. Fundamental Frequencies of Thin Flat Plates of Uniform Thickness (Ref. 5-11)

E = Young's Modulus, lb/in²
 I = Area Moment of inertia of Beam Cross Section, in⁴
 L = Length of Beam, inches
 m = Mass Per Unit Length of Beam, lb-sec²/in²

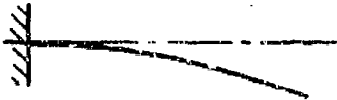
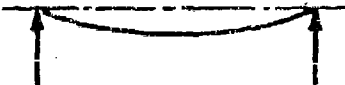
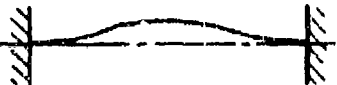

Fixed-Free (Cantilever)		$\omega_N = \frac{3.52}{L^2} \sqrt{\frac{EI}{m}}$
Hinged-Hinged (Simple)		$\omega_N = \frac{9.87}{L^2} \sqrt{\frac{EI}{m}}$
Fixed-Fixed (Built-in)		$\omega_N = \frac{22.4}{L^2} \sqrt{\frac{EI}{m}}$
Fixed-Hinged		$\omega_N = \frac{15.4}{L^2} \sqrt{\frac{EI}{m}}$

Figure 5-8. Natural Frequencies of Beams of Uniform Section and Uniformly Distributed Mass (Ref. 5-11)

where

a = radius of sphere, inches

ρ = mass density of sphere material, $\text{lb-sec}^2/\text{in}^4$

ν = Poisson's ratio for sphere material

E = modulus of elasticity for sphere material, lb/in^2

5.4 EQUIVALENT SINGLE DEGREE OF FREEDOM SYSTEMS

5.4.1 General

A rigorous dynamic analysis is feasible only for relatively simple structures where the loading and resistance functions can be expressed in simple mathematical terms. Although numerical analysis techniques are much more flexible, they also become tedious for more than a few degrees of freedom. Most real structures with distributed mass theoretically have an infinite number of degrees of freedom. For practical design purposes, it is necessary to develop approximate methods which allow rapid analysis of complex structures with reasonable accuracy. Fortunately, it is possible to reduce many common structural elements to an equivalent single degree of freedom system which can then be analyzed with accuracy sufficient for most engineering purposes. In view of the uncertainties in loads and material properties encountered in suppressive shield design, more complex analytical techniques are often not justified. The method used herein for reducing distributed mass systems to equivalent single degree of freedom systems is taken from Ref. 5-13.

Figure 5-9 shows a fixed end beam with a single degree of freedom replacement system. In order to define the equivalent single degree of freedom system, it is necessary to determine the parameters $F_{eq}(t)$, M_{eq} , K_{eq} and X_{eq} . The usual approach is to define the system as one in which the equivalent displacement, velocity and acceleration are equal

to that at some significant point in the actual system, e.g., the midspan of a beam. Stresses and forces in the equivalent system are not directly equivalent to those in the real system, but, if the deflections are known, the stresses in the real system can be calculated. It is also necessary to define equivalent resistance and forcing functions. The equivalent forcing function should have the same time dependence as the real load.

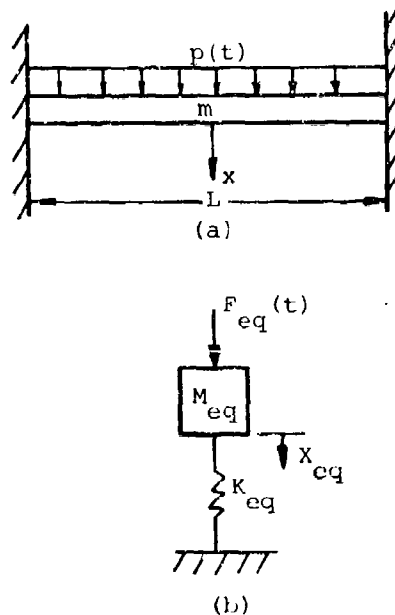


Figure 5-9. Equivalent Single Degree of Freedom System

The constants of the equivalent system are evaluated on the basis of an assumed deformed shape of the actual structure. This shape is usually taken as that resulting from the static application of the dynamic loads. This approach is not quite the same as that of using the first mode shape, but it yields more accurate results for many systems, especially for stress computations. These deflected shapes are more easily determined and described by simple mathematical functions than are mode shapes.

5.4.2 Transformation Factors for Beams and Slabs

It is convenient to develop transformation factors which convert the real system into the equivalent system. When the load, mass, resistance and stiffness of the real structure are multiplied by the corresponding transformation factors, these parameters are obtained for the equivalent single degree of freedom system. The mass transformation factor is defined to be

$$K_M = \frac{M_{eq}}{M_t} \quad (5-25)$$

where

M_t = total mass of the real structure

M_{eq} = mass of the equivalent single degree of freedom system

The load transformation factor is defined to be

$$K_L = \frac{F_{eq}}{F_t} \quad (5-26)$$

where

F_t = total force on the real structure

F_{eq} = force on the equivalent single degree of freedom system

Since the maximum resistance is the total load having the given distribution which the structure can support statically and the stiffness is equal to the total load of the same distribution required to cause a unit displacement at the significant point, it follows that the resistance factor, K_R , must always equal the load factor, K_L . Then

$$K_R = \frac{R_{meq}}{R_m} = K_L \quad (5-27)$$

and

$$K_R = \frac{K_{eq}}{K} = K_L \quad (5-28)$$

where R_m and K are the actual and R_{meq} and K_{eq} are the equivalent resistances and spring constants, respectively.

Transformation factors have been worked out for a number of common types of structural elements and support conditions. Tables 5-2 and 5-3 give factors for beams and one-way slabs, Tables 5-4 through 5-7 give factors for two-way slabs. Table 5-8 presents factors for circular slabs. The tables also include a load-mass factor which is defined to be the ratio of the mass and load-factors, i.e.,

$$K_{LM} = \frac{K_M}{K_L} \quad (5-29)$$

The ratio can be used to define the equations of motion for the equivalent system

$$K_{LM} M_t \ddot{X} + KX = F_t(t) \quad (\text{elastic region}) \quad (5-30)$$

$$K_{LM} M_t \ddot{X} + R_m = F_t(t) \quad (\text{plastic region}) \quad (5-31)$$

The natural frequency of both the real and idealized systems is

$$\omega_N = \left[\frac{K_{eq}}{M_{eq}} \right]^{1/2} = \left[\frac{K}{K_{LM} M_t} \right]^{1/2} \quad (5-32)$$

and the natural period is

$$T_n = 2\pi \left[\frac{K_{LM} M_t}{K} \right]^{1/2} \quad (5-33)$$

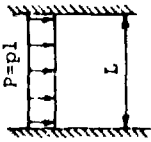
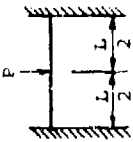
The maximum resistances and spring stiffnesses presented in Table 5-2 are those for the real system and are the conventional expressions for these quantities. They are given in terms of the total load on the system and, when multiplied by the load factor, they become the corresponding

Table 5-2
TRANSFORMATION FACTORS FOR BEAMS AND ONE-WAY SLABS (Refs. 5-6, 5-9, 5-10)

Loading Diagram	Strain Range	Load Factor K_L	Mass Factor K_M		Load-Mass Factor K_{LM}		Maximum Resistance R_m	Spring Constant K	Dynamic Reaction V
			Concentrated Mass*	Uniform Mass	Concentrated Mass*	Uniform Mass			
	Elastic	0.64		0.50			$2M_p/L$	$384EI/5L^3$	$0.39R + 0.11F$
	Plastic	0.50		0.33			$8M_p/L$	0	$0.39R_m + 0.12F$
	Elastic	1.0	1.0	0.49	1.0	0.49	$4M_p/L$	$48EI/L^3$	$0.78R - 0.28F$
	Plastic	1.0	1.0	0.33	1.0	0.33	$4M_p/L$	0	$0.75R_m - 0.25F$
	Elastic	0.87	0.76	0.52	0.87	0.60	$6M_p/L$	$56.4EI/L^3$	$0.62R - 0.12F$
	Plastic	1.0	1.0	0.56	1.0	0.56	$6M_p/L$	0	$0.52R_m - 0.02F$
	Elastic	0.4		0.26		0.65	$2M_{ps}/L$	$8EI/L^3$	$0.69R + 0.31F$
	Plastic	0.5		0.33		0.66	$2M_{ps}/L$	0	$0.75R_m + 0.25F$
	Elastic	1.0	1.0	0.24	1.0	0.24	M_{ps}/L	$3EI/L^3$	$1.36R - 0.36F$
	Plastic	1.0	1.0	0.33	1.0	0.33	M_{ps}/L	0	$1.5R_m - 0.5F$

* Equal parts of the concentrated mass are lumped at each concentrated load.

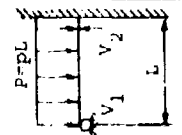
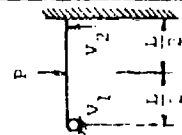
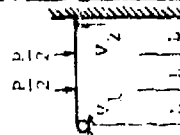
Table 5-3
TRANSFORMATION FACTORS FOR BEAMS AND ONE-WAY SLABS (Ref. 5-13)

Loading Diagram	Strain Range	Load Factor K_L	Mass Factor K_M		Load-Mass Factor K_{LM}		Maximum Resistance R_m	Spring Constant K	Effective Spring Constant K_E	Dynamic Reaction V
			Concentrated Mass*	Uniform Mass	Concentrated Mass*	Uniform Mass				
	Elastic	0.53	0.41	0.77	$12M_{ps}/L$	$384EI/L^3$	$0.36R + 0.14F$
	Elasto-Plastic	0.64	0.50	0.78	$\frac{8}{L}(M_{ps} + M_{pm})$	$384EI/5L^3$	$307EI/L^3$	$0.39R + 0.11F$
	Plastic	0.50	0.33	0.66	$\frac{8}{L}(M_{ps} + M_{pm})$	0	$0.38R_m + 0.12F$
	Elastic	1.0	1.0	0.37	1.0	0.37	$\frac{4}{L}(M_{ps} + M_{pm})$	$192EI/L^3$	$0.71R - 0.21F$
	Plastic	1.0	1.0	0.33	1.0	0.33	$\frac{4}{L}(M_{ps} + M_{pm})$	0	$0.75R_m - 0.25F$

* Concentrated mass is lumped at the concentrated load.

Table 5-3 (concluded)

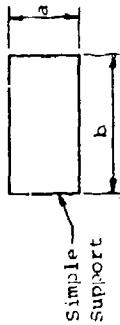
TRANSFORMATION FACTORS FOR BEAMS AND ONE-WAY SLABS (Ref. 5-6, 5-13)

Loading Diagram	Strain Range	Load Factor K_L	Mass Factor K_M		Load-Mass Factor K_{LM}		Maximum Resistance R_m	Spring Constant K	Effective Spring Constant K_E	Dynamic Reaction V
			Concentrated Mass*	Uniform Mass	Concentrated Mass*	Uniform Mass				
	Elastic	0.58	0.45	0.78	$8M_{ps}/L$	$185EI/L^3$	$V_1 = 0.26R + 0.12F$ $V_2 = 0.43R + 0.19F$
	Elasto-Plastic	0.64	0.50	0.78	$\frac{4}{L}(M_{ps} + 2M_{pm})$	$384EI/5L^3$	$160EI/L^3$	$V_1 = 0.39R + 0.11F - M_{ps}/L$ $V_2 = 0.39R + 0.11F + M_{ps}/L$
	Plastic	0.50	0.33	0.66	$\frac{4}{L}(M_{ps} + 2M_{pm})$	0	$V_1 = 0.36R_m + 0.12F - M_{ps}/L$ $V_2 = 0.36R_m + 0.12F + M_{ps}/L$
	Elastic	1.0	1.0	0.43	1.0	0.43	$16M_{ps}/3L$	$107EI/L^3$	$V_1 = 0.25R + 0.07F$ $V_2 = 0.54R + 0.14F$
	Elasto-Plastic	1.0	1.0	0.49	1.0	0.49	$\frac{2}{L}(M_{ps} + 2M_{pm})$	$48EI/L^3$	$160EI/L^3$	$V_1 = 0.78R - 0.28F - M_{ps}/L$ $V_2 = 0.78R - 0.28F + M_{ps}/L$
	Plastic	1.0	1.0	0.33	1.0	0.33	$\frac{2}{L}(M_{ps} + 2M_{pm})$	0	$V_1 = 0.75R_m - 0.25F - M_{ps}/L$ $V_2 = 0.75R_m - 0.25F + M_{ps}/L$
	Elastic	0.81	0.67	0.45	0.83	0.55	$6M_{ps}/L$	$132EI/L^3$	$V_1 = 0.17R + 0.17F$ $V_2 = 0.33R + 0.33F$
	Elasto-Plastic	0.87	0.76	0.52	0.87	0.60	$\frac{2}{L}(M_{ps} + 3M_{pm})$	$56EI/L^3$	$122EI/L^3$	$V_1 = 0.62R - 0.12F - M_{ps}/L$ $V_2 = 0.62R - 0.12F + M_{ps}/L$
	Plastic	1.0	1.0	0.56	1.0	0.56	$\frac{2}{L}(M_{ps} + 3M_{pm})$	$V_1 = 0.52R_m - 0.02F - M_{ps}/L$ $V_2 = 0.52R_m - 0.02F + M_{ps}/L$

* Equal parts of the concentrated mass are lumped at each concentrated load.

Table 5-4

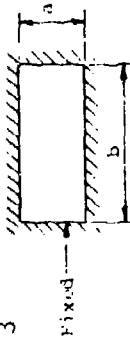
TRANSFORMATION FACTORS FOR TWO-WAY SLABS SIMPLE SUPPORTS, UNIFORM LOAD (Ref. 5-6, 5-13)
For Poissons Ratio = 0.3



Strain Range	a/b	Load Factor K_L	Mass Factor K_M	Load-Mass Factor K_{LM}	Maximum Resistance	Spring Constant K	Dynamic Reactions	
							V_A	V_B
Elastic	1.0	0.45	0.31	0.68	$\frac{12}{a}(M_{pfa} + M_{pfb})$	$252 EI_a / a^2$	$0.07F + 0.18R$	$0.07F + 0.18R$
	0.9	0.47	0.33	0.70	$\frac{1}{a}(12M_{pfa} + 11M_{pfb})$	$230 EI_a / a^2$	$0.06F + 0.16R$	$0.08F + 0.20R$
	0.8	0.49	0.35	0.71	$\frac{1}{a}(12M_{pfa} + 10.3M_{pfb})$	$212 EI_a / a^2$	$0.06F + 0.14R$	$0.08F + 0.22R$
	0.7	0.51	0.37	0.73	$\frac{1}{a}(12M_{pfa} + 9.8M_{pfb})$	$201 EI_a / a^2$	$0.05F + 0.13R$	$0.08F + 0.24R$
	0.6	0.53	0.39	0.74	$\frac{1}{a}(12M_{pfa} + 9.3M_{pfb})$	$197 EI_a / a^2$	$0.04F + 0.11R$	$0.09F + 0.26R$
	0.5	0.55	0.41	0.75	$\frac{1}{a}(12M_{pfa} + 9.0M_{pfb})$	$201 EI_a / a^2$	$0.04F + 0.09R$	$0.09F + 0.28R$
Plastic	1.0	0.33	0.17	0.51	$\frac{12}{a}(M_{pfa} + M_{pfb})$	0	$0.09F + 0.16R_m$	$0.09F + 0.16R_m$
	0.9	0.35	0.18	0.51	$\frac{1}{a}(12M_{pfa} + 11M_{pfb})$	0	$0.08F + 0.15R_m$	$0.09F + 0.18R_m$
	0.8	0.37	0.20	0.54	$\frac{1}{a}(12M_{pfa} + 10.3M_{pfb})$	0	$0.07F + 0.13R_m$	$0.10F + 0.20R_m$
	0.7	0.38	0.22	0.58	$\frac{1}{a}(12M_{pfa} + 9.8M_{pfb})$	0	$0.06F + 0.12R_m$	$0.10F + 0.22R_m$
	0.6	0.40	0.23	0.58	$\frac{1}{a}(12M_{pfa} + 9.3M_{pfb})$	0	$0.05F + 0.10R_m$	$0.10F + 0.25R_m$
	0.5	0.42	0.25	0.59	$\frac{1}{a}(12M_{pfa} + 9.0M_{pfb})$	0	$0.04F + 0.08R_m$	$0.11F + 0.27R_m$

Table 5-5

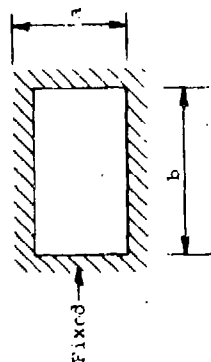
TRANSFORMATION FACTORS FOR TWO-WAY SLABS: FIXED SUPPORTS - UNIFORM LOAD (Ref. 5-6, 5-13)
For Poissons Ratio = 0.3



Strain Range	a/b	Load Factor K_L	Mass Factor K_M	Load-Mass Factor K_{LM}	Maximum Resistance	Spring Constant K	Dynamic Reactions	
							V_A	V_B
Elastic	1.0	0.33	0.21	0.63	$292 M_{psb}^0$	$810 EI_a / a^2$	$0.10F + 0.15R$	$0.10F + 0.15R$
	0.9	0.34	0.23	0.68	$274 M_{psb}^0$	$742 EI_a / a^2$	$0.09F + 0.14R$	$0.10F + 0.17R$
	0.8	0.36	0.25	0.69	$264 M_{psb}^0$	$703 EI_a / a^2$	$0.08F + 0.12R$	$0.11F + 0.19R$
	0.7	0.38	0.27	0.71	$262 M_{psb}^0$	$692 EI_a / a^2$	$0.07F + 0.11R$	$0.11F + 0.21R$
	0.6	0.41	0.29	0.71	$273 M_{psb}^0$	$724 EI_a / a^2$	$0.06F + 0.09R$	$0.12F + 0.23R$
	0.5	0.43	0.31	0.72	$302 M_{psb}^0$	$806 EI_a / a^2$	$0.05F + 0.08R$	$0.12F + 0.25R$
Elasto-Plastic	1.0	0.46	0.31	0.67	$\frac{1}{a} [12(M_{pfa} + M_{psa}) + 12(M_{pfb} + M_{psb})]$	$252 EI_a / a^2$	$0.07F + 0.18R$	$0.07F + 0.18R$
	0.9	0.47	0.33	0.70	$\frac{1}{a} [12(M_{pfa} + M_{psa}) + 11(M_{pfb} + M_{psb})]$	$230 EI_a / a^2$	$0.06F + 0.16R$	$0.08F + 0.20R$
	0.8	0.49	0.35	0.71	$\frac{1}{a} [12(M_{pfa} + M_{psa}) + 10.3(M_{pfb} + M_{psb})]$	$212 EI_a / a^2$	$0.06F + 0.14R$	$0.08F + 0.22R$
	0.7	0.51	0.37	0.73	$\frac{1}{a} [12(M_{pfa} + M_{psa}) + 9.8(M_{pfb} + M_{psb})]$	$201 EI_a / a^2$	$0.05F + 0.13R$	$0.08F + 0.24R$
	0.6	0.53	0.39	0.74	$\frac{1}{a} [12(M_{pfa} + M_{psa}) + 9.3(M_{pfb} + M_{psb})]$	$197 EI_a / a^2$	$0.04F + 0.11R$	$0.09F + 0.26R$
	0.5	0.55	0.41	0.75	$\frac{1}{a} [12(M_{pfa} + M_{psa}) + 9.0(M_{pfb} + M_{psb})]$	$201 EI_a / a^2$	$0.04F + 0.09R$	$0.09F + 0.28R$

Table 5-5 (concluded)

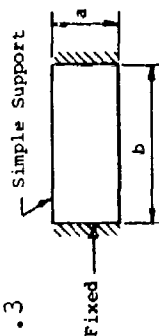
TRANSFORMATION FACTORS FOR TWO-WAY SLABS: FIXED SUPPORTS - UNIFORM LOAD (Ref. 5-13)
For Poissons Ratio = 0.3



Strain Range	a/b	Load Factor K_L	Mass Factor K_M	Load-Mass Factor K_{LM}	Maximum Resistance	Spring Constant K	Dynamic Reactions	
							V_A	V_B
Plastic	1.0	0.33	0.17	0.51	$\frac{1}{a} [12(M_{pfa} + M_{psa}) + 12(M_{pfb} + M_{psb})]$	0	$0.09F + 0.16R_m$	$0.09F + 0.16R_m$
	0.9	0.35	0.18	0.51	$\frac{1}{a} [12(M_{pfa} + M_{psa}) + 11(M_{pfb} + M_{psb})]$	0	$0.08F + 0.15R_m$	$0.09F + 0.18R_m$
	0.8	0.37	0.20	0.54	$\frac{1}{a} [12(M_{pfa} + M_{psa}) + 10.3(M_{pfb} + M_{psb})]$	0	$0.07F + 0.13R_m$	$0.10F + 0.20R_m$
	0.7	0.38	0.22	0.58	$\frac{1}{a} [12(M_{pfa} + M_{psa}) + 9.8(M_{pfb} + M_{psb})]$	0	$0.06F + 0.12R_m$	$0.10F + 0.22R_m$
	0.6	0.40	0.23	0.58	$\frac{1}{a} [12(M_{pfa} + M_{psa}) + 9.3(M_{pfb} + M_{psb})]$	0	$0.05F + 0.10R_m$	$0.10F + 0.25R_m$
	0.5	0.42	0.25	0.59	$\frac{1}{a} [12(M_{pfa} + M_{psa}) + 9.0(M_{pfb} + M_{psb})]$	0	$0.04F + 0.08R_m$	$0.11F + 0.27R_m$

Table 5-6

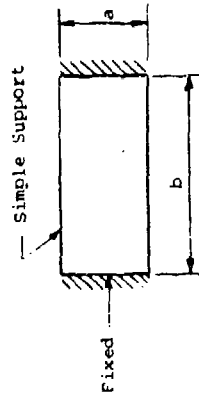
TRANSFORMATION FACTORS FOR TWO-WAY SLABS:
SHORT EDGES FIXED - LONG EDGES SIMPLY SUPPORTED (Ref. 5-13)
For Poissons Ratio = 0.3



Strain Range	a/b	Load Factor K_L	Mass Factor K_M	Load-Mass Factor K_{LM}	Maximum Resistance	Spring Constant K	Dynamic Reactions	
							V_A	V_B
Elastic	1.0	0.39	0.26	0.67	$20.4M_{psa}^0$	$575EI/a^2$	$0.09F + 0.16R$	$0.07F + 0.18R$
	0.9	0.41	0.28	0.68	$10.2M_{psa}^0 + \frac{11}{a} M_{pfb}$	$476EI/a^2$	$0.08F + 0.14R$	$0.08F + 0.20R$
	0.8	0.44	0.30	0.68	$10.2M_{psa}^0 + \frac{10.3}{a} M_{pfb}$	$396EI/a^2$	$0.08F + 0.12R$	$0.08F + 0.22R$
	0.7	0.46	0.33	0.72	$9.3M_{psa}^0 + \frac{9.7}{a} M_{pfb}$	$328EI/a^2$	$0.07F + 0.11R$	$0.08F + 0.24R$
	0.6	0.48	0.35	0.73	$8.5M_{psa}^0 + \frac{9.3}{a} M_{pfb}$	$283EI/a^2$	$0.06F + 0.09R$	$0.09F + 0.26R$
	0.5	0.51	0.37	0.73	$7.4M_{psa}^0 + \frac{9.0}{a} M_{pfb}$	$243EI/a^2$	$0.05F + 0.08R$	$0.09F + 0.28R$
Elasto-Plastic	1.0	0.46	0.31	0.67	$\frac{1}{a} [12(M_{pfa} + M_{psa}) + 12(M_{pfb})]$	$271EI/a^2$	$0.07F + 0.18R$	$0.07F + 0.18R$
	0.9	0.47	0.33	0.70	$\frac{1}{a} [12(M_{pfa} + M_{psa}) + 11(M_{pfb})]$	$248EI/a^2$	$0.06F + 0.16R$	$0.08F + 0.20R$
	0.8	0.49	0.35	0.71	$\frac{1}{a} [12(M_{pfa} + M_{psa}) + 10.3(M_{pfb})]$	$228EI/a^2$	$0.06F + 0.14R$	$0.08F + 0.22R$
	0.7	0.51	0.37	0.72	$\frac{1}{a} [12(M_{pfa} + M_{psa}) + 9.7(M_{pfb})]$	$216EI/a^2$	$0.05F + 0.13R$	$0.08F + 0.24R$
	0.6	0.53	0.37	0.70	$\frac{1}{a} [12(M_{pfa} + M_{psa}) + 9.3(M_{pfb})]$	$212EI/a^2$	$0.04F + 0.11R$	$0.09F + 0.26R$
	0.5	0.55	0.41	0.74	$\frac{1}{a} [12(M_{pfa} + M_{psa}) + 9.0(M_{pfb})]$	$216EI/a^2$	$0.04F + 0.09R$	$0.09F + 0.28R$

Table 5-6 (concluded)

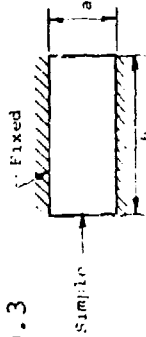
TRANSFORMATION FACTORS FOR TWO-WAY SLABS:
SHORT EDGES FIXED - LONG EDGES SIMPLY SUPPORTED (Ref. 5-13)
For Poissons Ratio = 0.3



Strain Range	L/b	Load Factor K_L	Mass Factor K_M	Load-Mass Factor K_{LM}	Maximum Resistance	Spring Constant K	Dynamic Reaction	
							V_A	V_B
Plastic	1.0	0.33	0.17	0.51	$\frac{1}{a} \left[12(M_{pfa} + M_{psa}) + 12M_{pfb} \right]$	0	$0.09F + 0.16R_m$	$0.09F + 0.16R_m$
	0.9	0.35	0.18	0.51	$\frac{1}{a} \left[12(M_{pfa} + M_{psa}) + 11M_{pfb} \right]$	0	$0.08F + 0.15R_m$	$0.09F + 0.18R_m$
	0.8	0.37	0.20	0.54	$\frac{1}{a} \left[12(M_{pfa} + M_{psa}) + 10.3M_{pfb} \right]$	0	$0.07F + 0.13R_m$	$0.10F + 0.20R_m$
	0.7	0.38	0.22	0.58	$\frac{1}{a} \left[12(M_{pfa} + M_{psa}) + 9.7M_{pfb} \right]$	0	$0.06F + 0.12R_m$	$0.10F + 0.22R_m$
	0.6	0.40	0.23	0.58	$\frac{1}{a} \left[12(M_{pfa} + M_{psa}) + 9.3M_{pfb} \right]$	0	$0.05F + 0.10R_m$	$0.10F + 0.25R_m$
	0.5	0.42	0.25	0.59	$\frac{1}{a} \left[12(M_{pfa} + M_{psa}) + 9.0M_{pfb} \right]$	0	$0.04F + 0.08R_m$	$0.11F + 0.27R_m$

Table 5-7

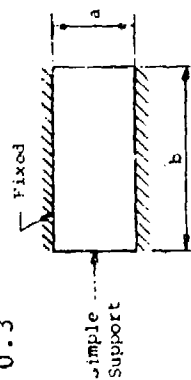
TRANSFORMATION FACTORS FOR TWO-WAY SLABS:
SHORT SIDES SIMPLY SUPPORTED - LONG SIDES FIXED (Ref. 5-13)
For Poissons Ratio = 0.3



Strain Range	a/b	Load Factor K_L	Mass Factor K_M	Load-Mass Factor K_{LM}	Maximum Resistance	Spring Constant K	Dynamic Reactions	
							V_A	V_B
Elastic	1.0	0.39	0.26	0.67	$20.4M_{psb}^0$	$575EI/a^2$	$0.07F + 0.18R$	$0.09F + 0.16R$
	0.9	0.40	0.28	0.70	$19.5M_{psb}^0$	$600EI/a^2$	$0.06F + 0.16R$	$0.10F + 0.18R$
	0.8	0.42	0.29	0.69	$19.5M_{psb}^0$	$610EI/a^2$	$0.06F + 0.14R$	$0.11F + 0.19R$
	0.7	0.43	0.31	0.71	$20.2M_{psb}^0$	$662EI/a^2$	$0.05F + 0.13R$	$0.11F + 0.21R$
	0.6	0.45	0.33	0.73	$21.2M_{psb}^0$	$731EI/a^2$	$0.04F + 0.11R$	$0.12F + 0.23R$
	0.5	0.45	0.34	0.72	$22.2M_{psb}^0$	$850EI/a^2$	$0.04F + 0.09R$	$0.12F + 0.25R$
Elasto-Plastic	1.0	0.46	0.31	0.67	$\frac{1}{a} \left[12M_{pfa} + 12(M_{psb} + M_{pfb}) \right]$	$271EI/a^2$	$0.07F + 0.18R$	$0.07F + 0.18R$
	0.9	0.47	0.33	0.70	$\frac{1}{a} \left[12M_{pfa} + 11(M_{psb} + M_{pfb}) \right]$	$248EI/a^2$	$0.06F + 0.16R$	$0.08F + 0.20R$
	0.8	0.49	0.35	0.71	$\frac{1}{a} \left[12M_{pfa} + 10.3(M_{psb} + M_{pfb}) \right]$	$228EI/a^2$	$0.06F + 0.14R$	$0.08F + 0.22R$
	0.7	0.51	0.37	0.73	$\frac{1}{a} \left[12M_{pfa} + 9.8(M_{psb} + M_{pfb}) \right]$	$216EI/a^2$	$0.05F + 0.13R$	$0.08F + 0.24R$
	0.6	0.53	0.39	0.74	$\frac{1}{a} \left[12M_{pfa} + 9.3(M_{psb} + M_{pfb}) \right]$	$212EI/a^2$	$0.04F + 0.11R$	$0.09F + 0.26R$
	0.5	0.55	0.41	0.74	$\frac{1}{a} \left[12M_{pfa} + 9.0(M_{psb} + M_{pfb}) \right]$	$216EI/a^2$	$0.04F + 0.09R$	$0.09F + 0.28R$

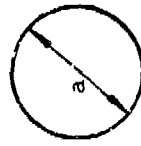
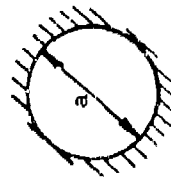
Table 5-7 (concluded)

TRANSFORMATION FACTORS FOR TWO-WAY SLABS
 SHORT SIDES SIMPLY SUPPORTED - LONG SIDES FIXED (Ref. 5-13)
 For Poissons Ratio = 0.3



Strain Range	a/b	Load Factor K_L	Mass Factor K_M	Load-Mass Factor K_{LM}	Maximum Resistance	Spring Constant K	Dynamic Reactions	
							V_A	V_B
Plastic	1.0	0.33	0.17	0.51	$\frac{1}{a} [12M_{pfa} + 12(M_{psb} + M_{pfb})]$	0	$0.09F + 0.16R_m$	$0.09F + 0.16R_m$
	0.9	0.35	0.18	0.51	$\frac{1}{a} [12M_{pfa} + 11(M_{psb} + M_{pfb})]$	0	$0.08F + 0.15R_m$	$0.09F + 0.18R_m$
	0.8	0.37	0.20	0.54	$\frac{1}{a} [12M_{pfa} + 10.3(M_{psb} + M_{pfb})]$	0	$0.07F + 0.13R_m$	$0.10F + 0.20R_m$
	0.7	0.38	0.22	0.58	$\frac{1}{a} [12M_{pfa} + 9.8(M_{psb} + M_{pfb})]$	0	$0.06F + 0.12R_m$	$0.10F + 0.22R_m$
	0.6	0.40	0.23	0.59	$\frac{1}{a} [12M_{pfa} + 9.3(M_{psb} + M_{pfb})]$	0	$0.05F + 0.10R_m$	$0.10F + 0.25R_m$
	0.5	0.42	0.25	0.59	$\frac{1}{a} [12M_{pfa} + 9.0(M_{psb} + M_{pfb})]$	0	$0.04F + 0.09R_m$	$0.11F + 0.27R_m$

Table 5-8
TRANSFORMATION FACTORS FOR CIRCULAR SLABS
FOR POISSONS RATIO = 0.3 (Ref. 5-9)



Fixed Edges a = Diameter of Slab							Simple Supports
Edge Condition	Strain Range	K_L	K_M	K_{LM}	Maximum Resistance	Spring Constant	Dynamic Reaction
Simple Supports	Elastic	0.46	0.30	0.65	$18.8M_{pc}$	$216EI/a^2$	$0.28F + 0.72R$
	Plastic	0.33	0.17	0.52	$18.8M_{pc}$	0	$0.36F + 0.64R_m$
	Elastic	0.33	0.20	0.61	$25.1M_{ps}$	$880EI/a^2$	$0.40F + 0.60R$
Fixed Supports	Elasto-Plastic	0.46	0.30	0.65	$18.8(M_{pc} + M_{ps})$	$216EI/a^2$	$0.28F + 0.72R$
	Plastic	0.33	0.17	0.52	$18.8(M_{pc} + M_{ps})$	0	$0.36F + 0.64R_m$

quantities for the equivalent system. Maximum resistances are expressed in terms of the fully plastic moment capacity, M_p , of the element and are based on the assumption that the member is proportioned so that a shear failure is prevented. Expressions for the fully plastic moment capacity of steel and reinforced concrete members are given in paragraph 5.3. The resistance-displacement function is a bilinear one similar to the elastic-plastic one shown in Fig. 5-1. Note that two mass factors are given for beams with concentrated loads. The concentrated mass factor is applied to those concentrated masses which occur at the point of application of the loads. The total equivalent mass would be the sum of the equivalent contributions from concentrated and distributed masses.

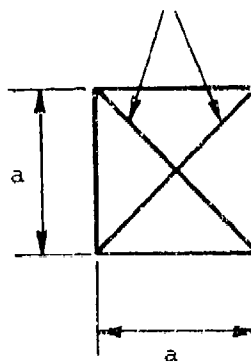
The maximum resistances and spring constants presented in Table 5-3 are for beams or one-way slabs with one end fixed and the other simply supported or with both ends fixed. In these cases, the element goes through three ranges of response since the fully plastic condition does not coincide with the formation of a plastic hinge at the supports. The resistance-displacement function for these elements is similar to that shown in Fig. 5-2. An exception is the fixed end beam with a concentrated load at midspan. For this case, the moments at midspan and the supports are equal and there is no elastic-plastic range. The maximum resistances given in Table 5-3 are those which occur at the upper limit of each range. In addition to the spring constant for each range, an effective spring constant covering all ranges is given. This effective spring constant allows the establishment of a bilinear resistance displacement function for use with the expressions given in paragraph 5.5. If plastic deformation is allowed (the normal case for most suppressive shield elements), the plastic K_{eq} is used. An equivalent elastic limit displacement can be obtained from

$$x_{eq} = \frac{R_{meq}}{K_{eq}} \quad (5-34)$$

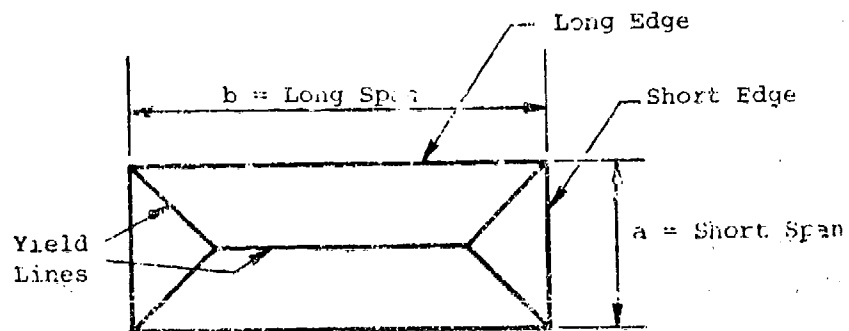
As in the case of Table 5-2, the maximum resistance and stiffnesses are in terms of the total load on the element. They must be multiplied by the appropriate load factor to obtain corresponding quantities for the equivalent system. The mass factors in Table 5-3 are used in the same manner as those in Table 5-2.

Maximum resistances, spring stiffnesses and transformation factors for two-way rectangular slabs with various edge conditions are presented in Tables 5-4 through 5-7. These quantities are also obtained from assumed deflected shapes of the slabs. In the elastic region, the deflected shapes are based upon approximations to classical plate theory. In the plastic region, they are based upon yield line theory. The assumed yield lines are as shown in Fig. 5-10. As in the case of the beams and slabs with fixed ends, the resistance-displacement function for two-way slabs can be divided into three ranges; elastic, elastic-plastic, and plastic. Reference 5-13 neglects the elastic-plastic range for simply supported two-way slabs. The elastic range for simply supported two-way slabs is assumed to exist until the development of plastic moment along the assumed yield lines. The elastic range for fixed-end, two-way slabs is assumed to exist until the support moment along the long edge of rectangular slabs, or all edges of square slabs, reaches the plastic resistance value. This is the beginning of the elastic-plastic range which is assumed to hold up to the plastic range. The plastic range is initiated with the development of plastic moment along each of the assumed yield lines. For two-way slabs, simply supported on two opposite sides and fixed on the other two sides, the elastic range is assumed to exist until the development of plastic moments along the fixed edges. The elastic-plastic range is assumed to hold up to the development of full plastic moments along all assumed yield lines. The maximum resistances given

Yield Lines



(a) Square Slab



(b) Rectangular Slab

Figure 5-10. Assumed Yield Lines for Two-Way Slabs

in Tables 5-4 through 5-7 represent the upper limits of each range. Spring stiffnesses are given for each range of response. Maximum resistances and spring stiffnesses are given in terms of the total load on the slab and must be multiplied by the load factor to obtain the corresponding quantities for the equivalent single degree of freedom system. These transformed quantities can be used to construct a resistance displacement diagram similar to that shown in Fig. 5-2. An effective spring stiffness over the entire displacement range can be calculated using the procedure described earlier in paragraph 5.2. A reasonable approximation can be obtained by visual inspection of the tri-linear plot.

Table 5-8 presents transformation factors for circular slabs. These factors were taken from Ref. 5-9 and were derived using the procedures outlined in Ref. 5-13.

As in the case of beams and one-way slabs, the maximum resistances for two-way slabs assume that the slabs are proportioned so that they do not fail in shear.

The notation used in Tables 5-2 through 5-8 is as follows.

- M_p = ultimate bending moment capacity
- M_{pfa} = total ultimate positive bending moment capacity along midspan section parallel to short edge, a
- M_{pfb} = total ultimate positive bending moment capacity along midspan section parallel to long edge, b
- M_{psa} = total ultimate negative moment capacity along short edge, a
- M_{psb} = total ultimate negative moment capacity along long edge, b
- M_{psa}^o = ultimate negative bending moment capacity per unit width at center of edge a in direction of long span, b

- M_{Psb}° = ultimate negative bending moment capacity per unit width at center of edge b in direction of short span, a
- M_{PC} = ultimate positive bending moment capacity per unit width at center of circular slab
- M_{Ps} = ultimate negative bending moment capacity per unit width at edge of circular slab or ultimate bending moment capacity of beam at support
- M_{Pm} = ultimate bending moment capacity of beam at mid-span
- I = moment of inertia of beam or moment of inertia of unit width of slab
- I_a = average of gross and cracked moment of inertia per unit width of concrete slabs (for short span in two-way slabs) or moment of inertia of plate per unit width
- E = modulus of elasticity
- V = dynamic reaction at ends of symmetric beams or simple cantilever
- V_1 = dynamic reaction at hinged end of non-symmetric beams
- V_2 = dynamic reaction at fixed end of non-symmetric beams
- V_A = total dynamic reaction along one short edge
- V_B = total dynamic reaction along one long edge

5.4.3 Dynamic Reactions

It is important to recognize that the dynamic reactions of the real structural element have no direct counterpart in the equivalent single degree of freedom system (Ref. 5-6). It is important to obtain some estimate of reactions since they are always related to the maximum shear in the

element, and they are also necessary for the design of the supporting structures.

Expressions for the reactions may be obtained by considering the dynamic equilibrium of the complete element. The dynamic equilibrium of the element includes consideration of loads acting on the element and inertia forces which are assumed to be proportional to the deflected shape. By assuming a deflected shape, the reactions can be defined in terms of the loads acting on the element and its resistance. Tables 5-2 through 5-8 include factors for calculating the dynamic reactions of the various structural elements. The general form of the expression is

$$V = C_1 F + C_2 R \quad (5-35)$$

where

V = the dynamic reaction at one end or edge of the element, except in the case of circular slabs where V represents the total reaction at the supports

C_1, C_2 = coefficients obtained from the tables

F = total force applied to the element

R = resistance of the element

In most cases, both F and R are functions of time. In the elastic range, the maximum resistance occurs at maximum displacement, and the loading and resistance at the time of maximum displacement are used in Eq. 5-35 with the appropriate coefficients to obtain the dynamic reactions. In the plastic range, as the load F decreases with time, the maximum reactions occur when the displacement first reaches its yield value and the resistance is equal to R_m . For these cases, the time to reach yield displacement can be obtained by numerical integration of the equation of motion or by a slightly conservative method discussed in the next paragraph. The loading at this time and R_m are used in Eq. 5-35 to obtain the dynamic reactions.

In those cases where the quasi-static load does not decrease significantly within a period of time approximately equal to the period of the structure and the peak reflected pressure pulse whose time of duration is much less than the period is neglected, the procedure is simplified somewhat. For both the elastic and plastic regions, the loading contribution is taken equal to the peak quasi-static load and the resistance is taken equal to R_m . The latter approach can also be used to obtain a conservative estimate of reactions for a decaying pulse. For rapidly decaying loads, the results can be overly conservative. Note that since F and R are expressed in terms of the total load and resistance, the reactions obtained from Eq. 5-35 represent the total at the ends of the beam or the total for an edge of the slab.

5.5 DYNAMIC RESPONSE OF STRUCTURAL SYSTEMS

5.5.1 Introduction

Most real structures are very complex in their behavior even under static loads, and their response to dynamic loads includes additional complications due to various combinations of elastic and inelastic vibrational modes. The usual approach to determining the dynamic response of a structure or structural element to some specific loading is to first model or represent the structure as a system of finite structural elements and masses connected together at a discrete number of nodal points. If the force-displacement relationships are known for the individual elements, various methods of structural analysis can be used to study the behavior of the assembled structure. Most structures are made up of beams, girders, columns, slabs, plates and shells, with each of these elements having distributed mass and stiffness. If certain assumptions are made regarding stiffness of connections, lumping of masses, stiffnesses and applied loads, it is possible to replace these structures and structural

elements with simpler equivalent systems. In general, the more complex the structure, the greater the number of individual elements required to accurately describe its response.

Methods of analysis for complex multiple degree of freedom systems are not considered in this handbook, except for those systems which can be represented by an equivalent single degree of freedom system. Approximate methods of analysis which reduce some common types of multiple degree of freedom systems to equivalent single degree of freedom systems were presented in paragraph 5.4. If the system is assumed to be vibrating in its fundamental mode only, its natural frequency can be computed using expressions from paragraph 5.3.6 and the system analyzed as a single degree of freedom system. Most suppressive shield structures consist of combinations of structural elements; however, it can be assumed in many cases that individual elements act independently of each other. For example, the peak response of a beam may be considered independent of the response of a girder which supports it. In this case, the beam and girder system can be analyzed independently as two uncoupled single degree of freedom systems. An approximate rule is that two such elements may be treated separately if their periods of vibration vary by a factor of 2 or more.

If the periods of vibration of the two elements are not sufficiently different, a multiple degree of freedom analysis should be made. The numerical integration technique which is applied to single degree of freedom systems in paragraph 5.5.3 can also be used for analysis of multiple degree of freedom systems. The calculations for systems with greater than two or three degrees of freedom become lengthy and tedious and should be programmed for high speed electronic computers. The elastic response of multiple degree of freedom systems is readily obtained using structural analysis programs such as STRUDL/DYNAL (MCAUTO), NASTRAN (NASA), STARDYNE (Mechanics Research, Inc.), and SAP IV (Univ. of Calif. at Berkeley). MARC-CDC (Control Data Corp.) and ANSYS (Swanson Analysis Systems, Inc.) are

general purpose finite element programs for the nonlinear analysis of structures with large displacements.

5.5.2 Energy Methods

Energy and momentum considerations can be used to develop general solutions for single degree of freedom systems. Assuming an elastic-plastic resistance function such as that shown in Fig. 5-1, solutions can be obtained for load cases which approximate those generated within suppressive shields. The first corresponds to the situation where the load rises suddenly to its maximum value and remains constant for all displacements of the structural element. This is the step pulse or long duration loading shown in Fig. 5-11. The second is the case where all of the force is applied as an impulse before the structural element can displace appreciably.

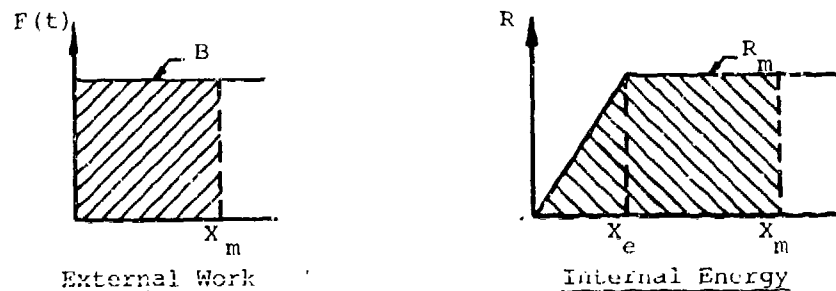


Figure 5-11. External Work and Internal Energy for Long Duration Load

In the first case, the external work done on the system is equal to the applied force times the displacement of its point of application in the direction of the force. At maximum displacement, the velocity of the mass is zero and the external work must be equal to the strain energy stored in the system. The external work and the internal energy are represented by the shaded areas of the diagrams shown in Fig. 5-11.

Equating the two areas

$$BX_m = R_m X_m - \frac{R_m X_e}{2} \quad (5-36)$$

the required maximum resistance is given by

$$R_m = B \left[\frac{2\mu}{2\mu-1} \right] \quad (5-37)$$

Rearranging terms in Eq. 5-37, the maximum displacement of the system is obtained from

$$\mu = \frac{X_m}{X_e} = \frac{1}{2 \left[1 - \frac{B}{R_m} \right]} \quad (5-38)$$

Equation 5-37 is applicable only to those problems where $\mu \geq 1$. It should also be noted from Eq. 5-38 that R_m must be greater than the peak load, B . If $R_m \leq B$, the internal energy will never equal the external work done by the step pulse.

In the case of the impulsive load shown in Fig. 5-12, the total impulse applied to the system is equal to the area under the load-time function, i.e.,

$$i = \frac{Bt_o}{2} \quad (5-39)$$

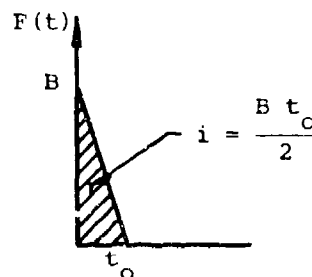


Figure 5-12. Impulsive Loading

Assuming the system is initially at rest, this impulse imparts an instantaneous velocity to the mass of

$$\dot{X} = \frac{i}{M} \quad (5-40)$$

and the kinetic energy of the mass is

$$K.E. = \frac{M(\dot{X})^2}{2} = \frac{i^2}{2M} \quad (5-41)$$

As in the case of the long duration load, this kinetic energy will be converted to strain energy at the time of maximum displacement of the system. Thus

$$\frac{1}{2M} \left[\frac{Bt_0}{2} \right]^2 = R_m X_m - \frac{R_m X_e}{2} \quad (5-42)$$

Substituting

$$M = \frac{K}{\omega_N^2} = \frac{R_m}{X_e} \left[\frac{T_N}{2\pi} \right]^2$$

and

$$\mu = \frac{X_m}{X_e}$$

into Eq. 5-42, the required maximum resistance is given by

$$R_m = B \left[\frac{\pi t_0}{T_N \sqrt{2\mu - 1}} \right] \quad (5-43)$$

Making the substitution

$$i = \frac{Bt_0}{2}$$

and

$$T_N = \frac{2\pi}{\omega_N}$$

results in a more general form of Eq. 5-43.

$$R_m = \frac{i\omega_N}{\sqrt{2\mu - 1}} \quad (5-44)$$

Maximum response of the system is obtained from

$$\mu = \frac{1}{2} \left[\left(\frac{B\pi t_o}{R_m T_N} \right)^2 + 1 \right] \quad (5-45)$$

or

$$\mu = \frac{1}{2} \left[\left(\frac{i\omega_N}{R_m} \right)^2 + 1 \right] \quad (5-46)$$

Equations 5-43 through 5-46 are also applicable only to problems where $\mu \geq 1$. In order for this condition to occur, the ratios

$$\frac{B\pi t_o}{R_m T_N} \quad \text{and} \quad \frac{i\omega_N}{R_m}$$

must be greater than or equal to 1. Equations 5-37 and 5-38 are most correct for larger values of t_o/T_N and Eqs. 5-43 through 5-46 for smaller values. Large and small have been somewhat arbitrarily defined to be ratios of 10 and 0.2 respectively. Reference 5-14 recommends the expression

$$\frac{B}{R_m} = \frac{T_N}{\pi t_o} \sqrt{2\mu - 1} + \frac{1 - \frac{1}{2\mu}}{1 + 0.7 \frac{T_N}{t_o}} \quad (5-47)$$

as applicable over the whole range of possible values of t_o/T_N . Equation 5-47 is reported to be in error by less than 8.4 percent over a range of values of t_o from 0 to infinity and of μ from 1 to infinity. At **large** values of t_o/T_N , it reduces to Eq. 5-37; at small values of t_o/T_N , it becomes Eq. 5-43.

The methods of analyses presented up to this point can only be applied to loadings which can be adequately represented by a simple triangular or step function. In some instances, a multiple triangle approximation of the actual loading will yield more accurate results. Figure 5-13 shows a three-triangle approximation of a loading function. Two, four or n-triangle approximations are also possible. A

reasonable approximation to the response of a single degree of freedom system to this loading can be obtained by treating each triangle as a partial load acting alone. For the three triangle approximation shown in Fig. 5-13, the relationship is

$$\frac{C_1 B/R_m}{F_1} + \frac{C_2 B/R_m}{F_2} + \frac{C_3 B/R_m}{F_3} = 1 \quad (5-48)$$

where F_1 , F_2 , and F_3 are the values of $C_1 B/R_m$, $C_2 B/R_m$ and $C_3 B/R_m$ for given values of μ and ratios of duration of load to period t_1/T_N , t_2/T_N and t_3/T_N , respectively. Equations 5-37, 5-43, 5-44 or 5-47, as appropriate, can be used to obtain F_1 , F_2 and F_3 . Identical values of μ and T_N are used for each partial load computation. The general relationship is

$$\sum \frac{C_n B/R_m}{F_n} = 1 \quad (5-49)$$

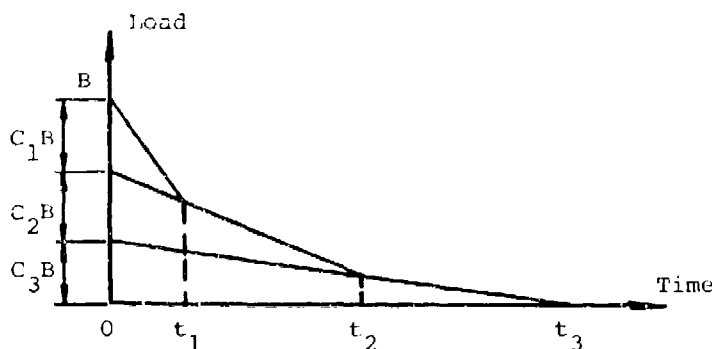


Figure 5-13. Multiple Triangle Approximation of Loading Function

Many airblast loadings of interest can be adequately represented by a two triangle approximation. Equations 5-47 and 5-48 can be combined to obtain a general solution for this case.

$$\frac{\frac{C_1 B}{R_m}}{\frac{T_N}{\pi t_1} \sqrt{2\mu-1} + \frac{1 - \frac{1}{2\mu}}{1 + 0.7 \frac{T_N}{t_1}}} + \frac{\frac{C_2 B}{R_m}}{\frac{T_N}{\pi t_2} \sqrt{2\mu-1} + \frac{1 - \frac{1}{2\mu}}{1 + 0.7 \frac{T_N}{t_2}}} = 1 \quad (5-50)$$

If both t_1 and t_2 are much larger than T_N , Eq. 5-50 reduces to

$$\frac{\frac{C_1 B}{R_m}}{1 - \frac{1}{2\mu}} + \frac{\frac{C_2 B}{R_m}}{1 - \frac{1}{2\mu}} = 1 \quad (5-51)$$

If both t_1 and t_2 are much smaller than T_N , Eq. 5-50 reduces to

$$\frac{\frac{C_1 B}{R_m}}{\frac{T_N}{\pi t_1} \sqrt{2\mu-1}} + \frac{\frac{C_2 B}{R_m}}{\frac{T_N}{\pi t_2} \sqrt{2\mu-1}} = 1 \quad (5-52)$$

The maximum error in this procedure occurs when an extremely short pulse is combined with an infinitely long one (see Fig. 5-14). For this case, a better approximation is obtained if the sum of the kinetic energy imparted by the impulse and the work done by the quasi-static pressure is equated to the strain energy in the system, i.e.,

$$\frac{1}{2M} \left[\frac{C_1 B t_1}{2} \right]^2 + C_2 B X_m = R_m X_m - \frac{R_m X_m^2}{2} \quad (5-53)$$

Making the same substitutions as were made for Eq. 5-43 and rearranging terms, it is found that

$$\left[\frac{\frac{C_1 B/R_m}{\frac{T_N}{\pi t_1} \sqrt{2\mu-1}}}{1 - \frac{1}{2\mu}} \right]^2 + \frac{C_2 B/R_m}{1 - \frac{1}{2\mu}} = 1 \quad (5-54)$$

where the subscript 1 refers to the impulse component and all other terms are as previously defined.

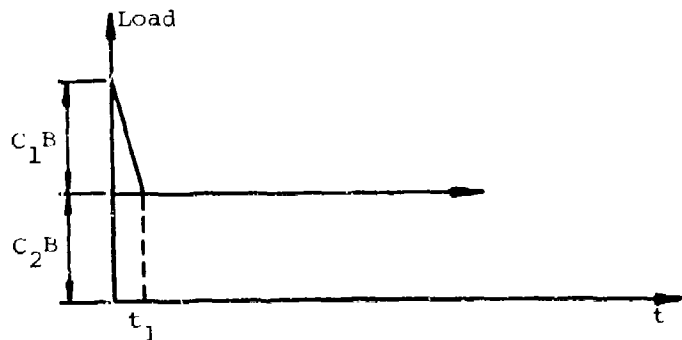


Figure 5-14. Impulsive Load Plus Long Duration Component

Although Eq. 5-54 is derived for a constant amplitude second pulse, it can be applied to other loadings where the duration of the initial pulse is less than one-fifth the period and the duration of the second pulse is greater than 10 times the period of the system. Alternatively, Eq. 5-55 can be used for those loadings where the initial pulse is less than one-fifth the period and the second pulse has a long, but finite duration.

$$\left[\frac{\frac{C_1 B}{R_n}}{\frac{T_N}{\pi t_1} \sqrt{2\mu-1}} \right]^2 + \frac{\frac{C_2 B}{R_m}}{\frac{T_N}{\pi t_2} \sqrt{2\mu-1} + \frac{1 - \frac{1}{2\mu}}{1 + 0.7 \frac{T_N}{t_2}}} = 1 \quad (5-55)$$

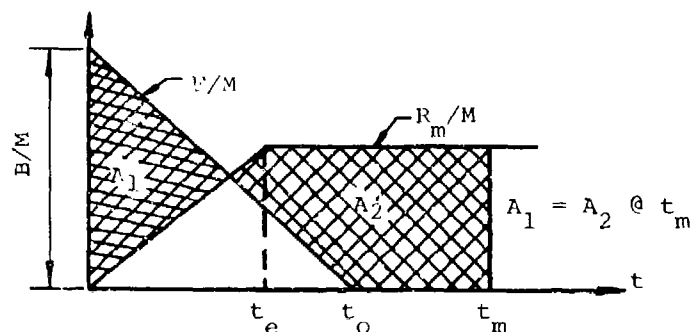
Appendix B includes charts of Eq. 5-54 which can be used for preliminary design or analysis.

The equations of this section and response charts of Appendix B can be used in two ways. If the properties of the system and load characteristics are specified, the maximum response can be obtained directly in terms of the ductility ratio, μ . For a single pulse approximation of the loading, the determination of response is straightforward. For multiple triangle approximations of the loading, it will be necessary to either assume various values of μ until the appropriate equation from Eqs. 5-49 through 5-55 is satisfied or to solve the equation for μ .

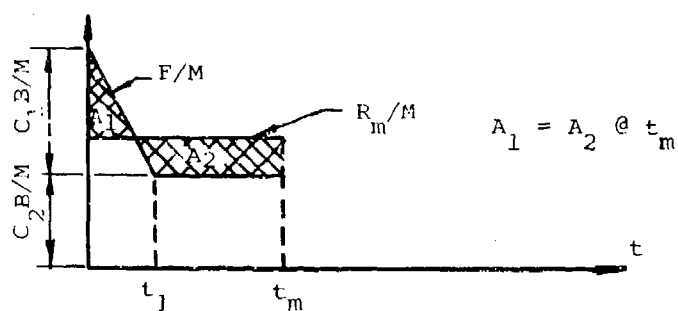
If only the load characteristics and a desired maximum response are specified, an iterative process is required for design. In order to start the process, it is necessary to assume some trial section properties. With these properties, the system can be designed and its maximum response obtained. If the required resistance is more than the trial section resistance, the process must be repeated until the required resistance is equal to or less than the trial section resistance.

Equations 5-37, 5-43, 5-44, and 5-47 through 5-55 are valid only if response extends beyond the elastic limit, i.e., $\mu \geq 1$. Inspection of these equations shows the benefit of allowing inelastic response to take place. Equation 5-37 indicates that, if a large value of μ is permitted, the required resistance of the element may be equal to B . For elastic response ($\mu=1$) the resistance must be equal to $2B$. Equation 5-44 shows that for the elastic case ($\mu=1$), the required resistance is equal to $i\omega_N$, but the required resistance approaches zero as μ increases. Note also that the load term " B " and the resistance term " R_m " may be either total load and total resistance (B, R_m) or unit load and unit resistance (P_r, r_m).

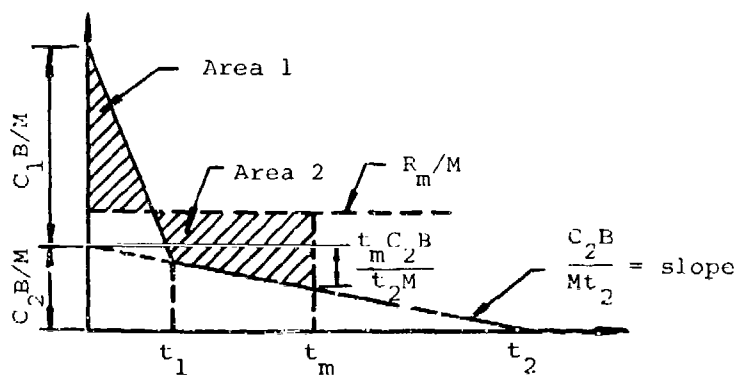
It is sometimes important to determine the time of maximum response of the structural element. If the ordinates of the loading and resistance functions are divided by the mass, M , they can be plotted as shown in Fig. 5-15. The loading can be considered an acceleration function and the resistance a deceleration function. The area under either plot is equal to the velocity change of the system due to the loading or resistance of the element. Since the velocity of the mass is equal to zero at t_m , the areas under the loading and resistance plots must be equal at this time. If one diagram is subtracted from the other, the net area must be equal to zero. If one area is subtracted from the other as shown in Fig. 5-15, then A_1 must equal A_2 . Although the concept is simple, a difficulty arises in determining the time, t_e , to reach maximum resistance. An iterative technique, such as numerical integration, can be used to determine t_e . Alternatively, a rigid-plastic resistance, i.e., $t_e=0$, might be assumed to obtain an approximation of t_m . The percent error in such an approximation decreases with increasing μ . Figure 5-15(b)



(a) Triangular Load



(b) Impulse Plus Quasi-Static Load with Rigid-Plastic Resistance



(c) Double Pulse Loading with Rigid-Plastic Resistance

Figure 5-15. Acceleration Versus Time Plots

demonstrates how this technique might be applied to an impulsive load superimposed on a quasi-static type loading and Fig. 5-15(c) applies the technique to a two-triangle representation of the airblast loading. Assuming a rigid-plastic resistance function, the areas under the loading and resistance plots in Fig. 5-15(b) will be equal at t_m , i.e.,

$$\frac{C_1 B t_1}{2M} + \frac{C_2 B t_m}{M} = \frac{R_m t_m}{M} \quad (5-56)$$

or

$$t_m = \frac{C_1 B t_1}{2(R_m - C_2 B)} \quad (5-57)$$

Assuming a rigid-plastic resistance function for the two triangle loading shown in Fig. 5-15(c), the areas under the loading and resistance functions can again be equated, i.e.,

$$\frac{C_1 B t_1}{2M} + \left[C_2 B - \frac{C_2 B t_m}{2t_2} \right] \frac{t_m}{M} = \frac{R_m t_m}{M} \quad (5-58)$$

Expanding Eq. 5-58 and solving for t_m , it is found that

$$t_m = \frac{C_2 B - R_m \pm \left[(R_m - C_2 B)^2 + \frac{(C_2 B)(C_1 B t_1)}{t_2} \right]^{0.5}}{C_2 B} \quad (5-59)$$

5.5.3 Numerical Integration

This analytical technique obtains the response of the system by numerical integration of the differential equation of motion. It is the most general and versatile method of analysis for many problems of interest. It can be applied to any system with a finite number of degrees of freedom and can treat any force-displacement-time relationship, ranging

from linear elastic to nonlinear, viscoelastic-plastic relations. Numerical integration has found wide application on electronic computing devices for compiling the solutions to simple problems, and for the rapid solution of problems in the dynamics of complicated systems. For hand computation, the method is best suited to systems of a few degrees of freedom with simple force-resistance relations, such as the bilinear elastic or elastic-plastic resistances.

Rewriting Eq. 5-30 in the form

$$\ddot{X} = \frac{F(t) - KX}{K_{LM}^M t} \quad (5-60)$$

it is seen that if $F(t)$ and X are known at any particular instant of time, the acceleration of the mass, M , can be calculated. The basis of the method of numerical integration is the subdivision of time into intervals, Δt , and an assumption of the nature of the variation of the acceleration during the time interval. The procedure recommended herein is presented in Refs. 5-15 and 5-16. It is convenient to adopt the notation developed in Ref. 5-15. If \ddot{X}_n , \dot{X}_n , X_n , are the acceleration, velocity and displacement, respectively, at time $t = t_n$, then the velocity and displacement of the mass at time $t = t_n + \Delta t$ are given by

$$\dot{X}_{n+\Delta t} = \dot{X}_n + \frac{1}{2} \Delta t (\ddot{X}_n + \ddot{X}_{n+\Delta t}) \quad (5-61)$$

$$X_{n+\Delta t} = X_n + \Delta t \dot{X}_n + \frac{(\Delta t)^2}{2} \ddot{X}_n + \beta (\ddot{X}_{n+\Delta t} - \ddot{X}_n) (\Delta t)^2 \quad (5-62)$$

If the variation of the acceleration over the time interval Δt is linear, β is taken equal to $1/6$. If a constant acceleration equal to the average of \ddot{X}_n and $\ddot{X}_{n+\Delta t}$ is assumed over the time interval, β is taken equal to $1/4$. Values of β of 0 and $1/12$ can also be given simple geometric interpretations.

The method proceeds as follows. The acceleration, velocity, and displacement at $t = 0$ are computed or obtained from the given initial conditions. Then for $t = \Delta t$, the

acceleration $\ddot{X}_{n+\Delta t}$ is assumed. Using Eqs. 5-61 and 5-62, the velocity and displacement at time $t_{n+\Delta t}$ are computed. Knowing the displacement $X_{n+\Delta t}$, the resistance KX can be evaluated. This value is then substituted into Eq. 5-60 and the assumed acceleration checked. If the assumed and resultant acceleration are not in agreement, the computed acceleration is used for the next trial and the computational process repeated until the procedure converges to the correct solution. When convergence is obtained, the next time increment is added and the process repeated.

The criteria which are important in the application of numerical integration are convergence, rate of convergence, stability, length of time interval, and choice of β . All of these criteria are interrelated and have been studied fairly extensively. The stability and convergence criteria for an undamped single degree of freedom system will generally be satisfied if the ratio $\Delta t/T_N$ is less than about 0.2. For systems with several degrees of freedom, the stability and convergence limits must be applied in terms of the natural period of the highest mode of vibration, i.e., the minimum natural period. The choice of a time interval also determines the number of iterations required to properly describe structural response and, therefore, affects the cost of the analysis in terms of computer time. Another consideration is that the time interval should be small enough to adequately describe the time variation of the forcing function.

The choice of β governs the accuracy and ease of application of the method. Extensive work in the application of this method has resulted in the following conclusions. A $\beta = 1/6$ is best suited for forced vibrations of systems with damping and with initial velocity and displacement. The best results in amplitude of response for an undamped system are obtained using $\beta = 1/4$. A $\beta = 1/12$ gives the most rapid and accurate results for an undamped system without initial

velocity. For very rapid results, where accuracy is not of primary importance, $\beta = 0$ often proves useful.

5.5.4 Spherical Chambers

Spherical chambers are used for some suppressive shield applications where the fragment hazards are minimal. If it is assumed that the sphere responds only in the fundamental mode, it can be analyzed as a single degree of freedom system using the techniques described earlier in this chapter. Its elastic period of vibration is given by Eq. 5-24. Its static resistance can be obtained from Eq. 5-17 or 5-21. Illustrative example 5.6.4 uses this approach to analyze a Group 6A shield.

Reference 5-12 proposes an approximate expression for the maximum stress in a spherical suppressive shield. It is based on computer solutions of the differential equation of motion for the sphere and applies only to the elastic case.

Reference 5-17 offers closed form solutions to the elastic-plastic response of thin spherical shells to internal blast loading. In order for results to be obtained, solutions to non-linear differential equations are required.

Reference 5-20 uses an energy method to obtain the plastic response; however, this report does not consider the effects of impulse and quasistatic pressure simultaneously.

For additional design information, references 5-21 and 5-22 discuss spherical chamber component parts, fabrication techniques, and test results for the Group 6A and 6B shields.

5.6 ILLUSTRATIVE EXAMPLES

5.6.1 Response of the Group 3 Suppressive Shield Walla. Given

A 48.8 pound charge of Pentolite is detonated inside the Group 3 Suppressive Shield. The Group 3 Shield is a cylindrical structure with a flat reinforced concrete roof and floor. The cylindrical body of the structure is fabricated from 296 interlocking S3x5.7 I-beams. The inner layer of I-beams has an inside radius of 5 feet 7.5 inches. The inside height of the structure is 10 feet. A layered steel reinforcing ring is placed around the outer circumference of the body at a distance of 5 feet above the floor.

b. Find

The maximum response of beam elements in the wall of the shield to airblast loading.

c. Solution

The first step is to determine the blast loading seen by the wall. The TNT equivalent for Pentolite is given in Table 3-1 as 1.129. The equivalent charge weight of TNT from Eq. 3-1, pg. 3-4 is

$$W = 1.129(48.8) = 55.1 \text{ lb TNT}$$

and

$$W^{1/3} = 3.805 \text{ lb}^{1/3}$$

The scaled distance from the charge to the mid-height of the wall from Eq. 3-2, pg. 3-6 is

$$Z = \frac{R}{W^{1/3}} = \frac{5.625}{3.805} = 1.478 \text{ ft/lb}^{1/3}$$

Values of peak reflected pressure and scaled specific impulse as a function of scaled distance are plotted in Fig. 3-6. For $Z = 1.478 \text{ ft/lb}^{1/3}$

$$P_r = 3350 \text{ psi}$$

and

$$\frac{i_r}{W^{1/3}} = 0.111 \text{ psi-sec/lb}^{1/3}$$

or

$$i_r = 0.422 \text{ psi-sec}$$

The duration of the reflected pulse is obtained from Eq. 3-4, pg. 3-14.

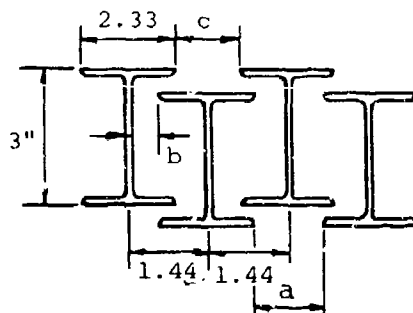
$$t_r = 2i_r/P_r = 0.00025 \text{ sec}$$

The peak quasi-static pressure is found from Fig. 3-9. For

$$\frac{W}{V} = \frac{55.1}{\pi (5.625)^2 (10)} = 0.0554 \text{ lb/ft}^3$$

$$P_{qs_{\max}} = 187 \text{ psi}$$

To determine the duration of the quasi-static pressure, the vent area ratio, α_e , of the structure must be found. Only the cylindrical wall provides venting. An idealized representation of the interlocking I-beams which make up the wall is shown below. Referring to Fig. 3-7(d),



Group 3 Shield Wall Section

$$a = c = 2 \left(1.44 - \frac{2.33}{2} \right) = 0.55 \text{ inch}$$

$$b = 1.44 - \frac{2.33}{2} - 0.5(0.19) = 0.179 \text{ inch}$$

Then,

$$A_{V_1} = 2 \ln a_i = 2(120)(148)(0.55) = 19,358.4 \text{ in}^2$$

$$A_{V_2} = A_{V_3} = 2 \ln b_i = 2(120)(148)(0.179) = 6358.1 \text{ in}^2$$

$$A_{V_4} = 2 \ln c_i = 2(120)(148)(0.55) = 19,358.4 \text{ in}^2$$

$$A_w = nL(2.33 + 0.545) = 148(120)(2.875) = 51,060 \text{ in}^2$$

and

$$\alpha_1 = \alpha_4 = \frac{A_{V_1}}{A_w} = \frac{19,358.4}{51,060} = 0.3791$$

$$\alpha_2 = \alpha_3 = \frac{A_{V_2}}{A_w} = \frac{6358.1}{51,060} = 0.1245$$

From Eq. 3-5, pg. 3-15,

$$\frac{1}{\alpha_e} = \sum_{i=1}^n \frac{1}{\alpha_i} = \frac{1}{0.3791} + \frac{1}{0.1245} + \frac{1}{0.1245} + \frac{1}{0.3791} = 21.34$$

or

$$\alpha_e = 0.0469$$

The scaled maximum pressure is

$$\bar{P} = \frac{P_{gs} + P_o}{P_o} = \frac{187 + 14.7}{14.7} = 13.72$$

The interior surface area of the shield wall is

$$A_i = 2\pi rh = 2(3.14)(5.625)(10) = 353.43 \text{ ft}^2$$

HNDM-1110-1-2

From Fig. 3-10 for a scaled maximum pressure of 13.72, the scaled blowdown time is

$$t_b a_o \alpha_e A_i / V = 1.23$$

Substituting the known parameters

V = volume of structure (994 ft^3)

α_e = vent area ratio (0.0469)

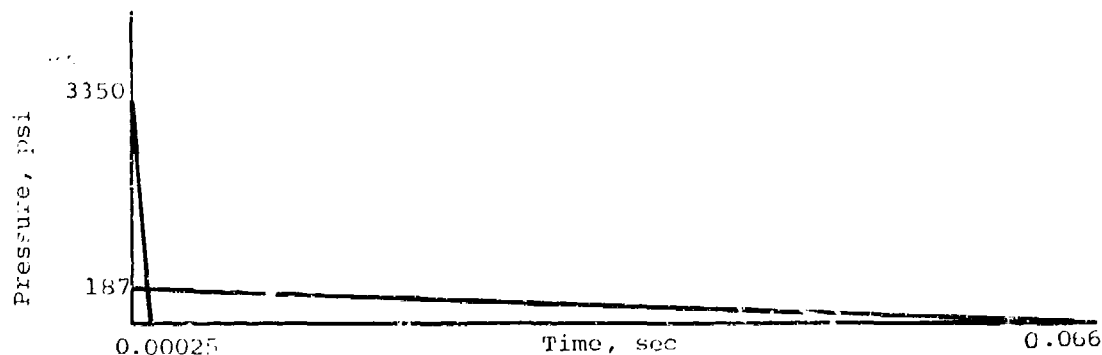
A_i = surface area of cylinder wall (353.43 ft^2)

a_o = sound velocity in air (1117 ft/sec)

and solving for t_b , it is found that the blowdown time is

$$t_b = 0.066 \text{ sec}$$

The blast pressure loading on the wall of the structure is approximated by a double triangular pressure pulse as shown below.



Blast Loading of Group 3 Shield I-Beam

$$C_1 = \frac{3350 - 187}{3350} = 0.944$$

$$C_2 = \frac{187}{3350} = 0.056$$

The structure responds dynamically to both the reflected pressure pulse and the quasi-static pressure. Response of the wall is determined by considering an individual I-beam. The beam is assumed to have fixed ends and a span of 5 feet. Because of the arrangement

of the interlocking I-beams, the effective width over which the blast load acts is assumed to be 1.44 inches per beam. (See previous sketch of Group 3 Shield wall section).

The section and material properties of the S3x5.7 beam are (Ref. 5-2)

$$\begin{aligned} w &= 5.7 \text{ lb/ft} & E &= 29 \times 10^6 \text{ psi} \\ I &= 2.52 \text{ in}^4 & f_y &= 36,000 \text{ psi} \\ S &= 1.68 \text{ in}^3 & f_{dy} &= 39,600 \text{ psi (Table 4-1)} \\ L &= 5 \text{ ft} = 60 \text{ inches} \end{aligned}$$

The natural period of a beam fixed at both ends is obtained from the expression for natural frequency in Fig. 5-8, i.e.,

$$T_N = \frac{2\pi}{\omega_N} = 0.28L^2 \sqrt{w/EIg}$$

where

$$w = \text{weight, lb/in} = 0.475 \text{ lb/in}$$

$$g = \text{gravitational acceleration, in/sec}^2 = 386 \text{ in/sec}^2$$

For the beam only, the natural period is

$$\begin{aligned} T_N &= 0.28(60)^2 \sqrt{0.475/[29(10)^6(2.52)(386)]} \\ &= 0.00414 \text{ sec} \end{aligned}$$

The maximum resistance of a uniformly loaded beam fixed at both ends is given in Table 5-3 as

$$R_m = \frac{16M_P}{L}$$

where the plastic moment

$$M_P = f_{dy} Z$$

Then the unit resistance (resistance per square inch of beam) is

$$r_m = \frac{16f_{dy}Z}{bL^2}$$

where

Z = plastic section modulus, 1.932 in³

f_{dy} = dynamic yield strength, 39,600 psi

b = effective beam width, 1.44 inches

L = length, 60 inches

Substituting in the above equation, it is found that

$$r_m = 236 \text{ psi}$$

The ratios t_1/T_N and t_2/T_N for the two triangles of the loading function meet the criteria for use of Eq. 5-55, pg. 5-58 to obtain the structural response, i.e.,

$$\left[\frac{C_1 P_r / r_m}{\frac{T_N}{\pi t_1} \sqrt{2\mu - 1}} \right]^2 + \frac{C_2 P_r / r_m}{\frac{T_N}{\pi t_2} \sqrt{2\mu - 1} + \frac{1 - \frac{1}{2\mu}}{1 + 0.7 \frac{T_N}{t_2}}} = 1$$

where

r_m = maximum unit resistance of member, psi

P_r = maximum pressure, psi

t_1 = time of duration of first pulse, sec

t_2 = time of duration of second pulse, sec

μ = ductility ratio

C_1 = ratio of peak pressure of first pulse to maximum pressure

C_2 = ratio of peak pressure of second pulse to maximum pressure

A solution of Eq. 5-55 is obtained by trial and error. Successive values of μ are assumed until Eq. 5-55 is satisfied. A table may be set up as follows:

trial No.	μ	$(C_1 P_r / r_m / F_1)^2$	$C_2 P_r / r_m / F_2$	Sum of Terms
1	14	.239	.774	1.013
2	16	.208	.766	.968
3	15	.223	.769	.992 O.K

The equivalent elastic deflection is given by

$$X_e = \frac{R_m}{K_e}$$

where, for the elastic-plastic range

$$K_e = K_E = \frac{307EI}{L^3} \text{ from Table 5-3}$$

$$R_m = \frac{16M_P}{L}$$

Then,

$$X_e = \frac{16M_P I^2}{307EI} = \frac{16(1.15)(1.68)(39,600)(60)^2}{307(29 \times 10^6)(2.52)}$$

$$= 0.1964 \text{ inch}$$

Maximum deflection is found from

$$X_m = \mu X_e = 0.1964\mu$$

and maximum strain is found from

$$\epsilon_m = c\mu_y = \mu \frac{f_{dy}}{E} = 0.00137\mu$$

Substituting the calculated ductility ratio of 15, the maximum deflection and strain for a beam are 2.95 inches and 0.02 inch/inch, respectively.

5.6.2 Numerical Integration Technique for Determining Response of a Steel Beam Subjected to Blast Loading

a. Given

A Group 3 Shield S3x5.7 I-beam 60 inches long, fixed at both ends, and subjected to the blast loading determined in illustrative example 5.6.1. Although a multiple degree

of freedom analysis of the beams using the numerical integration technique would provide more detailed information, it would require a computer. The approximate single degree of freedom approach is used here.

b. Find

(1) The time at which the beam begins to yield, (2) the load acting on the beam at time of yielding, and (3) the maximum displacement of the beam by numerical integration.

c. Solution

The equation of motion for an elastic equivalent single degree of freedom system is given by Eq. 5-30, pg. 5-32.

$$K_{LM} M_t \ddot{X} + KX = F_t(t)$$

where

K_{LM} = the load-mass transformation factor

M_t = total mass of the real element, lb-sec²/in

K = elastic spring constant, lb/in

F_t = total load acting on element, lb

\ddot{X} = acceleration of the mass, in/sec²

X = displacement of the mass, inches

The total mass of the beam is

$$M_t = \frac{wL}{g} = \frac{0.475(60)}{386} = 0.073834 \text{ lb-sec}^2/\text{in}$$

The load mass factor, K_{LM} , is given in Table 5-3 as 0.78. The effective spring constant, K_E , is also given in Table 5-3.

$$K_E = \frac{307EI}{L^3} = \frac{307(29)(10)^6(2.52)}{60^3} = 103,868 \text{ lb/in}$$

Equation 5-60, pg. 5-62, is used in the numerical integration process,

$$\ddot{X} = \frac{F_t(t) - K_E X}{K_{LM} M_t} = \frac{F(t) - 103,868X}{0.05759}$$

The total force acting on the beam is the product of the blast pressure times the effective area over which the pressure acts, i.e.,

$$F_t(t) = P_t L b_e$$

where

P_t = blast pressure at time t , psi

L = length of beam, inches

b_e = effective width of beam, inches

At each time interval in the numerical integration process, the total force is calculated using the blast pressure loading from example 5.6.1, a beam length of 60 inches and an effective width of 1.44 inches. The numerical integration technique also requires the use of Eqs. 5-61 and 5-62, pg. 5-62.

$$\dot{X}_{n+1} = \dot{X}_n + \frac{\Delta t}{2} (\ddot{X}_n + \ddot{X}_{n+1})$$

$$X_{n+1} = X_n + \Delta t \dot{X}_n + \frac{(\Delta t)^2}{2} \ddot{X}_n + \beta (\ddot{X}_{n+1} - \ddot{X}_n) (\Delta t)^2$$

where the subscripts $n+1$ indicate values of X , \dot{X} and \ddot{X} at the time $t+\Delta t$. $\beta = 1/4$ is assumed for this example.

At $t = 0$, it is assumed that the beam has a velocity and displacement equal to zero. The applied force at $t = 0$ is

$$F_t = P_t L b_e = 3350(60)(1.44) = 289,440 \text{ lb}$$

The acceleration of the mass is given by

$$a = \frac{F_t - 103,868X}{0.05759} = 5,025,813 \text{ in/sec}^2$$

For the next step, the acceleration is assumed to be equal to that calculated from the initial step. Then from Eq. 5-62 with $X_n = \dot{X}_n = 0$, $\Delta t = 0.0001 \text{ sec}$ and $\ddot{X}_n = \ddot{X}_{n+1} = 5,025,813 \text{ in/sec}^2$,

$$\begin{aligned}
 x_{n+1} &= 0 + 0.0001(0) + \frac{(0.0001)^2}{2} (5,025,813) \\
 &= 0.025129
 \end{aligned}$$

and the calculated acceleration at $t = 0.0001$ is

$$\begin{aligned}
 \frac{F_t - 103,868x}{0.05759} &= \frac{173,664 - (103,868)(0.025129)}{0.05759} \\
 &= 2,970,166 \text{ in/sec}^2
 \end{aligned}$$

Obviously, the initial assumption for the acceleration was in error. The calculated value is used as the new assumed acceleration, and the calculations are repeated until the calculated value agrees with the assumed value within the desired degree of accuracy.

The velocity is calculated from Eq. 5-61 using the last cycle value of acceleration.

$$\dot{x}_{n+1} = \dot{x}_n + \frac{\Delta t}{2} (\ddot{x}_n + \ddot{x}_{n+1})$$

These calculations are summarized in a following table entitled Numerical Integration Summary. A similar process is repeated for each time increment with the acceleration calculated for the previous time step used as the initial assumed acceleration for the next.

The calculations are repeated until the displacement reaches the yield displacement

$$x_E = \frac{R_m}{K_E}$$

From Table 5-3, the maximum resistance is

$$\begin{aligned}
 R_m &= \frac{16M_P}{L} = \frac{16f_{dy}Z}{L} = \frac{16(39,600)(1.932)}{60} \\
 &= 20,401 \text{ lb}
 \end{aligned}$$

NUMERICAL INTEGRATION SUMMARY

Time (sec)	Assumed \ddot{x}_{n+1} (in/sec ²)	\dot{x} (in/sec)	x (in)	$F_t - K_E \frac{x}{K_{LM} M_t}$ (in/sec ²)
0	N.A.	0	0	5,025,813.77
0.0001	5,025,813.77 2,970,166.44 2,979,435.15 2,979,393.36	400.2603661	0.0251291 0.0199900 0.0200131 0.0200130	2,970,166.44 2,979,435.15 2,979,393.36 2,979,393.55
0.0002361	2,979,393.55 95,439.71 119,524.40 119,323.26 119,324.94		0.1020781 0.0887241 0.0888356 0.0888347 0.0888347	95,439.71 119,524.40 119,323.26 119,324.94 119,324.93
0.0004	119,324.93 - 64,919.79 - 62,688.01 - 62,715.04 - 62,714.71	611.1197921	0.1906034 0.1893659 0.1893809 0.1893807 0.1893807	- 64,919.79 - 62,688.01 - 62,715.04 - 62,714.71 - 62,714.72
0.0004115	- 62,714.72 - 75,527.56 - 75,526.79	615.7591518 614.9642631	0.1964578 0.1964574 0.1964574	- 75,527.56 - 75,526.79 - 75,526.79

and the effective spring constant is

$$K_E = \frac{307EI}{L^3} = 103,866 \text{ lb/in}$$

Therefore, the displacement at yield is

$$X_E = \frac{20,401}{103,866} = 0.1964 \text{ in}$$

The yield displacement is reached at $t = 0.0004115$ seconds.

The load acting on the beam at time of yielding is 16,056 lb.

In the plastic range, the acceleration is obtained by rearranging Eq. 5-31, pg. 5-32.

$$\ddot{X} = \frac{F(t) - R_m}{0.05759} = \frac{F(t) - 20,401}{0.05759}$$

The load during this time period is defined by

$$F(t) = \left(-\frac{187}{0.066} t + 187 \right) (1.44) (60) = -244,800t + 16,156$$

The maximum deflection, X_m , occurs when the velocity is zero.

Therefore, from Eq. 5-61

$$0 = \dot{X}_n + \frac{\Delta t}{2} (\ddot{X}_n + \ddot{X}_{n+1})$$

Substituting, with $\Delta t = t - 0.0004115$,

$$0 = 614.9642631 + \frac{(t - 0.0004115)}{2} \left[-75,526.79142 + \left(\frac{-244,800t + 16,156.8 - 20,401.92}{0.05759} \right) \right]$$

Solving,

$$t_m = 0.007243$$

$$\Delta t = 0.006832$$

$$\ddot{X} = -104,499.67$$

The maximum deflection is found using Eq. 5-62.

$$X_{n+1} = X_n + \Delta t \dot{X}_n + \frac{(\Delta t)^2}{2} \ddot{X}_n + \frac{1}{4} (\ddot{X}_{n+1} - \ddot{X}_n) (\Delta t)^2$$

Substituting,

$$\begin{aligned} X_{n+1} &= 0.1964574085 + (0.006832)(614.9642631) \\ &\quad + \frac{(0.006832)^2}{2}(-75,526.79142) \\ &\quad + \frac{1}{4}(-104,499.6704 + 75,526.79142)(0.006832)^2 \end{aligned}$$

Solving,

$$X_{n+1} = 2.295 \text{ inches} = \text{maximum deflection}$$

Similar results could have been obtained by simply continuing the numerical integration process demonstrated in the summary table. For this example, the direct solution for t_m and X_m was more convenient.

5.6.3 Design of Roof Slab for Group 3 Type Suppressive Shield (Type I Construction Ref. 5-5)

a. Given

The same structure description and airblast loading as for illustrative example 5.6.1.

b. Find

Design a reinforced concrete roof slab for the shield using a ductility ratio of 6 (Ref Table 4-3).

c. Solution

Based on the airblast loading parameters of example 5.6.1,

$$i_r = 0.422 \text{ psi-sec}$$

$$C_1 = \frac{3350 - 187}{3350} = 0.944$$

$$C_2 = \frac{187}{3350} = 0.056$$

Some structural properties must be assumed or specified to start the design process. The designer can (1) assume trial section properties based on intuition or (2) use whatever aids are available to guide his choice of trial section

properties. The latter approach is chosen for this example. Since the quasi-static load is of fairly long duration, Eq. 5-37, pg. 5-53, might be used to obtain an initial estimate of the required R_m . The reflected impulse and the decay in pressure are neglected for this estimate.

$$r_m = p_{so} \left[\frac{2\mu}{2\mu-1} \right] = 187 \left[\frac{2(5)}{2(5)-1} \right] = 207.8 \text{ psi}$$

Select a somewhat lower resistance, e.g., 200 psi, for the first trial because of the anticipated larger influence in the decay in pressure. The following material properties are assumed from Table 4-1 and Table 4-2 for design purposes.

Concrete	$f'_c = 5000 \text{ psi}$
	$f'_{dc} = 6250 \text{ psi}$
Rebar	$f_y = 60,000 \text{ psi}$
	$f_{dy} = 72,000 \text{ psi}$
Structural Shapes	$f_y = 36,000 \text{ psi}$
	$f_{dy} = 39,600 \text{ psi}$

If the ends of the side wall beams are rigidly attached to the roof slab, they will provide some restraint of the outer edge of the slab. The moment capacity of the S3x5.7 beams is given by

$$M_{Ps} = \frac{f_{dy} Z}{\text{Beam Spacing}} = \frac{39,600(1.932)}{1.44} = 53,130 \text{ in-lb/in}$$

From Table 5-8, the maximum resistance of a circular slab with fixed edges is

$$R_m = 18.8(M_{PC} + M_{Ps})$$

Assuming the moment capacity of the slab at its edges is equal to the resistance provided by the beams, taking the radius of the slab to be 67.5 inches and $R_m = r_m A$, the required moment capacity at its center is

$$\begin{aligned}
 M_{PC} &= \frac{200\pi(a/2)^2}{18.8} - M_{PS} \\
 &= \frac{200(3.14)(67.5)^2}{18.8} - 53,130 = 99,145 \text{ in-lb/in}
 \end{aligned}$$

In order to determine the required depth of the slab, a reinforcing steel ratio must be assumed. Try

$$p = A_s/bd = 0.01$$

Equation 5-7, pg. 5-13, gives the moment capacity of a reinforced concrete member as

$$M_P = pf_{dy}bd^2 \left[1 - 0.59p \frac{f_{dy}}{f_{dc}} \right]$$

This equation may be solved directly for "d" but by manipulating, Equation 5-7 as shown above the following simple substitutions allow an easier solution.

$$m = \frac{f_{dy}}{0.85f_{dc}} = \frac{66000}{(0.85)(6250)} = 12.423$$

$$\begin{aligned}
 K_u &= pf_{dy} \left[1 - \frac{pm}{2} \right] = (0.01)(66000) \left[1 - \frac{(.01)(12.423)}{2} \right] \\
 &= 619.004
 \end{aligned}$$

$$bd^2 = \frac{M_{PC}}{K_u} \quad \text{where } b = 1"$$

$$d = \sqrt{\frac{99145}{619.004}} = 12.65"$$

Normally, the 12.65 inches would be rounded off to some practical depth like 13.0 inches; however, it will be retained for our first trial section.

From Eq. 5-8, pg. 5-14, the moment of inertia of the slab is

$$\begin{aligned}
 I_a &= \frac{bd^3}{2} [5.5p + 0.083] \\
 &= \frac{1(12.65)^3}{2} [5.5 \times 0.01 + 0.083] = 139.68 \text{ in}^4/\text{in}
 \end{aligned}$$

From Eq. 4-1, pg. 4-6, the modulus of elasticity for 150 lb/ft³ concrete is

$$E_c = 33w^{1.5}\sqrt{f'_c}$$

$$= 33(150)^{1.5}(5000)^{0.5} = 4.29 \times 10^6 \text{ psi}$$

From Table 5-8, the stiffness of the concrete slab is

$$K = \frac{216EI}{a^2} = \frac{216(4.29 \times 10^6)(139.68)}{(135)^2} = 7,101,952 \text{ lb/in}$$

$$K_{LM} = 0.65 \text{ (for elastic-plastic range)}$$

Assuming an overall slab thickness of 16", the total mass of the slab is

$$M_t = \frac{16(3.14)(67.5)^2(150)}{1728(386)} = 51.50 \text{ lb-sec}^2/\text{in}$$

From Eq. 5-33, pg. 5-32, the period of vibration of the slab is

$$T_N = 2\pi \left[\frac{K_{LM} M_t}{K} \right]^{1/2}$$

$$= 6.28 \left[\frac{0.65(51.50)}{7,101,952} \right]^{1/2} = 0.0136 \text{ sec}$$

The next step is to determine the response of the slab to the blast pressure loading. The ratios t_o/T_N for the two triangular components of the loading function indicate that Eq. 5-55, pg. 5-58, is the appropriate response equation to use.

$$\left[\frac{\frac{C_1 P_r}{r_m}}{\frac{T_N}{\pi t_1} \sqrt{2\mu-1}} \right]^2 + \frac{\frac{C_2 P_r}{r_m}}{\frac{T_N}{\pi t_2} \sqrt{2\mu-1} + \frac{1 - \frac{1}{2\mu}}{1 + \frac{0.7 T_N}{t_2}}} = 1$$

Substituting,

$$\left[\frac{\frac{0.944(3350)}{200}}{\frac{0.0136}{3.14(0.00025)} \sqrt{2(6)-1}} \right]^2 + \frac{\frac{0.056(3350)}{200}}{\frac{0.0136}{3.14(0.066)} \sqrt{2(6)-1} + \frac{1 - \frac{1}{2(6)}}{1 + \frac{0.7(0.0136)}{0.066}}} = 1$$

$$= 0.076 + 0.921 = 0.997$$

Additional trials are not necessary in this case. A value of $r_m = 200$ psi results in a required moment capacity of 99,145 in-lb/in, $d = 12.65$ inches, $I = 139.68$ in⁴/in, $K = 7,101,954$ lb/in. $T_N = 0.0136$ sec and Eq. 5-55 yields a sum of 0.997.

The shear capacity of the slab depends on the radial tension loads applied by the wall beams. If properly anchored and/or attached to the wall beams, it might be assumed that the circular col. base plates and reinforcing steel in the slab resist all radial forces and prevent tension cracks in the concrete. On the basis of this assumption, the full effective depth of the slab is available to resist the maximum shear force. From Table 5-8, the dynamic reaction at the edge of the slab is

$$V = 0.36F + 0.64R_m$$

where

$$R_m = 200(3.14)(67.5)^2 = 2,861,325 \text{ lbs}$$

For purposes of analysis, it is assumed that the load at the time of maximum response is equal to the quasi-static pressure. Then

$$F = 187(3.14)(67.5)^2 = 2,676,696 \text{ lbs}$$

Substituting in the above equation,

$$V = 0.36(2,676,696) + 0.64(2,861,325) = 2,794,858 \text{ lbs}$$

The reaction per inch of support is

$$\frac{2,794,858}{2(3.14)(67.5)} = 6593 \text{ lbs/in}$$

Using the criteria of Ref. 5-7 determine the required depth, d , for diagonal tension assuming ductile mode. The maximum allowable shear stress with shear reinforcing is

$$v_u = 11.5\sqrt{f'_c} = 11.5\sqrt{5000} = 813 \text{ psi}$$

Solving for d ,

$$d = \frac{6593}{(1)(813)} = 8.10 < 12.65 \text{ inches}$$

Next check the required depth of the roof slab for a possible direct shear failure as determined by Eq. 5-9, pg. 5-14

$$v_d = \frac{V_d}{bd} = 0.18f'_c$$

As direct shear is a brittle mode of failure a ductility ratio of only 1.3 (ref. Table 4-3, pg. 4-15) is allowed. Table 4-2 recommends a 10% increase in the direct shear strength of members due to rapid loading.

Substituting in Eq. 5-55, as noted on pg. 5-80, the value of μ of 1.3 and solving for a new r_m we see that $r_m = 300$ psi satisfies the equation

Determining our new shear reaction we have

$$V = 0.36F + 0.64R_m$$

where

$$R_m = 300 (3.14) (67.5)^2 = 4,291,987\#$$

and

$$F = 187 (3.14) (67.5)^2 = 2,861,325\#$$

therefore

$$V = (0.36)(2,676,696) + (0.64)(4,291,987) = 3,710,482\#$$

The reaction per inch of support is

$$\frac{3,710,482}{2(3.14)(67.5)} = 8753\#/"$$

Solving for d from Eq. 5-9 and allowing for the 10% increase in f'_c

$$d = \frac{V_d}{(1.1)(.18)(f'_c)} = \frac{8753}{(1.1)(.18)(5000)} = 8.84 < 12.65 \text{ inches}$$

Therefore bending controls the effective depth of the roof slab. For an effective depth of 12.65 inches and $M_{PC} = 99,145$ in-lb/in, the required steel ratio in the center of the roof (top steel) is also found from Eq. 5-7.

$$M_{PC} = pf_{dy}bd^2 \left[1 - 0.59p \frac{f_{dy}}{f'_{dc}} \right]$$

This equation may be solved directly for "b", but the following simple substitutions allow an easier solution.

$$\text{Let } m = \frac{f_{dy}}{0.85 f'_{dc}} = \frac{72000}{(0.85)(6250)} = 13.553$$

$$K_u = \frac{M_{PC}}{bd^2} = \frac{99145}{(1)(12.65)^2} = 619.569$$

$$p = \frac{1}{m} \left[1 - \sqrt{1 - \frac{2mK_u}{f_{dy}}} \right]$$

$$= \frac{1}{13.553} \left[1 - \sqrt{1 - \frac{(2)(13.533)(619.569)}{72000}} \right] = .0092$$

$$A_s = (0.0092)(1)(12.65) = .116 \text{ in}^2/\text{in} = 1.392 \text{ in}^2/\text{ft.}$$

Use two layers #5 @ 5" c.c. ($A_s = 1.44 \text{ in}^2/\text{ft.}$)

$$\text{Actual } p = 1.44/(12)(1)(12.65) = 0.0095$$

The wall beams provide a resistance of 53,130 in-lb/in and the moment capacity of the slab at the supports must be at least equal to that. Assume $M_{Ps} = 55,000 \text{ in-lb/in}$. For an effective depth of 12.65 inches, the required steel ratio at the support (bottom steel) is found from Eq. 5-7, pg. 5-13.

$$55,000 = p(72000)(1)(12.65)^2 \left[1 - 0.59p \frac{72,000}{6,250} \right]$$

or

$$p = 0.0049 \text{ (say } 0.0095 \text{ to provide additional restraint for radial reaction of wall beams.) See Example 5.6.6}$$

$$A_s = 0.0095(1)(12.65) = \underline{\underline{0.120 \text{ in}^2/\text{in}}}$$

The allowable shear stress in the concrete is given by Eq. 5-10, pg. 5-15.

$$v_c = (1.9\sqrt{f'_c} + 2500pdv_c/M_c)$$

where dv_c/M_c must be less than 1.0, and v_c less than $3.5\sqrt{f'_c}$ psi. Substituting previously calculated values,

$$dv_c/M_c = 12.65(6593)/55,000 = 1.52 > 1. \text{ Use } 1.0.$$

Then,

$$v_c = \left[1.9\sqrt{5000} + 2500(0.0095)(1) \right] = 158 \text{ psi} < 3.5\sqrt{f'_c} = 248 \text{ psi} \quad \underline{\text{OK}}$$

Therefore, the shear capacity of the concrete is

$$V_c = v_c b d = 158(1)(12.65) = 1999 \text{ lb/in}$$

The required shear reinforcing capacity is

$$V_s = V_u - V_c = 6593 - 1999 = 4594 \text{ lb/in}$$

The shear stress to be resisted by the shear reinforcing is

$$v_s = \frac{4594}{(1)(12.65)} = 363 \text{ psi} < 8\sqrt{5000} = 566 \text{ psi OK}$$

The size and spacing requirements are found from Eq. 5-11, pg. 5-15.

$$v_s = \frac{dA_v f_{dy}}{s}$$

and

$$\frac{A_v}{s} = \frac{4594}{12.6(72000)} = 0.0050 \text{ in}^2/\text{in for a 1 inch slab width}$$

In summary, the tensile reinforcing steel should be $0.120 \text{ in}^2/\text{in}$ at the center of the slab and at the supports. Vertical shear reinforcing should provide $0.0050 \text{ in}^2/\text{in}^2$ of slab surface area near the support. The overall depth of the slab must be sufficient to provide proper protection for the reinforcing steel and will depend upon the size and number of layers of reinforcing. This preliminary design could be made more conservative by neglecting the shear strength of the concrete in computing shear reinforcing requirements. It is possible that radial loads applied to the slab could cause cracking of the concrete and loss of shear strength, so care should be taken in detailing the reinforcing steel to assure full development of all bars through adequate embedment or mechanical anchorage. See Example 5.6.6 for reinforcing requirements due to radial loads applied by wall beams.

5.6.4 Analysis of Shield Group 6A Designa. Given

Shield Group 6A is a sphere with an inside diameter of 2 feet and a wall thickness of 1/4 inch. The shield is designed for a 13.63 ounce charge of Pentolite. It is made from mild steel with the following properties.

E = modulus of elasticity, 29×10^6 psi

ν = Poisson's ratio, 1/3

f_{dy} = dynamic yield strength, 39,600 psi

ρ = mass density, 7.36×10^{-4} lb-sec²/in⁴

b. Find

The strain and deformation due to detonation of the design charge weight.

c. Solution

The equivalent TNT charge weight for 13.63 ounces of Pentolite is obtained from Table 3-1 and Eq. 3-1, pg. 3-4.

$$W = \frac{13.63(1.129)}{16} = 0.962 \text{ lb TNT}$$

and

$$W^{1/3} = 0.987 \text{ lb}^{1/3}$$

Assuming the charge is at the center of the shield, the scaled distance to the wall is

$$Z = R/W^{1/3} = 1/0.987 = 1.013 \text{ ft/lb}^{1/3}$$

From Fig. 3-6, the peak reflected pressure, P_r , is 7000 psi and the scaled impulse is

$$i_r/W^{1/3} = 0.2 \text{ psi-sec/lb}^{1/3}$$

Then

$$i_r = 0.197 \text{ psi-sec}$$

and

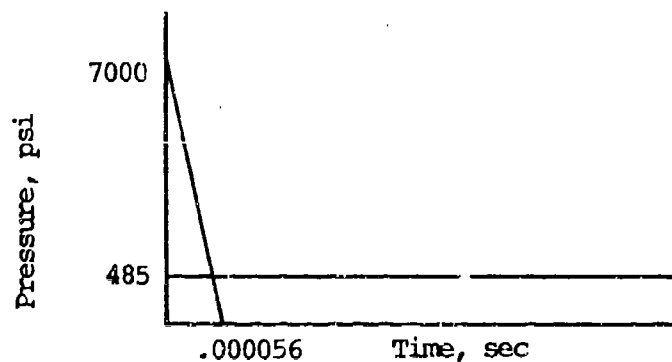
$$t_1 = 2i_r/P_r = (2)0.197/7000 = 0.000056 \text{ sec}$$

From Fig. 3-9, for

$$\frac{W}{V} = \frac{0.962}{4.188} = 0.230 \text{ lb/ft}^3$$

$$P_{qs} = 485 \text{ psi}$$

The blast pressure loading on the spherical chamber is as shown below. As indicated in the loading diagram, little or no venting would occur in this shield.



Blast Loading of a Group 6A Shield

$$C_1 = \frac{7000 - 485}{7000} = .931$$

$$C_2 = \frac{485}{7000} = .069$$

The structure responds dynamically to both the reflected pressure pulse and the quasi-static pressure. Assume the spherical chamber responds only in its fundamental mode of vibration, a simultaneous radial motion of all points on its surface. The natural period of the sphere is then obtained from Eq. 5-24, pg. 5-26, i.e.,

$$T_n = 2\pi \sqrt{\frac{\rho a^2 (1-2)}{2E}}$$

where

a = radius of sphere, 12 inches

The natural period of the sphere is

$$T_n = 2\pi \left[\frac{(7.36 \times 10^{-4}) (12)^2 (.667)}{(2) (29 \times 10^6)} \right]^{1/2}$$

$$= .000219 \text{ sec}$$

Assuming thin shell response, the unit resistance of the sphere is determined from Eq. 5-17, pg. 5-20, i.e.

$$f_{dy} = \frac{r_m a}{2t}$$

where

r_m = unit resistance, psi

t = wall thickness, .25 inches

Therefore

$$r_m = \frac{(2) (39600) (.25)}{12} = 1650 \text{ psi}$$

The next step is to determine the response of the sphere to blast pressure loading. The loading diagram indicates that Eq. 5-54, pg. 5-57, is the appropriate equation to use.

$$\left[\frac{C_1 P_r/r_m}{\frac{T_N}{\pi t_1} \sqrt{2\mu - 1}} \right]^2 + \frac{C_2 P_r/r_m}{1 - \frac{1}{2\mu}} = 1$$

The use of the charts of Appendix B simplifies the solution to this equation. From Fig. B-34, pg. B-40, for $C_1 = 0.93$ and $C_2 = 0.07$ with

$$P_r/r_m = 7000/1650 = 4.24$$

$$t_1/T_N = .000056/.000219 = .256$$

the ductility ratio, μ , is determined to be approximately 7.8.

The radial deflection, X_e , of the spherical chamber at the membrane yield stress is from Ref. 5-18.

$$\begin{aligned} X_e &= (f_{dy}) (a) (1-\nu) / E \\ &= (39600) (12) (.667) / (29 \times 10^6) = .011 \text{ inches} \end{aligned}$$

The maximum deflection is found from

$$X_m = \mu X_e = (7.8) (.011) = .086 \text{ inches}$$

5.6.5 Response of Removable Column in 81-mm Suppressive Shield

a. Given

The Milan 81-mm suppressive shield is a steel frame and panel structure with inside dimensions of 14 feet by 14 feet by 12.4 feet. All vertical frame members (except corners) are 8 x 6 x 1/4 structural steel tubing. Horizontal ceiling members are 8 x 6 x 3/8 structural steel tubing. Panels are mounted from the inside and restrained against the frame. One of the vertical frame members is removable to provide a larger access opening into the shield. Pages A-86 thru A-118 provide details of this shield.

A charge equivalent to 5.25 pounds of TNT is assumed to be located at the center of the shield. The effective vent ratio for the shield is $\alpha_{eff} = 0.043$. The volume of the structure is 2430.4 ft^3 and the vented surface area, A_i , 890.4 ft^2 . Atmospheric pressure, P_o , is assumed to be 14.7 psi, and the sound velocity in air, a_o , is 1117 ft/sec.

b. Find

The maximum axial tension in the removable column and its bending response to the blast loading.

c. Solution

The first step is to compute blast loads for both the roof and walls. For the roof, the scaled distance is

$$Z = R/W^{1/3} = 6.20/5.25^{1/3} = 3.57 \text{ ft/lb}^{1/3}$$

From Fig. 3-6, the peak reflected pressure, P_r , is 230 psi. Scaled reflected impulse, $i_r/W^{1/3}$, is 0.045 psi-sec/lb^{1/3}. Therefore, the impulse is

$$i_r = 0.045(1.738) = 0.078 \text{ psi-sec}$$

The duration of the reflected pulse is obtained from Eq. 3-4, pg. 3-14.

$$t_r = 2i_r/P_r = 2(0.078)/230 = 0.00068 \text{ sec}$$

For the walls, the scaled distance is

$$z = R/W^{1/3} = 7/5.25^{1/3} = 4.03 \text{ ft/lb}^{1/3}$$

and from Fig. 3-6

$$P_r = 175 \text{ psi}$$

$$i_r/W^{1/3} = 0.038 \text{ psi-sec/lb}^{1/3}$$

$$i_r = 0.066 \text{ psi-sec}$$

$$t_r = 2i_r/P_r = 0.00075 \text{ sec}$$

For

$$\frac{W}{V} = \frac{5.25}{(14)(14)(12.4)} = 0.0022 \text{ lb/cf}$$

Figure 3-9 indicates the quasi-static pressure to be

$$P_{qs} = 26 \text{ psi}$$

Next, substitute

$$P_{qs} = 26 \text{ psi}$$

$$P_o = 14.7 \text{ psi}$$

into the equation for scaled maximum pressure, pg. 3-23

$$\bar{P} = (P_{qs} + P_o)/P_o = (26 + 14.7)/14.7 = 2.77$$

Using 2.77 as the ordinate to the plot of Fig. 3-10, it is found that

$$t_b a_o \alpha A_i / V = 0.48$$

Substituting

$$\alpha_{\text{eff}} = 0.043$$

$$V = 2430.4 \text{ ft}^3$$

$$A_i = 890.4 \text{ ft}^2$$

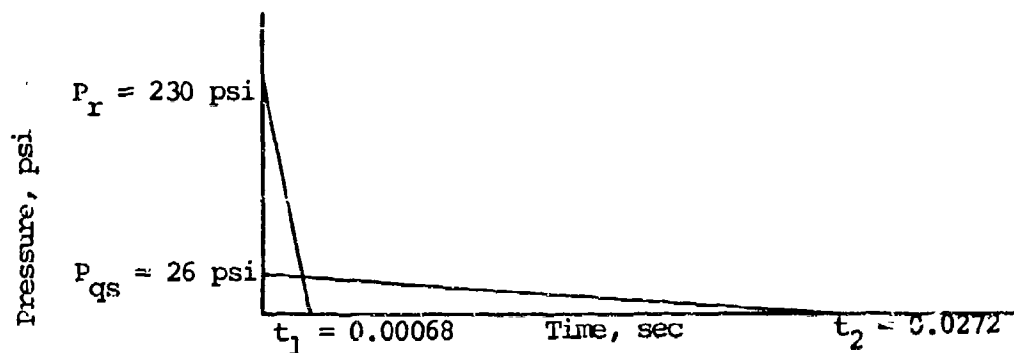
$$a_o = 1117 \text{ ft/sec}$$

and solving for the blowdown time, it is found that

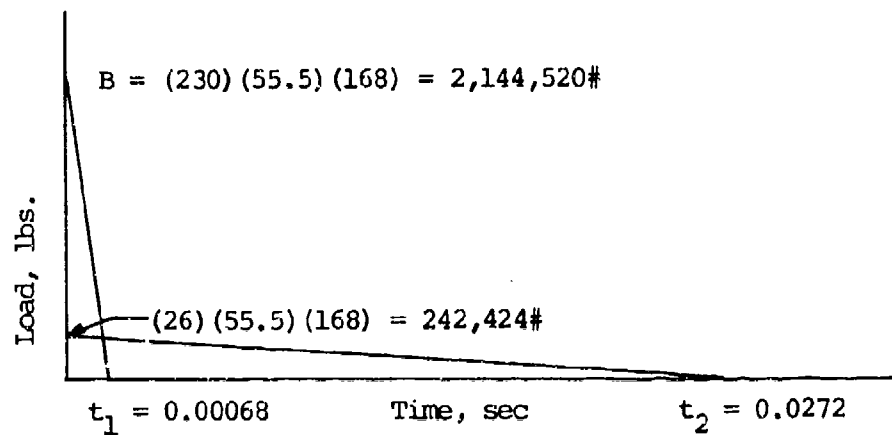
$$t_b = 0.0272 \text{ sec}$$

The shield panels are the primary means of transferring the blast pressure loads into the roof beams and side columns. As a conservative check of the loads applied to the removable column, assume that the panels are infinitely stiff.

The roof beam is 168 inches long and has a plastic section modulus, Z , equal to 27.02 inches³. The beam reacts the blast loads from two panels with a tributary width of 55.5 inches. Based on this data, the airblast loads acting on the roof beam are shown in the following sketches



Unit Airblast Loads Acting on the Roof Beam



Total Airblast Loads Acting on the Roof Beam

The maximum tension in the removable column is equal to the maximum dynamic reaction of the roof beam. The dynamic reaction for the uniformly loaded fixed end beam is given in Table 5-3, pg. 5-34,

$$V_{\max} = 0.38 R_m + 0.12F$$

The maximum bending resistance from Table 5-3 for the roof beam fixed at both ends is

$$R_m = \frac{16 M_p}{L} = \frac{162 f_{dy}}{L} = \frac{(16) (27.02) (39,600)}{168} = 101,904 \text{ lb}$$

The natural frequency of the roof beam is given in Fig. 5-8 as

$$\omega_N = 22.4 \frac{E I}{m L^4}$$

where

E = modulus of elasticity, 29×10^6 psi

I = moment of inertia, 79.7 in.^4

m = mass per linear inch of beam, $\text{lb-sec}^2/\text{in}^2$

L = length of beam, 168 inches

Since the panel weight is distributed along the beam, it must also be included. The weight of a panel is 32.6 lb/ft^2 , and its width is 49.5 inches. The $8" \times 6" \times 3/8"$ beam weighs 2.61 lb/in. The mass per inch is then

$$m = \left[2.61 + \frac{(49.5)(32.6)}{144} \right] / 386 = 0.0358 \text{ lb-sec}^2/\text{in}^2$$

and

$$\omega_N = 22.4 \left[\frac{(29 \times 10^6)(79.7)}{(0.0358)(168^4)} \right]^{1/2} = 201.658 \text{ rad/sec}$$

The natural period is

$$T_N = \frac{2\pi}{\omega_N} = 0.03116 \text{ sec}$$

The maximum tension in the removable column is equal to the maximum dynamic reaction of the roof beam. From Table 5-2, pg. 5-34,

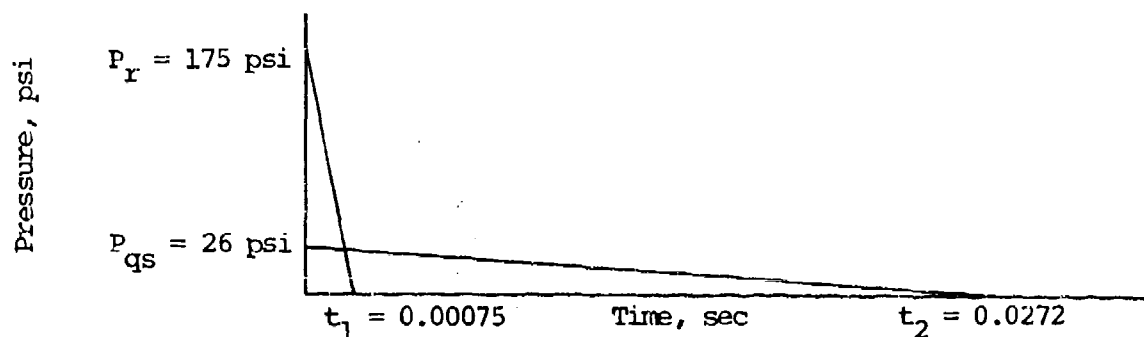
$$V_{\max} = 0.38 R_m + 0.12F$$

The total force, F , is time-dependent and its value at the time the roof beam yields should be used in the above equation; however, for a conservative estimate, the total quasi-static load is used. Since the natural period of the roof beam is very much longer than the duration of the peak reflected pressure, the peak reflected pressure is neglected.

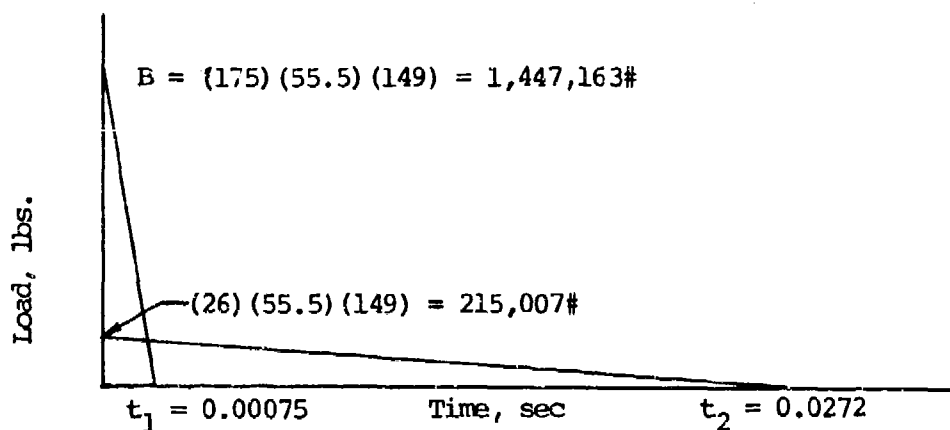
Therefore

$$V_{\max} = (0.38)(101,904) + (0.12)(215007) = 64,524 \text{ lg}$$

The horizontal load on the removable column is applied through the panels in the same fashion as described above for the roof beams. The removable column is 149 inches long and has a plastic section modulus, Z , equal to 18.66 in^3 . Based on this data, the blast loading on the removable column is shown in the following sketches.



Unit Airblast Loads Acting on the Removable Column



Total Airblast Loads Acting on the Removable Column

From the sketch,

$$C_1 = (1,447,163 - 215,007)/1,447,163 = .852$$

$$C_2 = 215,007/1,447,163 = .148$$

The column is assumed to be simply-supported at the base and fixed at the roof. From Table 5-3, the maximum bending resistance of the column is

$$R_m = \frac{12 M_p}{L} = \frac{12 \sum f_{dy}}{L} = \frac{(12)(18.66)(39,600)}{149} = 59,512 \text{ lb}$$

The natural frequency of the element is given in Fig. 5-8 as

$$\omega_N = 15.4 \sqrt{\frac{EI}{mL^4}}$$

where

E = modulus of elasticity, 29×10^6 psi

I = moment of inertia, 58.4 in^4

m = mass per linear inch of beam, $\text{lb-sec}^2/\text{in}^2$

L = length of beam, 149 inches

As with the roof beam, the panel weight is distributed along the beam. The weight of a panel is 32.6 lb/ft^2 , and its width is 49.5 inches. The $8" \times 6" \times 1/4"$ column weighs 1.84 lb/in . The mass per inch is then

$$m = \left[1.84 + \frac{49.5 (32.6)}{144} \right] / 386 = 0.0338 \text{ lb-sec}^2/\text{in}^2$$

and

$$\omega_N = 155.276 \text{ rad/sec}$$

The natural period is

$$T_N = \frac{2}{\omega_N} = 0.04046 \text{ sec}$$

The response of an elastic-plastic system to short duration and quasi-static triangular pulses is given by Eq. 5-55, pg. 5-58.

$$\left[\frac{C_1 B/R_m}{\frac{T_N}{\pi t_1} \sqrt{2\mu - 1}} \right]^2 + \left[\frac{C_2 B/R_m}{\frac{T_N}{\pi t_2} \sqrt{2\mu - 1} + \frac{1 - \frac{1}{2\mu}}{1 + 0.7 \frac{T_N}{t_2}} \frac{T_N}{t_2}} \right] = 1$$

where

R_m = maximum resistance of member, lb

B = maximum load on member, lb

T_N = natural period of element, sec

t_1 = time of duration of short pulse, sec

t_2 = time of duration of quasi-static pulse, sec

μ = ductility ratio

C_1 = ratio of the peak short duration force to the peak total force

C_2 = ratio of peak quasi-static force to the peak total force

A solution of Eq. 5-55 is obtained by trial and error. Successive values of μ are assumed until the equation is satisfied. Only the final calculation for $\mu = 23.8$ is shown below.

$$\begin{aligned}
 & \left[\frac{\frac{0.852(1,447,163)}{59,512}}{\frac{0.04046}{3.14(0.0075)} \sqrt{2(23.8)-1}} \right]^2 \\
 & \left[\frac{\frac{(.148)(1,447,163)}{59,512}}{\frac{0.04046}{3.14(0.0272)} \sqrt{2(23.8)-1} + \frac{1 - \frac{2(23.8)}{1 + 0.7 \frac{(0.04046)}{(0.0272)}}}{1 + 0.7 \frac{(0.04046)}{(0.0272)}}}} \right] \\
 & = 1.005
 \end{aligned}$$

The equivalent elastic displacement is given by

$$X_E = \frac{R_m}{K_E}$$

where for the elastic-plastic range

$$K_E = \frac{160 EI}{L^3} \text{ from Table 5-3}$$

or

$$K_E = \frac{160 (29 \times 10^6) (58.4)}{(149)^3} = 31,917 \text{ lb/in}$$

then

$$X_E = \frac{59,512}{31,917} = 0.726 \text{ inches}$$

and the maximum displacement is

$$X_m = \mu X_E = 23.8 (0.726) = 17.3"$$

Based on the assumption of infinitely stiff panels, the maximum displacement is conservative. A less conservative approach would involve determining the dynamic reactions of the panels as loads on the roof beams and columns.

5.6.6 Analysis of Base Plate Ring and Reinforcing Steel in Foundation Slab for Group 3 Suppressive Shield

a. Given

The same structure description and pressure loading as for illustrative example 5.6.1. The base plate ring has an outside diameter of 149 inches and an inside diameter of 128 inches. It is 1 inch thick. Pages A-12 thru A-27 provide details of the Group 3 Type Shield.

b. Find

The required reinforcing steel to resist the wall beam reactions.

c. Solution

Assume that the annular base plate and top rebars resist the entire radial load applied by the wall beams. From Table 5-3, the dynamic reaction at the ends of the interlocking I-beams is

$$V = 0.38R_m + 0.12F$$

where

$$R_m = \frac{16M_p}{L} = \frac{16Zf_{dy}}{L} = \frac{16(1.932)(39,600)}{60} = 20,401 \text{ lb/beam}$$

Since the natural period of the I-beam is much longer than the duration of the peak reflected pressure, only the quasi-static pressure load is considered in determining the load. Then

$$F = 187(1.44)(60) = 16,156 \text{ lb/beam}$$

Substituting in the above equation for the maximum reaction,

$$V = 0.38(20,401) + 0.12(16,156) = 9,692 \text{ lb/beam}$$

There are 296 beams at an effective diameter of 135 inches. The equivalent uniform radial load is

$$p = \frac{(\text{load/beam})(\text{number of beams})}{\text{circumference of ring}} = \frac{9692(296)}{135\pi} = 6764 \text{ lb/in}$$

The elastic deflection of the outer radius of the ring under a uniform radial pressure is (Ref. 5-18)

$$u_r = \frac{qR_o}{E} \left[\frac{2R_i^2}{R_o^2 - R_i^2} \right]$$

where

R_o = outer radius, 74.5 inches

R_i = inner radius, 64 inches

E = modulus of elasticity, 29×10^6 psi

q = uniform radial pressure, psi

The pressure q is multiplied by the 1 inch height, h , of the ring to obtain the radial load per inch of circumference of the ring, i.e.,

$$qh = F_R = \text{radial load per inch of ring}$$

or

$$q = \frac{F_R}{h} = \frac{F_R}{1.0}$$

Substituting

$$u_r = \frac{F_R(74.5)}{1.00(29 \times 10^6)} \left[\frac{2(64)^2}{(74.5)^2 - (64)^2} \right]$$

$$u_r = 14.471 \times 10^{-6} F_R$$

The elastic deflection of the reinforcement is

$$u_b = \frac{F_B L}{A_S E} = \frac{F_B R_O}{A_S E} = \frac{(74.5) F_B}{29(10)^6 A_S} = 2.569(10)^{-6} \frac{F_B}{A_S}$$

where

F_B = radial load carried by the reinforcement per inch of circumference assuming no radial deformation due to bending

A_S = cross sectional area of reinforcement available to resist tensile loads per inch of circumference

The area of reinforcement available to resist tensile forces is determined from example 5.6.3, pg. 5-82.

$$A_S = (.0095 - .0049)(1)(12.65) = 0.058 \text{ in}^2/\text{in}$$

Therefore

$$u_b = \frac{2.569(10)^{-6}}{0.058} F_B = 44.293(10)^{-6} F_B$$

Since the base plate and top layer of reinforcement are assumed to act together,

$$u_b = u_r$$

$$44.293(10)^{-6} F_B = 19.295(10)^{-6} F_R$$

$$F_R = 2.30 F_B$$

The above ratio of loads per inch of circumference in the ring and reinforcement is only good in the elastic range. The dynamic yield stresses for the ring and reinforcement are given in Table 4-1, pg. 4-5.

$$f_{dyR} = 39600 \text{ psi for the ring}$$

$$f_{dyB} = 72000 \text{ psi for the reinforcement}$$

The first step is to determine whether the combination of ring and reinforcement can resist the radial tension loads in the elastic range,

$$F_B + F_R = P$$

$$F_B + 2.30 F_B = 6764 \text{ lb/in}$$

$$F_B = 2050 \text{ lb/in in the reinf.}$$

then

$$F_R = 4714 \text{ lb/in in the ring}$$

The stress in the reinforcement is

$$v_B = \frac{F_B}{A_S} = 35345 \text{ psi} < 72000 \text{ psi}$$

The maximum stress in the steel ring is given by Case 1a, page 504, Ref. 5-18.

$$v_R = \frac{F_R}{r} \left[\frac{2R_O^2}{R_O^2 - R_i^2} \right]$$

$$= \frac{4714}{1.0} \left[\frac{2(74.5)^2}{(74.5)^2 - (64)^2} \right] = 35,983 \text{ psi} < 39,600 \text{ psi}$$

The stresses for both the ring and reinforcement are below the yield point, so the combined system is adequate to resist the radial beam reactions.

An economical redesign would allow the ring, with its lower dynamic yield stress, to respond in the plastic range. This would allow a reduction in the reinforcing steel.

In general the reaction of the ring and reinforcing steel to the radial tensile loads could be developed in three stages.

1. The elastic range response for both the ring and reinforcement.
2. The combination of plastic range response for the ring ($f_{dyR} = 39600$ psi) and the elastic range for the reinforcing steel ($v_{max} < f_{dyB} = 72000$ psi).
3. The plastic range response for both the ring and reinforcement.

5.6.7 Design of Upper Connection for Removable Column in 81-mm Suppressive Shield

a. Given

The Milan 81-mm suppressive shield is a steel frame and panel structure with inside dimensions of 14 feet by 14 feet by 12.4 feet. The side columns in the shield area are 8 x 6 x 1/4 structural tubes. A description of the shield and its design parameters are given in Example 5.6.5.

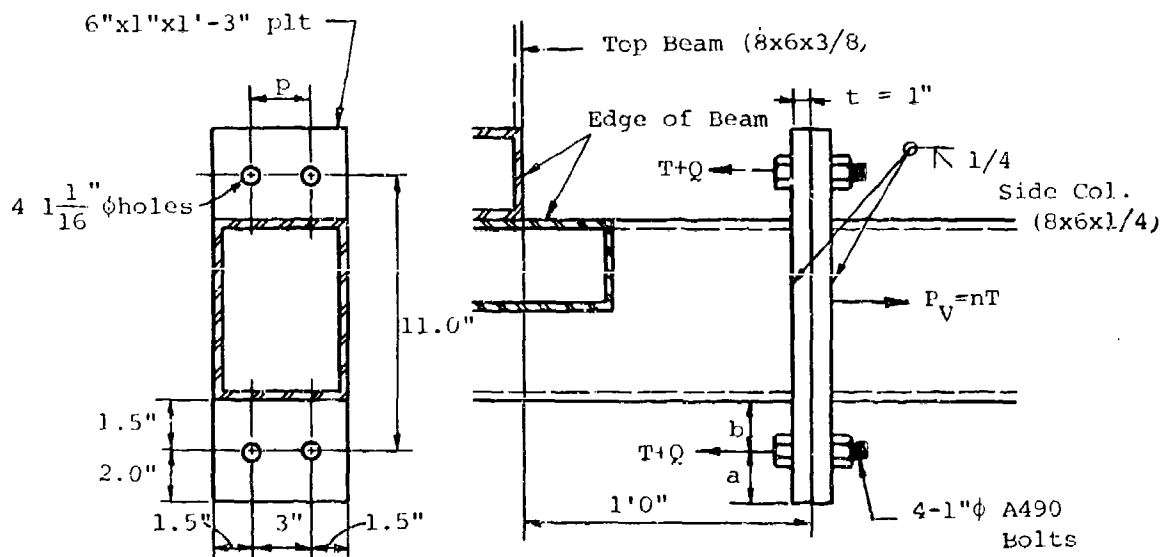
b. Find

Using the loads derived in Example 5.6.5, analyze the upper connection of the removable column. Assume the upper end of the column is fixed and the lower end is simply supported. The upper connection is located 1 foot below the roof beam.

c. Solution

Without a finite element dynamic analysis of the shield, it is difficult to predict the exact phasing of the various axial and bending components of loads applied to the connection. For this reason, the analysis presented here evaluates the connections ability to develop separately the columns full plastic moment, full axial load capacity, and the combination of bending plus axial load from Example 5.6.5.

Details of the upper connection are shown below.



Removable Column Upper Connection Details

The axial load capacity of the column is

$$P_e = f_{dy} A = 6.48(39,600) = 256,608 \text{ lbs}$$

Approximate load per bolt without prying action is

$$P_b = \frac{256,608}{4} = 64,152 \text{ lbs}$$

The fully plastic moment capacity of the 8 x 6 x 1/4 column is

$$M_P = f_{dy} Z = 39,600(18.66) = 738,936 \text{ in-lb}$$

The load per bolt without prying action for an 11.0-inch lever arm is

$$P_b = \frac{738,936}{2(11)} = 33,588 \text{ lbs}$$

Bolt tension increase, Q , due to prying action is found from Eq. 13.6.37 of Ref. 5-3.

$$\frac{Q}{P_b} = \frac{\frac{1}{2} - \frac{pt^4}{30ab^2A_b}}{\frac{a}{b}\left(\frac{a}{3b} + 1\right) + \frac{pt^4}{6ab^2A_b}}$$

where, referring to the sketch of the connection,

$$p = 3 \text{ inches}$$

$$a = 2 \text{ inches}$$

$$b = 1.5 \text{ inches}$$

$$A_b = \text{area of bolt} = 0.785 \text{ in}^2$$

$$t = 1 \text{ inch}$$

Then

$$\frac{Q}{P_b} = \frac{\frac{1}{2} - \frac{3(1.0)^4}{30(2)(1.5)^2(0.785)}}{\frac{2}{1.5}\left(\frac{2}{3 \times 1.5} + 1\right) + \frac{3(1.0)^4}{6(2)(1.5)^2(0.785)}} = 0.223$$

and bolt tension with prying action is

$$P_{ba} = 64,152(1.228) = 78,788 \text{ lbs for pure axial load}$$

$$P_{bm} = 33,588(1.228) = 41,251 \text{ lbs for pure bending load}$$

The most probable load is the axial tension applied by the roof beam acting simultaneously with the ultimate moment capacity of the column. The bolts will also be subjected to a total shear equal to the column reaction. Because of the proximity of the connection to the fixed end, the connection is designed for the loads applied at that point. That is, $M = 738,936 \text{ in-lb}$ and $T = 64,524 \text{ lb}$.

From paragraph 5.6.5, the maximum resistance of the column is 59,512 lb, and the maximum horizontal load is 215,007 lbs (assuming only the quasi-static load component need be considered). The dynamic reaction of the column at its upper (fixed) end is (Table 5-3)

$$\begin{aligned} V &= 0.38R_m + 0.12F_v + M_{ps}/L \\ &= 0.38(59,512) + 0.12(215,007) + 738,936/149 \\ &= 53,375 \text{ lb} \end{aligned}$$

The shearing stress in the bolts is

$$f_v = \frac{53,375}{4(0.785)} = 16,998 \text{ psi}$$

The total bolt tension is

$$P_b = 1.228[P_{ba} + P_{bm}] = 1.228\left[\frac{64,524}{4} + 33,588\right] = 61,055 \text{ lb}$$

Reference 5-2 allows a bolt tensile stress of

$$\begin{aligned} F_t &= 1.7[70 - 1.6f_v] \leq 1.7(54) \\ &= 1.7[70 - 1.6(17.0)] \leq 91.8 \text{ ksi} \\ &= 72.8 \leq 91.8 \text{ ksi} \end{aligned}$$

Actual maximum tensile stress in the bolts is

$$F_t = \frac{61,055}{0.785} = 77,777 \text{ psi} = 77.7 \text{ ksi} > 72.8 \text{ ksi}$$

and the bolts appear somewhat overstressed but will not be changed at this time. Using an allowable tensile stress of 72.8 ksi, the capacity of each bolt is

$$P_b = 72.8 A_b = 72.8(0.785) = 57.2 \text{ kips}$$

The bending moment in the connection plate at the bolt line is

$$M = Qa = 0.228 \left[\frac{61,055}{4} + 33,588 \right] [2.0] = 22,276 \text{ in-lb}$$

Subtracting the 1.0625-inch hole from the plate, the allowable bending at the bolt line is

$$M_{all} = \frac{f_{dy}(p - 1.0625)t^2}{4} = \frac{39,600(3.0 - 1.0625)(1)^2}{4} = 19,181 \text{ in-lb}$$

The bending moment in the plate at the face of the column is

$$M = T_b - Qa = \left[\frac{61,055}{4} + 33,588 \right] 1.5 - 22,276 = 51,002 \text{ in-lb}$$

Allowable bending at the column, assuming $p = 6$ inches, is

$$M_{all} = \frac{f_{dy}pt^2}{4} = \frac{39,600(6)(1.0)^2}{4} = 59,400 \text{ in-lb}$$

Therefore, bending of the plate is within the allowable limits at the column line but exceeded at the bolt line. In view of the conservatism of using end moments and shears in this analysis, the plate is considered satisfactory.

The shear load per bolt is

$$V = \frac{53,375}{4} = 13,344 \text{ lb}$$

The bearing stress is

$$f_b = \frac{V}{A_b} = \frac{13,344}{1(1)} = 13,344 \text{ psi}$$

The allowable bearing stress is

$$F_p = 1.35 f_{dy} = 1.35(39,600) = 53,460 \text{ psi}$$

5.6.8 Structural Response of Group 3 Suppressive Shield Steel Hoop

a. Given

The steel hoop of the Group 3 shield is located midway between the foundation slab and the roof slab. The hoop is placed around the outer circumference of the cylinder to support the S3x5.7 interlocking beams. It consists of ten continuous straps 5 inches wide by 1/2 inch thick to make a hoop cross section 5 inches wide by 5 inches thick.

b. Find

The response of the steel hoop using the blast loads given in illustrative example 5.6.1.

c. Solution

The first step is to determine the natural period of vibration of the hoop and that portion of the vertical beams it supports. The vertical beams are assumed to be fixed at the roof and foundation slab and supported at mid span by the steel hoop. The weight of the steel hoop is

$$W_R = \rho A = 0.283(25) = 7.075 \text{ lb/in}$$

From Table 5-3, one-third of the mass of the beam between supports is assumed concentrated at midspan for single degree of freedom analyses. It appears logical to assume the remaining two-thirds is distributed equally to each support. Since there are two beams bearing on the steel hoop, assume that 2/3 of the weight of a vertical beam is included in the weight of the steel hoop. The additional uniformly distributed weight contributed to the steel hoop by the beams is

$$W_B = 2/3 \frac{wLN}{2\pi R}$$

$$W_B = 2/3 \left(\frac{5.7}{12} \right) (60) \left(\frac{296}{2\pi(72.5)} \right) = 12.35 \text{ lb/in}$$

where

w = weight of beam per inch

L = length of beam, inches

N = total number of beams

R = radius to center of wall, inches

The total distributed steel hoop mass is

$$M = \frac{7.08 + 12.35}{386} = 0.0503 \text{ lb-sec}^2/\text{in}^2$$

The natural period of the ring is obtained from

$$T_N = 2\pi \left[\frac{mR^2}{EA} \right]^{1/2} = 6.28 \left[\frac{0.0503(72.5)^2}{29 \times 10^6 (25)} \right]^{1/2} = 0.0038 \text{ sec}$$

The maximum unit resistance of the ring beam is given by

$$r_m = \frac{f_{dy} A}{L_B R_i}$$

where

f_{dy} = dynamic yield strength, 39,600 psi

A = 25 in²

L_B = supported length of beam, 60 inches

R_i = inside radius of structure, 67.5 inches

Substituting,

$$r_m = \frac{39,600(25)}{60(67.5)} = 244.44 \text{ psi}$$

From example 5.6.1, the peak reflected pressure, P_r , is 3350 psi and its duration, t_1 , is 0.00025 seconds.

The peak quasi-static pressure, P_{qs} , is 187 psi and its duration, t_2 , is 0.066 seconds. The ratio of the durations of the two pulses to the period of the hoop are such that the structural response of the steel hoop is found from

$$\left[\frac{\frac{C_1 P_r}{r_m}}{\frac{T_N}{\pi t_1} \sqrt{2\mu-1}} \right]^2 + \frac{\frac{C_2 P_r}{r_m}}{\frac{T_N}{\pi t_2} \sqrt{2\mu-1} + \frac{1 - \frac{1}{2\mu}}{1 + 0.7 \frac{T_N}{t_2}}} = 1$$

where

$$r_m = 244.44 \text{ psi}$$

$$P_r = 3350 \text{ psi}$$

$$t_1 = 0.00025 \text{ sec}$$

$$t_2 = 0.066 \text{ sec}$$

$$C_1 = 0.944$$

$$C_2 = 0.056$$

$$T_N = 0.0038 \text{ sec}$$

A solution is obtained by trial and error and a ductility ratio, μ , of 15 was found to satisfy the equation. Substituting in the equation

$$\left[\frac{0.944(3350)}{244.44(25.987)} \right]^2 + \frac{0.056(3350)}{244.44(1.0277)} = 0.99 \approx 1.0$$

The circumferential stretching of the hoop at the elastic limit is

$$\Delta_L = \frac{f_{dy} A (2\pi R_R)}{AE} = \frac{39,600(25)(6.28)(72.5)}{25(29)(10)^6}$$

$$\Delta_L = 0.622 \text{ inch}$$

and the radial deflection is

$$\Delta_R = \frac{0.622}{2\pi} = 0.099 \text{ inch}$$

Since $\mu = X_m/X_y$, the maximum radial deflection of the hoop is

$$X_m = 15(0.099) = 1.485 \text{ inches}$$

5.7 LIST OF SYMBOLS

a	(1) Side of square plate (inches) (2) Plate dimension (inches)
A, A_1, A_2, \dots	Area (in^2)
A_s	Area of tensile steel (in^2)
A_v	Area of vertical web reinforcing (in^2)
A_{vH}	Area of horizontal web reinforcing over distance S_H (in^2)
b	(1) Width of cross section (inches) (2) Plate dimension (inches)
B	Peak total load (lbs)
C, C_1, C_2, C_3, \dots	Equation constants
d	(1) Effective depth of concrete member (inches)
d_w	Web depth (inches)
D	Diameter (inches)
E	Modulus of elasticity (psi)
f'_c	Static unconfined compressive strength of concrete (psi)
f'_{dc}	Dynamic compressive strength of concrete (psi)
f_{dy}	Dynamic tensile yield stress (psi)
f_y	Static tensile yield stress (psi)
F	Force (lbs)
F_{eq}	Force on equivalent single degree of freedom system (lbs)
F_t	(1) Total force (lbs) (2) Tensile load on bolt (lbs)
$F_t(t)$	Time varying force (lbs)
F_1, F_2, F_3, F_i	Ratios of $C_i B/R_m$ for given load characteristics and ductility ratio
H	Force per unit length (lbs)
i	Impulse (lbs-sec)
i_r	Reflected pressure impulse (psi-sec)
I	Moment of inertia of beam or moment of inertia of unit width of one-way slab (in^4)
I_a	Average of gross and cracked moment of inertia per unit width of concrete slabs (for short span in two-way slabs) or plastic section modulus of plate per unit width (in^4)

K, K_1, K_2, \dots	Spring constant (lb/inch)
K_e	Spring constant for elastic range (lb/inch)
K_{ep}	Spring constant for elastic-plastic range (lb/inch)
K_{eq}	Spring constant of equivalent single degree of freedom system (lb/inch)
K_E	Equivalent spring constant (lb/inch)
K_L	Load transformation factor
K_{LM}	Load-mass factor
K_M	Mass transformation factor
K_R	Resistance factor
K.E.	Kinetic energy (in-lb)
ℓ, L	Length (inches)
L_D	Deformed rebar required development length (inches)
m	Mass per unit length/area (lb-sec ² /in ²)
M	Mass (lb-sec ² /in)
M_b	Total mass of beam (lb-sec ² /in)
M_c	Total moment at critical section (inch/lb)
M_{eq}	Mass of equivalent single degree of freedom system (lb-sec ² /in)
M_p	Ultimate bending moment capacity (inch/lbs)
M_{Pc}	Ultimate positive bending moment capacity per unit width at center of circular slab (in-lb/in)
M_{Pfa}	Total ultimate positive bending moment capacity along midspan section parallel to short side, a (in-lb)
M_{Pfb}	Total ultimate positive bending moment capacity along midspan section parallel to long side, b (in-lb)
M_{Pm}	Ultimate bending moment capacity of beam at midspan (in-lb)
M_{Ps}	Ultimate negative bending moment capacity per unit width at center of circular slab or ultimate bending moment capacity of beam at support (in-lb/in or in-lb)
M_{Psa}	Total ultimate negative bending moment capacity along short edge, a (in-lb)

M_{Psa}°	Ultimate negative bending moment capacity per unit width at center of edge a in direction of long span, b (in-lb/in)
M_{Psb}	Total ultimate negative bending moment capacity along long edge, b (in-lb)
M_{Psb}°	Ultimate negative bending moment capacity per unit width at center of edge b in direction of short span, a (in-lb/in)
M_s	Total mass of spring (lb-sec ² /in)
M_t	Total mass (lb-sec ² /in)
p	(1) Pressure (psi) (2) Tensile reinforcing steel ratio
$p(t)$	Pressure as a function of time (psi)
P	Force (lbs)
r_m	Maximum unit resistance (psi)
R	(1) Radius (inches) (2) Resistance of element (lbs)
R_e	Elastic resistance (lbs)
R_i	Inside radius (inches)
R_m	Maximum resistance (lbs)
R_{meq}	Maximum resistance of equivalent single degree of freedom system (lbs)
R_o	Outside radius (inches)
s	Spacing of vertical web reinforcing (inches)
s_H	Vertical spacing of horizontal web reinforcing (inches)
S	(1) Section modulus (in ³) (2) Slope of strain hardening curve
t	Thickness (inches)
t_f	Flange thickness (inches)
t_m	Time of maximum displacement (inches)
t_o	Duration of positive pressure pulse (sec)
t_w	Web thickness (inches)
t_1, t_2, \dots	Pulse durations (sec)
T_N	Natural period of vibration (sec)
U	Strain energy (in-lb)
v_d	Direct shear stress (psi)

V	(1) Dynamic reaction at end or edge of symmetric element (lbs) (2) Total shear acting on section (lbs)
V_c	Ultimate shear force in concrete (lbs)
V_d	Total shear at support (lbs)
V_s	Shear capacity added by shear reinforcing (lbs)
V_u	Ultimate shear capacity (lbs)
V_y	Total shear acting on section (lbs)
V_A	Total dynamic reaction along one short edge, a (lbs)
V_B	Total dynamic reaction along one long edge, b (lbs)
V_1	Dynamic reaction at hinged end of nonsymmetric beams (lbs)
V_2	Dynamic reaction at fixed end of nonsymmetric beams (lbs)
W	Charge weight of explosive (lbs)
X	Displacement (inches)
\dot{X}	Velocity (in/sec)
\ddot{X}	Acceleration (in/sec ²)
X_e	Elastic limit displacement (inches)
X_{eq}	Displacement of equivalent single degree of freedom system (inches)
X_m	Maximum displacement (inches)
X_p	Elasto-plastic displacement (inches)
X_E	Equivalent elastic limit displacement (inches)
Z	(1) Scaled distance (ft/lb ³) (2) Plastic section modulus (in ³)
ϵ	Strain (in/in)
ϵ_{dy}	Dynamic yield strain (in/in)
μ	Ductility ratio
ν	Poisson's ratio
ρ	Mass density (lb-sec ² /in ⁴)
σ	Stress (psi)
σ_h	Hoop stress (psi)

σ_l
 σ_r
 ω_N

Longitudinal stress (psi)

Radial stress (psi)

Circular natural frequency (rad/sec)

5.7 REFERENCES

- 5-1 Beedle, L.S., Plastic Design of Steel Frames, John Wiley and Sons, Inc., New York N.Y., 1958. (U)
- 5-2 Manual of Steel Construction, Seventh Edition, American Institute of Steel Construction, Inc., New York, N.Y., 1970. (U)
- 5-3 Salmon, C.G. and Johnson, J.E., Steel Structures-Design and Behavior, Intext Educational Publishers, Scranton, Pa., 1971. (U)
- 5-4 Winter, G., et al, Design of Concrete Structures, McGraw-Hill Book Co., New York, N.Y., 1964. (U)
- 5-5 Structures to Resist the Effects of Accidental Explosions, TM 5-1300, Department of the Army, Washington, D.C., June 1969. (U)
- 5-6 Biggs, J.M., Introduction to Structural Dynamics, McGraw-Hill Book Co., New York, N.Y., 1964. (U)
- 5-7 Building Code Requirements for Reinforced Concrete, ACI 318-71, American Concrete Institute, Detroit, Mich., 1971. (U)
- 5-8 Shear and Diagonal Tension, Report of ACI-ASCE Committee 326, ACI Manual of Concrete Practice-Part 2, American Concrete Institute, Detroit, Mich., 1968. (U)
- 5-9 Crawford, R.E., Higgins, C.J. and Bultmann, E.H., The Air Force Manual for Design and Analysis of Hardened Structures, AFWL-TR-74-102, Air Force Weapons Laboratory, Kirtland AFB, N.M., October 1974. (U)
- 5-10 Seely, F.B. and Smith, J.O., Advanced Mechanics of Materials, Second Edition, John Wiley and Sons, Inc., New York, N.Y., August 1961. (U)
- 5-11 Harris, C.M., and Crede, C.E., Shock and Vibration Handbook, McGraw-Hill Book Co., New York, N.Y., 1961. (U)
- 5-12 Trott, B. Dale, et al, Design of Explosion Blast Containment vessels for Explosive Ordnance Disposal Units, Picatinny Arsenal, Dover, N.J., June 1975. (U)

- 5-13 Design of Structures to Resist the Effects of Atomic Weapons, Structural Elements Subjected to Dynamic Loads, U.S. Army Corps of Engineers Manual TM5-856-4 December 1965. (U)
- 5-14 Design of Structures to Resist Nuclear Weapon Effects, American Society of Civil Engineers Manual of Engineering Practice No. 42, ASCE, New York, N.Y. (U)
- 5-15 Newmark, N.M., "Computation of Dynamic Structural Response in the Range Approaching Failure," Proceedings of the Symposium on Earthquake and Blast Effects on Structures, Los Angeles, Calif., 1952. (U)
- 5-16 Melin, J.W., Numerical Integration by Beta Method, ASCE Conference on Electronic Computation, Kansas City, Mo., 1968. (U)
- 5-17 Baker, W.E., The Elastic Plastic Response of Thin Spherical Shells to Internal Blast Loading, Paper No. 59-A-95, Applied Mechanics Division, American Society of Mechanical Engineers, February 1959. (U)
- 5-18 Roark, R.J. and Young, W.C., Formulas for Stress and Strain, McGraw-Hill Co., New York, N.Y. 5th Edition, 1975. (U)
- 5-19 Design of Structures to Resist the Effects of Atomic Weapons, Strength of Materials and Structural Elements, U.S. Army Corps of Engineers Manual, TM5-856-2, August 1965. (U)
- 5-20 Baker, W.E., et al, Analysis and Preliminary Design of a Suppressive Structure for a Melt Loading Operation, EM-CR-76056, Edgewood Arsenal, Aberdeen Proving Ground, Md., May 1976. (U)
- 5-21 Trott, B. Dale, et al, The Blast and Fragment Containment Capability of Portable Chambers, N00174-74-C-0219, Naval Explosive Ordnance Disposal Facility, Indian Head, Md., September 1975. (U)
- 5-22 Nelson, K.P., Spherical Shields for the Containment of Explosions, EM-TR-76096, Edgewood Arsenal, Aberdeen Proving Ground, Md., March 1977. (U)

CHAPTER VI

STRUCTURAL DETAILS

6.1 INTRODUCTION

Suppressive shields used for ammunition manufacturing and other hazardous operations require provisions for gaining access to the operation being protected. Personnel must be able to enter the shield to accomplish routine and emergency maintenance and clean-up and other essential operations. An opening of sufficient size must be provided to enable the installation or removal of equipment in realistically large subassemblies. Openings for conveyors and chutes must also be provided and properly configured to prevent excessive pressure and fragments from escaping. Provisions must be made to provide all utilities and satisfy all environmental conditioning needs which may be essential to the operations inside the shield.

Utility penetrations, ventilating and air conditioning ducts, and vacuum lines must not diminish the overall protective capability of the shield. They must not alter the basic mode of structural failure of the suppressive shield and should be small compared to the general size of the shield.

Operations that produce explosive dust may require the use of liners both inside and outside the shield to prevent the accumulation of dust within shield panels. With configurations such as the Group 5 shield, which is primarily designed for use with propellants or pyrotechnic materials, liners must not inhibit the venting characteristics of the shield.

6.2 UTILITY PENETRATIONS

6.2.1 General

Utility penetrations for water, compressed air, and electricity are basic to the manufacturing process of munitions.

Explosive dust and chips are a waste product produced during the manufacture of various munitions. Water is needed for wash down/cooling and deluge operations which safely remove these products. Most deluge lines will be 2 to 2.5-inch diameter industrial hose. Compressed air is needed for the operation of pneumatic tools. A typical requirement might be for 100 psig of dry compressed air at 25 to 30 cubic feet per minute. Electrical power is needed for the prime movers of the manufacturing equipment and peripherals, i.e., motors, air handling units and lights. Depending on the amperage requirements, the size of conduits might vary from 0.5-inch diameter for 120V single phase (lights) to as large as 2 to 3-inch diameter for 440-480 volt three phase service. Penetrations can be routed through the side walls of a shield or through the roof depending on the specific operational requirements.

6.2.2 Design Concept and Rationale

Utility lines passing through suppressive shields are vulnerable to both airblast and fragment hazards. The airblast could push unprotected utility penetrations through the walls of the shield and create secondary fragments. Fragments from an accidental explosion could perforate the thin walls of an unprotected utility pipe and escape from the shield. To eliminate the threat of airblast and fragments, a protective box is used to cover the area where the utility lines pass through the shield wall. The box is configured to rest on the inside surface of the shield and is welded to the shield. The size of the wall penetrations is limited to that required for the utilities, i.e., pipes of 0.5 to 3 inches in diameter. Each pipe is bent at a right angle inside the shield within the protective box. The penetrations of the shield wall are reinforced with a sleeve or box section welded to the shield panel through which the utility line passes. The penetration box is designed to maintain the structural integrity of the shield area penetrated. A typical protective box design is shown in Fig. 6-1. The cover plate thickness is selected to stop the worst case fragment.

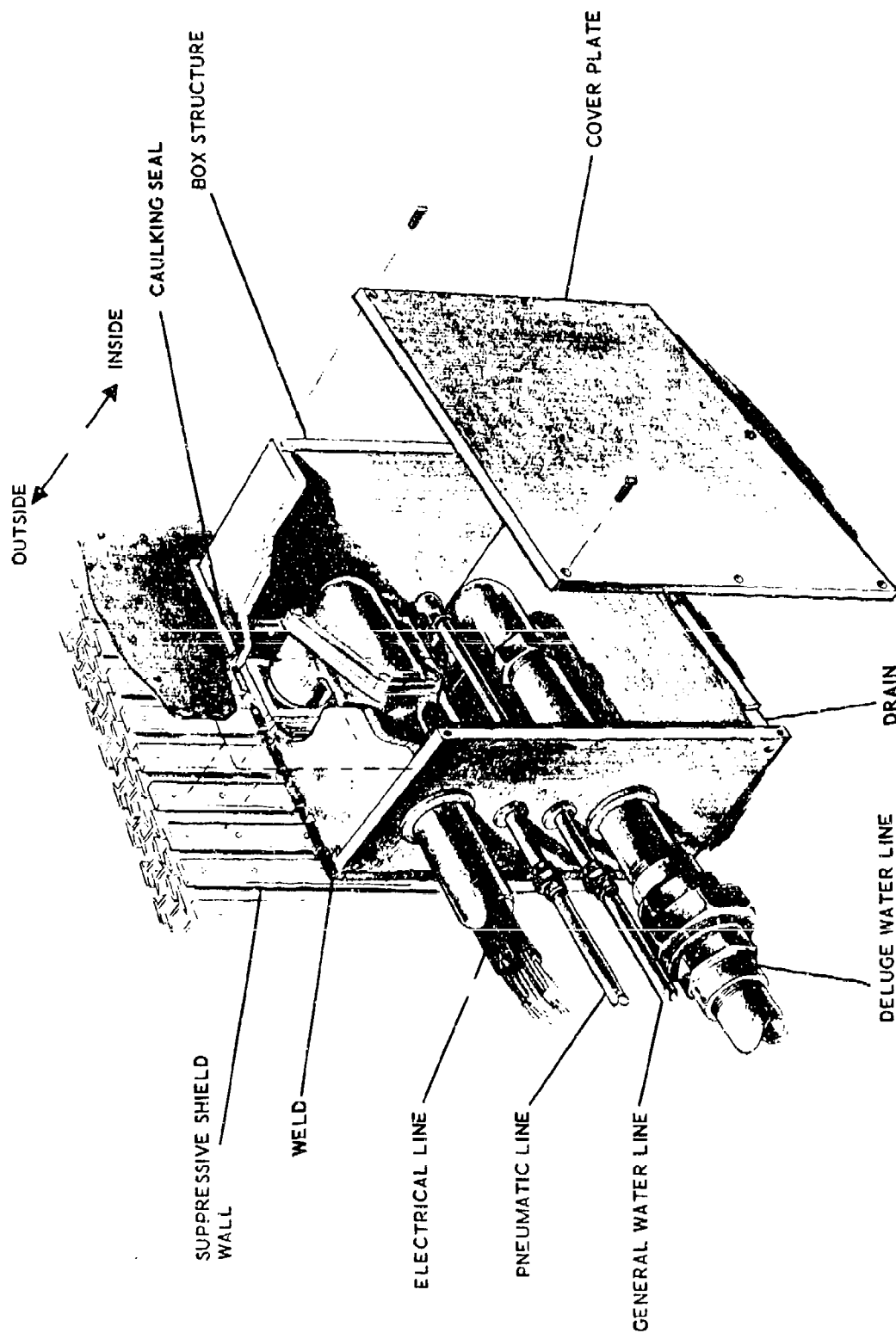


Figure 6-1. Typical Utility Penetration

For the safety approved shields, the minimum cover plate thickness is equal to the nominal steel thickness of the shield wall.

The individual utility lines are arranged with the lowest being deluge water, next highest the general water service, then compressed air and finally the electrical line in the topmost position. This arrangement is recommended to prevent water, leaking from loose or faulty connections, from saturating the electrical line and causing a short circuit. Water accumulation inside the protective box can be avoided by incorporating a suitable drain. Figure 6-1 shows a short slot in the bottom plate which is large enough for drainage yet small enough to prevent fragment entry.

6.2.3 Method of Structural Analysis

The initial step in the design analysis is the determination of the fragment hazard to allow selection of the cover plate thickness. Representative primary fragment hazards for standard ammunitions are listed in Ref. 6-1. If Ref. 6-1 is not available, fragment hazards for standard ammunitions and unusual shapes and combinations can be approximated using the methods presented in Chapter 3. Chapter 3 also provides procedures for computing the material thickness required to prevent fragment perforation.

Once a minimum cover plate thickness has been chosen, the protective box can be designed for the airblast loading. The box consists of a cover plate and four side members. The cover plate is mechanically fastened to the side members, and the complete assembly is welded to the shield panel. The analytical procedure presented here is for the protective box design shown in Fig. 6-1. Alternate designs may be used, provided acceptable analytical procedures are employed to determine the dynamic response of the structural components. To verify the structural integrity of the protective box design, the following analyses must be performed.

- Bending of cover plate
- Buckling of side members

a. Bending of Cover Plate

The cover plate is loaded by the reflected pressure and the quasi-static pressure which causes bending stresses. Procedures for analyzing this member are presented in paragraph 5.5. The ductility ratio must be less than 6 for an acceptable design. Example 6.7.1 demonstrates the method of analysis of a cover plate.

b. Buckling of Side Plates

The side plates of the box structure are assumed to be simply supported along the edges attached to the cover plate and shield panel. Joints connecting side members at the corners of the box are assumed to be clamped. The critical buckling stress is (Ref. 6-2),

$$\sigma_{cr} = \frac{K_b E}{1-\nu^2} \left[\frac{t_s}{b_c} \right]^2 \quad (6-1)$$

where K_b depends on the ratio h/b_c and is determined from the following table.

$\frac{h}{b_c}$	0.4	0.5	0.6	0.7	0.8	1.0	1.2	1.4	1.6	1.8	2.1	∞
K_b	7.76	6.32	5.80	5.76	6.00	6.32	5.80	5.76	6.00	5.80	5.76	5.73

E = modulus of elasticity, psi

ν = Poissons ratio

h = height of side member, inches

The side plate thickness should be equal to or greater than the nominal steel thickness of the safety approved shields or that computed by the methods of Chapter 3 to prevent fragment perforation.

The compressive stress developed, e.g., in the side members b, by the blast pressure is determined from

$$\sigma_b = \frac{V_B}{b_c t_s} \quad (6-2)$$

where

V_B = dynamic reaction along side b, lbs
(see Table 5-4)

The compressive stress from Eq. 6-2 must be less than the critical buckling stress from Eq. 6-1.

c. Effect of Protective Box on Shield Wall Members

The members of shield wall panels are designed without consideration of penetrations and appurtenances. Penetrations (holes) weakens the members; however, pipes and the protective box, because of their weights, attenuate the loads. The protective box serves two functions.

- Protects the pipes
- Redistributes the loads which would have been carried by the weakened members to adjacent members

The longest side plate along the length of the box distributes the load from the box to the panel members as concentrated loads. As shown in Section "A-A", pg. 6-11, at least 80% of the members must be effective in resisting the concentrated loads. Since the box cover is relatively flexible compared to the panel members and the concentrated loads are usually away from the midspan of the panel members, the resulting net effect on the panel member from the typical box is negligible.

The shortest side plate along the width of the box, as shown in Section "B-B", pg. 6-11, results in a local overload in

the panel member on which it reacts. This overload effect is also considered negligible.

Increase in panel deflection is not expected to be excessive due to the influence of the protective box as the panel members have an inherent built-in safety factor. If the protective box is not located and configured as recommended, serious problems, i.e., excessive deflections, may result. Under special conditions, complex and sophisticated analysis techniques are required such as the use of finite elements or finite differences in the solution of such problems. These techniques are beyond the scope of this handbook.

6.2.4 Location of Utility Penetrations

In rectangular type shields, such as the Group 4, 5 and 81-mm, the utility penetration should be made adjacent to a column or beam at the floor or the ceiling. Figure 6-3 shows a typical installation.

For Group 3 type shields with interlocked I-beam configurations, utility penetrations can be located in the I-beam side walls, the concrete roof, or the foundation. Utility penetrations in the side wall should be located above the floor stiffeners or below roof stiffeners. This procedure is shown in Fig. 6-4. Attachment details and engineering drawings are provided in Ref. 6-3.

6.3 VACUUM LINE PENETRATION

6.3.1 Design Requirements

In the process of manufacturing various munitions, explosive dust and chips are generated and must be safely removed as waste products. A common practice is to use a vacuum line for this function. The vacuum line penetration through the shield must prevent the escape of fragments and attenuate the side-on pressure to less than 2.3 psi at any adjacent operator location.

There are three hazards associated with the use of a vacuum line that must be analyzed in the design of a safe waste removal system.

- Detonation of the munition during production operations
- Detonation of airborne dust in the vacuum line
- Detonation of dust sediment in the vacuum line

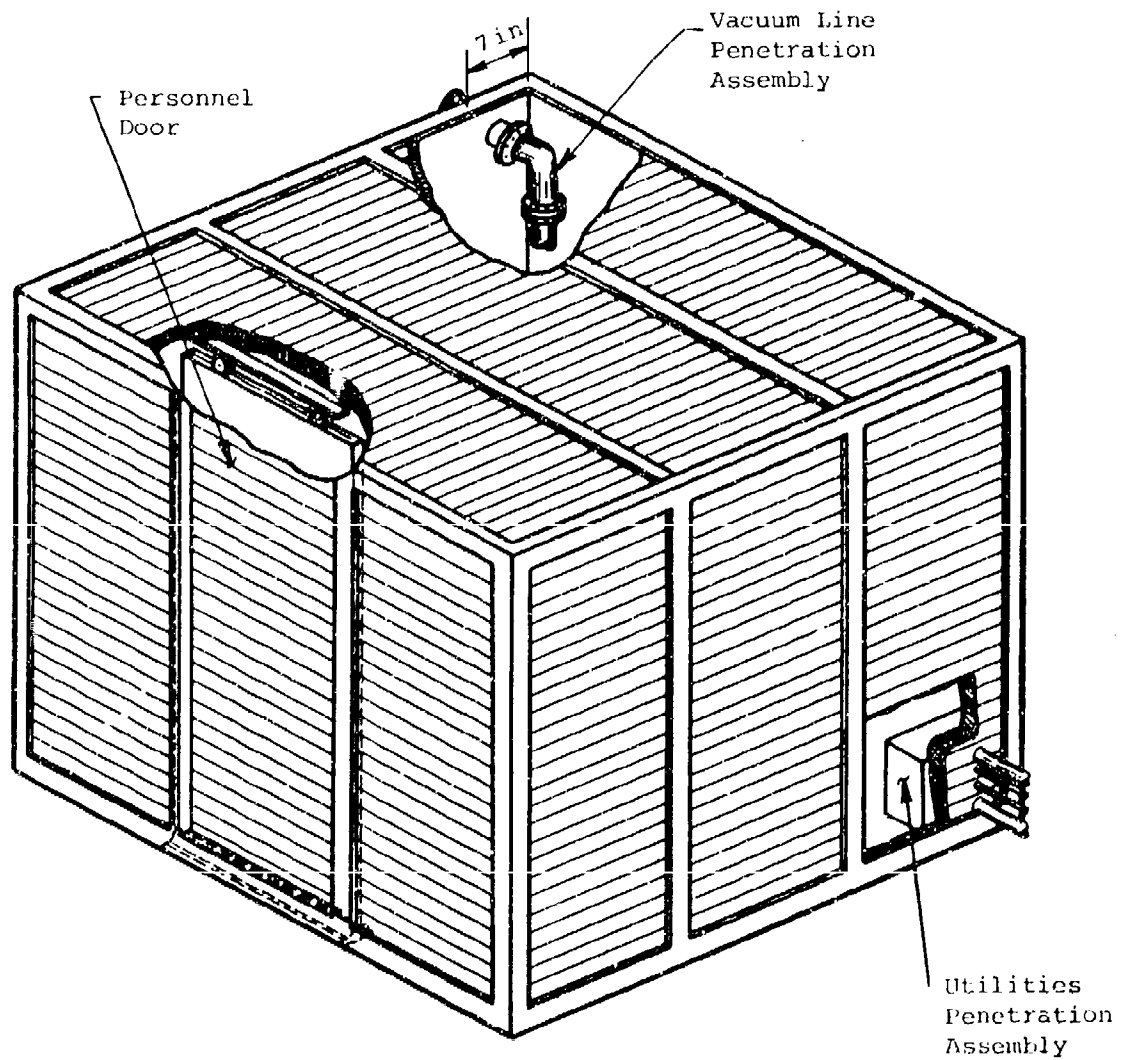


Figure 6-3. Typical Location of Utility Penetration in Shield Groups 4, 5 and 81-mm

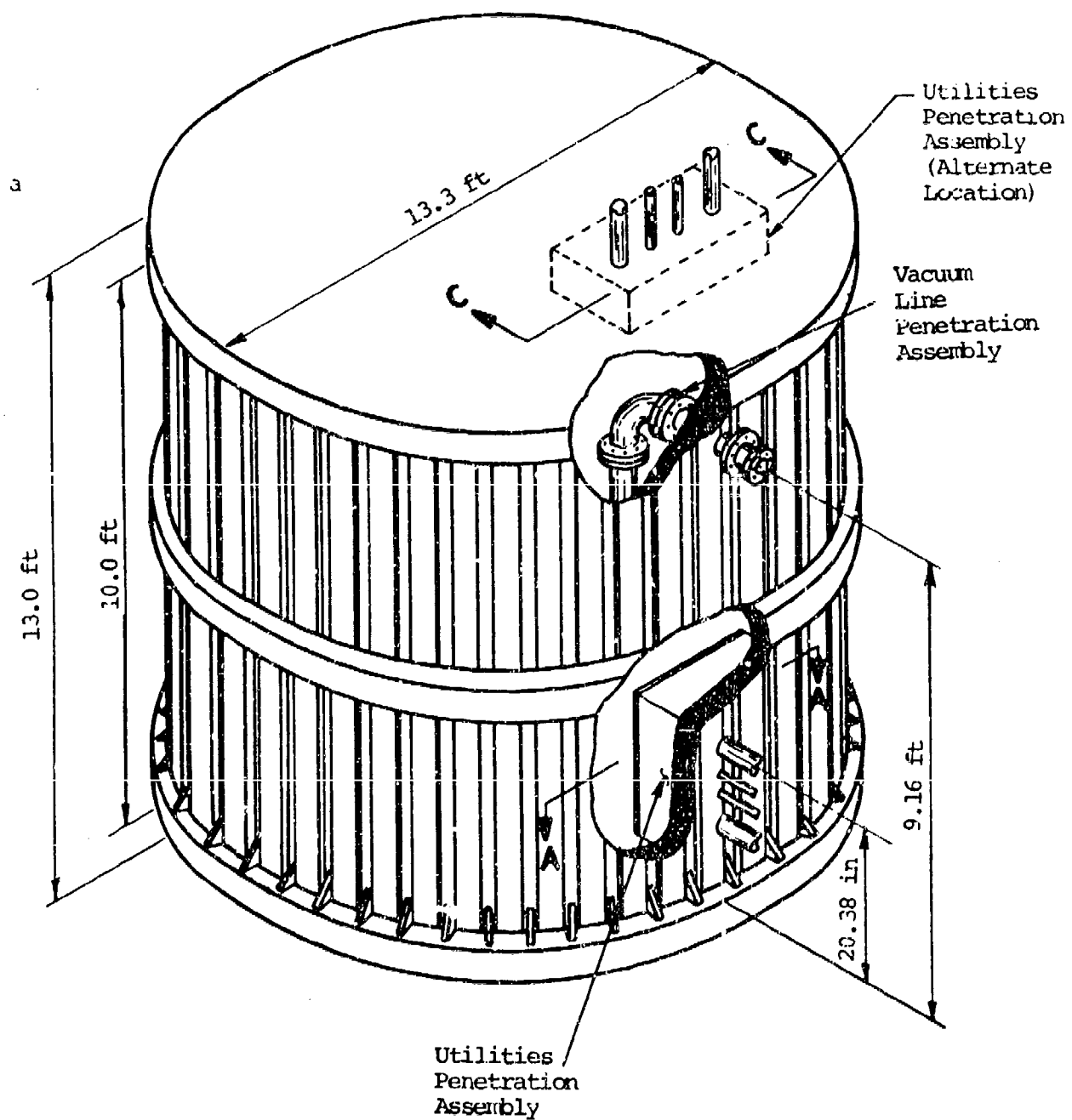


Figure 6-4. Typical Location of Utility Penetrations in Shield Group 3

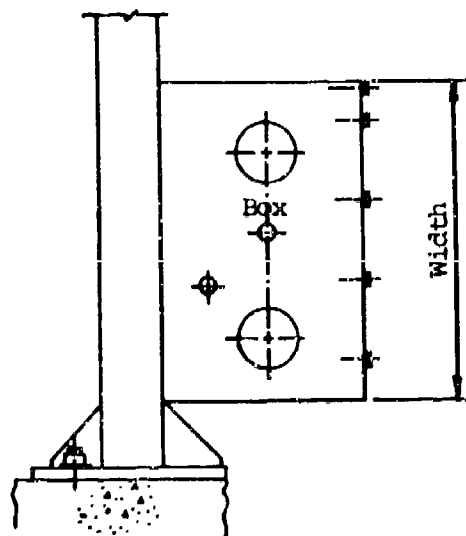
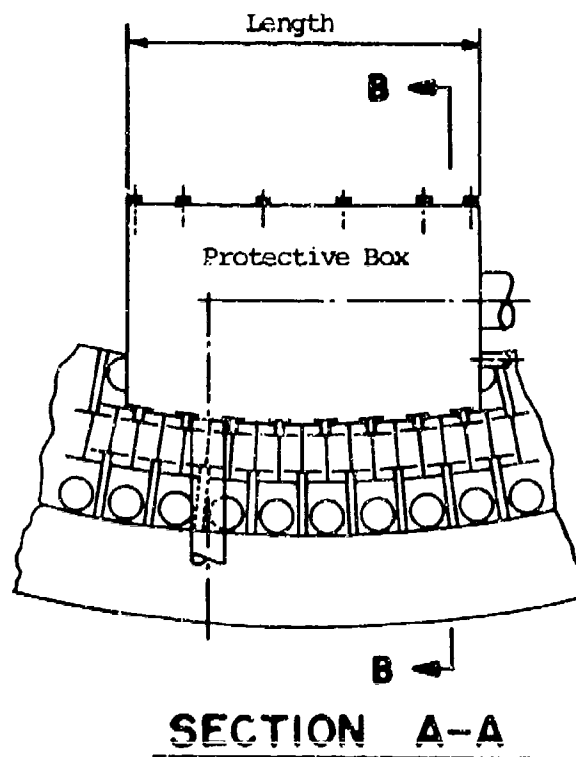


Figure 6-4. Typical Location of Utility Penetrations in Shield Group 3 (continued)

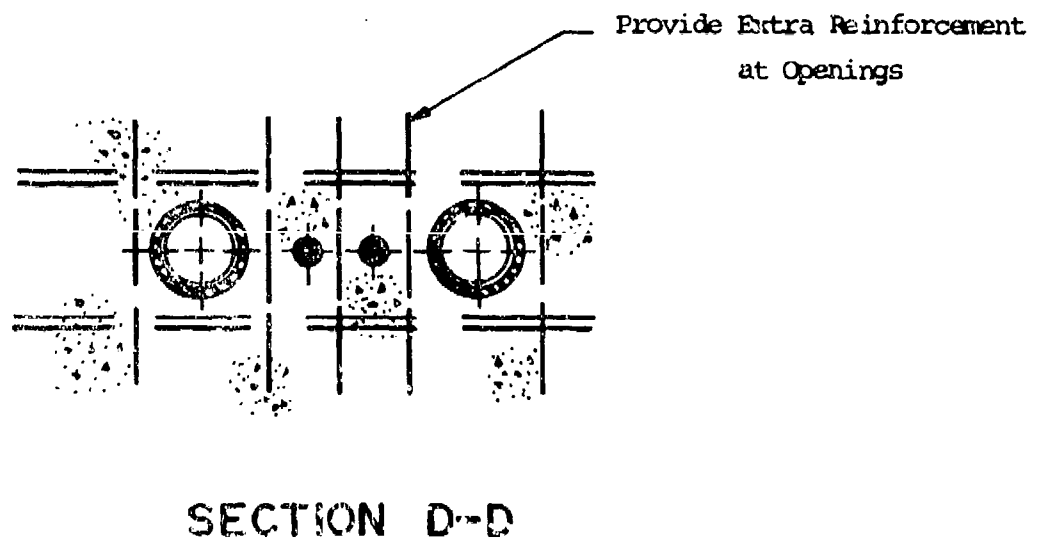
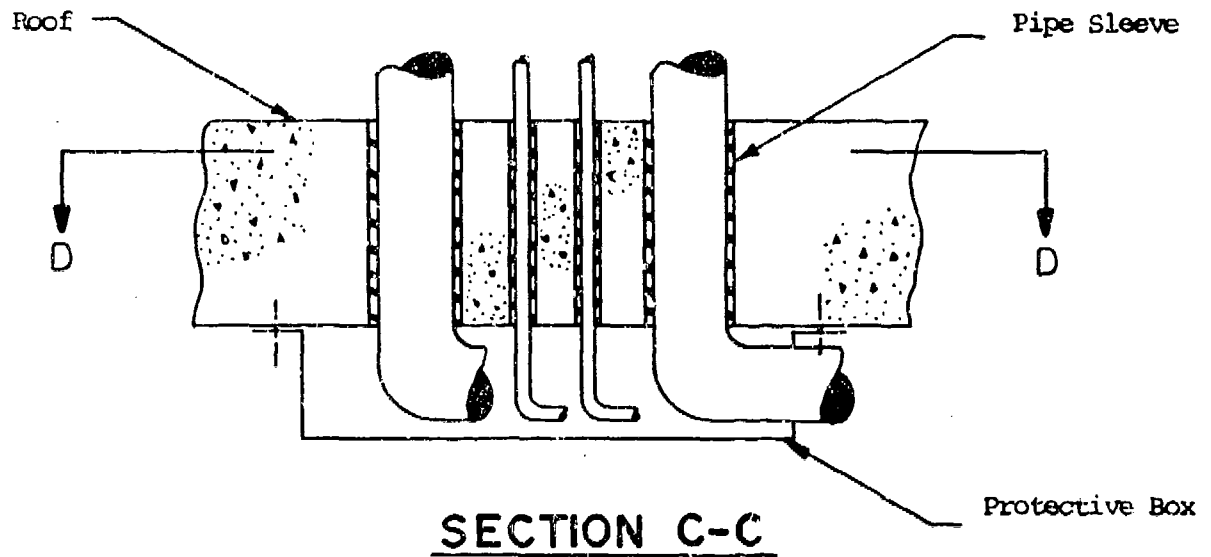


Figure 6-4. Typical Location of Utility Penetrations in Shield Group 3 (continued)

The vacuum line must be designed to allow for periodic disassembly for decontamination. At the shield penetration interface, provisions must be made to prevent the accumulation of dust in joints. All directional changes should be made with a large radius of curvature to preclude dust accumulation.

6.3.2 Design Concept and Rationale

The vacuum line penetration concept used in shield applications is shown penetrating the Group 3 shield in Fig. 6-5. This design satisfies the requirements established in paragraph 6.3.1 and is adaptable to all safety approved shields. Alternate designs were investigated and are described in detail in Ref. 6-4. For special situations when the design concept shown in Fig. 6-5 cannot be used, one of the alternate configurations should be considered. The recommended system consists of a thin-walled aluminum tube (disposal line) encased by a larger diameter aluminum tube which functions as a shield to contain all fragments and airblast effects.

The disposal line is located eccentrically within the shield tube so as to locate explosive dust residue in the approximate center of the shield tube and cause uniform airblast loading. The thickness of the shield tube must be sufficient to defeat fragments from the disposal line. The shielded disposal line extends from the waste disposal area to the shield and terminates just outside the suppressive shield.

The portion of the line which actually passes through and into the shield comprises a number of short, thick-walled steel sections connected by bolted flanges. The bushing in the suppressive shield must be large enough to clear the disposal line flange diameter. The space between the bushing and the disposal line is closed by a pair of split collars which encircle the disposal line and are bolted to the inner and outer faces of the bushing. The split collars support the disposal line where it passes through the shield wall and block the passage of fragments through the clearance space.

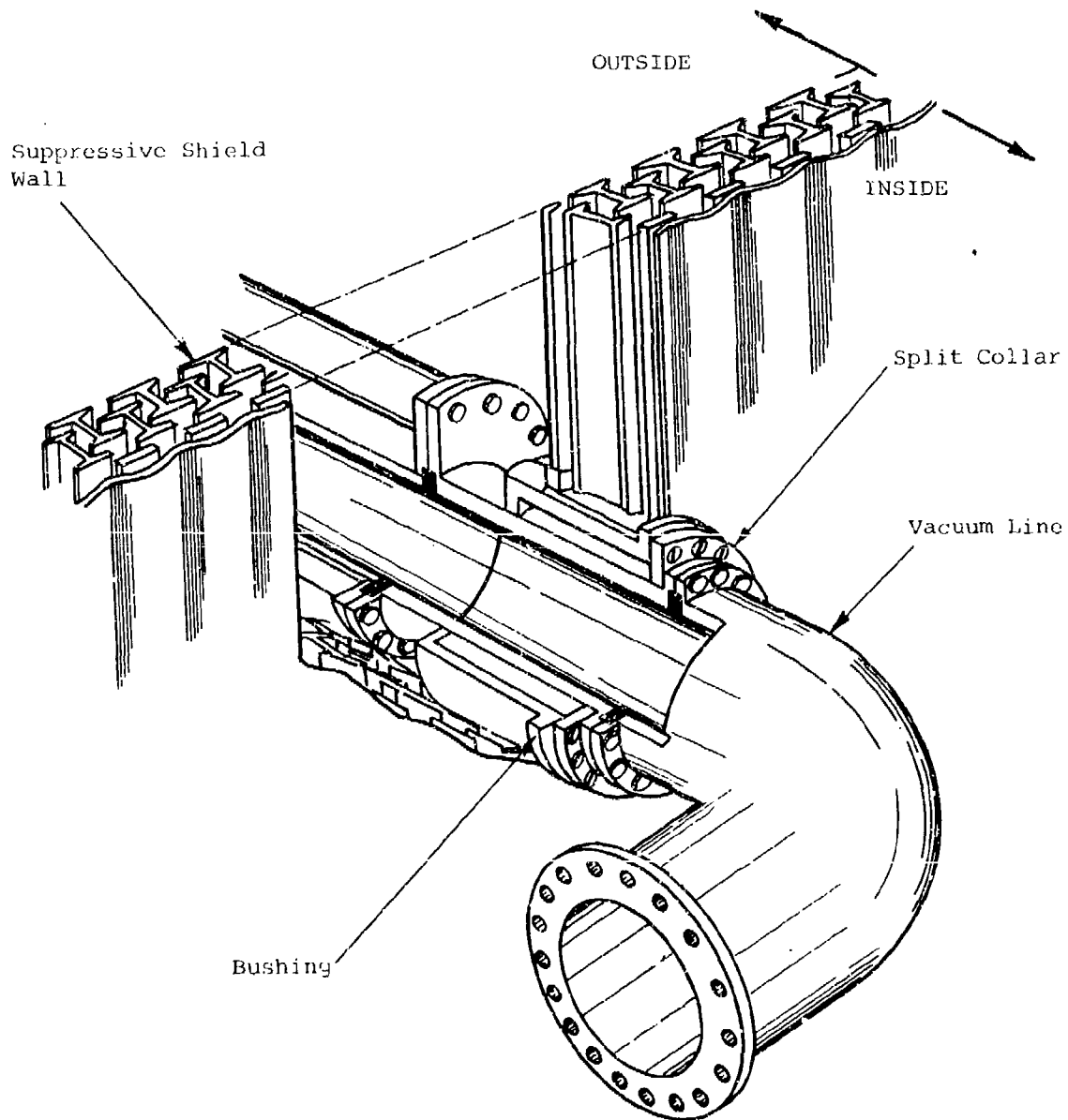


Figure 6-5. Typical Vacuum Line Penetration

Figure 6-6 illustrates the important details of a waste disposal vacuum line penetration through a suppressive shield wall. First, a circular hole is cut through the shield wall and a heavy steel bushing is welded into place. The thickness of this bushing must be sufficient to stop any fragments. All layers of the shield wall are welded to the bushing to retain their structural integrity. This procedure should be incorporated at the time of manufacture of the shield panel. In situations requiring the addition of a vacuum line to an existing suppressive shield, it will be necessary to make the bushing from a number of short tubular sections. The length of each section is at least equal to the spacing between panel layers. Sections are installed one at a time, welding each successive piece to the preceding section and to the appropriate panel layer.

Immediately inside the suppressive shield, the vacuum line contains a 90-degree elbow. This elbow is oriented to prevent the entrance of fragments into the disposal line without at least one ricochet. The elbow has the same inside diameter as the disposal line and is designed with a generous radius of curvature to promote free flow of waste material. The flanged connections are fitted with specially shaped elastomeric compression seals to prevent explosive dust from lodging at the joints. Flanges are bolted together. An alignment pin or pair of witness marks should be provided at each joint to insure that the inner tubes will be properly aligned after assembly. Figure 6-7 illustrates the joint design.

6.3.3 Method of Structural Analysis

a. Detonation of Munition

Two conditions must be satisfied for the waste disposal line to be considered safe under the loads imposed by the explosion of munitions during the manufacturing process.

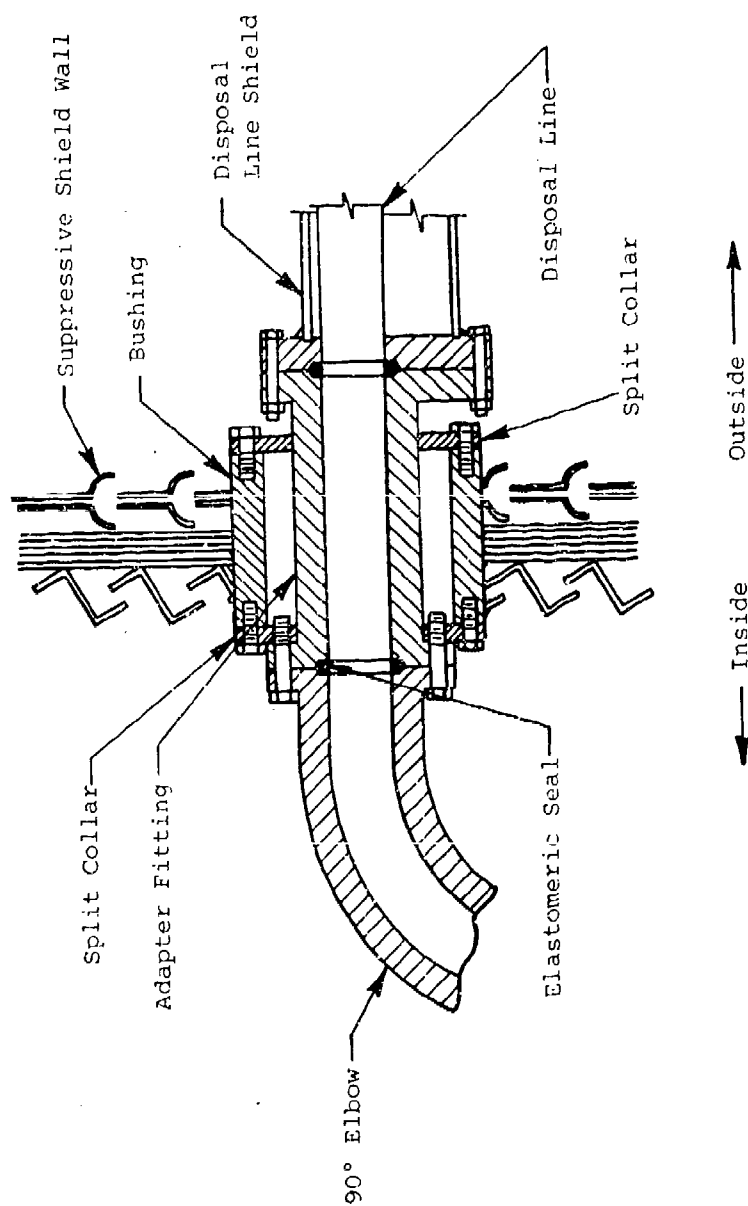


Figure 6-6. Waste Disposal Vacuum Line Entry Into Suppressive Shield

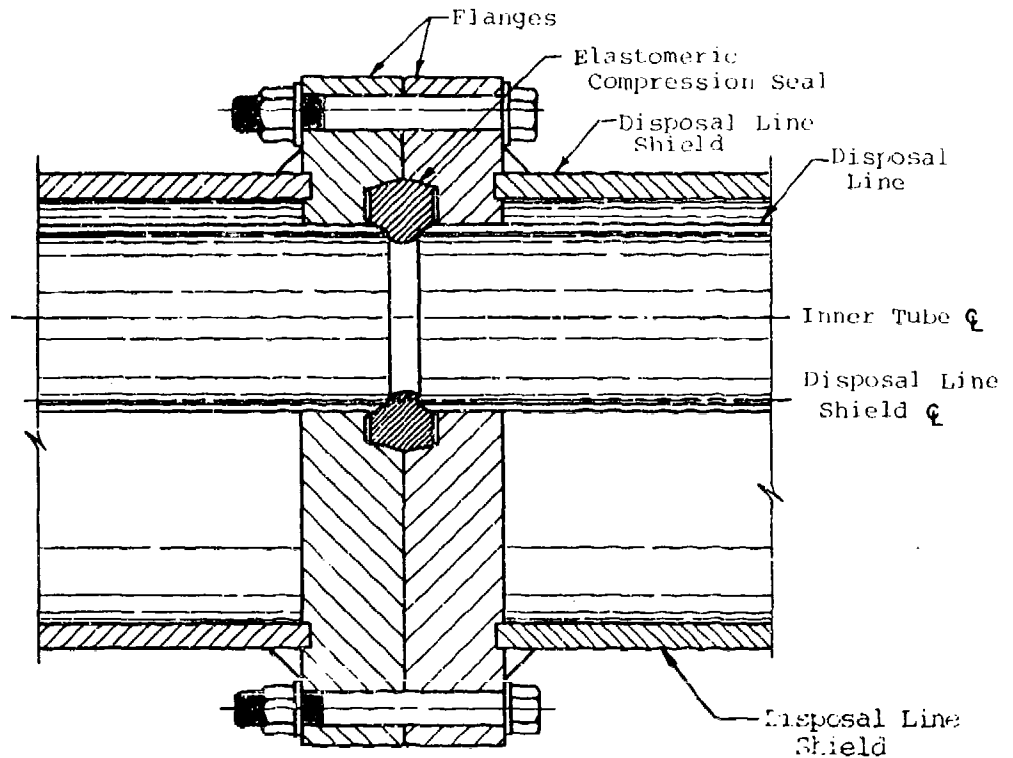


Figure 6-7. Joint Design for the Shielded Disposal Vacuum Line

- The vacuum line/suppressive shield interface must not fail and endanger personnel outside the shield.
- The disposal line shield extending outside the suppressive shield must remain intact in the event that the disposal line itself bursts under a load propagating through it.

Analysis methods for these conditions are presented below.

(1) Vacuum Line/Suppressive Shield Interface

Two modes of failure are possible at the interface between the vacuum line and the suppressive shield wall. The first is a shear failure in the split collar at the location identified as Shear Area 1 in Fig. 6-8. Although the split collar could be subjected to a detailed dynamic analysis, it is a low cost component in the shield. Uncertainties in loading also make any analysis questionable. It is recommended that the required shear strength of the split collar be determined from

$$\tau_s A_{SHC} = A_{VL} f_{dy} \quad (6-3)$$

where

τ_s = shear yield stress for collar material, psi

A_{SHC} = collar area resisting shear, in²

A_{VL} = cross section area of vacuum line, in²

f_{dy} = dynamic yield strength of vacuum line material, psi

The shear area should be determined at Shear Area 1 indicated in Fig. 6-8. The split collar should also meet the nominal shield wall thickness criteria for containment of fragments. Since two collars are used at each penetration, their thicknesses should be at least one-half the nominal wall thickness of the suppressive shield wall panel.

A second possible mode of failure is a punching through of the bushing and bushing flange. This would result from a shear failure in the shield wall along the lines marked Shear Area 2 in Fig. 6-8. In order to insure integrity of the penetration, the shield panel cross section area must meet the shear criteria of Eq. 6-3.

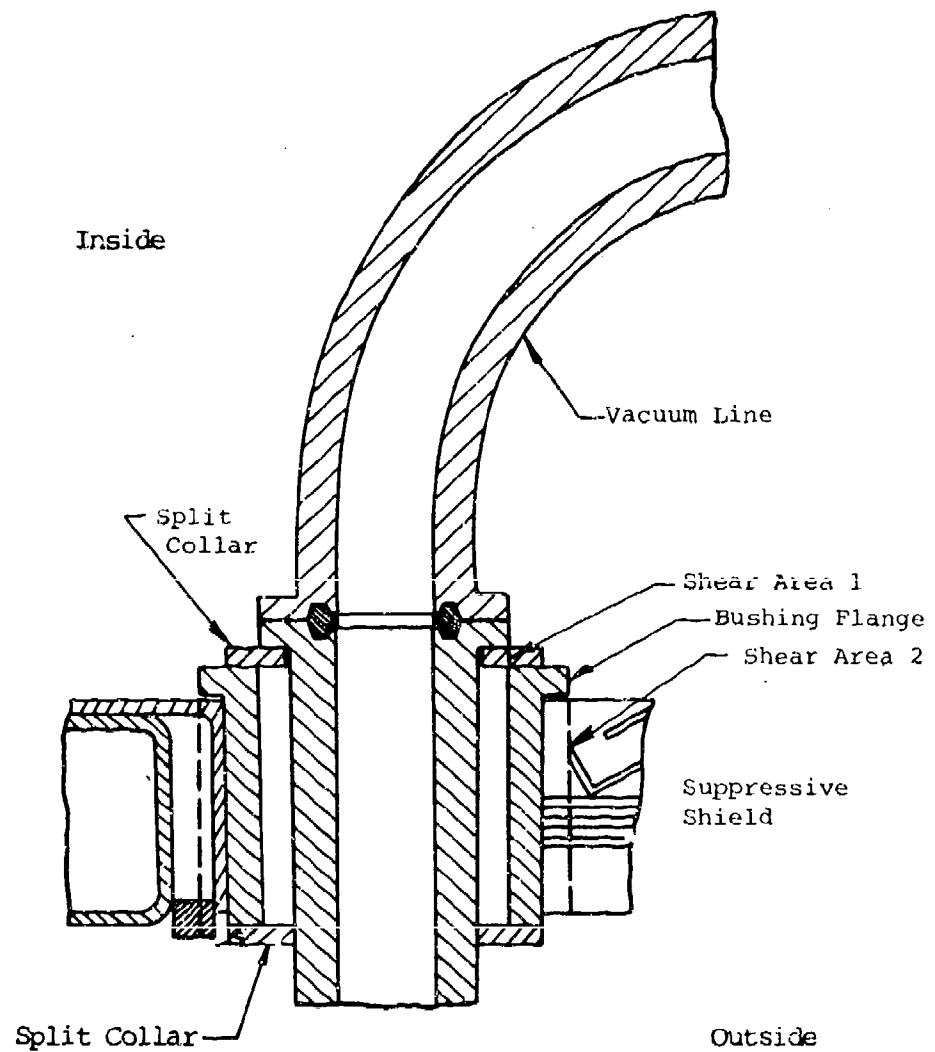


Figure 6-8. Typical Vacuum Line - Suppressive Shield Interface

(2) External Disposal Line Shield

In order to adopt a conservative posture in the analysis, it is assumed that the disposal line does not offer any restraint to the airblast, i.e., the disposal line shield alone must contain the airblast. The dynamic response of the shield tube to the impulsive loading will be affected by the natural period of vibration of the tubing. If the duration of the load is greater than about 5 times the natural period, the load may be considered a dynamically applied long duration load with a dynamic load factor of 2. However, if the duration of the impulse is much less than the natural period of the structure, the load can be considered a pure impulse and the effective stresses and deflections will be increased by a dynamic load factor of less than 2.

The natural period of vibration of the shield tube for internal pressure loading can be obtained from Eq. 5-23 for the natural frequency of a steel hoop.

$$T_N = 2\pi \sqrt{\frac{mR^2}{Et}}$$

where

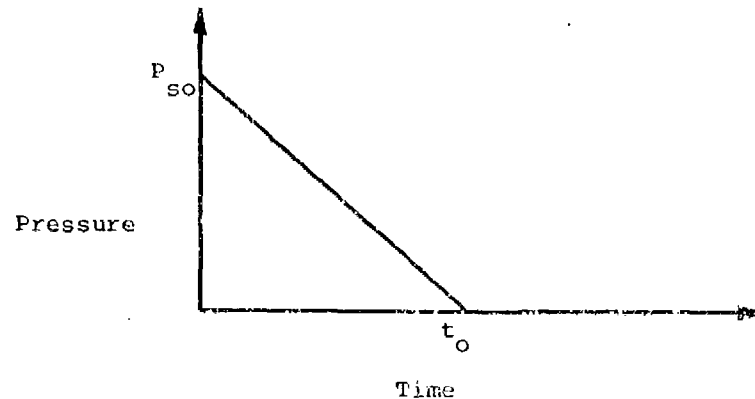
R = average radius, inches

E = modulus of elasticity, psi

t = wall thickness, inches

m = mass per unit surface area of cylinder, lb-sec²/in³

Assume that the impulse load from the air-blast pressure is due to incident overpressure and is triangular as shown below.



From Fig. 3-3, find the peak overpressure, P_{so} , and impulse, i_s , at a scaled distance

$$Z = R/W^{1/3}$$

Select R as the distance to a point just outside of the suppressive shield; W is the TNT equivalent charge weight of the detonating munition.

The positive duration given in Fig. 3-3 is the actual duration of the blast wave and represents an exponential-type decay from the peak pressure. This duration cannot be used in the simplified methods of analysis presented in this chapter. An equivalent duration which conserves the total impulse can be obtained from

$$t_o = \frac{2i_s}{P_{so}} \quad (6-4)$$

Compute the ratio t_o/T_N and, depending on the value of this ratio, use Eq. 5-47, pg. 5-55, to determine the required maximum unit resistance r_m of the shield tube for $\mu = 1$ (elastic case). Then, calculate the tensile stress in the disposal line shield from

$$\sigma = r_m R_i / t \quad (6-5)$$

where R_i is the interior radius and t is the thickness of the disposal line shield.

If σ is less than the dynamic yield stress of the material, no further analysis is necessary, because the material remains elastic. In the case of aluminum tubing, there is no increase in yield strength for dynamic loads, i.e., the dynamic yield stress is equal to the static yield stress. If $\sigma > f_{dy}$, the plastic response of the disposal line shield must be examined.

Using the equation for stress in a thin walled tube and the dynamic yield stress of the material, compute the maximum resistance.

$$r_m = f_{dy} t / R_i \quad (6-6)$$

Using this r_m and P_{so} and Eq. 5-47, compute a ductility ratio μ .

For a conservative design, the calculated stress should be less than the yield stress of the material ($\sigma < f_{dy}$). However, the tube is satisfactory if the stress is less than the ultimate stress of the material and if

$$\mu = \frac{X_m}{X_e} \leq 6.0$$

b. Response to Airborne Dust Explosion

Detailed data concerning dust explosions for many materials are presented in Ref. 6-5. A portion of the

data is presented in Table 6-1. As in the preceding discussion, a conservative approach is taken which assumes that the disposal line shield must withstand the full force of an airborne dust explosion.

The response of the disposal line shield is dependent upon the peak pressure, the ratio of rise time to natural period of the structure and the ratio of the load pulse duration to the natural period of the structure. The preceding paragraph considers a shock wave impulse loading caused by explosion of a munition at the end of the disposal line and propagating through it. In contrast, the load imposed by an airborne dust explosion in the line is a radial pressure load increasing from time zero. Table 6-1 summarizes peak pressures and rate of pressure increase for various types of explosives and a range of dust concentration levels characteristic of disposal lines. If it is assumed that the load increases linearly as a function of time and that the rate of pressure decay from peak is much slower than the rate of increase, Fig. 6-9 may be used to determine the maximum response or required maximum resistance of the disposal line shield.

The loading pulse rise time is

$$t_r = \frac{P_{ro}}{r_p} \quad (6-7)$$

where

P_{ro} = peak overpressure from the explosion, psi

r_p = rate of pressure rise, psi/sec

The first step is to compute the natural period of the disposal line shield using Eq. 5-23. Next, calculate r_m from Eq. 6-6 and the ratio r_m/P_{ro} (equivalent to R_m/B on Fig. 6-9). For this ratio and the t_r/T_N ratio, find the ductility ratio from Fig. 6-9. If designing for a given maximum response, find the required maximum resistance from the ratio R_m/B in Fig. 6-9 and the required line thickness from Eq. 6-6.

Table 6-1
PRESSURE AND PRESSURE INCREASE RATES FOR AIRBORNE DUST EXPLOSIONS (Ref. 6-5)

Explosive Dust	Minimum Explosive Concentration (oz/cu in)	0.20 oz/cu ft		0.50 oz/cu ft		1.00 oz/cu ft	
		Maximum Pressure (psi)	Maximum Rate of Pressure Rise (psi/sec)	Maximum Pressure (psi)	Maximum Rate of Pressure Rise (psi/sec)	Maximum Pressure (psi)	Maximum Rate of Pressure Rise (psi/sec)
Ammonium picrate (comp D)	0.200			74	2,400	141	8,800
Dinitrobenzamide	0.040	73	5,000	94	6,500	118	6,000
Dinitrobenzoic acid	0.050	59	2,300	92	4,300	111	4,100
Nitrostarch	0.070	35	1,600	116	10,000		
Trinitrotoluene (TNT)	0.070	32	700	63	2,100		

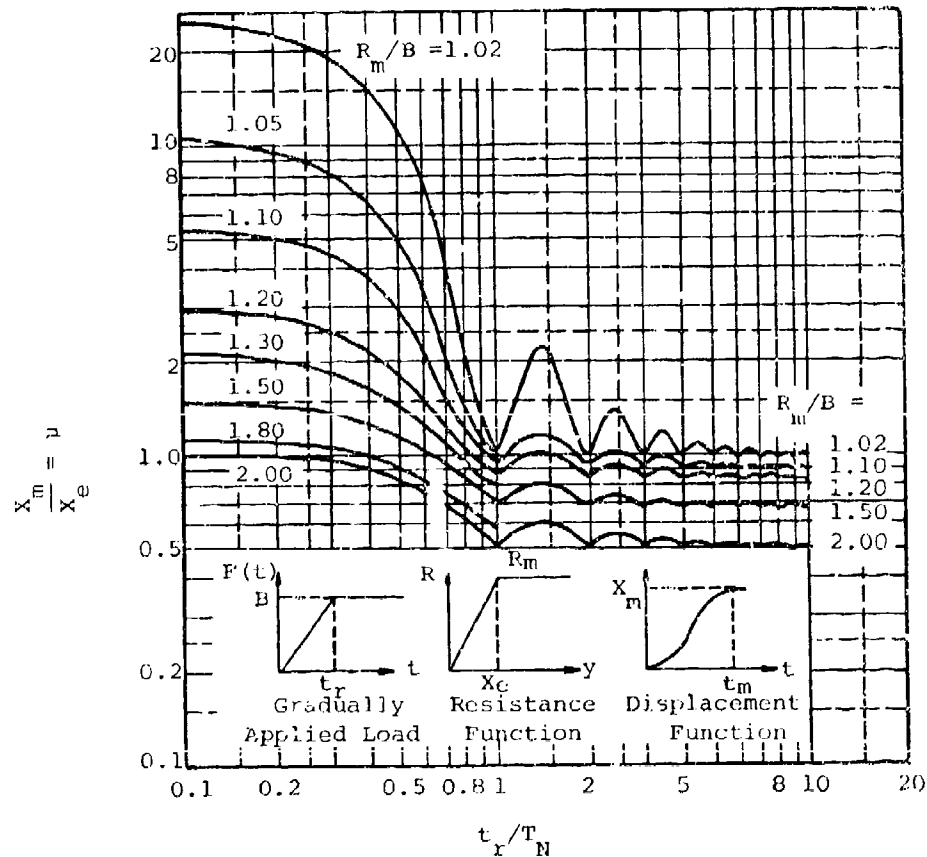


Figure 6-9. Maximum Response of Elasto-Plastic One-Degree Systems (undamped) Due to Constant Force With Finite Rise Time (Ref. 6-6)

Because the disposal line shield is outside of the suppressive shield, safety considerations indicate that the stress should not exceed the yield stress. However, a design in which the ratio $\mu = X_m/X_e \leq 6.0$ is acceptable.

c. Response to Dust Sediment Explosion

A third hazard that must be considered is the possibility of an explosion of dust which has collected on the bottom of the disposal line. The amount of dust sediment that might accumulate in the line depends upon the velocity of air through the line, the size of the dust particles, the shape of the line, etc. Although an accurate analytical determination of the amount of sediment is difficult, an estimate can be made on the basis of inspection of similar facilities and the disposal line cross section shown in Fig. 6-10.

For purposes of analysis, it is assumed that the density of the explosive dust is 0.8 gm/cm^3 and that the sediment behaves like a solid spherical charge of TNT. This is a conservative approach because the dust probably will not be compressed and the airblast parameters computed for a solid charge represent the maximum obtainable. Because the dust sediment explosion is treated as a detonation of solid explosive rather than a relatively mild explosion of airborne dust, the analytical technique proposed is similar to that of paragraph 6.2.3.a. For each inch of line length, the airblast energy imparted to the disposal line shield is equated to the strain energy which can be stored in the shield in order to find the maximum radial deflection.

Using the procedure outlined in Chapter 3, calculate

- The scaled distance $z = R/W^{1/3}$ for the radius of the disposal line shield (R) and the weight of explosive per inch of line (W)

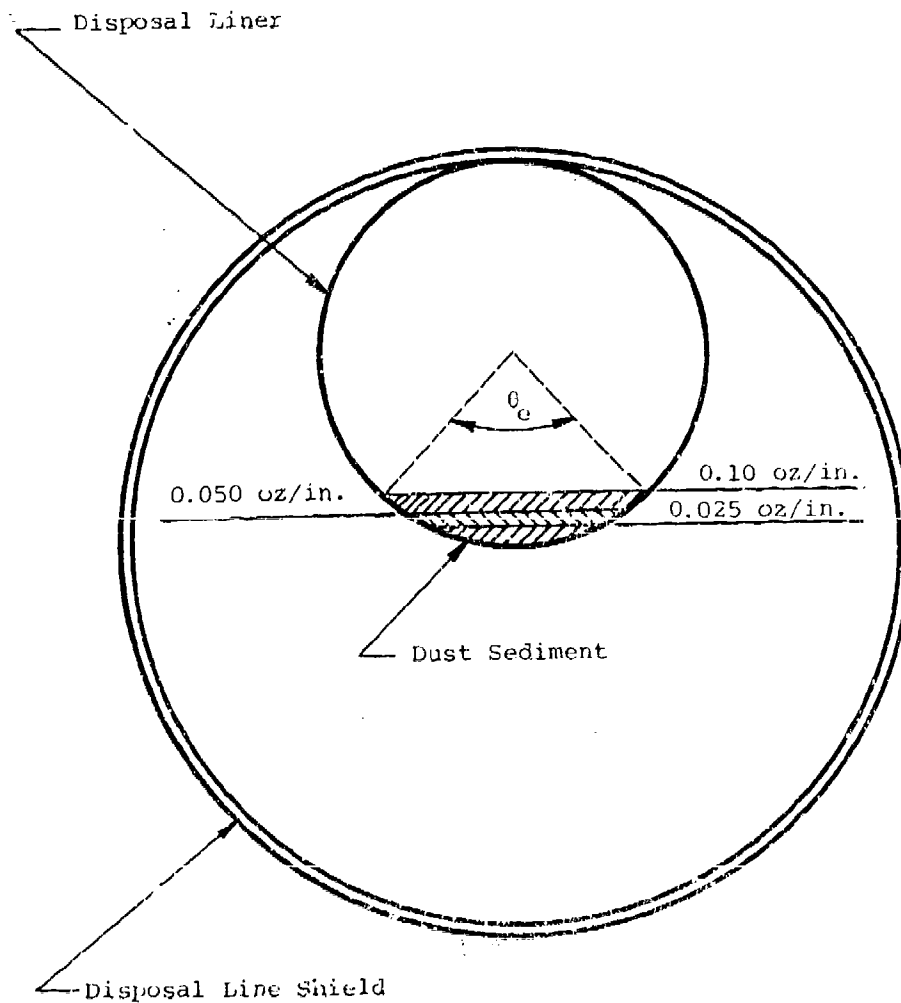


Figure 6-10. Estimate of Dust Sediment on Bottom of Disposal Liner - Shielded Disposal Line Concept

- The pulse duration $t_o = 2i_r/P_r$, where i_r and P_r are the peak reflected impulse and pressure, respectively, from Fig. 3-6.

Once the internal airblast parameters have been established, the design or analysis of the disposal line shield proceeds as described in paragraph 6.3.3.a.(2).

For a safe design, the calculated stress should be less than the yield stress of the material, i.e., $\sigma < f_{dy}$. However, the structure is acceptable if the stress is less than the ultimate stress of the material and if

$$\mu = \frac{X_m}{X_e} \leq 6.0$$

d. Fragment Hazard Analysis

The explosion of dust within the disposal line will propel fragments outward. These fragments must be contained by the disposal line shield. In order to evaluate the fragment hazard, the quantity of metal involved in the process and fragment velocity must be determined.

The weight of metal per unit length of tube subtended by the explosive (see Fig. 6-11) is a function of the depth of the sediment. It can be calculated from

$$W_c = \frac{\rho_m \theta_e}{2} [R_o^2 - R_i^2] \quad (6-8)$$

where

ρ_m = density of tube material, lb/in³

R_o = tube outside radius, inch

R_i = tube inside radius, inch

θ_e = angle which the explosive subtends (see Fig. 6-11), radians.

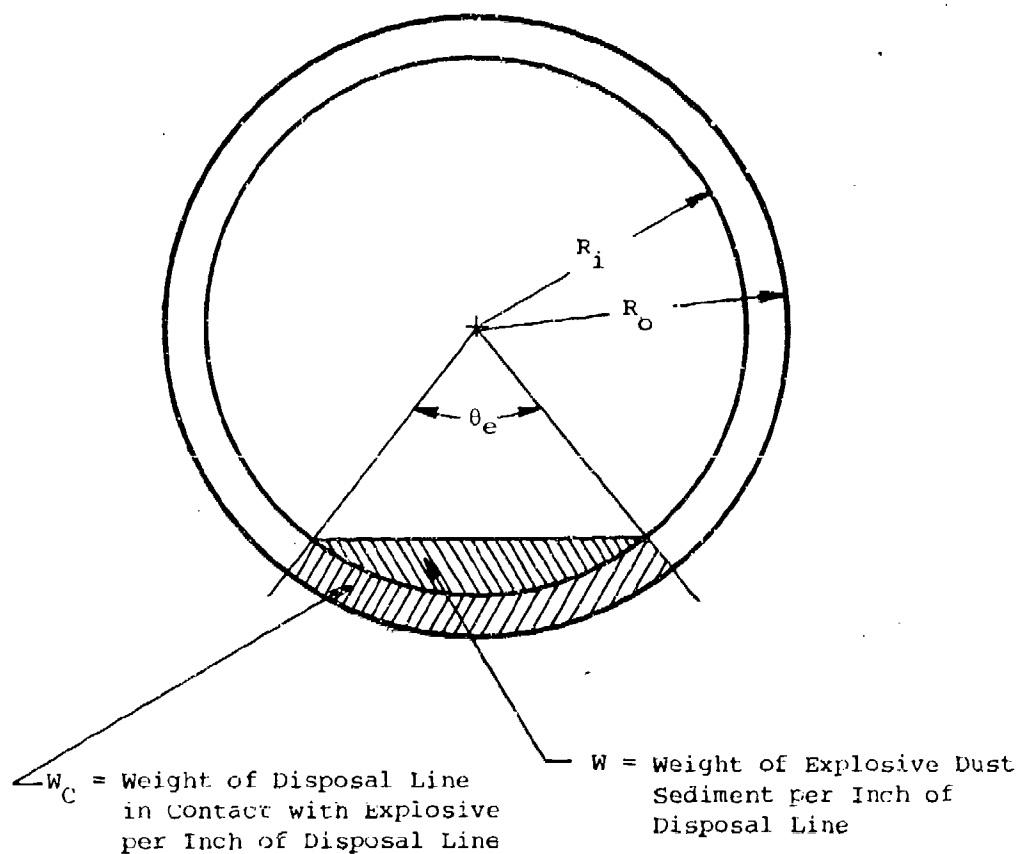


Figure 6-11. Cross Section of Disposal Line With Explosive Dust Sediment

The weight of explosion per unit length is given by

$$W_T = \rho_e \left[\frac{R_i^2 (\theta_e - \sin \theta_e)}{2} \right] \quad (6-9)$$

where

W_T = weight of explosive per unit length of tube, oz/in

ρ_e = density of explosive, oz/in³

The partially filled tube does not meet the criteria for the Gurney cylindrical charge equation for calculating fragment speed since explosive products can flow freely into the unfilled region of the tube during the metal acceleration process. An alternative and more appropriate approach would be to treat the process as an approximation to an open-faced sandwich. In that case, the fragment speed is given by

$$v_o = \sqrt{2E'} \sqrt{\frac{3}{1 + (5W_c/W_T) + 4(W_c/W_T)^2}} \quad (6-10)$$

Fragment velocity predictions were made for the three cases shown in Fig. 6-10. The following constants were assumed

$$R_i = 0.94 \text{ inch}$$

$$R_o = 1.00 \text{ inch}$$

$$\rho_e = 0.462 \text{ oz/in}^3$$

$$\sqrt{2E'} = 8900 \text{ ft/sec}$$

The results of the calculations are

W_i oz/in	W_c oz/in	W_c/W_i —	v_o ft/sec
0.025	0.0853	3.41	1910
0.050	0.1083	2.17	2770
0.100	0.1384	1.38	3880

The minimum fragment velocity required to penetrate a known thickness of material is

$$v_{\ell} = \frac{A_o A_p^m (t_t \sec \theta)^n}{\sqrt{W_s}} \quad (6-11)$$

where

A_o = constant related to material being penetrated,
see Table 3-5

A_p = presented area of fragment in the direction of
penetration, in²

t_t = thickness of material being penetrated, inch

θ = angle of impact relative to the normal to the
surface of impact

W_s = weight of fragment, lb

m, n = exponents related to material being penetrated,
see Table 3-5

Rearranging equation 6-11, the minimum thickness of metal needed to stop a compact fragment impacting normal to the disposal line shield becomes

$$t_t = \left[\frac{v_{\ell} \sqrt{W_s}}{A_o A_p^m} \right]^{1/n} \quad (6-12)$$

The problem which arises in using this method of analysis is the prediction or assumption of fragment properties and the establishment of the various constants and exponents. The constants and exponents presented in Table 3-5 are applicable to the case of compact steel fragments impacting upon mild steel plate. The absence of data for aluminum fragments impacting upon aluminum plate requires the assumption that the constants and exponents of Table 3-5 are applicable to this case also.

This handbook does not include methods for predicting the dimensions of fragments for use in Eqs. 6-11 and 6-12. In the absence of better guidance, it is suggested that the fragments be assumed square in shape with a thickness equal to the thickness, t , of the vacuum line. The dimensions of the square can be taken equal to that portion of the vacuum line circumference in contact with the explosive, i.e.,

$$L = R_i \theta_e \quad (6-13)$$

The weight of the fragment is then given by

$$W_s = \rho_m t L^2 \quad (6-14)$$

where all terms are as previously defined.

It is suggested that the presented area be taken equal to

$$A_p = L^2 \quad (6-15)$$

If the thickness of metal required to stop a fragment computed from Eq. 6-12 is less than that of the vacuum line shield, the shield is satisfactory. If the thickness computed from Eq. 6-12 is larger, a thicker shield is required.

There is some question as to whether a detonation could be propagated in the sediment quantities evaluated above. The maximum thicknesses of explosive in each of the three cases considered are 0.098, 0.154 and 0.248 inch. These are probably less than the critical charge thickness required to sustain the propagation of a detonation under the reduced charge density condition.

6.3.4 Location of Vacuum Line

Depending upon the details of the operation requiring a vacuum line, the location of the penetration could be either in the side walls or ceiling of the shield. The vacuum

line penetration is designed to be located in the corner of the Shield Groups 4, 5, and 81-mm adjacent to a beam and column, two beams, or a column and the base of the shield. For the Group 3 shield, the vacuum line penetration is designed to pass through the wall at the web of the I-beam. The vacuum line could also penetrate the concrete foundation or the concrete roof in the Group 3 shield, if required for a special application. Procedures defined in Ref. 6-4 should be used in these situations. Figures 6-3 and 6-4 show typical installations of the vacuum line.

6.4 ENVIRONMENT CONDITIONING PENETRATION

6.4.1 Design Concept and Rationale

Certain hazardous operations require special control of air temperature and humidity and require periodic air changes inside a suppressive shield. Since operating personnel are not present inside a shield during operation, it is not necessary to meet the air change requirements of OSHA for occupied spaces.

The air can be introduced inside the suppressive shield in several ways. The method selected will depend upon the air conditioning requirements for a particular operation. It may be sufficient to use conditioned air around the outside of the shield and have it leak through to the inside via the spaces around shield penetrations such as personnel and product doors. Where the air flow requirements cannot be satisfied in this manner, inlet ducts of sufficient thickness to withstand the airblast loading and configured to prevent fragment escape are required. The equipment which supplies air to the shield must be located so that airblast effects will not endanger personnel in the surrounding area. The inlet duct penetration design is the same as the vacuum line penetration. Design procedures provided in paragraph 6.3 should be applied.

Air is removed from the suppressive shield by a duct penetrating the shield roof. This duct or stack must extend beyond the roof of the building housing the suppressive shield and be of sufficient height to prevent excessive airblast pressures from acting on the building roof. This concept is shown in Fig. 6-12. In operations which generate explosive dust, filters should be located in the stack. Operations having a waste disposal (vacuum line) system may not require an alternate method for exhausting air, provided sufficient air is exhausted from the shield through the disposal system.

6.4.2 Design Procedure

The design procedure for the inlet duct penetration has been presented previously in paragraph 6.3. A design procedure for the exit duct/stack is presented below.

The first step is to determine the required number of air changes per unit of time for the operation being shielded. In the absence of other specific requirements, assume that two complete air changes per hour will be provided. This is consistent with industrial practice for enclosures which are not occupied during operations.

The exhaust area required is a function of the air flow rate and velocity

$$A_{ex} = \frac{Q}{v_a}$$

where

$$\begin{aligned} Q &= \text{air flow rate, ft}^3/\text{min} \\ &= V \times N_a \end{aligned}$$

and

$$\begin{aligned} V &= \text{shield internal volume, ft}^3 \\ N_a &= \text{number of air changes per minute} \\ v_a &= \text{air flow velocity, ft/min} \end{aligned}$$

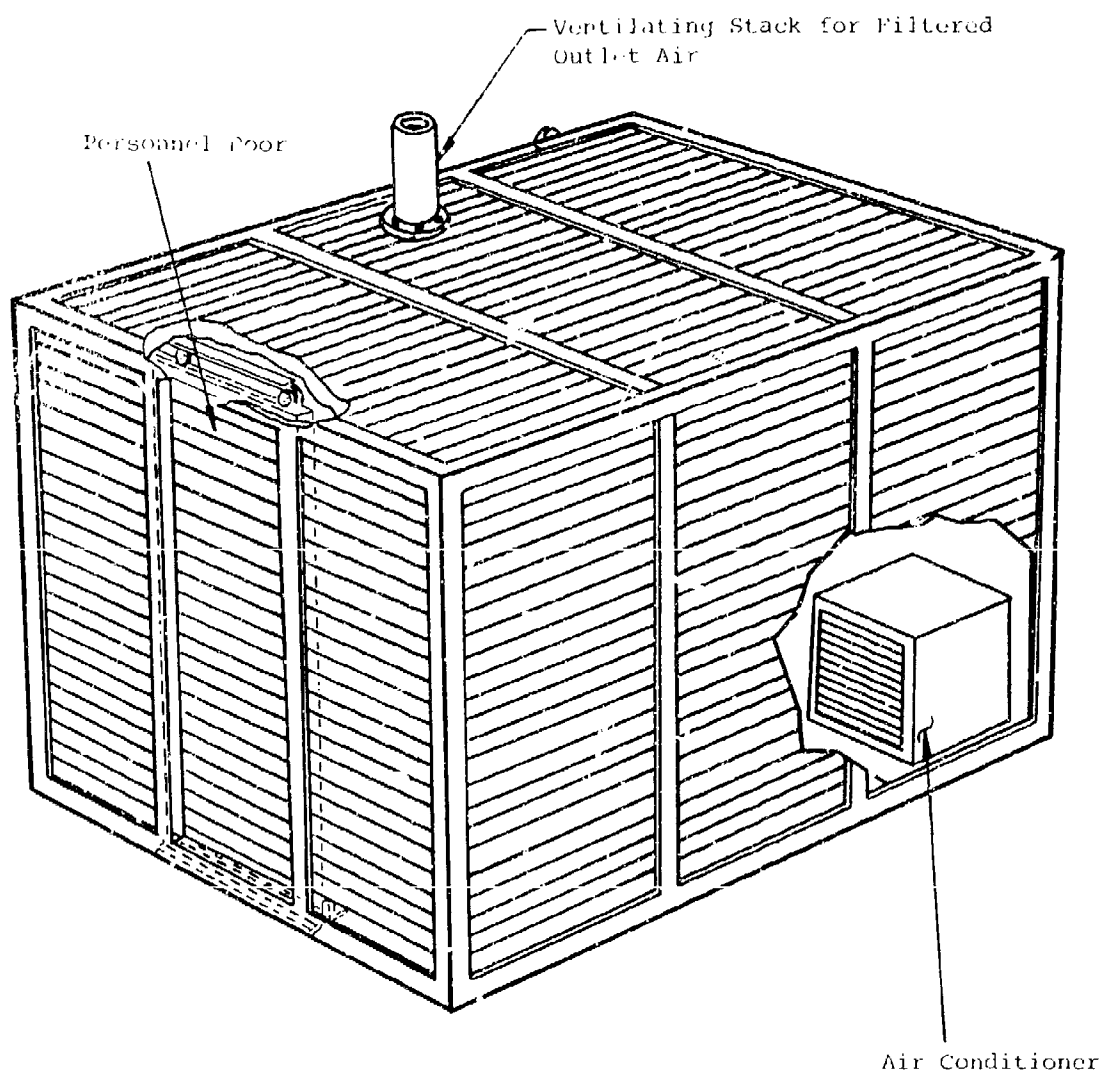


Figure 6-12. Typical Environmental Conditioning Penetration

There are no experimental data pertaining to the airblast pressure field outside a stack emanating from the roof of a suppressive structure. Tests have been performed and a predictive model developed for four walled cubicles with a square vent hole in the roof (Ref. 6-7). By making several assumptions, the model shown in Fig. 6-13 can be applied to an exhaust stack. It is assumed that no pressure decay occurs in the stack and that the pressure decay outside the stack is the same as that occurring outside the four walled vented cubicle of Fig. 6-13. The incident pressure outside the stack is determined from

$$P_s = 290 \left[\frac{A_{ex}}{V^{2/3}} \right]^{0.401} \left[\frac{W^{1/3}}{R} \right]^{1.496} \quad (6-16)$$

where

R = horizontal distance from stack exit to point of interest, ft

W = charge weight, lb

Equation 6-16 is a curve fit to data and is applicable to the conditions within the range of test parameters, i.e.,

$$\begin{aligned} 0.063 &\leq W/V &\leq 0.375 \text{ lb/ft}^3 \\ 0.0198 &\leq A/V^{2/3} &\leq 1.000 \\ 1.59 &\leq R/W^{1/3} &\leq 63.0 \text{ ft/lb}^{1/3} \end{aligned}$$

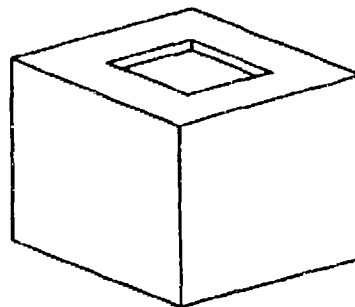


Figure 6-13. Cubicle with Partial Roof

Equation 6-16 was used to develop the design curves shown in Fig. 6-14. The dashed lines on Fig. 6-14 represent approximately the above limits of experimental data. These curves can be used to size a vent to limit peak pressure at a given distance or to predict what the peak pressure will be for a given size vent.

It is important to note that Eq. 6-16 and Fig. 6-14 are for predicting the pressures outside a cubicle on a horizontal plane located at the elevation of the vent area. If the horizontal plane of interest lies below the elevation of the vent area, pressures at points located within several cubicle heights are less than those given by Fig. 6-14 and the differences increase with W/V . Reference 6-7 discusses a semi-empirical method for modifying the pressures obtained from Eq. 6-16 and Fig. 6-14 when the planes of interest and vent area are not at the same elevation. The procedure was proposed for open-top, four-wall cubicles and its application to vent openings is uncertain. It is suggested that the procedure be used if the point of interest is closer than 3 times the difference in elevation between the vent opening and the plane of interest. An alternative is to take R equal to the radial distance from the vent opening to the point of interest.

Stresses in the stack can be obtained by first predicting the peak overpressure and duration at a point just outside of the suppressive shield wall or roof. Figure 3-3 is applicable. Next compute the natural period of vibration of the stack from Eq. 5-23 and follow the procedure described in paragraph 6.3.3.a.(2) to obtain maximum stresses and displacements.

6.5 ACCESS PENETRATIONS

6.5.1 Requirements

In the munition plant environment, suppressive shields are designed to protect category III or IV hazardous operations as defined in Table 1-1, Pg. 1-7. Remote operation is required,

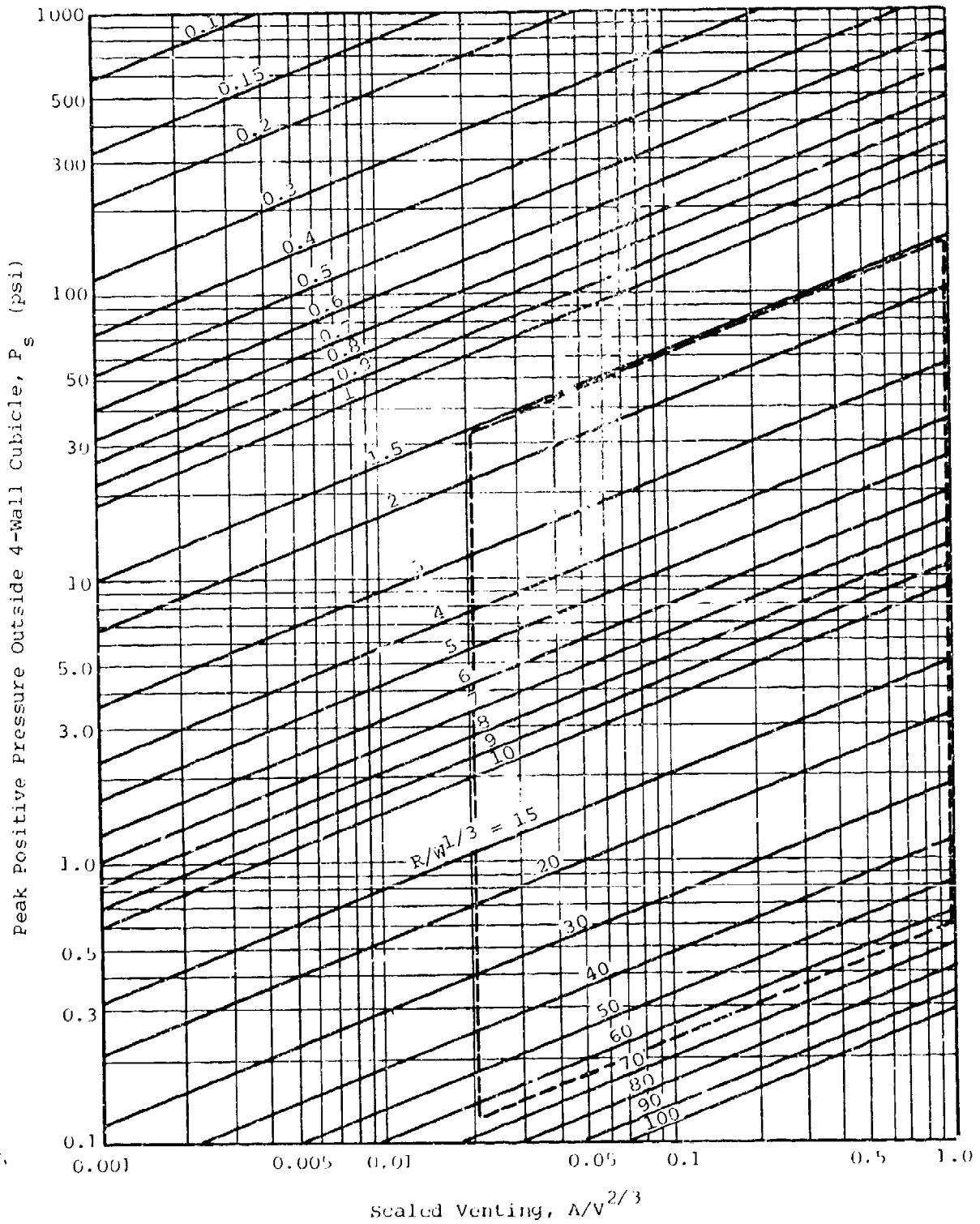


Figure 6-14. Design Chart for Vent Area Required to Limit Pressures at Any Range Outside a 4-Wall Cubicle

and personnel will not be inside the shield during operation. However, access to the equipment must be provided to allow for maintenance, repair, and inspection as required. Personnel doors which satisfy the above requirements have been designed for each of the safety approved shields. These doors also provide large openings to enable most equipment to be installed or removed in realistically large subassemblies. Exits from these shields have not been designed in accordance with Ref. 6-8, since no personnel are in the shield during the operation. The door remains open for conditions requiring personnel access.

Access is also required for munition components, explosives and assembled munitions to pass through the suppressive shield. In the case of conveyor transporting systems, consideration must be given to the proper pass-through of the conveyor. Requirements for this type of access depend on the configuration of the munition product, transporting pallets and conveyors as well as production rates and other factors unique to each operation. For these reasons, definition of specific design requirements is not possible. Design of a rotary type door which allows pass-through of projectiles is discussed in paragraph 6.5.4.

6.5.2 Safety Considerations

All access doors are designed to provide the same level of protection as the suppressive shield, i.e., attenuation of airblast pressure and fireball and containment of all fragments.

Safety considerations require an interlock system on personnel access doors to prevent a hazardous operation from being conducted with a door open. The door should be fitted with two limit switches such that both the switches are activated when the door is closed. Moreover, the interlock circuit should be designed to indicate the closure of both switches sequentially within a finite time interval of

each other. This feature prevents tampering of the type where one switch is taped closed and the other can be used to simulate door opening and closing by manual operation.

6.5.3 Personnel Door

a. Design Concepts

Three different types of doors have been developed for use in suppressive shields: sliding, hinged, and double leaf. The hinged door was designed to swing inward. This undesirable feature reduces the useable space inside the shield. A sliding door is preferred for personnel access to munition operations. Figure 6-15 illustrates a typical sliding door. This type door is used with the Group 4, 5 and Milan 81-mm shields. The sliding door consists of an entire shield panel suspended from a monorail system. The panel is inside the shield and is not rigidly attached to the column members. Special consideration was given to the air gap between the door panel and the column to assure that excessive pressure leakage would not occur and that fragments could not pass through the gap.

The cylindrical Group 3 shield contains a two-leaf door, hinged at each side. It swings inward as shown in Fig. A-3. The door is curved to match the shield wall contour and is fabricated from S5 x 10 I-beams. Pressure loading restraint is provided by the door bearing on the external support rings of the shield at the top and bottom of the door. An external latch provides restraint during rebound of the door.

b. Design Procedure

(1) Sliding Door

The shield panel in the location selected for the sliding door is replaced by the door panel. The door panel is of the same construction as the other shield panels;

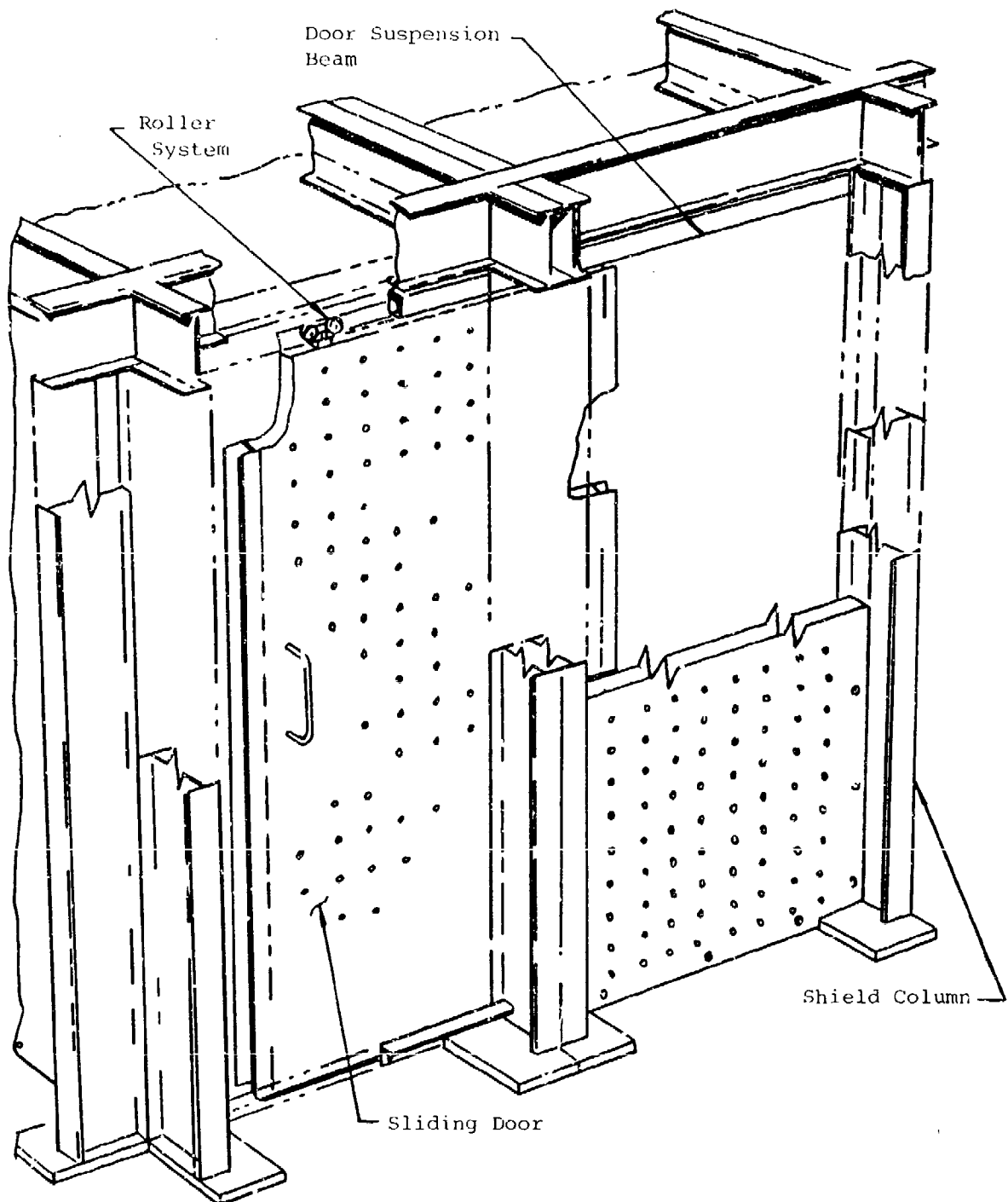


Figure 6-15. Sliding Personnel Door

therefore, it provides the same airblast and fireball attenuation and fragment containment capability. A commercial track and trolley system is selected based on the door weight. Standard assembly procedures are followed for installation of the track and trolley system.

(2) Leaf Door

The beams comprising the leaf door are designed as simply supported elements spanning the vertical dimension of the door. They are heavier sections than those in the Group 3 shield wall because of the single layer and loss of continuity at the supports.

6.5.4 Product Door

a. Design Concept

Only one type of product door has been developed conceptually for use in suppressive shields. It is the rotary, three lobed configuration shown in Fig. 6-16. The design procedure for this door is described to illustrate the type of analysis required. It can be used as a guide for analysis of similar alternate design concepts for product doors.

b. Safety Considerations

The airblast will most severely load the rotating product door when the munition opening is coincident with the pocket in the rotary door. A nonoverriding clutch prevents the door from counterrotating. The angular impulsive load is

$$T_i = i_r A_d r_d \quad (6-17)$$

where

i_r = reflected impulse, psi-sec

A_d = door area, in²

r_d = radius from center of impulse load to center of door rotation, inches

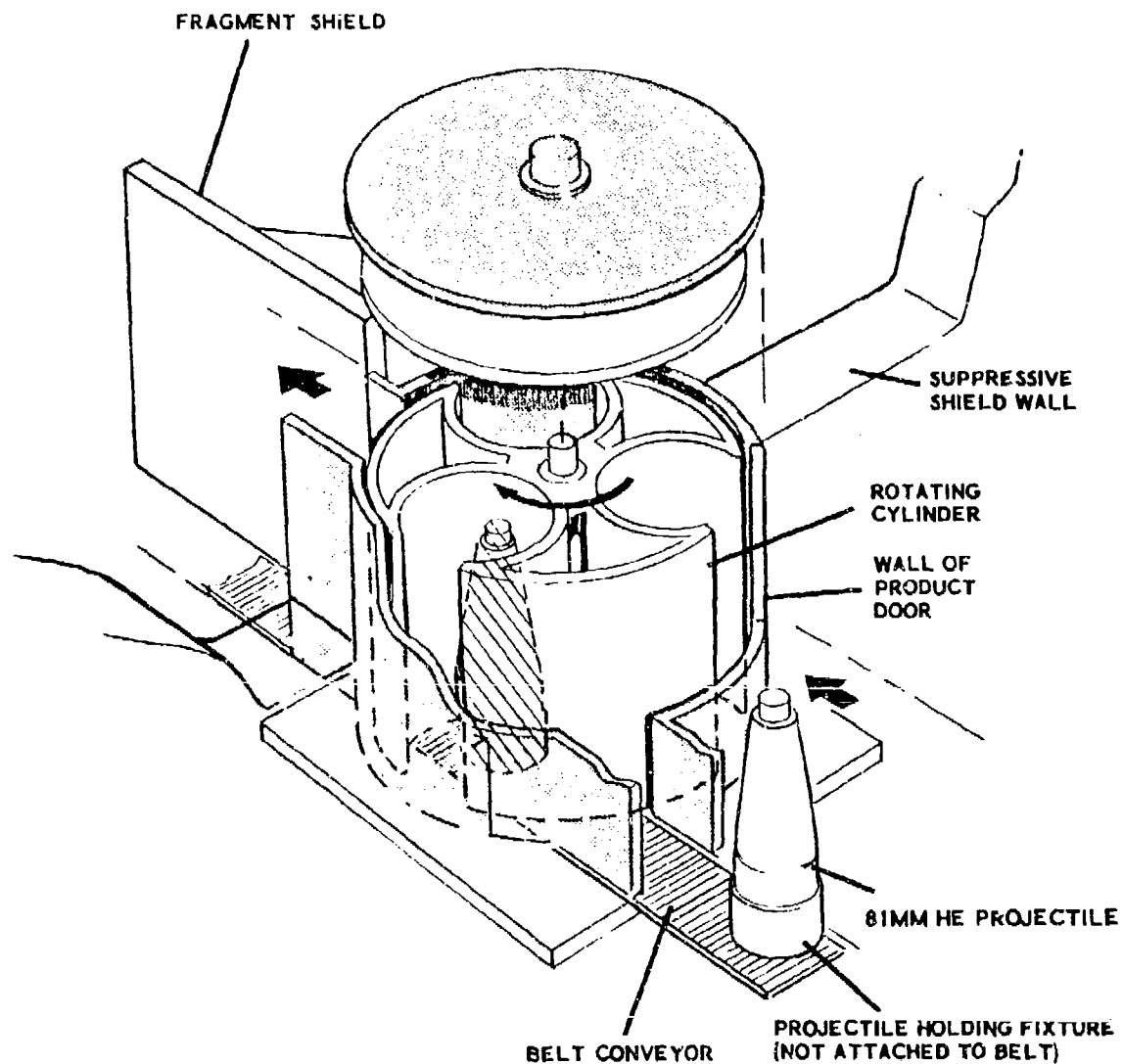


Figure 6-16. Rotating Product Door

Assuming the product door to be initially at rest, the rotational velocity imparted to the door is given by (Ref. 6-9)

$$\omega = \frac{T_i}{I_m} \quad (6-18)$$

where

ω = angular velocity, rad/sec

I_m = mass moment of inertia of door about shaft axis,
lb-sec²-inch

The kinetic energy imparted to the door is given by

$$K.E. = \frac{I_m \omega^2}{2} = \frac{T_i^2}{2I_m} \quad (6-19)$$

The strain energy absorbed by a circular shaft is given by

$$U_s = \frac{\pi L_s}{4G} (r_s \tau_s)^2 \quad (6-20)$$

where

L_s = length of shaft, inches

G = shear modulus of shaft material, psi

r_s = radius of shaft, inches

τ_s = maximum shear stress in shaft, psi

Equating the kinetic energy of the rotating door to the strain energy in the shaft and solving for the shear stress yields

$$\tau_s = \frac{T_i}{r_s} \sqrt{\frac{2G}{\pi I_m L_s}} \quad (6-21)$$

where

I_m = mass moment of inertia of door, lb-sec²-inch

The computed shear stress in the shaft must be less than the dynamic shear stress of the shaft material, i.e.,

$$\tau_s < 0.55f_{dy}$$

6.6 SHIELD LINERS

6.6.1 Functional Requirements

The vented or porous nature of the suppressive shield wall creates a potential for explosive and/or flammable dust to filter into and accumulate within the interior of the shield wall. Removal of such accumulations can be extremely difficult. The dust could originate from an operation being performed inside the shield or from an exterior source. A means for sealing both the interior and exterior of the vented panels must be provided. One way to prevent the accumulation of dust in the shield wall is to provide liners which cover the inner and outer surfaces of the vented panels. Special attention should be given to the joints of the inner and outer liners to assure that the joints will not provide a route for explosive dust entry into the shield wall structure and that the joints themselves will not create an additional location for the accumulation of explosive dusts.

6.6.2 Design Considerations

The addition of liners to a suppressive shield could have an adverse effect on the performance of shields of certain groups. When shielding hazardous operations which involve pyrotechnic materials or propellants, the ventilating properties of the shield must be designed to minimize too rapid a pressure buildup within the structure. A liner for such applications must break or burn away so that ventilating properties are retained.

For explosive materials, the ventilation requirements are different. If the structure is designed to withstand

the combined impulsive and quasi-static pressure loads, fragment impact and thermal effects, a continuous metal liner which remains in place during the incident is acceptable. Such continuous metal liners must not seal the shield sufficiently to prevent the products of combustion from venting, causing the shield to become a pressure vessel. Some suppressive shields are not designed to withstand the loads they would experience with a continuous metal liner. Liners for these shields must be designed so that the initial pressure blows out the liner to provide the venting properties designed into the shield. In all designs with liners which break away, care must be taken that hazardous secondary fragments are not produced outside the shield by pieces of the liner.

6.6.3 Recommended Configurations

a. Rigid Liners

Explosive materials can be confined within a suppressive shield with a rigid liner that does not allow venting of the airblast pressure only if the structure is designed to take the loads. These liners may be attached expeditiously with sheet metal screws to inside surfaces only.

The final installation of metal liners, such as in the Group 3 shield, should include a soft gasket material or caulking compound to seal the liner-panel interface and to prevent accumulation of explosive dust at inaccessible locations. Typical installation details are shown in Fig. 6-17.

b. Frangible Liners

A frangible plastic liner can be used on shields containing explosive materials without affecting their venting characteristics. A number of plastic film materials have been investigated as possible candidates for frangible internal liners. The material selected is Velostat plastic film. This material exhibits the following properties.

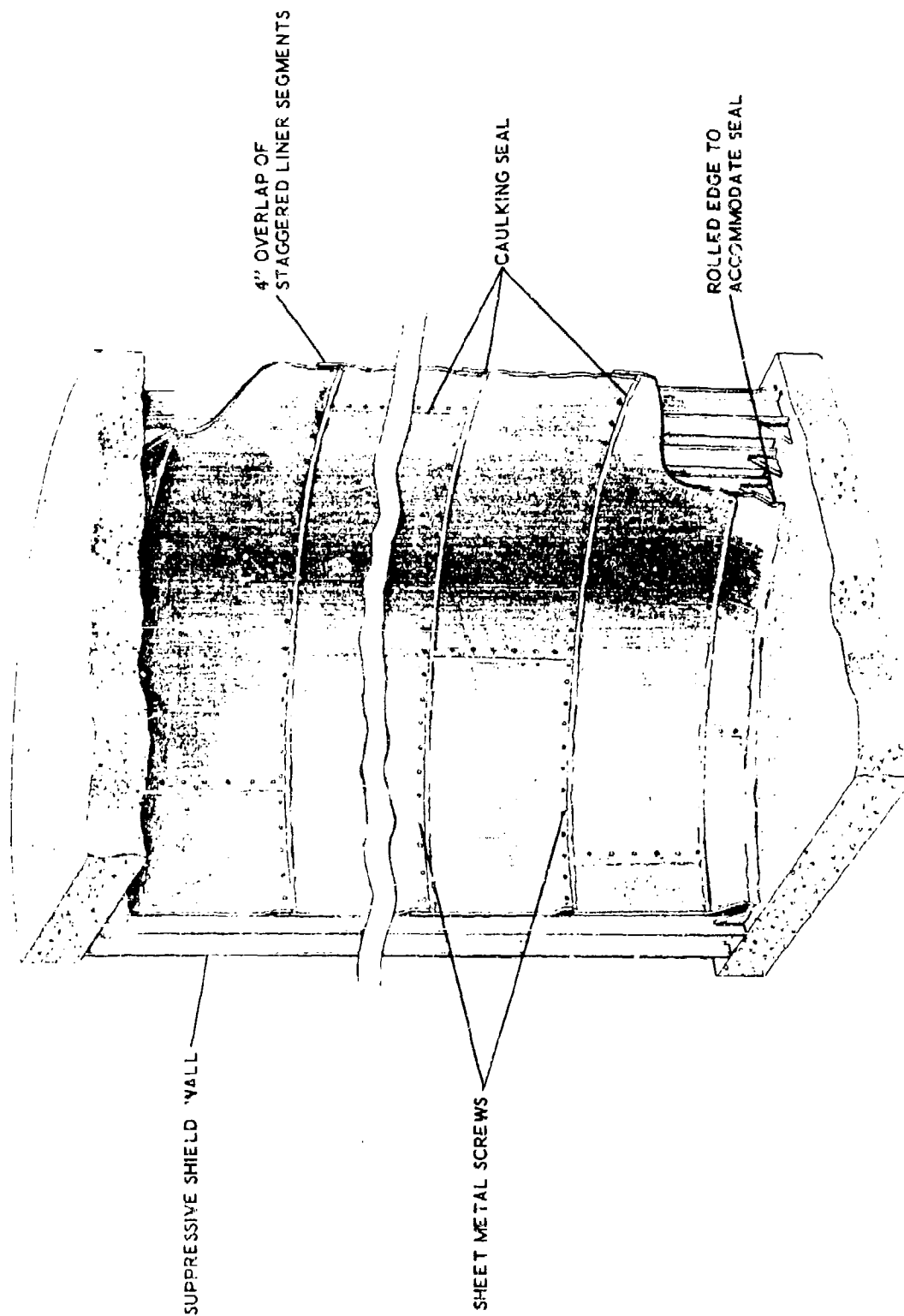


Figure 6-17. Typical Installation of Sheet Metal Liners

- Conductive
- Abrasive/tear resistant
- Disintegrates rapidly under flame
- Workable

Velostat or equal can be purchased with an adhesive applied to one side to allow easy attachment to the panel surface. Attachment can be accomplished as shown in Fig. 6-18.

Care must be taken to prepare the shield surface when installing adhesive-backed plastic liners so that a good bond is achieved. The material must be attached without wrinkles or gaps through which hazardous material can enter inaccessible regions of the panels.

For pyrotechnic materials, venting is essential to prevent shield damage. Tests indicate that the Group 5 shield requires internal and external liners fabricated from a lightweight material which will disintegrate, decompose, or fracture when a pyrotechnic material reacts in the shield. This will allow the rapidly expanding gases to bleed off as they are produced by the reaction, thus preventing excessive pressure buildup in the structure.

c. Summary

Table 6-2 summarizes the recommended internal and external liner systems for each of the safety approved shields. In all cases, a sealing system has been proposed which will preclude dust accumulation or leakage around the liner. This will also keep the extreme edges of the Velostat material from pulling loose and curling.

The liner material for external application requires the same characteristics as the internal liner material plus the additional requirement of being incapable of producing lethal or damaging fragments. The Velostat material meets all these requirements.

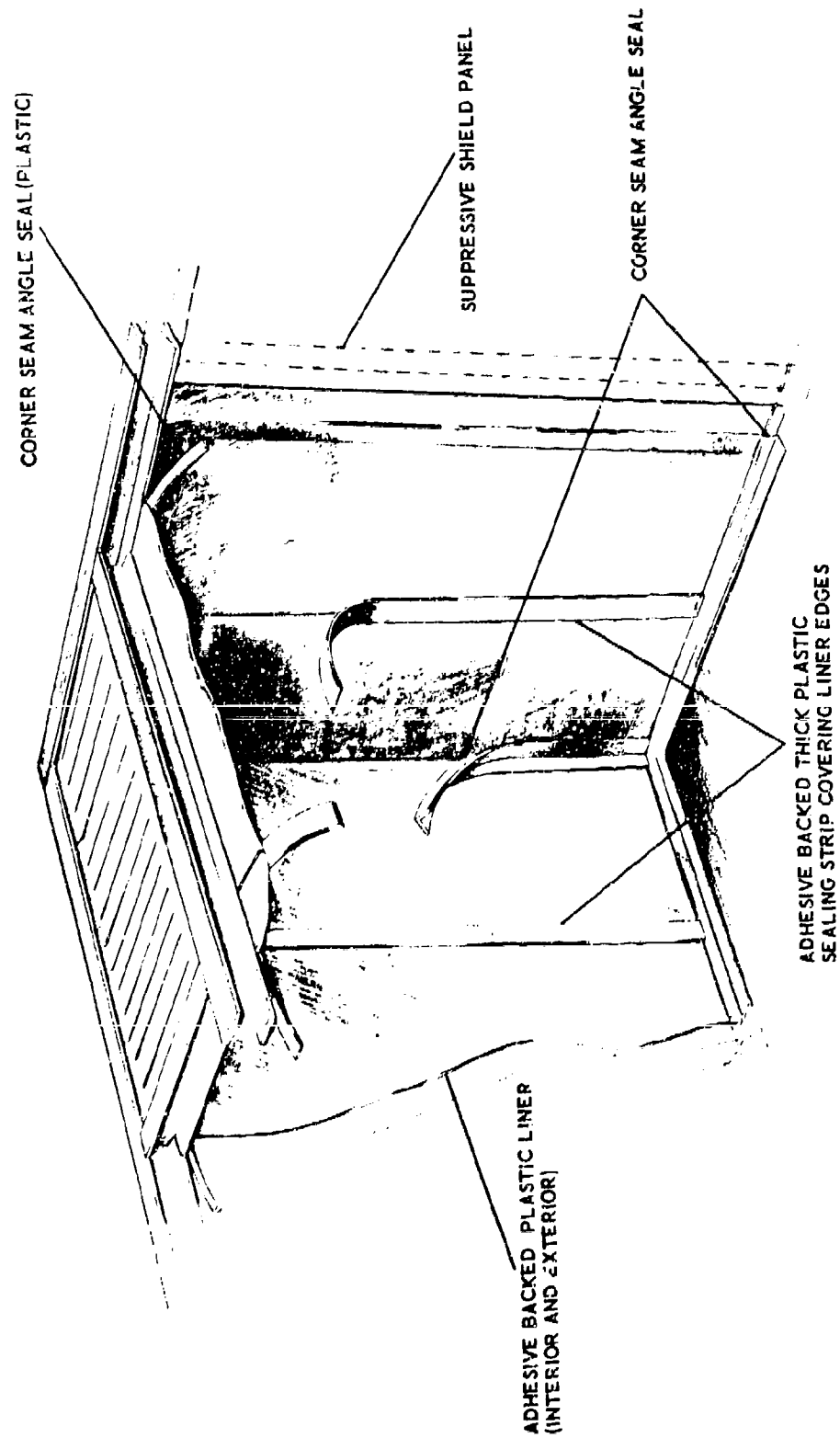


Figure 6-18. Typical Installation of Thin Plastic Liners

Table 6-2
SUMMARY OF PROPOSED LINERS FOR SUPPRESSIVE SHIELDS*

Shield Group	Interior Liner	Exterior Liner	Attachment Method	
			Internal	External
3	Sheet Metal	Velostat	Screws & Gasket	Adhesive & Cemented Plastic Strips
4	Velostat	Velostat	Adhesive & Cemented Plastic Strips	Adhesive & Cemented Plastic Strips
5	Velostat	Velostat	Adhesive & Cemented Plastic Strips	Adhesive & Cemented Plastic Strips
81-mm	Velostat	Velostat	Adhesive & Cemented Plastic Strips	Adhesive & Cemented Plastic Strips

* Velostat may be substituted for by an equivalent liner

6." ILLUSTRATIVE EXAMPLES

6.7.1 Bending in Box Structure Cover Platea. Given

The Group 3 shield has internal dimensions of 11.25 ft in diameter by 10 ft high. A utility penetration protective box attached to the wall of the shield has length, b_c ; width, a_c ; and cover thickness, t_c ; dimensions of 20, 10 and 1 inches, respectively. The side plates are 8 inches high by 1 inch thick. Thicknesses were selected to correspond to the nominal wall thickness of the Group 3 shield. The box structure is fabricated from mild steel which has a modulus of elasticity, E , of 29×10^6 psi and a Poisson's ratio, ν , of 0.33. Its static yield strength is 36,000 psi.

b. Find

The response of the cover plate to an explosion of the proof charge weight of 45.7 lbs of 50-50 Pentolite.

c. Solution

Entries in Table A-3 show that the proof charge is equivalent to 51.6 lb of TNT. The sidewalls are at a scaled range of $1.511 \text{ ft/lb}^{1/3}$. At this range, Figs. 3-6 and 3-9 indicate the reflected impulse is 447 psi-msec, the peak reflected pressure equals 3200 psi, and the quasi-static pressure is 180 psi.

The side plates are bolted to the cover plate which coincides with the discussion in Section 6.2.3.c which assumes the connection to be a simple support. Therefore, the cover plate is analyzed as a plate simply supported along its four edges. The total mass of the plate is

$$\begin{aligned} M_t &= (10)(20)(1)(0.29)/386 \\ &= 0.15 \text{ lb-sec}^2/\text{in} \end{aligned}$$

Its moment of inertia per unit width is

$$I_a = t_c^3/12 = (1)^3/12 = 0.083 \text{ in}^4/\text{in}$$

For a width to length ratio of 0.5 and the assumed edge conditions, Table 5-4 gives a load-mass factor of 0.59. An expression for the spring constant for the plate is also obtained from Table 5-4.

$$\begin{aligned} K &= 201EI_a/a_c^2 = 201(29 \times 10^6)(0.083)/(10)^2 \\ &= 4.84 \times 10^6 \text{ lb/in} \end{aligned}$$

The fundamental frequency of vibration for the plate is obtained from Eq. 5-32, pg. 5-32.

$$\begin{aligned} \omega_N &= \left[\frac{K}{K_{LM} t} \right]^{1/2} = \left[\frac{4.84 \times 10^6}{0.59 \times 0.15} \right]^{1/2} \\ &= 7395 \text{ rad/sec} \end{aligned}$$

The natural period for the fundamental mode is

$$\begin{aligned} T_N &= \frac{2\pi}{\omega_N} = \frac{2(3.14)}{7395} \\ &= 0.00085 \text{ sec} \end{aligned}$$

Assuming a 10 percent increase in yield strength under dynamic loading, the plastic moment capacity of the cover plate is given by Eq. 5-3, pg. 5-7.

$$\begin{aligned} M_p &= f_{dy} Z = 36,000(1.1)(1)^3/4 \\ &= 9900 \text{ in-lb/in} \end{aligned}$$

The total moment capacity across the 10-inch width is

$$M_{pfa} = 10(9900) = 99,000 \text{ in-lb}$$

Across the 20-inch length it is

$$M_{pfb} = 20(9900) = 198,000 \text{ in-lb}$$

The maximum resistance of the simply supported rectangular plate is obtained from the equation in Table 5-4

$$\begin{aligned} R_m &= \frac{1}{a_c} (12M_{Pfa} + 9.0M_{Pfb}) \\ &= \frac{1}{10} (12 \times 99,000 + 9.0 \times 198,000) \\ &= 297,000 \text{ lb} \end{aligned}$$

The duration of the triangular pressure pulse is given by Eq. 3-4, pg. 3-13.

$$\begin{aligned} t_r &= t_1 = 2i_r/P_r \\ &= 2 \times 0.447/3200 \\ &= 0.000279 \text{ sec} \end{aligned}$$

and

$$\begin{aligned} t_o/T_N &= 0.000279/0.00085 \\ &= 0.328 \end{aligned}$$

The duration of the reflected pressure pulse is short compared to the period of vibration of the plate and Eq. 5-54 is appropriate for determining its maximum response.

$$\left[\frac{C_1 B/R_m}{\frac{T_N}{\pi t_1} \sqrt{2\mu-1}} \right]^2 + \left[\frac{C_2 B/R_m}{1 - \frac{1}{2\mu}} \right] = 1$$

For the given loading pulse,

$$C_1 = \frac{3200 - 180}{3200} = 0.944$$

$$t_1 = 0.000279 \text{ sec}$$

$$C_2 = 1.0 - C_1 = 1.0 - 0.944 = 0.056$$

$$B = (3200)(20)(10) = 640,000 \text{ lb}$$

By rearranging Eq. 5-54 the value of μ can be obtained:

$$\mu = \frac{\left[\frac{C_1 B}{R_m} \right]^2 + 1}{2 \left[1 - \frac{C_2 B}{R_m} \right]} = 3.07$$

Since μ is less than 6.0, the cover plate will survive the proof airblast in the Group 3 shield and experience a small plastic deformation. The maximum deformation is estimated using additional information from Table 5-4.

Since

$$R_m = KX_e$$

then

$$\begin{aligned} X_e &= R_m / K \\ &= 297,000 / 4.84 \times 10^6 \\ &= 0.061 \text{ inch} \end{aligned}$$

and the maximum displacement is

$$\begin{aligned} X_m &= \mu X_e \\ &= 3.07 \times 0.061 \\ &= 0.187 \text{ inches} \end{aligned}$$

6.7.2 Buckling of utility Box Side Members

a. Given

The structural and airblast parameters for this example are as described in Ex. 6.7.1.

b. Find

Check the sideplates of the utility penetration protective box for buckling resistance.

c. Solution

The dynamic reaction along the edge of the cover plate is calculated using information from Table 5-4. Recall from Ex. 6.7.1 that

$$R_m = 297,000 \text{ lb}$$

The airblast loading at the time of yield is assumed to be equal to the quasi-static overpressure. This assumption was investigated in Ex. 5.6.2 and 5.6.3 and found to be reasonable for impulsive type loadings combined with long duration quasi-static overpressures. In other problems where the time of maximum response, t_m , is less than the duration of the reflected pressure pulse, t_o , the pressure can be approximated as

$$P_{\text{approx}} = P_r \left(\frac{t_o - t_m}{t_o} \right)$$

For this example

$$\begin{aligned} F &= P_{qs} A \\ &= 180 \times 10 \times 20 \\ &= 36,000 \text{ lb} \end{aligned}$$

From Table 5-4, the total reactions along the short and long sides of the cover plate are

$$\begin{aligned}
 V_a &= 0.04F + 0.08R_m \\
 &= 0.04 \times 36,000 + 0.08 \times 297,000 \\
 &= 25,200 \text{ lb} \\
 V_b &= 0.11F + 0.27R_m \\
 &= 0.11 \times 36,000 + 0.27 \times 297,000 \\
 &= 84,150 \text{ lb}
 \end{aligned}$$

The height of the sideplate, h , is given as 8 inches in Ex. 6.7.1. Its thickness, t_s , is 1 inch. The coefficient, K_b , to be used in Eq. 6-1, pg. 6-5 is selected from the table following the equation. For the long side a value of h/b_c equal to the value of K_b is 7.76. The critical buckling stress is obtained from Eq. 6-1.

$$\begin{aligned}
 \sigma_{cr} &= \frac{K_b E}{1-\nu^2} \left[\frac{t_s}{b_c} \right]^2 \\
 &= \frac{7.76 \times 29 \times 10^6}{1 - (0.33)^2} \left[\frac{1}{20} \right]^2 \\
 &= 631,354 \text{ psi} > f_{dy}
 \end{aligned}$$

The shear reaction of the cover plate along the long side is 84150 lb, thus the largest reaction is 4208 lb/in. The side members are 1 inch thick, and the compressive stress is 4208 psi. This stress is less than the yield strength of the material, and buckling is not a factor in the design of the side members.

6.7.3 Shear in Shield Group 81-mm Split Collar at the Vacuum Line/Suppressive Shield Interface

a. Given

The geometry of a typical waste disposal vacuum

line is illustrated in Fig. 6-19. The vacuum line is shown passing through a Shield Group 81-mm wall panel.

The material in the bushing, split collars, and adapter fittings is mild steel; $f_y = 36,000$ psi, $f_{dy} = 39,600$ psi, $E = 29 \times 10^6$ psi, $\nu = 0.33$. The vacuum line is specified to have a nominal internal diameter of 2.0 inches. A 300-pound steel flanged 90 degree elbow has an inside diameter of 2.0 inches, a wall thickness of 0.25 inch, a flange diameter of 6.5 inches, a flange thickness of 0.875 inch, and a radius of curvature equal to 6.5 inches. Since the elbow thickness is less than the 1 inch required to defeat the fragment threat, an additional plate will be required to cover the region in front of the opening through the adapter fitting.

b. Find

Minimum thickness required for the split collar to (1) remain elastic until the elbow begins to yield in compression, and (2) satisfy the minimum thickness requirement specified to defeat the fragment threat.

c. Solution

If it is assumed that the vacuum line penetration is subjected to axial loads only, the compressive force developed in the elbow at the onset of yielding is calculated by multiplying the elbow cross sectional area, A , by the yield stress, f_{dy} . The cross sectional area is

$$\begin{aligned} A_{VL} &= \frac{\pi}{4} (D_o^2 - D_i^2) \\ &= \frac{\pi}{4} (2.5^2 - 2^2) \\ &= 1.77 \text{ in}^2 \end{aligned}$$

and the compressive force is

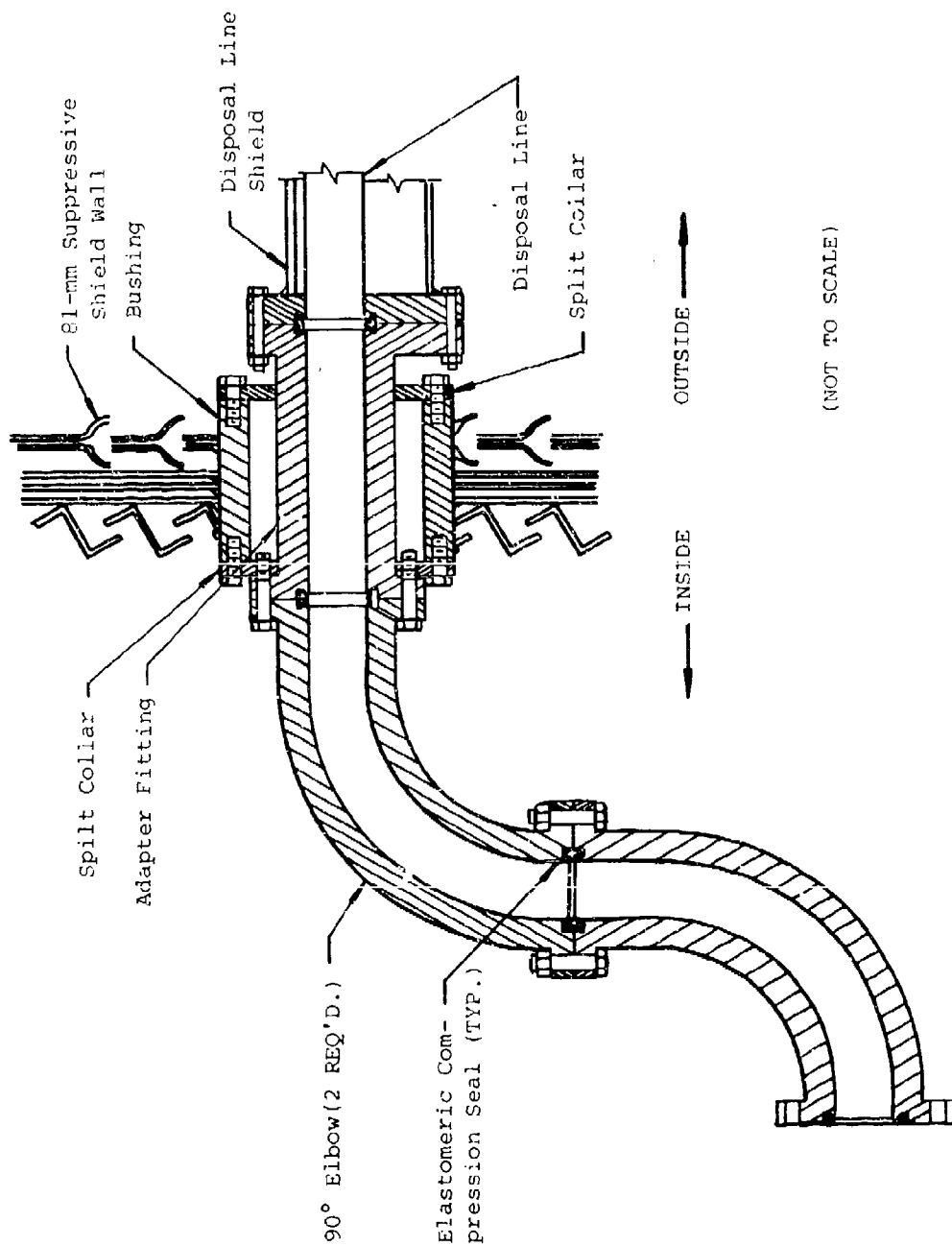


Figure 6-19. Waste Disposal Line Entry Into Suppressive Shield

$$\begin{aligned}
 F &= A_{VL} f_{dy} \\
 &= 1.77 \times 39,600 \\
 &= 70,092 \text{ lb}
 \end{aligned}$$

The shear area, A_{sh} , through the collar is

$$A_{sh} = \pi D_{\text{flange}} t$$

where t is the split collar thickness. The allowable shear stress, τ_s equals $0.55 f_{dy}$, or 21,780 psi, and the allowable shear force is

$$F_{\text{allowable}} = A_{sh} \tau_s$$

Equating the applied force to the allowable force and substituting the allowable stress yields the required shear area and, hence, the split collar thickness.

$$\begin{aligned}
 A_{sh} &= F / \tau_s \\
 &= 70,092 / 21,780 \\
 &= 3.2 \text{ in}^2 \\
 t &= 3.2 / (3.14 \times 6.5) \\
 &= 0.16 \text{ inch}
 \end{aligned}$$

Half of the nominal wall thickness for the Group 81-mm shield equals 0.5 inch. Therefore, the minimum recommended thickness for the split collars is 0.5 inches to defeat fragments.

6.7.4 Stress in Group 3 Shield External Disposal Line Shield Caused by Munition Explosion

a. Given

A waste disposal vacuum line is installed on the Group 3 shield considered in the first 2 example problems in this chapter. The vacuum line performance requirements dictate that the vacuum line should be about 2.0 inches and the vacuum line shield about 4 inches in diameter. The tubing selected for the shield measures 4.5 inches outside diameter by 0.188 inch

wall thickness. Tubing material is 6061-T6 extruded and drawn aluminum tubing; $f_y = 35,000$ psi, $\nu = 0.33$, $E = 10 \times 10^6$ psi, $\rho = 0.098$ lb/in³.

b. Find

Verify that the tensile stress in the Group 3 external vacuum line shield caused by an accidental explosion equal to the proof charge weight of 45.7 lbs of 50-50 Pentolite will not exceed its yield strength.

c. Solution

The mass of the tube per unit of surface area is

$$\begin{aligned} m &= \frac{t\rho}{g} \\ &= \frac{(0.188)(0.098)}{386} \\ &= 4.77 \times 10^{-5} \text{ lb-sec}^2/\text{in}^3 \end{aligned}$$

The natural period of vibration of the vacuum line in the extensional mode is calculated using Eq. 5-23, pg. 5-26.

$$\begin{aligned} T_N &= 2\pi \sqrt{\frac{mR^2}{Et}} \\ &= 2\pi \sqrt{\frac{4.77 \times 10^{-5} \times (2.156)^2}{10 \times 10^6 \times 0.188}} \\ &= 6.82 \times 10^{-5} \text{ sec} \end{aligned}$$

The critical location for stress in the disposal line is at a point just outside of the suppressive shield wall. The interior radius of the suppressive shield is 5.625 ft. Assuming a wall thickness of 3 inches the radius to a point on the outer surface of the shield is

$$R = 5.625 + \frac{3}{12} = 5.875 \text{ ft}$$

As noted in a previous example, 45.7 lbs of 50-50 Pentolite is equivalent to 51.6 lbs of TNT, therefore, the scaled distance is

$$Z = \frac{R}{W^{1/3}} = \frac{5.875}{(51.6)^{1/3}} \\ = 1.578 \text{ ft/lb}^{1/3}$$

From Fig. 3-3, the peak overpressure is

$$P_{so} = 400 \text{ psi}$$

and the scaled positive impulse is

$$0.018 \text{ psi-sec/lb}^{1/3}$$

The impulse is

$$i_s = 0.018(51.6)^{1/3} = 0.067 \text{ psi-sec}$$

The effective duration of an equivalent triangular pulse is

$$t_o = \frac{2i_s}{P_{so}} = \frac{2(0.067)}{400} = 0.000335 \text{ sec}$$

and

$$\frac{t_o}{T_N} = \frac{0.000335}{0.0000682} = 4.91$$

Compute the maximum resistance of the shield using Eq. 6-6, pg. 6-22

$$r_m = f_{dy} t / R_i = 35,000(0.188)/2.06 \\ = 3194 \text{ psi}$$

Use Eq. 5-47, pg. 5-55 to determine the required maximum resistance for $\mu = 1$. Substituting $\mu = 1$ in

$$\frac{P_r}{r_m} = \frac{T_N}{\pi t_o} \sqrt{2\mu-1} + \frac{1 - \frac{1}{2\mu}}{1 + 0.7 \frac{T_N}{t_o}}$$

$$\frac{P_r}{r_m} = \frac{0.0000682}{3.14(0.000335)} \sqrt{2(1) - 1} + \frac{1 - \frac{1}{2(1)}}{1 + 0.7 \left(\frac{0.0000682}{0.000335} \right)}$$

$$= 0.502$$

or the required r_m is

$$r_m = \frac{400}{0.502} = 796 \text{ psi}$$

Since 3194 psi is provided, the shield will remain elastic under the airblast generated by an internal explosion of 45.7 lbs of 50-50 Pentolite.

6.7.5 Stress in Group 3 Shield Disposal Line Shield Caused by an Airborne Dust Explosion

a. Given

The vacuum disposal line shield for the Group 3 shield considered in the previous problem experiences an internal airblast pressure due to the detonation of airborne dust particles. Without specific information as to the actual concentration levels and types of HE dust that might be encountered in the vacuum line, the most severe condition is assumed. The worst explosion shown in Table 6-1 will result from a concentration of 1.0 oz/cu ft of Comp. D (ammonium picrate). From Table 6-1,

$$\text{max pressure} = P = 141 \text{ psi}$$

$$\text{max rate of pressure rise} = r_p = 8800 \text{ psi/sec}$$

b. Find

Investigate tensile stress in the Group 3 external disposal shield caused by an explosion of airborne HE dust.

c. Solution

The loading pulse rise time is calculated from Eq. 6-7, pg. 6-23.

$$\begin{aligned}
 t_r &= \frac{P}{r_p} \\
 &= 141/8800 \\
 &= 0.016 \text{ sec}
 \end{aligned}$$

The natural period of the disposal line was calculated in Ex. 6.7.4 as 6.82×10^{-5} sec, yielding a ratio of t_r/T_N of 234, a very long rise time relative to the natural period. The maximum resistance for the thin wall cylinder is approximated using Eq. 6-6, pg. 6-22.

$$\begin{aligned}
 r_m &= f_{dy} t / R_i \\
 &= 35,000 \times 0.188 / 2.06 \\
 &= 3194 \text{ psi}
 \end{aligned}$$

The ratio of peak pressure to element resistance is

$$\begin{aligned}
 r_m / p_r &= 3194 / 141 \\
 &= 22.6
 \end{aligned}$$

The values of r_m / p_r and t_r / T_N are well off the chart shown in Fig. 6-9, but they are off in the direction that indicates the ductility ratio will be much less than unity. Hence,

$$\mu \ll 1$$

and the vacuum line shield selected is acceptable.

This problem could also have been solved using the approach outlined in Ex. 6.7.4 where the actual r_m is shown to be greater than that required for elastic response.

6.7.6 Stress in Disposal Line Shield Caused by Dust Sediment Explosion

a. Given

The largest accumulation of explosive dust shown in Fig. 6-10 is assumed to be present and detonate in the disposal line. The disposal line shield considered in this and the

previous two examples is 4.12 inches inside diameter by 0.188 inch wall thickness 6061-T6 extruded and drawn aluminum tubing.

b. Find

Determine the response of the Group 3 external disposal line shield to an explosion of HE dust sediment in the vacuum disposal line.

c. Solution

The largest amount of dust estimated to collect on the bottom surface of the vacuum line is shown as 0.10 oz/inch in Fig. 6-10. The internal radius for the vacuum line shield is 2.06 inches, therefore, the scaled range is

$$\begin{aligned} Z &= R/W^{1/3} \\ &= (2.06/12.0)/(0.1/16.0)^{1/3} \\ &= 0.932 \text{ ft/lb}^{1/3} \end{aligned}$$

From Fig. 3-6, the following values are obtained for peak positive reflected pressure and positive reflected impulse.

$$\begin{aligned} P_r &= 8000 \text{ psi} \\ i_r/W^{1/3} &= 0.23 \\ i_r &= 0.23 \times (0.1/16.0)^{1/3} \\ &= 0.0424 \text{ psi sec} \end{aligned}$$

The duration of the equivalent triangular representation for the reflected pressure/time curve is

$$\begin{aligned} t_0 &= 2 \times i_r/P_r \\ &= 2 \times 0.0424/8000 \\ &= 1.06 \times 10^{-5} \text{ sec} \end{aligned}$$

From Ex. 6.7.4, the natural period of vibration for the chosen vacuum line shield is $T_N = 6.82 \times 10^{-5} \text{ sec}$. The ratio

$$\begin{aligned} t_o/T_N &= \frac{1.06 \times 10^{-5}}{6.82 \times 10^{-5}} \\ &= 0.16 \end{aligned}$$

indicates that the load is impulsive. The maximum resistance provided by the tube shield is obtained from Eq. 6-6, pg. 6-22.

$$\begin{aligned} r_m &= f_{dy} t/R_i \\ &= 35,000 \times 0.188/2.06 \\ &= 3194 \text{ psi} \end{aligned}$$

The required maximum resistance that the tubing must develop to remain elastic is obtained from Eq. 5-43, pg. 5-54 by setting the ductility ratio equal to unity.

$$\begin{aligned} r_m &= P_r \left[\frac{\pi t_o}{T_N \sqrt{2\mu-1}} \right] \\ &= 3200 \left[\frac{\pi \times 1.06 \times 10^{-5}}{6.82 \times 10^{-5} \sqrt{2-1}} \right] \\ &= 1560 \text{ psi} \end{aligned}$$

Since the required maximum resistance is less than that provided, the disposal line shield will remain elastic and is acceptable. In those cases where r_m provided is less than r_m required to remain elastic and the load is impulsive, the peak response can be calculated in terms of the ductility ratio by using Eq. 5-45 or 5-47, pg. 5-55.

6.7.7 Fragment Hazard From Detonation of Explosive Dust Sediment in Disposal Line

a. Given

The Group 3 disposal line and disposal line shield are subjected to an explosion of dust sediment in the disposal line.

b. Find

Evaluate the ability of the disposal line shield to stop fragments produced by the explosion of Comp B dust sediment in the disposal line.

c. Solution

From Fig. 6-10, it is estimated that the maximum weight of explosive dust per inch of disposal line is

$$W = 0.10 \text{ oz/in}$$

The interior radius of the disposal line is 0.94 inch and it is assumed that the density of the explosive dust sediment is $\rho_e = 0.0289 \text{ lb/in}^3$. Substituting these values in Eq. 6-9, pg. 6-30,

$$W = \rho_e \left[\frac{R_1^2 (\theta_e - \sin \theta_e)}{2} \right]$$

$$\frac{0.1}{16} = 0.0289 \left[\frac{(0.94)^2 (\theta_e - \sin \theta_e)}{2} \right]$$

it is found that $\theta_e = 1.4858$ radians.

The density of aluminum is taken to be 0.10 lb/in³. The outer radius of the disposal line is 1.0 inch. The weight of metal per inch of aluminum disposal line in contact with the dust sediment is obtained from Eq. 6-8, pg. 6-28.

$$W_c = \frac{\rho_m}{2} \theta_e [R_o^2 - R_i^2] = \frac{0.1(1.4858)}{2} [(1.0)^2 - (0.94)^2]$$

$$= 0.0086 \text{ lb/in} = 0.1384 \text{ oz/in}$$

The empirical constant $\sqrt{2E'}$ is taken as 8900 fps for Comp B, and the fragment velocity is obtained from Eq. 6-10, pg. 6-30.

$$\begin{aligned}
 v_o &= \sqrt{2E'} \sqrt{\frac{3}{1 + (5W_c/W) + 4(W_c/W)^2}} \\
 &= 8900 \sqrt{\frac{3}{1 + \left(\frac{5 \times 0.1384}{0.1}\right) + 4\left(\frac{0.1384}{0.1}\right)^2}} \\
 &= 3905 \text{ fps}
 \end{aligned}$$

The thickness of the fragment is taken equal to the thickness of the vacuum disposal line shield. The side dimensions of the fragment are obtained from Eq. 6-13, pg. 6-32.

$$L = R_i \theta_e = 0.94(1.4858) = 1.3967 \text{ inches}$$

The weight of the fragment is obtained from Eq. 6-14, pg. 6-32.

$$W_s = \rho_m t L^2 = 0.1(0.06)(1.3967)^2 = 0.0117 \text{ lb}$$

The presented area of the fragment is given by Eq. 6-15, pg. 6-32.

$$A_p = L^2 = (1.3967)^2 = 1.95 \text{ in}^2$$

From Table 3-5 for $L/t > 5$,

$$A_o = 1261$$

$$m = 0.427$$

$$n = 0.647$$

Substituting in Eq. 6-12, pg. 6-31, the thickness of vacuum line shield required to stop the fragment is

$$\begin{aligned}
 t_t &= \left[\frac{v_1 \sqrt{W_s}}{A_o A_p^m} \right]^{1/n} = \left[\frac{3905 \sqrt{0.0117}}{1261 (1.95)^{0.427}} \right]^{1/0.647} \\
 &= 0.119 \text{ inch}
 \end{aligned}$$

From Ex. 6.7.4, the shield wall thickness is 0.188 inch, so the shield should contain the fragment. If an edge-on impact is assumed, a shield thickness of 0.95 inch is required for containment.

6.7.8 Determine the Area of the Environmental Conditioning Exhaust Stack for the Milan 81-mm Suppressive Shield

a. Given

The Milan 81-mm suppressive shield has inside dimensions of 14 feet wide by 14 feet long by 12.4 feet high. The design charge weight for incident and reflected overpressure and impulse is 4.53 lb TNT.

b. Find

The exhaust stack area required to provide two complete air changes per hour at a maximum velocity of 400 ft/min.

c. Solution

The required exhaust stack area is

$$A_{ex} = Q/v_a$$

where

$$Q = VN_a$$

and

Q = air flow rate, ft^3/min

V = shield internal volume, 2430.4 ft^3

N_a = number of changes per minute, 0.0333

v_a = air flow velocity, 400 ft/min

Substituting, the required area is

$$A_{ex} = \frac{2430.4(0.0333)}{400} = 0.2 \text{ ft}^2 = 29.1 \text{ in}^2$$

6.7.9 Determination of Exhaust Stack Height

a. Given

A frangible structure is located immediately adjacent to the Milan 81-mm suppressive shield described in the

previous problem. The height to the roof of the frangible structure is the same as that of the shield.

b. Find

The height of the exhaust stack required to limit the overpressure on the roof of the frangible structure to 0.3 psi.

c. Solution

The required stack height is determined from Eq. 6-16, pg. 6-36.

$$P_{so} = 290 \left[\frac{A_{ex}}{V^{2/3}} \right]^{0.401} \left[\frac{W^{1/3}}{R} \right]^{1.496}$$

where

P_{so} = peak overpressure = 0.3 psi

A_{ex} = exhaust stack area = 0.2 ft²

V = internal volume of shield = 2430.4 ft³

W = charge weight = 4.53 lb

R = distance from exhaust exit, ft

Rearranging and substituting,

$$\begin{aligned} R^{1.496} &= \frac{290}{0.3} \left[\frac{0.2}{(2430.4)^{2/3}} \right]^{0.401} \left[(4.53)^{1/3} \right]^{1.496} \\ &= 133.986 \end{aligned}$$

and

$$R = 26.41 \text{ ft}$$

Therefore, the minimum stack height to limit overpressure on the roof of the frangible structure to 0.3 psi is 26.4 feet.

6.7.10 Stress in Environmental Conditioning Exhaust Stack

a. Given

The exhaust stack of the Milan 81-mm suppressive shield described in previous problems is a steel tube with the following properties.

$$E = 29 \times 10^6 \text{ psi}$$

$$\nu = 1/3$$

$$\rho = 0.286 \text{ lb/in}^3$$

$$f_y = 36,000 \text{ psi}$$

$$f_{dy} = 39,600 \text{ psi}$$

b. Find

The stress in the exhaust stack caused by an explosion inside the shield.

c. Solution

From Ex. 6.7.11, the exhaust stack requires a cross sectional area of 29.1 in^2 . The inside radius is

$$R_1 = \sqrt{\frac{A}{\pi}} = \sqrt{\frac{29.1}{3.14}} \approx 3.0 \text{ inches}$$

Use a 6.25 inch O.D. tube with a 0.125 inch wall. The natural period of the tube is given by Eq. 5-23, pg. 5-26.

$$T_N = 2\pi \sqrt{\frac{mR^2}{Et}}$$

Since

$$m = \frac{t\rho}{g}$$

Equation 5-23 can be written in the form

$$T_N = 2\pi \sqrt{\frac{\rho R^2}{Eg}}$$

where

ρ = density of tube material, 0.286 lb/in³

R = mean radius of tube, 3.0625 inches

E = modulus of elasticity, 29×10^6 psi

g = gravitational acceleration, 386 in/sec²

Substituting

$$T_N = 2\pi \sqrt{\frac{0.286(3.0625)^2}{29(10)^6(386)}}$$

$$= 0.000097 \text{ sec}$$

The peak overpressure, P_{so} , and positive impulse, i_s , at a point just outside the suppressive shield is obtained from Fig. 3-3. For a scaled distance

$$Z = R/W^{1/3} = 7.5/4.53^{1/3} = 4.53 \text{ ft/lb}^{1/3}$$

the peak overpressure, P_{so} , is 30 psi. The scaled positive impulse is 0.011 psi-sec/lb^{1/3}. The positive impulse is

$$i_s = 0.011W^{1/3} = 0.011(4.53)^{1/3} = 0.0182 \text{ psi-sec}$$

Therefore, the pulse duration of an equivalent triangular pulse is

$$t_c = \frac{2i_s}{P_{so}} = \frac{2(0.0182)}{30} = 0.00121 \text{ sec}$$

The ratio of the pulse duration to the natural period of the tube is

$$\frac{t_o}{T_N} = \frac{0.00121}{0.000097} = 12.5$$

Since the ratio is greater than 10, the required maximum resistance of the exhaust stack is given by Eq. 5-37, pg. 5-53.

$$r_m = p_{so} \left[\frac{2\mu}{2\mu-1} \right] = 30 \left[\frac{2\mu}{2\mu-1} \right]$$

For the elastic case, $\mu = 1$. Therefore,

$$r_m = 30 \left[\frac{2}{1} \right] = 60 \text{ psi}$$

The membrane stress in the exhaust stack is

$$\sigma = r_m R_i / t = \frac{60(3)}{0.125} = 1440 \text{ psi}$$

This stress is well below the dynamic yield stress of the tube. No further analysis is necessary.

6.7.11 Stress in the Shaft of the Rotary Product Door Caused by the Accidental Detonation of Munitions During Production

a. Given

The rotary product door that has been conceived and tested for the 81-mm shield group is illustrated pictorially in Fig. 6-16. It is desired to analytically investigate the response of the product door to an accidental detonation equal to the Prototype 81-mm Shield proof charge. Maximum torque will be transferred to the product door when the munition opening is coincident with a pocket in the rotating door. The area of the product door, A_d , exposed to the airblast is 38.9 in^2 . The effective moment arm, r_d , from the center of rotation to the centroid of the area A_d is 4.32 inches. Analysis of the rotary product door prototype has revealed that the moment of inertia, I_m , of the assembly is about 6.23 in-lb-sec^2 . The shaft is constructed of 1025 carbon steel with an allowable yield stress, f_y , of 36,000 psi, a modulus of elasticity, E , of 29×10^6 psi, and a Poisson ratio, ν , of 0.333. The shaft radius, r_s , is 0.75 inch and its length, L_s , is 6.0 inches

b. Find

The shear stress in the shaft of a rotary product door in the Prototype 81-mm Shield caused by the detonation of a proof charge.

c. Solution

The proof charge is equivalent to 125 percent of the design charge listed in Table A-8a.

$$\begin{aligned} W_{\text{TNT}} &= 7.24 \times 1.25 \\ &= 9.05 \text{ lb} \end{aligned}$$

Scaled range to the sidewall located 7.0 feet from the shield centerline is

$$\begin{aligned} Z &= \frac{R}{W^{1/3}} \\ &= \frac{7}{(9.05)^{1/3}} \\ &= 3.36 \text{ ft/lb}^{1/3} \end{aligned}$$

The scaled reflected impulse is read from Fig. 3-6 as

$$i_r/W^{1/3} = 4.6 \times 10^{-2} \text{ psi-sec/lb}^{1/3}$$

Hence,

$$\begin{aligned} i_r &= 4.6 \times 10^{-2} \times (9.05)^{1/3} \\ &= 0.096 \text{ psi-sec} \end{aligned}$$

The angular impulsive load, T_i , is calculated from Eq. 6-17, pg. 6-42.

$$\begin{aligned} T_i &= i_r A_d r_d \\ &= 0.096 \times 38.9 \times 4.32 \\ &= 16.13 \text{ lb-sec-in} \end{aligned}$$

The modulus of rigidity, G , is a function of the modulus of elasticity, E , and calculated as follows.

$$\begin{aligned}
 G &= \frac{E}{2(1 + \nu)} \\
 &= \frac{29 \times 10^6}{2(1 + 1/3)} \\
 &= 10.9 \times 10^6 \text{ psi}
 \end{aligned}$$

The shear stress can now be calculated from Eq. 6-21, pg. 6-44.

$$\begin{aligned}
 \tau_s &= \frac{T_i}{r_s} \sqrt{\frac{2G}{\pi I_m L_s}} \\
 &= \frac{16.13}{0.75} \sqrt{\frac{2 \times 10.9 \times 10^6}{\pi \times 6.23 \times 6}} \\
 &= 9,300 \text{ psi}
 \end{aligned}$$

The allowable shear stress as indicated in Chapter 4 is

$$\begin{aligned}
 \tau &= 0.55f_{dy} \\
 &= 0.55 \times 1.1 \times 36,000 \\
 &= 21,780 \text{ psi}
 \end{aligned}$$

The allowable shear stress for the material is greater than the expected shear stress. Therefore, the shaft should not yield.

6.8 LIST OF SYMBOLS

a_c	Width of cover plate (inches)
A_d	Door area (in^2)
A_{ex}	Exhaust duct area (ft^2)
A_o	Equation constant
A_p	Area of fragment (in^2)
A_{SHC}	Collar area resisting shear (in^2)
A_{VL}	Cross section area of vacuum line (in^2)
b_c	Length of cover plate (inches)
B	Peak total load (lbs)
E	Modulus of elasticity (psi)
f_{dy}	Dynamic tensile yield stress (psi)
G	Modulus of rigidity (psi)
h	Height of side plate (inches)
i_r	Reflected pressure impulse (psi-sec)
i_s	Positive incident impulse (psi-sec)
I_m	Mass moment of inertia of door ($\text{lb-sec}^2\text{-inch}$)
k	Number of different types of plates in shield panel
K_b	Plate buckling constant
$K.E.$	Kinetic energy (in-lb)
$2, L$	Length (inches)
L_1	Length of transverse mounted protective box side plate (inches)
L_2	Length of longitudinal mounted protective box side plate (inches)
L_s	Length of shaft, inches
m	(1) Mass per unit surface area of cylinder ($\text{lb-sec}^2/\text{in}^3$) (2) Equation constant

n	(1) Number of different types or sizes of panel members (2) Equation constant
N _a	Number of air changes per minute
P _r	Peak reflected overpressure (psi)
P _{ro}	Peak overpressure (psi)
P _s	Incident pressure outside stack (psi)
P _{so}	Peak positive incident pressure (psi)
Q	Air flow rate (ft ³ /min)
r _d	Radius from center of impulse load to center of door rotation (inches)
r _m	Maximum unit resistance (psi)
r _p	Rate of pressure rise (psi/sec)
r _s	Radius of shaft (inches)
R	Average radius (inches)
R _i	Inside radius (inches)
R _m	Maximum resistance (lbs)
R _o	Outside radius (inches)
t	Wall thickness (inches)
t _c	Thickness of cover plate (inches)
t _o	Duration of positive pressure pulse (sec)
t _r	Duration of positive reflected pressure (sec)
t _s	Thickness of side plate (inches)
t _t	Thickness of material being penetrated (inches)
T _i	Angular impulsive load (lb-sec-in)
T _N	Natural period of vibration (sec)

U_s	Torsional shear strain energy (in-lb)
V_a	Air flow velocity (ft/min)
V_o	Initial fragment velocity (ft/sec)
V_L	Minimum velocity for penetration (ft/sec)
V	(1) Volume (ft ³) (2) Dynamic reaction at end or edge of symmetric element (lbs)
V_B	Total dynamic reaction along one long edge, b (lbs)
V_C	Dynamic load along transverse plate (lbs)
V_L	Dynamic load along longitudinal plate (lbs)
W	Charge weight of explosive (lbs)
W_C	Weight of unit length of tube (lbs)
W_S	Striking weight of fragment (lbs)
W_T	Weight of explosive per unit length of tube (oz/in)
X_e	Elastic limit displacement (inches)
X_m	Maximum displacement (inches)
Z	Scaled distance (ft/lb ^{1/3})
θ_e	Angle which explosive subtends (radians)
μ	Ductility ratio
ν	Poisson's ratio
ρ_e	Density of explosive (oz/in ³)
ρ_m	Density of tube material (lb/in ³)
σ	Stress (psi)
σ_b	Compressive stress in side plate (psi)
σ_{cr}	Critical buckling stress (psi)
τ_{cp}	Shear stress in cover plate (psi)
τ_s	Dynamic shear yield stress (psi)
τ_{SP}	Average shear stress around perimeter of protective box (psi)
ω	Angular velocity (radians/sec)
$\sqrt{2E'}$	Gurney energy constant (ft/sec)

6.9 REFERENCES

- 6-1 Joint Munitions Effectiveness Manual, FM101-62-3, Manual of Fragmentation Data, 15 September 1973.
(C-XGDS-3)
- 6-2 Roark, R.J. and Young, W.C., Formulas for Stress and Strain, McGraw-Hill Book Co., New York, N.Y., 5th Edition, 1975. (U)
- 6-3 Schroeder, F.J., Kachinski, R.L., Schnapfe, R.W., Reger, D.M., McKivriga, J.L. and Jezek, B.W., Engineering Design Guidelines, Drawings and Specifications for Support Engineering of Suppressive Shields, EM-CR-76097, Edgewood Arsenal, Aberdeen Proving Ground, Md., December 1976. (U)
- 6-4 Hubich, H.O. and Kachinski, R.L., Explosive Waste Removal Systems for Suppressive Shields, EM-CR-76002, Edgewood Arsenal, Aberdeen Proving Ground, Md., August 1975. (U)
- 6-5 Nagy, J., et al, Explosibility of Miscellaneous Dusts, United States Department of the Interior, Bureau of Mines, Report of Investigations 7208, December 1968. (U)
- 6-6 Crawford, R.E., Higgins, C.J. and Bultmann, E.H., The Air Force Manual for Design and Analysis of Hardened Structures, AFWL TR 74-102, Air Force Weapons Laboratory, Kirtland AFB, N.M., October 1974. (U)
- 6-7 Keenan, W.A. and Tancreto, J.E., Blast Environment from Fully and Partially Vented Explosions in Cubicles, Technical Report R828, Civil Engineering Laboratory, Naval Construction Battalion Center, Port Hueneme, California, November 1975. (U)
- 6-8 Safety Manual, AMCR 385-100, Headquarters, U.S. Army Materiel Command, Alexandria, Va., Latest Edition. (U)
- 6-9 Seely, F.B. and Ensign, N.E., Analytical Mechanics for Engineers, John Wiley & Sons, Inc., New York, N.Y., 3rd Edition, 1948. (U)

CHAPTER VII

ECONOMIC ANALYSIS

7.1 THE PROBLEM

The objective of an economic analysis is to determine the most cost effective configuration from among the set of workable design alternatives considered to be technically feasible. Selection of the most economical solution requires a detailed investigation of these feasible alternative system configurations.

The complete series of events involved in a munitions operation must be studied in a stepwise sequence to determine where the greatest hazards exist. Each identified hazard is then isolated for determination of methods of reducing the hazard. In some cases, proven protective systems capable of reducing the hazard may be applied without modification. In other cases, alternate systems must be designed to fit the particular requirements of interest.

The final selection of a protective, or hazard reduction, system may be based partially on considerations which do not have a definable dollar value. For example, items such as time lost in repair of munition lines damaged by an accidental detonation may enter into the final choice. Generally, however, the alternatives will all be designed to provide the desired level of reliability and safety, and dollar costs will be the determining factor in selecting one system or another.

7.2 CONSIDERATIONS

The number of factors entering into the process for evaluating the merits of different methods of providing adequate protection to a hazardous operation can be quite extensive. Although each installation may be unique in its requirements, there are certain considerations which are common to all applications. For example, the general methods of providing protection require consideration in every application. These are

- Dispersal based on unbarricaded quantity-distance requirements.
- Dispersal based on barricaded quantity-distance requirements using reinforced concrete blast walls.
- Using suppressive shields to reduce quantity-distance requirements.

The first two methods listed above have been in existence for some time and have been successfully utilized many times in the past. Reference 7-1 provides guidance on quantity-distance requirements; design of reinforced concrete blast walls is covered in Ref. 7-2. Suppressive shields, the subject of this handbook, have also been proven successful in safely reducing separation requirements between hazardous operations and providing the required safety in the operating plant environment.

In the most general of terms, it may be found that a plant designed on the basis of unbarricaded quantity-distance requirements is most economical in areas where real estate, utilities, and labor are abundant at low cost. Suppressive shields may be found to be the most economical approach where the inverse is true and the hazardous operations must be kept as near each other as possible. The use of reinforced concrete barricades may be the most economical solution in areas of intermediate real estate, utilities and labor cost. One must also remain alert to the possible advantages of combining two or all three of the methods in particular situations.

Representative items which can be expected to require consideration in any economic analysis of munitions plant alternative designs are listed in Table 7-1. Although by no means all-inclusive, the list in Table 7-1 is furnished as a starting point for items to be considered in the preparation of an economic analysis.

Table 7-1

REPRESENTATIVE ITEMS TO CONSIDER
IN AN ECONOMIC ANALYSIS

- ACCESS ROADS
- BUILDINGS
 - Production
 - Igloos
 - Office
 - Change Rooms
 - Cafeteria
 - Laundry
- COVERED RAMPS
- PAVING
 - Concrete
 - Asphalt
 - Improved
- STORM DRAINS
- LIGHTING
 - Street
 - Parking
- FIRE PROTECTION
- RAILROAD
- SITE ROADS
- FENCE
- GUARD HOUSE
- PARKING
- LANDSCAPING
- BARRICADES
- SUPPRESSIVE SHIELDS
- CONVEYORS
- UTILITIES
 - Electrical
 - Communications
 - Water
 - Steam and Condensate
 - Compressed Air
 - Sanitary Sewage
 - Heating, Ventilating and Air Conditioning
- LAND

7.3 METHOD

It has probably become apparent at this point that the only realistic basis upon which to base an economic analysis is investigation of the available alternative systems in the criteria development stage. To begin the process, the entire sequence of operations that must be performed is separated into discrete steps. The operations are then combined into compatible groups which can be safely consolidated into separate buildings or areas of the same building. The number of operations and the desired production capacity will determine the area and the size of the building, or buildings, required.

One or more layouts to accomplish the required functions are then developed based on the protective method, or combination of methods, being utilized. The compatible hazardous operations are located by unbarricaded quantity-distance requirements, barricaded quantity-distance requirements, and/or suppressive shield separation distances. The investigation is now at the point where criteria will be required. Reinforced concrete barricades should be designed. Suppressive shields should be selected or designed by the procedures described in preceding chapters. Reference 7-3 can be very helpful in estimating reinforced concrete barricade costs. Reference 7-4 is suggested for estimating all other construction costs.

With the various alternative layouts and preliminary facility designs established as outlined above, it will be possible to estimate initial real estate and facilities costs. Subsequently, estimates of the recurring costs for the candidate designs can be made.

Recurring costs include operating and maintenance costs which continue throughout the life of the facility, as opposed to the one-time nonrecurring costs which include all labor, material, plant and equipment costs required to initiate production. It may be found in some cases that the recurring costs

are insignificant with respect to the nonrecurring costs. This will not necessarily always be the case, however, and recurring costs should be considered until analysis shows that they can be safely neglected.

There will be overriding factors in some cases that will rule out possible alternative layouts and designs. The most common of such factors are limited real estate availability and the requirement to utilize existing facilities. These factors may make the economic analyses simpler or more complex, depending upon the particular circumstances.

7.4 EXAMPLE ECONOMIC ANALYSES

An economic analysis of hazardous operation facilities is not notably different from economic analysis of more conventional plant facilities. Alternative acceptable configurations must be conceived; the usual as well as the unusual items must be designed; and the various alternative designs must be developed to the extent that valid economic comparisons can be made between the candidate configurations.

Since there are a number of possibilities and considerations that will arise in economic analyses of munitions plant facilities, it is believed that the best way to illustrate the methods and procedures involved is by specific examples. These examples are presented in Refs. 7-5 and 7-6. The first example is an analysis of an improved conventional munition LAP facility (Ref. 7-5). The second example is an analysis of a 105-mm high explosive melt-pour facility (Ref. 7-6).

The first example analysis evaluates layouts and develops alternative layouts using suppressive shields around hazardous explosive operations with the objective of determining the most economical facility that will meet production requirements for both peak production and for guaranteed production in case of

an accidental detonation. The second example analysis develops five alternative layouts which employ suppressive shielding and compares these five designs with a proposed design concept which did not utilize suppressive shields. Recurring operating, maintenance and energy use costs are included in the second example analysis.

Both example analyses find that the use of suppressive shielding technology can result in meaningful savings in the cost of munitions plant construction.

7.5 REFERENCES

- 7-1 Safety Manual, AMCR 385-100, U.S. Army Material Command, Alexandria, Va., Latest Edition. (U)
- 7-2 Structures to Resist the Effects of Accidental Explosions, TM5-1300, Department of the Army, Washington, D.C., June 1969. (U)
- 7-3 Dede, M., et al, Preliminary Estimate of Concrete Thicknesses and Construction Costs of Laced Reinforced Concrete Structures, Technical Report No. 4441, Picatinny Arsenal, Dover, N.J., October 1972. (U)
- 7-4 Building Construction Cost Data, Robert Snow Means Co., Inc., 100 Construction Plaza, Duxbury, Mass., Latest Edition. (U)
- 7-5 Nelson, K.P., The Economics of Applying Suppressive Shielding to the M483A1 Improved Conventional Munition LAP Facility, EM-TR-76087, Edgewood Arsenal, Aberdeen Proving Ground, Md., January 1977. (U)
- 7-6 Wenzel, A.B., et al, An Economic Analysis of the Use of Suppressive Structures in the Lone Star Army Ammunition Plant 105-mm High Explosive Melt-Pour Facility, EM-CR-76032, Edgewood Arsenal, Aberdeen Proving Ground, Md., November 1975. (U)

CHAPTER VIII

ASSURING STRUCTURAL QUALITY

8.1 INTRODUCTION

Control of fabrication quality is important if a suppressive shield is to be constructed with the full strength intended in design. Quality control is exercised by various methods throughout construction. Materials are purchased according to specifications; the construction is performed by certified individuals or companies using qualified procedures; the final product is inspected; and, in some cases, the structure is proof tested.

This chapter contains references to the material and fabrication specifications required to fabricate suppressive shields with full design capability. It includes reference to specific quality control requirements which experience in the suppressive shield design and technology program has indicated are significant factors in shield integrity. Steel and steel fabrication procedures are discussed first, followed by a presentation of considerations applicable to specifications for both standard and fiber reinforced concrete.

9.2 STEEL

8.2.1 Structural Steel

Steel is the most commonly used material in suppressive shields. Structural steels are specified by many organizations and the Federal Government and are categorized for intended use. The American Society for Testing and Materials (ASTM) publishes specifications that cover steels of all strength levels, mill conditions (wrought, forged or cast) and shapes. Other organizations such as the American Institute for Steel Construction (AISC), the American Iron and Steel Institute (AISI), the Society of Automotive Engineers

(SAE), and American Petroleum Institute (API) also specify steels. The API specifications cover piping. In suppressive shield structures, ductility is one of the most important material properties since shields must undergo large deflections beyond the elastic limit without failure. Therefore, the more ductile low carbon structural grade steels are required in this type of structure instead of high strength steels. The structural grade steel ASTM A36 is the most readily available and is the most commonly used.

8.2.2 Reinforcing Steel

Reinforcing bars for use with concrete are specified by ASTM, the Concrete Reinforcing Steel Institute (CRSI), and the American Concrete Institute (ACI). The bars are categorized by strength level and diameter. The CRSI specification provides guidance for the reinforcing steel details such as bending, embedments, splices, etc. Reference 8-1 cites numerous ASTM specifications for reinforcing steel.

8.3 WELDING

8.3.1 General

The requirement for strict quality control of welds became apparent early in the suppressive shield test program when the regular occurrence of weld failures was noted. It was thought at first that the weld failures occurred despite following established welding procedures and that new welding procedures were needed for welds exposed to an explosive environment. However, it was discovered that the occurring weld deficiencies such as undercutting, insufficient fusion, and inadequate joint penetration were the result of not following established welding procedures. It thus becomes apparent in the

suppressive shield program that structural integrity is a function of quality control as well as the correct design and analytical procedures.

8.3.2 Welding Processes

Two welding processes are common for field welding applications such as required in suppressive shield construction. Shielded metal-arc welding (SMAW) is the most common process and is used about twice as often as gas metal-arc welding (GMAW). Both processes offer advantages in field applications. The SMAW process is versatile and can be used in all positions with relative ease. The equipment required, power supply, electrode holder and cable, and ground cable are simple to use and field portable. The SMAW process leaves a slag covering on the deposited weld bead which must be removed before the application of another weld bead or paint. GMAW on the other hand provides better quality weld beads with little or no slag covering. The equipment, however, is more cumbersome and less field portable than SMAW equipment. For welding procedures, certified welder requirements, electrode requirements and other information concerning both processes, the AWS Welding Code, AWS D1.1-75, should be consulted.

8.3.3 Welding Defects

In addition to mechanical property changes, especially in the heat affected zone (HAZ), and dimensional defects due to incorrect weld sizes or profiles, improper use of welding procedures as occurred in early suppressive shield construction can introduce defects such as porosity, slag inclusions, incomplete fusion, inadequate joint penetration, undercutting, and cracking into the weld joint. The welding procedures used are governed by the structure being welded, the position of the weld (i.e., flat, overhead, horizontal, or vertical), and the chemical composition of the metal. Carbon levels in the

base metal govern the level of preheat temperature used. As a rule, the higher the carbon level, the higher the preheat temperature used. Recommended practices are contained in AWS D1.1-75.

a. Cracking

Cracking is one of the most frequently detected flaws occurring in a weldment (see Fig. 8-1). Cracks occur when the temperature of the cooling weld and base plate is within either of two ranges. One range is at or slightly below the solidification temperature of the weld metal, and the other is from about 400°F to ambient temperature. The high-temperature cracking is called hot tearing and occurs because the metal is weak and has limited plasticity at this temperature. Fillet welds, weld craters, and the heat affected zone (HAZ) display this type of cracking. Low-temperature cracking or cold cracking occurs in root passes of butt welds and in the HAZ. Cracking in this range is invariably associated with the presence of hydrogen as a dissolved impurity.



Figure 8-1. Cracking of Weld

(1) Hot Tearing

High-temperature cracks are intercrystalline tears that occur at or near the range of solidification for the metal. They are attributed to low-freezing compounds such as iron sulfide, or solid impurities that have little or no ductility at high temperatures. These tears are located in the metal that is last to freeze. Sulfur contributes significantly to hot tearing, while silicon, phosphorus, carbon, copper, and nickel contribute to a lesser degree. Manganese, on the other hand, has a beneficial effect on hot ductility because it has a greater affinity to sulfur than iron does and forms manganese sulfides. Manganese sulfides have a higher melting temperature than steel and will form globular inclusions rather than the intergranular film that iron sulfide forms. If the ratio of manganese to sulfur in steel is 60 or greater, then hot tearing is not likely to occur. The stresses required to induce hot tearing can be introduced by welding highly restrained joints and by shrinkage due to cooling weld metal and base metal.

(2) Cold Cracking

Cold cracking is induced by the high stresses resulting from the cooling weld metal. When the weld cools, the metal contracts and tends to get smaller in length, width, and height. This contraction puts the weld metal into tension because the shortening and lateral contraction are resisted by the surrounding colder base metal. The resulting tensile stresses can cause plastic deformation of the weld, especially at higher temperatures when the metal is weak. When the temperature reaches the transformation range, the metal becomes stronger but less plastic. Below the transformation range, the plastic flow is similar to cold working, which tends to use up the ductility of the metal.

Since most mild steels are susceptible to strain aging effects in the temperature range below 1000°F, which causes them to lose ductility quickly when cold worked, the danger of cracking rises continuously as the metal cools to room temperature. If there is a notch of some type present, such as the root of the joint, it will act as a stress riser and will also inhibit plastic flow.

As previously mentioned, hydrogen is a contributing factor in cold cracking. There are three factors acting simultaneously in the generation of hydrogen-induced cracking: dissolved hydrogen, tensile stresses, and a low-ductility microstructure such as martensite. The source of hydrogen is the shield gas, flux, or surface contamination. The hydrogen is carried to the arc and converted to the atomic or ionized state, which readily dissolves in the weld metal. As the weld metal cools, it becomes super-saturated and the hydrogen diffuses to the HAZ and the atmosphere. Under rapid cooling conditions, when the steel transforms to martensite, the hydrogen becomes trapped. Since hydrogen has a very low solubility in the martensite structure, it is at a very high energy level and seeks discontinuities in the microstructure where it can decrease its energy levels. The hydrogen concentrates in these discontinuities and, in conjunction with external stresses, enlarges them to crack size.

Joint design and attention to joint fit-up can reduce the chances of cold cracking. To reduce the tendency toward hydrogen-induced cracking, a post-weld temperature of 400°F for up to 10 hours (depending on weld thickness) is recommended. Joint cleaning and the use of low hydrogen electrodes are also recommended to limit the source of hydrogen.

b. Porosity

The AWS defines porosity as cavity type discontinuities formed by gas entrapment during solidification (see Fig. 8-2). The gases that form porosity are either

driven from solution because of low solubility at lower temperature or are produced by chemical reactions in the molten weld puddle. These gases are trapped in the weld metal because there is insufficient time to rise to the surface of the puddle before solidification occurs. The formation of porosity can be avoided by not using excessively high currents or long arc lengths. This is especially true for shielded metal-arc welding (SMAW) because high currents and long arc lengths will consume large amounts of deoxidants in the electrode covering, leaving little to combine with excess gases in the weld pool. The distribution of porosity will give some indication of the cause.



Figure 8-2. Porosity in Weld

Uniformly scattered porosity can be found in many weldments and is of little concern, because there are usually large distances of sound metal between the pores. Clustered porosity is often associated with changes in arc conditions. Starting and stopping areas frequently contain clustered porosity. Linear porosity is usually found in the

root pass and is considered a special case of inadequate joint penetration.

c. Incomplete Fusion

Incomplete fusion is the condition in which two weld beads have not fused together or the base metal and a weld bead have not fused (see Fig. 8-3). Incomplete fusion is caused by failure to raise the adjoining material to the fusion temperature or failure to dissolve any oxides or other foreign material on the surface that the new weld bead must fuse to. Incomplete fusion can be avoided by proper cleaning of the weld joint before depositing a new bead and by proper use of welding procedures.



Figure 8-3. Incomplete Fusion at Sidewall and Incomplete Joint Penetration at Root

d. Inadequate Joint Penetrations

Inadequate joint penetration is the condition in which fusion of the weld and base metal at the root of the

joint is less than specified by design (see Figs. 8-3 and 8-4). Although the cause may be a poorly cleaned joint, it is more often heat transfer conditions in the joint that cause inadequate penetration. Heat transfer can be increased by using wider angles for V-grooves or using a root opening. Poor penetration is detrimental to weld joints that will be stressed in service because the root forms a notch that acts as a stress concentrator, which leads to an early failure of the joint.



Figure 8-4. Undercut Weld and Incomplete Penetration at Root

e. Undercutting

Undercutting refers to either a sharp recess in the sidewall of a weld joint or the reduction in thickness of the base plate at the toe of the last weld bead on the surface of the plate (see Fig. 8-4). In both cases, the primary cause of undercutting is the welder's technique. High currents or high voltage, as well as low current and fast travel speeds, may increase the tendency to undercut. If the undercutting is a sharp recess in the joint sidewall, it should be smoothed out.

by grinding or chipping. The surface undercut can easily be detected. The AWS Welding Code has limitations for undercutting.

f. Slag Inclusions

Slag inclusions are oxides or nonmetallic solids that become trapped in the solidifying weld metal. The inclusions can be either completely surrounded by weld metal or be between the weld metal and the base plate. In the SMAW process, chemical reactions between the weld metal and coating materials produce a nonmetallic slag that has low solubility in the weld metal and generally will float to the surface. In some instances, the slag is forced into the weld metal by the stirring action of the arc, or flows ahead of the arc and is covered by the weld metal. Slag inclusions can be prevented by proper cleaning and preparation of the weld joint, by using good technique, or by increasing the heat input and preheat to make the weld metal less viscous and slow the solidification rate. Increasing the heat input provides more energy to melt the slag and the metal and gives the slag more time to float to the surface.

8.3.4 Weld Inspection Methods

A family of methods for investigating the quality, integrity, and dimensions of materials and components without damaging or impairing their serviceability is called nondestructive testing. Any of the following methods may be used in the fabrication of Suppressive Shields.

a. Visual Methods

Visual inspection is always required in weld inspection. Although visual inspection of a weld is the quickest, easiest and cheapest method, internal defects and minute surface defects cannot be detected. The specified size of a weld can be rapidly checked visually by using a welding gage to measure the dimensions of the weld metal. Visual inspection

may be the only type of inspection required for welds which are designed primarily to hold parts together and are not significantly stressed in service. A more efficient method is required if survivability of the structure depends upon the integrity of the weldment.

b. Penetrant Inspection Method

Penetrant inspection is a nondestructive test for discontinuities open to the surface in parts of nonporous materials. This is done by treating the whole area with a fluid which penetrates into the surface discontinuity by capillary action. The surplus penetrant not in the discontinuity is removed. The penetrant remaining in the discontinuity is returned to the surface by an absorbant developer. It is a quick and positive method for detecting many different types of surface discontinuities.

c. Magnetic Particle Inspection Method

Magnetic particle inspection is a rapid non-destructive means of detecting discontinuities in materials having ferromagnetic properties, principally iron and steel. Magnetic particle inspection is accomplished by inducing a magnetic field into a part. A defect will interrupt this field creating new north and south poles with the magnetic flux bridging the defect. This flux leaking attracts the magnetic particles to form the indication. In addition to cracks, the types of flaws that can be detected by an experienced observer include seams, laps, folds, and nonmetallic inclusions that are either surface or slightly subsurface.

d. Ultrasonic Inspection Method

Ultrasonic inspection is a method of inspection using sound waves above the audible range. High frequency sound is induced into the part by a transducer. This ultrasonic energy travels through the part. Any marked changes

in acoustic properties (flaws, interface or back surface) will reflect the sound back to the transducer while a weld without defects will not impede passage of the sound waves. This information is normally displayed on an oscilloscope. Proper selection of transducer, frequency, sensitivity, angle, etc., will enable inspection of the surface, subsurface, and back surface of the part.

e. Radiographic Inspection Method

Radiographic inspection is a nondestructive inspection method utilizing a source of X-rays or gamma rays to detect discontinuities in materials and components. X-rays penetrate metallics and nonmetallics and are differentially absorbed. Discontinuities, which are less dense than metal absorb less radiation and thus are shown on the recording medium as dark shadows. The recording medium is usually film, but it can be any means that converts radiation energy into a visible image. Radiography is used to inspect both metallic and nonmetallic materials. It has the capability of inspecting the interior of opaque objects or assemblies without access to the inside. This method is expensive to use but very reliable and provides a permanent record of the weld quality. Special precautions must be taken to contain the hazardous radiation that is emitted.

8.3.5 Weld Repairs

Repairability of defective welds is probably one of weldings greatest virtues. The quality of a welded structure must be insured by producing sound welds, but flaws in the initial placement of welds are readily repaired as long as adequate inspection methods are used for detection. There is a limit to the amount of weld repair that is advisable in lieu of rejecting a part. Generally, the amount of weld repairs can be quite extensive without affecting the strength of the joint. This is possible because the repair process involves removing

the defect by grinding, chipping, cutting, gas gouging, etc., to expose clean sound surfaces and then replacing the removed material with new weld metal. The metal is, therefore, joined together by weld metal which develops the full strength and cross sectional area of the structural members. Often the appearance of the repaired section is such that it cannot readily be distinguished from the original material.

8.4 CONCRETE

8.4.1 General

Concrete is a much more variable construction material than steel and its final properties are much more dependent on its constituents and methods of mixing, placing and curing. Hydraulic cements are used almost exclusively for the manufacture of structural concrete and the most common type used is portland cement. Concrete tensile strength is very low compared to its compressive strength and, therefore, it is always combined with steel reinforcing in suppressive shield applications. Quality assurance requires close inspection at all stages of mixing, placing and curing. This would reduce the problem of voids, a problem in some suppressive shield foundations.

8.4.2 Mixing

Quality control in the mixing operations must begin with the selection of materials. Cements, aggregate admixtures and mixing water must meet the standard specifications of the American Society for Testing Materials. Reference 8-1 contains a list of the applicable specifications. Mixture designs can be obtained using standard procedures and should be verified by a suitable test program.

The cement-water ratio is the chief factor controlling the strength of concrete. It also affects the workability

of the concrete and an inspector must be vigilant to prevent the addition of water to a mix to improve its workability at the expense of its compressive strength. Once a mix design has been developed, the slump test provides a reasonably quick field check on quality control.

The principal purpose of mixing is to produce an intimate mixture of cement, water, fine and coarse aggregate. This is achieved in machine mixers of the revolving-drum type. Minimum mixing time is 1.5 minutes. Mixing can be continued for a considerable time without adverse effect. This fact is particularly important in connection with ready-mixed concrete.

On large projects, where ample space is available, mixing plants are installed and operated at the site. On smaller jobs, ready-mixed concrete is used. Such concrete is batched in a stationary plant and then hauled to the site in trucks in various ways. The most common method is transit-mixed, i.e., batched at the plant but mixed in a truck mixer. Concrete should be discharged from the mixer or agitator within at most one and a half hours after the water is added to the batch.

8.4.3 Placing

Most structural concrete is carried from the mixer or truck to the form in wheelbarrows or buggies or by pumping through pipelines. The chief danger during conveying is that of segregation. The individual components of concrete tend to segregate because of their dissimilarity. In overly wet concrete standing in containers or forms, the heavier gravel components tend to settle, and the lighter materials, particularly water, tend to rise. Lateral movement within the forms tends to separate the coarse gravel from the finer components of the mix. The danger of segregation has caused the discarding of some previously common means of conveying, such as chutes and conveyor belts, in favor of methods which minimize this tendency.

Prior to placing, loose rust must be removed from reinforcement, forms must be cleaned, and hardened surfaces of previous concrete lifts must be cleaned and treated appropriately. Proper placement must avoid segregation, displacement of forms or of reinforcement in the forms, and poor bond between successive layers of concrete. Immediately upon placing, the concrete should be compacted by means of hand tools or vibrators. Such compacting prevents honeycombing, assures close contact with forms and reinforcement, and serves as a partial remedy to possible prior segregation. Compacting is achieved most commonly with high-frequency, power-driven vibrators. These are of the internal type, immersed in the concrete, or of the external type, attached to the forms. The former are preferable, but must be supplemented by the latter where narrow forms or other obstacles make immersion impossible.

8.4.4 Curing

Fresh concrete gains strength most rapidly during the first few days and weeks. Structural design is generally based on the 28-day strength, about 70 percent of which is reached at the end of the first week after placing. The final concrete strength depends greatly on the conditions of moisture and temperature during this initial period. Thirty per cent or more of the strength can be lost by premature drying out of the concrete; similar amounts may be lost by permitting the concrete temperature to drop to 40°F or lower during the first few days, unless the concrete is maintained continuously moist for a long time thereafter. Freezing of fresh concrete may reduce its strength by as much as 50 percent.

Concrete should be protected from loss of moisture for at least 7 days and, in more sensitive work, up to 14 days. When high-early-strength cements are used, curing periods can be reduced. Curing can be achieved by keeping exposed surfaces

continually wet through sprinkling, ponding, covering with wet burlap, or the like. Sealing compounds, when properly used, form evaporation-retarding membranes. In addition to improved strength, proper moist curing provides better shrinkage control. To protect the concrete against low temperature during cold weather, the mixing water and, occasionally, the aggregates are heated. Temperature insulation is used where possible and when air temperatures are very low, external heat may have to be supplied in addition to insulation.

8.4.5 Quality Control

Because of the variability in the properties of concrete, a systematic quality control program must be instituted at the construction site. The primary measure of the structural quality of concrete is its compression strength. Tests for this property are made on cylindrical specimens prepared in accordance with ASTM C172, Method of Sampling Fresh Concrete, and ASTM C31, Method of Making and Curing Concrete Specimens in the Field. The cylinders are moist-cured, generally for 28 days, and then tested in the laboratory at a specified rate of loading. The compression strength obtained from such tests is known as the unconfined compressive strength, f'_c and is the main property specified for design purposes.

Inspection during construction should be carried out by a competent engineer, preferably the one who produced the design or one who is responsible to the design engineer. The inspector's main functions in regard to materials quality control are sampling, examination, and field testing of materials, control of concrete proportioning, inspection of batching, mixing, conveying, placing, compacting, and curing, and supervision of preparation of specimens for laboratory tests. In addition, he must inspect formwork, placing of reinforcing steel, and other embedded items. Deficiencies in these items are impossible to detect after placement of concrete. The importance of thorough inspection to the correctness and adequate

quality of the finished structure cannot be emphasized too strongly.

8.5 FIBER REINFORCED CONCRETE

The low tensile strength and brittle character of conventional concrete can be improved by the addition of metallic, organic or inorganic fibers. Several investigators have found that the energy absorption capacity of fiber reinforced concrete is at least an order of magnitude higher than that of plain concrete (Ref. 8-2). Studies and tests have indicated that randomly distributed fibers in concrete increase considerably the spalling and shatter resistance of concrete members which are subjected to explosive loadings such as those of suppressive shields. Steel fibers, up to about 4 percent by volume, were found to increase the first crack flexural strength of concrete up to 2.5 times that of the unreinforced materials and slightly improve the compressive strength. The steel fibers used in concrete have lengths ranging from 0.25 to 3 inches. The round fibers have diameters between 6 and 30 mils. Flat steel fibers have cross sections ranging from 6 to 16 mils in thickness by 10 to 35 mils in width.

Although the fibers can enhance the properties of concrete, they can present problems in mixing and placement. Fibrous concrete requires a considerably greater amount of fine material than does plain concrete to achieve the same degree of workability. Reference 8-2 discusses some alternate techniques for adjusting workability.

The addition of steel fibers to concrete greatly influences its mixing characteristics. Each piece of mixing equipment has its own operating characteristics and will require a procedure tailor-made for the type of equipment to be used. The equipment should be checked out if it has not been previously used to mix fibrous concrete. Excess mixing has a tendency to develop fiber

balls in certain types of mixers, and, generally, additional mixing will not break up the balls. To alleviate this problem, the fibers may be dispersed in and among the coarse aggregate prior to the addition of the fine aggregate, cement, and water.

The aspect ratio (ratio of fiber diameter or width to length) also affects the tendency toward balling. The higher the ratio, the more likely balling will occur. If balling occurs, the fiber balls should be picked out before they reach the forms. The addition of fibers decreases the mobility of concrete mixes, and problems with consolidation can occur if the spacing between the reinforcing bars is too small. The time to consolidate the concrete increases drastically when the bar spacing is less than twice the length of the fibers.

Fiber reinforced concrete was utilized in the Group 3 Suppressive Shield roof and foundation with great success. The use of fiber reinforced concrete in all new suppressive shield construction is highly recommended as an additional safety precaution.

8.6 REFERENCES

- 8-1 Building Code Requirements for Reinforced Concrete,
ACI Standard 318-71, American Concrete Institute,
Detroit, Mich., 1971. (U)
- 8-2 Gray, B.H., Williamson, G.R., and Batson, G.B.,
Fibrous Concrete Construction Material for the
Seventies, Construction Engineering Research Labor-
atory, Champaign, Ill., May 1972. (U)

APPENDIX A

SAFETY APPROVED SUPPRESSIVE SHIELDS

APPENDIX A

SAFETY APPROVED SUPPRESSIVE SHIELDS

A.1 INTRODUCTION

This appendix describes the safety approved suppressive shield designs in some detail and provides guidance concerning acceptable modifications. Brief information is provided in Tables A-1 through A-8 concerning each design group's physical size, weight, construction, and cost. Charge weights used for design and to proof test each shield group are listed in the tables for various types of explosives. The explosive quantities are also shown in terms of their TNT equivalent. The calculated values for reflected impulse, reflected pressure, and quasi-static pressure were obtained from Chapter 3 using the TNT equivalent weight. Measured values are included in the tables where data were available. Most of the information contained in Tables A-3 through A-6 and Table A-8 has been extracted from safety approval documentation (Ref. A-1). Additional information on the approved safety shield designs is presented in the following paragraphs of this appendix.

In general, the methods used for designing suppressive shields have always been conservative. However, some of the suppressive shields were designed and proof tested early in the development of suppressive shielding technology and may be over-designed. The methods of analysis presented in this handbook are current design techniques which were not used in the earlier design developments. Some of the earliest designs were the Shield Groups 4, 5 and the Prototype 81-mm Shield. Later designs which used the methods of analysis presented in this handbook include Shield Groups 3, 6 and Milan 81-mm Suppressive Shield.

Copies of the fabrication drawings for each approved shield

Table A-1

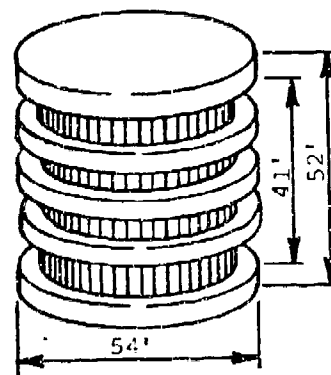
SUPPRESSIVE SHIELD GROUP 1

Inside dimensions: 46 ft diameter,
41 ft high

Weight: 5,760,000 lb

Type construction: Interlocked I-beam
walls with steel
liner and reinforced
concrete base and top.

Unit cost: 84,144 man-hours, ap-
proximately \$1,100,000
(est) (1975 costs)



Charge weight (Comp B):

- a. Design 2,500 lb (2870 lb TNT equiv.)
- b. Proof (25% overcharge) 3,125 lb (3588 lb TNT equiv.)

Reflected impulse (sidewall):

	<u>Calculated</u>	<u>Measured</u>
a. Design	1364 psi-ms	N/A
b. Proof	1647 psi-ms	Not tested

Reflected pressure (sidewall):

	<u>Calculated</u>	<u>Measured</u>
a. Design	2800 psi	N/A
b. Proof	3200 psi	Not tested

Quasi-static pressure:

	<u>Calculated</u>	<u>Measured</u>
a. Design	160 psi	N/A
b. Proof	185 psi	Not tested

Blowdown time (design): 58 msec with $\alpha = 5.0\%$ (total w/o liner)
600 msec with $\alpha_e = 0.4\%$ (total w/ liners)

Nominal wall thickness (fragment stopping): 4 inches steel

Status: Preliminary design concept complete; not safety approved;
testing may be required for approval.

Table A-2

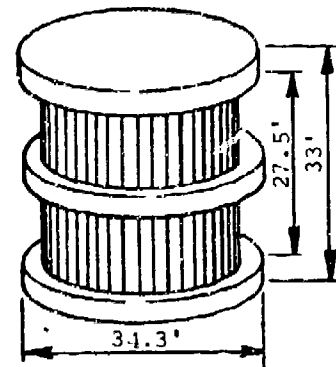
SUPPRESSIVE SHIELD GROUP 2

Inside dimensions: 31 ft diameter,
27.5 ft high

Weight: 1,581,840 lb

Type construction: Interlocked I-beam
walls with steel
liner and reinforced
concrete base and top.

Unit cost: 32,496 man-hours, ap-
proximately \$475,000
(est) (1975 costs)



Charge weight (Comp B):

- a. Design 750 lb (861 lb TNT equiv.)
- b. Proof (25% overcharge) 937.5 lb (1076 lb TNT equiv.)

Reflected impulse (sidewall):

		<u>Calculated</u>	<u>Measured</u>
a.	Design	913 psi-ms	N/A
b.	Proof	1102 psi-ms	Not tested

Reflected pressure (sidewall):

		<u>Calculated</u>	<u>Measured</u>
a.	Design	2800 psi	N/A
b.	Proof	3200 psi	Not tested

Quasi-static pressure:

		<u>Calculated</u>	<u>Measured</u>
a.	Design	160 psi	N/A
b.	Proof	185 psi	Not tested

Blowdown time (design): 58 msec with $\alpha_e = 5.0\%$ (total w/o liner)
600 msec with $\alpha_e = 0.4\%$ (total w/ liners)

Nominal wall thickness (fragment stopping): 2.7 inches steel

Status: Preliminary design concept complete; not safety approved;
testing may be required for approval.

Table A-3

SUPPRESSIVE SHIELD GROUP 3

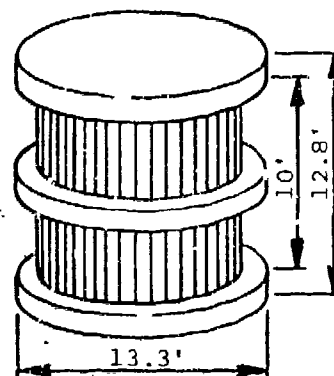
Note: Shield Group 3 is a one-quarter geometrical scale model of Shield Group 1.

Inside dimensions: 11.25 ft diameter,
10 ft high

Weight: 90,000 lb

Type construction: Interlocked I-beam
walls with steel
liner and reinforced
concrete base and top.

Unit cost: 5,259 man-hours, ap-
proximately \$75,000 (1975 costs)



Charge weight (50-50 pentolite):

- a. Design 36.6 lb (41.32 lb TNT equiv.)
- b. Proof (25% overcharge) 45.7 lb (51.6 lb TNT equiv.)

Reflected impulse (sidewall):

	<u>Calculated</u>	<u>Measured</u>
a. Design	333 psi-ms	N/A
b. Proof	402 psi-ms	435 psi-ms

Reflected pressure (sidewall):

	<u>Calculated</u>	<u>Measured</u>
a. Design	2800 psi	N/A
b. Proof	3200 psi	2386 psi

Quasi-static pressure:

	<u>Calculated</u>	<u>Measured</u>
a. Design	160 psi	N/A
b. Proof	185 psi	187 psi

Blowdown time (design): 52 msec with $\alpha_e = 5.0\%$ (total w/o liner)
600 msec with $\alpha_e = 0.4\%$ (total w/ liners)

Nominal wall thickness (fragment stopping): 1 inch steel

Status: Safety approved

Table A-4

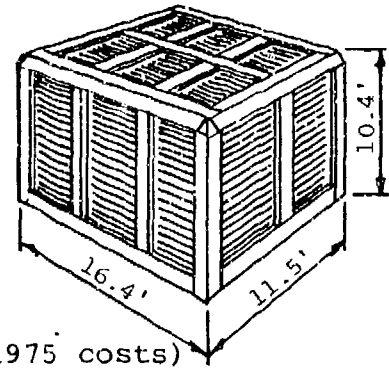
SUPPRESSIVE SHIELD GROUP 4

Inside dimensions*: 9.2 ft wide
x 13.1 ft long
x 9.3 ft high

Weight: 79,159 lb

Type construction: I-beam frame with
panels of nested angles
and perforated plates.

Unit cost: 6,500 man-hours, ap-
proximately \$105,000 (1975 costs)



Charge Weight (50/50 Pentolite):

- a. Design 9 lb (10.16 lb TNT equiv.)
- b. Proof (25% overcharge) 11.25 lb (12.7 lb TNT equiv.)

Reflected impulse (sidewall):

	<u>Calculated</u>	<u>Measured</u>
a. Design	147 psi-ms	N/A
b. Proof	170 psi-ms	-

Reflected pressure (sidewall):

	<u>Calculated</u>	<u>Measured</u>
a. Design	1150 psi	N/A
b. Proof	1480 psi	1143 psi

Quasi-static pressure:

	<u>Calculated</u>	<u>Measured</u>
a. Design	62 psi	N/A
b. Proof	70 psi	44 psi

Blowdown time (design): 51 ms with $\alpha_e = 3.0\%$ (total)

Nominal wall thickness (fragment stopping): 1.46 inches steel

Status: Safety approved

* Dimensions given are for equipment clearance; dimensions for pressure calculations are 9.48'H x 9.66'W x 14.56'L.

Table A-5

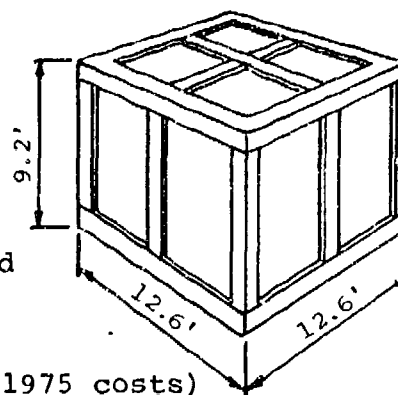
SUPPRESSIVE SHIELD GROUP 5

Inside dimensions: 10.4 ft wide
x 10.4 ft long
x 8.5 ft high

Weight: 16,772 lb

Type construction: Steel frame with
panels of angles,
perforated plates and
screens.

Unit Cost: 3,174 man-hours, ap-
proximately \$55,000 (1975 costs)



Charge weight (C-4):

- a. Design 1.84 lb (1.98 lb TNT equiv.)
- b. Proof (25% overcharge) 2.44 lb (2.63 lb TNT equiv.)

Reflected impulse (sidewall):

	<u>Calculated</u>	<u>Measured</u>
a. Design	46.5 psi-ms	N/A
b. Proof	56.6 psi-ms	68 psi-ms

Reflected pressure (sidewall):

	<u>Calculated</u>	<u>Measured</u>
a. Design	150 psi	N/A
b. Proof	192 psi	346 psi

Quasi-static pressure:

	<u>Calculated</u>	<u>Measured</u>
a. Design	26 psi	N/A
b. Proof	32 psi	33 psi

Blowdown time (design): 5 ms with $\alpha_e = 15.5\%$ (panels)

Nominal wall thickness (fragment stopping): 0.427 inch steel

Status: Safety approved

Table A-6a

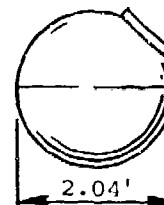
SUPPRESSIVE SHIELD GROUP 6A

Inside dimensions: 2 ft diameter

Weight: 165 lb

Type construction: Mild steel sphere
(no venting)

Unit cost: 130 man-hours, approximately \$2,500 (1975 costs)



Charge weight (50-50 pentolite):

- a. Design 13.63 oz (0.962 lb TNT equiv.)*
- b. Proof (25% overcharge) 17.04 oz (1.202 lb TNT equiv.)

Reflected impulse:

	<u>Calculated</u>	<u>Measured</u>
a. Design	195 psi-ms	N/A
b. Proof	234 psi-ms	-

Reflected pressure:

	<u>Calculated</u>	<u>Measured</u>
a. Design	6900 psi	N/A
b. Proof	7800 psi	-

Quasi-static pressure:

	<u>Calculated</u>	<u>Measured</u>
a. Design	480 psi	N/A
b. Proof	570 psi	600 psi

Blowdown time (design): N/A

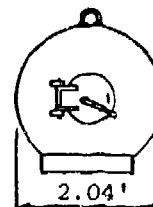
Nominal wall thickness (fragment stopping): 0.25 inch steel

Status: Safety approved

* The design charge can be a single charge or multiple charges which do not exceed the total specified charge weight. See paragraph A.5.2.a for multiple charge criteria.

Table A-6b (concluded)
SUPPRESSIVE SHIELD GROUP 6B

Inside dimensions: 2 ft diameter
Weight: 165 lb
Type construction: Stainless steel sphere
(no venting)
Unit cost: 130 man-hours, approximately \$2,500 (1975 costs)



Charge weight (C-4):

- a. Design 8.23 oz (0.5545 lb TNT equiv.)*
- b. Proof (25% overcharge) 10.29 oz (0.693 lb TNT equiv.)

Reflected impulse:

	<u>Calculated</u>	<u>Measured</u>
a. Design	119 psi-ms	N/A
b. Proof	144 psi-ms	-

Reflected pressure:

	<u>Calculated</u>	<u>Measured</u>
a. Design	4900 psi	N/A
b. Proof	5700 psi	-

Quasi-static pressure:

	<u>Calculated</u>	<u>Measured</u>
a. Design	330 psi	N/A
b. Proof	390 psi	-

Blowdown time (design): N/A

Nominal wall thickness (fragment stopping): 0.25 inch steel

Status: Safety approved

*The design charge can be a single charge or multiple charges which do not exceed the total specified charge weight. See paragraph A.5.2.b for multiple charge criteria.

Table A-7

SUPPRESSIVE SHIELD GROUP 7

Final design criteria have not been established for the Group 7 shield, and its further development is currently unfunded.

Table A-8a

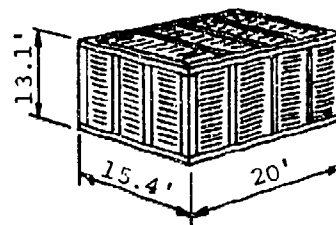
PROTOTYPE 81-mm SHIELD

Inside dimensions: 14 ft wide
x 18.7 ft long
x 12.4 ft high

Weight: 50,000 lb

Type construction: Box-beam frame with
panels of Z-shapes and
perforated plates.

Unit cost: 4,095 man-hours, ap-
proximately \$80,000 (1975 costs)



Design charge weight:

- a. 6.72 lb C-4 (7.24 lb TNT equiv.) for incident and reflected overpressure and impulse.
- b. 10.1 lb C-4 (10.9 lb TNT equiv.) for quasi-static pressure; $W/V = 0.0034 \text{ lb/ft}^3$ (for TNT equiv.)
- c. 4 ea. M374, 81-mm mortar projectiles

Reflected pressure (sidewall):

	<u>Calculated</u>	<u>Measured</u>
a. Design	220 psi	N/A
b. Proof	260 psi	-

Quasi-static pressure:

	<u>Calculated</u>	<u>Measured</u>
a. Design	36 psi	N/A
b. Proof	42 psi	-

Blowdown time (design): 85 ms with $\alpha_e = 4.3\%$ (total)

Nominal wall thickness (fragment stopping): 1.23 inches steel

Status: Safety approved

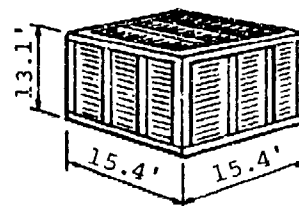
Table A-8b (concluded)

MILAN 81-mm SUPPRESSIVE SHIELD

Inside dimensions: 14 ft wide
 x 14 ft long
 x 12.4 ft high

Weight: 40,625 lb

Type construction: Box-beam frame with
 panels of Z-shapes and
 perforated plates.



Unit cost: To be determined

Design charge weight:

- a. 4.2 lb C-4 (4.53 lb TNT equiv.) for incident and reflected overpressure and impulse.
- b. 6.3 lb C-4 (6.79 lb TNT equiv.) for quasi-static pressure; $W/V = 0.0028 \text{ lb/ft}^3$ (for TNT equiv.)
- c. 3 ea M374, 81-mm mortar projectiles

Reflected pressure (sidewall):

	<u>Calculated</u>	<u>Measured</u>
a. Design	150 psi	N/A
b. Proof	180 psi	N/A

Quasi-static pressure:

	<u>Calculated</u>	<u>Measured</u>
a. Design	32 psi	N/A
b. Proof	37 psi	N/A

Blowdown time (design): 78 ms with $\alpha_e = 4.3\%$ (total)

Nominal wall thickness (fragment stopping): 1.23 inches steel

Status: Safety approved

design are included in this appendix. Authorized agencies may obtain full-size copies of the drawings from the U.S. Army Engineer Division, Huntsville, HNDED-CS, P. O. Box 1600, West Station, Huntsville, Alabama 35807.

A.2 SHIELD GROUP 3

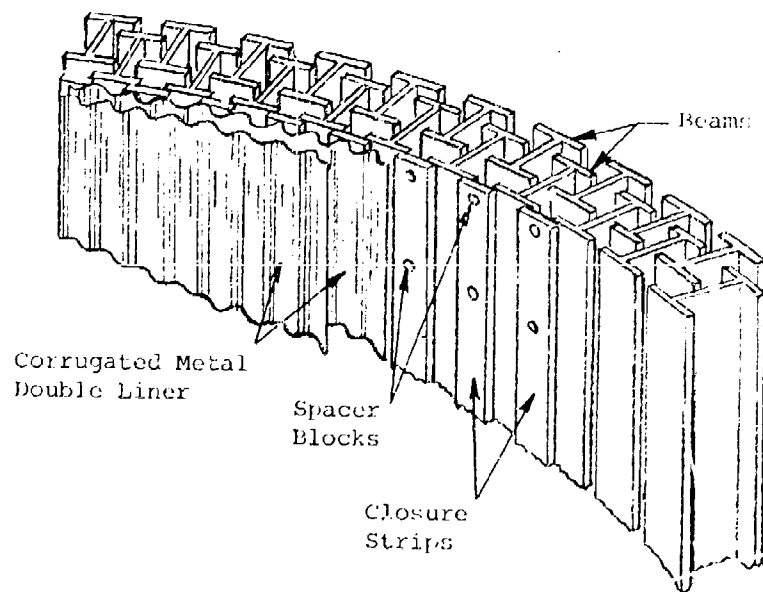
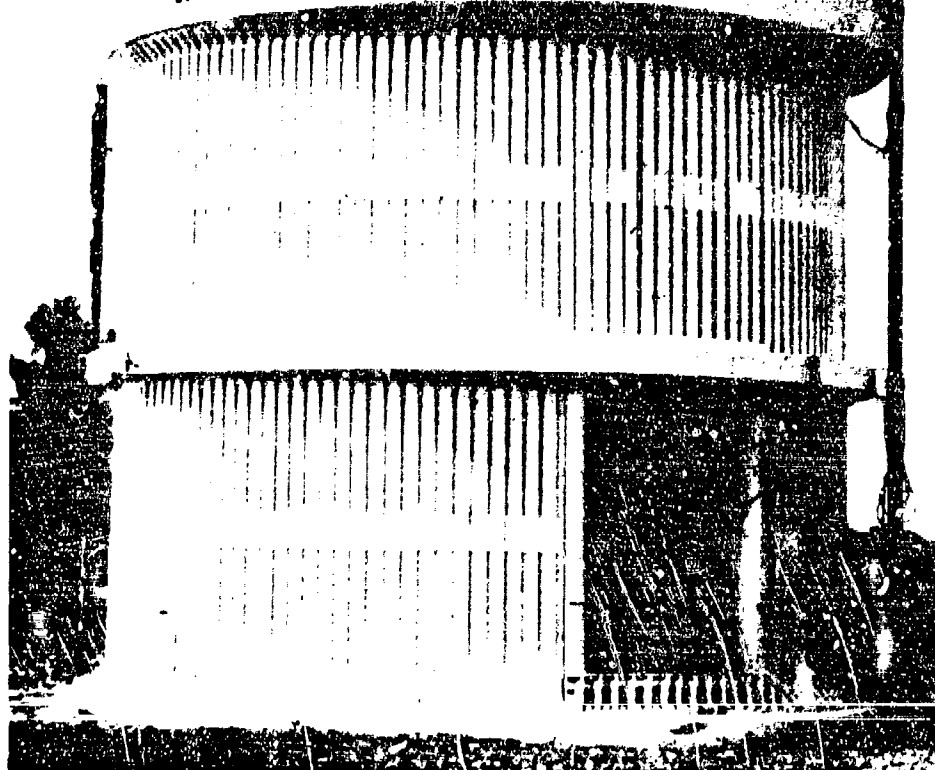
A.2.1 Description

The Group 3 suppressive shield is of cylindrical configuration with walls of interlocked I-beams and a reinforced concrete roof and foundation as illustrated in Fig. A-1. The inside dimensions are 11.25-foot diameter and 10 feet high; the outside dimensions are 13.3-foot diameter and 12.8 feet high.

The sidewalls of the cylinder are assembled by using S3 x 5.7 beams interlocked as illustrated in Fig. A-1. Reinforced concrete slabs attach to and support the upper and lower ends of the vertical beams. In addition to the support provided the beams by the roof and foundation, there is an intermediate steel hoop encircling the middle of the cylinder. The hoop is fabricated from 10 layers of 5-inch wide by 1/2-inch thick steel plates. Joints in each 1/2-inch plate of a hoop are welded together to ensure continuity around the hoop. The construction details are shown in Fig. A-2.

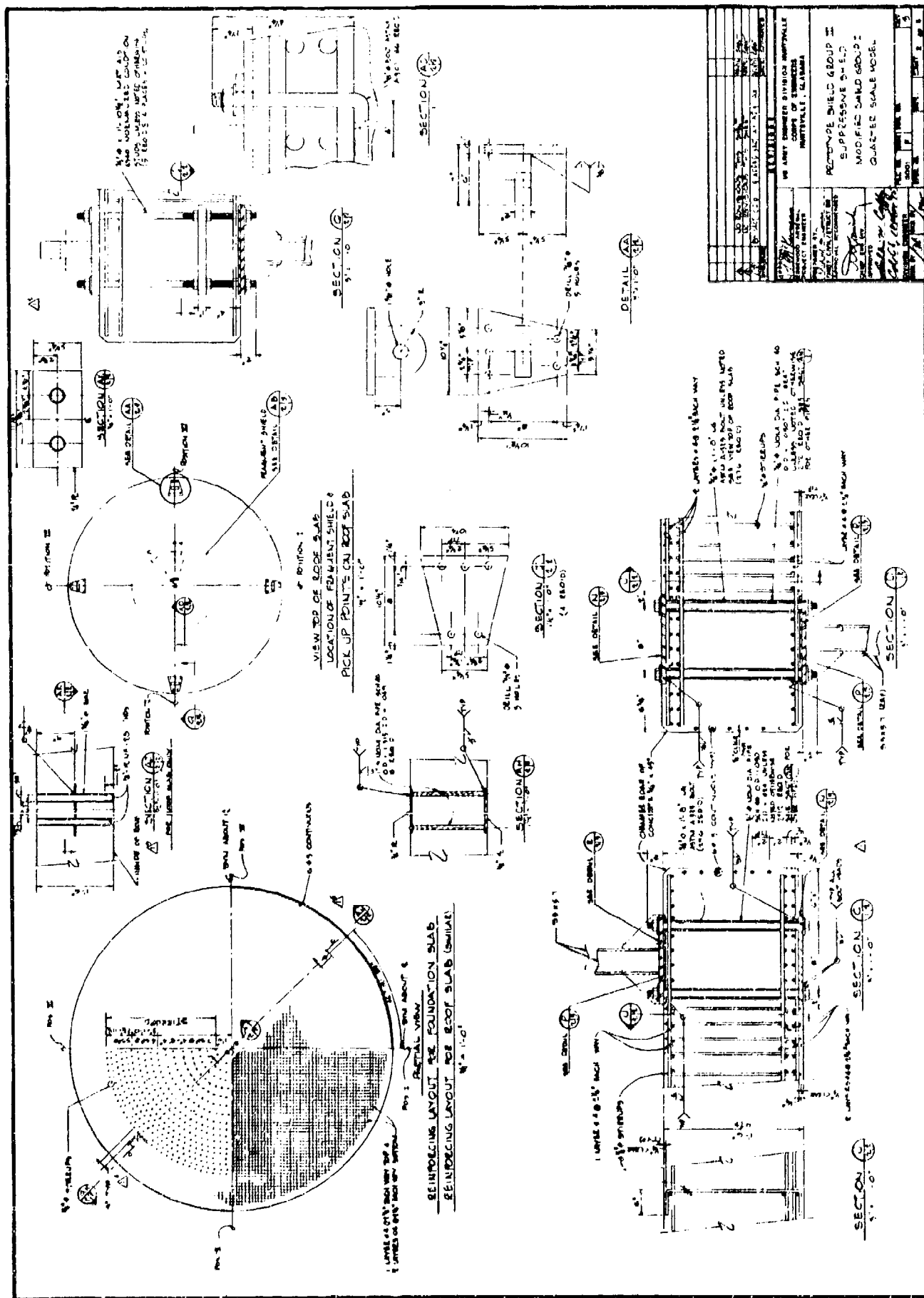
Access to the interior of the shield is provided by double-leaf doors swinging inward. The door leaves shown in Fig. A-3 are curved to match the contour of the shield walls and fabricated using deeper beam sections than those of the walls; see Fig. A-2c. Top and bottom plates of 1/2-inch steel maintain the individual beams in their relative positions. Edges of the opening for the door are reinforced with square steel tubing which also serves as a hinge support for each door half. When the doors are closed, the upper edge is restrained from blowing outward by the band circling the middle of the shield. The lower edge butts against a restraint constructed from a piece of

BRL-TEST 198



Wall Cross Section Detail

Figure A-1. Group 3 Suppressive Shield

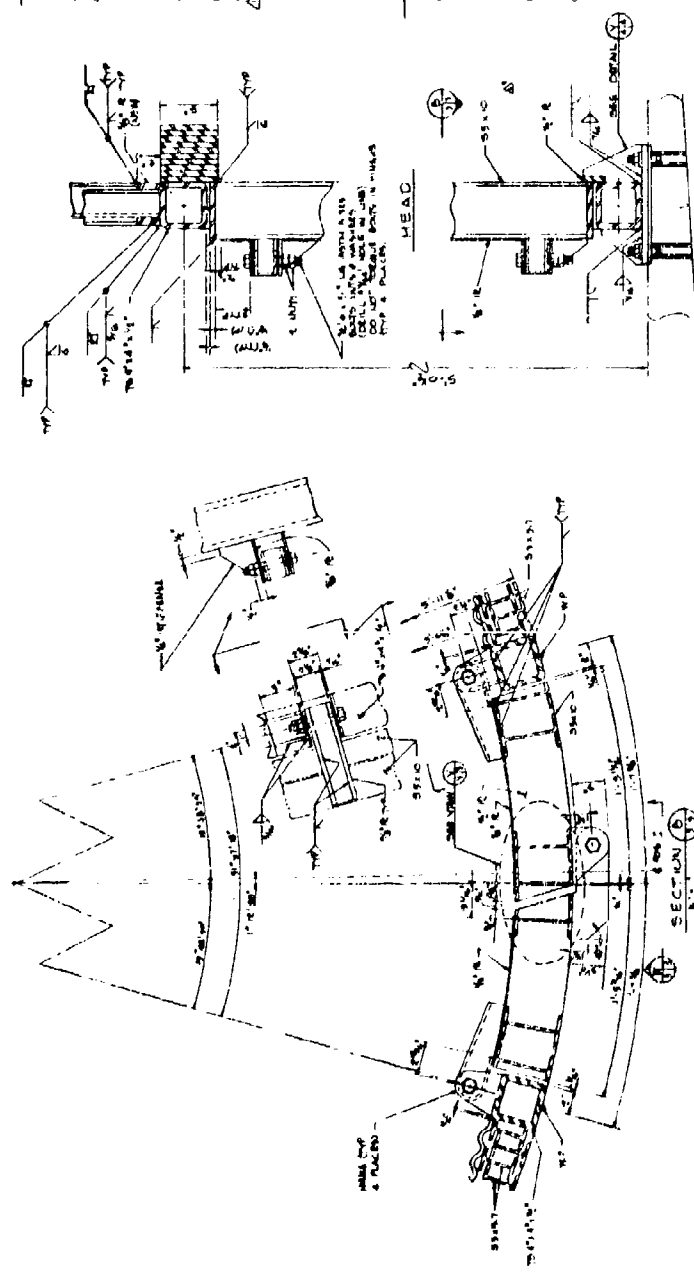


STRUCTURAL STEEL NOTES

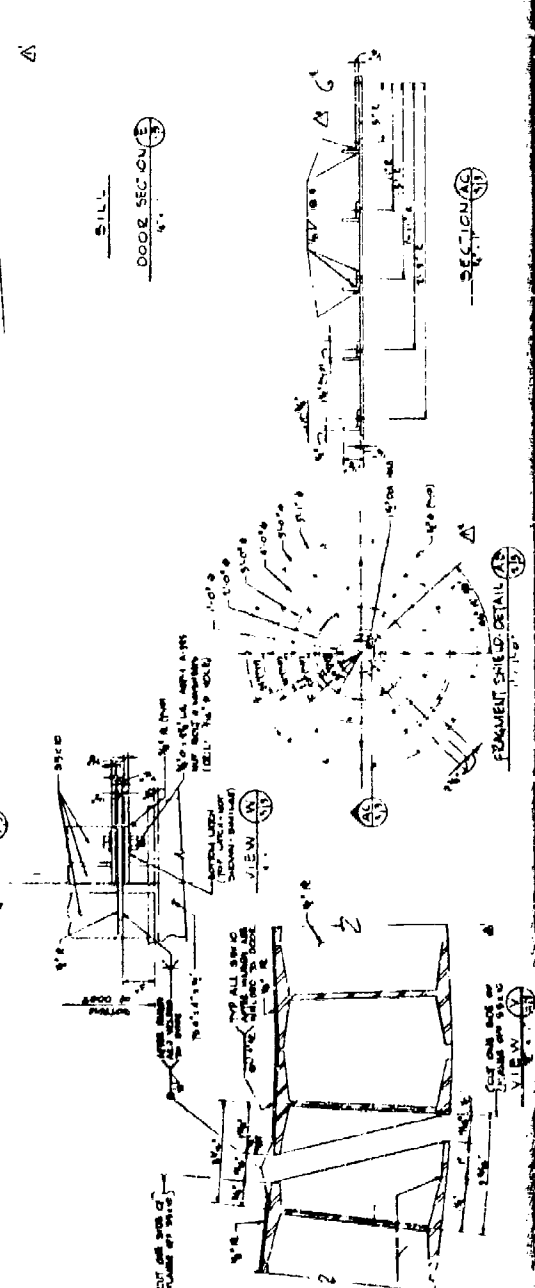
- [illegible]

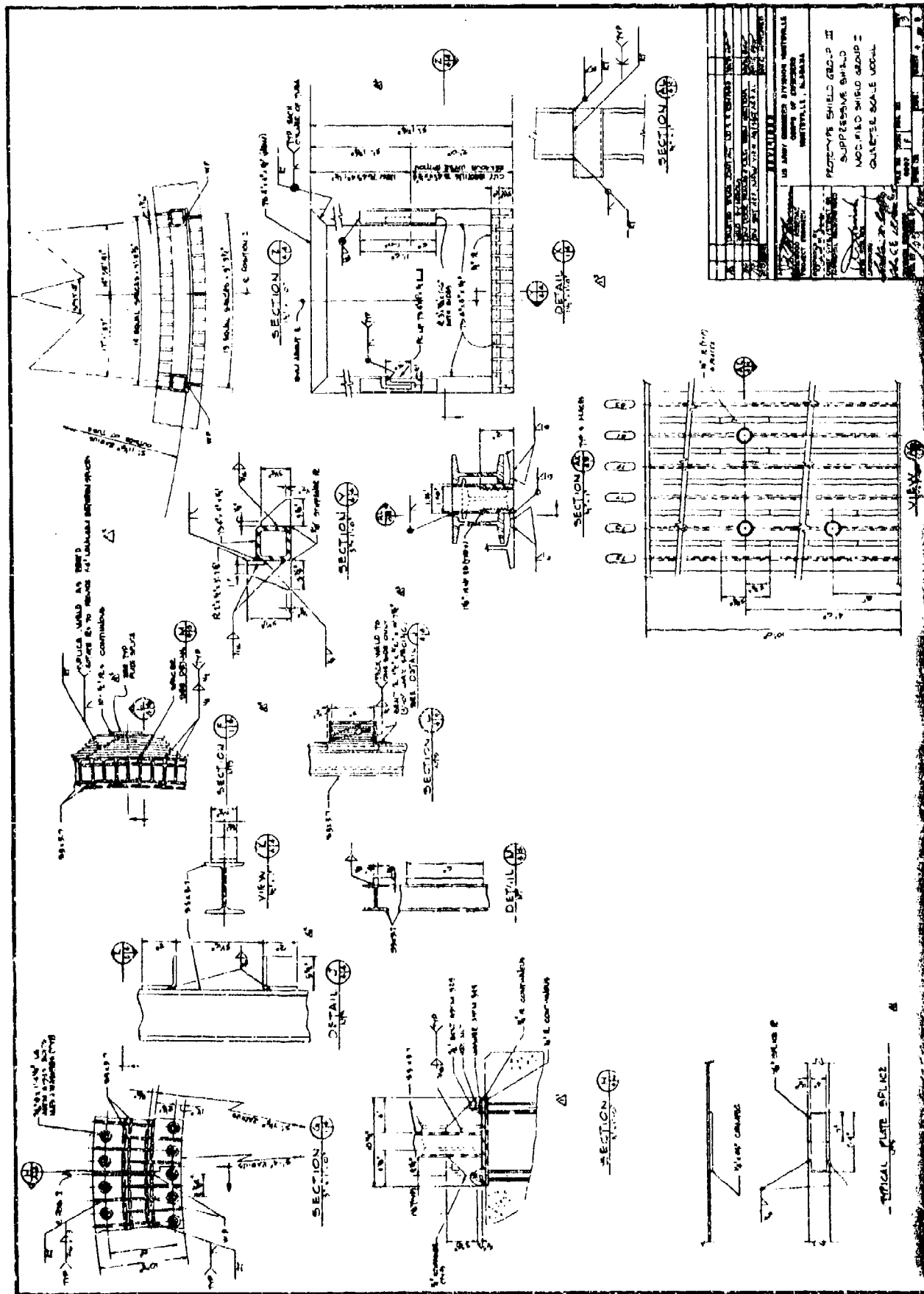
PAINTING VOTES

- [illegible]



51715
DOOR SEC NO 3

[illegible]



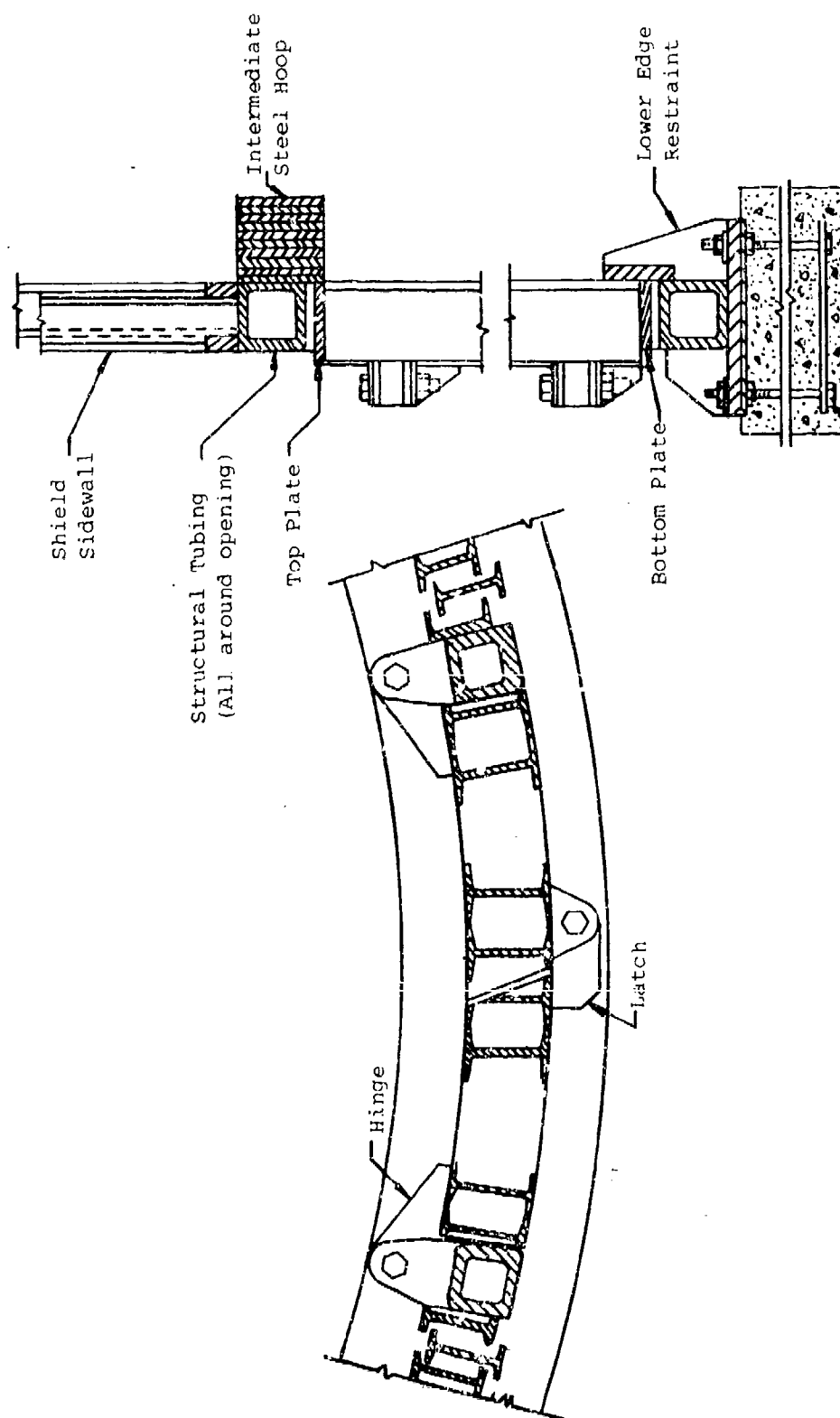


Figure A-3. Door - Group 3 Shield

square steel tubing anchored to the shield foundation. A latch between the two leaves maintains the door in the closed position.

Gaps between exposed flanges inside the shield are covered with closure strips. The strips are 1-1/2 inches wide by 1/4 inch thick and have 1/4-inch diameter holes along their centerlines for plug welding to the outer layers of the staggered beams. Edges of the closure strips are tack welded to the beam flanges onto which they overlap.

Dust from a manufacturing process could cause accumulation of explosive materials in hazardous amounts. To prevent explosive dust from accumulating in the interior of the structure walls or escaping outside the shield, two liners of 1/2 x 2-inch x 22 gauge corrugated steel plate are placed on the inside surface of the shield. Two liners were chosen based on results of the proof-test series. One liner was adequate for the shielding function but was severely distorted by the detonation. Subsequently, the two-liner concept was tested with good results and adopted for future use. A frangible liner of Velostat plastic is applied to the exterior surface of the shield to prevent the entry and accumulation of explosive dust within the shield wall.

The Group 3 shield foundation and roof are circular monolithic reinforced concrete slabs; details of the slab designs are shown in Fig. A-2. The slabs are 13 feet 4 inches in diameter, 18 inches thick and designed in accordance with TM5-1300 procedures. The foundation and roof exhibited only superficial cracking during proof tests of the Group 3 shield.

A.2.2 Application

The Group 3 shield design has been tested and safety approved for 36.6 pounds of 50/50 pentolite (41.32 lb TNT equivalent). Typical applications of this design are (a) 5.56-mm blank cartridge loading and (b) 20/30-mm HEI (High Explosive Incendiary) projectile fill and press operations.

Based on the test results, external pressure will be reduced to 2.3 psi at a distance of 6.2 feet from the exterior of the shield. The fireball is restricted to within four feet of the shield wall.

The Group 3 suppressive shield design can be utilized for operations that

- Require a maximum 100 square feet of floor area with a 10-foot maximum clear height.
- Involve bare charge weights equivalent to 36.6 pounds of 50/50 pentolite (41.32 lb TNT equiv.; maximum W/V ratio = 0.04157 lb/ft³; minimum Z = 1.627 ft/lb^{1/3} to side-wall and minimum Z = 1.446 ft/lb^{1/3} for roof).
- Produce no fragments that cannot be defeated by one inch of mild steel.
- Are compatible with a fireball at four feet and external pressure of 2.3 psi at 6.2 feet from the exterior of the shield.

A.2.3 Modification

The height of the shield may be increased or decreased modularly by adding or removing bands and using longer or shorter beam lengths. However, the free span cannot be changed, the ratio of W/V may not be increased, and Z cannot be decreased. The shield size may be scaled down provided the stress levels calculated using the analysis methods provided in Chapter 5 are equal to or lower than those in the safety approved shield design.

In addition to the structural adequacy of a proposed Group 3 shield modification, the fragment threat for any application must be such that the threat is defeated by one inch of mild steel.

A.3 SHIELD GROUP 4

A.3.1 Description

The Group 4 suppressive shield shown in Fig. A-4 employs a modular configuration consisting of a steel frame with panels made up of nested angles and perforated plates. The nominal outside dimensions are 11.5 feet wide by 16.4 feet long by 10.4 feet high; the inside dimensions are 9.2 feet wide by 13.1 feet long by 9.3 feet high.

Construction details for the Group 4 suppressive shield are shown in Fig. A-5. The structural framing members are W14 x 61 wide flange steel sections. A schematic of the structural frame is shown in Fig. A-6. The lower ends of the vertical members are attached to a 3/4-inch base plate which covers the entire floor of the shield.

The panels spanning between the framing members have the cross section shown in Fig. A-4. There are four layers of 3/16-inch perforated steel plate. One plate is on the innermost face of the panels, and three are spaced slightly apart near the panel centerline. The two layers of interlaced structural steel angles provide stiffness to the panel and resistance against fragment penetration. The panels are installed in the frame and wedged into place as shown in Fig. A-6b.

The Group 4 shield will typically utilize a slab on grade foundation such as shown in Fig. A-5f. High speed motion pictures of the Group 4 proof tests showed an upward movement of the structure of from 1 to 2 inches because the structure was not rigidly attached to its foundation. This movement could cause problems in an operating environment if utility penetrations are not appropriately designed. Foundation tiedown procedures used in the Group 5 or 81-mm shield may be applied to this shield if rigid tiedown is required.

Access to the Group 4 shield is provided by a sliding door. The cross section of the door is identical to the sidewall

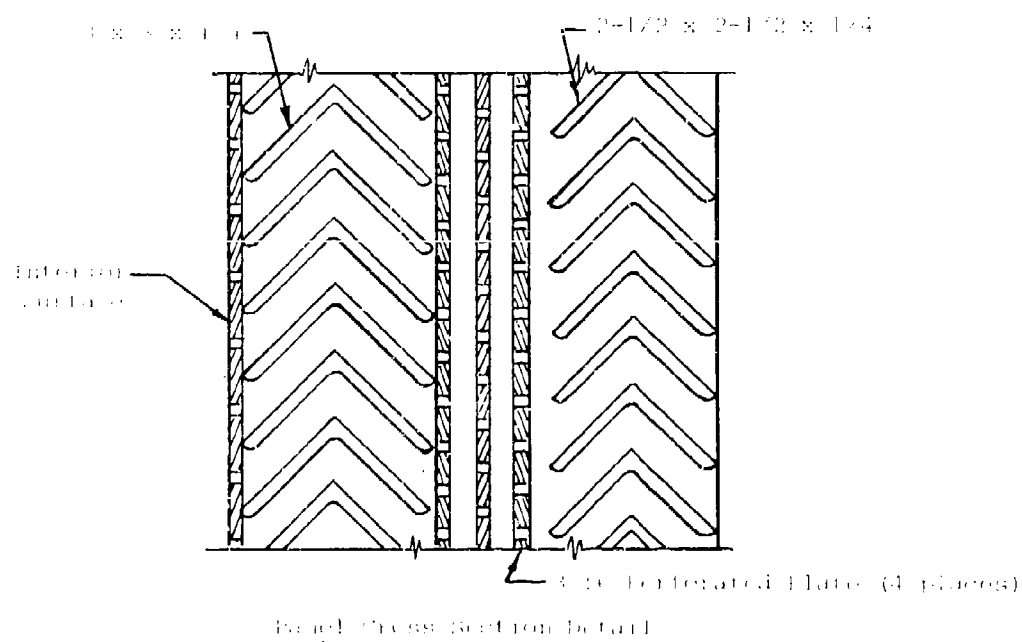
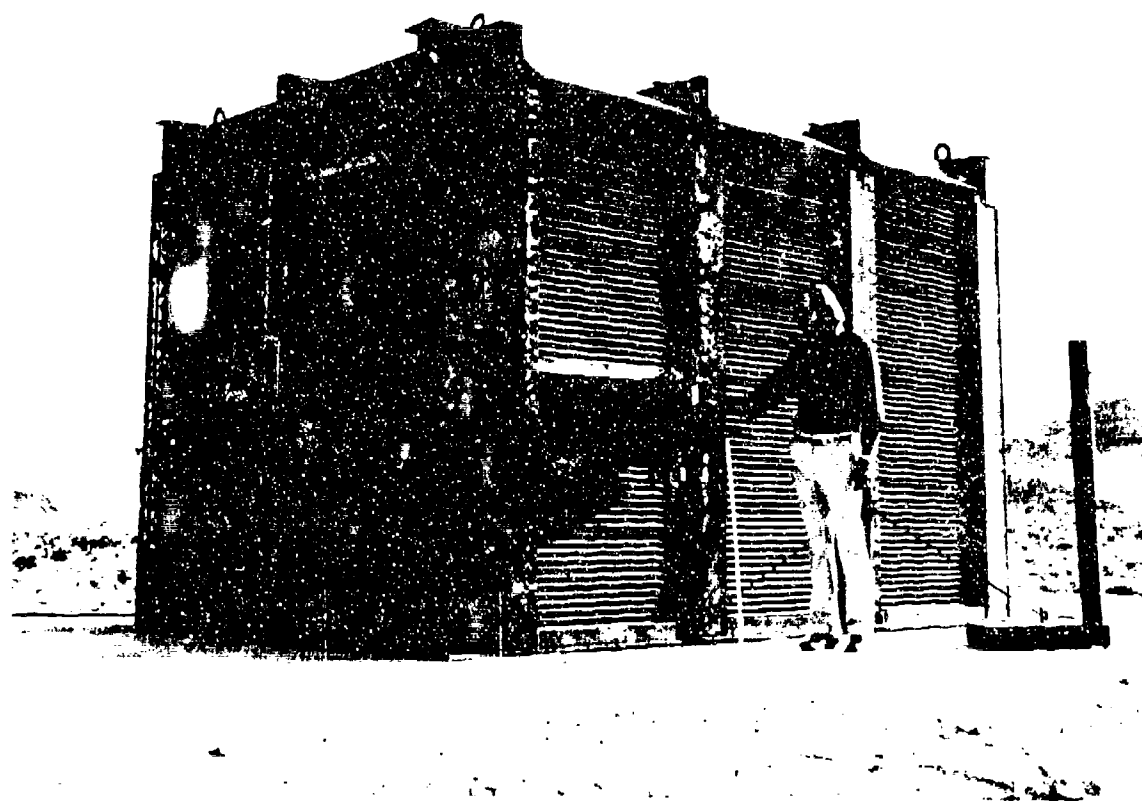
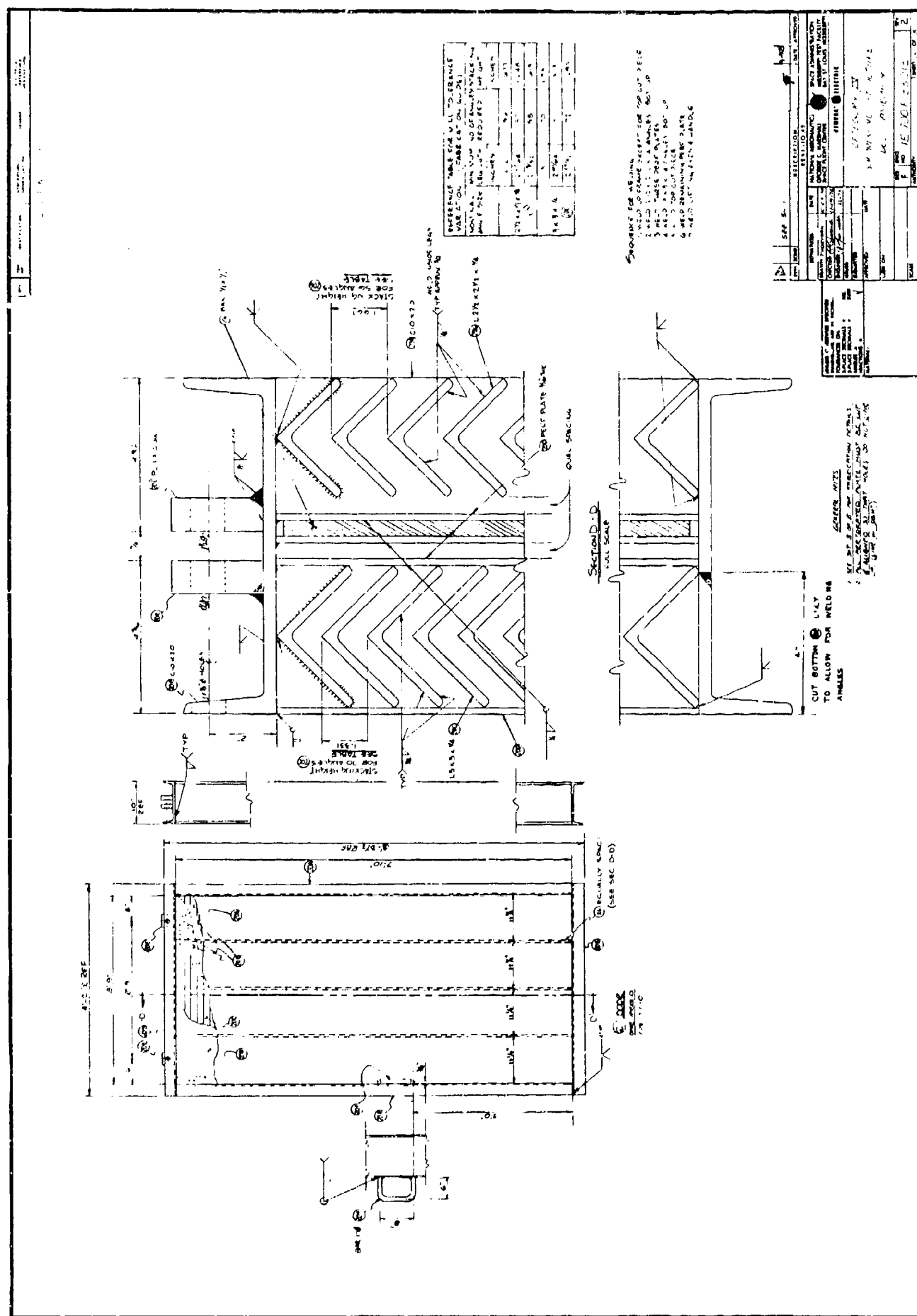


Figure A-4. Group 4 Suppressive Shield



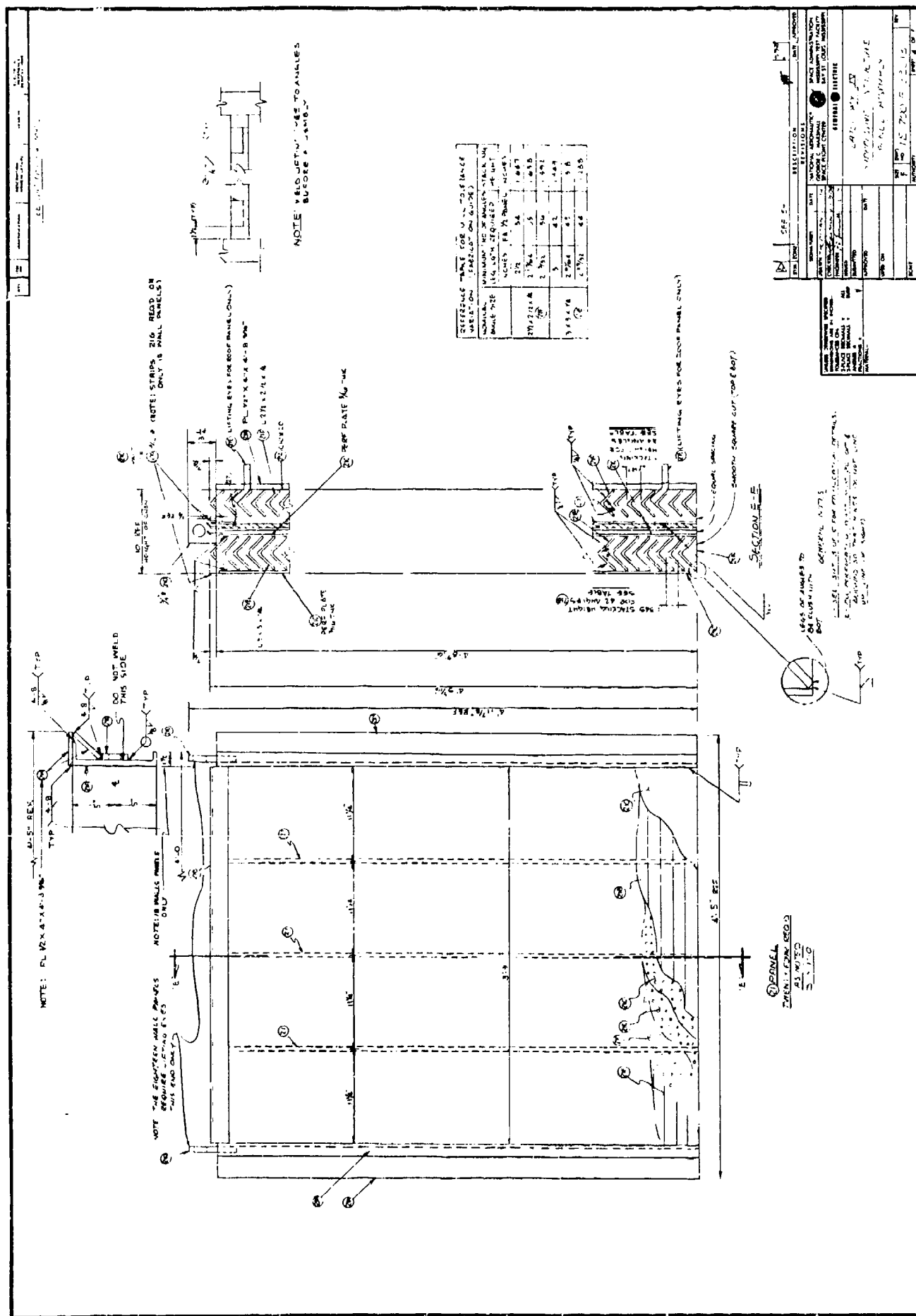
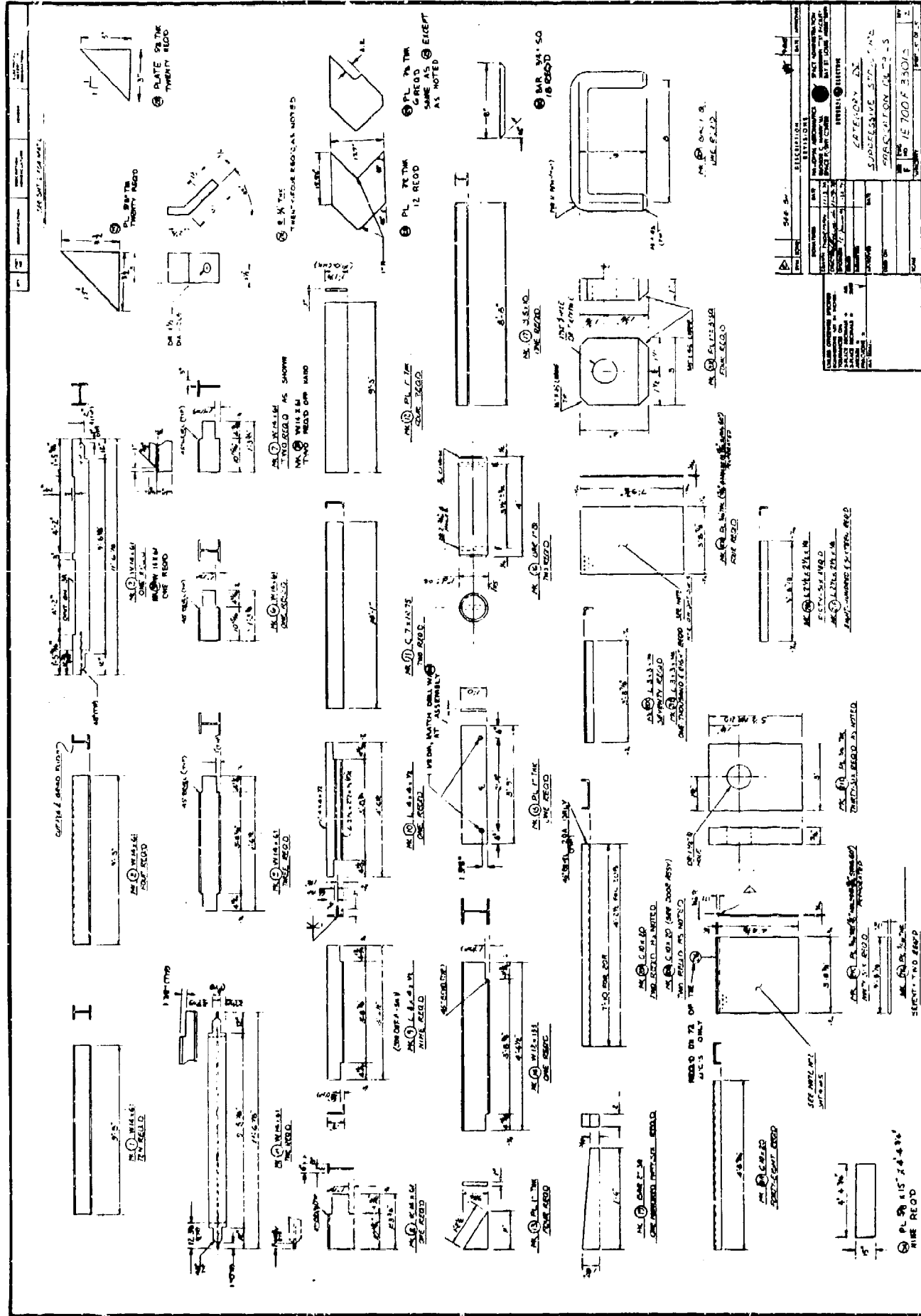


Figure A-5d. Group 4 Shield Construction Details (continued)



(continued)

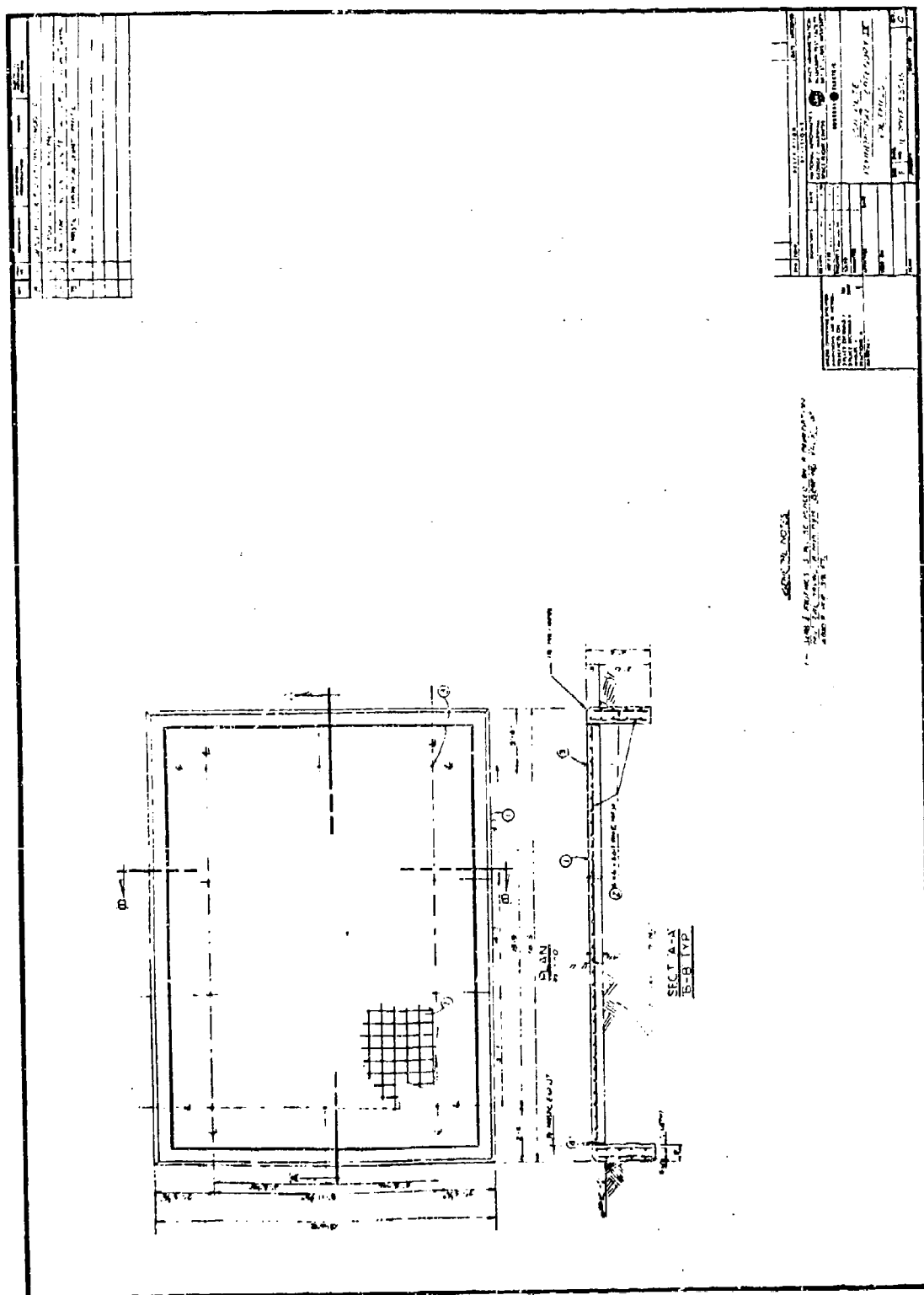


Figure A-5f. Group 4 Shield Construction Details (concluded)

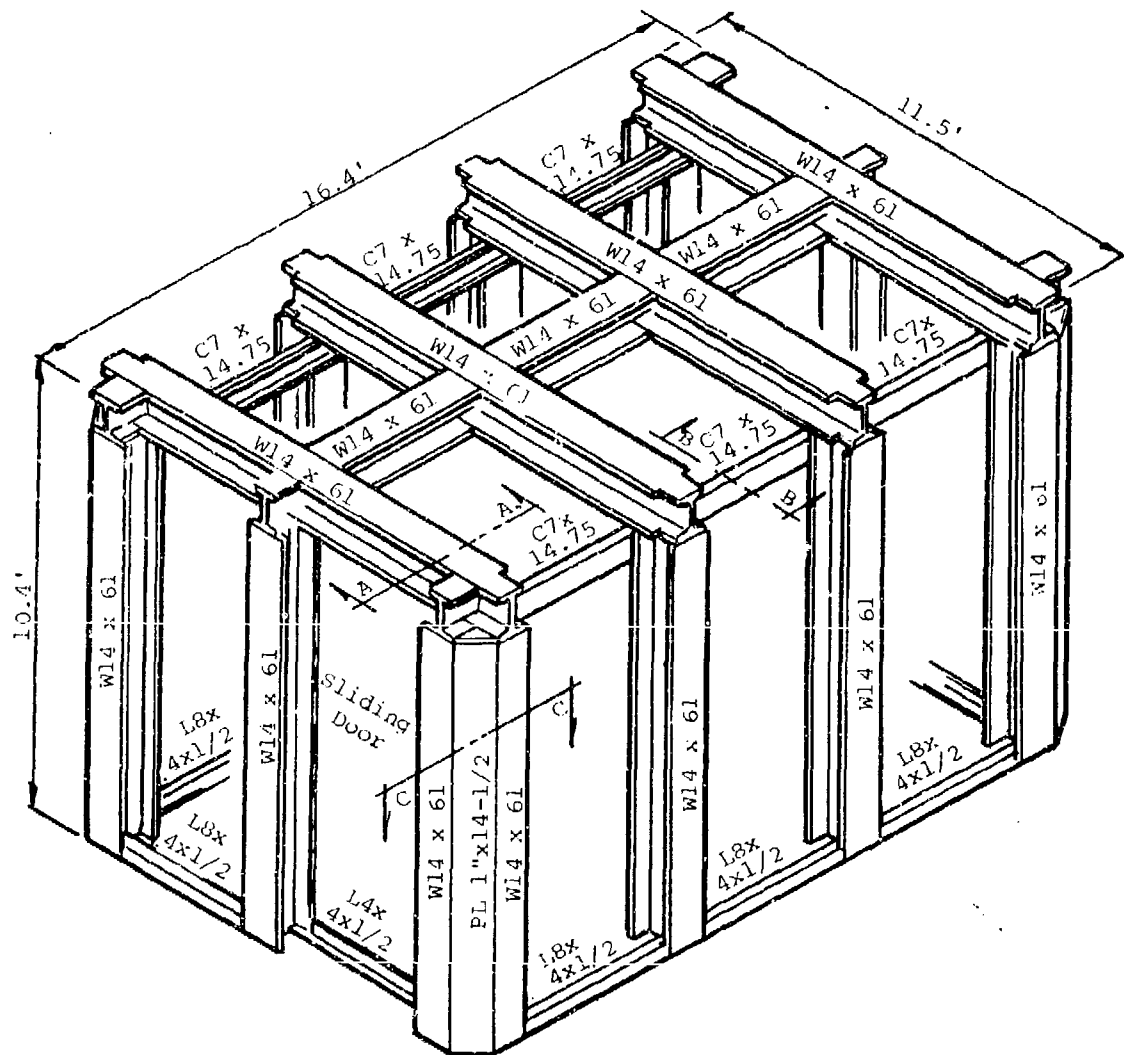
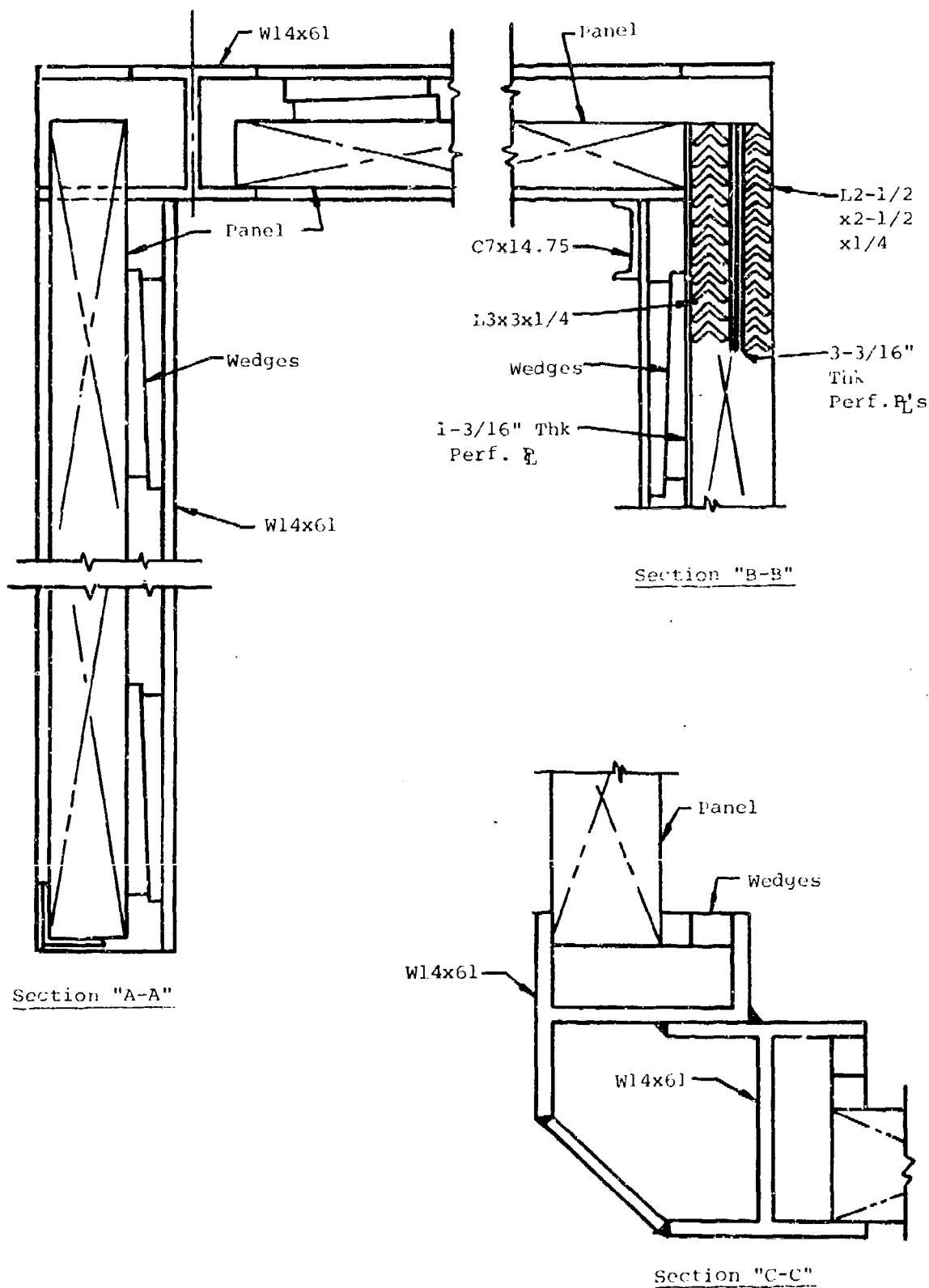


Figure A-6a. Schematic of Group 4 Shield Frame



Figures A-6b. Schematic of Group 4 Shield Frame (concluded)

panels. A view of the door cross section and its monorail support system may be seen in Fig. A-5b.

A.3.2 Application

This design is applicable to munition operations involving up to nine pounds of bare charge of 50/50 pentolite, or equivalent. A typical application would be a 105-mm high explosive projectile fuze-insert-and-torque operation.

The Group 4 shield has been tested and safety approved for a 9-pound bare charge of 50/50 pentolite (10.16 lb TNT equivalent) and fragments from the simultaneous detonation of two 105-mm projectiles located on simulated fuze-insert-and-torque equipment. The shield contains all fragments resulting from the specified detonation (minimum steel thickness along any fragment path is 1.45 inches), restricts the fireball to within 10 feet of the shield, and prevents external pressures greater than 2.3 psi at any point beyond 19 feet from the exterior walls.

Group 4 shields can be considered for operations that

- Require a maximum rectangular floor area 9.2 feet wide by 13.1 feet long with a maximum ceiling height of 9.3 feet (inside dimensions).
- Employ bare charge weights equivalent to nine pounds of 50/50 pentolite (10.16 lb TNT equiv; maximum W/V ratio = 0.00762 lb/ft³; minimum Z = 2.23 ft/lb^{1/3} to side-wall and minimum Z = 2.19 ft/lb^{1/3} for roof).
- Produce fragments incapable of perforating 1.46 inches of steel.
- Are compatible with a fireball 10 feet from the shield and external pressure of 2.3 psi up to 19 feet from the shield exterior walls.

A.3.3 Modification

The length of this particular shield design could be increased with modular extensions almost indefinitely for its rated charge weight. This is due to the way the airblast loading is resisted by the structural system. Each module (wall and roof panels and frames) is capable of carrying its rated loading independent of the adjacent modules since this loading is carried primarily by one-way flexural action in the direction of the short panel dimension. Shield length can be decreased modularly by reducing the number of panels in the sidewall, provided W/V is not increased and scaled distances Z are not decreased.

Changing the span or the height of the Group 4 shield design for the rated charge weight would be subject to the same restrictions discussed above for the Group 3 design. The fragment threat for any proposed application must be such that the threat is defeated by 1.46 inches of mild steel.

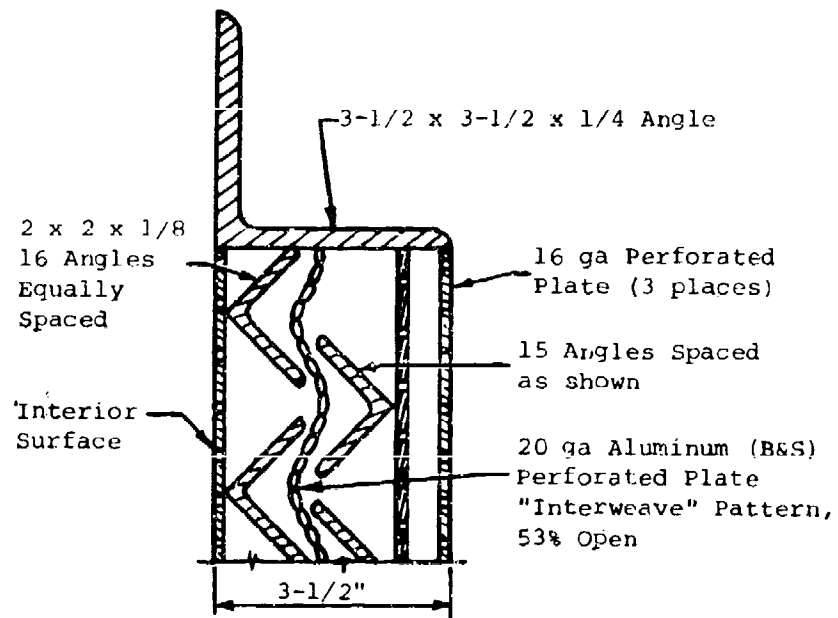
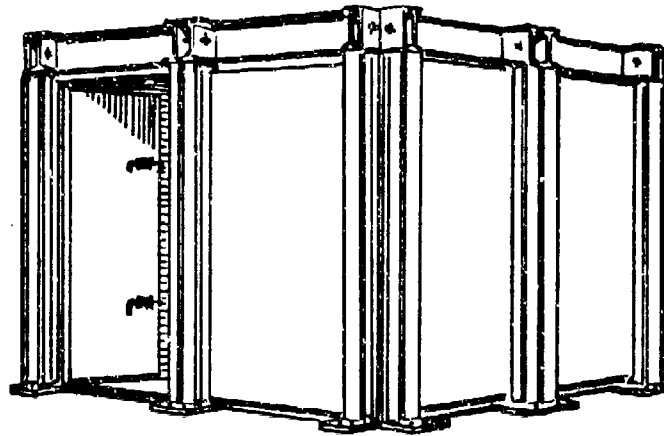
A.4 SHIELD GROUP 5

A.4.1 Description

The Group 5 design shown in Fig. A-7 employs a steel frame with panels made up of perforated plate, angles and screen. The outside dimensions are 12.6 feet square by 9.2 feet high, and the inside dimensions are 10.4 feet square by 8.5 feet high.

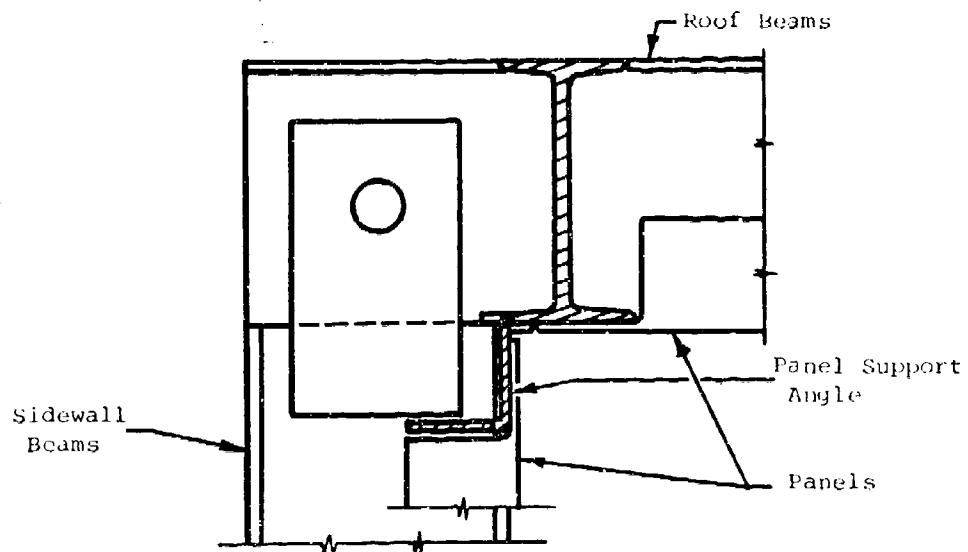
The Group 5 shield wall and roof panels include the basic structural frame members as integral parts of the panel, i.e., the frame columns and roof beams are part of the panels. The shield is assembled by bolting or welding the various panels together. Pertinent connection details are illustrated in Figs. A-8 through A-10; the Group 5 shield fabrication drawings are shown in Fig. A-11.

A typical Group 5 panel cross section is shown in Fig. A-7. Each panel contains three layers of 16 gauge perforated steel plates. One plate is on the inner panel surface and

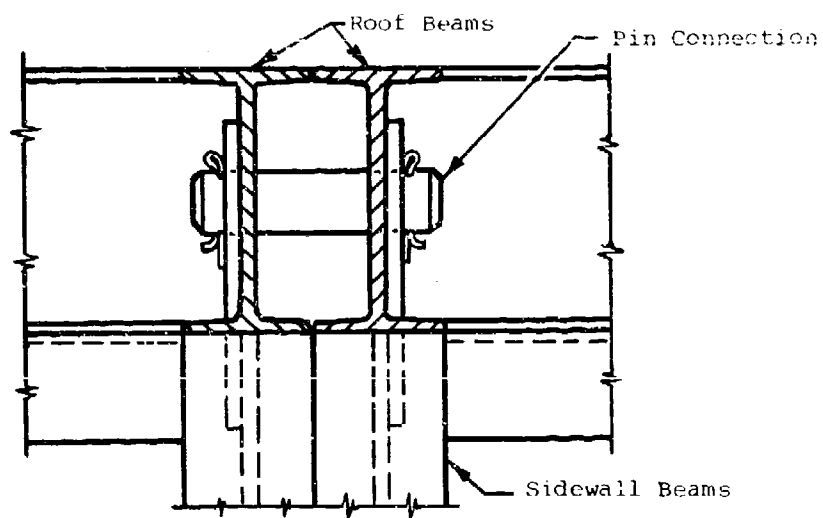


Panel Cross Section Detail

Figure A-7. Group 5 Suppressive Shield



a. Side View



b. End View

Figure A-8. Center Framework Connection - Group 5 Shield

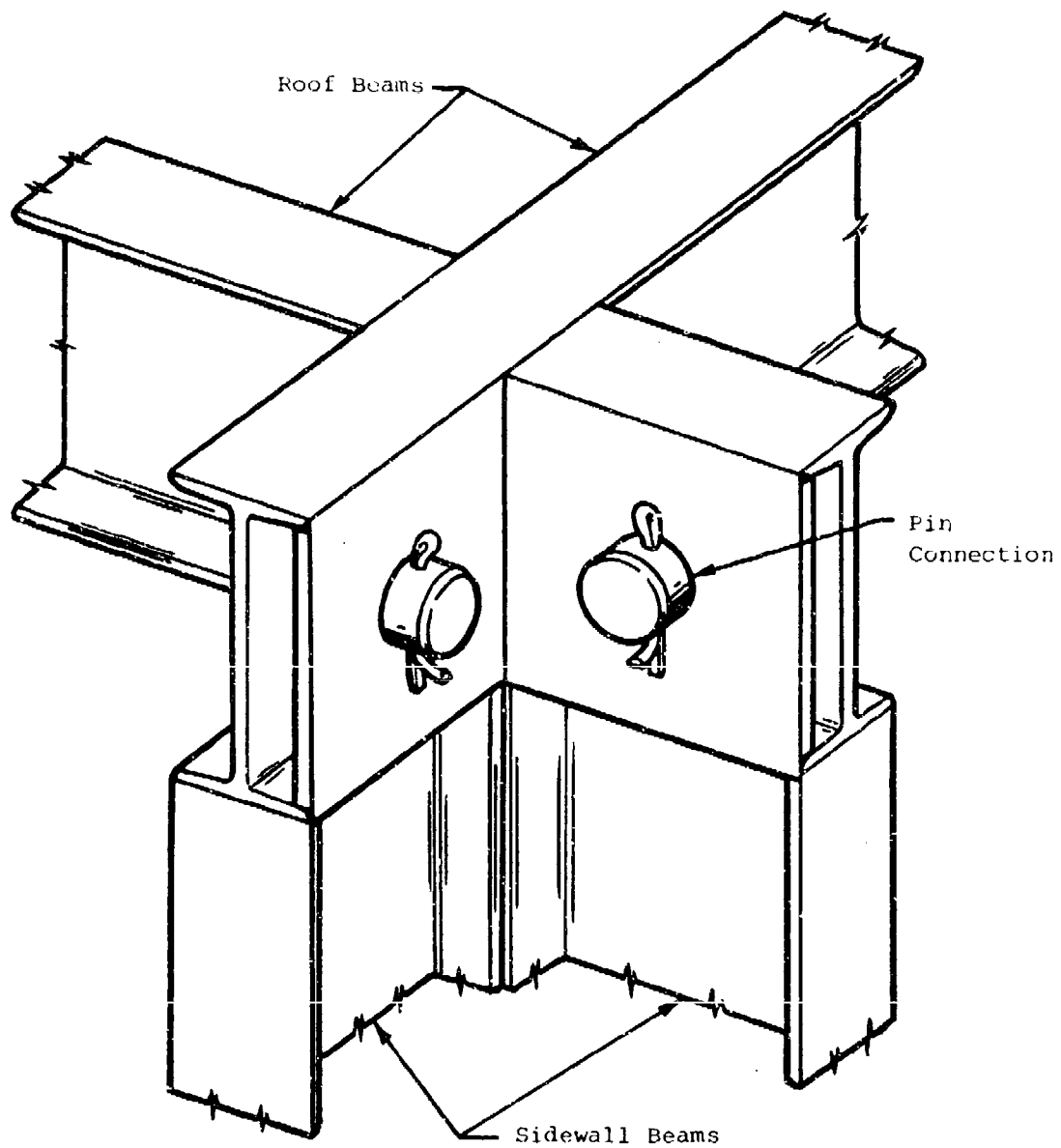


Figure A-9. Edge Framework - Group 3 Shield

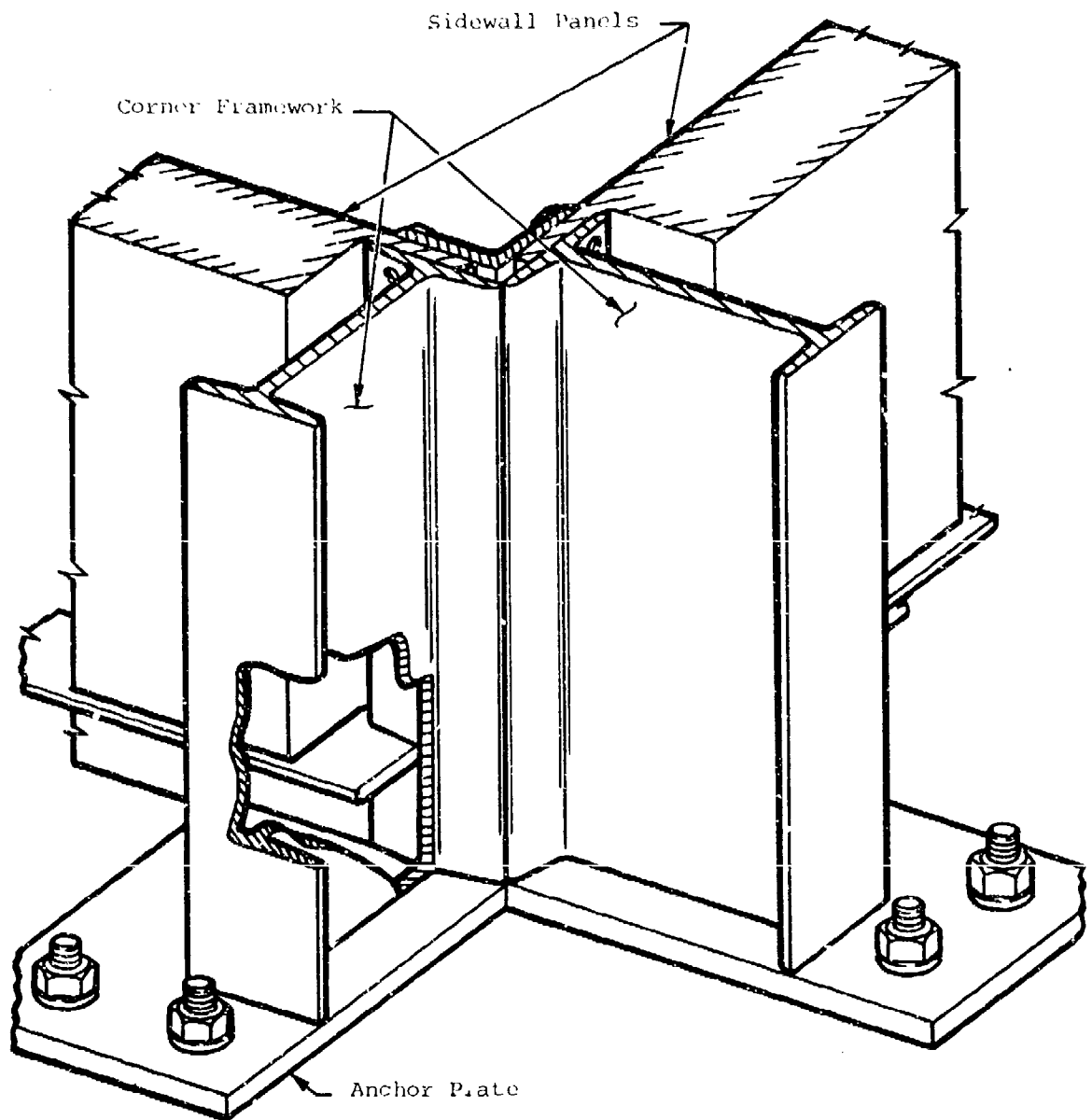
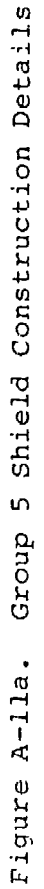
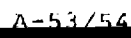
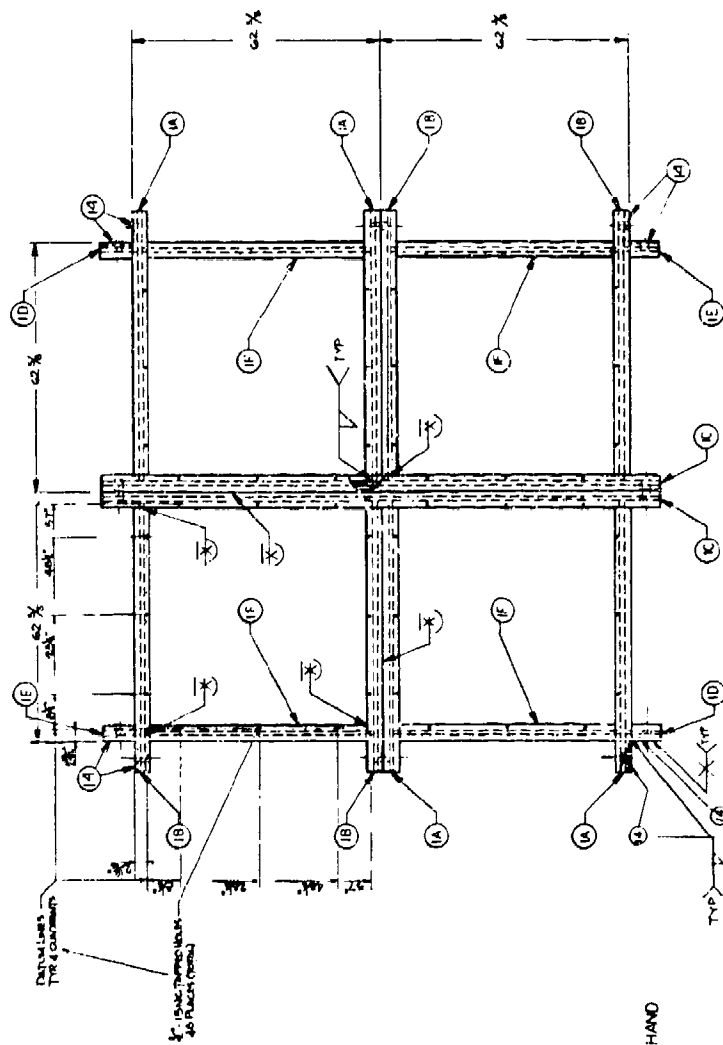


Figure A-10. Corner Anchor Plate - Group 5 Shield

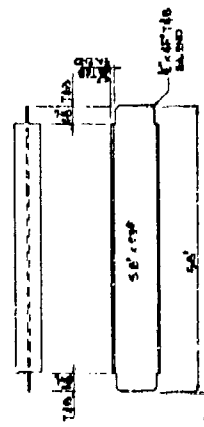
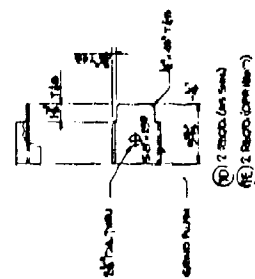
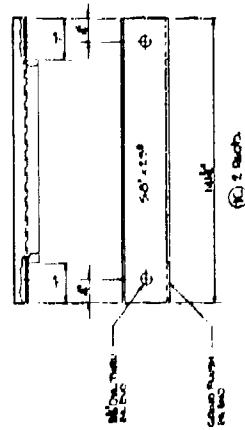
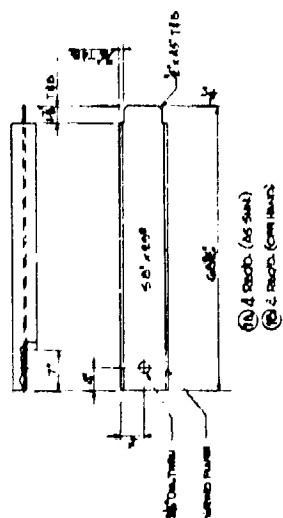
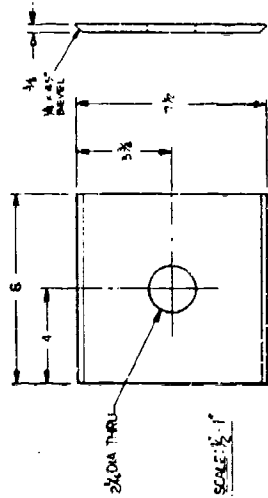




1	2	3	4	5	6	7	8	9	10	11	12	13	14	15	16	17	18	19	20	21	22	23	24	25	26	27	28	29	30	31	32	33	34	35	36	37	38	39	40	41	42	43	44	45	46	47	48	49	50	51	52	53	54	55	56	57	58	59	60	61	62	63	64	65	66	67	68	69	70	71	72	73	74	75	76	77	78	79	80	81	82	83	84	85	86	87	88	89	90	91	92	93	94	95	96	97	98	99	100
---	---	---	---	---	---	---	---	---	----	----	----	----	----	----	----	----	----	----	----	----	----	----	----	----	----	----	----	----	----	----	----	----	----	----	----	----	----	----	----	----	----	----	----	----	----	----	----	----	----	----	----	----	----	----	----	----	----	----	----	----	----	----	----	----	----	----	----	----	----	----	----	----	----	----	----	----	----	----	----	----	----	----	----	----	----	----	----	----	----	----	----	----	----	----	----	----	----	----	-----



(10) 2 AS SHOWN
 (12) 2 OPPOSITE HAND



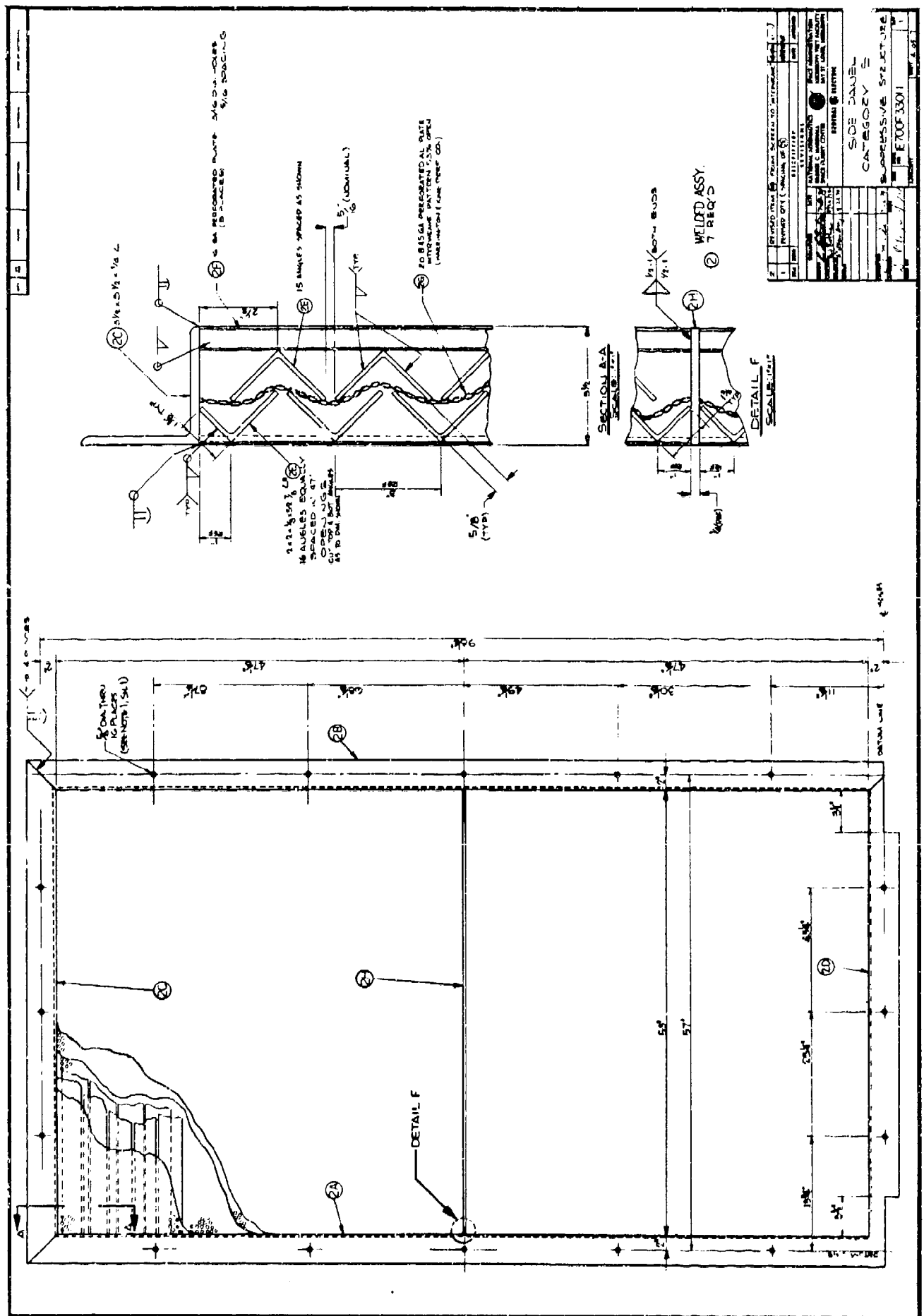
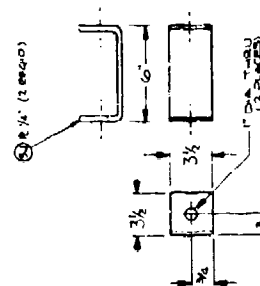
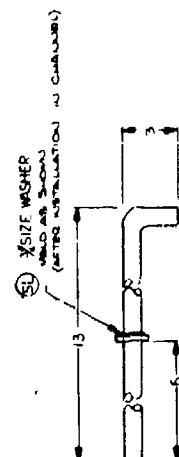
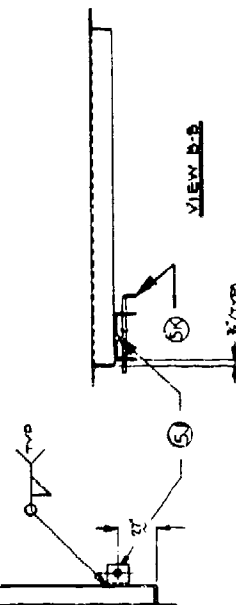
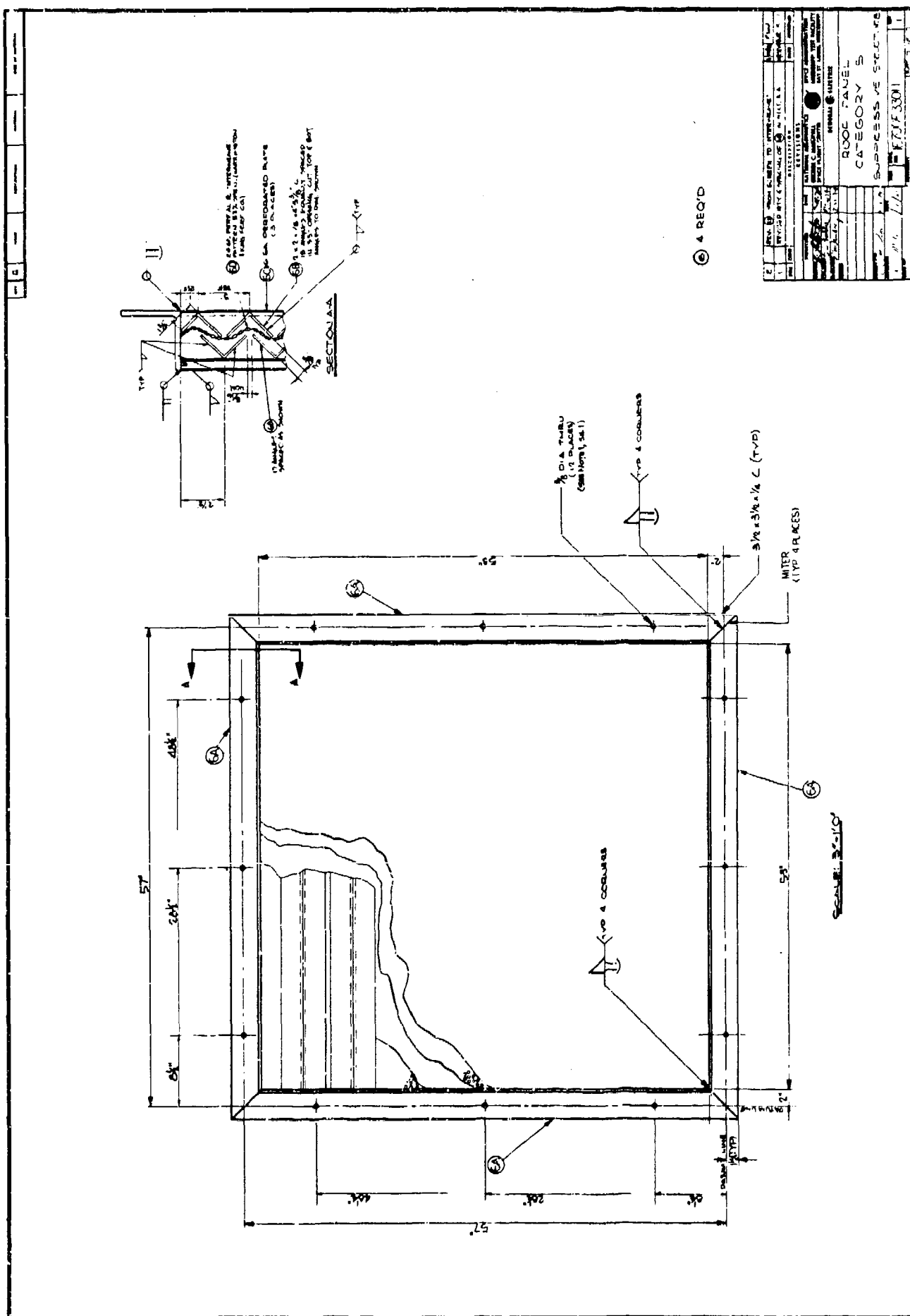


Figure A-1d. Group 5 Shield Construction Details (continued)



1. THIS DOOR PANEL IS IDENTICAL TO SIDE PANEL, SHEET 4, EXCEPT AS SHOWN IF NOTED

[illegible]



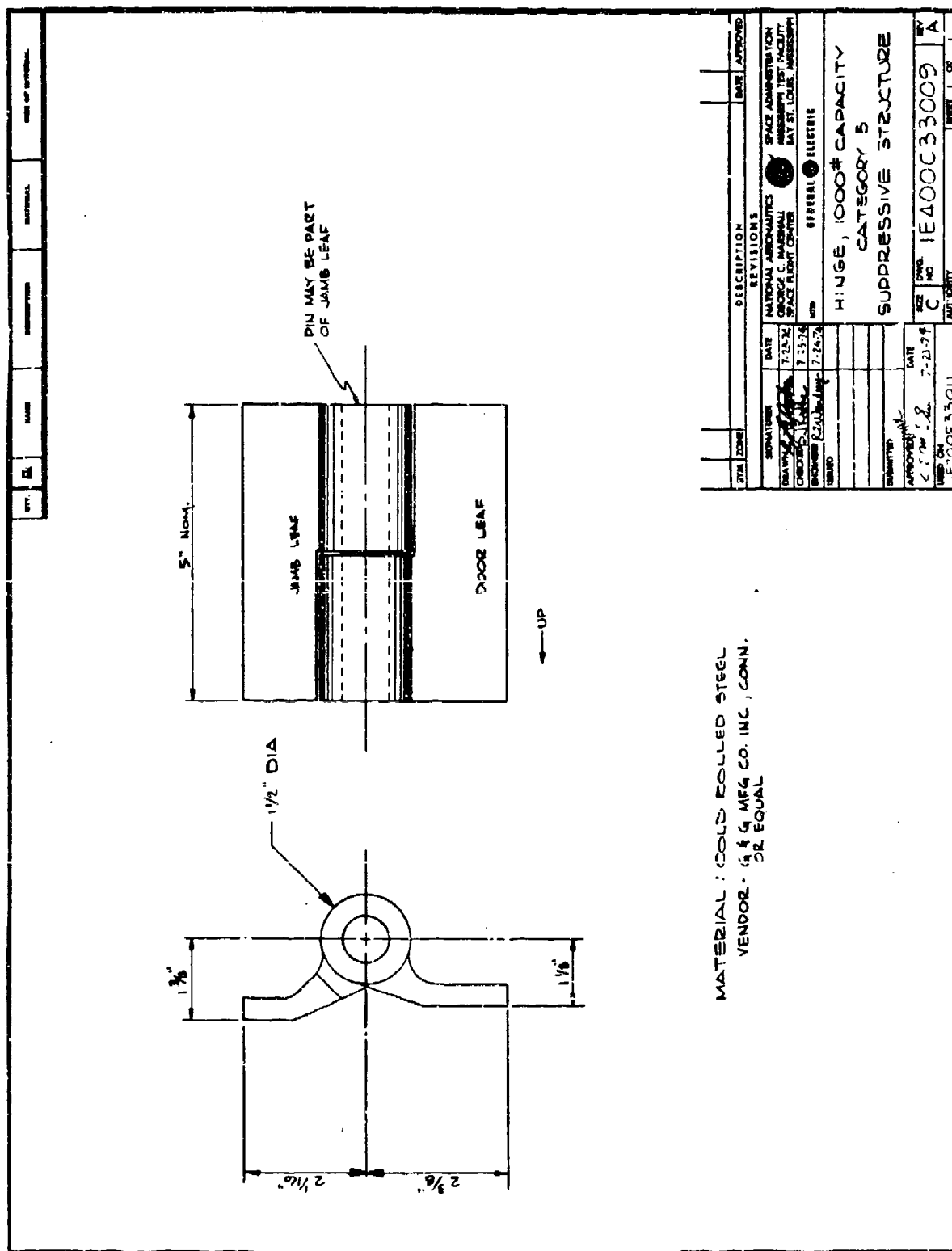


Figure A-11h. Group 5 Shield Construction Details (continued)

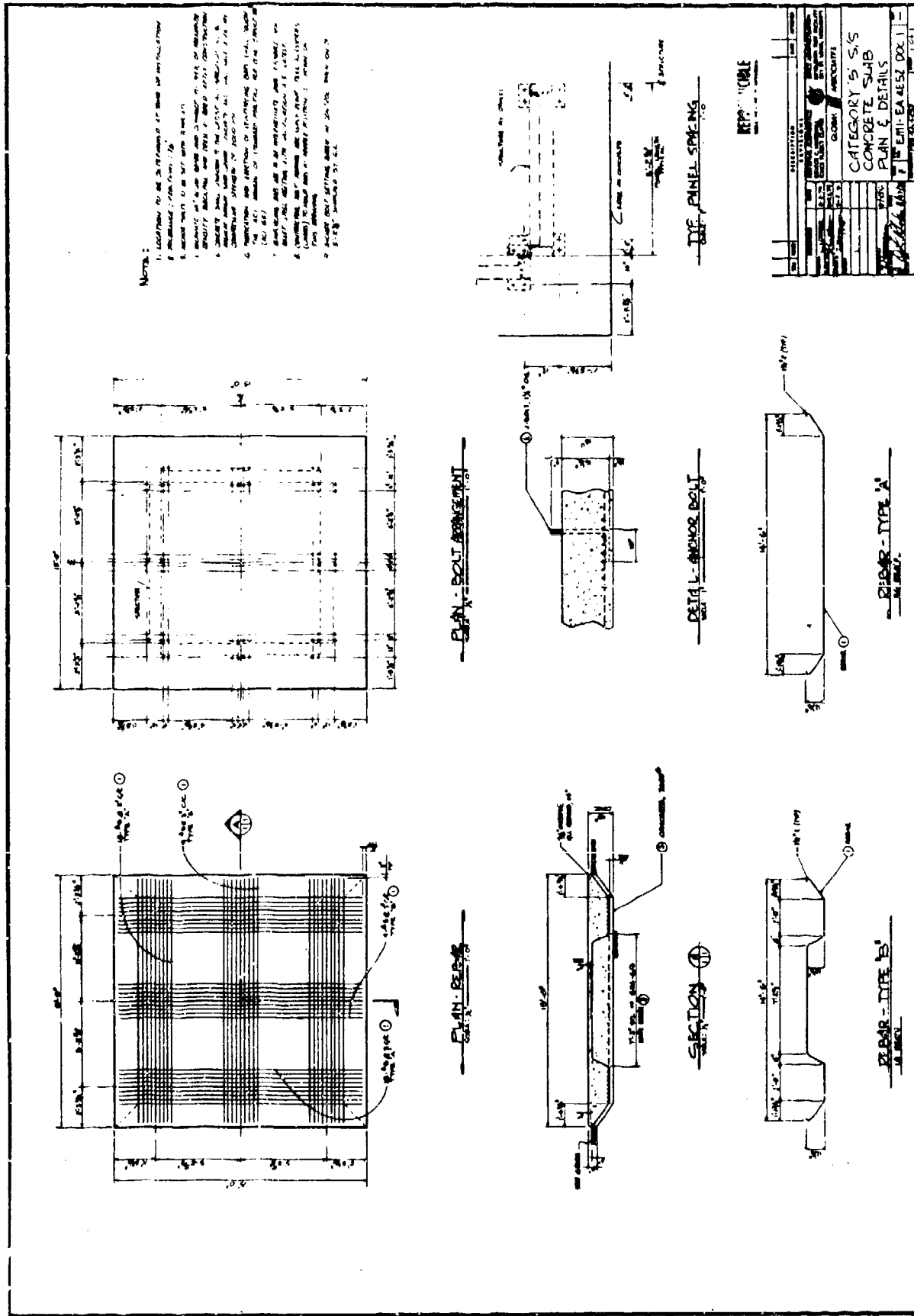


Figure A-11i. Group 5 Shield Construction Details (concluded)

two on the outer, with the outer two spaced slightly apart. Between the perforated plates are two rows of structural angles. The two layers of angles are reversed and staggered so that the gap left between individual angles in a layer is covered by angles in the other layer. A sheet of 20 gauge perforated aluminum plate interweave pattern is placed between the layers of angles. The complete assembly is surrounded by 3-1/2 x 3-1/2 x 1/4 inch structural angle which is attached to the S8 x 23 wall or roof members.

The foundation for the Group 5 shield consists of a reinforced concrete slab on grade as shown in Fig. A-11i. Anchor bolts cast into the foundation restrain the bottom of the shield. An anchor plate for a corner is shown in Fig. A-10. Anchors for the sidewall members are similar.

The doorway shown in Figs. A-7 and A-11 is a hinged door and depicts the shield configuration that was proof tested. A sliding door such as utilized with the Group 4 shield would be preferable for an operational installation. Such a sliding door for the Group 5 shield has been designed and is described in Chapter 6.

A.4.2 Application

The Group 5 shield has been developed primarily for operations involving propellants and pyrotechnics. Since unconfined propellant tends to burn at a constant rate and confined propellant tends to burn at a faster rate with increasing pressure and temperature, venting is very important when the shield is used for a propellant application. The Group 5 shield design has been tested and safety approved for up to 30 pounds of pyrotechnic material. Ignition of 30 pounds of pyrotechnic (55 percent NaNO_3 and 45 percent magnesium granules) resulted in no blast pressure outside the shield. The fireball was restricted to within two feet of the shield, and small acceptor batches (≤ 1 lb) of illuminant composition three feet from the shield were not ignited.

Since the Group 5 shield is designed primarily to suppress large fireballs resulting from deflagration/burning of pyrotechnic materials, a typical application would be for an igniter slurry mixing operation. It is suitable for use in connection with munition operations or storage involving up to 30 pounds of pyrotechnic material in a working volume of 10.4 x 10.4 x 8.5 feet, or more. Such use must be compatible with ignition of illuminant composition within three feet of the shield and a fireball that extends two feet beyond the shield exterior walls.

The design is also suitable for operations involving detonating munitions up to 1.84 pounds of C-4 explosive, or equivalent, and a fragment threat that can be defeated by 0.427 inch of mild steel. Such application would be limited to the same working volume specified above and must be compatible with an external pressure of 2.3 psi up to 3.7 feet from the exterior of the shield.

The Group 5 shield can be used in installations where the requirements are compatible with

- A maximum square floor plan measuring 10.4 feet on a side clear internal working space with a maximum clear working height of 8.5 feet.
- Charge weights up to 1.84 pounds of C-4 explosive, or equivalent (1.98 lb TNT equiv; maximum W/V ratio = 0.00215 lb/ft^3 ; minimum $Z = 4.14 \text{ ft/lb}^{1/3}$ at sidewalls and minimum $Z = 6.79 \text{ ft/lb}^{1/3}$ for roof. Note that the charge is not located at mid-height of the shield in this case.)
- An external pressure of 2.3 psi up to 3.7 feet from the exterior of the shield and a fireball that extends two feet outside the shield.

- Fragments that are incapable of perforating 0.427 inch of mild steel.
- 30 pounds of pyrotechnic materials.

A.4.3 Modification

Modification of the Group 5 shield design as safety approved would be subject to the same considerations discussed above for the Group 4 shield. That is, the length could be increased in modular panel increments provided Z is not decreased and W/V is not increased. The fragment threat for the application of interest must be defeated by the Group 5 shield nominal wall thickness (0.427 in).

A.5 SHIELD GROUP 6

A.5.1 Description

Shield Group 6 consists of two designs which have been safety approved. These two designs, designated Group 6A and 6B, are shown in Figs. A-12 and A-13, respectively. Both shields are spherical in configuration with a 24-inch interior diameter and a nominal steel wall thickness of 1/4 inch.

a. Group 6A

The Group 6A design consists of two hemispherical shells of 1/4-inch mild steel welded together. The shield is shown schematically in Fig. A-14; the fabrication drawings are presented in Fig. A-15. An access opening to the interior is provided by a 7-1/2-inch diameter hole. The opening is reinforced by an external ring proportioned in accordance with standard penetration reinforcing methods such as the ASME pressure vessel code. The closure for the access opening is an 8-inch diameter circular plate 3/8 inch thick which hinges inward. There is an external bar to securely latch the closure shut.

A vertical pipe on the centerline of the sphere supports a revolving tray for ease in dispensing the hazardous



Figure A-12. Group 6A Suppressive Shield

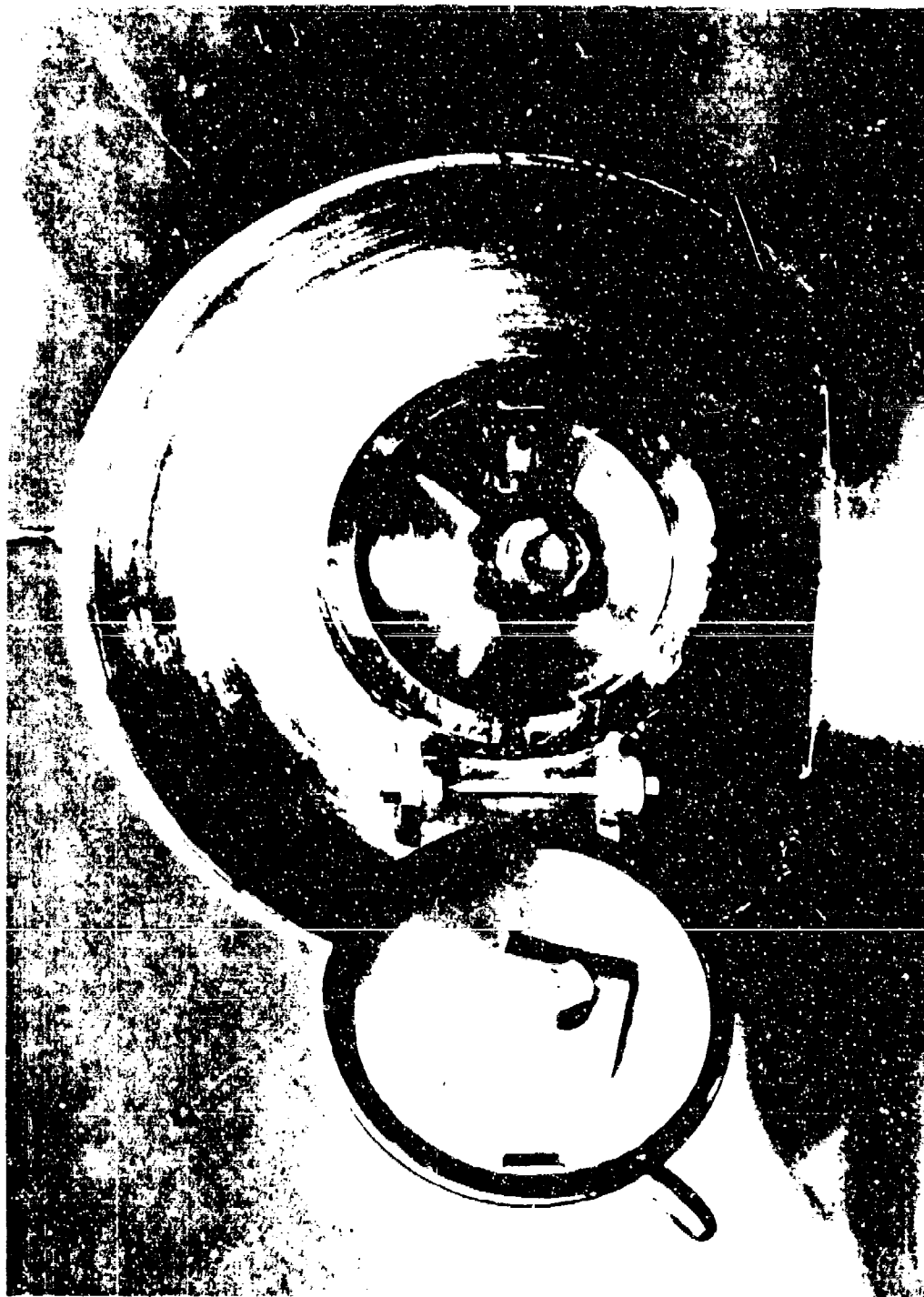


Figure A-13. Group 6B Suppressive Shield

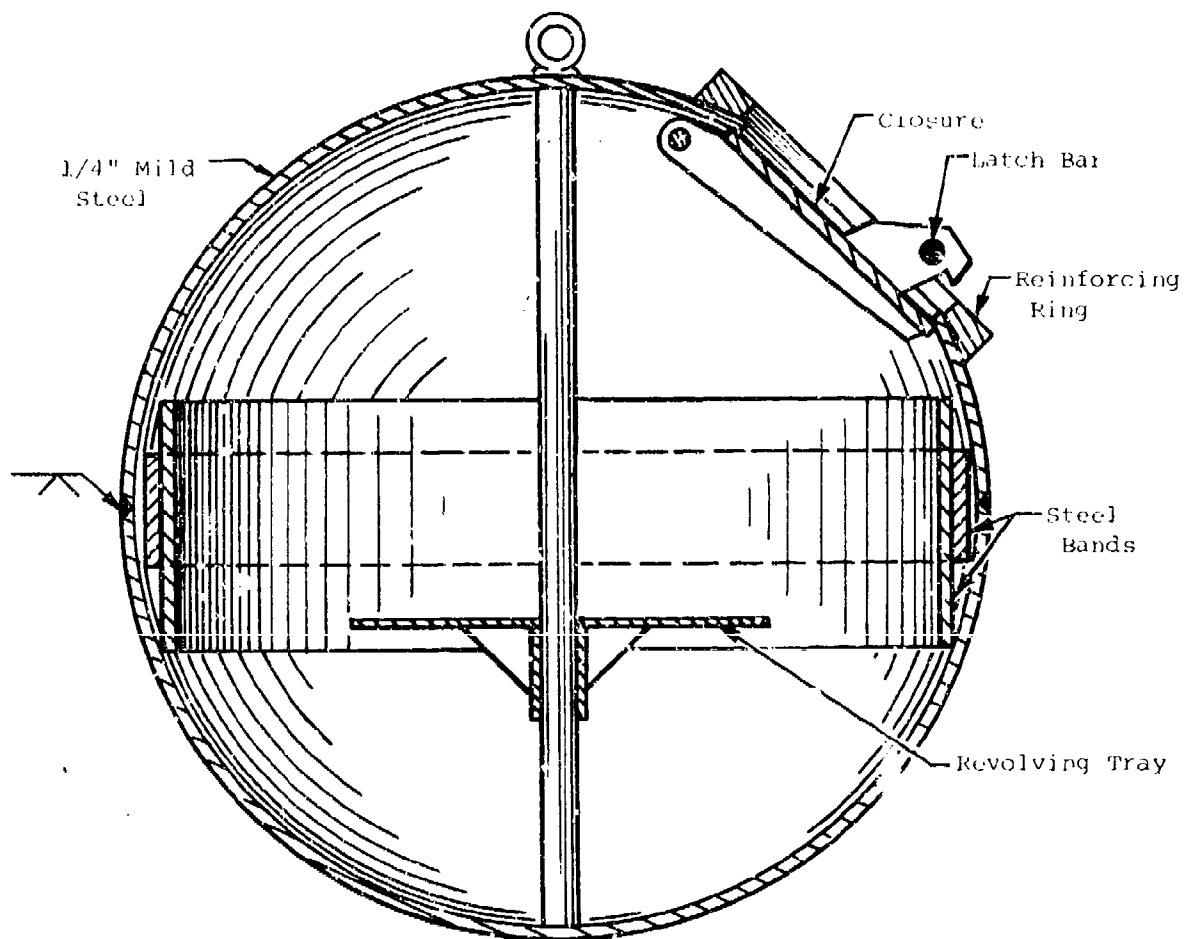


Figure A-14. Group 6A Shield Schematic



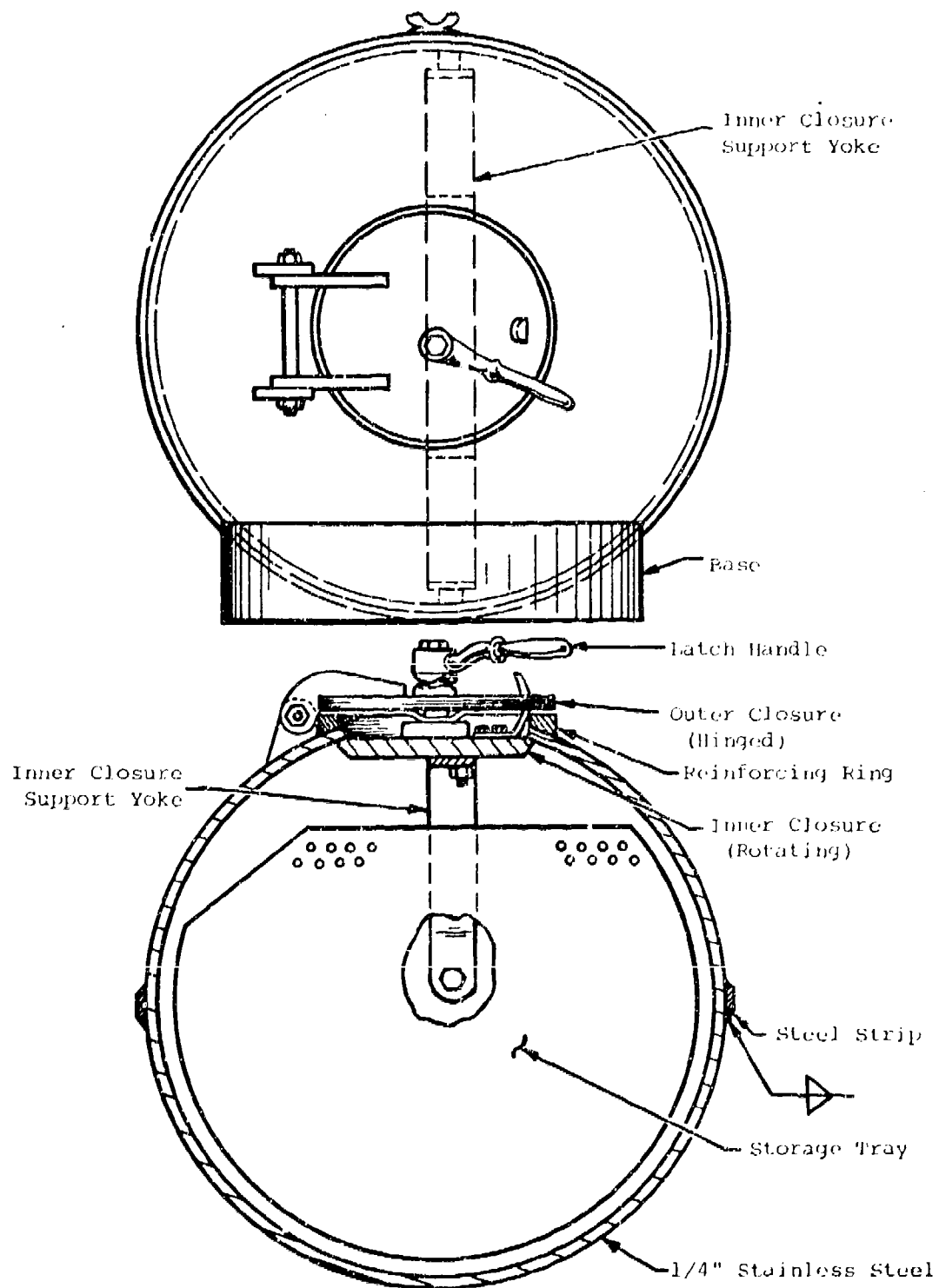
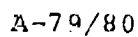
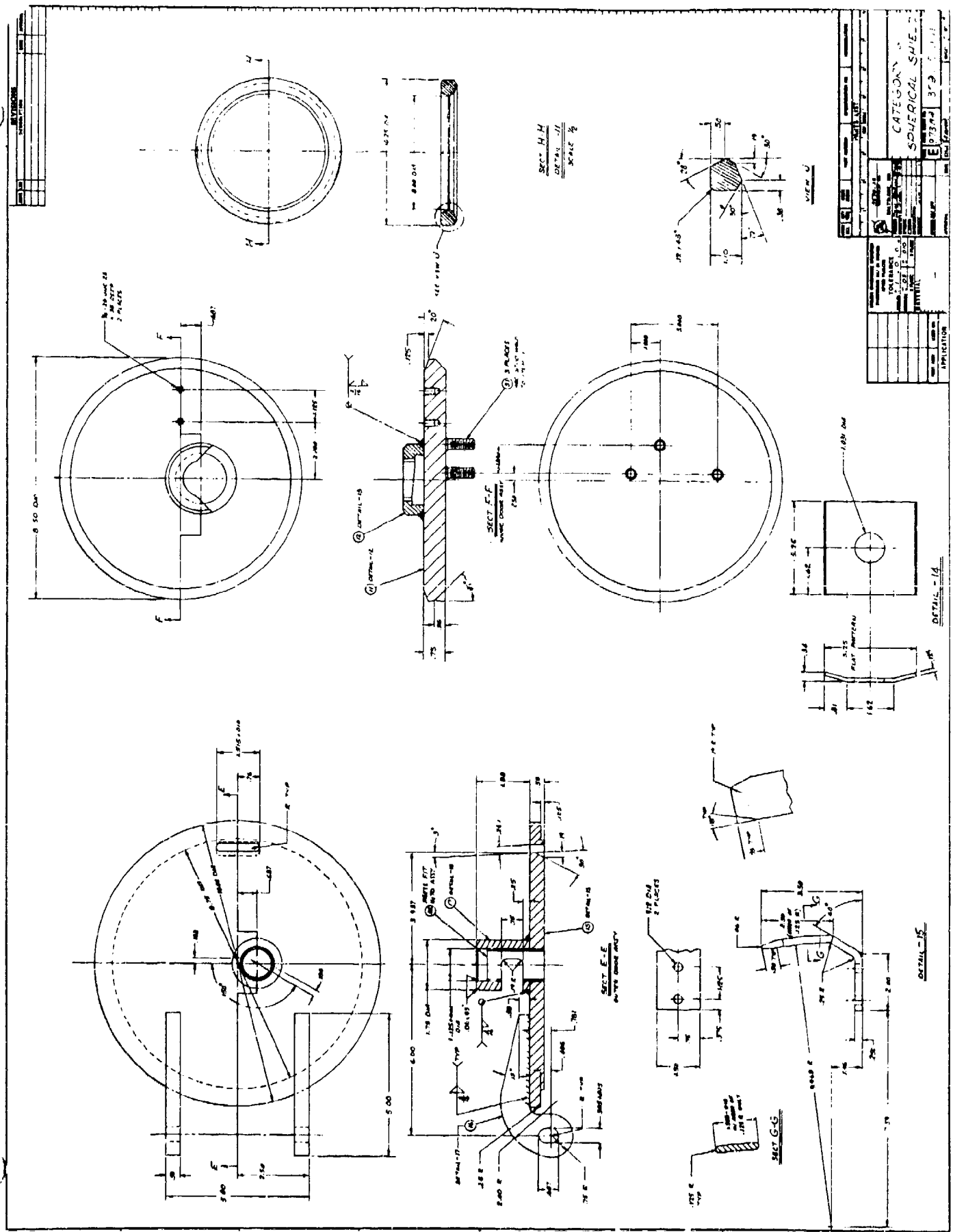


Figure A-16. Group 6B Shield Schematic







A.5.2 Application

Typical applications of these shield designs would be to safely transport or store small quantities of explosives between operations such as in a detonator loading facility or in a laboratory.

a. Group 6A

The group 6A design has been tested and safety approved for detonation of a single charge of 13.63 ounces of 50/50 pentolite, or equivalent, and a maximum reflected pressure on the interior shield surface of 6900 psi. The charge weight may also be made up of equally spaced 1/2-ounce 50/50 pentolite charges located 3 inches or more from the wall so that the calculated reflected overpressure on the wall does not exceed 11,400 psi. The fireball and fragments, if any, from the test charge are completely contained by the shield. External pressure is considerably less than 2.3 psi (approximately 1 psi) at a distance of two feet from the shield.

The Group 6A design would be applicable to munition operations that

- Utilize 13.63 ounces of 50/50 pentolite, or equivalent (0.962 lb TNT equiv; maximum W/V ratio = 0.2297 lb/ft^3 ; minimum $Z = 1.013 \text{ ft/lb}^{1/3}$; W/V ratio and Z values will be different for 0.5 oz distributed charges.)
- Require a maximum working volume equal to a 2-foot diameter sphere.
- Are compatible with external pressure less than 2.3 psi two feet from the shield.
- Produce fragments that will not perforate one-quarter inch of mild steel.

b. Group 6B

The Group 6B design has been tested and approved for use as a storage container in applications requiring a safety shield to contain 8.23 ounces of C-4 explosive, or equivalent. The charge weight may be made up of equally spaced 0.4-ounce C-4 charges located 3 inches or more from the wall so that the calculated reflected overpressure does not exceed 9800 psi. Larger charges (up to a total of 8.23 ounces) must be located far enough from the shield wall so that the calculated reflected overpressure does not exceed 4900 psi. Blast pressure is reduced well below 2.3 psi (approximately 0.2 psi) at a distance of one foot from the shield; the fireball is completely contained within the shield.

The Group 6B design is adaptable to applications that

- Involve 8.23 ounces of C-4 explosive
(0.5545 lb TNT equiv.; maximum W/V ratio
= 0.132 lb/ft³; minimum Z = 1.217 ft/
lb^{1/3}; W/V ratio and Z values will be
different for 0.4-oz distributed charges.)
- Require a working volume available in a
2-foot maximum spherical diameter.
- Are compatible with an external pressure
less than 2.3 psi two feet from the shield.
- Are located in a corrosive environment
requiring a stainless steel vessel.
- Produce no fragments that cannot be de-
feated by one-quarter inch of stainless
steel.

A.5.3 Modification

There are no simple, straightforward rules for modifying the Group 6 shield designs. They may not, of course,

be used for applications involving a larger charge or more severe fragment threat than that for which the designs have been approved. Similarly, the diameter may not be decreased for the rated charge weight. Increasing the diameter for the rated charge weight would require careful analysis using the methods presented in Chapter 5.

A.6 SHIELD GROUP 81-mm

The Group 81-mm shield was the first suppressive shield design to be safety approved. This shield group has two design versions, both of which are rectangular parallelopipeds made up of a structural steel frame supporting vented panels. One version will be designated the Prototype 81-mm Shield; the other will be called the Milan 81-mm Suppressive Shield.

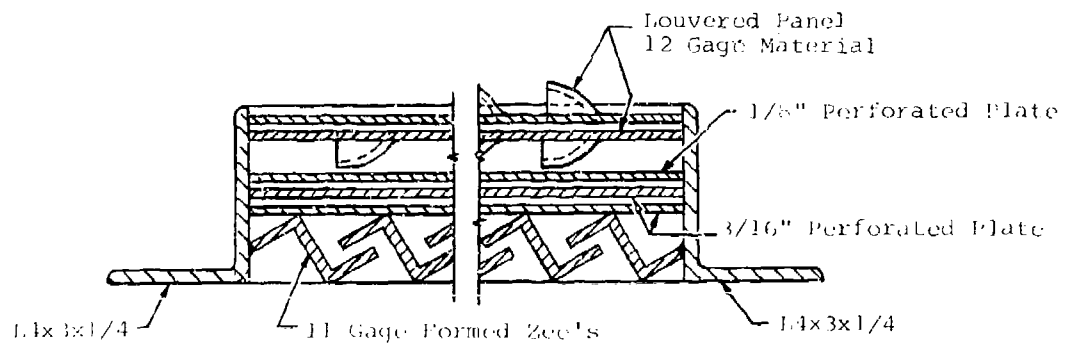
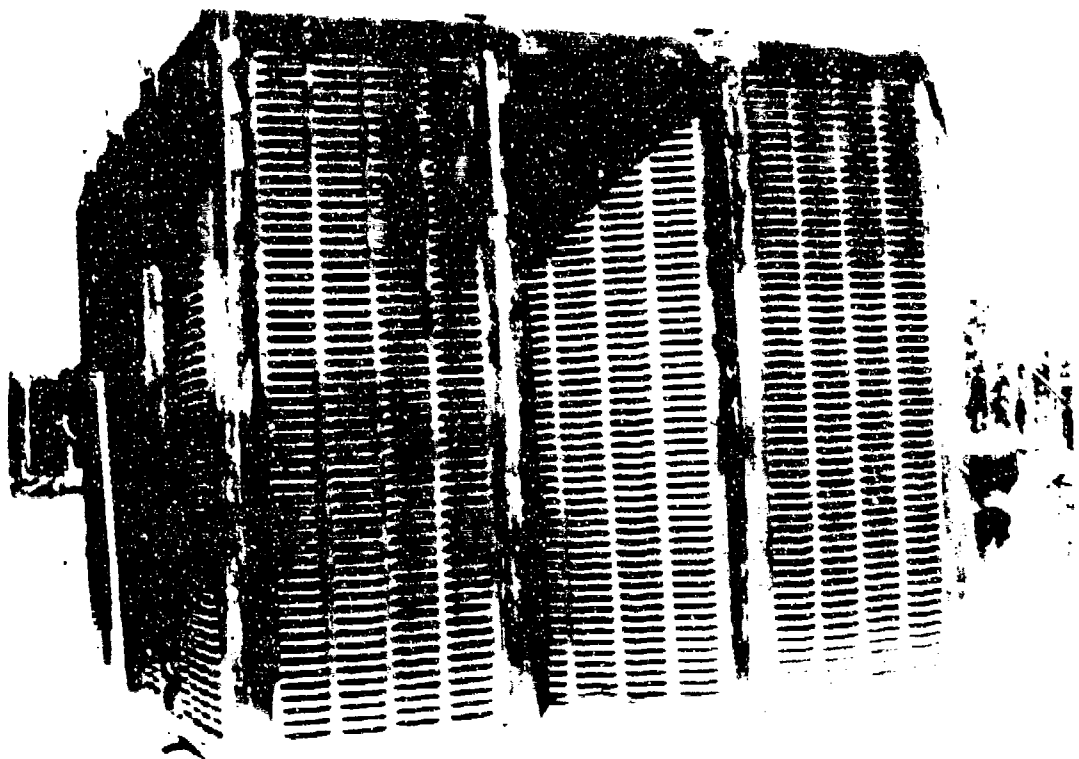
A.6.1 Description

a. Prototype 81-mm Shield

The Prototype 81-mm Shield design shown in Fig. A-18 is approximately 15.4 feet wide by 13.1 feet high by 20 feet long on the outside and 14 feet wide by 12.4 feet high by 18.7 feet long on the inside.

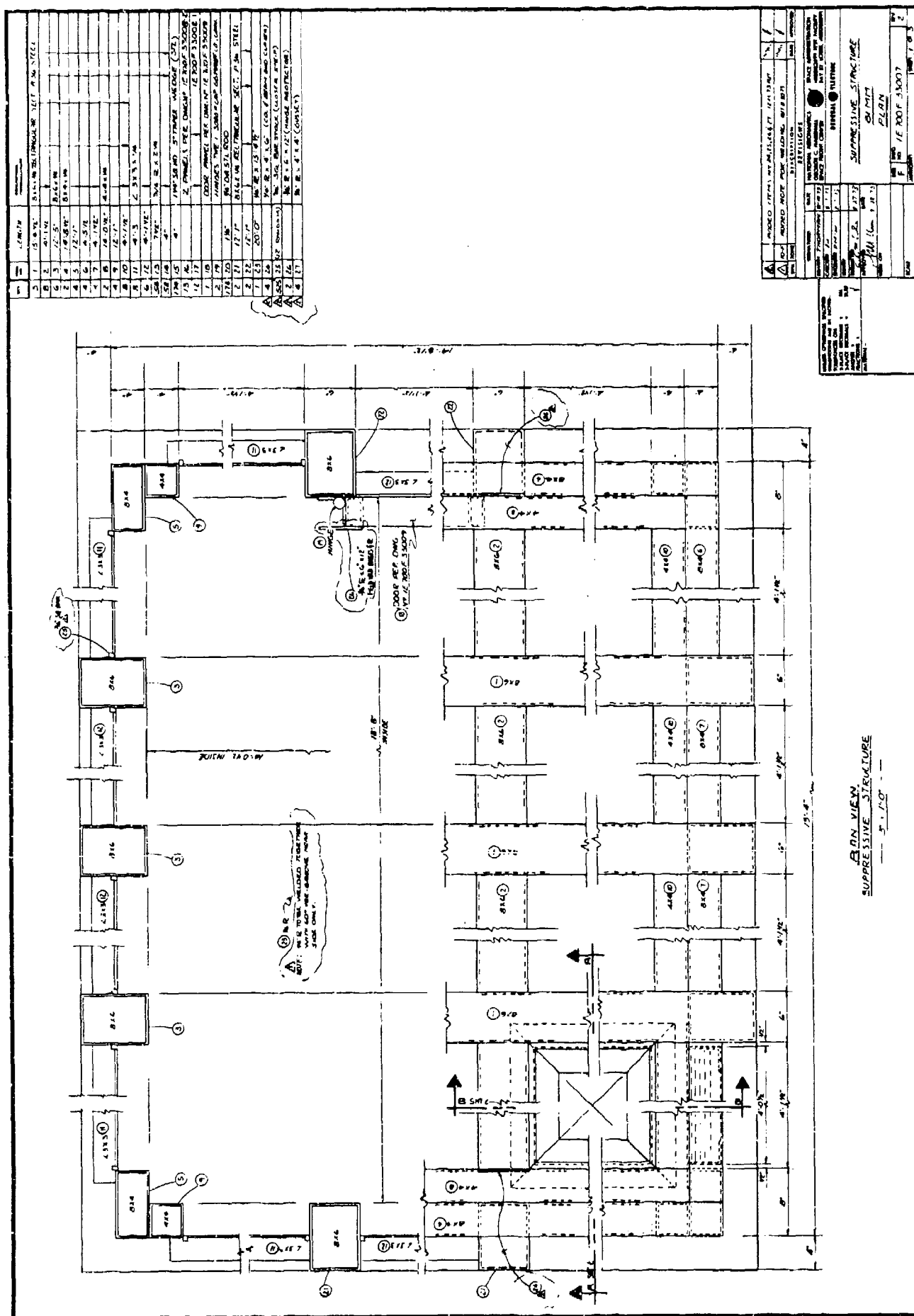
The frame consists of structural steel tubes. All corner members, including ceiling corner members, are constructed of two 1/4 inch thick tubes, one of which is 8 inches by 4 inches and the other 4 inches square. These tubes are welded together the full length of the tubes to form an L as shown in Fig. A-19, the shield fabrication drawings. All vertical members of the frame (except corners) are 8 x 6 x 1/4 structural steel tubes. The horizontal ceiling members (except corners) are 8 x 6 x 3/8 structural steel tubes.

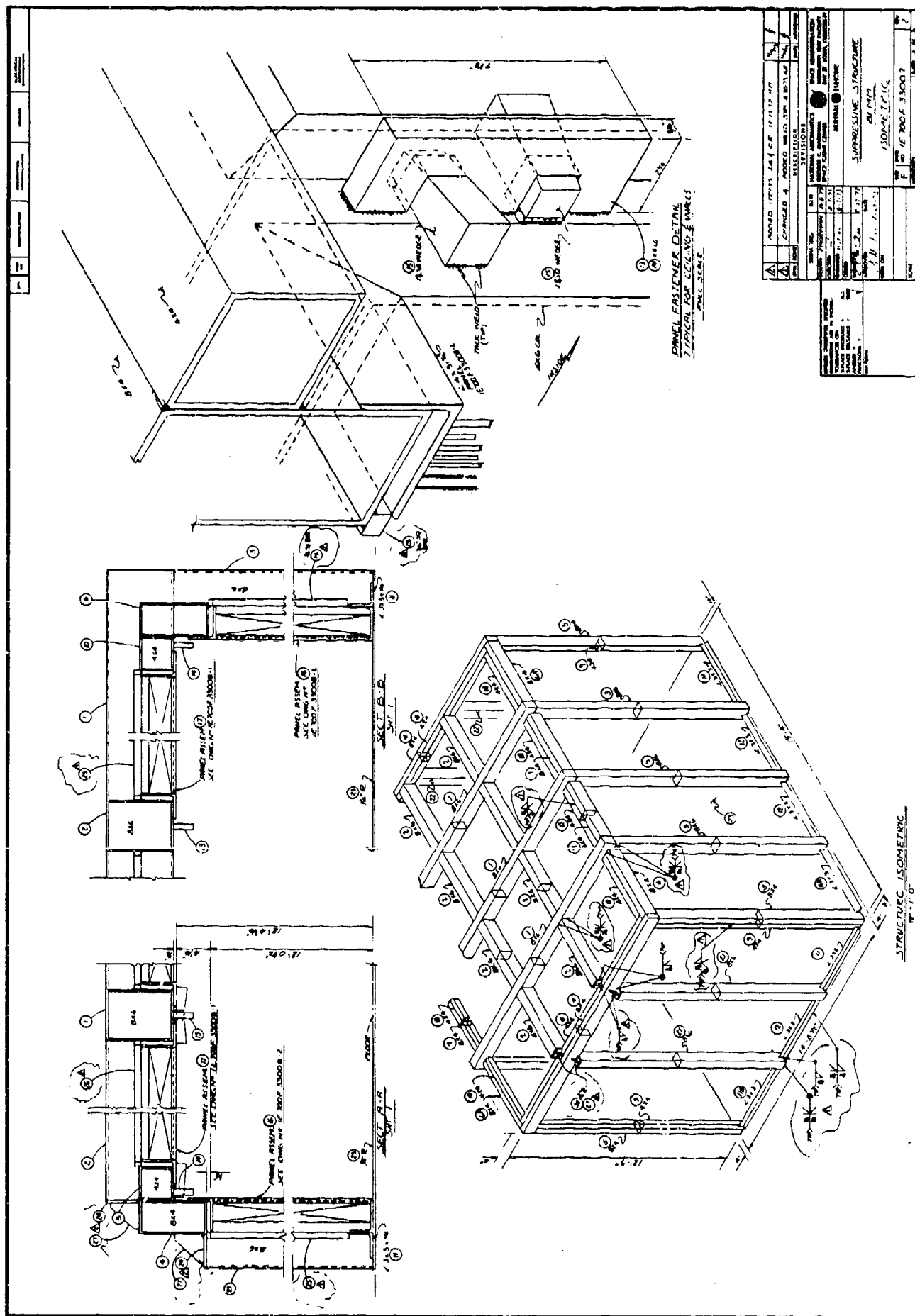
The wall panels are 4 feet by 12 feet and the ceiling panels are 4 feet square. The panel cross section is shown in Fig. A-18 and is the same for both wall and ceiling

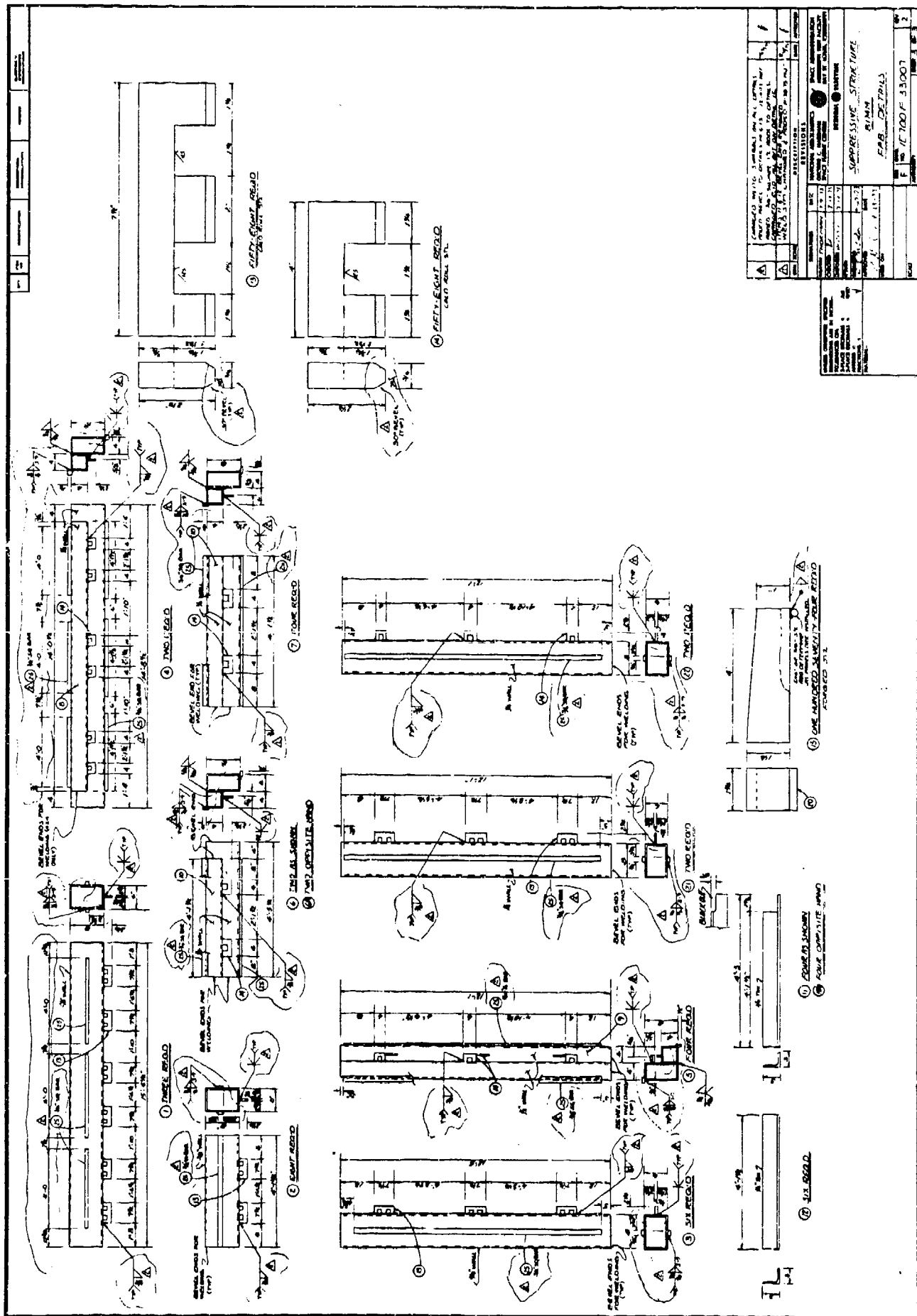


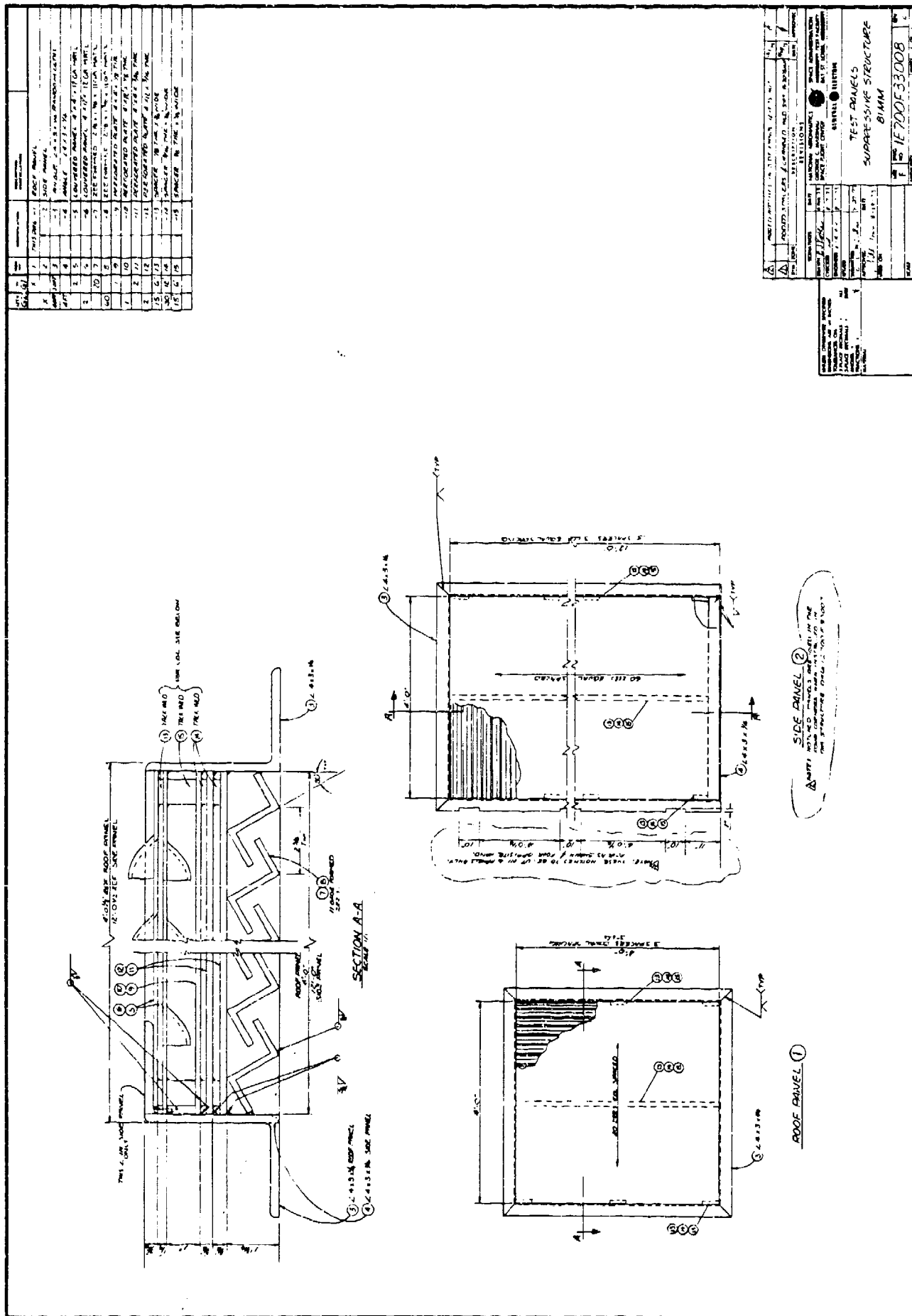
Panel Cross Section Detail

Figure A-18. Prototype 81-mm Suppressive Shield

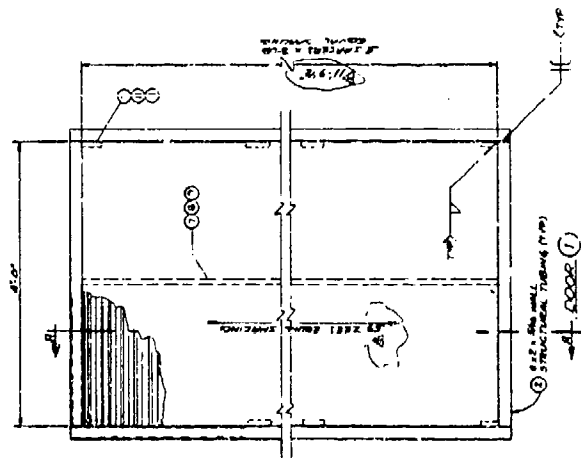
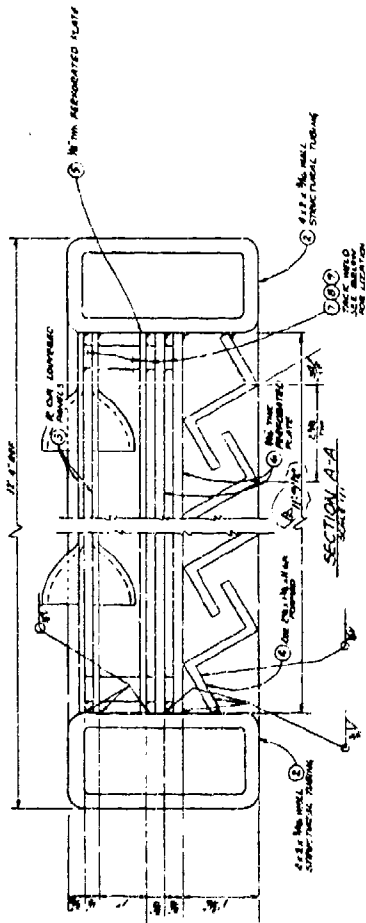








NO.	DESCRIPTION	QUANTITY	UNIT
1	1" x 12" x 1/2" PLATE	1	PC
2	2" x 12" x 1/2" PLATE	1	PC
3	3" x 12" x 1/2" PLATE	1	PC
4	4" x 12" x 1/2" PLATE	1	PC
5	5" x 12" x 1/2" PLATE	1	PC
6	6" x 12" x 1/2" PLATE	1	PC
7	7" x 12" x 1/2" PLATE	1	PC
8	8" x 12" x 1/2" PLATE	1	PC
9	9" x 12" x 1/2" PLATE	1	PC
10	10" x 12" x 1/2" PLATE	1	PC
11	11" x 12" x 1/2" PLATE	1	PC
12	12" x 12" x 1/2" PLATE	1	PC
13	13" x 12" x 1/2" PLATE	1	PC
14	14" x 12" x 1/2" PLATE	1	PC
15	15" x 12" x 1/2" PLATE	1	PC
16	16" x 12" x 1/2" PLATE	1	PC
17	17" x 12" x 1/2" PLATE	1	PC
18	18" x 12" x 1/2" PLATE	1	PC
19	19" x 12" x 1/2" PLATE	1	PC
20	20" x 12" x 1/2" PLATE	1	PC
21	21" x 12" x 1/2" PLATE	1	PC
22	22" x 12" x 1/2" PLATE	1	PC
23	23" x 12" x 1/2" PLATE	1	PC
24	24" x 12" x 1/2" PLATE	1	PC
25	25" x 12" x 1/2" PLATE	1	PC
26	26" x 12" x 1/2" PLATE	1	PC
27	27" x 12" x 1/2" PLATE	1	PC
28	28" x 12" x 1/2" PLATE	1	PC
29	29" x 12" x 1/2" PLATE	1	PC
30	30" x 12" x 1/2" PLATE	1	PC
31	31" x 12" x 1/2" PLATE	1	PC
32	32" x 12" x 1/2" PLATE	1	PC
33	33" x 12" x 1/2" PLATE	1	PC
34	34" x 12" x 1/2" PLATE	1	PC
35	35" x 12" x 1/2" PLATE	1	PC
36	36" x 12" x 1/2" PLATE	1	PC
37	37" x 12" x 1/2" PLATE	1	PC
38	38" x 12" x 1/2" PLATE	1	PC
39	39" x 12" x 1/2" PLATE	1	PC
40	40" x 12" x 1/2" PLATE	1	PC
41	41" x 12" x 1/2" PLATE	1	PC
42	42" x 12" x 1/2" PLATE	1	PC
43	43" x 12" x 1/2" PLATE	1	PC
44	44" x 12" x 1/2" PLATE	1	PC
45	45" x 12" x 1/2" PLATE	1	PC
46	46" x 12" x 1/2" PLATE	1	PC
47	47" x 12" x 1/2" PLATE	1	PC
48	48" x 12" x 1/2" PLATE	1	PC
49	49" x 12" x 1/2" PLATE	1	PC
50	50" x 12" x 1/2" PLATE	1	PC
51	51" x 12" x 1/2" PLATE	1	PC
52	52" x 12" x 1/2" PLATE	1	PC
53	53" x 12" x 1/2" PLATE	1	PC
54	54" x 12" x 1/2" PLATE	1	PC
55	55" x 12" x 1/2" PLATE	1	PC
56	56" x 12" x 1/2" PLATE	1	PC
57	57" x 12" x 1/2" PLATE	1	PC
58	58" x 12" x 1/2" PLATE	1	PC
59	59" x 12" x 1/2" PLATE	1	PC
60	60" x 12" x 1/2" PLATE	1	PC
61	61" x 12" x 1/2" PLATE	1	PC
62	62" x 12" x 1/2" PLATE	1	PC
63	63" x 12" x 1/2" PLATE	1	PC
64	64" x 12" x 1/2" PLATE	1	PC
65	65" x 12" x 1/2" PLATE	1	PC
66	66" x 12" x 1/2" PLATE	1	PC
67	67" x 12" x 1/2" PLATE	1	PC
68	68" x 12" x 1/2" PLATE	1	PC
69	69" x 12" x 1/2" PLATE	1	PC
70	70" x 12" x 1/2" PLATE	1	PC
71	71" x 12" x 1/2" PLATE	1	PC
72	72" x 12" x 1/2" PLATE	1	PC
73	73" x 12" x 1/2" PLATE	1	PC
74	74" x 12" x 1/2" PLATE	1	PC
75	75" x 12" x 1/2" PLATE	1	PC
76	76" x 12" x 1/2" PLATE	1	PC
77	77" x 12" x 1/2" PLATE	1	PC
78	78" x 12" x 1/2" PLATE	1	PC
79	79" x 12" x 1/2" PLATE	1	PC
80	80" x 12" x 1/2" PLATE	1	PC
81	81" x 12" x 1/2" PLATE	1	PC
82	82" x 12" x 1/2" PLATE	1	PC
83	83" x 12" x 1/2" PLATE	1	PC
84	84" x 12" x 1/2" PLATE	1	PC
85	85" x 12" x 1/2" PLATE	1	PC
86	86" x 12" x 1/2" PLATE	1	PC
87	87" x 12" x 1/2" PLATE	1	PC
88	88" x 12" x 1/2" PLATE	1	PC
89	89" x 12" x 1/2" PLATE	1	PC
90	90" x 12" x 1/2" PLATE	1	PC
91	91" x 12" x 1/2" PLATE	1	PC
92	92" x 12" x 1/2" PLATE	1	PC
93	93" x 12" x 1/2" PLATE	1	PC
94	94" x 12" x 1/2" PLATE	1	PC
95	95" x 12" x 1/2" PLATE	1	PC
96	96" x 12" x 1/2" PLATE	1	PC
97	97" x 12" x 1/2" PLATE	1	PC
98	98" x 12" x 1/2" PLATE	1	PC
99	99" x 12" x 1/2" PLATE	1	PC
100	100" x 12" x 1/2" PLATE	1	PC



PROJECT NO. 1700-33009	
DOOR	
SUPPORTIVE STRUCTURE	
DATE 1/1/77	
BY 1700-33009	
CHECKED BY 1700-33009	
APPROVED BY 1700-33009	
REVISIONS	
NO.	DESCRIPTION
1	DOOR
2	DOOR
3	DOOR
4	DOOR
5	DOOR
6	DOOR
7	DOOR
8	DOOR
9	DOOR
10	DOOR
11	DOOR
12	DOOR
13	DOOR
14	DOOR
15	DOOR
16	DOOR
17	DOOR
18	DOOR
19	DOOR
20	DOOR
21	DOOR
22	DOOR
23	DOOR
24	DOOR
25	DOOR
26	DOOR
27	DOOR
28	DOOR
29	DOOR
30	DOOR
31	DOOR
32	DOOR
33	DOOR
34	DOOR
35	DOOR
36	DOOR
37	DOOR
38	DOOR
39	DOOR
40	DOOR
41	DOOR
42	DOOR
43	DOOR
44	DOOR
45	DOOR
46	DOOR
47	DOOR
48	DOOR
49	DOOR
50	DOOR
51	DOOR
52	DOOR
53	DOOR
54	DOOR
55	DOOR
56	DOOR
57	DOOR
58	DOOR
59	DOOR
60	DOOR
61	DOOR
62	DOOR
63	DOOR
64	DOOR
65	DOOR
66	DOOR
67	DOOR
68	DOOR
69	DOOR
70	DOOR
71	DOOR
72	DOOR
73	DOOR
74	DOOR
75	DOOR
76	DOOR
77	DOOR
78	DOOR
79	DOOR
80	DOOR
81	DOOR
82	DOOR
83	DOOR
84	DOOR
85	DOOR
86	DOOR
87	DOOR
88	DOOR
89	DOOR
90	DOOR
91	DOOR
92	DOOR
93	DOOR
94	DOOR
95	DOOR
96	DOOR
97	DOOR
98	DOOR
99	DOOR
100	DOOR

panels. The panels are mounted from the inside of the structure and wedged tight against the frame as shown in the Panel Fastener Detail on Fig. A-19b.

The base of the shield consists of a 1/4-inch steel plate. The lower ends of the vertical frame members and the bottom support angles for the wall panels are welded to this base plate.

A 4 x 12-foot door is provided at the center of one end of the shield. The door has the same cross section as the wall and roof panels, except that it is framed with 4 x 2 x 5/16 structural steel tube instead of angles.

b. Milan 81-mm Suppressive Shield

The Milan adaptation is quite similar to the Prototype 81-mm Shield; see Fig. A-20. The primary differences between the two versions are

- Square, rather than rectangular, floor plan.
- Revised design of the structural frame corners.
- Sliding access door.
- Inclusion of provisions for anchoring the shield to a reinforced concrete foundation.
- Inclusion of provisions for a removable vertical frame member (column) to permit a larger access opening.

The outside dimensions of the Milan 81-mm shield are approximately 15.4 feet wide by 15.4 feet long by 13.1 feet high. The inside dimensions are 14 feet wide by 14 feet long by 12.4 feet high.

The structural frame corner design was modified as a result of the tests conducted on the Prototype 81-mm

BEST AVAILABLE COPY

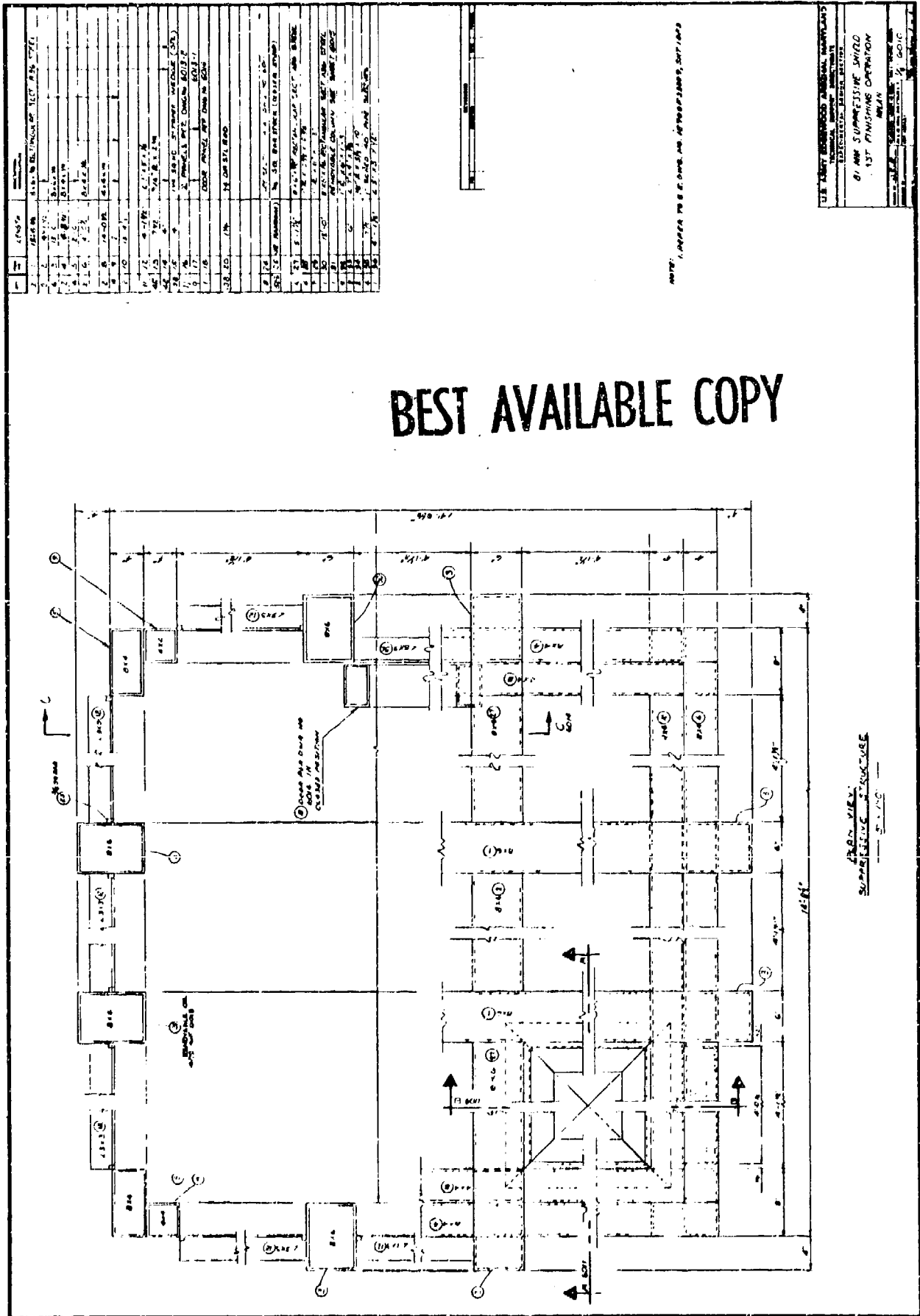
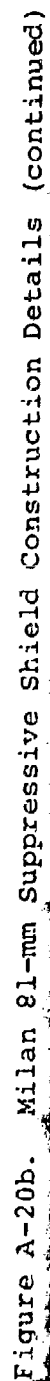


Figure A-20a. Milan 81-mm Suppressive Shield Construction Details



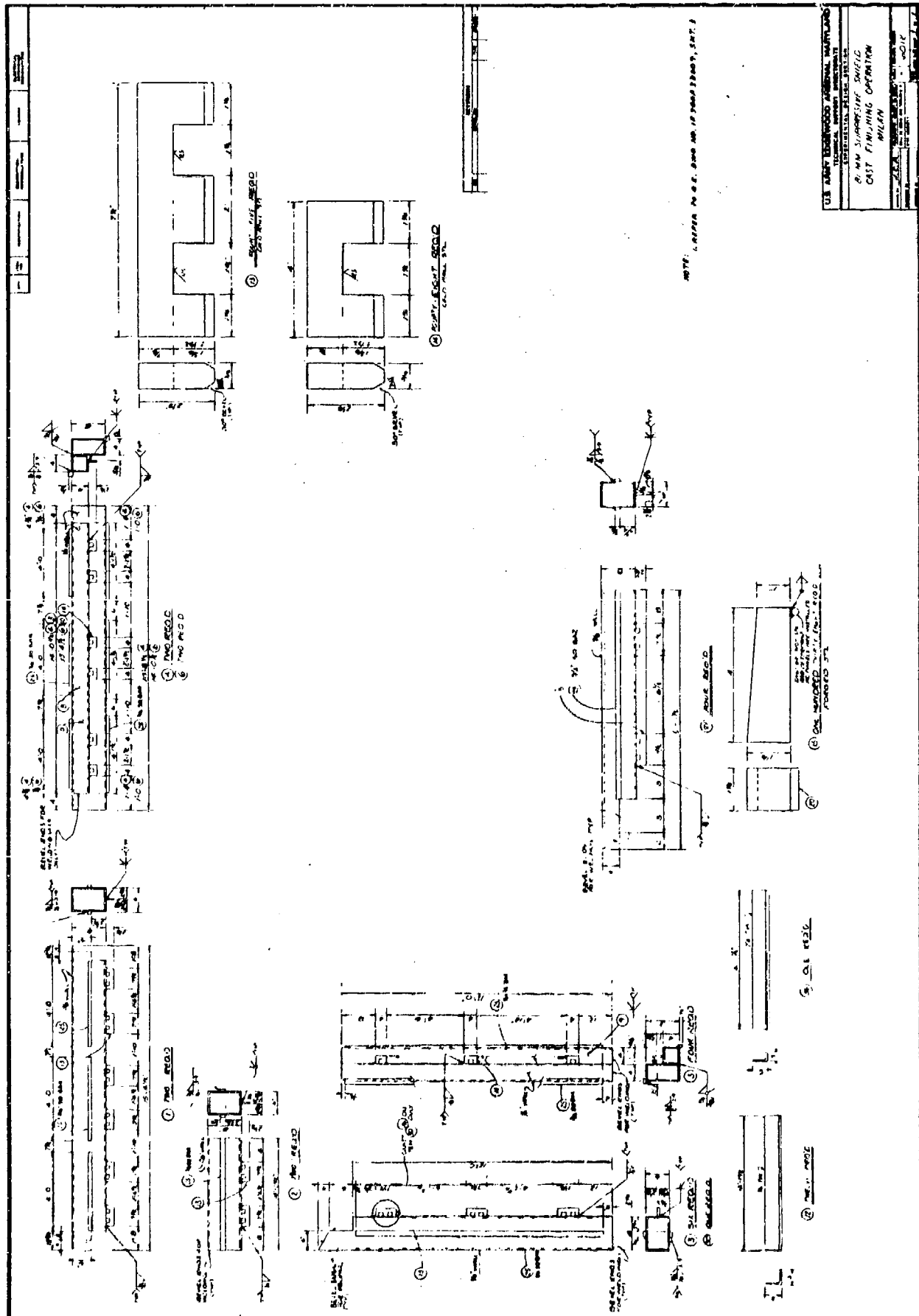
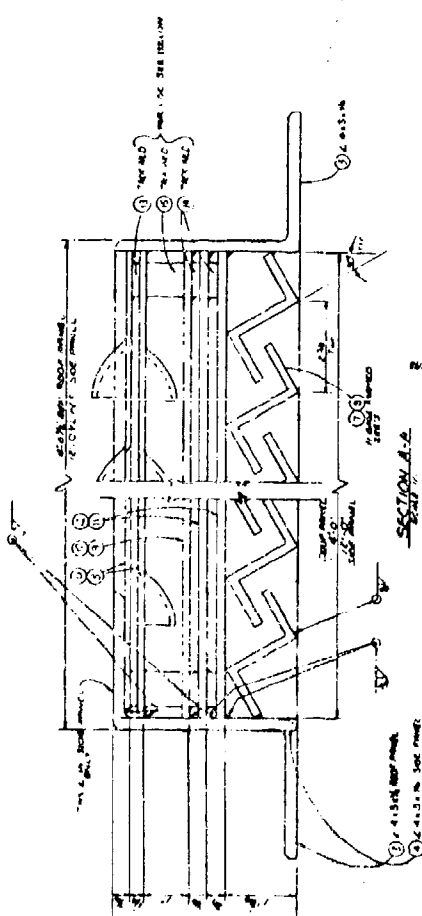
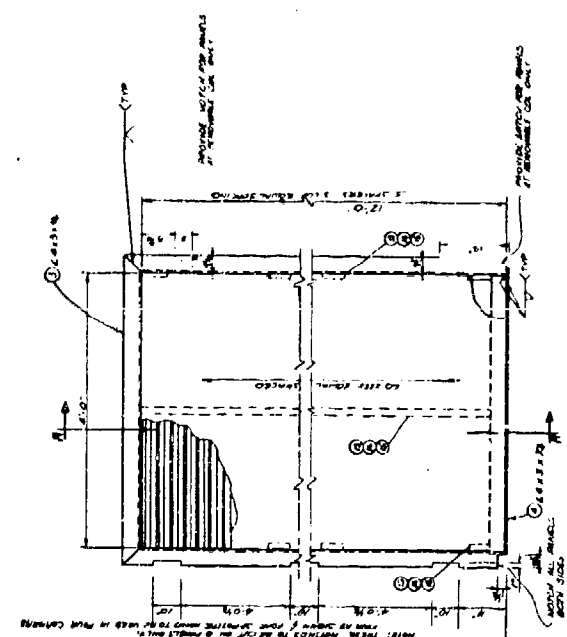


Figure A-20c. Milan 81-mm Suppressive Shield Construction Details (continued)

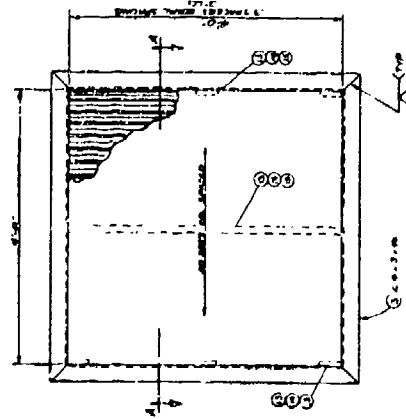
ITEM	DESCRIPTION	QUANTITY	UNIT
1	ROOF PANEL	1	SQ. YD.
2	ROOF PANEL	1	SQ. YD.
3	ROOF PANEL	1	SQ. YD.
4	ROOF PANEL	1	SQ. YD.
5	ROOF PANEL	1	SQ. YD.
6	ROOF PANEL	1	SQ. YD.
7	ROOF PANEL	1	SQ. YD.
8	ROOF PANEL	1	SQ. YD.
9	ROOF PANEL	1	SQ. YD.
10	ROOF PANEL	1	SQ. YD.
11	ROOF PANEL	1	SQ. YD.
12	ROOF PANEL	1	SQ. YD.
13	ROOF PANEL	1	SQ. YD.
14	ROOF PANEL	1	SQ. YD.
15	ROOF PANEL	1	SQ. YD.
16	ROOF PANEL	1	SQ. YD.
17	ROOF PANEL	1	SQ. YD.
18	ROOF PANEL	1	SQ. YD.
19	ROOF PANEL	1	SQ. YD.
20	ROOF PANEL	1	SQ. YD.
21	ROOF PANEL	1	SQ. YD.
22	ROOF PANEL	1	SQ. YD.
23	ROOF PANEL	1	SQ. YD.
24	ROOF PANEL	1	SQ. YD.
25	ROOF PANEL	1	SQ. YD.
26	ROOF PANEL	1	SQ. YD.
27	ROOF PANEL	1	SQ. YD.
28	ROOF PANEL	1	SQ. YD.
29	ROOF PANEL	1	SQ. YD.
30	ROOF PANEL	1	SQ. YD.
31	ROOF PANEL	1	SQ. YD.
32	ROOF PANEL	1	SQ. YD.
33	ROOF PANEL	1	SQ. YD.
34	ROOF PANEL	1	SQ. YD.
35	ROOF PANEL	1	SQ. YD.
36	ROOF PANEL	1	SQ. YD.
37	ROOF PANEL	1	SQ. YD.
38	ROOF PANEL	1	SQ. YD.
39	ROOF PANEL	1	SQ. YD.
40	ROOF PANEL	1	SQ. YD.
41	ROOF PANEL	1	SQ. YD.
42	ROOF PANEL	1	SQ. YD.
43	ROOF PANEL	1	SQ. YD.
44	ROOF PANEL	1	SQ. YD.
45	ROOF PANEL	1	SQ. YD.
46	ROOF PANEL	1	SQ. YD.
47	ROOF PANEL	1	SQ. YD.
48	ROOF PANEL	1	SQ. YD.
49	ROOF PANEL	1	SQ. YD.
50	ROOF PANEL	1	SQ. YD.
51	ROOF PANEL	1	SQ. YD.
52	ROOF PANEL	1	SQ. YD.
53	ROOF PANEL	1	SQ. YD.
54	ROOF PANEL	1	SQ. YD.
55	ROOF PANEL	1	SQ. YD.
56	ROOF PANEL	1	SQ. YD.
57	ROOF PANEL	1	SQ. YD.
58	ROOF PANEL	1	SQ. YD.
59	ROOF PANEL	1	SQ. YD.
60	ROOF PANEL	1	SQ. YD.
61	ROOF PANEL	1	SQ. YD.
62	ROOF PANEL	1	SQ. YD.
63	ROOF PANEL	1	SQ. YD.
64	ROOF PANEL	1	SQ. YD.
65	ROOF PANEL	1	SQ. YD.
66	ROOF PANEL	1	SQ. YD.
67	ROOF PANEL	1	SQ. YD.
68	ROOF PANEL	1	SQ. YD.
69	ROOF PANEL	1	SQ. YD.
70	ROOF PANEL	1	SQ. YD.
71	ROOF PANEL	1	SQ. YD.
72	ROOF PANEL	1	SQ. YD.
73	ROOF PANEL	1	SQ. YD.
74	ROOF PANEL	1	SQ. YD.
75	ROOF PANEL	1	SQ. YD.
76	ROOF PANEL	1	SQ. YD.
77	ROOF PANEL	1	SQ. YD.
78	ROOF PANEL	1	SQ. YD.
79	ROOF PANEL	1	SQ. YD.
80	ROOF PANEL	1	SQ. YD.
81	ROOF PANEL	1	SQ. YD.
82	ROOF PANEL	1	SQ. YD.
83	ROOF PANEL	1	SQ. YD.
84	ROOF PANEL	1	SQ. YD.
85	ROOF PANEL	1	SQ. YD.
86	ROOF PANEL	1	SQ. YD.
87	ROOF PANEL	1	SQ. YD.
88	ROOF PANEL	1	SQ. YD.
89	ROOF PANEL	1	SQ. YD.
90	ROOF PANEL	1	SQ. YD.
91	ROOF PANEL	1	SQ. YD.
92	ROOF PANEL	1	SQ. YD.
93	ROOF PANEL	1	SQ. YD.
94	ROOF PANEL	1	SQ. YD.
95	ROOF PANEL	1	SQ. YD.
96	ROOF PANEL	1	SQ. YD.
97	ROOF PANEL	1	SQ. YD.
98	ROOF PANEL	1	SQ. YD.
99	ROOF PANEL	1	SQ. YD.
100	ROOF PANEL	1	SQ. YD.



SECTION A-A



SIDE PANEL 2



ROOF PANEL 1

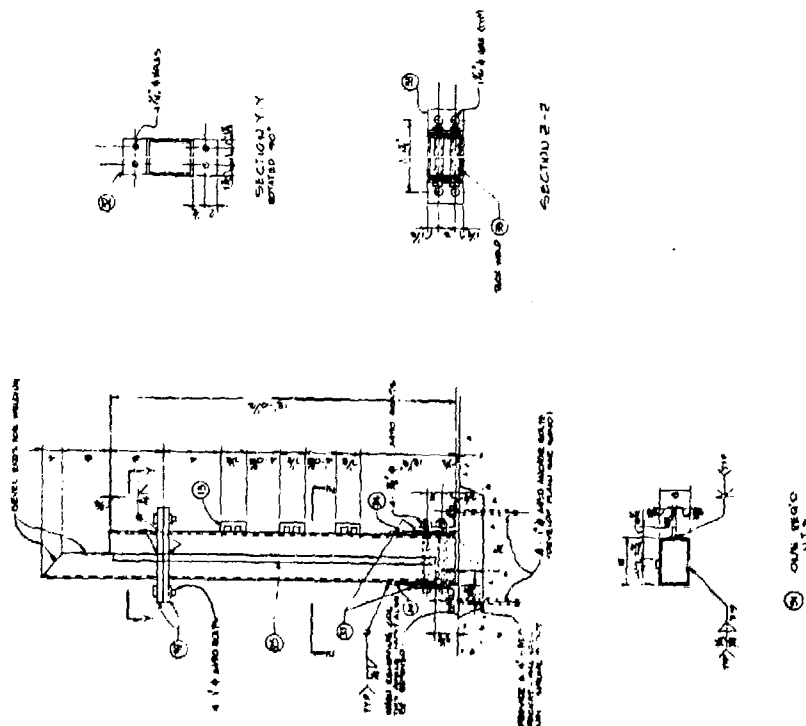
NOTE: REFER TO THE DRAWING FOR DIMENSIONS.

US ARMY ENGINEERING CENTER, FORT MONMOUTH, NEW JERSEY	
PROJECT: 81-MM SUPPRESSIVE SHIELD	
TASK: CAST FINISHING OPERATION	
DRAWING NO.: 81-107/108	
DATE: 1968	

BEST AVAILABLE COPY

Figure A-20d Milan 81-mm Suppressive Shield Construction Details (continued)

BEST AVAILABLE COPY



AD 18:

U.S. ARMY EDGEWOOD ARSENAL, MARYLAND TECHNICAL PROJECT AND TOWNSHIP IDENTIFICATION, 313 MAR. 1962-2000	BR. 1000 SUPERPRESSIVE 300000 CASE FINISHING OPERATIONS MIL. AR.	6015
--	--	------

Figure A-20f. Milan 81-mm Suppressive Shield Construction Details (continued)

Shield design. These modifications are shown in Fig. A-21.

The Milan 81-mm shield utilizes a sliding access door. The door section, which is shown on Fig. A-20e, is the same as the original design.

The Milan 81-mm shield does not utilize the 1/4-inch steel base plate employed with the original design. The columns of the revised design are anchored to either the existing plant foundation or to a prepared foundation as illustrated in Fig. A-22.

It was deemed desirable to be able to provide access to the interior of the shield for equipment too large to pass through the personnel door. Accordingly, a removable column has been designed which will permit opening up an area approximately 8 x 12 feet. This column modification is shown in Fig. A-23.

A.6.2 Application

a. Prototype 81-mm Shield

The Prototype 81-mm Suppressive Shield Design was tested and safety approved for 6.72 pounds of C-4 explosive, (10.1 pounds of C-4 for quasi-static pressure) or equivalent. A typical application of this shield would be for 81-mm mortar drill-and-face and/or cast-finishing operations. The charge must be located so that the maximum reflected pressure on any panel does not exceed 220 psi.

The test results show that external pressures are reduced to 2.3 psi or less at three feet from any exterior wall, that the fireball is contained essentially within the shield, and that all fragments are contained by the shield. The test fragment threat consisted of two tests: (a) simultaneous detonation of two each M374, 81-mm mortar projectiles with simulated process equipment, and (b) simultaneous detonation of six each M374, 81-mm mortar projectiles.

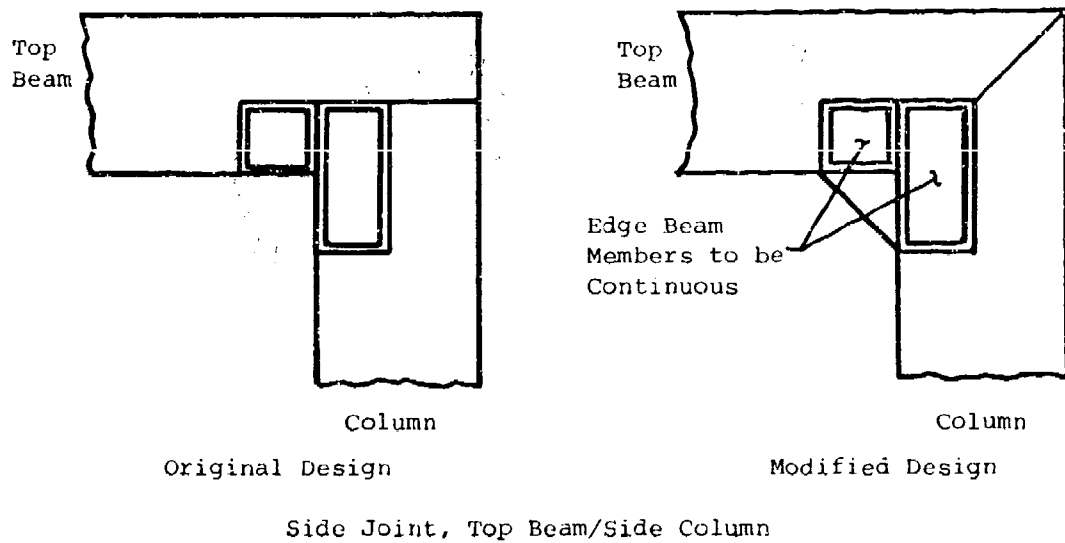
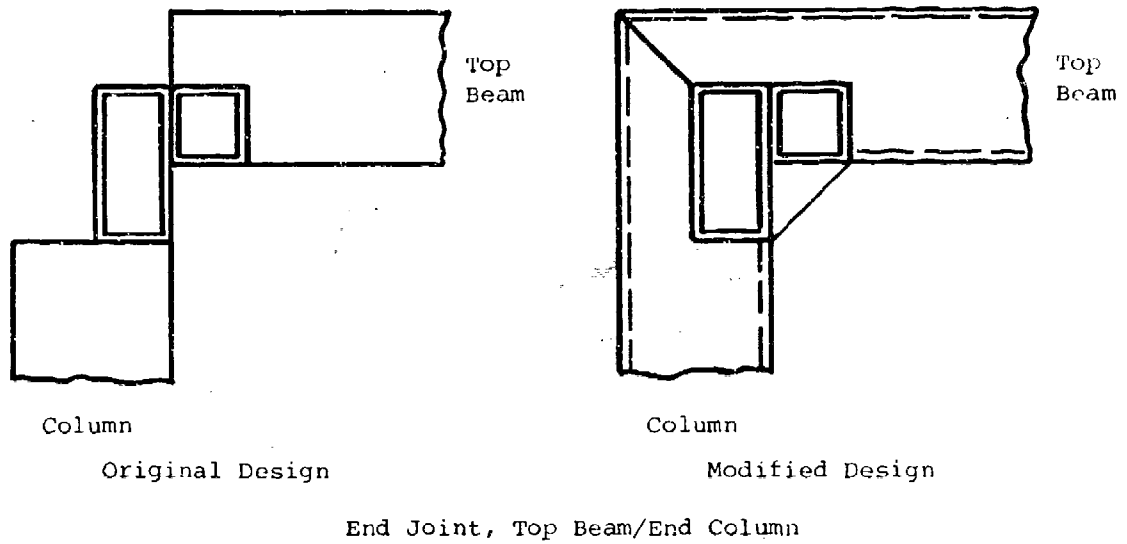


Figure A-21. Revised Structural Frame Corner Design

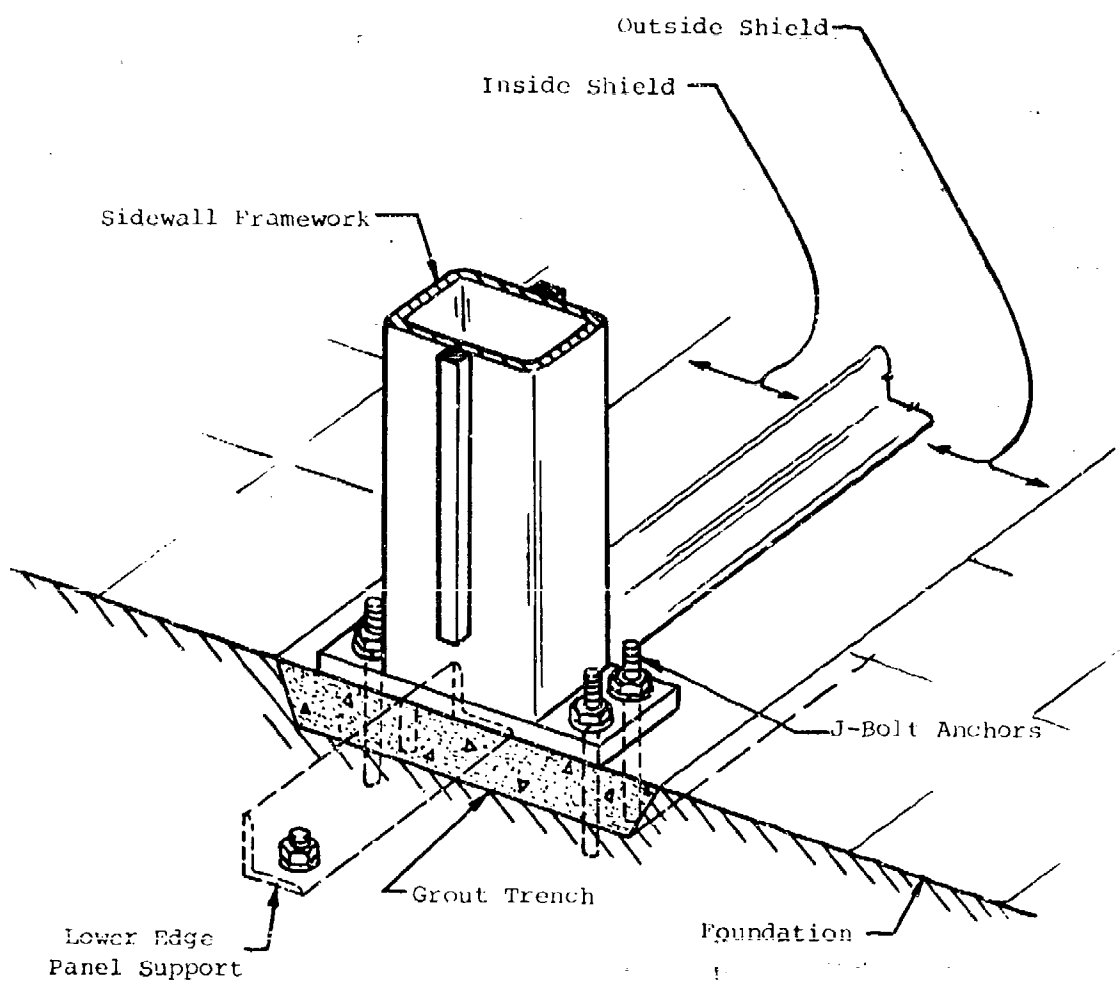


Figure A-22. Milan 81-mm Suppressive Shield Foundation Attachment

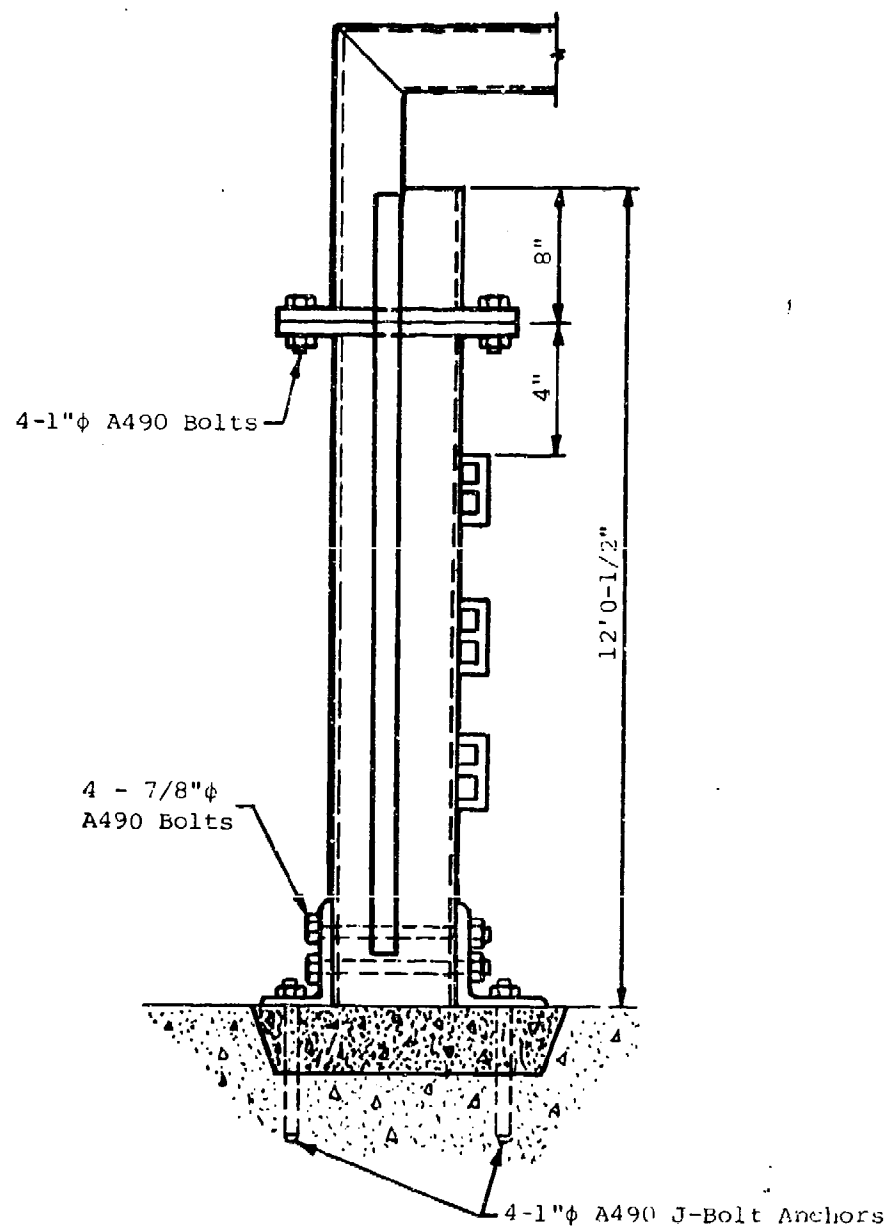


Figure A-23. Milan 81-mm Suppressive Shield Removable Column

The Prototype 81-mm Shield design would be appropriate for munition operations

- Requiring a maximum rectangular floor area 14 feet by 18.7 feet with a maximum 12.4-foot clear height (inside dimensions).
- Involving a charge weight equivalent to 6.72 pounds of C-4 explosive (7.24 lb TNT equiv.; maximum W/V ratio = 0.0034 lb/ft³; minimum Z = 3.62 ft/lb^{1/3} to sidewall and minimum Z = 3.20 ft/lb^{1/3} for roof).
- That produce no fragments which cannot be defeated by 1.23 inches of mild steel.
- That are compatible with 2.3 psi peak external pressure at three feet from any exterior shield wall.

Utilization of the prototype 81-mm design for any application may incorporate the design improvements of the Milan 81-mm adaptation, i.e., the revised frame corner design, sliding door, shield anchors, and removable column.

b. Milan 81-mm Suppressive Shield

This adaptation of the Prototype 81-mm Shield design is appropriate for applications which do not require as much floor area as the prototype design and which involve a smaller charge weight. The Milan 81-mm Suppressive Shield is appropriate for munition operations

- Requiring a maximum floor area 14 feet square with a 12.4-foot maximum clear height (inside dimensions).

- Involving a charge weight equivalent to 4.2 pounds (6.3 pounds of C-4 for quasi-static pressure) of bare C-4 explosive (4.53 lb TNT equiv.; maximum W/V ratio = 0.0028 lb/ft^3 ; minimum $Z = 4.23 \text{ ft/lb}^{1/3}$ at sidewalls and minimum $Z = 3.75 \text{ ft/lb}^{1/3}$ for roof).
- That produce no fragments which cannot be defeated by 1.23 inches of mild steel.
- That are compatible with 2.3 psi peak external pressure at 7.3 feet from any exterior shield wall.

A.6.3 Modification

The Milan 81-mm shield design is an example of modification of a safety approved shield design for which safety approval may be obtained without further testing. The Milan 81-mm design did not alter the fundamental hazard-defeating components of the shield that had been proof-tested, i.e., the panels and the structural frame, except to make the frame stronger. The panels resist airblast loads primarily by one-way flexural response of the Z shapes in the 4-foot direction. These loads are then transmitted to the vertical and/or horizontal frame members. Therefore, since the panel and frame cross sectional properties remain the same and since the 4-foot modular spacing and frame member spans are unchanged, the airblast load carrying capacity of the design has not been diminished. The fragment defeating capability of the design is the same, since the same thickness of steel has been maintained.

Assurance that the proof-test airblast loading will not be exceeded is provided by the increased Z value and the decreased W/V ratio. The structural frame corner design revision clearly provides increased load-carrying capability and does not require further testing. Similarly, it can be shown with proven and accepted analytical methods that the shield anchoring system

HNDM-1110-1-2

and the removable column design are as strong as, or stronger than, the corresponding elements of the tested design. Changing the access door method of support from hinged to monorail does not alter the basic door configuration that was successfully proof tested. In addition, the monorail support system utilized was successfully proof tested with the Group 4 shield design.

A.7 REFERENCES

- A-1 Katsanis, D.J., Safety Approval of Suppressive Shields, EM-TR-76088, Edgewood Arsenal, Aberdeen Proving Ground, Md., August 1976. (U)

APPENDIX B

RESPONSE CHARTS

APPENDIX B RESPONSE CHARTS

B.1 INTRODUCTION

The response charts presented in this appendix were prepared as a design aid alternative to the use of equations in Chapter 5. They should only be used for preliminary design or analysis. The charts are plots of Eq. 5-54 for a range of values of B/R_m or P_r/r_m (the load term "B" and the resistance term " R_m " as shown on the charts may be either total load and total resistance (B/R_m) or unit load and unit resistance (P_r/r_m)), t_1/T_N , C_1 , C_2 and the ductility ratio μ , where

- B = peak total load, pounds
- P_r = peak unit pressure, psi
- R_m = maximum resistance of structural element, pounds
- r_m = maximum unit resistance of structural element, psi
- t_1 = duration of reflected pressure pulse, sec
- T_N = fundamental period of vibration of element, sec
- $C_1 = (P_r - P_{qs})/P_r$
- $C_2 = P_{qs}/P_r$
- P_{qs} = peak quasi-static pressure, psi
- $\mu = X_m/X_e$ = ductility ratio
- X_m = maximum displacement of single degree of freedom system, in
- X_e = yield displacement of single degree of freedom system, in

The chart solutions are based upon the same assumptions stated for Eq. 5-54, i.e.,

- A short duration impulsive load superimposed on a long duration quasi-static loading.
- An elastic-plastic resistance function for the structural element.
- No structural damping in system.

Since they are derived for an infinite duration quasi-static pressure, the charts yield conservative results for a decaying quasi-static pressure component. The degree of conservatism depends on the actual pulse duration. For cases where the duration of the reflected pressure is of the same order of magnitude as the period of the structure, the charts of this appendix will yield unconservative results and the charts should not be extrapolated beyond the values plotted. The charts can always be used, however, for initial selection of a trial section for further analysis.

B.2 USE OF CHARTS

The charts of this appendix can be used in various ways.

- Class 1 - Find the maximum response of a given structural element to a specified loading function.
- Class 2 - Find the required maximum resistance for a given loading and specified maximum response.
- Class 3 - Find the maximum allowable peak pressure for a given structural element and specified maximum response.

Except for the first class of problems where the loading function and structural properties are specified, an iterative process is required to obtain a solution. For the first class of problems, one must compute C_1 , C_2 , B/R_m and t_1/T_N . Next, locate the appropriate chart for the computed values of C_1 and C_2 . On this chart, locate the curved line for the computed value of B/R_m . At the intersection of this curve with the vertical line representing the computed value t_1/T_N , read the ductility ratio μ on the vertical scale at the left side of the chart.

For the second class of problems, it is necessary to assume a trial section or a period of vibration. Then C_1 , C_2 and t_1/T_N are computed as before. Select the appropriate chart for the computed values of C_1 and C_2 . At the intersection of the vertical line representing the computed value of t_1/T_N and the horizontal line representing the specified ductility ratio μ , read the value B/R_m . From this ratio, compute the required R_m , select or design the element, and then recompute its period of vibration. If the new period differs significantly from the first value, the entire process must be repeated with a new value of t_1/T_N . Repeat the iterations until satisfactory agreement is achieved.

The last class of problems is perhaps the most difficult because of the greater number of parameters describing the loading function. The characteristics of the loading function must be assumed and the parameters C_1 , C_2 , t_1/T_N and B/R_m computed. The appropriate chart is selected and the maximum response (ductility ratio) determined. If the maximum response does not agree with that specified, a new loading function is assumed and the process repeated until the desired agreement is achieved.

Illustrative examples which demonstrate use of the response charts are presented below. These examples utilize given data from selected examples in Chapter V and, therefore, provide some comparison of the accuracy of the response charts for a range of problem parameters. As might be expected, where the problem parameters fit the criteria for use of Eq. 5-54, the agreement is good.

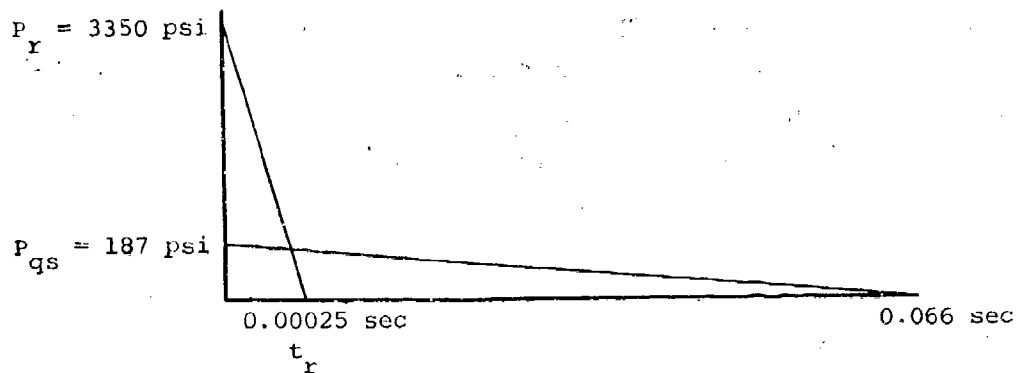
B.3 ILLUSTRATIVE EXAMPLES

B.3.1 Response of Group 3 Wall Beam Element to Airblast Loading

a. Given

From Example 5.6.1, a 48.8 pound charge of

Pentolite is detonated inside the Group 3 Suppressive Shield. The resulting airblast loading on the interior surfaces of the wall is shown below.



b. Find

The maximum response of beam elements in the shield wall using the response charts of Appendix B.

c. Solution

The following beam element properties were established in Ex. 5.6.1.

$$\text{Maximum resistance} = r_m = 236.13 \text{ psi}$$

$$\begin{aligned} \text{Fundamental period of vibration of beam elements} &= T_N \\ &= 0.00414 \text{ sec} \end{aligned}$$

From the given airblast loading function,

$$C_1 = \frac{P_r - P_{qs}}{P_r} = \frac{3350 - 187}{3350} = 0.944 \rightarrow \text{say } 0.94$$

$$C_2 = \frac{P_{qs}}{P_r} = \frac{187}{3350} = 0.056 \rightarrow \text{say } 0.06$$

$$t_r = t_1 = 0.00025 \text{ sec}$$

and

$$t_1/T_N = 0.00025/0.00414 = 0.0604$$

$$P_r/r_m \text{ (same as } B/R_m) = \frac{3350}{236.13} = 14.19$$

In order to use the response charts, it is necessary to assume an infinite duration for the quasi-static pressure rather than the load duration predicted by blow-down time computations.

From Fig. B-35 for $C_1 = 0.94$, $C_2 = 0.06$ with P_r/r_m (same as B/R_m) = 14.19 and $t_1/T_N = 0.0604$, the ductility ratio, $\mu = 24$.

Using Eq. 5-55 in Ex. 5.6.1, it was found that $\mu = 15$. The greater response obtained from using the charts is largely due to the assumption of an infinite duration load. For this example, the difference is

$$100 \frac{24-15}{15} = 57 \text{ percent increase in computed maximum response.}$$

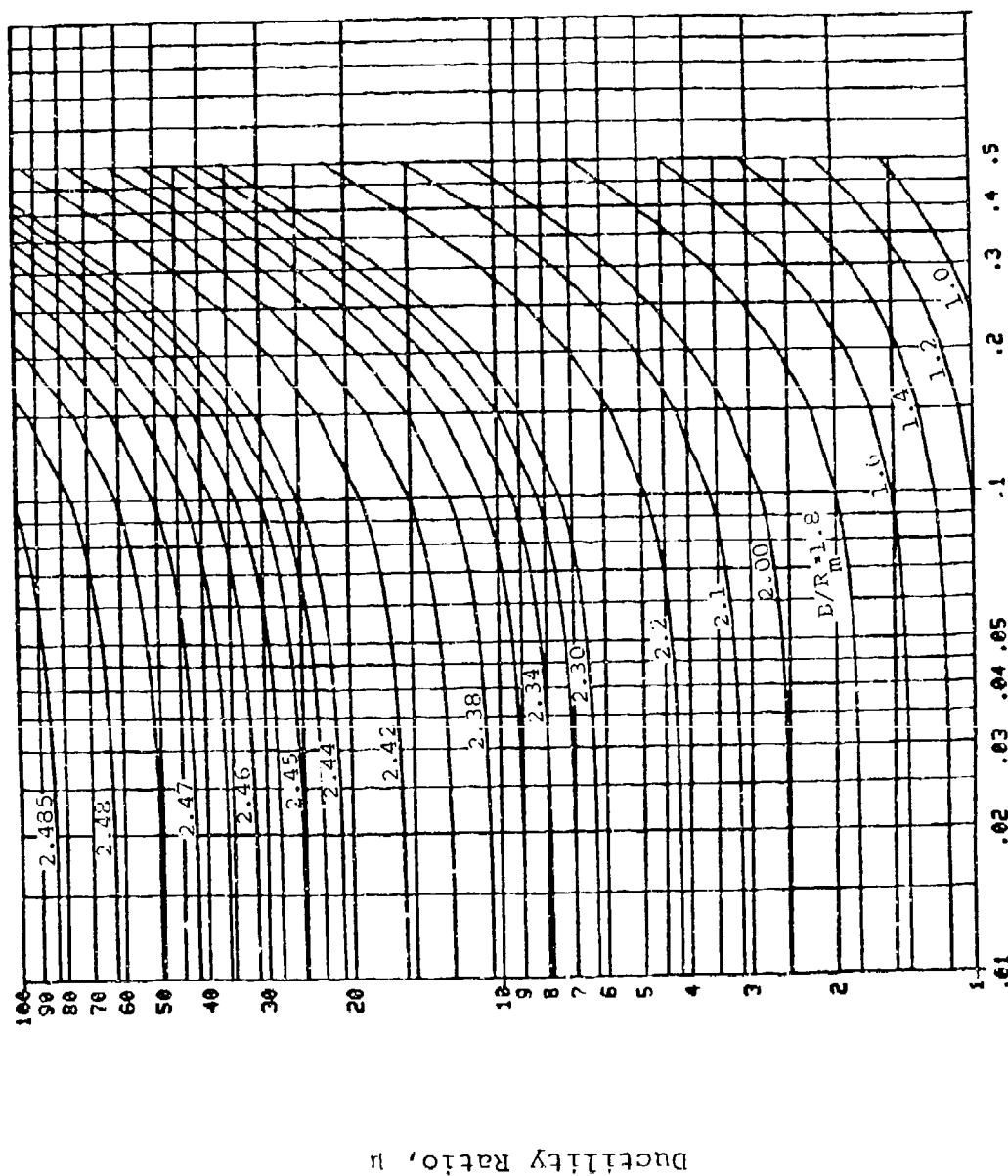


Figure B-1. Response Chart for $C_1 = 0.60$ and $C_2 = 0.40$

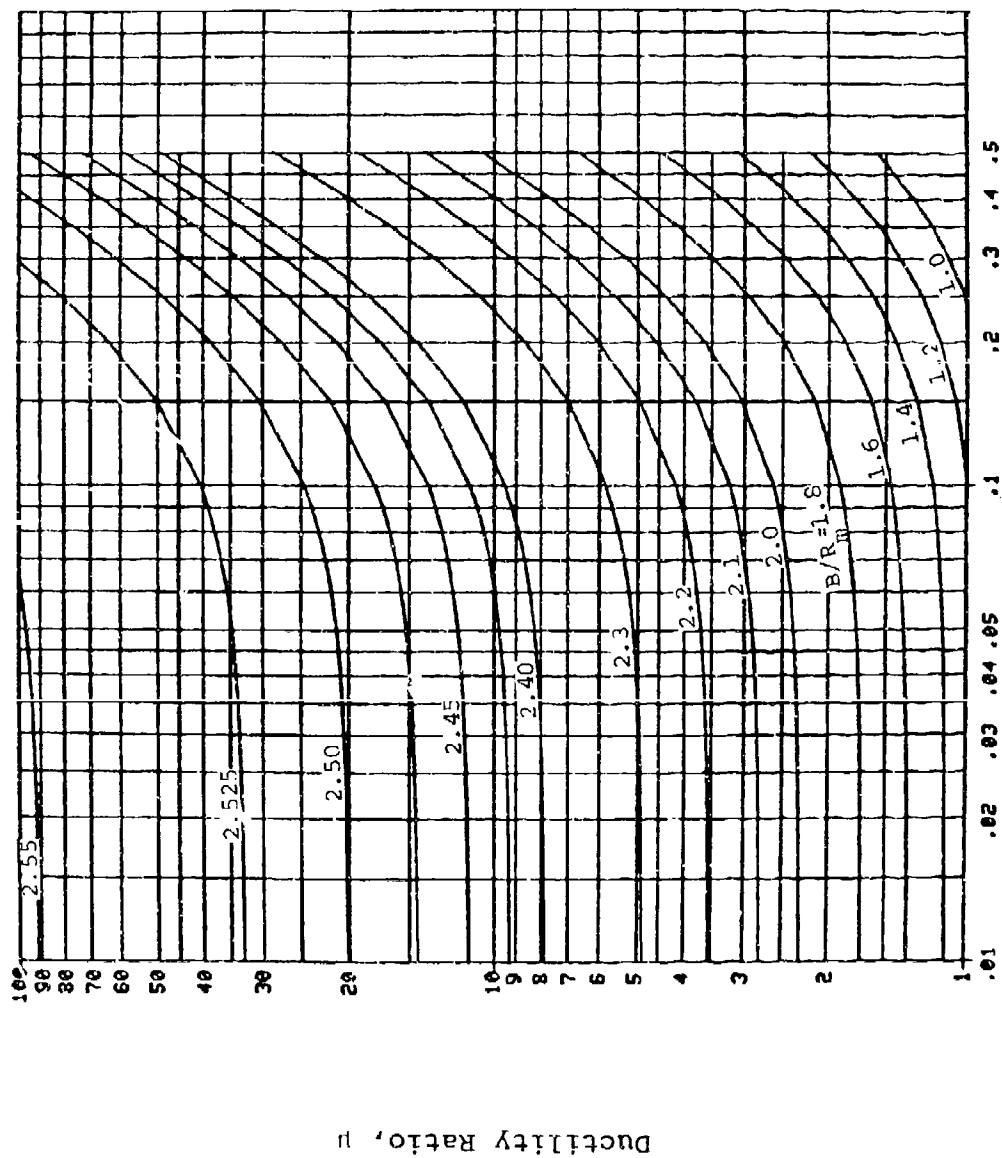


Figure B-2. Response Chart for $C_1 = 0.61$ and $C_2 = 0.39$

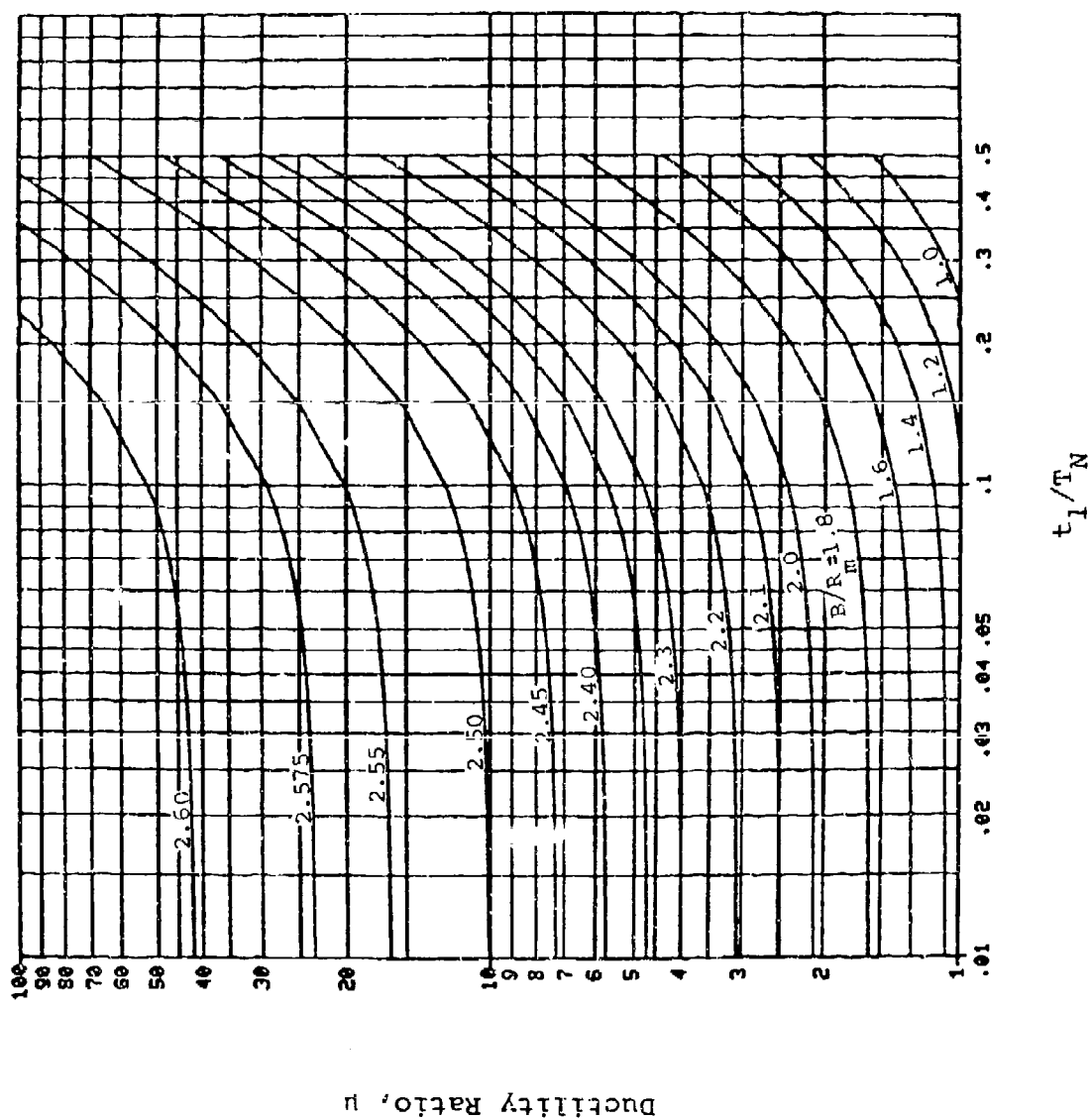


Figure B-3. Response Chart for $C_1 = 0.62$ and $C_2 = 0.38$

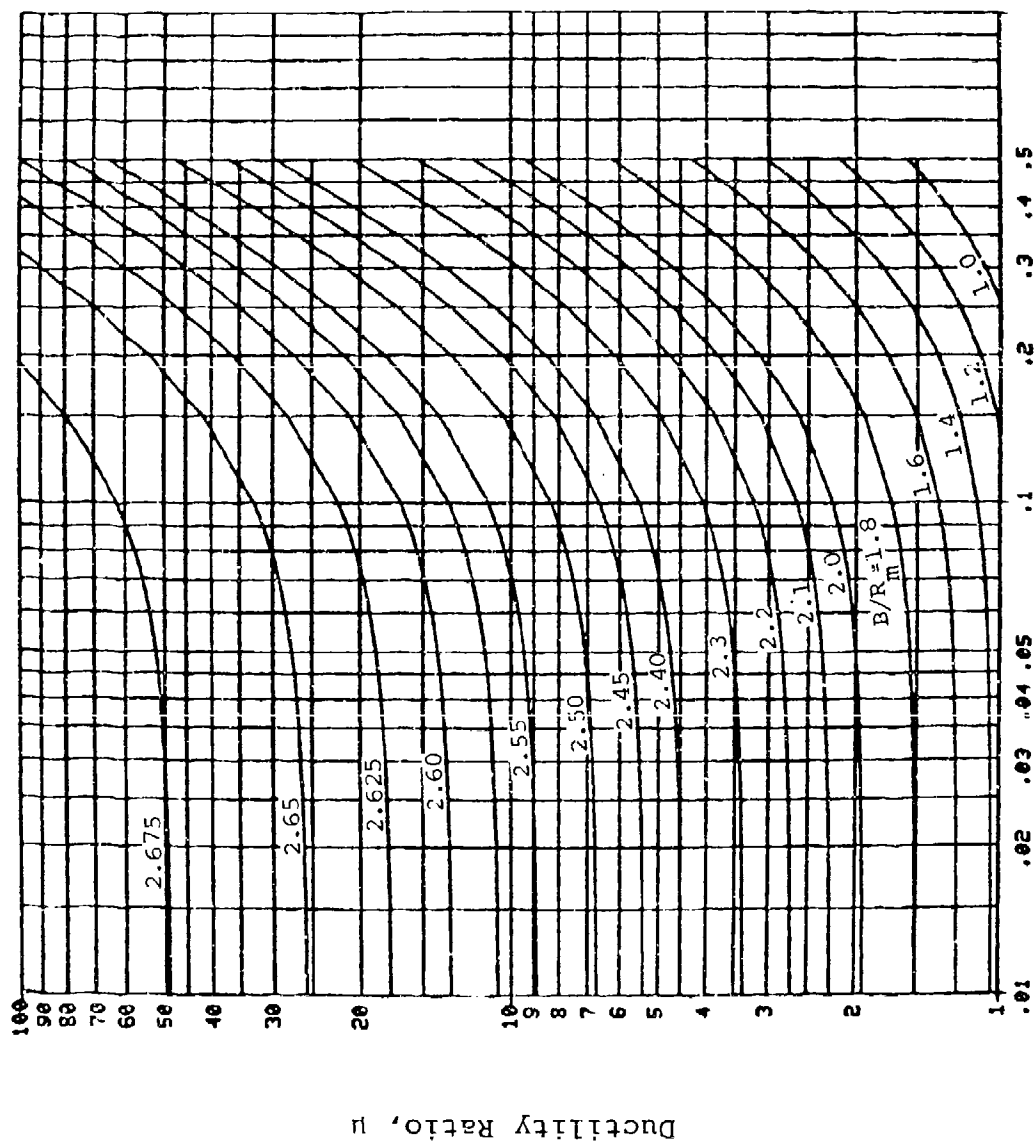


Figure B-4. Response Chart for $C_1 = 0.63$ and $C_2 = 0.37$

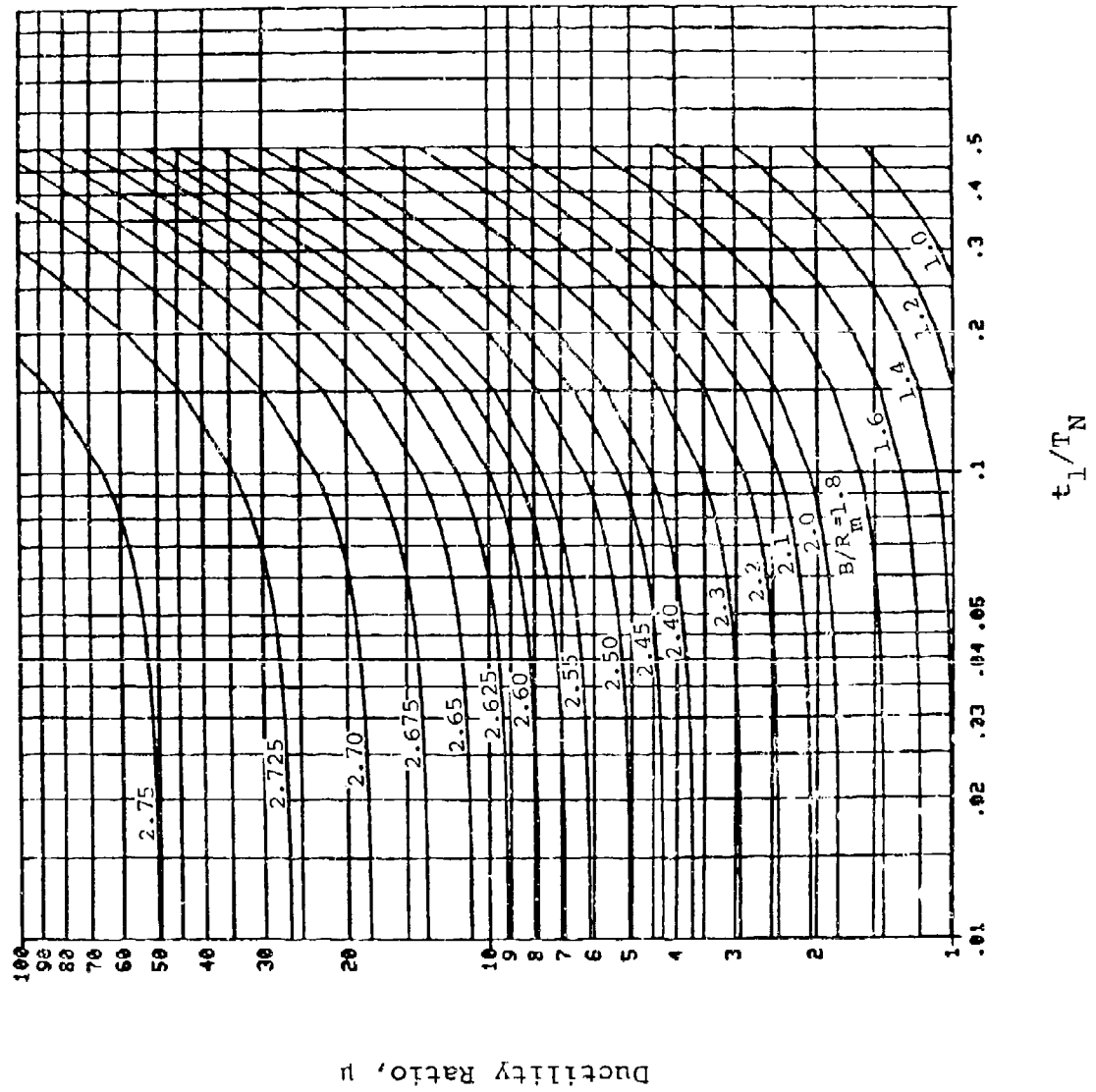


Figure B-5. Response Chart for $C_1 = 0.64$ and $C_2 = 0.36$

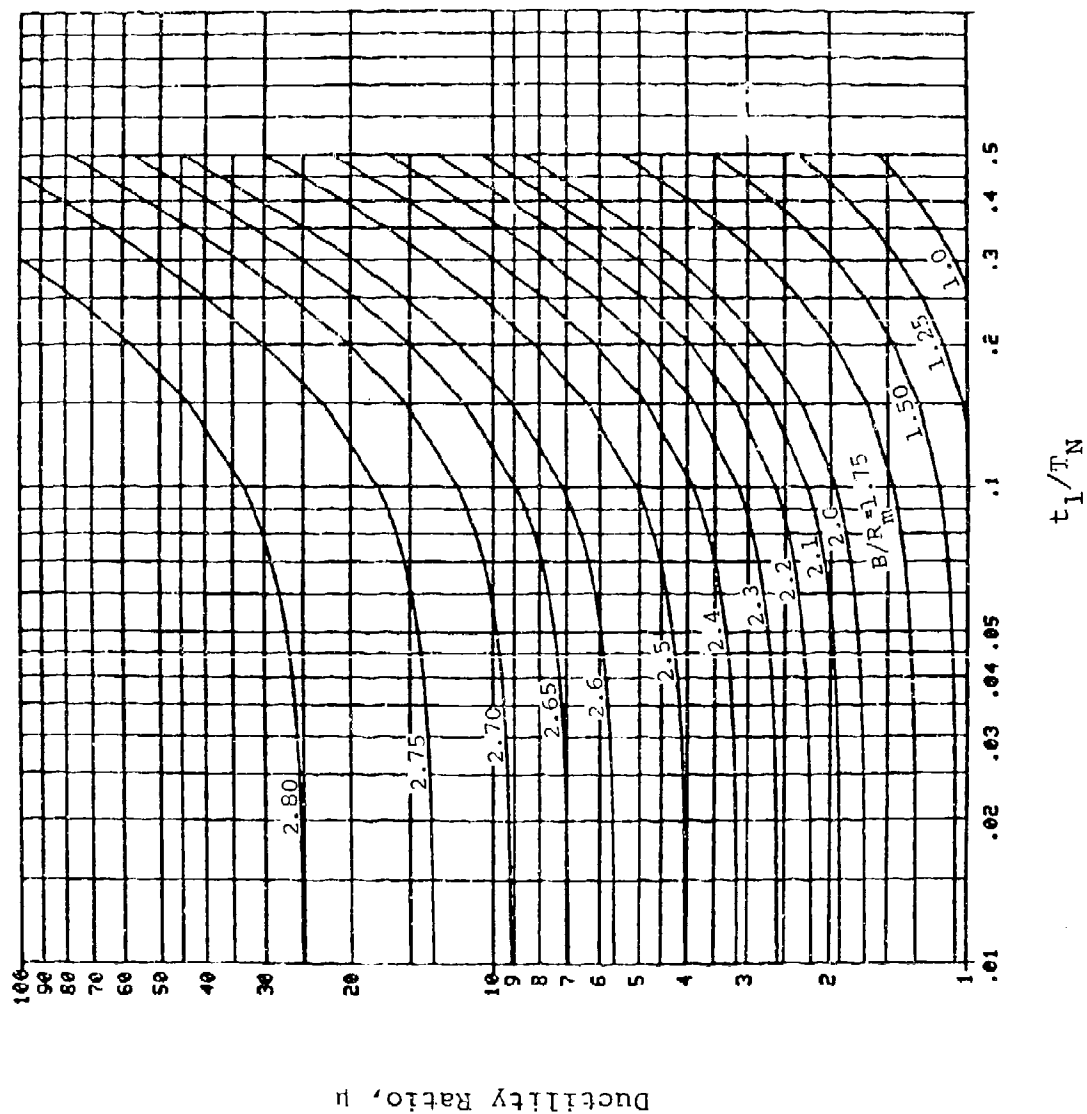


Figure B-6. Response Chart for $C_1 = 0.65$ and $C_2 = 0.35$

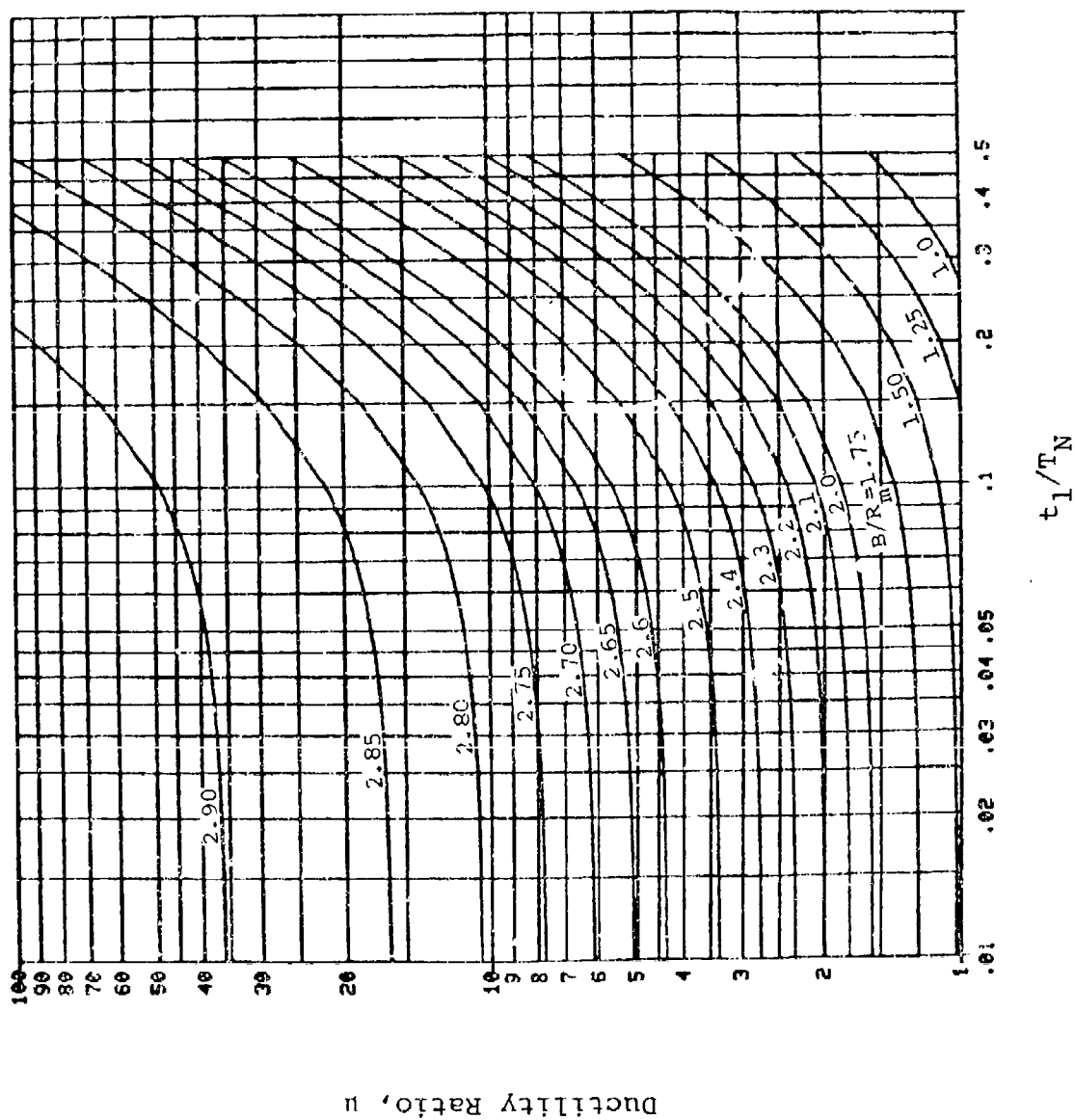


Figure B-7. Response Chart for $C_1 = 0.66$ and $C_2 = 0.34$

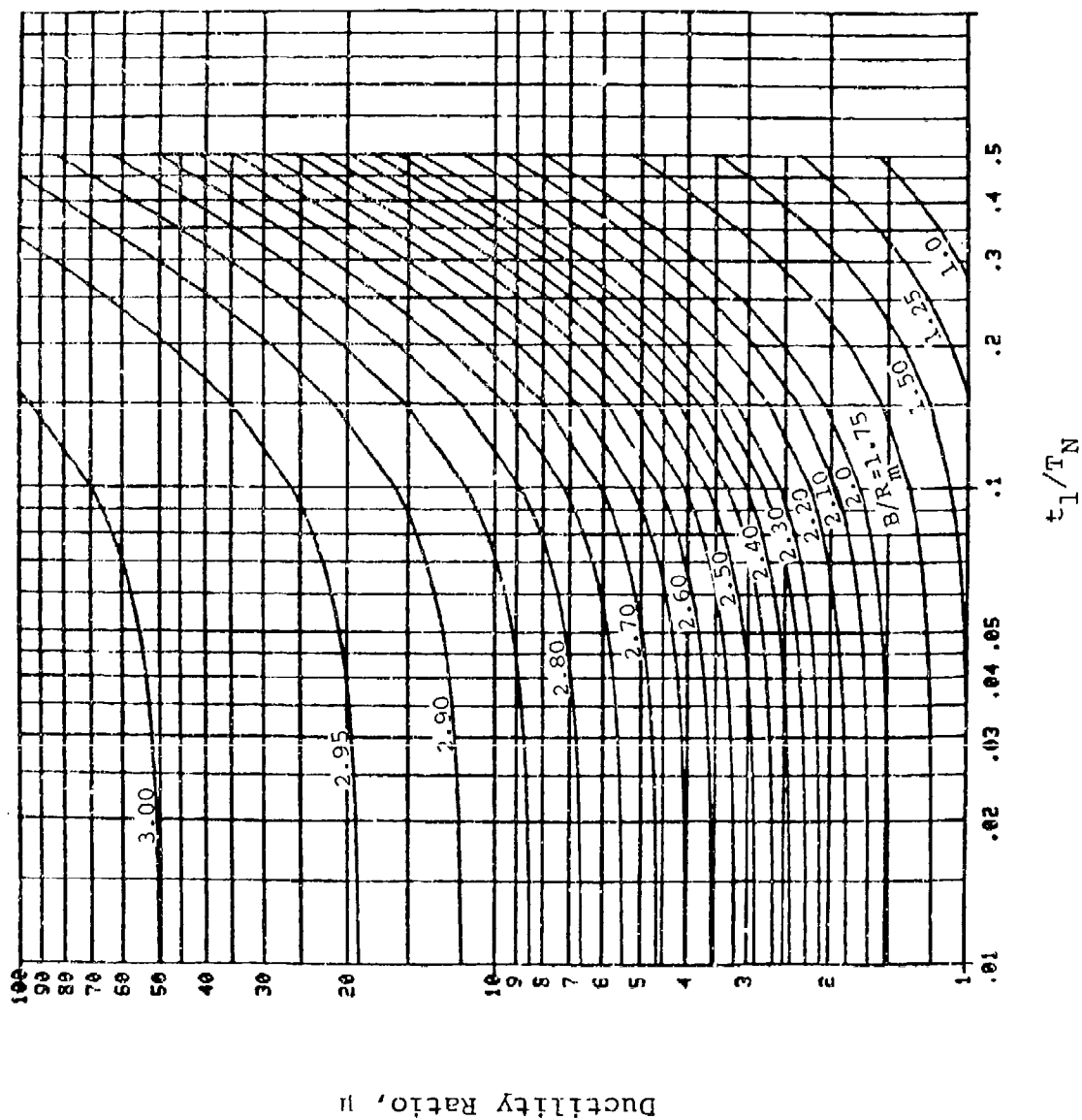


Figure B-8. Response Chart for $C_1 = 0.67$ and $C_2 = 0.33$

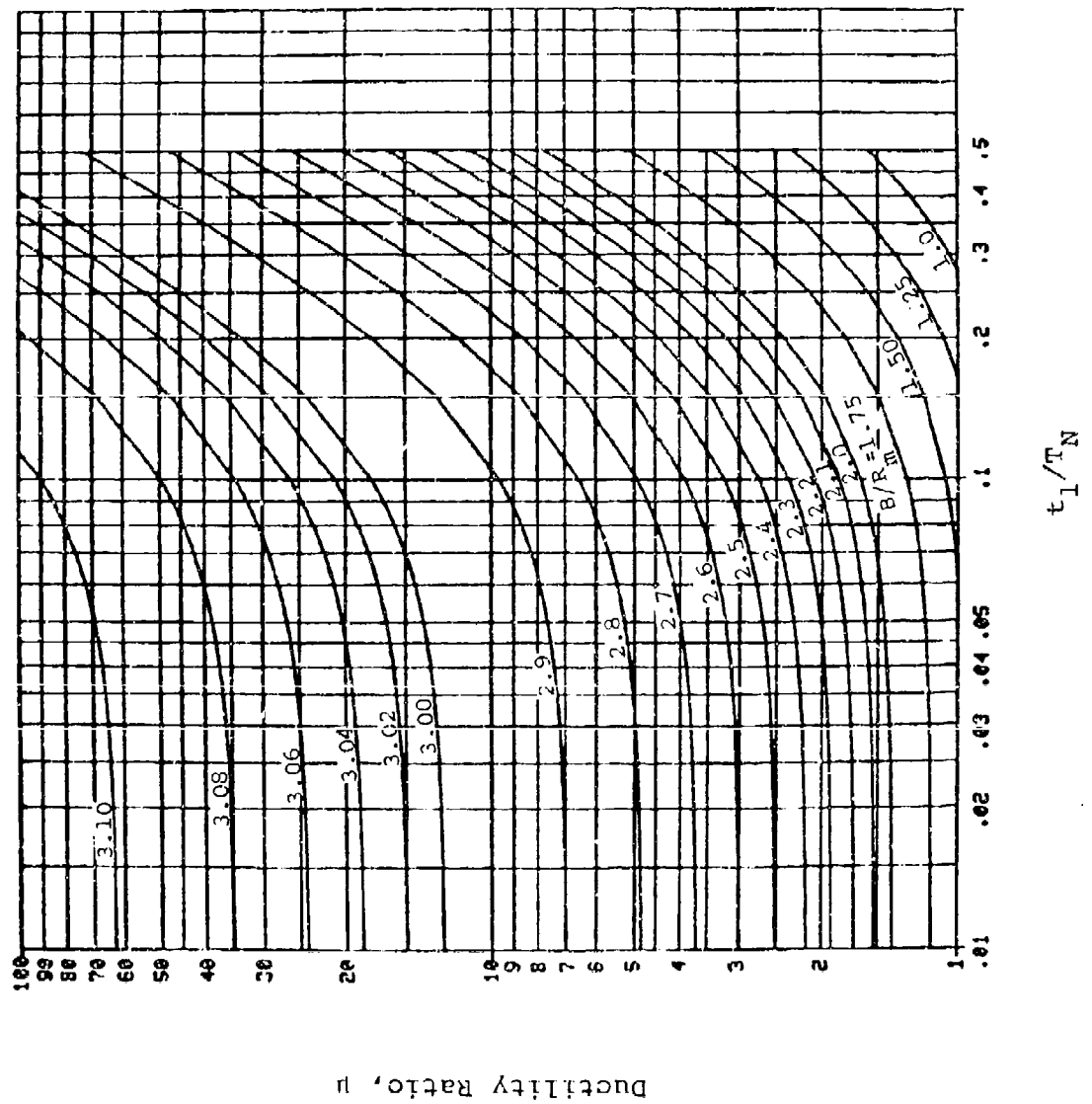


Figure B-9. Response Chart for $C_1 = 0.68$ and $C_2 = 0.32$

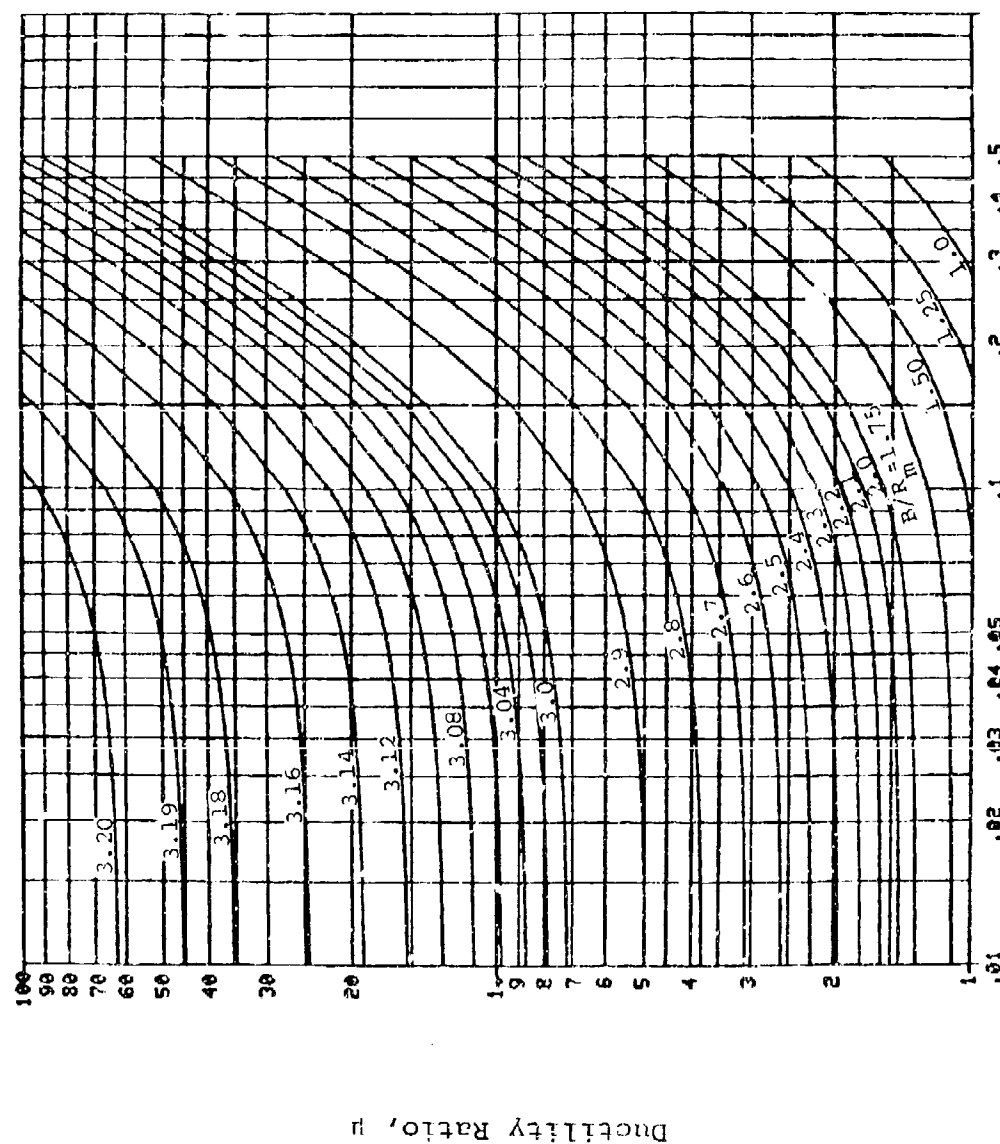


Figure B-10. Response Chart for $C_1 = 0.69$ and $C_2 = 0.31$

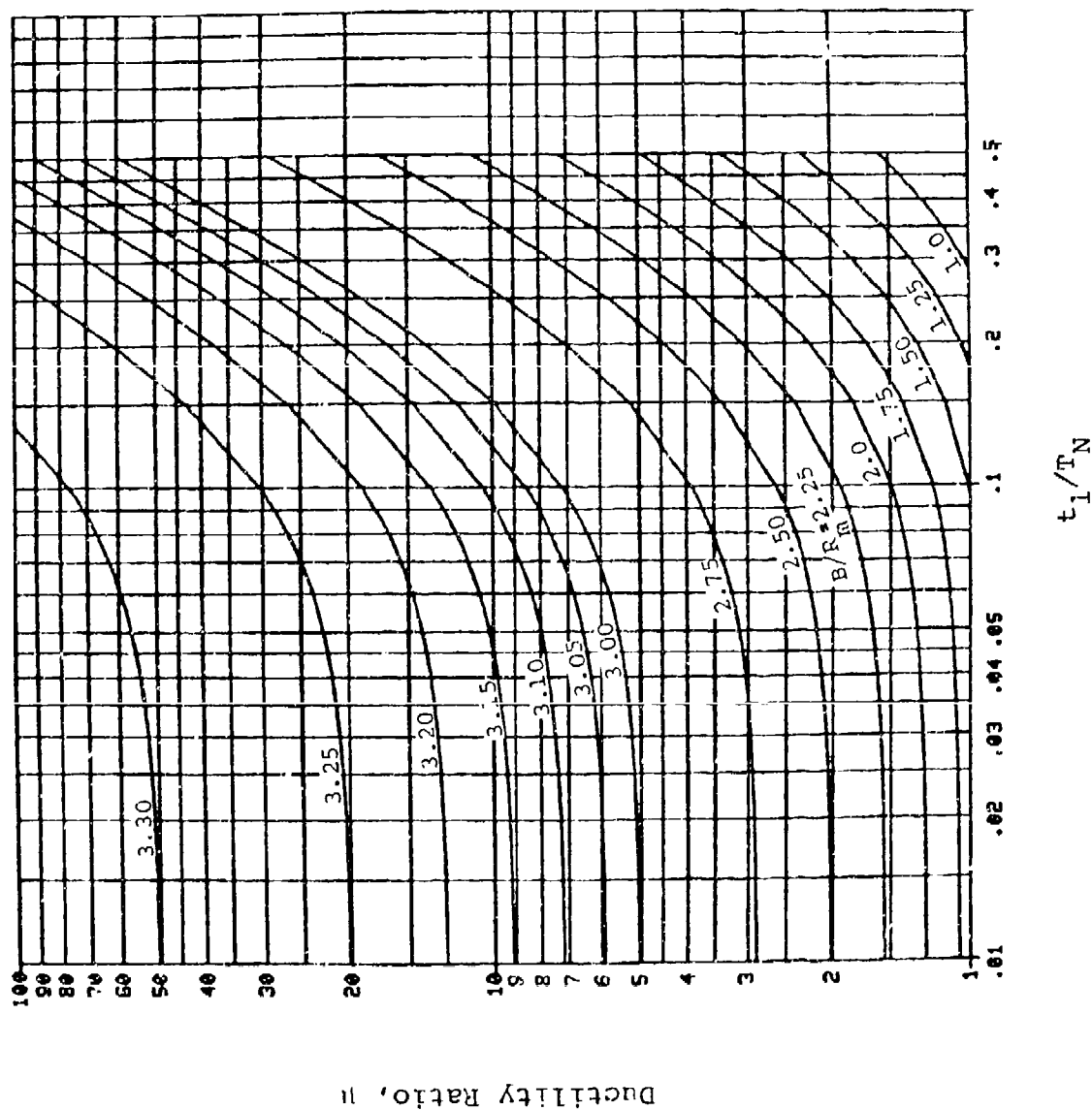


Figure B-11. Response Chart for $C_1 = 0.70$ and $C_2 = 0.30$

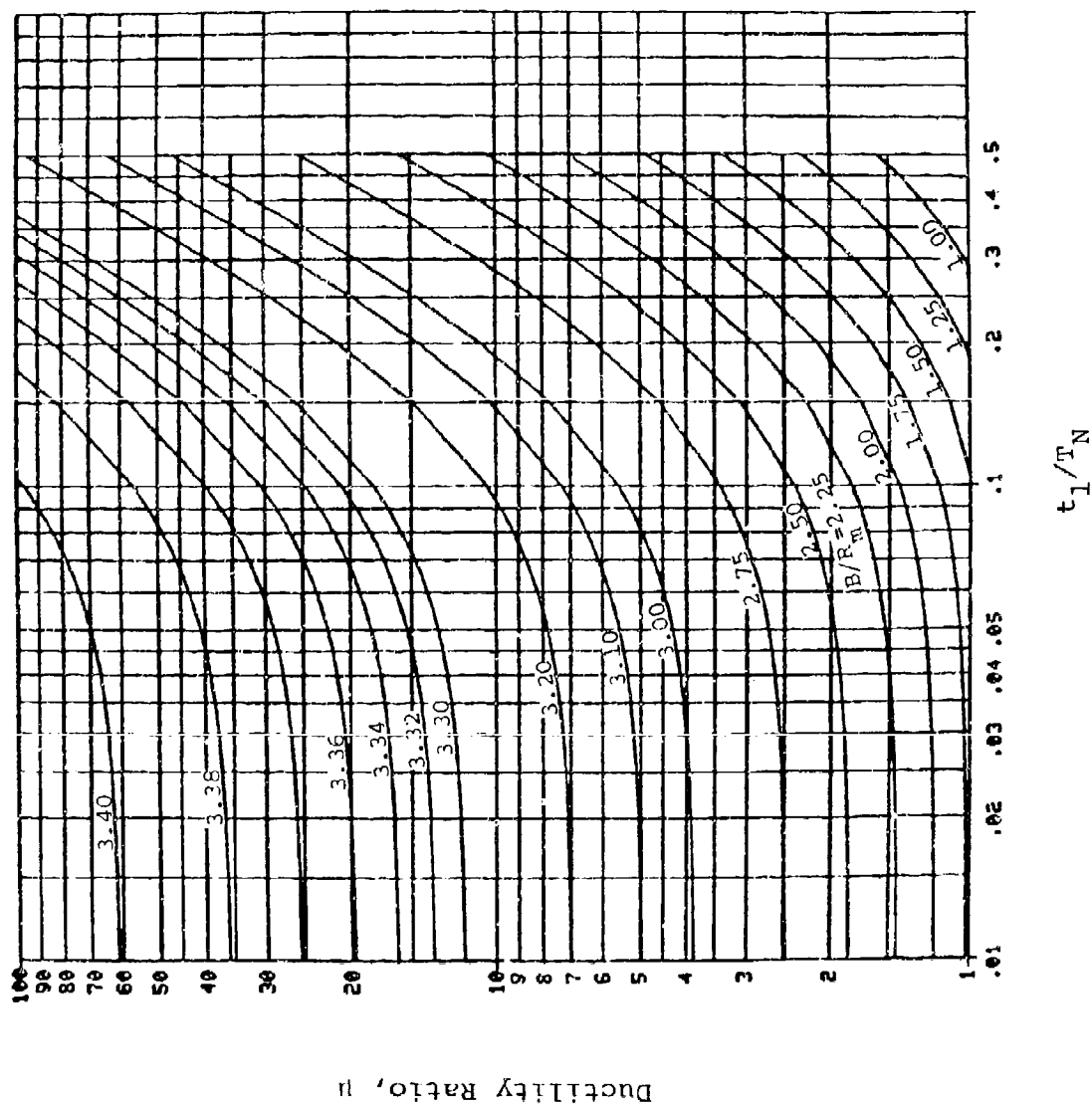


Figure B-12. Response Chart for $C_1 = 0.71$ and $C_2 = 0.29$

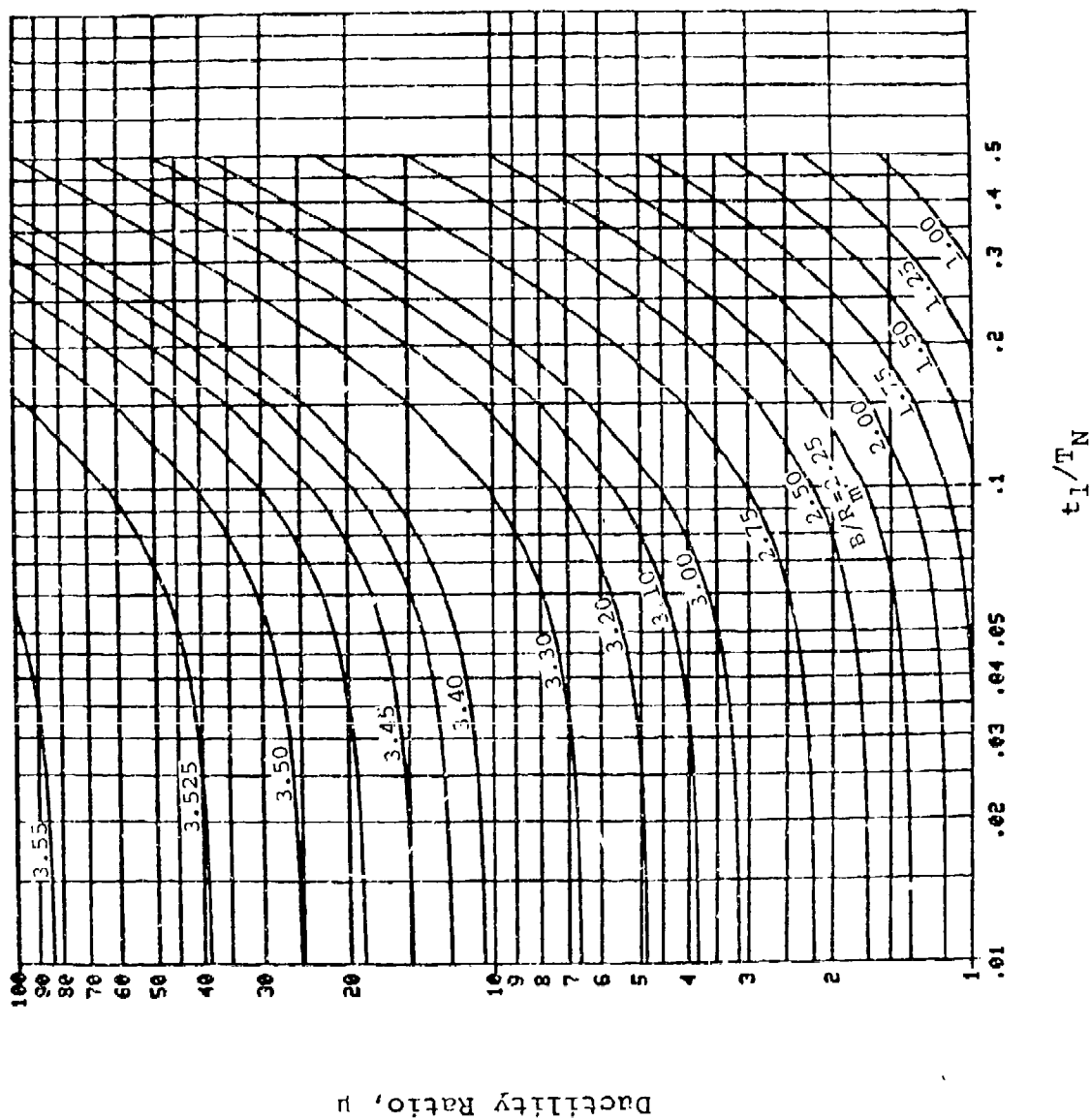


Figure B-13. Response Chart for $C_1 = 0.72$ and $C_2 = 0.28$

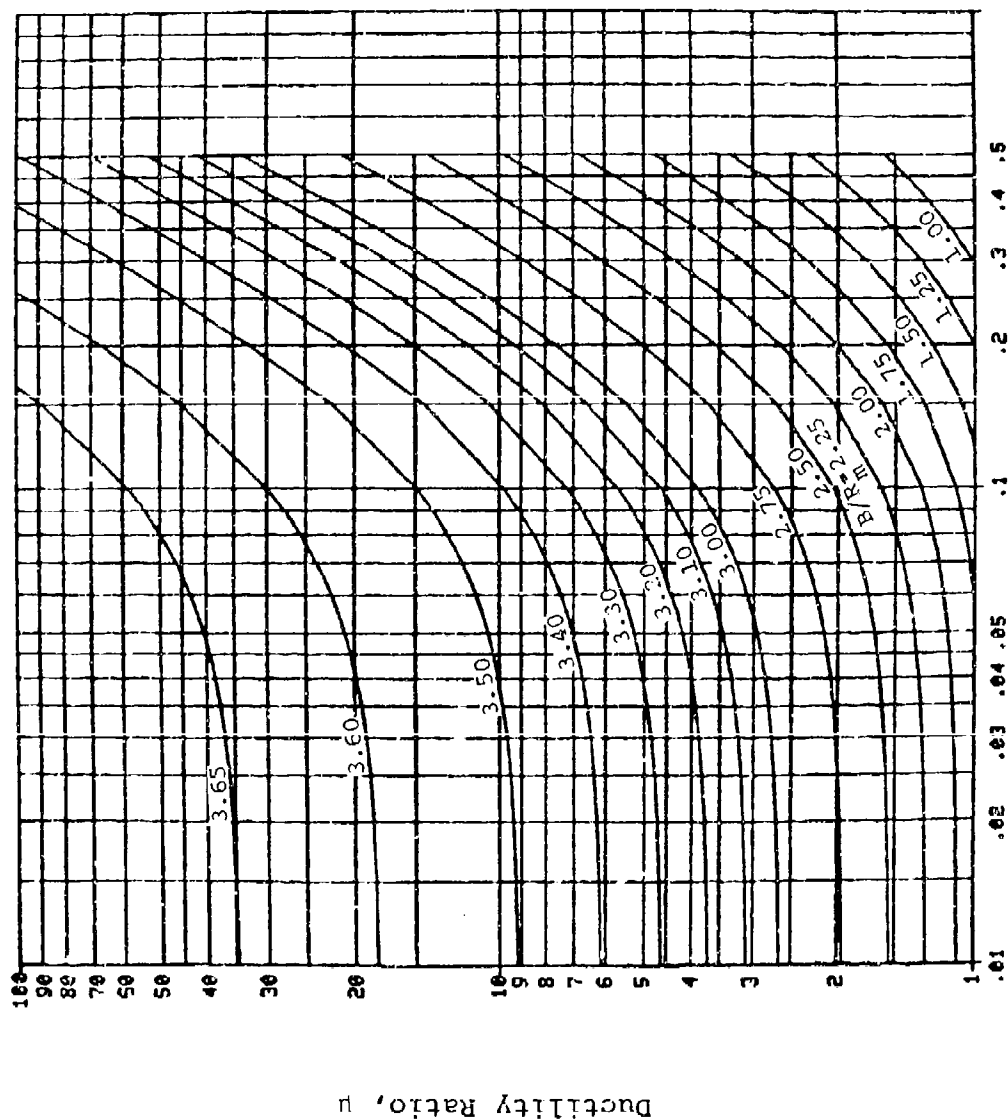


Figure B-14. Response Chart for $C_1 = 0.73$ and $C_2 = 0.27$

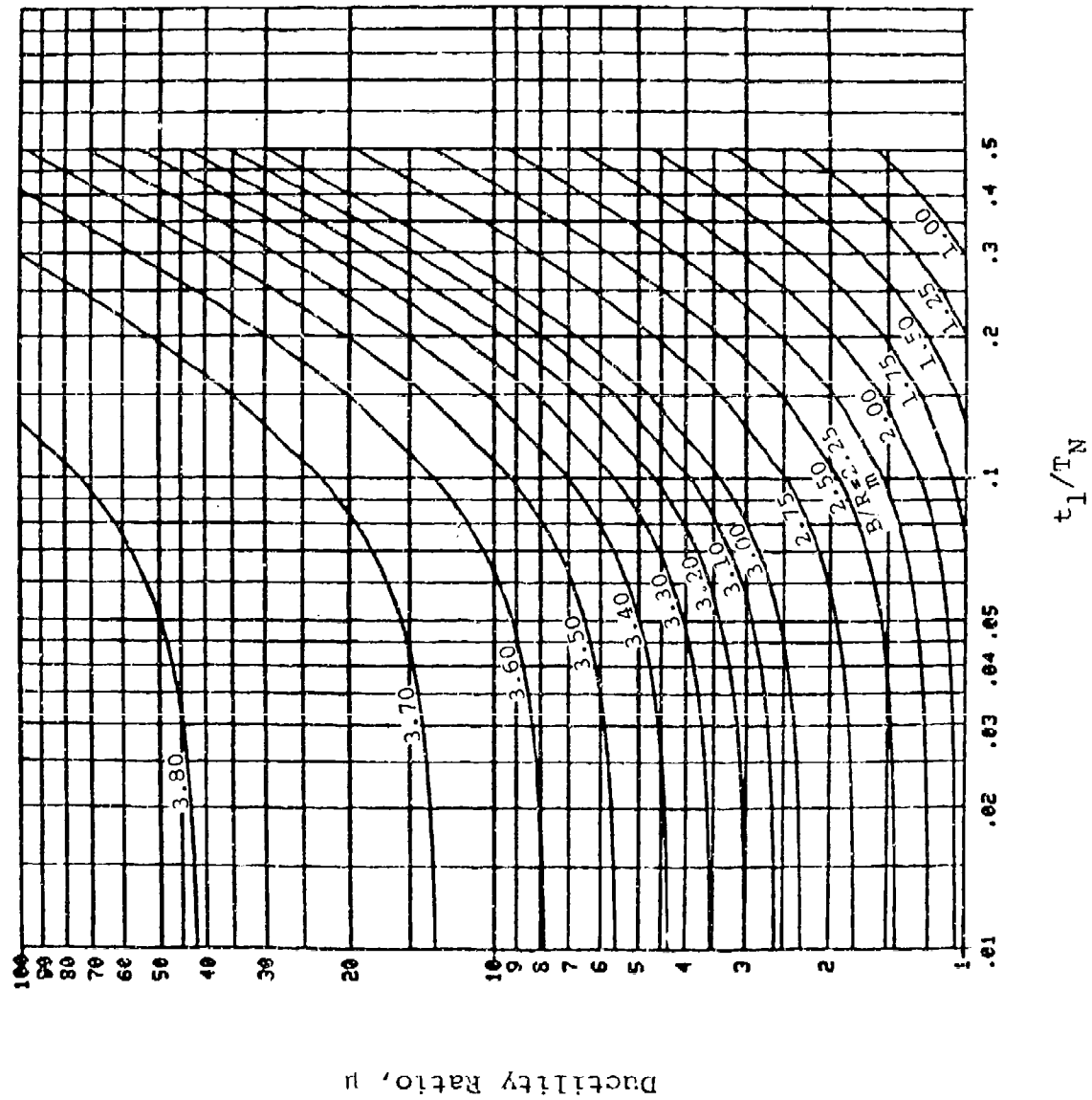


Figure B-15. Response Chart for $C_1 = 0.74$ and $C_2 = 0.26$

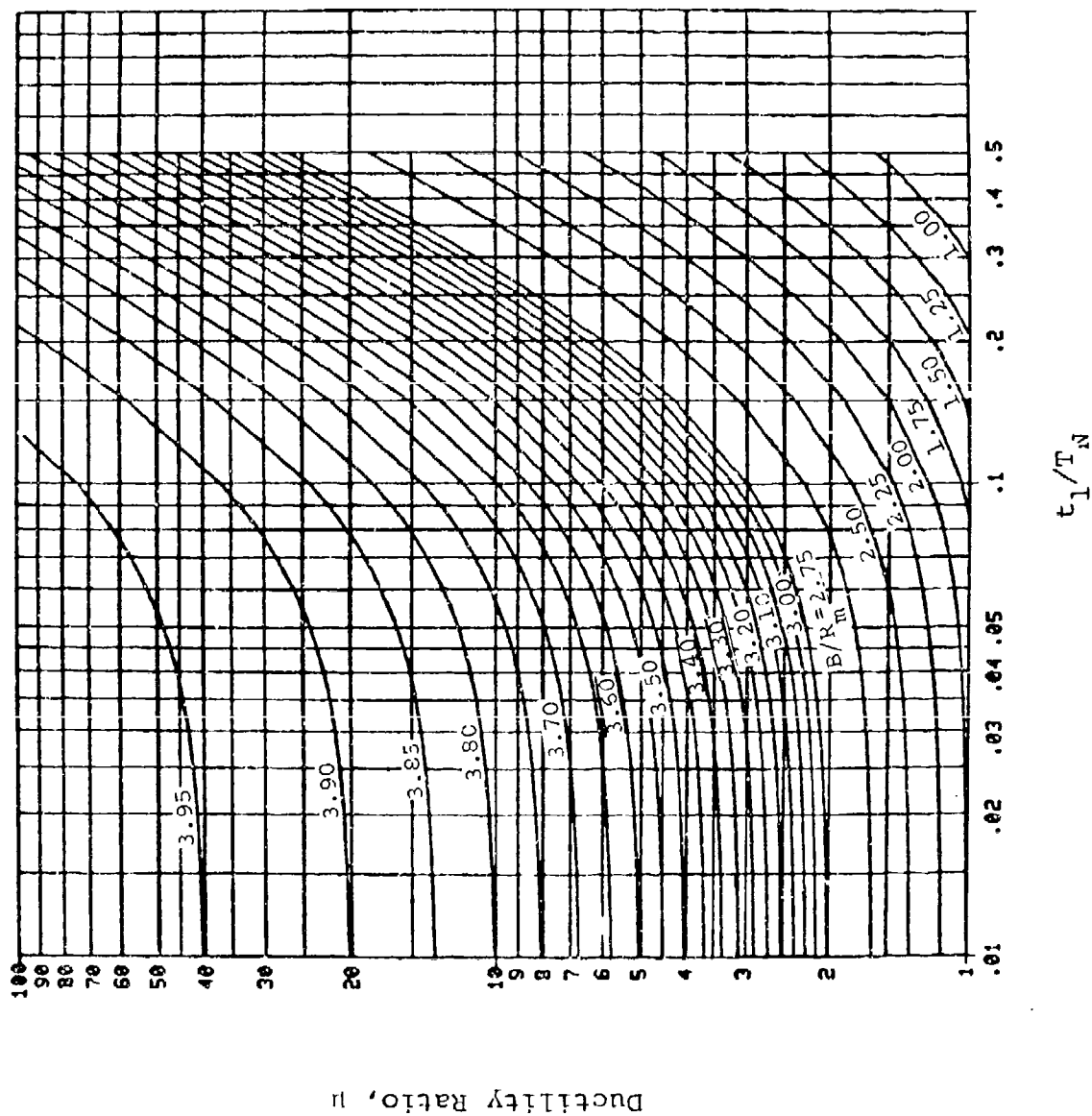


Figure B-16. Response Chart for $C_1 = 0.75$ and $C_2 = 0.25$

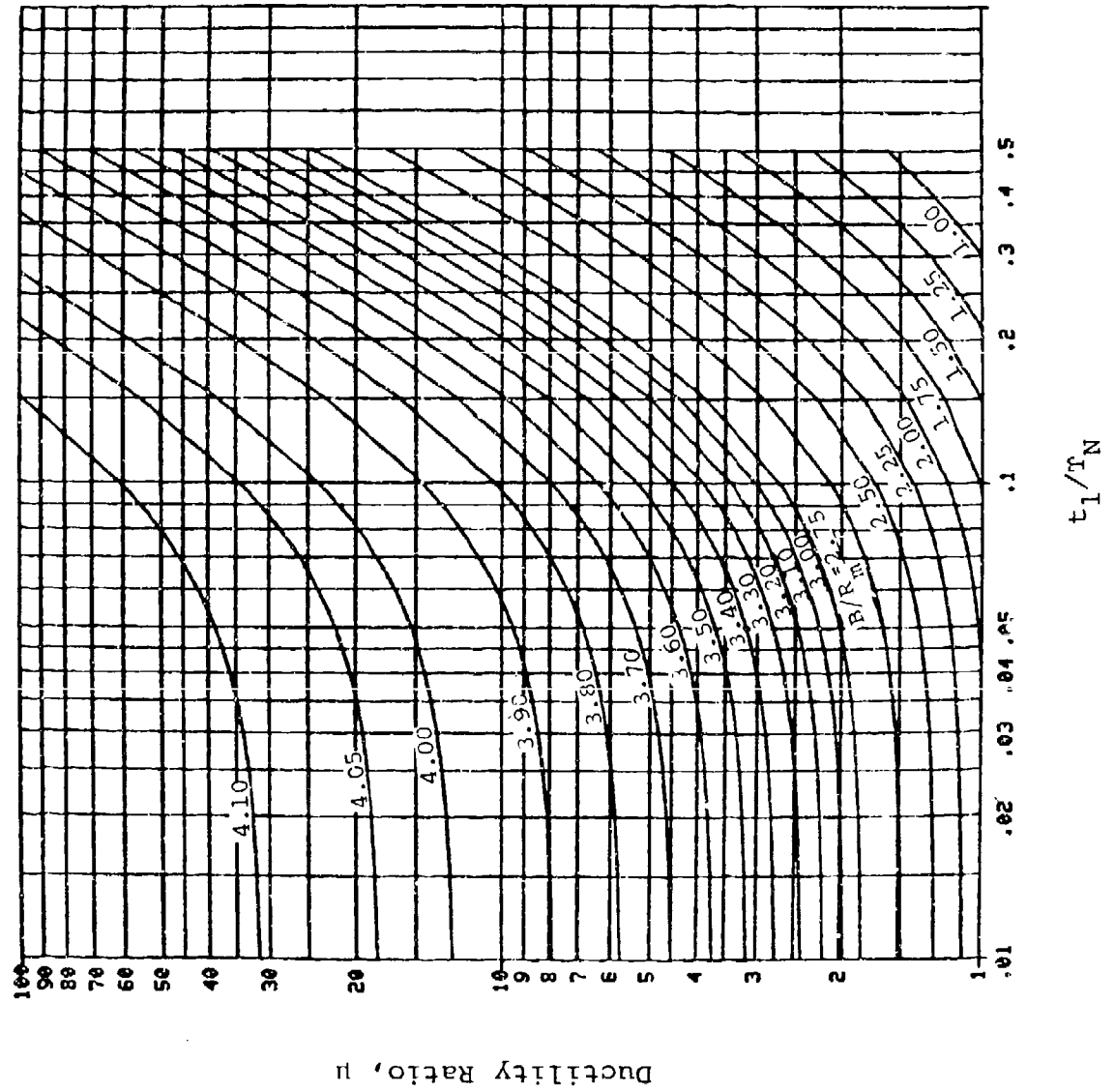


Figure B-17. Response Chart for $C_1 = 0.76$ and $C_2 = 0.24$

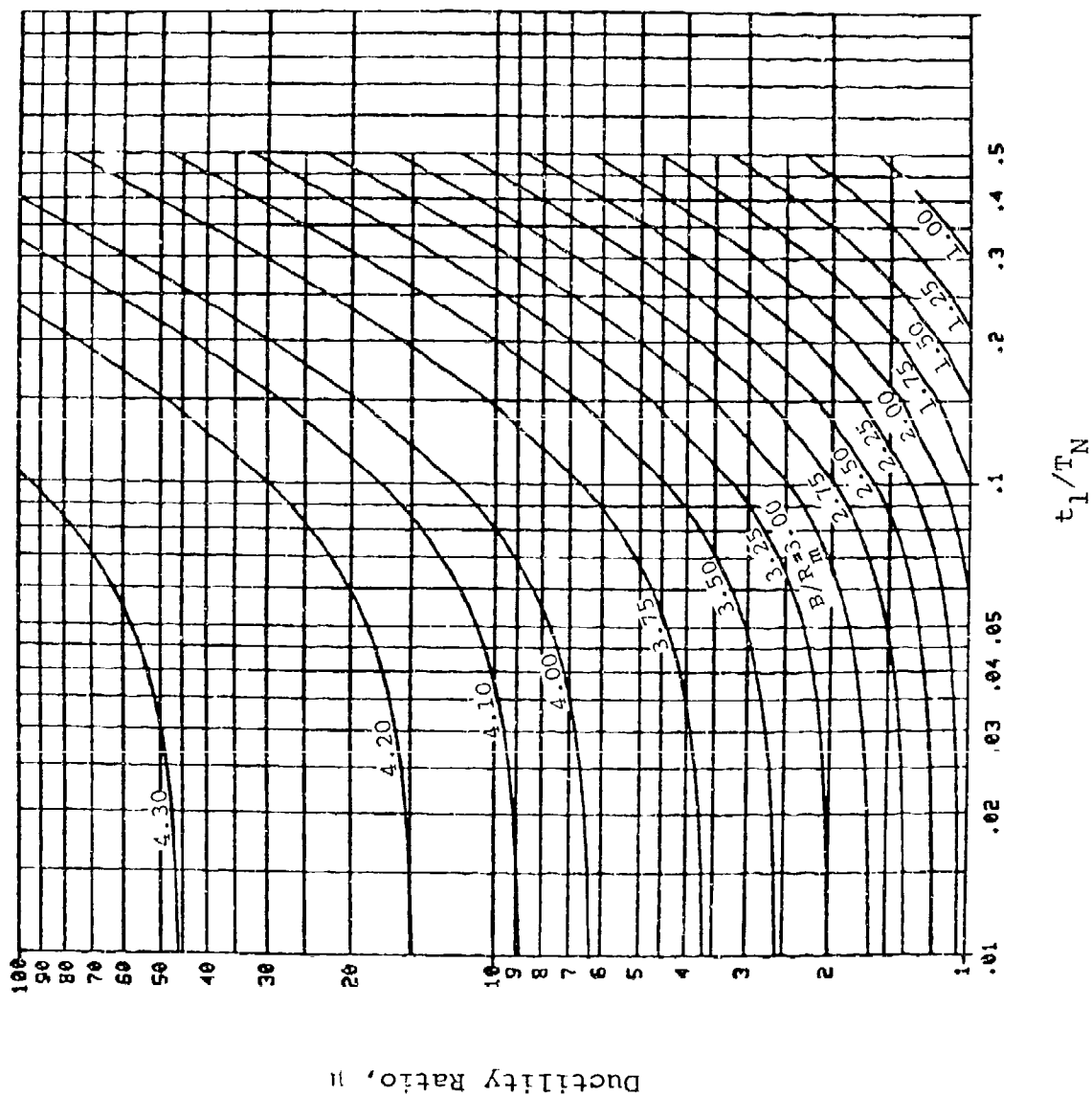


Figure B-18. Response Chart for $C_1 = 0.77$ and $C_2 = 0.23$

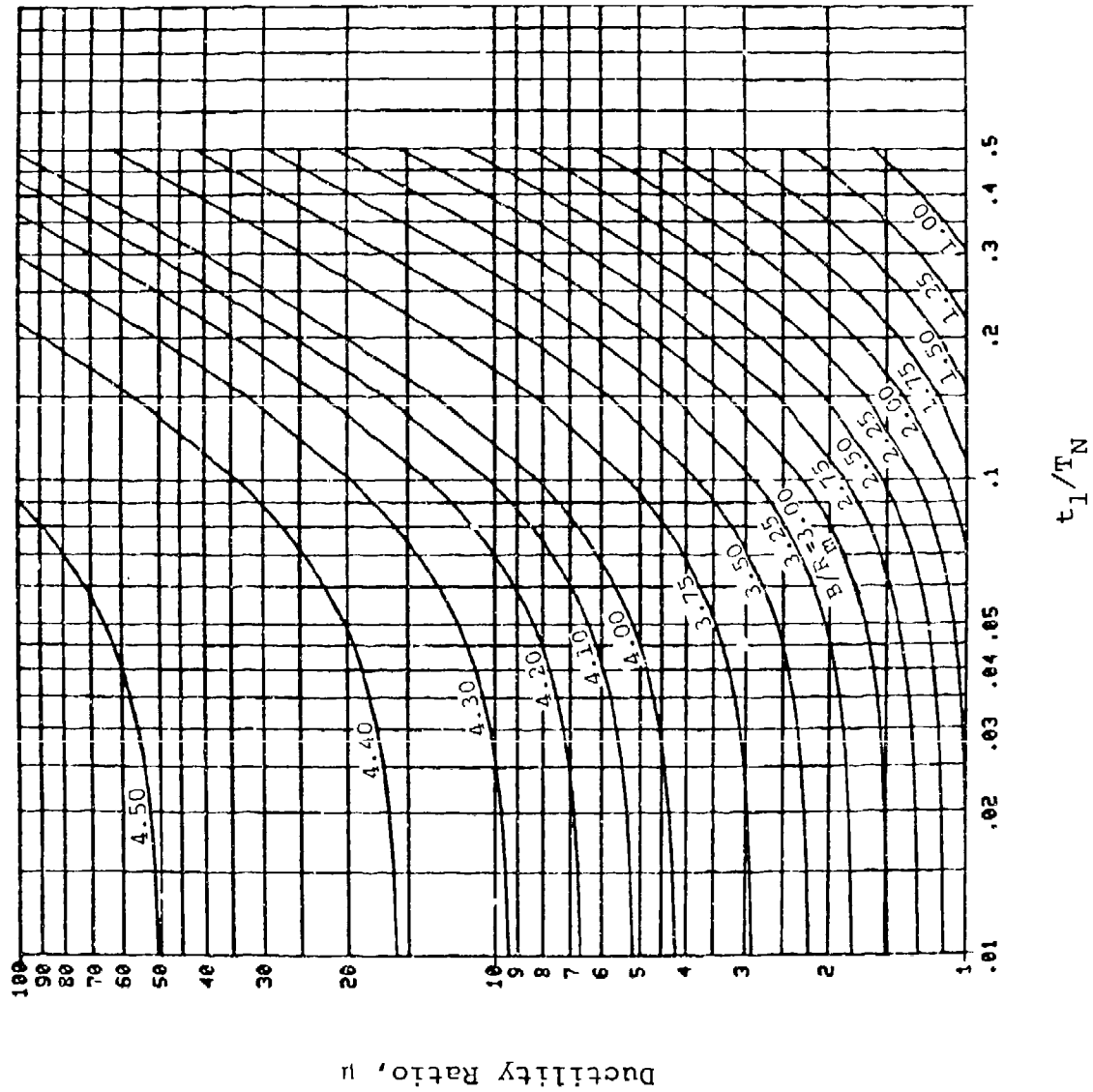


Figure B-19. Response Chart for $C_1 = 0.78$ and $C_2 = 0.22$

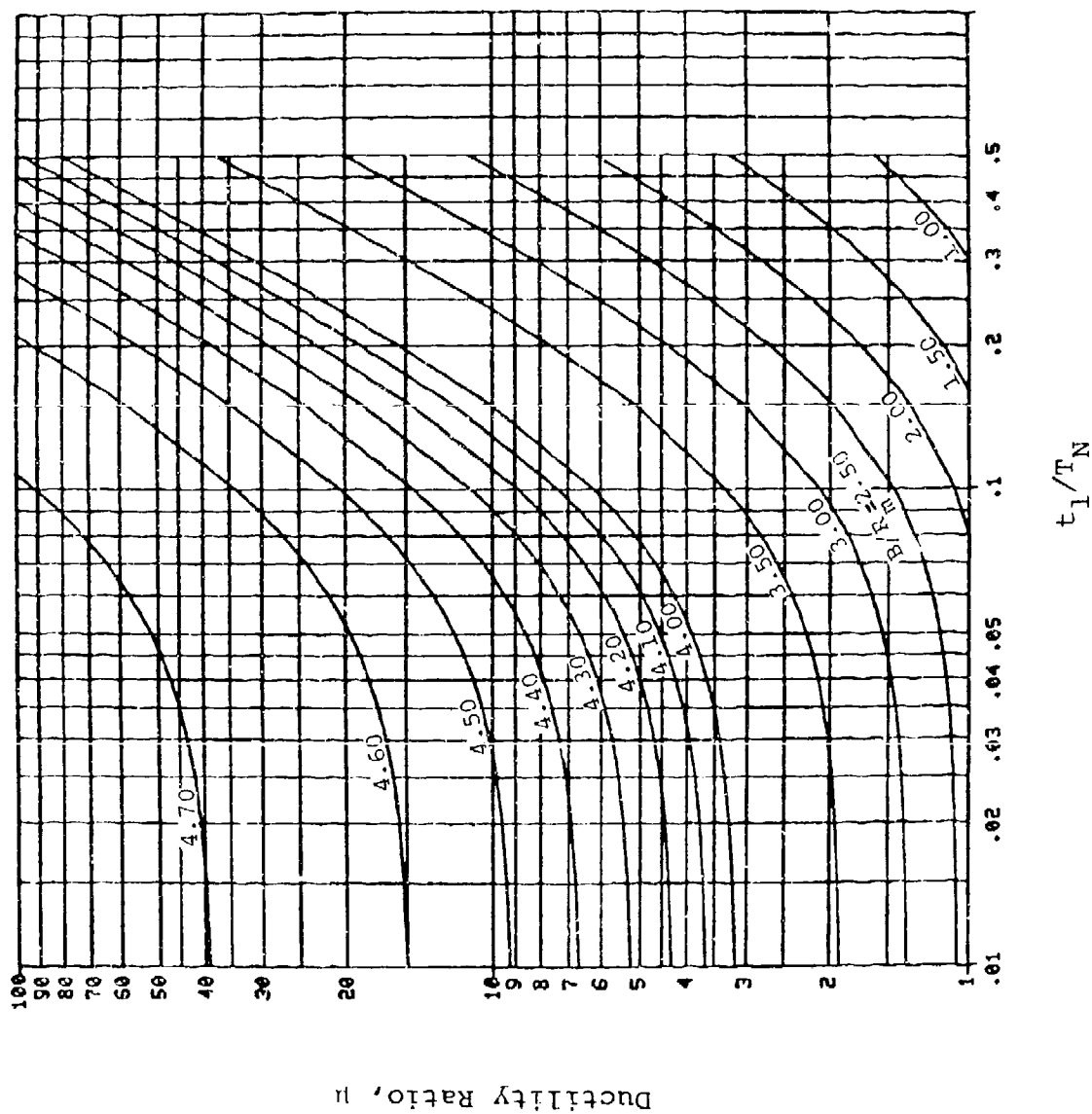


Figure B-20. Response Chart for $C_1 = 0.79$ and $C_2 = 0.21$

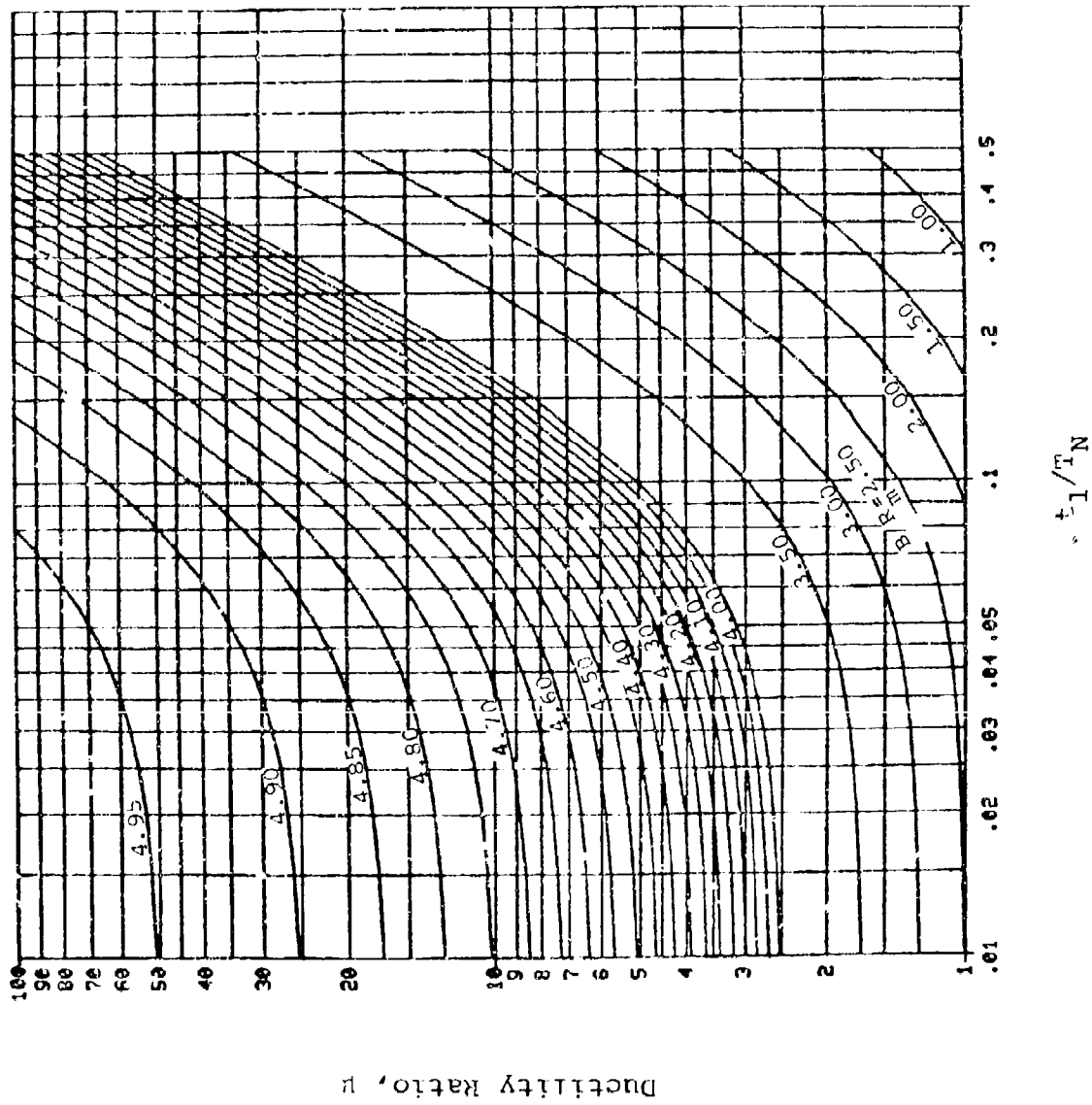


Figure B-21. Response Chart for $C_1 = 0.80$ and $C_2 = 0.20$

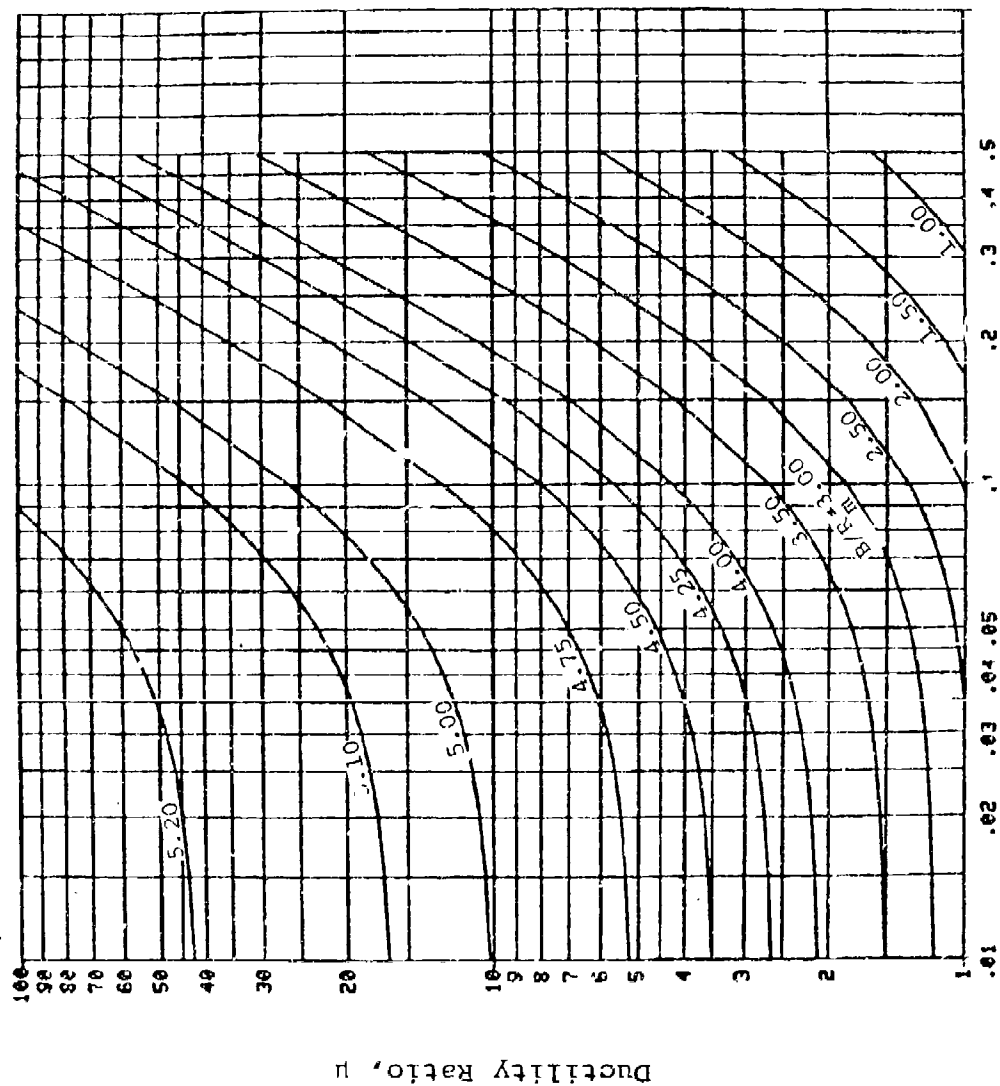


Figure B-22. Response Chart for $C_1 = 0.81$ and $C_2 = 0.19$

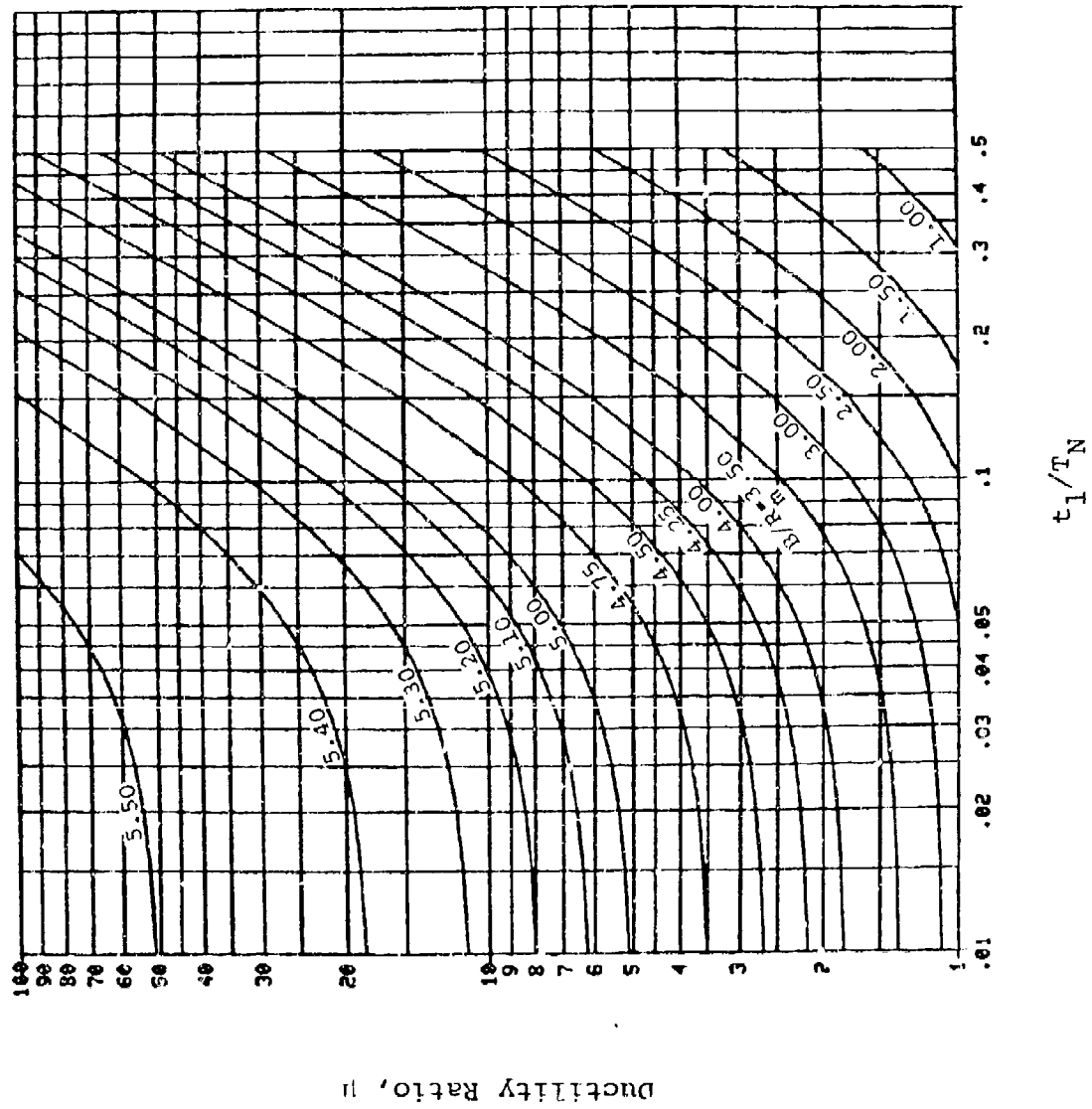
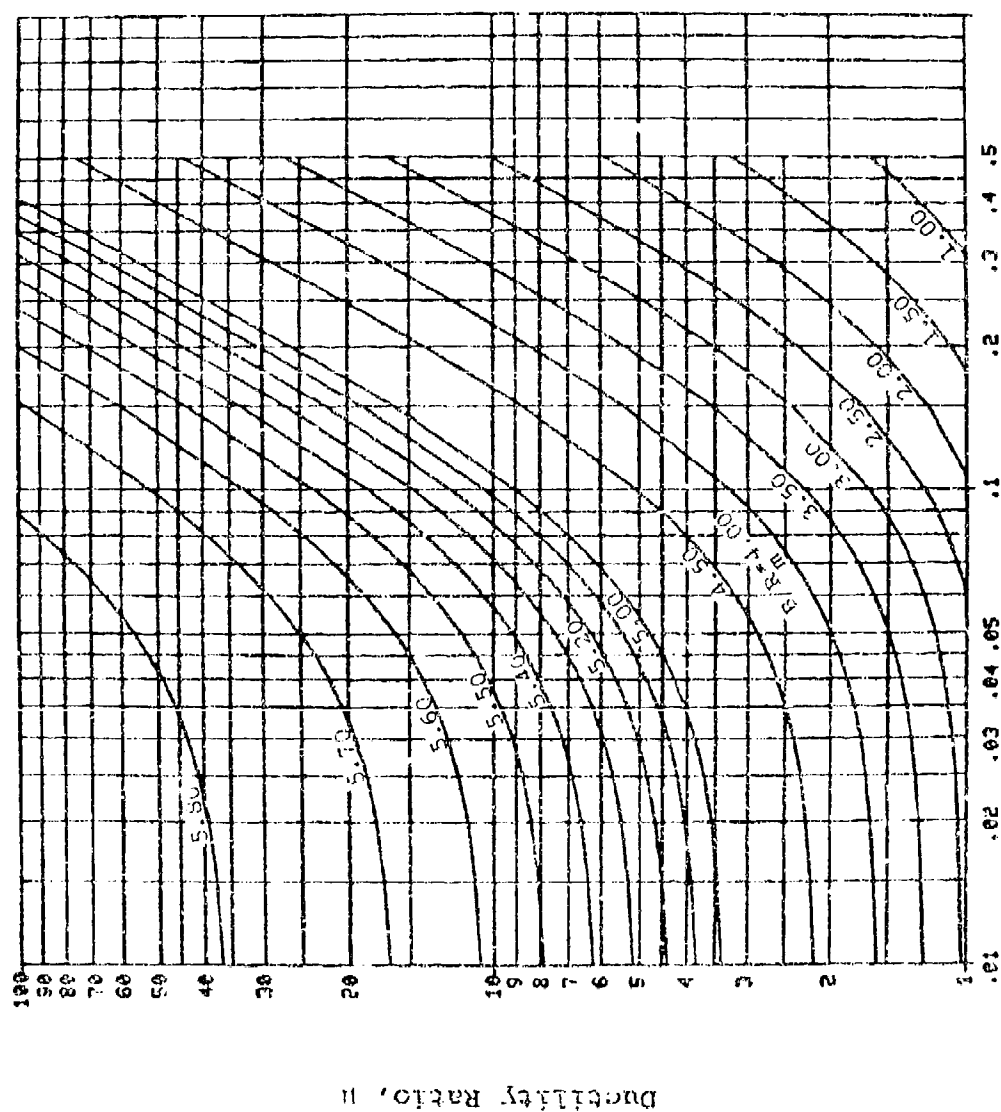
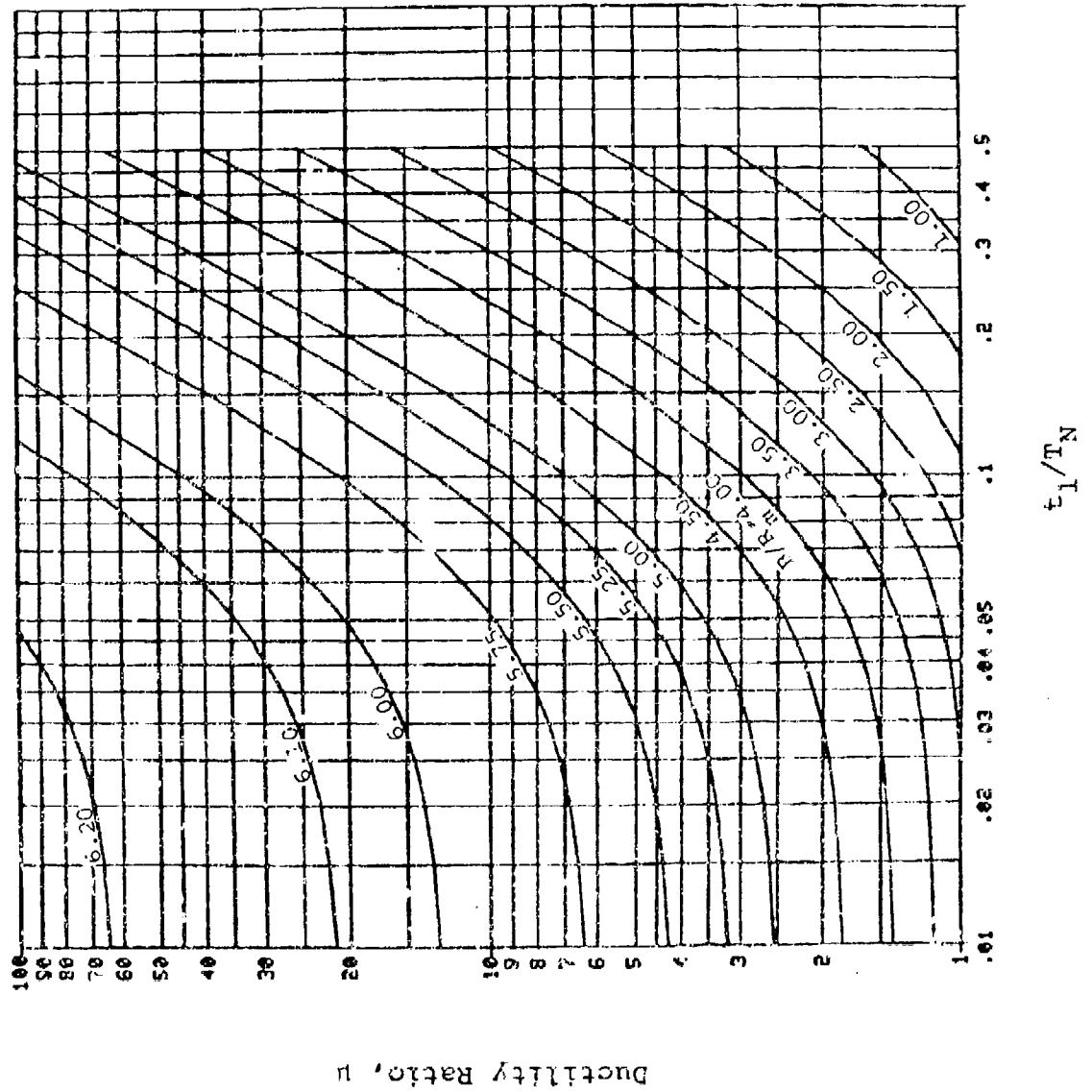


Figure B-23. Response Chart for $C_1 = 0.82$ and $C_2 = 0.18$



t_1/T_N

Figure B-24. Response Chart for $C_1 = 0.83$ and $C_2 = 0.17$



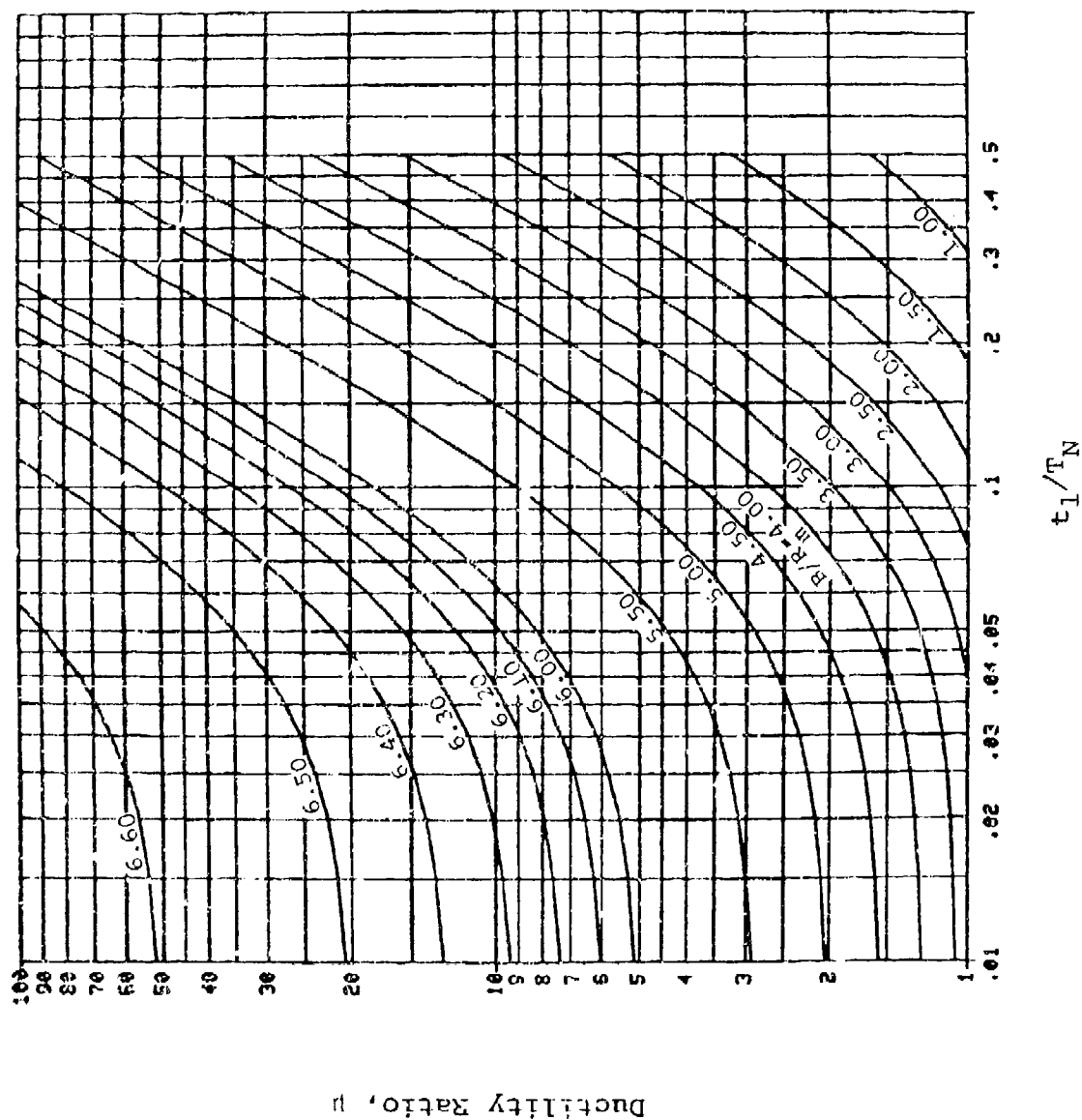


Figure B-26. Response Chart for $C_1 = 0.85$ and $C_2 = 0.15$

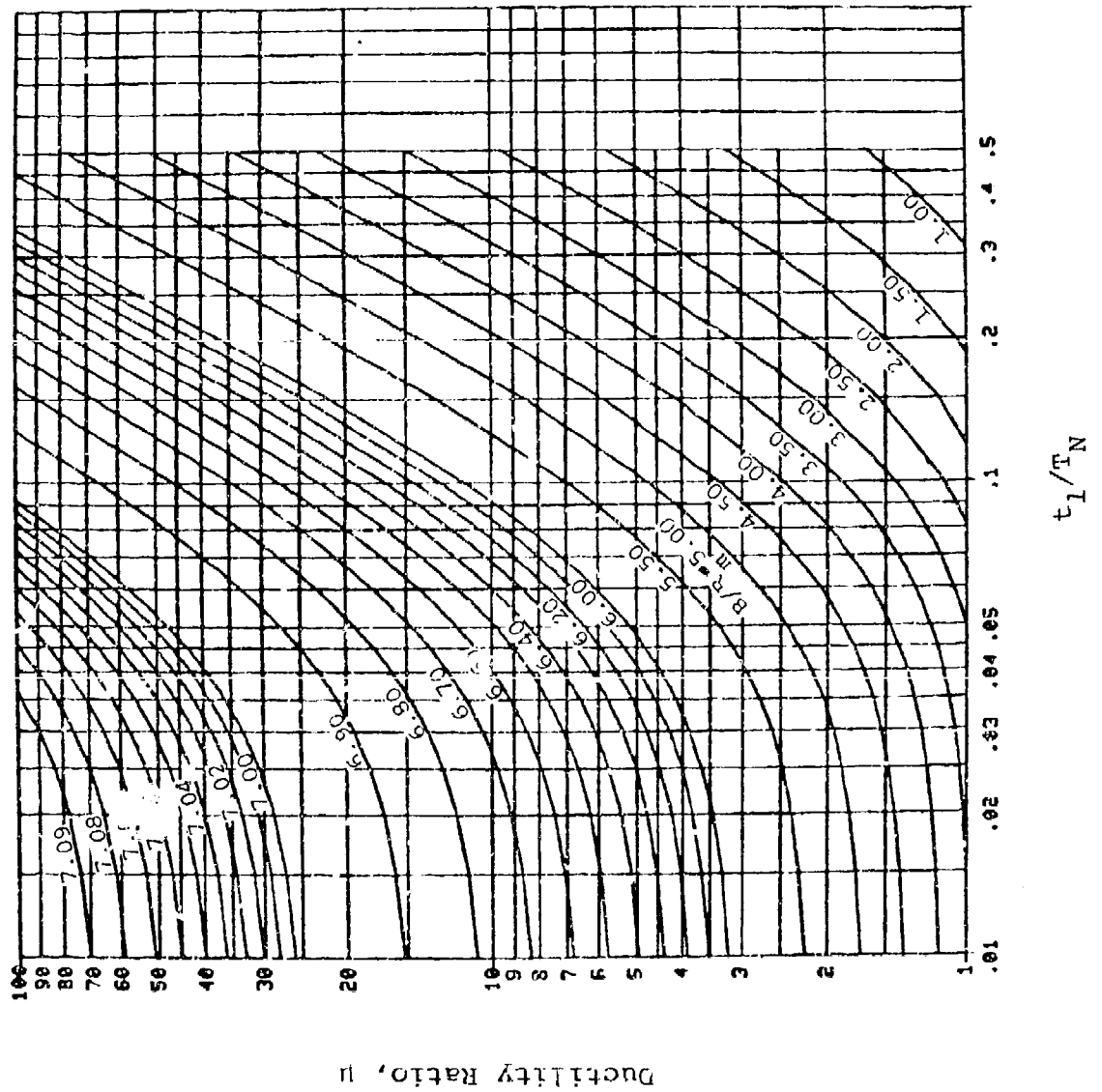


Figure B-27. Response Chart for $C_1 = 0.86$ and $C_2 = 0.14$

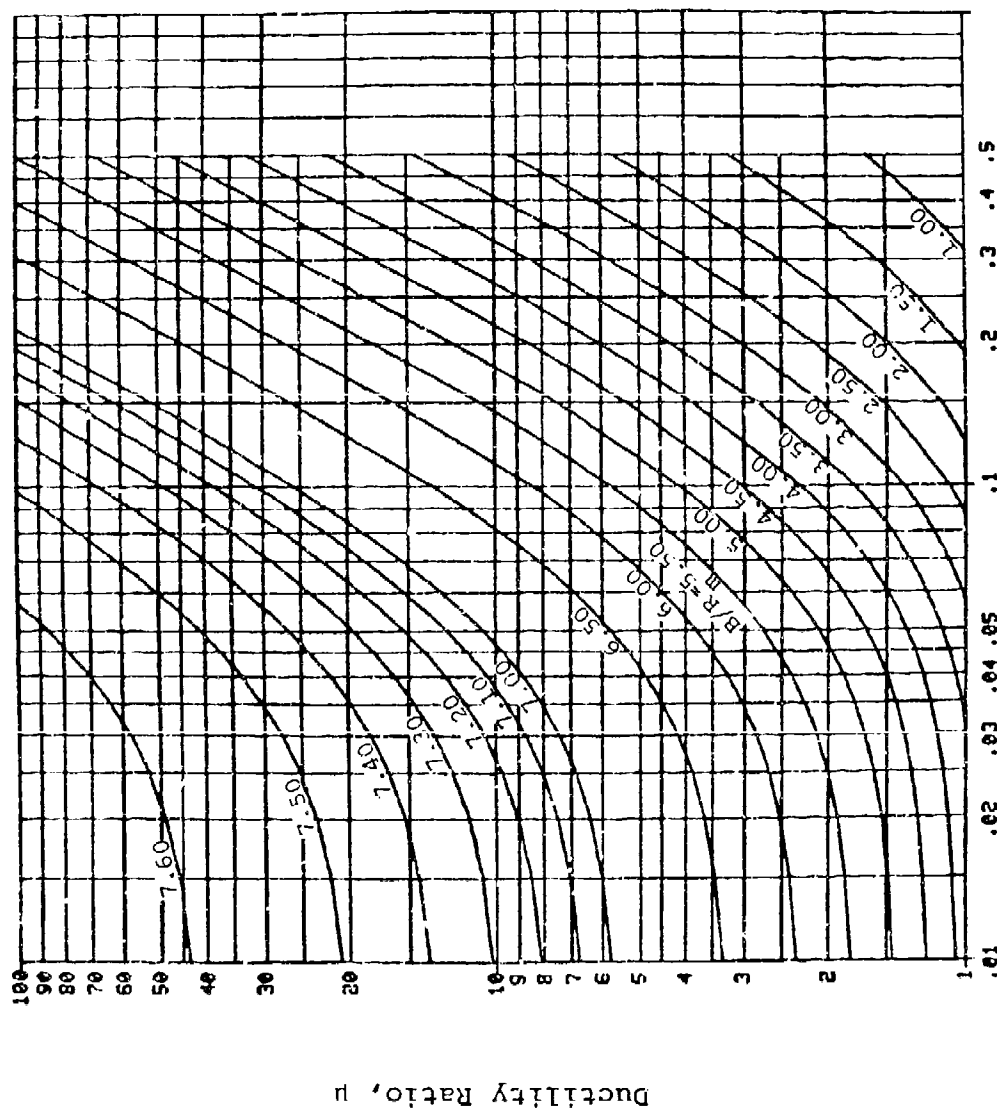


Figure B-28. Response Chart for $C_1 = 0.87$ and $C_2 = 0.13$

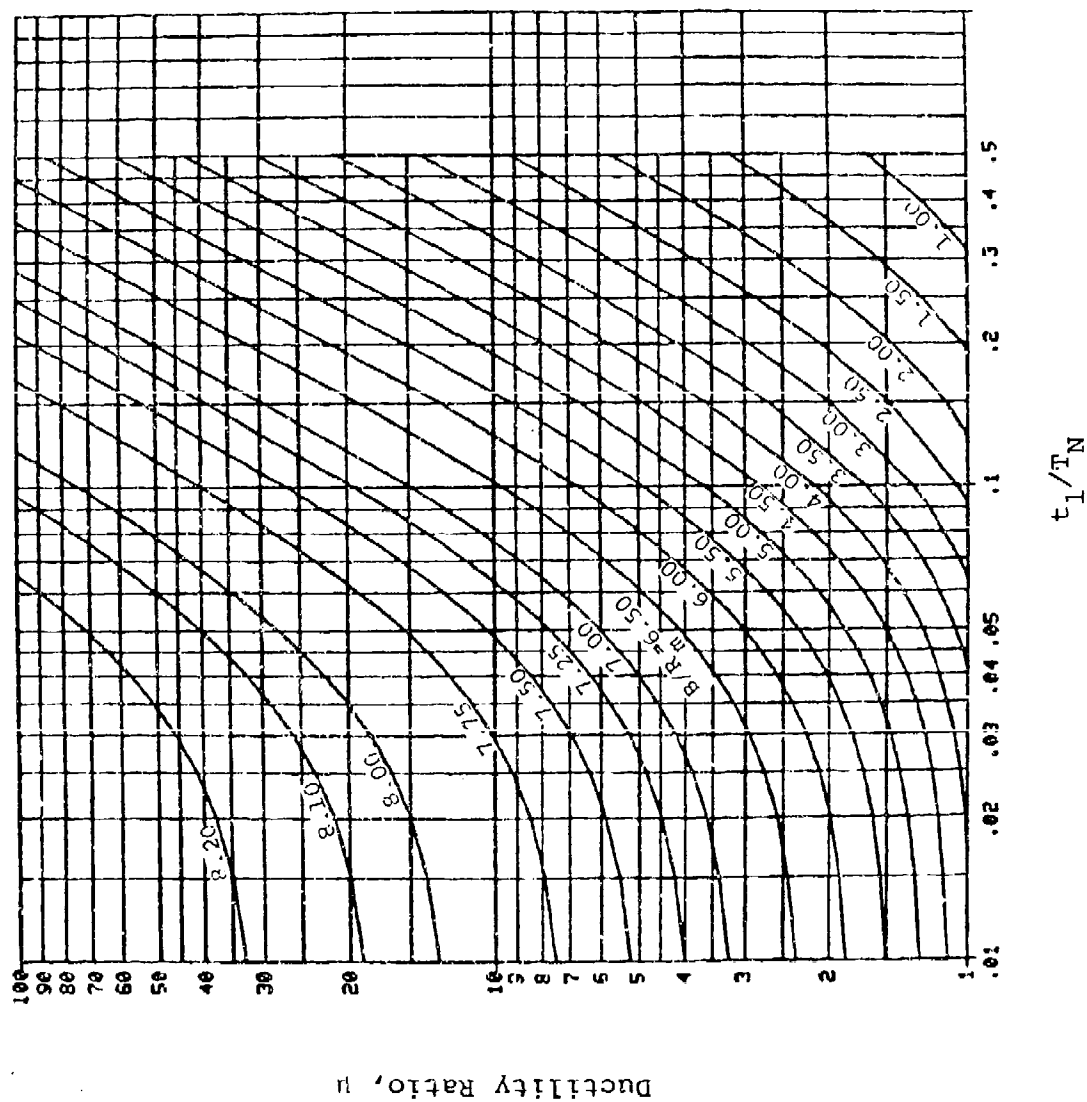


Figure B-29. Response Chart for $C_1 = 0.88$ and $C_2 = 0.12$

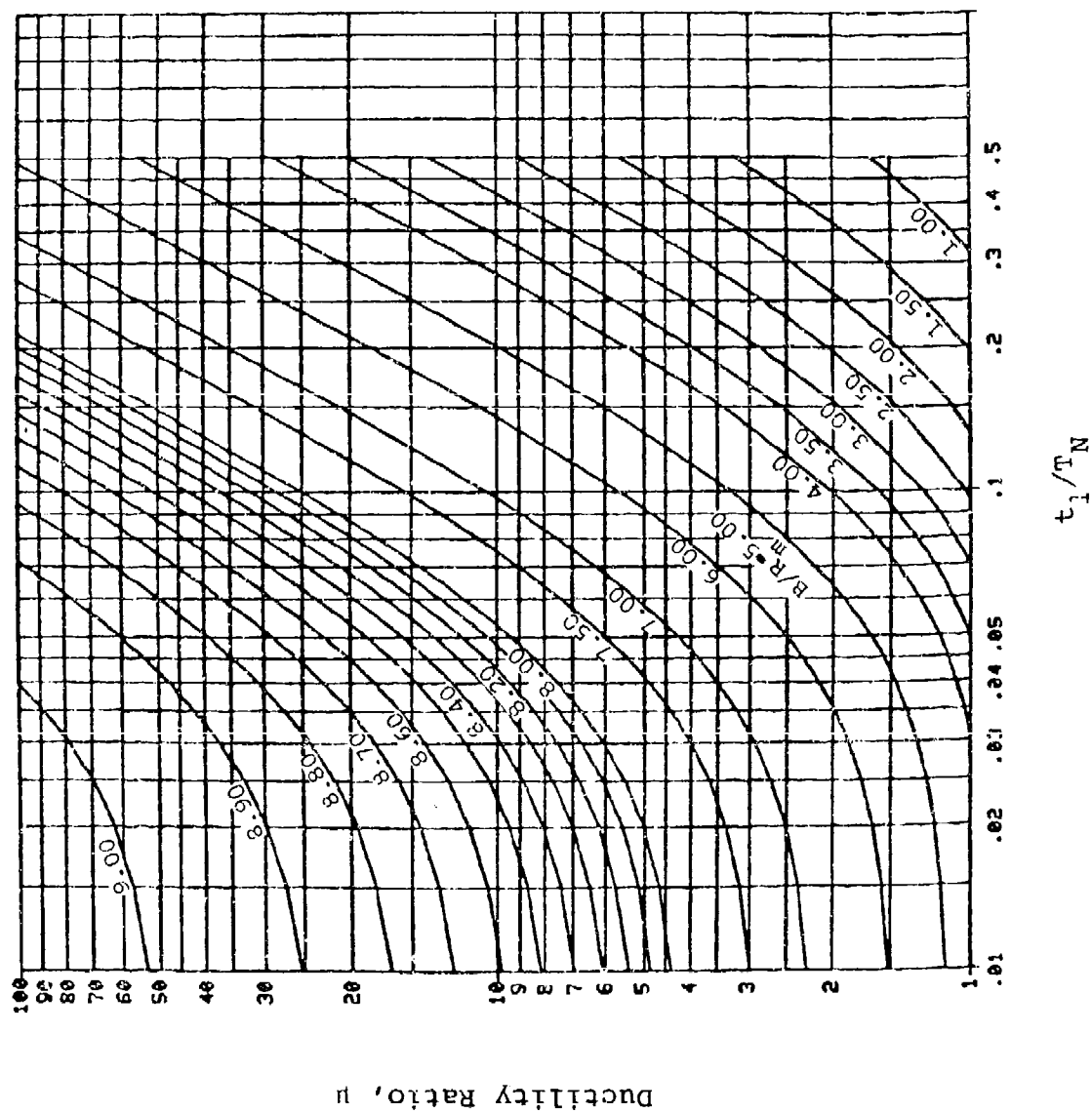


Figure B-30. Response Chart for $C_1 = 0.89$ and $C_2 = 0.11$

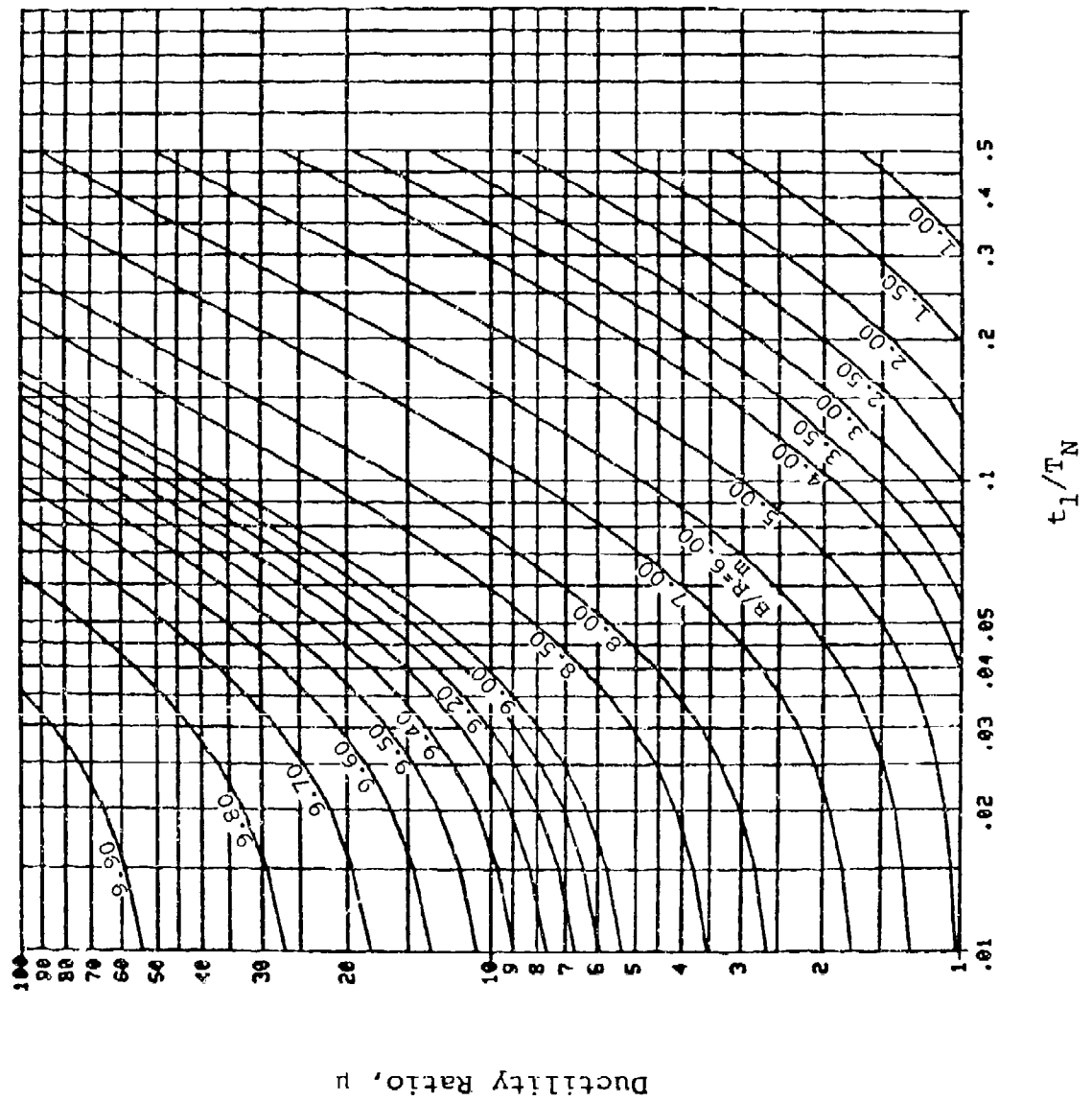


Figure B-31. Response Chart for $C_1 = 0.90$ and $C_2 = 0.10$

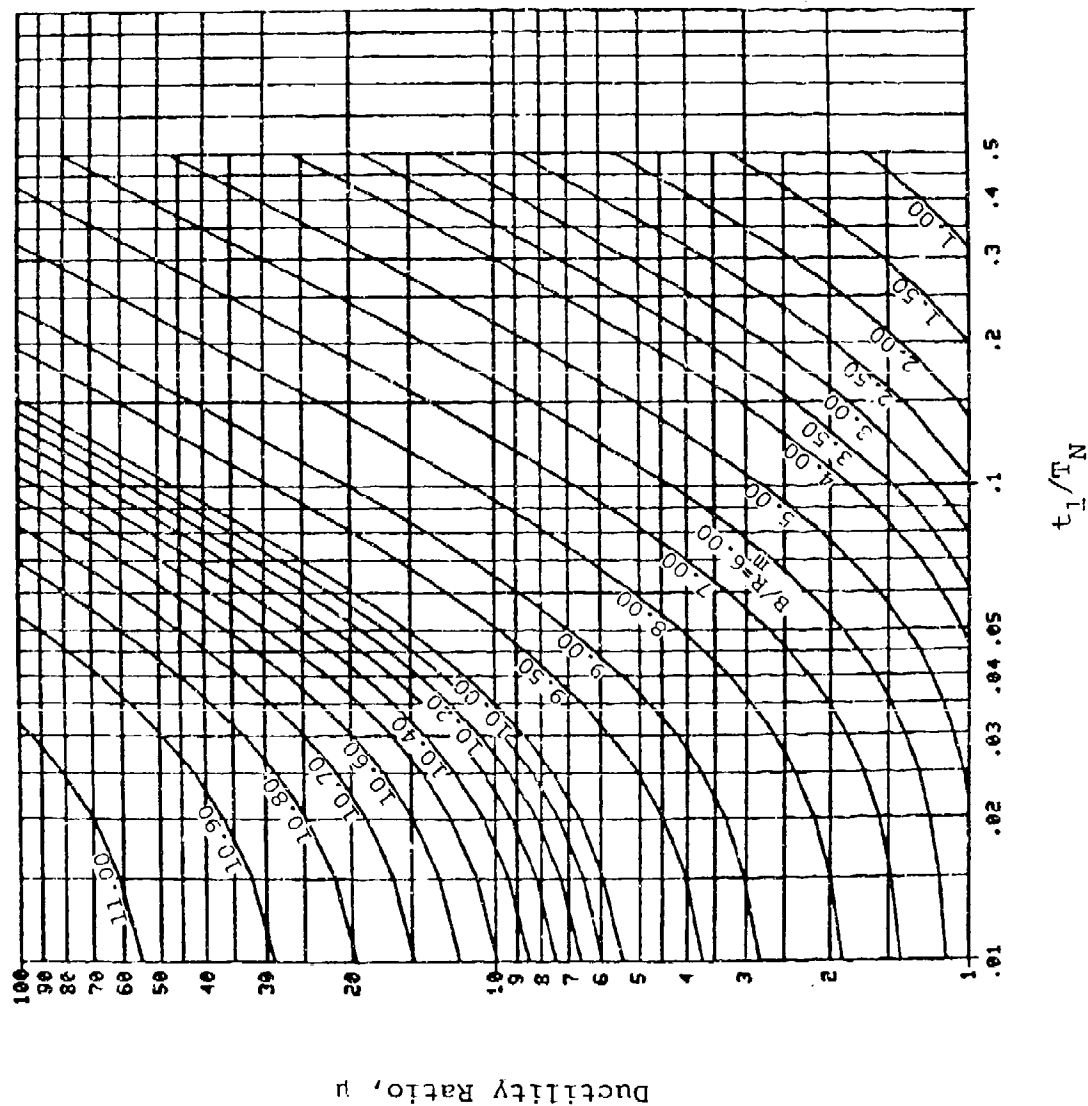


Figure B-32. Response Chart for $C_1 = 0.91$ and $C_2 = 0.09$

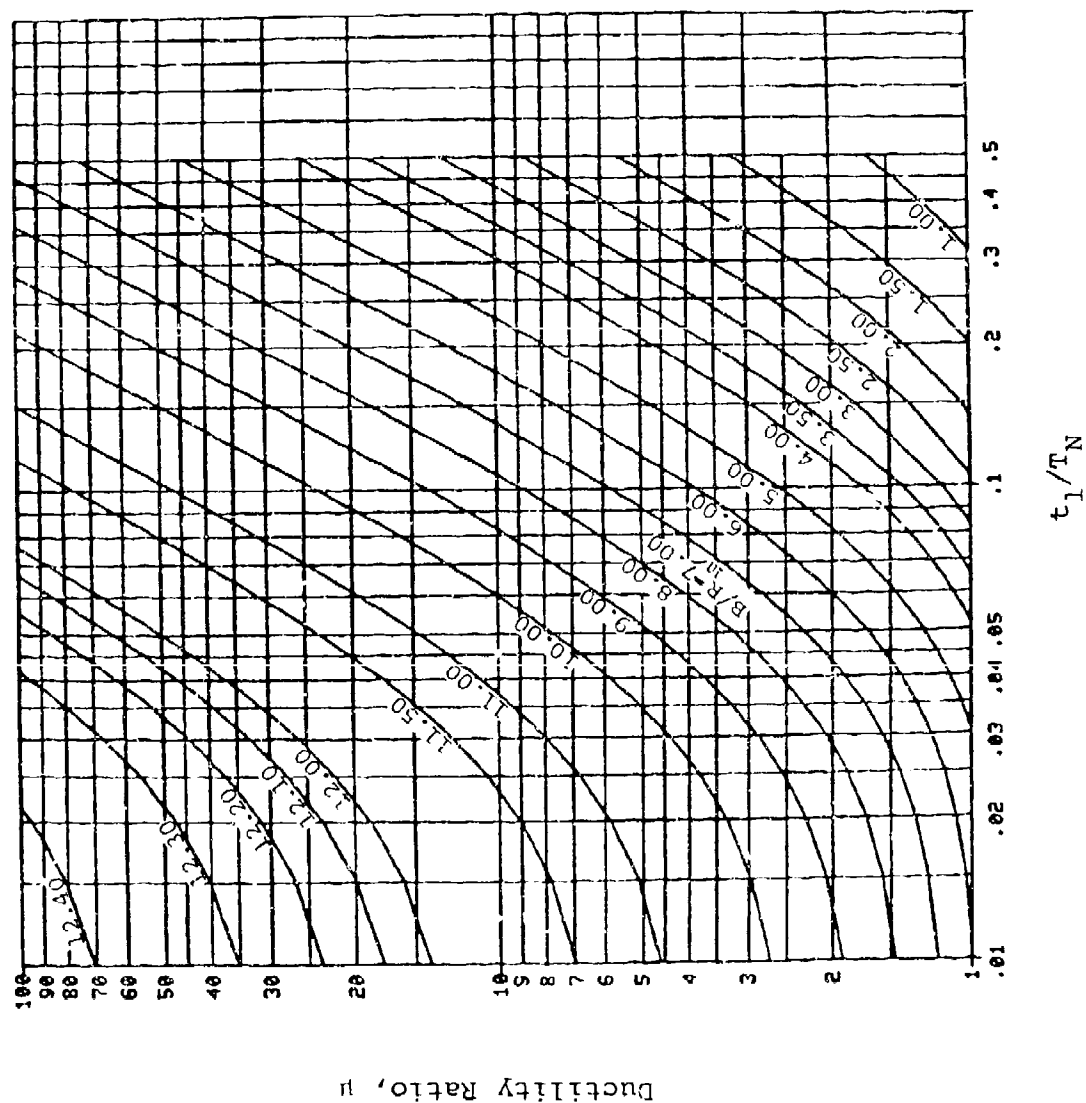


Figure B-33. Response Chart for $C_1 = 0.92$ and $C_2 = 0.08$

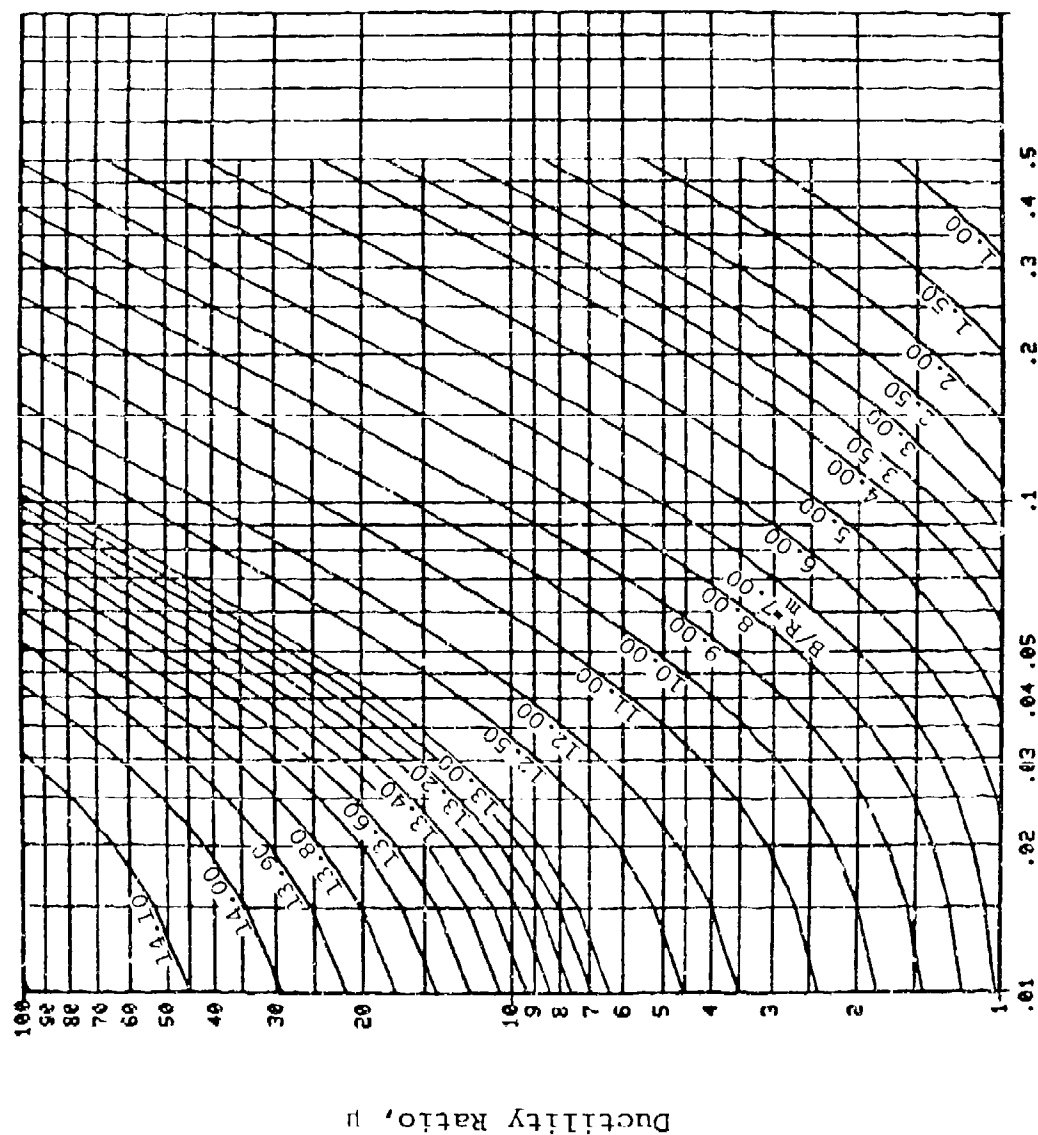


Figure B-34. Response Chart for $C_1 = 0.93$ and $C_2 = 0.07$

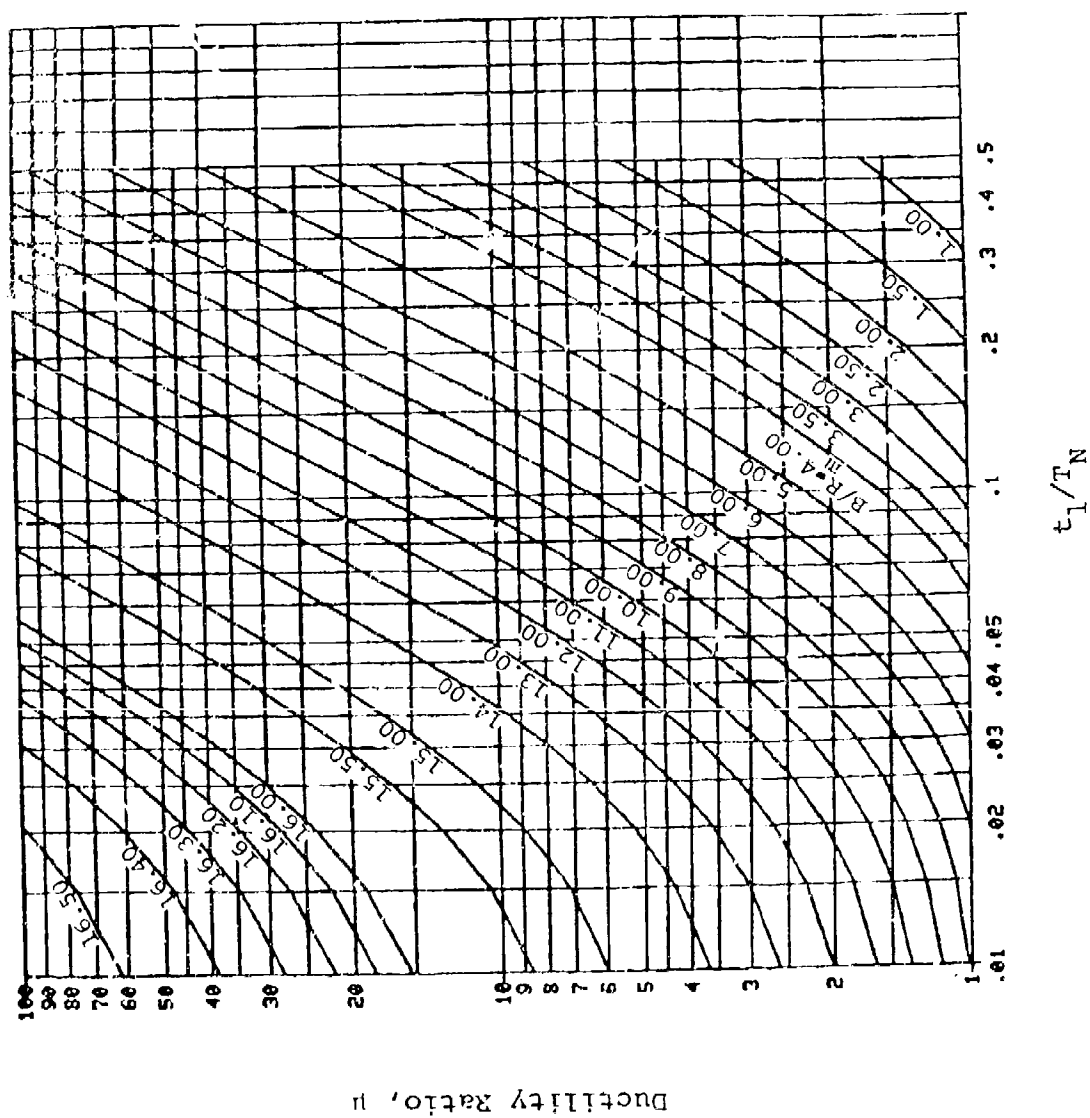


Figure B-35. Response Chart for $C_1 = 0.94$ and $C_2 = 0.06$

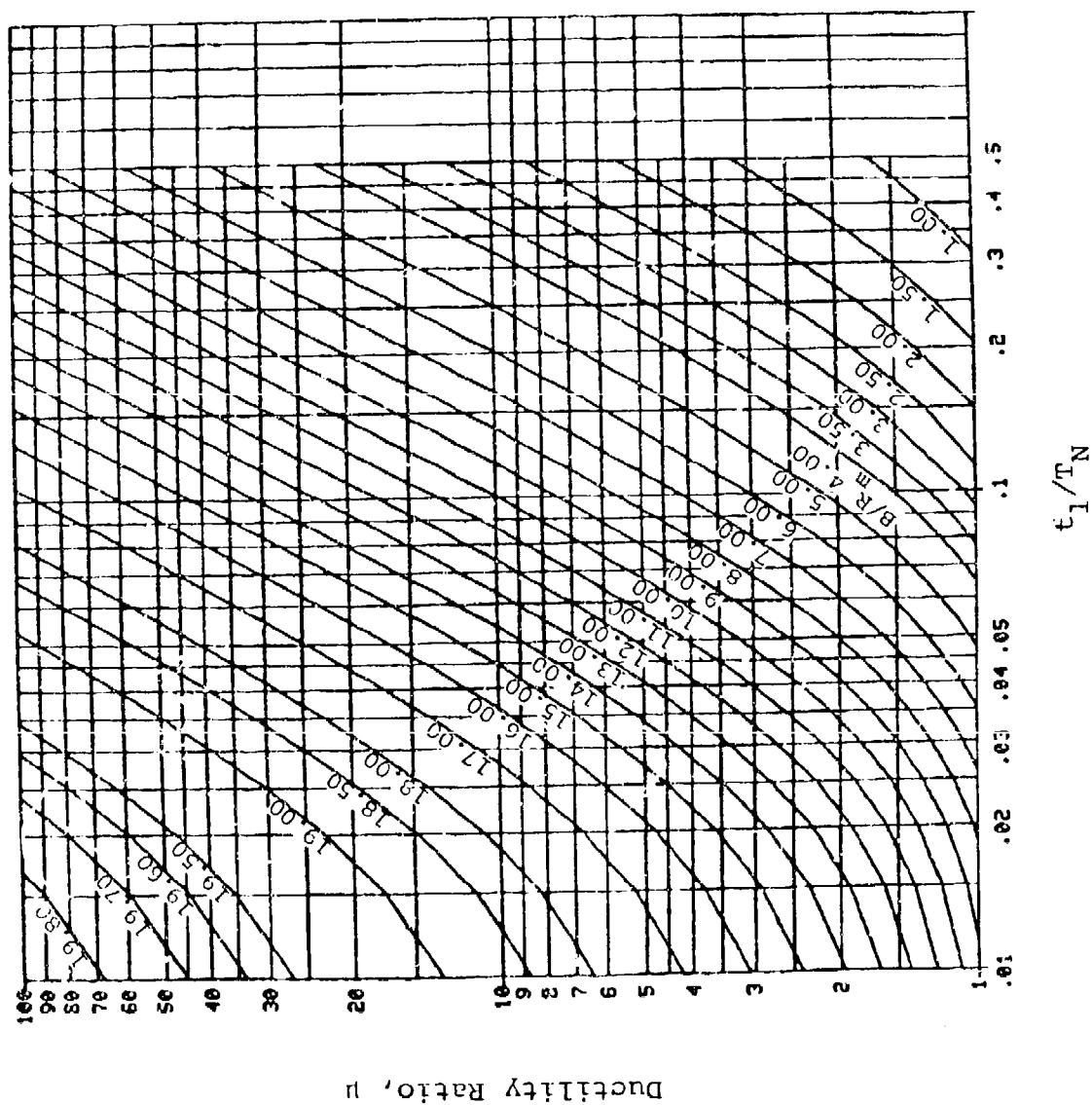


Figure B-36. Response Chart for $C_1 = 0.95$ and $C_2 = 0.05$

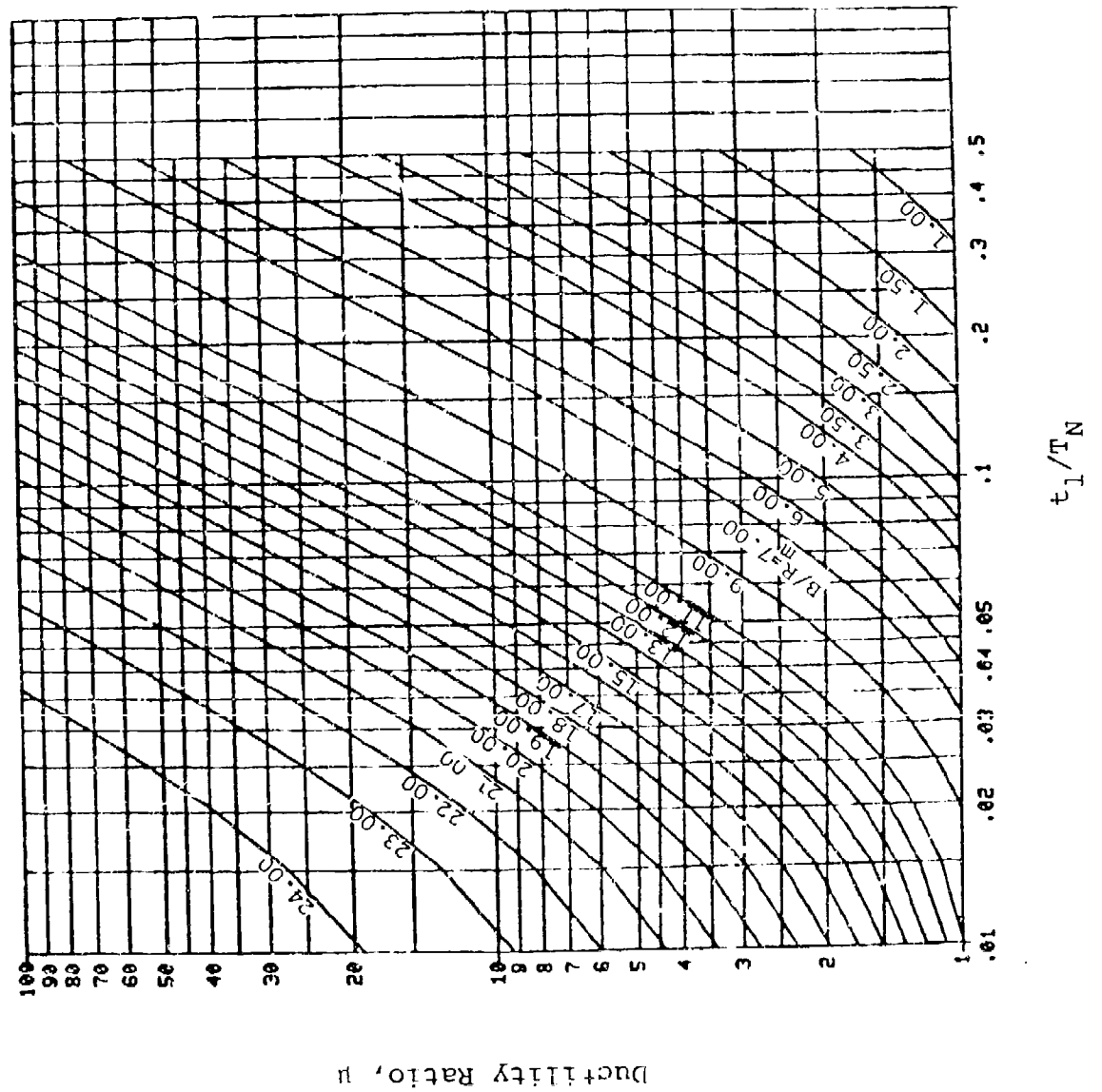


Figure B-37. Response Chart for $C_1 = 0.96$ and $C_2 = 0.04$

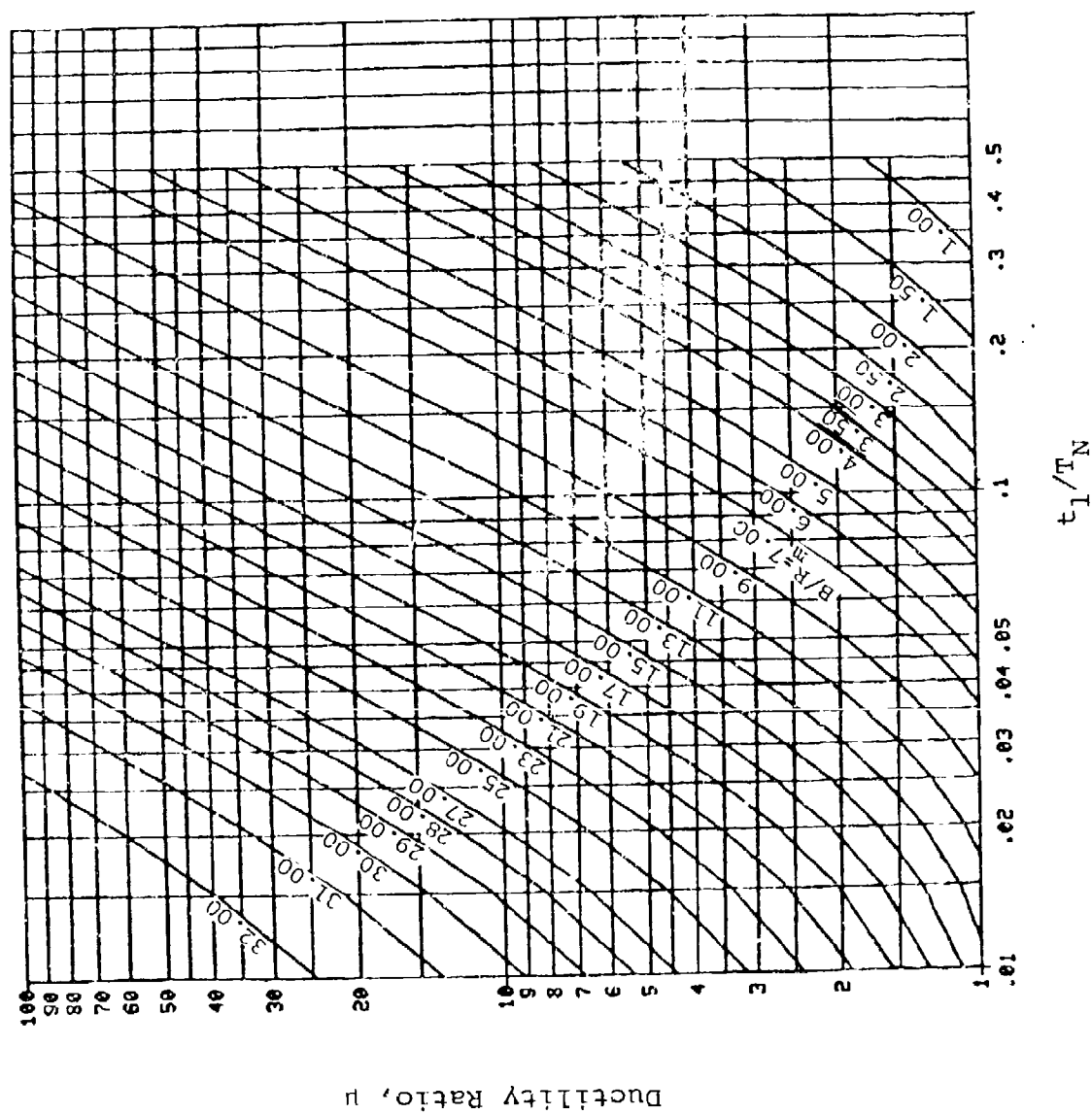


Figure B-32. Response Chart for $C_1 = 0.97$ and $C_2 = 0.03$

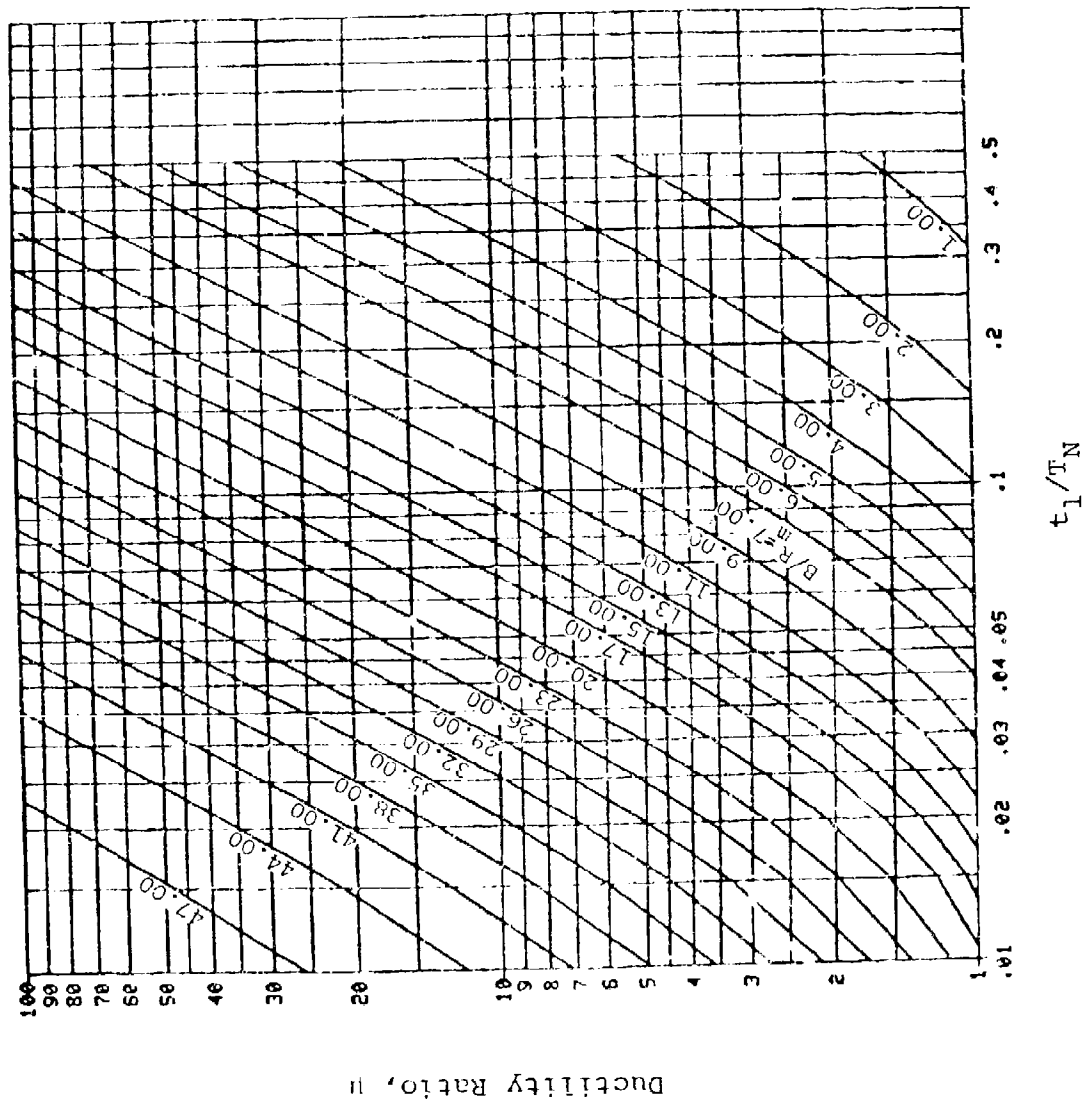


Figure B-39. Response Chart for $C_1 = 0.98$ and $C_2 = 0.02$

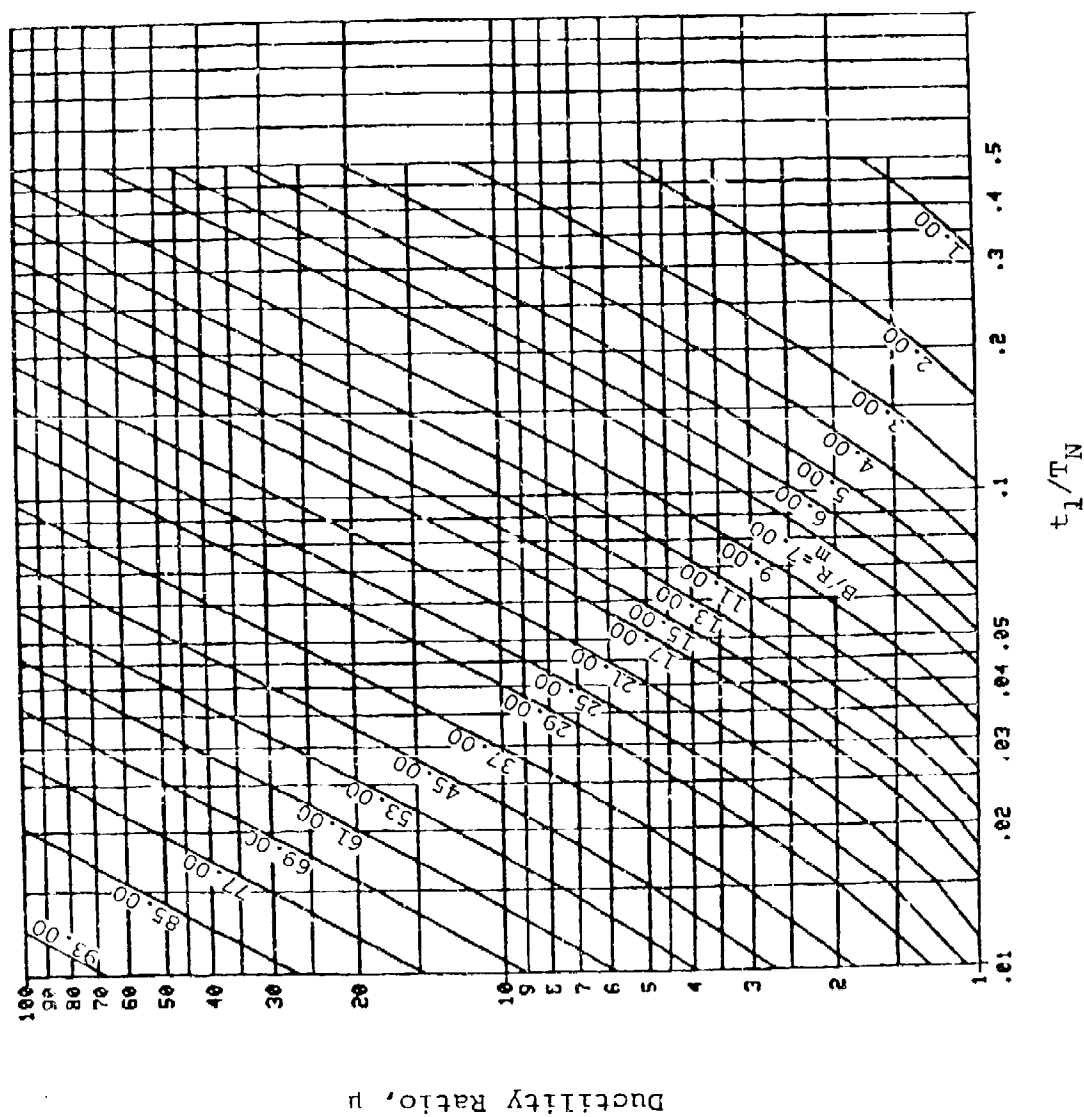


Figure B-40. Response Chart for $C_1 = 0.99$ and $C_2 = 0.01$

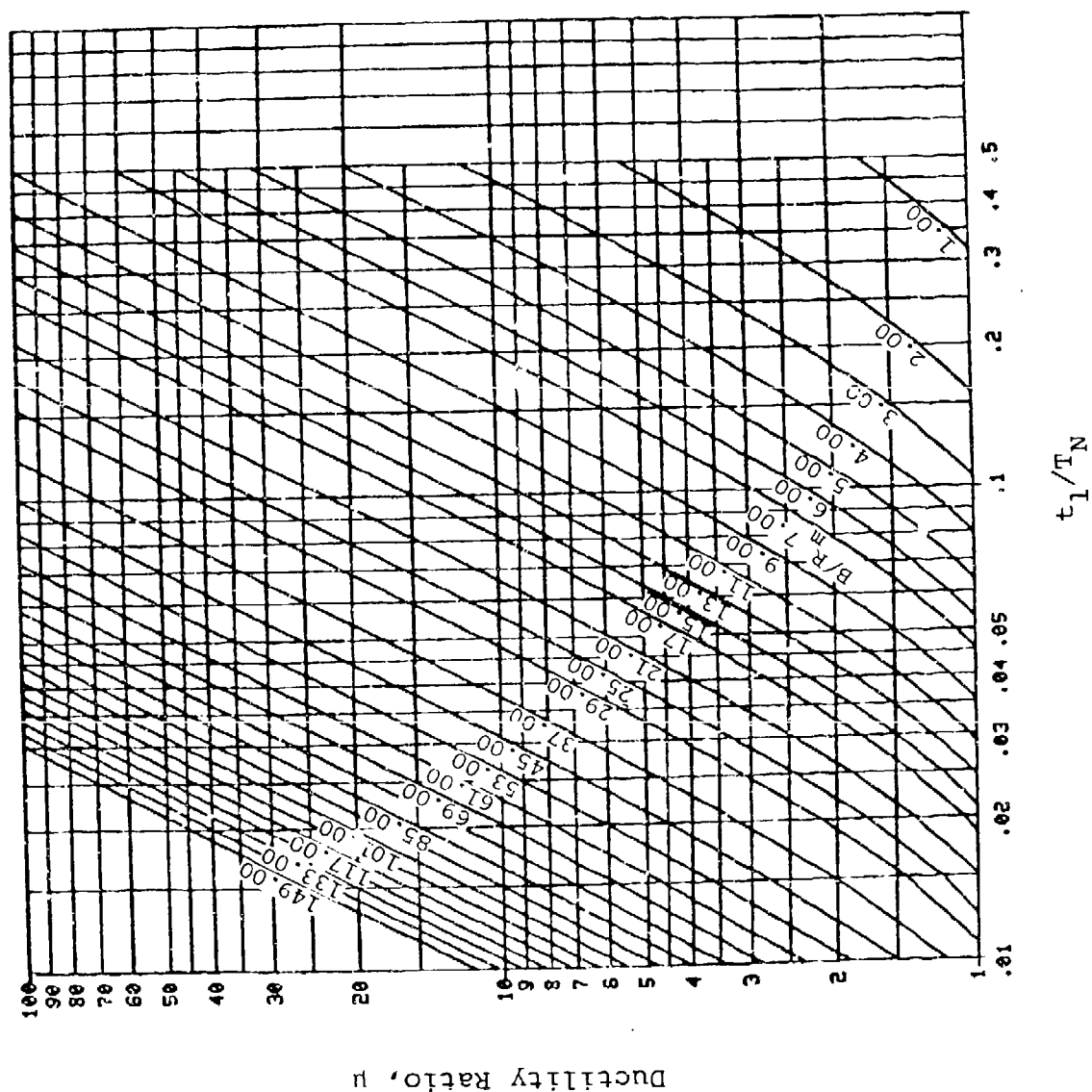


Figure B-41. Response Chart for $C_1 = 1.00$ and $C_2 = 0.00$

APPENDIX C

METRIC CONVERSION FACTORS

APPENDIX C
METRIC CONVERSION FACTORS
BASED ON THE INTERNATIONAL (SI) METRIC SYSTEM

To Convert From	To	Multiply By
<u>Acceleration</u>		
foot/second ²	meter/second ² (m/s ²)	3.0480 x 10 ⁻¹
inch/second ²	meter/second ² (m/s ²)	2.5400 x 10 ⁻²
<u>Area</u>		
acre	meter ² (m ²)	4.0469 x 10 ³
foot ²	meter ² (m ²)	9.2903 x 10 ⁻²
inch ²	meter ² (m ²)	6.4516 x 10 ⁻⁴
mile ² (U.S. Statute)	meter ² (m ²)	2.5900 x 10 ⁶
yard ²	meter ² (m ²)	8.3613 x 10 ⁻¹
<u>Energy (Work)</u>		
foot-pound force	joule (J)	1.3558 x 10 ⁰
foot-poundal	joule (J)	4.2140 x 10 ⁻²
<u>Force</u>		
kip	newton (N)	4.4482 x 10 ³
ounce force (avoir.)	newton (N)	2.7801 x 10 ⁻¹
pound force (avoir.)	newton (N)	4.4482 x 10 ⁰
poundal	newton (N)	1.3826 x 10 ⁻¹

To Convert From	To	Multiply By
<u>Force/Area (Pressure or Stress)</u>		
atmosphere (normal)	pascal (Pa)	1.0133×10^5
foot of water (39.2°F)	pascal (Pa)	2.9890×10^3
inch of mercury (32°F)	pascal (Pa)	3.3864×10^3
inch of water (39.2°F)	pascal (Pa)	2.4908×10^2
kip/inch ² (ksi)	pascal (Pa)	6.8948×10^6
poundal/foot ²	pascal (Pa)	1.4882×10^0
pound force/foot ²	pascal (Pa)	4.7880×10^1
pound force/inch ² (psi)	pascal (Pa)	6.8948×10^3
<u>Force/Length</u>		
kip/foot	newton/meter (N/m)	1.4594×10^4
pound force/inch	newton/meter (N/m)	1.7513×10^2
pound force/foot	newton/meter (N/m)	1.4594×10^1
<u>Length</u>		
fathom	meter (m)	1.8288×10^0
foot	meter (m)	3.0480×10^{-1}
inch	meter (m)	2.5400×10^{-2}
inch	centimeter (cm)	2.5400×10^0
mile (U.S. statute)	meter (m)	1.6093×10^3
mile (U.S. nautical)	meter (m)	1.8520×10^3
yard	meter (m)	9.1440×10^{-1}

To Convert From	To	Multiply By
<u>Mass</u>		
Hundredweight (short)	kilogram (kg)	4.5359×10^1
ounce mass (avoir.)	kilogram (kg)	2.8350×10^{-2}
pound mass (avoir.)	kilogram (kg)	4.5359×10^{-1}
slug	kilogram (kg)	1.4594×10^1
ton (short)	kilogram (kg)	9.0718×10^2
ton (short)	metric ton (m ton)	9.0718×10^{-1}
<u>Mass/Area</u>		
ounce mass/foot ²	kilogram/meter ² (kg/m ²)	3.0515×10^{-1}
ounce mass/inch ²	kilogram/meter ² (kg/m ²)	4.3942×10^1
ounce mass/yard ²	kilogram/meter ² (kg/m ²)	3.3906×10^{-2}
pound mass/foot ²	kilogram/meter ² (kg/m ²)	4.8824×10^0
pound mass/inch ²	kilogram/meter ² (kg/m ²)	7.0307×10^2
pound mass/yard ²	kilogram/meter ² (kg/m ²)	5.4249×10^{-1}
tons (short)/foot ²	kilogram/meter ² (kg/m ²)	9.7649×10^3
tons (short)/yard ²	kilogram/meter ² (kg/m ²)	1.0850×10^3
<u>Mass/Length</u>		
pound mass/foot	kilogram/meter (kg/m)	1.4882×10^0
pound mass/inch	kilogram/meter (kg/m)	1.7858×10^1
pound mass/yard	kilogram/meter (kg/m)	4.9605×10^{-1}

To Convert From	To	Multiply By
<u>Mass/Volume</u>		
ounce (avoir.) / gallon (U.S. liq.)	kilogram/meter ³ (kg/m ³)	7.4892 x 10 ⁰
ounce (avoir.) mass/inch ³	kilogram/meter ³ (kg/m ³)	1.7300 x 10 ³
pound mass/foot ³	kilogram/meter ³ (kg/m ³)	1.6018 x 10 ¹
pound mass/inch ³	kilogram/meter ³ (kg/m ³)	2.7680 x 10 ⁴
pound mass/gallon (U.S. liq.)	kilogram/meter ³ (kg/m ³)	1.1983 x 10 ²
slug/foot ³	kilogram/meter ³ (kg/m ³)	5.1538 x 10 ²
ton (short)/foot ³	kilogram/meter ³ (kg/m ³)	3.2037 x 10 ⁴
ton (short)/yard ³	kilogram/meter ³ (kg/m ³)	1.1856 x 10 ³
<u>Moment or Torque</u>		
kip force-foot	newton-meter (N.m)	1.3558 x 10 ³
ounce force-inch	newton-meter (N.m)	7.0616 x 10 ⁻³
pound force-inch	newton-meter (N.m)	1.1298 x 10 ⁻¹
pound force-foot	newton-meter (N.m)	1.3558 x 10 ⁰
<u>Power</u>		
foot-pound force/hour	watt (W)	3.7662 x 10 ⁻⁴
foot-pound force/minute	watt (W)	2.2597 x 10 ⁻²
foot-pound force/second	watt (W)	1.3558 x 10 ⁰
horsepower (550 ft-lb/sec)	watt (W)	7.4570 x 10 ²
horsepower (boiler)	watt (W)	9.8095 x 10 ³

To Convert From	To	Multiply By
<u>Plane Angle</u>		
degree (angle)	radian (rad)	1.7453×10^{-2}
minute (angle)	radian (rad)	2.9089×10^{-4}
second (angle)	radian (rad)	4.8481×10^{-6}
<u>Section Property</u>		
moment of inertia in ⁴	meter ⁴ (m ⁴)	4.1623×10^{-7}
section modulus in ³	meter ³ (m ³)	1.6387×10^{-5}
<u>Temperature</u>		
degree Celsius	kelvin (K)	$tk = tc + 273.15$
degree Fahrenheit	kelvin (K)	$tk = (t_F + 459.67)/1.8$
degree Fahrenheit	degree Celsius	$tc = (t_F - 32)/1.8$
<u>Velocity</u>		
foot/hour	meter/second (m/s)	8.4667×10^{-5}
foot/minute	meter/second (m/s)	5.0800×10^{-3}
inch/minute	meter/second (m/s)	4.2333×10^{-4}
knot	meter/second (m/s)	5.1444×10^{-1}
knot	kilometer/hour (km/hr)	1.8520×10^0
mile/hour (U.S. statute)	meter/second (m/s)	4.4704×10^{-1}
mile/hour (U.S. statute)	kilometer/hour (km/hr)	1.6093×10^0
mile/minute (U.S. statute)	meter/second (m/s)	2.6822×10^1

To Convert From	To	Multiply By
<u>Volume (Capacity)</u>		
acre-foot	meter ³ (m ³)	1.2335 x 10 ³
barrel (oil, 42 gal.)	meter ³ (m ³)	1.5899 x 10 ⁻¹
board foot	meter ³ (m ³)	2.3597 x 10 ⁻³
bushel (U.S.)	meter ³ (m ³)	3.5239 x 10 ⁻²
foot ³	meter ³ (m ³)	2.8317 x 10 ⁻²
gallon (U.S. dry)	meter ³ (m ³)	4.4049 x 10 ⁻³
gallon (U.S. liquid)	meter ³ (m ³)	3.7854 x 10 ⁻³
inch ³	meter ³ (m ³)	1.6387 x 10 ⁻⁵
ounce (U.S. fluid)	meter ³ (m ³)	2.9573 x 10 ⁻⁵
peck (U.S.)	meter ³ (m ³)	8.8098 x 10 ⁻³
pint (U.S. dry)	meter ³ (m ³)	5.5061 x 10 ⁻⁴
pint (U.S. liquid)	meter ³ (m ³)	4.7318 x 10 ⁻⁴
quart (U.S. dry)	meter ³ (m ³)	1.1012 x 10 ⁻³
quart (U.S. liquid)	meter ³ (m ³)	9.4635 x 10 ⁻⁴
ton (register)	meter ³ (m ³)	2.8317 x 10 ⁰
yard ³	meter ³ (m ³)	7.6455 x 10 ⁻¹
<u>Volume/Time</u>		
barrel/day	meter ³ /second (m ³ /s)	1.8401 x 10 ⁻⁶
barrel/hour	meter ³ /second (m ³ /s)	4.4163 x 10 ⁻⁵
barrel/minute	meter ³ /second (m ³ /s)	2.6498 x 10 ⁻³
foot ³ /hour	meter ³ /second (m ³ /s)	7.8658 x 10 ⁻⁶

To Convert From	To	Multiply By
<u>Volume/Time (continued)</u>		
foot ³ /minute	meter ³ /second (m ³ /s)	4.7195 x 10 ⁻⁴
gallon (U.S. liquid)/day	meter ³ /second (m ³ /s)	4.3813 x 10 ⁻⁸
gallon (U.S. liquid)/hour	meter ³ /second (m ³ /s)	1.0515 x 10 ⁻⁶
gallon (U.S. liquid)/minute	meter ³ /second (m ³ /s)	6.3090 x 10 ⁻⁵
inch ³ /hour	meter ³ /second (m ³ /s)	4.5520 x 10 ⁻⁹
inch ³ /minute	meter ³ /second (m ³ /s)	2.7312 x 10 ⁻⁷
yard ³ /day	meter ³ /second (m ³ /s)	8.8490 x 10 ⁻⁶
yard ³ /hour	meter ³ /second (m ³ /s)	2.1238 x 10 ⁻⁴
yard ³ /minute	meter ³ /second (m ³ /s)	1.2743 x 10 ⁻²

SI PREFIXES AND MULTIPLICATION FACTORS

Prefix	Symbol	Factor	Prefix	Symbol	Factor
tera	T	10 ¹²	centi	c	10 ⁻²
giga	G	10 ⁹	milli	m	10 ⁻³
mega	M	10 ⁶	micro	μ	10 ⁻⁶
kilo	k	10 ³	nano	n	10 ⁻⁹
hecto	h	10 ²	pico	p	10 ⁻¹²
deka	da	10 ¹	femto	f	10 ⁻¹⁵
deci	d	10 ⁻¹	atto	a	10 ⁻¹⁸

BASE AND SUPPLEMENTARY SI UNITS

<u>Quantity</u>	<u>Name</u>	<u>Symbol</u>	<u>Formula</u>
Length	meter	m	-
Mass	kilogram	kg	-
Temperature	kelvin	K	-
Time	second	s	-
Energy	joule	J	N.m
Force	newton	N	kg.m/s ²
Frequency	hertz	Hz	s ⁻¹
Power	watt	W	J/s
Pressure	pascal	Pa	N/m ²
Work	joule	J	N.m

DISTRIBUTION LIST

Names	Copies
CHEMICAL SYSTEMS LABORATORY	
Commander	
Chemical Systems Laboratory	
Aberdeen Proving Ground, MD 21010	
Technical Director	
Attn: SAREA-TD-E	1
Foreign Intelligence Officer	1
Chief, Legal Office	1
Chief, Safety Office	1
CDR, US Army Technical Escort Center	1
DRDAR-CLN-TM, Dr. D.J. Katsanis	50
DEPARTMENT OF DEFENSE	
Administrator	
Defense Documentation Center	
Attn: Accessions Division	12
Cameron Station	
Alexandria, VA 22314	
Defense Supply Agency	
Attn: Mr. John Komos	1
Cameron Station	
Alexandria, VA 22314	
Chairman	
Department of Defense	
Explosives Safety Board	
Attn: COL P. Kelley, Jr.	5
Forrestal Bldg. GB-145	
Washington, DC 20314	
DEPARTMENT OF THE ARMY	
HQDA (DAMC-ODC)	1
Washington, DC 20310	
HQDA (DAEN-MCC-I/Mr. L. Foley)	1
Washington, DC 20314	
HQDA (DAEN-MCE-D/Mr. R. Wight)	1
Washington, DC 20314	
US ARMY MATERIEL DEVELOPMENT AND READINESS COMMAND	
Director	
US Army Materiel Development	
and Readiness Command	
Attn: DRXOS-TA/Mr. Olson/Mr. R. B. Henry	2
Attn: DRXOS-ES/Mr. Myers	50
Field Safety Activity	
Charlestown, IN 47111	

DISTRIBUTION LIST (continued)

Names	Copies
Commander	
US Army Materiel Development and Readiness Command	
Attn: DRCCG	1
Attn: DRCSE/Mr. W. Queen	2
Attn: DRCPM-CS/COL Morris	1
5001 Eisenhower Avenue Alexandria, VA 22333	
Project Manager for Chemical Demilitarization and Installation Restoration	
Attn: DRCPM-DR	2
APG-Edgewood Area	
Project Manager for Munitions Production Base Modernization and Expansion	
US Army Materiel Development and Readiness Command	
Attn: DRCPM-PBM-EC/Mr. A Dybacki	3
Dover, NJ 07801	
Director	
US Army Materiel Development and Readiness Command	
Intern Training Center	1
Red River Depot Texarkana, TX 75502	
US Army Armament Materiel Readiness Command	
Attn: Director, IBEA, DRXIB-MT	2
Attn: DRSAR-EN	1
Attn: HQS, ARRCOM, DRSAR-IMB-C	2
Attn: HQS, ARRCOM, DRSAR-SF	2
Rock Island, IL 61201	
Commander	
DARCOM Ammunition Center	
Attn: SARAC-DE/Mr. J. Byrde	1
Attn: SARAC-DEM/Mr. Huddleston	1
Savanna, IL 61074	
Commander	
US Army Armament Research & Development Command	
Attn: DRDAR-SF	1
Attn: DRDAR-ICM-SP/Mr. Forsten, Mr. Moroney	4
Dover, NJ 07801	

DISTRIBUTION LIST (continued)

Names	Copies
Joint Army-Navy-Air Force Conventional Ammunition Production Coordinating Grp US Army Armament Materiel Readiness Command Attn: Mr. E. Jordan Rock Island, IL 61201	7
Commander Cornhusker Army Ammunition Plant Grand Island, NE 68801	1
Commander Indiana Army Ammunition Plant Charleston, IN 47111	1
Commander Iowa Army Ammunition Plant Burlington, IA 52502	1
Commander Joliet Army Ammunition Plant Joliet, IL 60436	1
Commander Kansas Army Ammunition Plant Parsons, KS 67357	1
Commander Longhorn Army Ammunition Plant Marshall, TX 75671	1
Commander Lone Star Army Ammunition Plant Texarkana, TX 75502	1
Commander Louisiana Army Ammunition Plant Shreveport, LA 71102	1
Commander Milan Army Ammunition Plant Milan, TN 38358	1
Commander Radford Army Ammunition Plant Radford, VA 24141	1
Commander Sunflower Army Ammunition Plant Lawrence, KS 66044	1
Commander Lake City Army Ammunition Plant Attn: Mr. J. Jacobi Independence, MO 64056	1

DISTRIBUTION LIST (continued)

Name	Copies
Commander Ravenna Army Ammunition Plant Ravenna, OH 44266	1
Commander Pine Bluff Arsenal Pine Bluff, AR 71611	1
US ARMY TEST AND EVALUATION COMMAND	
Commander US Army Test and Evaluation Command Attn: AMSTE-NB APG-Aberdeen Area	1
Commander Dugway Proving Ground Attn: Mr. P. Miller Attn: Dr. Rothenburg Dugway, UT 84022	1 1
DEPARTMENT OF THE NAVY	
Commander Naval Ordnance Systems Command Attn: Code ORD 43B/Mr. A. Fernandes Washington, DC 20360	1
Commander Bureau of Naval Weapons Department of the Navy Attn: Code F121/Mr. E. Dougherty Washington, DC 20360	1
Commander Naval Ship Research and Development Center Attn: Code 17417/Mr. A. Wilner Bethesda, MD 20034	1
Commander Naval Explosive Ordnance Disposal Facility Attn: Code 501/Mr. L. Wolfson Indian Head, MD 20640	1
Commander Naval Ordnance Systems Command NAPEC-Ammunition Depot Attn: ORD-04M/B/X-5/Mr. L. Leonard Crane, IN 47522	1

DISTRIBUTION LIST (continued)

Names	Copies
Commander Naval Surface Weapons Center White Oak Laboratory Silver Spring, MD 20910	1
Commander Naval Weapons Laboratory Attn: Mr. Sanches Dahlgren, VA 22448	1
Commander Naval Sea Systems Command Washington, DC 20315	1
DEPARTMENT OF THE AIR FORCE	
Commander Explosives Safety Division Attn: ADTC/SEV/Mr. R. Allen Eglin AFB, FL 32542	1
HQ, Armament Development and Test Center Attn: DOM/Mr. S. Reither Eglin AFB, FL 32542	1
Commander Rocket Propulsion Laboratory Attn: Mr. M. Raleigh Edwards AFB, CA 93523	1
HQ, Ogden Attn: MMNTR/Mr. Cummings Hill AFB, UT 84406	1
Commander Norton AFB Attn: AFISC-SEV San Bernardino, CA 92409	1
Commander Air Force Civil Engineering Center Attn: AFCEC-DE/LTC Walkup Tyndall AFB Panama City, FL 32401	1
HQ, Air Force Logistics Command Attn: MMWM/CPT D. Rideout	1
Attn: IGYE/Mr. K. Shopher Wright-Patterson AFB, OH 45433	1

DISTRIBUTION LIST (continued)

Names	Copies
ADDED ADDRESSES	
Commander US Army Mechanic and Material Research Center Attn: DRXMR-D/Dr. C. Lakshmi-Kantham Watertown, MA 02172	1
Director US Army Materiel Systems Analysis Activity APG-Aberdeen Area	3
Director US Army Ballistics Research Laboratories Attn: Mr. R. Vitali APG-Aberdeen Area	5
Division Engineer US Army Engineer Division, Huntsville Attn: HNDED/CS/Mr. Dembo Attn: Mr. W. Char P.O. Box 1600, West Station Huntsville, AL 35807	1 1
Director US Army Engineer Division Waterways Experimental Station P.O. Box 631 Vicksburg, MS 39180	1
Deputy Manager for Engineering Atomic Energy Commission Attn: Mr. W. H. Jackson P. O. Box E Oak Ridge, TN 37830	1
US Department of Transportation Office of Hazardous Materials Operations Attn: Mr. Erskine Harton, Jr. Transpoint Bldg 2100 Second St., SW Washington, DC 20590	1
Mr. Frank Neff Mound Laboratory Monsanto Research Corp. Miamisburg, OH 45342	1
Dr. W. E. Baker Southwest Research Institute San Antonio, TX 78284	1

DISTRIBUTION LIST (continued)

Names	Copies
Division Engineer US Army Engineer Division Fort Belvoir, VA 22060	1
Chief ARRADCOM Operations Offices NASA National Space Technology Laboratories Bay St. Louis, MS 39520	1
Battelle Columbus Laboratories Attn: Dr. Dale Trott 505 King Avenue Columbus, OH 43201	1
Thiokol Corp Attn: Dr. Dillehay Longhorn Army Ammunition Plant Marshall, TX 75671	1
Bermite Corp Attn: R.E. Guy Sargus, CA	1
Illinois Technical Research Institute Attn: Mr. Sidney Katz Chicago, IL	1
Denver Research Institute Attn: Dr. Robert Blunt University Park Denver, CO 80210	1
Civil/Nuclear Systems Corporation Attn: Dr. Robert E. Crawford 1200 University Blvd., NE Albuquerque, NM 87102	10
Mr. James Vacca DCAS/MA/QS 45 So. Front Street Reading, PA 19002	1
Commander Air Force Systems Command Attn: AFSC/IGFG, Mr. Robert Newbern Andrews Air Force Base, MD 20334	1
Commander/Director US Army Construction Engineering Research Laboratory Attn: Mr. Robert Weber P.O. Box 4005 Champaign, IL 61820	1

DISTRIBUTION LIST (concluded)

Names	Copies
HQDA (DAEN-SOD, Mr. Tom Bower) Washington, DC 20314	1
Commander Civil Engineering Laboratory/NCBC Attn: Mr. William Keenan Port Hueneme, CA 93043	1
AFISC/SEV Attn: Mr. Robert Alg Norton Air Force Base, CA	1
AAI Corporation P. O. Box 6767 Baltimore, MD 21204	1
Commander 548th Ordnance Detachment (EODCC) Presidio of San Francisco, CA 94129	1

Unclassified

SECURITY CLASSIFICATION OF THIS PAGE (When Data Entered)

REPORT DOCUMENTATION PAGE		READ INSTRUCTIONS BEFORE COMPLETING FORM	
1. REPORT NUMBER HNDM-1110-1-2	2. GOVT ACCESSION NO.	3. RECIPIENT'S CATALOG NUMBER 9 rept.	
4. TITLE (and Subtitle) Suppressive Shields Structural Design and Analysis Handbook.		5. TYPE OF REPORT & PERIOD COVERED Final Sep 76 - Nov 77.	
7. AUTHOR(s) 12 497p.		8. CONTRACT OR GRANT NUMBER(s) 15 DACA87-76-C-0057	
9. PERFORMING ORGANIZATION NAME AND ADDRESS Civil/Nuclear Systems Corporation 1200 University Blvd, NE Albuquerque, New Mexico 87102		10. PROGRAM ELEMENT, PROJECT, TASK AREA & WORK UNIT NUMBERS	
11. CONTROLLING OFFICE NAME AND ADDRESS US Army Corps of Engineers, Huntsville Division, HNDED-CS, PO Box 1600 Huntsville, AL 35807		12. REPORT DATE 18 November 1977	
14. MONITORING AGENCY NAME & ADDRESS (if different from Controlling Office) Director, Chemical Systems Laboratory ATTN: DRDAR-CLN-TM Aberdeen Proving Ground, Maryland 21010 (CPD: Dr. David J. Katsanis, 671-3328/4219)		13. NUMBER OF PAGES 564	
15. DISTRIBUTION STATEMENT (of this Report) Approved for public release; distribution unlimited.		15. SECURITY CLASS. (of this report) UNCLASSIFIED	
16. DECLASSIFICATION/DOWNGRADING SCHEDULE			
17. DISTRIBUTION STATEMENT (of the abstract entered in Block 20, if different from Report)			
18. SUPPLEMENTARY NOTES			
19. KEY WORDS (Continue on reverse side if necessary and identify by block number) Suppressive Shield Design Fragment Parameters Suppressive Shield Analysis Safety Approval of New Shields Safety Approved Suppressive Shields Explosive Environments Hazard Identification Blast Waves Charge Parameters Internal Airblast			
20. ABSTRACT (Continue on reverse side if necessary and identify by block number) Procedures for the design, analysis, quality control, and economic analysis of suppressive shields are given. A suppressive shield is a vented steel structure designed to resist the effects of accidental explosions. Eight groups of shields are discussed. The factors necessary for the correct selection and modification of an existing safety approved suppressive shield or the design of a new shield are presented. Explosive environments, fragmentation, fragment penetration, fireball, thermal environment, dynamic material			

DD FORM 1 JAN 73 1473

EDITION OF 1 NOV 65 IS OBSOLETE

Unclassified

SECURITY CLASSIFICATION OF THIS PAGE (When Data Entered)

390 945

13

Unclassified

SECURITY CLASSIFICATION OF THIS PAGE(When Data Entered)

19. (cont.)

Vent Area Ratio

Fireball

Material Properties

Structural Ductility

Structural Resistance

Equivalent Single Degree of Freedom

Fragmentation

Dynamic Response

Energy Methods

Numerical Integration

Structural Details

Structural Penetrations

Economic Analysis

Structural Quality

Welding

Fiber-Reinforced Concrete

Safety Approved Drawings

20. (cont.)

properties and structural ductility are explained. A simplified method of structural dynamic analysis of new designs, including structural details, is discussed. Illustrative examples are presented to assist in any new design. Drawings and design data for all safety approved suppressive shields are included. ←

Unclassified

SECURITY CLASSIFICATION OF THIS PAGE(When Data Entered)